INORGANIC HALOGEN OXIDIZERS

FINAL REPORT

RI/RD 94 - 271

Period 1 June 1991 - 31 August 1994

Prepared for:

U.S. ARMY RESEARCH OFFICE
RESEARCH TRIANGLE PARK, NC   27709

A Report on Work Sponsored by the U.S. Army Research Office, under Contract DAAL03-91-C-0025

AUTHOR: K.O. Christe and W.W. Wilson

Rockwell International Corporation
Rocketdyne Division
6633 Canoga Avenue, Canoga Park, CA   91303

Date of Report: 23 September 1994

MASTER COPY   KEEP THIS COPY FOR REPRODUCTION PURPOSES

REPORT DOCUMENTATION PAGE	Form Approved OMB No. 0704-0188

Public reporting burden for this collection of information is estimated to average 1 hour per response, including the time for reviewing instructions, searching existing data sources, gathering and maintaining the data needed, and completing and reviewing the collection of information. Send comments regarding this burden estimate or any other aspect of this collection of information, including suggestions for reducing this burden, to Washington Headquarters Services, Directorate for Information Operations and Reports, 1215 Jefferson Davis Highway, Suite 1204, Arlington, VA 22202-4302, and to the Office of Management and Budget, Paperwork Reduction Project (0704-0188), Washington, DC 20503.

1. AGENCY USE ONLY (Leave blank)	2. REPORT DATE 23 September 1994	3. REPORT TYPE AND DATES COVERED FINAL: 1 Jun 91–30 Nov 94

4. TITLE AND SUBTITLE	5. FUNDING NUMBERS
INORGANIC HALOGEN OXIDIZERS	DAAL03-91-C-0025

6. AUTHOR(S)

K.O. CHRISTE AND W.W. WILSON

7. PERFORMING ORGANIZATION NAME(S) AND ADDRESS(ES)	8. PERFORMING ORGANIZATION REPORT NUMBER
ROCKWELL INTERNATIONAL CORPORATION Rocketdyne Division 6633 Canoga Avenue Canoga Park, CA 91303	RI/RD94-271

9. SPONSORING/MONITORING AGENCY NAME(S) AND ADDRESS(ES)	10. SPONSORING/MONITORING AGENCY REPORT NUMBER
U. S. Army Research Office P. O. Box 12211 Research Triangle Park, NC 27709-2211	ARO 28655.24-CH

11. SUPPLEMENTARY NOTES

The view, opinions and/or findings contained in this report are those of the author(s) and should not be construed as an official Department of the Army position, policy, or decision, unless so designated by other documentation.

12a. DISTRIBUTION/AVAILABILITY STATEMENT	12b. DISTRIBUTION CODE
Approved for public release; distribution unlimited.	

13. ABSTRACT (Maximum 200 words)

A research program was carried out in novel energetic materials. This program was highly successful and resulted in 28 major publications. Highlights of this effort include: the characterization of the XeF_5^- anion which is the first example of a pentagonal planar XY_5 structure, completion of our work on a quantitative oxidizer strength scale, the synthesis and characterization of new compounds at the limits of coordination and oxidation, such as $XeOF_5^-$, $TeOF_6^{2-}$, IOF_6^-, IF_8^-, TeF_8^{2-}, TeF_7^-, and XeF_7^+, the study of fluxionality and steric repulsion effects in hexa- and hepta- coordinated species, such as IF_7, HPF_5^-, HSF_5, and IOF_5, the controlled replacement of two fluorine ligands by one doubly bonded oxygen ligand, studies of the thermal instability of NF_5 and the F_3^- anion, the characterization of the N_2F^+ cation, $N(CH_3)_4N_3$, $H_2N_3^+$ cation and the SF_4^- and SOF_4^- radical anions, the synthesis and characterization of a new $Os(+VIII)$ compound, OsF_4O_2, theoretical studies on ONOF and a new family of polynitrogen compounds, the synthesis and characterization of the novel PF_4^- anion and its hydrolysis products, and the electrophilic fluorination of CH_4 with F^+ equivalent N_2F^+ and NF_4^+ salts.

14. SUBJECT TERMS XeF_5^- salts, fluorine-oxygen exchange, high coordination number and oxidation state chemistry, quantitative oxidizer strength scale, IOF_6^-, $TeOF_6^{2-}$, TeF_7^-, TeF_8^{2-}, IF_8^-, $XeOF_5$, HPF_5^-, (cont.)	15. NUMBER OF PAGES	
	16. PRICE CODE	

17. SECURITY CLASSIFICATION OF REPORT	18. SECURITY CLASSIFICATION OF THIS PAGE	19. SECURITY CLASSIFICATION OF ABSTRACT	20. LIMITATION OF ABSTRACT
UNCLASSIFIED	UNCLASSIFIED	UNCLASSIFIED	UL

NSN 7540-01-280-5500

Standard Form 298 (Rev. 2-89)
Prescribed by ANSI Std. Z39-18
298-102

14. SUBJECT TERMS

PF_4^- salts, OsF_4O_2, $ONOF$, NF_5, Br_3^+ and Br_5^+ salts, N_2F^+, $H_2N_3^+$ and XeF_7^+ salts, electrophilic fluorination of CH_4, azidamines, NF_5, the F_3^- anion, and $N(CH_3)_4^+N_3^-$.

Accesion For		
NTIS CRA&I		☒
DTIC TAB		☐
Unannounced		☐
Justification _____		
By _____		
Distribution /		
Availability Codes		
Dist	Avail and / or Special	
A-1		

TABLE OF CONTENTS

FOREWORD

The research reported herein was supported by the U.S. Army Research Office with Dr. R. Husk and Dr. R. Ghirardelli as Scientific Officers. This report covers the period 1 June 1991 through 31 August 1994. The program has been directed by Dr. K.O. Christe. The scientific effort was carried out mainly by Drs. K.O. Christe, W.W. Wilson, C.J. Schack, E.C. Curtis and Mr. R.D. Wilson. The program was administered by Dr. S.C. Hurlock.

Other contributors to these research efforts, at no cost to the contract were:

Dr. D.A. Dixon (DuPont)

Drs. G.J. Schrobilgen, J.C.P, Sanders, and H.P. Mercier (McMaster University)

Drs. G.A. Olah, G.K.S. Prakash, N. Hartz, G. Rasul, Q. Wang, and J. Casanova (USC).

Drs. R. Bau, D. Zhao, S. Sukumar, S.W. Bunte, R. Lu, and T. Metzenthin (USC)

Dr. R. Bougon (CEN Saclay, France)

Dr. Minkwitz (Universität Dortmund, Germany)

Drs. F. Williams, B.W. Walther, and J.T. Wang (University of Tennessee, Knoxville)

Dr. S. Khan (UCLA)

Drs. K. Seppelt and A.R. Mahjoub (Freie Universität Berlin, Germany)

Dr. A. Pagelot (Bruker France)

Drs. H. Oberhammer and H.G. Mack (Universität Tübingen, Germany)

INTRODUCTION

This is the final report of a research program carried out at Rocketdyne between 1 June 1991 and 31 August 1994. The purpose of this program was to explore the synthesis and properties of energetic inorganic halogen oxidizers. Although the program was directed toward basic research, applications of the results were continuously considered.

Only the completed items of research, which have been summarized in manuscript form, are included in this report. A total of 23 technical papers were published and 5 papers are in press in major scientific journals. In addition, 12 papers were presented at international and national conferences. The technical papers are given as Appendices A through BB.

PUBLICATIONS GENERATED UNDER THIS PROGRAM

Published Papers

1. "The Pentafluoroxenate (IV) Anion, XeF_5^-; the First Example of a Pentagonal Planar AX_5 Species," <u>J. Amer. Chem. Soc.</u>, <u>113</u>, 3351 (1991) with E. C. Curtis, H. P. Mercier, J. C. P. Sanders, G. J. Schrobilgen, and D. Dixon.

2. "X-ray Crystal Structure and Raman Spectrum of Tribromine(1+) Hexafluoroarsenate(V), $Br_3^+AsF_6^-$, and Raman Spectrum of Pentabromine(1+) Hexafluoroarsenate(V), $Br_5^+AsF_6^-$," <u>Z. anorg. allg. Chem.</u> <u>593</u>, 46 (1991) with R. Bau, and D. Zhao.

3. "High-coordination Number Fluoro- and Oxofluoro-anions; IF_6O^-, TeF_6O^{2-}, TeF_7^-, IF_8^-, and TeF_8^{2-}," <u>J. Chem. Soc. Chem. Commun.</u>, 837 (1991) with J.C.P. Sanders, G.J. Schrobilgen and W.W. Wilson.

4. "The N_2F^+ Cation. An Unusual Ion Containing the Shortest Presently Known Nitrogen-Nitrogen and Nitrogen-Fluorine Bonds," <u>J. Amer. Chem. Soc.</u>, <u>113</u>, 3795 (1991) with R. D. Wilson, W. W. Wilson, R. Bau, and S. Sukumar, and D.A. Dixon.

5. "New Synthesis, Crystal Structure, and Vibrational Spectra of Tetramethylammonium Azide and Reactions of the Fluoride Anion with HN_3 and of the Azide Anion with HF," <u>J. Amer. Chem. Soc.</u>, <u>114</u>, 3411 (1992) with W.W. Wilson, R. Bau and S. Bunte.

6. "A Quantitative Scale for the Oxidizing Strength of Oxidative Fluorinators," <u>J. Amer. Chem. Soc.</u>, <u>114</u>, 2978 (1992) with D.A. Dixon.

7. "Controlled Replacement of Fluoride by Oxygen in Fluorides and Oxyfluorides," Chapter contributed to a book on "Synthetic Fluorine Chemistry," G.A. Olah, R.D. Chambers and G.K.S. Prakash, Edit. John Wiley & Sons, Inc. (1992) with W.W. Wilson and C.J. Schack.

8. "Osmium Tetrafluoride Dioxide, OsO_2F_4," a New Osmium (VIII) Oxide Fluoride," <u>J. Chem. Soc. Chem. Commun.</u>, 1056 (1992) with R. Bougon.

9. "The Pentabromine (1+) Cation, Br_5^+. Local Density Functional Calculations and Vibrational Spectra," <u>Z. Anorg. Allg. Chem.</u>, <u>612</u>, 1 (1992) with D.A. Dixon and R. Minkwitz.

10. "Nitrogen Pentafluoride: Covalent NF_5 versus Ionic $NF_4^+F^-$ and Studies on the Instability of the Latter," <u>J. Amer. Chem. Soc.</u>, <u>114</u>, 9934 (1992) with W.W. Wilson.

11. "Nitrosyl Hypofluorite: Local Density Functional Study of a Problem Case for Theoretical Methods," J. Phys. Chem., 96, 1018 (1992) with D.A. Dixon.

12. "The Tetrafluorosulfate (1-) and Tetrafluorooxosulfate (1-) Radical Anions, SF_4^- and SF_4O^-," J. Amer. Chem. Soc., 115, 1129 (1993) with J.T. Wang, B. Walther, F. Williams, I.B. Goldberg, D.A. Dixon, and C.J. Schack.

13. "On the Problem of Heptacoordination: Vibrational Spectra, Structure, and Fluxionality of Iodine Heptafluoride" J. Amer. Chem. Soc., 115, 1520 (1993) with E.C. Curtis and D.A. Dixon.

14. "The Aminodiazonium Cation, $H_2N_3^+$," J. Amer. Chem. Soc., 115, 1836 (1993) with W.W. Wilson, D.A. Dixon, S.I. Khan, R. Bau, T. Metzenthin, and R. Lu.

15. "The IOF_6^- Anion: The First Example of a Pentagonal Bipyramidal AX_5YZ Species," J. Amer. Chem. Soc., 115, 2696 (1993) with D.A.Dixon, A.R. Mahjoub, H.P.A. Mercier, J.C.P. Sanders, K. Seppelt, G.J. Schrobilgen, and W.W. Wilson.

16. "Heptacoordination: Pentagonal Bipyramidal TeF_7^- and XeF_7^+ Ions," J. Amer. Chem. Soc., in press with D.A. Dixon, J.C.P. Sanders, G.J. Schrobilgen, and W.W. Wilson.

17. "On the Structure of IOF_5," J. Amer. Chem. Soc., 115, 9655 (1993) with E.C. Curtis and D. A. Dixon.

18. "The $TeOF_6^{2-}$ Anion: The First Example of a Divalent, Pentagonal Bipyramidal "Osmium Tetrafluoride Dioxide, OsO_2F_4," submitted to J. Amer. Chem. Soc., with D.A. Dixon, H.G. Mack, H. Oberhammer, A. Pagelot, J.C.P. Sanders, and G.J. Schrobilgen.

20. "The Tetrafluorophosphite, PF_4^-, Anion," J. Am. Chem. Soc., 116, 2850 (1994) with D.A. Dixon, H.P.A. Mercier, J.C.P. Sanders, G.J. Schrobilgen, and W.W. Wilson.

21. "Heptacoordinated Main-Group Fluorides and Oxofluorides," Chapter 5 in "Inorganic Fluorine Chemistry Toward the 21st Century" ACS Symposium Series 555 (1994), with E.C. Curtis, D.A. Dixon, H.P.A. Mercier, J.C.P. Sanders, G.J. Schrobilgen, and W.W. Wilson.

22. "Electrophilic Fluorination of Methane with "F^+" Equivalent N_2F^+ and NF_4^+ Salts," J. Am. Chem. Soc., 116, 5671 (1994) with J.A. Olah, N. Hartz, G. Rasul, Q Wang, G.K.S. Prakash, and J. Casanova.

23. "Vibrational Spectra and Mutual Ligand Interactions in the Hydrogen Substituted Main Group Hexafluorides HPF_5^- and HSF_5," J. Am. Chem. Soc., 116, 7123 (1994) D.A. Dixon and W.W. Wilson.

Submitted Papers

24. "On the Hydrolysis and Methanolysis of PF_4^- and Nuclear Magnetic Resonance and Vibrational Spectra of the POF_2^- and HPO_2F^- Anions," Inorg. Chem., in press, with D.A. Dixon, J.C.P. Sanders, G.J. Schrobilgen, and W.W. Wilson.

25. "On the Instability of Salts Containing the Trifluoride Anion," J. Fluorine Chem., in press.

26. "Theoretical Prediction of the Structures and Stabilities of Azidamines," J. Phys. Chem., in press, with H.H. Michels, J.A. Montgomery, and D.A. Dixon.

27. "Chemical Methods for the Generation of Fluorine," chapter contributed to the new Fluorine Chemistry edition of Houben-Weyl's Methods of Organic Chemistry.

28. "On the Structure of the $XeOF_5^-$ Anion and of Heptacoordinated Complex Fluorides containing One or Two Highly Repulsive Ligands of Sterically Active Free Valence Electron Pairs," Inorg. Chem., in press, with D.A. Dixon, J.C.P. Sanders, G.J. Schrobilgen, S.S. Tsai, and W.W. Wilson.

Papers Presented at Meetings

29. "A Quantitative Scale for the Oxidizing Strength of Oxidative Florinators," by K.O. Christe and D.A. Dixon, XIIIth International Symposium on Fluorine Chemistry, Bochum, Germany, September, 1991.

30. "Lewis Acid Behavior of Xenon (II) Cations and the Synthesis and Characterization of Fluoro- and Oxofluoro- Xenon Anions at the Limits of Coordination," by K.O. Christe, H.P. Mercier, J.C.P. Sanders, G.J. Schrobilgen, J.S. Thrasher, and W.W. Wilson, XIIIth International Symposium on Fluorine Chemistry, Bochum, Germany, September, 1991.

31. "Syntheses and Characterization of the New PF_4^- and HPO_2F^- Anions," by W.W. Wilson, K.O. Christe, J.P.C. Sanders, G.J. Schrobilgen, D.A. Dixon, and R. Bau, 203rd National Meeting of the American Chemical Society, San Francisco, CA, April, 1992.

32. "From Heptacoordiation to Fulleronium Salts," by K.O. Christe, W.W. Wilson, 203rd National Meeting of the American Chemical Society, San Francisco, CA, April, 1992.

33. "Application of Local Density Functional Theory to Fluorinated Systems," by D.A. Dixon and K.O. Christe, 203rd National Meeting of the American Chemical Society, San Francisco, CA, April, 1992.

34. "Novel Fluorine Oxidizers," by K.O. Christe, High Energy Density Matter Conference, Lancaster, CA, April, 1992.

35. "Osmium Tetrafluoride Dioxide, OsF_4O_2. A new Osmium (+VIII) Fluoride Oxide," by K.O. Christe, Xth European Symposium on Fluorine Chemistry, Padua, Italy, September, 1992.

36. "Computational Studies of Fluorinated Systems," by D.A. Dixon, K.D. Dobbs, and K.O. Christe, ACS 11th Winter Fluorine Conference, St. Petersburg, FA, January, 1993.

37. "Experimental and Computational Chemistry. A Marriage Made in Heaven," by K.O. Christe, W.W. Wilson, and D.A. Dixon, ACS 11th Winter Fluorine Conference, St. Petersburg, FA, January, 1993.

38. "In Search of Novel High Energy Density Materials," by K.O. Christe, High Energy Density Matter Conference, Woods Hole, MA, June, 1993.

39. "On Mutual Ligand Interactions in Monosubstituted Main-Group Hexafluoride," by K.O. Christe, W.W. Wilson, and D.A. Dixon, 207th ACS National Meeting, San Diego, CA, March, 1994.

40. "Novel High Energy Compounds," by K.O. Christe and W.W. Wilson, High Energy Density Matter Conference, Crystal Bay, NV, June, 1994.

RESULTS AND DISCUSSION

The present report follows our tradition [Ref. 1,2] of highly successful research programs under Army sponsorship. In view of the vast amount of technical data generated under this program, this discussion will be limited to a highlight of some of the major achievements. For more details, the reader is referred to the publications given in the Appendices.

Novel Chemistry at the Limits of Coordination and Oxidation

Most of this chemistry is based on our discovery of a synthesis of truly anhydrous tetramethylammonium fluoride in 1990 [Ref. 3]. This compound provides a source of highly soluble fluoride ion while possessing a cation which has excellent kinetic stability toward strong oxidizers. Using CH_3CN as an oxidizer resistant solvent, we have succeeded to prepare and isolate $N(CH_3)_4^+$ salts of strongly oxidizing anions such as ClF_4^- [Ref. 4], ClF_6^- [Ref. 5], IOF_6^- (Appendix O) or $XeOF_5^-$ (Appendix BB). The ability to prepare with this approach highly coordinated fluoro anions in their highest oxidation states has led to a worldwide renaissance in high coordination chemistry, and the structures of many compounds with coordination numbers in excess of 6 have been explored [Appendices C,O,P,R, and U and Ref. 6].

A particularly interesting case is that of heptacoordination. Depending on the presence or absence of free valence electron pairs and unequal ligand repulsions, these compounds can exhibit fluxionality, dynamic puckering effects, and either steric activity or inactivity of the free valence electron pair (see Appendices A,C,M,O,P,R, and BB). Of the numerous novel ions prepared under this program, the most unique one is the XeF_5^- anion (Appendix A). This ion is the first known example of a pentagonal planar XY_5 species.

Nitrogen Fluoride Chemistry

Since recent ab initio calculations [Ref. 7,8] had suggested that NF_5 is a vibrationally stable molecule, and our Born Haber cycles had indicated that the energy difference between covalent NF_5 and ionic $NF_4^+F^-$ should be very small, we examined the thermal stability of $NF_4^+F^-$ by metathetical syntheses at low temperatures. It was found that even at -142°C, $NF_4^+F^-$ is unstable toward decomposition to NF_3 and F_2, a process which we calculated to be exothermic by about 32 kcal mol^{-1} (Appendix J).

In collaboration with Prof. Olah's group from USC, the electrophilic fluorination of methane with "F^+" equivalent N_2F^+ and NF_4^+ salts was studied (Appendix V). It was shown that CH_4 can be fluorinated electrophilicly in high yields to give CH_3F, CH_2F_2 and CHF_3, and the mechanistic consequences of these reactions were discussed.

Azide Chemistry

Recently, there has been considerable interest in the possible existence of new allotropic forms of nitrogen, i.e. polynitrogen compounds [9]. All of these studies were theoretical studies and dealt with cyclic or polycyclic compounds which would be very difficult to synthesize. In collaboration with Dr. Michels from UTC and Dr. Dixon from DuPont we have now shown that a new class of noncyclic polynitrogen compounds the azidamines, are vibrationally stable, and feasible synthetic routes for these materials were proposed (Appendix Z).

We have also found a new synthesis for $N(CH_3)_4^+N_3^-$ and have determined its crystal structure and vibrational spectra. In addition we have studied the reaction chemistry of the F^- anion with HN_3 and of the N_3^- anion with HF. It was found that even at -80°C HN3 displaces F^- from M^+F^- with formation of equimolar amounts of $M^+N_3^-$ and HF. The latter reacts with M^+F^- to give $M^+HF_2^-$. On the other hand, HF quantitatively displaces

N_3^- from $M^+N_3^-$ with formation of HN_3 and $M^+H_2^-$. This apparent discrepancy can be explained by the vast difference in basicity between F^- and HF_2^- (Appendix E).

By protonation of HN_3 in super acids, the new aminodiazonium salts $H_2N_3^+SbF_6^-$, $H_2N_3^+AsF_6^-$, and $H_2N_3^+BF_4^-$ were prepared, and the crystal structure of $H_2N_3^+SbF_6^-$ was determined in collaboration with Prof. Bau from USC. It was shown that both hydrogen atoms are connected to the same nitrogen atom and that $H_2N_3^+$ is isostructural with cyanamide H_2NCN (Appendix N).

High Oxidation State Transition Metal Fluorides

The new Os(+VIII) oxofluoride, OsO_2F_4, was prepared from OsO_4 and KrF_2. It is a stable compound and its structure was determined by electron diffraction, NMR and vibrational spectroscopy. Also, its [187]Os chemical shift was determined by indirect methods in collaboration with Dr. Pagelot from Bruker-France. [187]Os NMR spectra are very difficult to measure because [187]Os is the least sensitive nuclide in the Periodic Table (Appendix S).

Miscellaneous

In the area of polyhalogen chemistry, it was shown that the F_3^- anion, which had previously been observed at 15°K in Ar matrix [Ref. 10], is unstable at temperatures as low as 131°K (Appendix Y). Furthermore, the crystal structure and vibrational spectra of the Br_3^+ cation were determined (Appendix B) and the Br_5^+ cation was studied by Raman spectroscopy and local density functional calculations (Appendix I). Using anhydrous $N(CH_3)_4F$ as a convenient source of soluble F^- ions, the novel PF_4^- anion was prepared and characterized (Appendix T), and its hydrolysis and methanolysis products were studied (Appendix X). Also, the novel SF_4^- and SF_4O^- radical anions were prepared by

γ-irradiation of SF_5^- and SF_5O^- salts and characterized by ESR spectroscopy (Appendix L). The nitrosyl hypofluorite molecule, FONO, which is a problem case for theoretical calculations, was successfully calculated by local density functional methods and the experimentally observed vibrational spectra were successfully duplicated (Appendix K). Our work on a quantitative scale for the oxidizing strength of oxidative fluorination (Appendix F) and systematic fluorine-oxygen exchange reactions (Appendix G) were completed and published. The previously published [Ref. 11] structure of IOF_5 was revised and it was shown that there is no evidence for the existence of a so called "secondary relaxation effect" (Appendix Q).

REFERENCES

[1]   K.O. Christe, "Research in Inorganic Fluorine Chemistry," Final Report under Contract DAAG29-84-C-0001 (March 1, 1987).

[2]   K.O. Christe, "Research in Inorganic Fluorine Chemistry," Final Report under Contract DAAL03-88-C-0005 (May 28, 1991).

[3]   K.O. Christe, W.W. Wilson, R.D. Wilson, R. Bau, and J. Feng, *J. Am. Chem. Soc.*, 112, 7619 (1990).

[4]   W.W. Wilson, R.D. Wilson, R. Bau, and J. Feng, *J. Am. Chem. Soc.*, 112, 7619 (1990).

[5]   K.O. Christe, W.W. Wilson, R.V. Chirakal, J.C.P. Sanders, and G.J. Schrobilgen, *Inorg. Chem.*, 29, 3506 (1990).

[6]   K. Seppelt, Chapter 4 in "Inorganic Fluorine Chemistry Toward the 21st Century," *ACS Symposium Series 555* (1994), J.S. Thrasher and S.H. Strauss edit.

[7]   C.S. Ewig and J.R. VanWazer, *J. Am. Chem. Soc.*, 111, 4172 (1989).

[8]   H.H. Michels and J. Montgomery, *J. Chem. Phys.*, 93, 1805 (1993).

[9]   R. Janoschek, *Angew. Chem. Int. Ed. Engl.*, 32, 230 (1993).

[10] B.S. Ault and L. Andrews, *Inorg. Chem.*, 16, 2024 (1977).

[11] L.S. Bartell, F.B. Clippard, and E.J. Jacob, *Inorg. Chem.*, 15, 3009 (1976).

APPENDICES

A   "The Pentafluoroxenate (IV) Anion, XeF_5^-; the First Example of a Pentagonal Planar AX_5 Species," J. Amer. Chem. Soc., 113, 3351 (1991) with E. C. Curtis, H. P. Mercier, J. C. P. Sanders, G. J. Schrobilgen, and D. Dixon.

B   "X-ray Crystal Structure and Raman Spectrum of Tribromine(1+) Hexafluoroarsenate(V), $Br_3^+AsF_6^-$, and Raman Spectrum of Pentabromine(1+) Hexafluoroarsenate(V), $Br_5^+AsF_6^-$," Z. anorg. allg. Chem. 593, 46 (1991) with R. Bau, and D. Zhao.

C   "High-coordination Number Fluoro- and Oxofluoro-anions; IF_6O^-, TeF_6O^{2-}, TeF_7^-, IF_8^-, and TeF_8^{2-}," J. Chem. Soc. Chem. Commun., 837 (1991) with J.C.P. Sanders, G.J. Schrobilgen and W.W. Wilson.

D   "The N_2F^+ Cation. An Unusual Ion Containing the Shortest Presently Known Nitrogen-Nitrogen and Nitrogen-Fluorine Bonds," J. Amer. Chem. Soc., 113, 3795 (1991) with R. D. Wilson, W. W. Wilson, R. Bau, and S. Sukumar, and D.A. Dixon.

E   "New Synthesis, Crystal Structure, and Vibrational Spectra of Tetramethylammonium Azide and Reactions of the Fluoride Anion with HN_3 and of the Azide Anion with HF," J. Amer. Chem. Soc., 114, 3411 (1992) with W.W. Wilson, R. Bau and S. Bunte.

F   "A Quantitative Scale for the Oxidizing Strength of Oxidative Fluorinators," J. Amer. Chem. Soc., 114, 2978 (1992) with D.A. Dixon.

G   "Controlled Replacement of Fluoride by Oxygen in Fluorides and Oxyfluorides," Chapter contributed to a book on "Synthetic Fluorine Chemistry," G.A. Olah, R.D. Chambers and G.K.S. Prakash, Edit. John Wiley & Sons, Inc. (1992) with W.W. Wilson and C.J. Schack.

H   "Osmium Tetrafluoride Dioxide, OsO_2F_4," a New Osmium (VIII) Oxide Fluoride," J. Chem. Soc. Chem. Commun., 1056 (1992) with R. Bougon.

I   "The Pentabromine (1+) Cation, Br_5^+. Local Density Functionanl Calculations and Vibrational Spectra," Z. Anorg. Allg. Chem., 612, 1 (1992) with D.A. Dixon and R. Minkwitz.

J   "Nitrogen Pentafluoride: Covalent NF_5 versus Ionic $NF_4^+F^-$ and Studies on the Instability of the Latter," J. Amer. Chem. Soc., 114, 9934 (1992) with W.W. Wilson.

K   "Nitrosyl Hypofluorite: Local Density Functional Study of a Problem Case for Theoretical Methods," J. Phys. Chem., 96, 1018 (1992) with D.A. Dixon.

L   "The Tetrafluorosulfate (1-) and Tetrafluorooxosulfate (1-) Radical Anions, SF_4^- and SF_4O^-," J. Amer. Chem. Soc., 115, 1129 (1993) with J.T. Wang, B. Walther, F. Williams, I.B. Goldberg, D.A. Dixon, and C.J. Schack.

M   "On the Problem of Heptacoordination: Vibrational Spectra, Structure, and Fluxionality of Iodine Heptafluoride" J. Amer. Chem. Soc., 115, 1520 (1993) with E.C. Curtis and D.A. Dixon.

N   "The Aminodiazonium Cation, $H_2N_3^+$," J. Amer. Chem. Soc., 115, 1836 (1993) with W.W. Wilson, D.A. Dixon, S.I. Khan, R. Bau, T. Metzenthin, and R. Lu.

O   "The IOF_6^- Anion: The First Example of a Pentagonal Bipyramidal AX_5YZ Species," J. Amer. Chem. Soc., 115, 2696 (1993) with D.A.Dixon, A.R. Mahjoub, H.P.A. Mercier, J.C.P. Sanders, K. Seppelt, G.J. Schrobilgen, and W.W. Wilson.

P   "Heptacoordination: Pentagonal Bipyramidal TeF_7^- and XeF_7^+ Ions," J. Amer. Chem. Soc., in press with D.A. Dixon, J.C.P. Sanders, G.J. Schrobilgen, and W.W. Wilson.

Q   "On the Structure of IOF_5," J. Amer. Chem. Soc., 115, 9655 (1993) with E.C. Curtis and D. A. Dixon.

R   "The $TeOF_6^{2-}$ Anion: The First Example of a Divalent, Pentagonal Bipyramidal AX_5YZ Species and the Vibrational Spectra of the $TeOF_5^-$ Anion," Inorg. Chem., 32, 4089 (1993) with D.A. Dixon, J.C.P.Sanders, G.J. Schrobilgen, and W.W. Wilson.

S   "Osmium Tetrafluoride Dioxide, cis-OsO_2F_4," J. Am. Chem. Soc., 115, 11279 (1993) with D.A. Dixon, H.G. Mack, H. Oberhammer, A. Pagelot, J.C.P. Sanders, and G.J. Schrobilgen.

T   "The Tetrafluorophosphite, PF_4^-, Anion," J. Am. Chem. Soc., 116, 2850 (1994) with D.A. Dixon, H.P.A. Mercier, J.C.P. Sanders, G.J. Schrobilgen, and W.W. Wilson.

U   "Heptacoordinated Main-Group Fluorides and Oxofluorides," Chapter 5 in "Inorganic Fluorine Chemistry Toward the 21st Century" ACS Symposium Series 555 (1994), with E.C. Curtis, D.A. Dixon, H.P.A. Mercier, J.C.P. Sanders, G.J. Schrobilgen, and W.W. Wilson.

V   "Electrophilic Fluorination of Methane with "F^+" Equivalent N_2F^+ and NF_4^+ Salts," J. Am. Chem. Soc., 116, 5671 (1994) with J.A. Olah, N. Hartz, G. Rasul, Q Wang, G.K.S. Prakash, and J. Casanova.

W   "Vibrational Spectra and Mutual Ligand Interactions in the Hydrogen Substituted Main Group Hexafluorides HPF_5^- and HSF_5^-," J. Am. Chem. Soc., 116, 7123 (1994) D.A. Dixon and W.W. Wilson.

X   "On the Hydrolysis and Methanolysis of PF_4^- and Nuclear Magnetic Resonance and Vibrational Spectra of the POF_2^- and HPO_2F^- Anions," <u>Inorg. Chem.</u>, in press, with D.A. Dixon, J.C.P. Sanders, G.J. Schrobilgen, and W.W. Wilson.

Y   "On the Instability of Salts Containing the Trifluoride Anion," <u>J. Fluorine Chem.</u>, in press.

Z   "Theoretical Prediction of the Structures and Stabilities of Azidamines," <u>J. Phys. Chem.</u>, in press, with H.H. Michels, J.A. Montgomery, and D.A. Dixon.

AA   "Chemical Methods for the Generation of Fluorine," chapter contributed to the new Fluorine Chemistry edition of Houben-Weyl's Methods of Organic Chemistry.

BB   "On the Structure of the $XeOF_5^-$ Anion and of Hetacoordinated Complex Fluorides containing One or Two Highly Repulsive Ligands of Sterically Active Free Valence Electron Pairs," <u>Inorg. Chem.</u>, in press, with D.A. Dixon, J.C.P. Sanders, G.J. Schrobilgen, S.S. Tsai, and W.W. Wilson.

Appendix A

Reprinted from the Journal of the American Chemical Society, 1991, *113.*
Copyright © 1991 by the American Chemical Society and reprinted by permission of the copyright owner.

The Pentafluoroxenate(IV) Anion, XeF$_5^-$: The First Example of a Pentagonal Planar AX$_5$ Species

Karl O. Christe,*[1] Earl C. Curtis,[1] David A. Dixon,[2] Hélène P. Mercier,[3]
Jeremy C. P. Sanders,[3] and Gary J. Schrobilgen*[3]

*Contribution from Rocketdyne, A Division of Rockwell International, Canoga Park,
California 91303, the Department of Chemistry, McMaster University, Hamilton,
Ontario L8S 4M1, Canada, and the Central Research and Development Department,
E. I. du Pont de Nemours and Company, Inc., Experimental Station,
Wilmington, Delaware 19880-0328. Received September 28, 1990*

Abstract: Xenon tetrafluoride forms stable 1:1 adducts with N(CH$_3$)$_4$F, CsF, RbF, KF, and NaF and an unstable 1:1 adduct with FNO. All these adducts are ionic salts containing pentagonal planar XeF$_5^-$ anions as shown by a crystal structure determination of N(CH$_3$)$_4^+$XeF$_5^-$, Raman and infrared spectra, and ^{19}F and ^{129}Xe NMR spectroscopy. The X-ray crystal structure of N(CH$_3$)$_4^+$XeF$_5^-$ was determined at −86 °C. This compound crystallizes in the orthorhombic system, space group *Pmcn*, with four molecules in a unit cell of dimensions $a = 6.340$ (2) Å, $b = 10.244$ (3) Å, and $c = 13.896$ (4) Å with $R = 0.0435$ for 638 observed [$I > 3\sigma(I)$] reflections. In addition to four N(CH$_3$)$_4^+$ cations, the structure contains four pentagonal planar XeF$_5^-$ anions per unit cell with D_{5h} symmetry. The Xe–F distances are 1.979 (2)–2.034 (2) Å with F–Xe–F angles of 71.5 (4)–72.3 (4)°. The D_{5h} structure of the XeF$_5^-$ anion is highly unusual and represents the first example of an AX$_5$E$_2$ (E = valence electron lone pair) species in which all six atoms are coplanar. The results from the crystal structure determination and a normal coordinate analysis show that the XeF$_5$ plane of XeF$_5^-$ is considerably more rigid than that in the fluxional IF$_7$ molecule due to the increased repulsion from the xenon free valence electron pairs. Local density functional calculations were carried out for XeF$_5^-$ and XeF$_4$ with a double-numerical basis set augmented by polarization functions and confirm the experimentally observed geometries and vibrational spectra. It is shown that the bonding in XeF$_5^-$ closely resembles that in XeF$_4$. In a valence bond description, it can be visualized as the two axial positions being occupied by two sp-hybridized free valence electron pairs and the equatorial fluorines being bound by two Xe 5p electron pairs through semiionic multicenter four-electron bonds.

Introduction

Recent work in our laboratories has shown that anhydrous N(CH$_3$)$_4$F[4] holds great potential for the synthesis and characterization of novel, high oxidation state, complex fluoro anions.[5-7] An area of special interest to us is the problem of maximum coordination numbers and their influence on the steric activity of free valence electron pairs. For example, it was shown that nitrogen(V) cannot accommodate five fluorine ligands,[8] whereas the iodine in IF$_6^-$, which had long been thought to have a distorted octahedral structure,[9,10] has recently been confirmed to possess a sterically active lone valence electron pair.[10] In contrast, the central atom free valence electron pairs in the smaller ClF$_6^-$ and BrF$_6^-$ anions become sterically inactive due to space limitations, as demonstrated in very recent vibrational[6,10] and single-crystal X-ray structure studies.[11]

In this context, the likely structures of the XeF$_5^-$ and XeF$_6^{2-}$ anions posed an interesting problem, since both anions contain two free valence electron pairs on the xenon central atom. Therefore, they are representatives of the novel AX$_5$E$_2$ and AX$_6$E$_2$ geometries, respectively, where E stands for a free valence electron pair. Whereas no reports have been published on the existence or possible structure of XeF$_5^-$ or any other AX$_5$E$_2$ species, Kiselev and co-workers[13-15] recently reported the synthesis of M$_2$XeF$_6$ salts (M = Cs, Rb, K, Na) from XeF$_4$ and MF. On the basis of vibrational spectra, they surprisingly assigned an octahedral structure to XeF$_6^{2-}$. However, a closer inspection of their published

(1) Rockwell International, Rocketdyne Division.
(2) E. I. du Pont de Nemours and Company, Inc.
(3) McMaster University.
(4) Christe, K. O.; Wilson, W. W.; Wilson, R. D.; Bau, R.; Feng, J. *J. Am. Chem. Soc.* **1990**, *112*, 7619.
(5) Wilson, W. W.; Christe, K. O. *Inorg. Chem.* **1989**, *28*, 4172.
(6) Christe, K. O.; Wilson, W. W.; Chirakal, R. V.; Sanders, J. C. P.; Schrobilgen, G. J. *Inorg. Chem.* **1990**, *29*, 3506.
(7) Wilson, W. W.; Christe, K. O.; Feng, J.; Bau, R. *Can. J. Chem.* **1989**, *67*, 1988.
(8) Christe, K. O.; Wilson, W. W.; Schrobilgen, G. J.; Chirakal, R. V.; Olah, G. A. *Inorg. Chem.* **1988**, *27*, 789.
(9) Klamm, H.; Meinert, H.; Reich, P.; Witke, P. *Z. Chem.* **1968**, *8*, 469.
(10) Christe, K. O.; Wilson, W. W. *Inorg. Chem.* **1989**, *28*, 3275 and references cited therein.

(11) Mahjoub, A. R.; Hoser, A.; Fuchs, J.; Seppelt, K. *Angew. Chem., Int. Ed. Engl.* **1989**, *28*, 1526.
(12) Reference deleted in proof.
(13) Spitzin, V. I.; Kiselev, Yu. M.; Fadeeva, N. E.; Popov, A. I.; Tchumaevsky, N. A. *Z. Anorg. Allg. Chem.* **1988**, *559*, 171.
(14) Kiselev, Yu. M.; Goryachenkov, S. A.; Martynenko, L. I.; Spitsyn, V. I. *Dokl. Akad. Nauk SSSR* **1984**, *278*, 881.
(15) Kiselev, Yu. M.; Fadeeva, N. E.; Popov, A. I.; Korobov, M. V.; Nikulin, V. V.; Spitsyn, V. I. *Dokl. Akad. Nauk SSSR* **1987**, *295*, 378.

0002-7863/91/1513-3351$02.50/0   © 1991 American Chemical Society

spectra[13] revealed that both the frequency separations and relative intensities of the observed bands are incompatible with an octahedral species.[16] Furthermore, it was noted that the Raman spectrum attributed to Cs_2XeF_6 was identical with that previously observed during the laser photolysis of $CsXeF_7$ and tentatively assigned to Cs_2XeF_8.[17] In view of these discrepancies we decided to investigate the fluoride-acceptor properties of XeF_4 using $N(CH_3)_4F$ as a fluoride ion source and to reinvestigate the XeF_4-MF systems.

Experimental Section

Apparatus and Materials. Volatile materials were handled in stainless steel–Teflon and Pyrex glass vacuum lines, as previously described.[18,19] Nonvolatile materials were handled in the dry nitrogen atmosphere of a glovebox.

Literature methods were used for the syntheses of anhydrous $N(CH_3)_4F$,[4] XeF_4,[20] and FNO[21] and the drying of CH_3CN.[4,22] The LiF (Research Inorganic Chemicals, Research Organic Chemicals), NaF (Matheson), and BaF_2 (Baker and Adamson) were dried under vacuum at 125 °C prior to their use. The KF (Allied), RbF (American Potash), and CsF (KBI) were dried by fusion in a platinum crucible, followed by transfer of the hot clinkers to the dry nitrogen atmosphere of the glovebox where the fluoride samples were ground prior to use.

Syntheses of $M^+XeF_5^-$ (M = Cs, Rb, K, Na). The dry, finely powdered alkali metal fluorides (2 mmol) and XeF_4 (4–8 mmol) were loaded inside the drybox into prepassivated (with ClF_3), 10-mL, stainless steel Hoke cylinders that were closed by metal valves. The cylinders were evacuated at −78 °C on the vacuum line and then heated in an oven to 190 °C for 14 h. Unreacted XeF_4 was pumped off at 30 °C and collected in a tared Teflon U-trap at −196 °C until the cylinders reached a constant weight. The combining ratios of MF with XeF_4 were obtained from the observed material balances, i.e., the weights of MF, XeF_4 used, XeF_4 recovered, and the products. Under the above conditions, the following combining ratios were observed: $CsF:XeF_4$ = 1:0.99, $RbF:XeF_4$ = 1:0.95, $KF:XeF_4$ = 1:0.65, and $NaF:XeF_4$ = 1:0.32. Additional heating of the $KF–XeF_4$ and $NaF–XeF_4$ adducts with more XeF_4 to 135 °C for 10 days increased the conversion of KF and NaF to the corresponding XeF_5^- salts to 73% and 36%, respectively.

Synthesis of $NO^+XeF_5^-$. In the drybox, XeF_4 (1.03 mmol) was loaded into a prepassivated 0.5-in.-o.d. Teflon–FEP ampule that was closed by a stainless steel valve. On the vacuum line, FNO (6.77 mmol) was added to the ampule at −196 °C. The ampule was allowed to warm to 0 °C and was kept at this temperature for 10 min with agitation, and the unreacted FNO was then pumped off at −78 °C. The white solid residue (265 mg, weight calculated for 1.03 mmol of $NO^+XeF_5^-$ = 264 mg) had a dissociation pressure of 10 Torr at 0 °C.

Synthesis of $N(CH_3)_4^+XeF_5^-$. In a typical synthesis, $N(CH_3)_4F$ and XeF_4 (2.01 mmol each) were loaded into a Teflon–FEP ampule in a drybox and CH_3CN (3 mL liquid) was vacuum distilled onto the solid at −196 °C. The mixture was warmed to −40 °C for 30 min with agitation and then allowed to warm to room temperature, followed by removal of the solvent in vacuo at this temperature. The white solid residue [605 mg, weight calculated for 2.01 mmol of $N(CH_3)_4^+XeF_5^-$ = 604 mg] was identified as $N(CH_3)_4^+XeF_5^-$ by vibrational and NMR spectroscopy and a crystal structure determination. When isolated from CH_3CN solution, the compound is stable indefinitely at room temperature.

Caution! When solutions of $N(CH_3)_4^+XeF_5^-$ in CH_3CN are frozen in liquid nitrogen, they may detonate. Similar, but milder, detonations were also found to occur when XeF_4 solutions were frozen at −196 °C. Exposure of solid samples of $N(CH_3)_4^+XeF_5^-$ to atmospheric moisture for even brief periods has resulted in the violent detonation of bulk samples.

Crystal Structure Determination of $N(CH_3)_4^+XeF_5^-$. Crystal Growing. Single crystals of $N(CH_3)_4^+XeF_5^-$ suitable for X-ray analysis were grown from CH_3CN solution by vacuum distilling ca. 2.5 mL of dry CH_3CN onto ca. 50 mg of $N(CH_3)_3^+XeF_5^-$ in a $^1/_4$-in.-o.d. FEP reaction vessel equipped with a Kel-F valve. The mixture was warmed to 65 °C to effect

Table I. Summary of Crystal Data and Refinement Results for $[N(CH_3)_4]^+[XeF_5]^-$ [a]

space group	*Pmcn* (orthorhombic)
a (Å)	6.340 (2)
b (Å)	10.244 (3)
c (Å)	13.896 (4)
V (Å³)	902.55
molecules/unit cell	4
molec wt (g mol⁻¹)	300.44
calcd density (g cm⁻³)	2.153
T (°C)	−86
color	colorless
cryst decay (%)	0.6
μ (cm⁻¹)	35.77
wavelength (Å) used for data collectn	0.710 69
sin θ/λ limit (Å⁻¹)	0.538
total no. of reflcns measured	1414
no. of independent reflcns	641
no. of reflcns used in struct anal. $I > 3\sigma(I)$	638
no. of variable params	83
final agreement factors	$R(F)$ = 0.0435
	$R(WF)$ = 0.0435

[a] Unit cell parameters obtained at 23 °C were a = 6.400 Å, b = 10.321 Å, and c = 14.029 Å; volume, 926.71 Å³.

dissolution and allowed to cool slowly to room temperature (ca. 5 °C/h). Colorless crystals up to 5 mm in length, having a needle-like morphology, formed overnight. The mother liquor was syringed off the crystals in a dry nitrogen atmosphere and residual solvent was removed under dynamic vacuum. Several crystals were cleaved perpendicular to their long axes to give fragments measuring ca. 0.2 mm × 0.2–0.3 mm and transferred in a drybox to 0.2-mm-o.d. Lindemann glass capillaries (previously dried under dynamic vacuum at 250 °C for 1 day) and sealed under a dry nitrogen atmosphere. The crystals were shown to be identical with the bulk sample prior to recrystallization by obtaining the single-crystal Raman spectrum at room temperature (see Figure 5b) and were found to be stable at room temperature in glass indefinitely.

Collection and Reduction of X-ray Data. Crystals of $N(CH_3)_4^+XeF_5^-$ were centered on a Syntex P_3 diffractometer. Accurate cell dimensions were determined at T = 23 °C and at T = −86 °C from a least-squares refinement of the setting angles (χ, φ, and 2θ) obtained from 15 accurately centered reflections (with $22.14° < 2\theta < 28.11°$) chosen from a variety of points in reciprocal space. At T = 23 °C, and after several hours in the X-ray beam, the crystal appeared to be totally decomposed, resulting in an opaque white coloration. Integrated diffraction intensities were collected on a new crystal at T = −86 °C using a θ–2θ scan technique (slowest rate 5.0°/min) with $0 \le h \le 10$, $0 \le k \le 15$, and $-15 \le l \le 15$, using molybdenum radiation monochromatized with a graphite crystal (λ = 0.710 69 Å). Throughout the data collection, two standard reflections were monitored every 48 reflections; a decay of 0.6% was observed; the intensities were adjusted accordingly. A total of 1414 reflections were collected out of which 641 reflections, satisfying the condition $I > 3\sigma(I)$, were chosen for structure solution. The intensities of these reflections were corrected for Lorentz polarization effects.

Solution and Refinement of the Structure. There were two space groups that were consistent with the reflection pattern: the noncentrosymmetric space group $P2_1cn$ (No. 33) and the centrosymmetric space group *Pmcn* (No. 62). The structure has been solved in both centrosymmetric (*Pmcn*) and noncentrosymmetric (*P2₁cn*) space groups. The direct method of structure solution in the computer program SHELX-76[23] was used to locate the positions of the Xe atom and the five F atoms. Successive Fourier synthesis yielded all the remaining non-hydrogen atoms. The structure was refined by using the full-matrix least-squares technique with isotropic thermal parameters for individual atoms. In the case of the *Pmcn* space group and after full convergence of the isotropic refinement (R = 0.1265), the atoms were assigned anisotropic thermal parameters and further refined by the full-matrix least-squares technique (R = 0.0714). The positions of the hydrogen atoms were calculated and the fixed hydrogen atoms were given an isotropic temperature factor of 0.05 Å². [24] The R factor obtained was 0.0652, with the unit weights. There was significant disagreement between the F_o and F_c values of three reflections, 110, 312, and 413, and these values were consequently omitted in a further refinement. This resulted in a global improvement of the structure and a final value for the R factor of 0.0435.

(16) Weidlein, J.; Müller, U.; Dehnicke, K. *Schwingungsspektroskopie*; Georg Thieme Verlag: Stuttgart, Germany, 1982.

(17) Christe, K. O.; Wilson, W. W. *Inorg. Chem.* **1982**, *21*, 4113.

(18) Christe, K. O.; Wilson, R. B.; Schack, C. J. *Inorg. Synth.* **1986**, *24*, 3.

(19) Syvret, R. G.; Schrobilgen, G. J. *Inorg. Chem.* **1989**, *28*, 1564.

(20) (a) Bartlett, N.; Sladky, F. O. *J. Am. Chem. Soc.* **1968**, *90*, 5316. (b) Malm, J. G.; Chernick, C. L. *Inorg. Synth.* **1966**, *8*, 254.

(21) Christe, K. O. *Inorg. Chem.* **1972**, *12*, 1580.

(22) Winfield, J. M. *J. Fluorine Chem.* **1984**, *25*, 91.

(23) Sheldrick, G. M. *SHELX-76 Program for Crystal Structure Determination*; University of Cambridge: Cambridge, England, 1976.

(24) Hall, S. R.; Stewart, J. H. *XTAL 2.6 User's Manual*; University of Western Australia and University of Maryland.

The Pentafluoroxenate(IV) Anion, XeF$_5^-$

J. Am. Chem. Soc., Vol. 113, No. 9, 1991 3353

Table II. Final Atomic Coordinates for [N(CH$_3$)$_4$]$^+$[XeF$_5$]$^-$

atom	x	y	z	pop.^{a}
Xe1	0.2500	0.1233 (1)	0.0155 (1)	0.5
F1	0.2500	0.1876 (9)	0.1497 (6)	0.5
F2	0.2500	−0.0324 (8)	0.1025 (6)	0.5
F3	0.2500	−0.0399 (8)	−0.0673 (6)	0.5
F4	0.2500	0.1799 (9)	−0.1236 (6)	0.5
F5	0.2500	0.3217 (8)	0.0110 (6)	0.5
N1	0.2500	−0.403 (1)	0.172 (1)	0.5
C1	0.2500	0.628 (2)	0.068 (1)	0.5
C2	0.2500	−0.281 (2)	0.231 (1)	0.5
C3	0.437 (5)	−0.483 (2)	0.196 (1)	1.0

^{a} The site occupation factor.

The same procedure was used for the *P*21*cn* space group, which gave rise to a final *R* factor of 0.0763. The ratio of agreement factors *R*-(7.63/4.35) = 1.75 is sufficient by Hamilton's *R* factor ratio test[7] to state that the correct space group is *Pmcn*.

An empirical absorption correction was also applied, but no significant improvement in the refinement was observed; in particular there was no change in the anisotropic thermal parameters.

Details of the data collection parameters and other crystallographic information for the *Pmcn* space group are given in Table I, and the final atomic coordinates are summarized in Table II. The following programs were used: XTAL,[24] data reduction; SHELX-76,[23] structure refinement; SNOOPI,[25] diagrams.

Vibrational Spectroscopy. Raman spectra were recorded on either a Cary Model 83 or a Spex Model 1403 spectrophotometer using a 488-nm exciting line of an Ar ion or the 647.1-nm line of a Kr ion laser, respectively. Baked-out Pyrex melting point capillaries or thin-walled Kel-F tubes were used as sample containers. A previously described[26] device was used for recording the low-temperature spectra (at −150 °C). Single-crystal spectra of N(CH$_3$)$_4^+$XeF$_5^-$ were recorded at room temperature on a Instruments S.A. Mole S-3000 triple spectrograph system equipped with a microscope for focusing the excitation laser to a one-micrometer spot. The Ar laser line at 514.5 nm was selected for excitation of the sample. Crystals were sealed in Lindemann glass capillaries as described below.

Infrared spectra were recorded by using AgBr disks on a Perkin-Elmer Model 283 spectrophotometer. The finely powdered samples were sandwiched between two thin AgBr disks and pressed together in a Wilks minipress inside the drybox.

Nuclear Magnetic Resonance Spectroscopy. The ^{19}F and ^{129}Xe NMR spectra were recorded unlocked (field drift < 0.1 Hz h^{-1}) with Bruker WM-250 and Bruker AM-500 spectrometers equipped with 5.8719-T and 11.744-T cryomagnets, respectively. Fluorine-19 spectra were obtained by using a 5-mm combination ^{1}H/^{19}F probe operating at 235.36 MHz. The spectra were accumulated in 16K memory. Spectral width settings of 5000 and 30000 Hz were employed, yielding data point resolutions of 0.61 and 3.6 Hz/data point and acquisition times of 1.638 and 0.279 s, respectively. No relaxation delays were applied. Typically 300–7000 transients were accumulated. The pulse width corresponding to a bulk magnetization tip angle, θ, of approximately 90° was equal to 1 μs. No line broadening parameters were applied in the exponential multiplication of the free induction decays prior to Fourier transformation.

Xenon-129 NMR spectra were obtained by using a broad-band VSP probe tunable over the range 23–202 MHz; spectra were recorded at 139.05 MHz. The spectra were accumulated in a 16K memory. A spectral width setting of 50 kHz was employed, yielding a data point resolution of 6.1 Hz/data point and an acquisition time of 0.164 s. No relaxation delays were applied. Typically 10000 transients were accumulated. The pulse width corresponding to a bulk magnetization tip angle, θ, of approximately 90° was equal to 18 μs. Line-broadening parameters of 4 Hz were applied in the exponential multiplication of the free induction decays prior to Fourier transformation.

The ^{19}F and ^{129}Xe NMR spectra were referenced to neat external samples of CFCl$_3$ and XeOF$_4$, respectively, at ambient temperature. The chemical shift convention used is that a positive (negative) sign signifies a chemical shift to high (low) frequency of the reference compound.

The ^{129}Xe NMR samples of saturated solutions of N(CH$_3$)$_4^+$XeF$_5^-$ in CH$_3$CN were prepared in 25-cm lengths of $^3/_8$-in.-o.d., $^1/_{32}$-in. wall FEP plastic tubing that had been reduced to 9-mm o.d. by squeezing in a heated precision brass mold. The FEP tubing was heat sealed at one

end with the open end flared (45° SAE) and joined, by means of compression fittings, to a Kel-F valve. The FEP tubes were heat sealed under dynamic vacuum with their contents frozen at −78 °C. The sealed FEP sample tubes were inserted into 10-mm thin-walled precision NMR tubes (Wilmad) in order to run their spectra.

The ^{19}F NMR samples were prepared in precision 5-mm glass NMR tubes (Wilmad). Solid N(CH$_3$)$_4^+$XeF$_5^-$ [or N(CH$_3$)$_4^+$XeF$_5^-$ and N-(CH$_3$)$_4^+$F$^-$] was loaded into the NMR tube in the drybox and CH$_3$CN solvent distilled in vacuo into the tube at −78 °C. The tube was flame sealed. On warming to room temperature, a colorless saturated solution resulted containing some solid N(CH$_3$)$_4^+$XeF$_5^-$, which was decanted into the top of the tube prior to obtaining the NMR spectrum.

Computational Method. The calculations described below were done by using the local density functional theory[27-30] with the program system DMol.[31] DMol employs numerical functions for the atomic basis sets. The atomic basis functions are given numerically as an atom-centered, spherical, polar mesh. The radial portion of the grid is obtained from the solution of the atomic LDF equations by numerical methods. The radial functions are stored as sets of cubic spline coefficients so that the radial functions are piecewise analytic, a necessity for the evaluation of gradients. The use of exact spherical atom results offers certain advantages. Because of the quality of the atomic basis sets, basis set superposition effects should be minimized, correct behavior at the nucleus is obtained, and radial nodal properties of the wave function are present.

Because the basis sets are numerical, the various integrals arising from the expression for the energy need to be evaluated over a grid. The integration points are generated in terms of angular functions and spherical harmonics. The number of radial points N_R is given as

$$N_R = 1.2 \times 14(Z + 2)^{1/3} \qquad (1)$$

where Z is the atomic number. The maximum distance for any function is 12 au. The angular integration points N_0 are generated at the N_R radial points to form shells around each nucleus. The value of N_0 ranges from 14 to 302 depending on the behavior of the density.[32] The Coulomb potential corresponding to the electron repulsion term could be solved by evaluation of integrals. However, since the method is based on the density, it was found to be more appropriate to determine the Coulomb potential directly from the electron density by solving Poisson's equation

$$-\nabla^2 V_c(r) = 4\pi e^2 \rho(r) \qquad (2)$$

In DMol, the form for the exchange–correlation energy of the uniform electron gas is that derived by von Barth and Hedin.[33]

All of the DMol calculations were done with a double-numerical basis set augmented by *d* polarization functions. This can be thought of in terms of size as a polarized double-ζ basis set. However, because exact numerical solutions are employed for the atom, this basis set is of significantly higher quality than a normal molecular orbital polarized double-ζ basis set. The fitting functions have an angular momentum number one greater than that of the polarization function, resulting in a value of $l = 3$ for the fitting functions.

Geometries were determined by optimization using analytic gradient methods.[34] First derivatives in the LDF framework can be calculated efficiently and only take on the order of three to four SCF iterations or 10–25% of an energy evaluation. There are two problems with evaluating gradients in the LDF framework, which are due to the numerical methods that are used. The first is that the energy minimum does not nec-

(27) Parr, R. G.; Yang, W. *Density Functional Theory of Atoms and Molecules*; Oxford University Press: New York, 1989.

(28) Salahub, D. R. In *Ab Initio Methods in Quantum Methods in Quantum Chemistry*, 2nd ed.; Lawley, K. P., Ed.; J. Wiley & Sons: New York, 1987; p 447.

(29) (a) Wimmer, E.; Freeman, A. J.; Fu, C.-L.; Cao, P.-L.; Chou, S.-H.; Delley, B. In *Supercomputer Research in Chemistry and Chemical Engineering*; Jensen, K. F., Truhlar, D. G., Eds.; ACS Symposium Series: American Chemical Society: Washington, DC, 1987; p 49. (b) Dixon, D. A.; Andzelm, J.; Fitzgerald, G.; Wimmer, E.; Delley, B. In *Science and Engineering on Cray Supercomputers. Proceedings of the Fifth International Symposium*; Cray Research: Minneapolis, MN, 1990; p 285.

(30) Jones, R. O.; Gunnarsson, O. *Rev. Mod. Phys.* **1989**, *61*, 689.

(31) Delley, B. *J. Chem. Phys.* **1990**, *92*, 508. DMol is available commercially from BIOSYM Technologies, San Diego, CA.

(32) This grid can be obtained by using the FINE parameter in DMol.

(33) von Barth, U.; Hedin, L. *J. Phys. Chem.* **1972**, *5*, 1629.

(34) (a) Versluis, L.; Ziegler, T. *J. Chem. Phys.* **1988**, *88*, 3322. (b) Andzelm, J.; Wimmer, E.; Salahub, D. R. In *The Challenge of d and f Electrons: Theory and Computation*; Salahub, D. R., Zerner, M. C., Eds.; ACS Symposium Series 394; American Chemical Society: Washington, DC, 1989; p 228. (c) Fournier, R.; Andzelm, J.; Salahub, D. R. *J. Chem. Phys.* **1989**, *90*, 6371.

(35) Pauling, L. *The Nature of the Chemical Bond*, 3rd ed.; Cornell University Press: Ithaca, NY, 1960; p 260.

(36) Bondi, A. *J. Phys. Chem.* **1964**, *68*, 441.

(25) Davies, K. *CHEMGRAF Suite: SNOOPI*; Chemical Design Ltd.: Oxford, England, 1983.

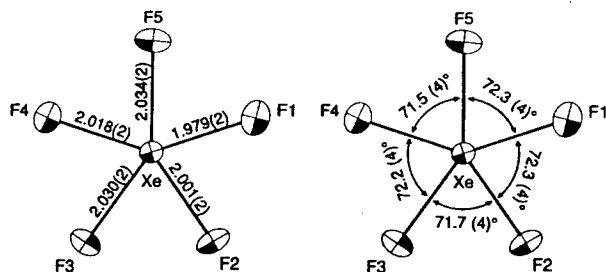(26) Miller, F. A.; Harney, B. M. *Appl. Spectrosc.* **1969**, *23*, 8.

Figure 1. Atom numbering scheme, bond lengths (Å) and angles (deg) for XeF_5^- at -86 °C in $[N(CH_3)_4]^+[XeF_5]^-$. Projection of the XeF_5^- anion on (111). Esd's are given in parentheses; thermal ellipsoids are shown at the 50% probability level.
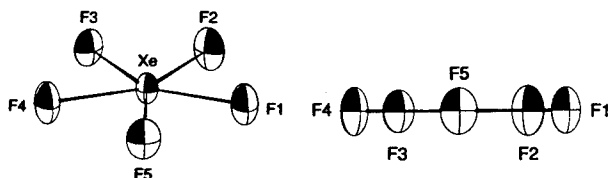

Figure 2. Projections of the XeF_5^- anion on (130) (left) and (010) (right). Thermal ellipsoids are shown at the 50% probability level.

Table III. Bond Distances (Å) and Bond Angles (deg) in $[N(CH_3)_4]^+[XeF_5]^-$

Bond Lengths			
Xe1–F1	1.979 (2)	N1–C1	1.481 (6)
Xe1–F2	2.001 (2)	N1–C2	1.488 (6)
Xe1–F3	2.030 (2)	N1–C3	1.524 (4)
Xe1–F4	2.018 (2)		
Xe1–F5	2.034 (2)		

Bond Angles			
F2–Xe1–F1	72.3 (4)	C2–N1–C1	110.7 (3)
F3–Xe1–F2	71.7 (4)	C3–N1–C1	108.9 (5)
F4–Xe1–F3	72.2 (4)	C3–N1–C2	109.6 (4)
F5–Xe1–F1	72.3 (4)		
F5–Xe1–F4	71.5 (4)		

essarily correspond exactly to the point with a zero derivative. The second is that sum of the gradients may not always be zero as required for translational invariance. These tend to introduce errors on the order of 0.001 Å in the calculation of the coordinates if both a reasonable grid and basis set are used. This gives bond lengths and angles with reasonable error limits. The difference of 0.001 Å is about an order of magnitude smaller than the accuracy of the LDF geometries as compared to experiment.

Results and Discussion

Syntheses and Properties of XeF_5^- Salts. The reactions of the alkali-metal fluorides with XeF_4 were studied under conditions (190 °C, 14 h) very similar to those previously reported by Kiselev and co-workers.[13-15] It was found that XeF_4 combines with either CsF or RbF in a clean 1:1 mole ratio to form the corresponding, previously unidentified XeF_5^- salts. In the case of KF and NaF the same anion was formed; however, the percentage conversion of MF to $MXeF_5$ decreased with decreasing atomic weight of M (CsF = 99%, RbF = 95%, KF = 65%, and NaF = 32%) and increased reaction times were required for higher conversions.

The interactions of LiF and BaF_2 with XeF_4 were also examined, but in neither case was evidence for the formation of a stable adduct obtained.

The XeF_5^- salts of Cs^+, Rb^+, K^+, and Na^+ are white, stable solids. Their physical properties, thermal stabilities, etc. are those previously attributed by Kiselev and co-workers to the corresponding M_2XeF_6 salts.[13-15] As will be shown below, they all contain pentagonal planar XeF_5^- anions.

Attempts to prepare $CsXeF_5$ from CsF and XeF_4 at room temperature in CH_3CN solutions were unsuccessful because of the very low solubility of CsF in this solvent. However, the highly soluble $N(CH_3)_4F$ readily forms $N(CH_3)_4^+XeF_5^-$ under these

conditions. Even with a 2:1 molar ratio of $N(CH_3)_4F:XeF_4$ in CH_3CN solvent and a large excess of MF in the XeF_4–MF systems, only XeF_5^-, and no XeF_6^{2-}, was observed, indicating that XeF_5^- is the favored anion. The $N(CH_3)_4^+XeF_5^-$ salt is a white, stable solid whose structure was established by a crystal structure determination and vibrational and NMR spectroscopy (see below).

The lack of XeF_6^{2-} formation in these systems was further demonstrated by a study of the FNO–XeF_4 system. Even when a large excess of FNO was used, only $NO^+XeF_5^-$, and no $(NO^+)_2XeF_6^{2-}$, was formed at temperatures as low as -78 °C. The $NO^+XeF_5^-$ salt is a white solid having a dissociation pressure of 10 Torr at 0 °C. It is ionic, containing NO^+ and XeF_5^- ions as shown by vibrational spectroscopy (see below).

In view of the above results and the structural evidence presented below, it appears quite clear that the salts obtained by the reactions of XeF_4 with fluoride ion sources are XeF_5^-, and not XeF_6^{2-}, salts. The fact that some of the products reported[13-15] by the Soviet workers gave elemental analyses approaching the M_2XeF_6 composition might be attributed to incomplete conversion of MF to $MXeF_5$ thus resulting in MF + $MXeF_5$. There is also no doubt that the products observed during the laser photolysis of either $CsXeF_7$ or NF_4XeF_7 were not XeF_8^{2-} but XeF_5^- salts.[17]

X-ray Crystal Structure of $N(CH_3)_4^+XeF_5^-$. The crystal structure consists of well-separated $N(CH_3)_4^+$ and XeF_5^- ions. The $N(CH_3)_4^+$ cation is tetrahedral with the expected bond lengths. Different views of the XeF_5^- anion are shown in Figures 1 and 2, while a stereoview of the packing in the unit cell is given in Figure 3 in which the hydrogen atoms have been omitted in the cation. Important bond lengths and angles are listed in Table III. The xenon and five fluorines of the XeF_5^- anion and the nitrogen and two carbons of the cation are located on special positions that are on the mirror plane, resulting in an anion that is planar by crystal symmetry. The closest anion–cation distance occurs between F2 and C2, which lies in the anion plane, at 3.105 (5) Å, whereas the remaining closest F···C distances occur at 3.237 (5) (F5···C1), 3.354 (5) (F3···C2), 3.370 (5) (F1···C3), and 3.651 (5) Å (F4···C2). The sum of the van der Waals radii of CH_3 (2.00 Å[35]) and F (1.35[35]–1.40[36] Å) is 3.35–3.40 Å. The F2···C2 distance suggests weak hydrogen bonding between the C2 methyl group and F2 and is somewhat shorter than the shortest F···C
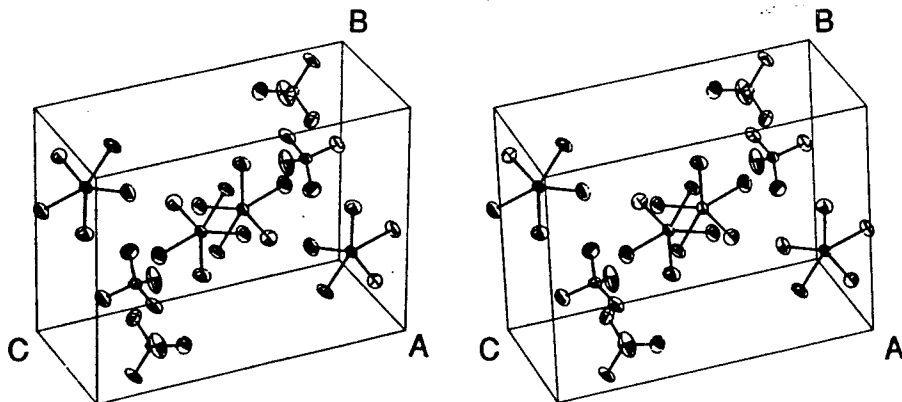

Figure 3. Stereoview [111] of the unit cell of $[N(CH_3)_4]^+[XeF_5]^-$; hydrogen atoms are excluded.

Table IV. Vibrational Spectra of the XeF₅⁻ Anion in Different Salts

NOXeF₅[b] R		N(CH₃)₄XeF₅[c]		NaXeF₅		KXeF₅		RbXeF₅		CsXeF₅		assignments for XeF₅⁻ in point group D_{5h}
25 °C	−150 °C	R	IR	R	IR	R	IR	R	IR	R	IR	
							860 vw		970 vw		955 vw	$\nu_1 + \nu_3(E_1')$
									882 vw		870 sh	$\nu_3 + \nu_5(E_2' + E_2')$
							800 vw				850 vw	$2\nu_5(A_1' + E_1' + A_2')$
									808 vw		795 vw	$\nu_5 + \nu_6(A_1' + E_1' + A_2')$
									752 vw		740 sh	$2\nu_6(A_1' + E_1')$
							740 vw		728 vw		724 vw	$\nu_4 + \nu_5(E_1' + E_2')$
											705 sh	
						544 (0.1)		550 (0.1)		547 (0.1)	650 sh	$\nu_4 + \nu_6(E_1' + E_2')$
				519 (10)		505 (10)		509 (10)		504 (10)		$2\nu_2(A_1')$
503 (10)	506 (10)	502 (10)	509 sh		525 sh	498 sh		489 sh	668 vw			$\nu_1(A_1')$
	498 (1)											
482 (0+)	475 (0.5)		465 vs	473 (0.1)	450 vs, br		480 vs	471 (0.1)	470 vw, br		450 vs, br	$\nu_3(E_1')$
			420 sh		415 s		410 s	453 sh	418 s		415 s	
440 sh	445 (1.8)	423 (2.1)		444 (1.8)		438 (1.4)		440 (1.6)		432 (1.5)		$\nu_5(E_2')$
429 (1.1)	424 (1)			422 (1.3)		424 (1.2)		437 sh		422 (1.6)		
382 sh	384 (1)	377 (3.3)		386 (2.0)		388 (2.4)	379 sh	389 (2.2)	372 w	380 (2.2)		$\nu_6(E_2')$
374 (2.3)	373 (2.5)			383 sh		381 (1.9)		379 (1.6)		369 (2.3)		
290 (0+)	282 (0.5)		278 s	293 (0+)	276 s	290 (0+)	275 s	299 (0+)	288 sh	312 (0+)	288 sh	$\nu_4(E_1')$
240 (0.2)	244 (0.6)							278 (0+)	275 s		274 s	$\nu_2(A_2'')$
						147 (1.5)		169 (0.7)				
						113 sh		131 (1.1)		124 (1.2)		
135 (1)	144 (1.5)	90 (1)		144 (1.4)		102 (0.5)		107 (0.4)		104 (1.5)		lattice vibrations
97 (0.8)	100 (1.5)					90 (2)		91 (1.3)		57 (0.3)		
75 (1.5)	82 (3.0)					65 sh		77 (1)				
35 (0.5)	42 (1)					52 sh		59 (1.4)				
						42 sh		52 sh				
								47 sh				
								35 (0.6)				

Table V. Symmetry Coordinates and Approximate Mode Descriptions for a Pentagonal Planar XY_5 Molecule

$S_1 = \frac{1}{\sqrt{5}} (\Delta r_1 + \Delta r_2 + \Delta r_3 + \Delta r_4 + \Delta r_5)$ symmetric stretch

$S_2 = \frac{1}{\sqrt{10}} \left[\sum_{i=1}^{5} (\Delta \gamma_{i6} - \Delta \gamma_{i7}) \right]$ symmetric out of plane (umbrella) deformation

$S_{3a} = \sqrt{\frac{2}{5}} [\Delta r_1 + \cos\alpha (\Delta r_2 + \Delta r_5) + \cos 2\alpha (\Delta r_3 + \Delta r_4)]$ asymmetric stretch

$S_{3b} = \sqrt{\frac{2}{5}} [\sin\alpha (\Delta r_2 - \Delta r_5) + \sin 2\alpha (\Delta r_3 - \Delta r_4)]$

$S_{4a} = \sqrt{\frac{2}{5}} [\Delta\alpha_{34} + \cos\alpha (\Delta\alpha_{45} + \Delta\alpha_{23}) + \cos 2\alpha (\Delta\alpha_{15} + \Delta\alpha_{12})]$ asymmetric in plane deformation

$S_{4b} = \sqrt{\frac{2}{5}} [\sin\alpha (\Delta\alpha_{45} - \Delta\alpha_{23}) + \sin 2\alpha (\Delta\alpha_{15} - \Delta\alpha_{12})]$

$S_{5a} = \sqrt{\frac{2}{5}} [\Delta r_1 + \cos 2\alpha (\Delta r_2 + \Delta r_5) + \cos\alpha (\Delta r_3 + \Delta r_4)]$ asymmetric stretch

$S_{5b} = \sqrt{\frac{2}{5}} [\sin 2\alpha (\Delta r_2 + \Delta r_5) + \sin\alpha (\Delta r_3 + \Delta r_4)]$

$S_{6a} = \sqrt{\frac{2}{5}} [\Delta\alpha_{34} + \cos 2\alpha (\Delta\alpha_{45} + \Delta\alpha_{23}) + \cos\alpha (\Delta\alpha_{15} + \Delta\alpha_{12})]$ in plane (scissor) deformation

$S_{6b} = \sqrt{\frac{2}{5}} [\sin 2\alpha (\Delta\alpha_{45} - \Delta\alpha_{23}) - \sin\alpha (\Delta\alpha_{15} - \Delta\alpha_{12})]$

$S_{7a} = \frac{1}{\sqrt{5}} [(\Delta\gamma_{16} - \Delta\gamma_{17}) + \cos 2\alpha (\Delta\gamma_{26} - \Delta\gamma_{27} + \Delta\gamma_{56} - \Delta\gamma_{57})$ asymmetric out of plane deformation
$\qquad + \cos\alpha (\Delta\gamma_{36} - \Delta\gamma_{37} + \Delta\gamma_{46} - \Delta\gamma_{47})]$

$S_{7b} = \sqrt{\frac{1}{5}} [\sin 2\alpha (\Delta\gamma_{26} - \Delta\gamma_{27} - \Delta\gamma_{56} + \Delta\gamma_{57})$
$\qquad - \sin\alpha (\Delta\gamma_{36} - \Delta\gamma_{37} - \Delta\gamma_{46} + \Delta\gamma_{47})]$

Table VI. G Matrix[a] for Pentagonal Planar XeF_5^- of Symmetry D_{5h}

A_1'	$G_{11} = \mu_y = 5.2637 \times 10^{-2}$
A_2''	$G_{22} = (2/r^2)(\mu_y + 5\mu_x) = 4.4802 \times 10^{-2}$
E_1'	$G_{33} = \mu_y + 5\mu_x/2 = 7.1677 \times 10^{-2}$
	$G_{34} = 5(5^{1/2})\mu_x/(4r \sin\alpha) = 1.1123 \times 10^{-2}$
	$G_{44} = (1/r^2)(5\mu_y \sin^2 2\alpha + \mu_x) = 2.4333 \times 10^{-2}$
E_2'	$G_{55} = \mu_y = 5.2637 \times 10^{-2}$
	$G_{56} = 0$
	$G_{66} = (1/r^2)(4\mu_y \sin^2\alpha) = 4.7026 \times 10^{-2}$
E_2''	$G_{77} = 2\mu_y/r^2 = 2.5995 \times 10^{-2}$

[a] The following geometry was used for the calculation of the G matrix: $r = 2.0124$ Å and $\alpha = 72°$.

had not previously been carried out for such a species. Force constants were calculated by the Wilson FG matrix method.[44] Figure 7 shows our choice of internal coordinates to describe the vibrations of such a molecule. Two imaginary ligands, E_6 and E_7, have been placed in the axial positions to define the angles γ, required for the definition of the out-of-plane deformation modes. The symmetry coordinates and approximate mode descriptions are given in Table V and are derived from those previously reported for the IF_7 molecule after correction for two apparent typographical errors.[45] The analytical G and F matrices, together with the computed numerical values, are given in Tables VI and VII, respectively. The correctness of our G matrix was verified by an independent calculation of the numerical G matrix by using a computational method that gave identical values.

Vibrational Assignments. In agreement with the above predictions for XeF_5^- of symmetry D_{5h}, three mutually exclusive Raman and two infrared bands were observed in the 200–700-cm^{-1} region expected for the fundamental vibrations. The $N(CH_3)_4^+$ salt, containing the largest cation and, hence, the best isolated XeF_5^- anion, shows three narrow Raman lines at 502, 423, and 377 cm^{-1}. On the basis of their relative intensities and frequencies, which are similar to those of the three closely related Raman-active modes of octahedral molecules, the 502-, 423-, and 377-cm^{-1} bands are assigned to the symmetric stretch, $\nu_1(A_1')$, the antisymmetric stretch, $\nu_5(E_2')$, and the symmetric in-plane deformation, $\nu_6(E_2')$, respectively. The rigorous adherence of the observed Raman spectrum to the vibrational selection rules for symmetry D_{5h} and the failure to observe further splittings of the vibrational bands serve to underscore that the vibrational modes of the XeF_5^- anion

(44) Wilson, E. B. *J. Chem. Phys.* **1941**, *9*, 76.
(45) Khanna, R. K. *J. Mol. Spectrosc.* **1962**, *8*, 134.

Table VII. F Matrix and Force Field for Pentagonal Planar XeF_5^- of Symmetry D_{5h}

assign-ment		freq, cm^{-1}	symmetry force constants[a]
A_1'	ν_1	502	$F_{11} = f_r + 2f_{rr} + 2f_{rr}' = 2.820$
A_2''	ν_2	274	$F_{22} = r^2(f_\gamma + 2f_{\gamma\gamma} \cos\alpha + 2f_{\gamma\gamma}' \cos 2\alpha) = 0.996$
E_1'	ν_3	465	$F_{33} = f_r + 2f_{rr} \cos\alpha + 2f_{rr}'' \cos 2\alpha = 1.830$
			$F_{34} = r(f_{r\alpha} + 2f_{r\alpha}' \cos\alpha + 2f_{r\alpha}'' \cos 2\alpha) = -0.342$
	ν_4	290	$F_{44} = r^2(f_\alpha + 2f_{\alpha\alpha} \cos\alpha + 2f_{\alpha\alpha}' \cos 2\alpha) = 2.212$
E_2'	ν_5	423	$F_{55} = f_r + 2f_{rr} \cos 2\alpha + 2f_{rr}' \cos\alpha = 2.003$
			$F_{56} = r(f_{r\alpha} + 2f_{r\alpha}' \cos 2\alpha + 2f_{r\alpha}'' \cos\alpha) = 0$
	ν_6	377	$F_{66} = r^2(f_\alpha + 2f_{\alpha\alpha} \cos 2\alpha + 2f_{\alpha\alpha}' \cos\alpha) = 1.797$
E_2''	ν_7	79[b]	$F_{77} = r^2(f_\gamma + 2f_{\gamma\gamma} \cos 2\alpha + 2f_{\gamma\gamma}' \cos\alpha) = 0.143$

[a] Stretching constants in mdyn/Å, deformation constants in mdyn Å/rad^2, and stretch–bend interaction constants in mdyn/rad. [b] Value taken from the ab initio calculation.

in its $N(CH_3)_4^+$ salt are only very weakly coupled.[46] It also justifies the use of the assumed free anion symmetry in the subsequent vibrational analysis and force field calculations.

In the salts with smaller cations, stronger coupling of the XeF_5^- motions or slight distortions of the anions can occur, resulting in a splitting of the two E_2' modes into their doubly degenerate components. As expected, the anion–cation interaction is strongest for the NO^+ salt, causing some of the infrared-active modes, such as $\nu_3(E_1')$ and $\nu_4(E_1')$, also to become weakly active in the Raman spectrum.

In the infrared spectra two strong anion bands were observed above 250 cm^{-1}. The first one was a very intense broad band extending from 400 to 550 cm^{-1}, which must be due to the antisymmetric stretching mode $\nu_3(E_1')$. The second one is an intense band at 274 cm^{-1}, which, on the basis of its frequency and relative intensity, must be the symmetric out-of-plane (umbrella) deformation, $\nu_2(A_2'')$.

The third predicted infrared-active mode is the antisymmetric in-plane deformation, $\nu_4(E_1')$. Assuming the F_{66} and F_{44} symmetry force constants to be identical (both modes involve f_α and different combinations of $f_{\alpha\alpha}$ and $f_{\alpha\alpha}'$, with the latter being small due to the large mass of the xenon central atom), a frequency of 274 cm^{-1} was calculated for $\nu_4(E_1')$. Therefore, $\nu_4(E_1')$, which should be of medium infrared intensity, might either be hidden underneath the intense $\nu_2(A_2'')$ band at 274 cm^{-1} or occur just below the 250-cm^{-1} cutoff frequency of the AgBr windows used for our study. A frequency range 240–290 cm^{-1} for $\nu_4(E_1')$ is also supported by the Raman spectrum of $NO^+XeF_5^-$ (see Table IV). In this compound, where the anion–cation interaction is the strongest and the infrared-active modes become also weakly Raman active, two weak Raman bands were observed at 244 and 282 cm^{-1}, respectively. Furthermore, the infrared spectra of $RbXeF_5$ and $CsXeF_5$ exhibit a 288-cm^{-1} shoulder on the strong 275-cm^{-1} band, and the Raman spectra of all the alkali-metal XeF_5^- salts show an extremely weak band at about 290 cm^{-1}. Consequently, a frequency of 290 cm^{-1} was chosen by us for $\nu_4(E_1')$ and used for the force field computations. Our choice of 290 cm^{-1} for ν_4 is also supported by ab initio calculations for XeF_5^- (see below) and IF_7.[47] Assuming the frequency differences between calculated and observed frequencies to be the same for the two in-plane deformation modes in XeF_5^-, a value of 291 cm^{-1} is predicted for ν_4. Similarly, the

(46) A factor-group analysis of the vibrational modes of the unit cell was carried out by use of the correlation chart method (Carter, R. L. *J. Chem. Educ.* **1971**, *48*, 297 and references therein). The free anion symmetry (D_{5h}) was correlated to the site symmetry of the anion (C_s), which, in turn, was correlated to the crystal symmetry (D_{2h}). Assuming complete vibrational coupling occurs in the unit cell of $N(CH_3)_4^+XeF_5^-$, all the vibrational modes of the XeF_5^- anion are found to be Raman- and infrared-active under the crystal symmetry. Moreover, ν_3, ν_4, ν_5, ν_6, and ν_7 will be split into four and three components in their Raman (A_g, B_{1g}, B_{2g}, B_{3g}) and infrared (B_{1u}, B_{2u}, B_{3u}) spectra, respectively; ν_1 will be split into two components in both the Raman (A_g, B_{3g}) and infrared (B_{1u}, B_{2u}) spectra and ν_2 will not be split in the infrared (B_{3u}) but will be split into two components in the Raman (B_{1g}, B_{2g}) spectrum.

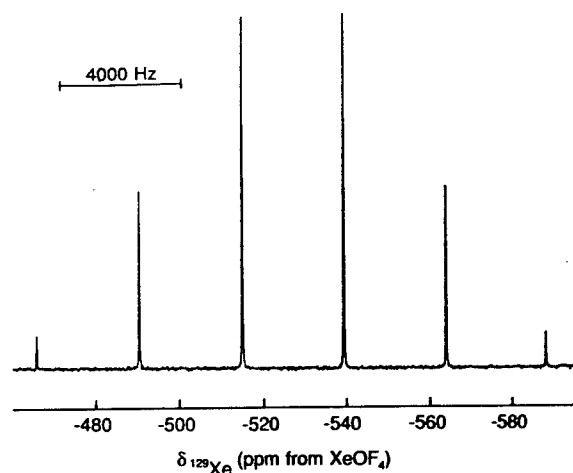(47) Bartell, L. S.; Rothman, M. J.; Gavezzotti, A. *J. Chem. Phys.* **1982**, *76*, 4136 and references cited therein.

Figure 4. ^{129}Xe NMR spectrum (139.05 MHz) at 24 °C of a saturated solution of N(CH$_3$)$_4$$^+XeF_5$$^-$ in CH$_3$CN containing a 1 M excess of N-(CH$_3$)$_4$$^+F^-$.

distance in N(CH$_3$)$_4$$^+HF_2^-$ [3.313 (5) Å],[7] which appears to be at the limit of the van der Waals distance. The short F2···C2 distance appears to account for the greater elongation of the thermal ellipsoid of F2 (in the direction of the C_5-axis of the anion; Figure 2).

Although the site symmetry of the XeF$_5^-$ anion is C_s, the five fluorines are clearly equivalently bonded to the xenon, giving a pentagonal planar structure of D_{5h} symmetry. The average F–Xe–F angle of 72.0 (4)° is essentially the ideal angle of 72°. The average Xe–F bond length [2.012 (2) Å] is significantly longer than the average bond length of XeF$_4$ [1.953 (2) Å][37] and the average equatorial bond length of IF$_7$ [1.858 (4) Å].[38] The nearest-neighbor F···F contacts in the XeF$_5^-$ anion are 2.35–2.38 Å and are substantially less than twice the nominal van der Waals radius for fluorine, i.e., 2.70[35]–2.80[38] Å, indicating that the fluorines of the pentagon are significantly congested and are consistent with the long Xe–F bond length in XeF$_5^-$. This contrasts with the shorter Xe–F bond length of XeF$_4$, where the fluorines in the plane are not contacting, and the intramolecular F···F distances (2.76 Å) are at the limit of the sum of the fluorine van der Waals radii. The short I–F bond lengths for the equatorial belt of five fluorines in IF$_7$ relative to the Xe–F bond length of XeF$_5^-$ may be attributed to relief of the congestion in the IF$_5$ belt by means of a 7.5° puckering, which has been deduced from electron diffraction studies[38] but not corroborated by an independent study. The fact that XeF$_5^-$ does not relieve its steric congestion by a puckering distortion may be attributed to the presence of the two axial lone pairs of electrons, which exert greater repulsive forces than the two axial fluorines in the IF$_7$ molecule, thus forcing the XeF$_5^-$ anion to be planar. Moreover, the formal negative charge on XeF$_5^-$ leads to a greater Xe–F bond polarity and elongation of the Xe–F bond, as is evident from a comparison with the Xe–F bond length of XeF$_4$, and serves to alleviate some of the steric congestion in the anion plane.

The steric crowding in the XeF$_5^-$ molecular plane is further illustrated by the thermal parameters, which remain essentially unaltered before and after empirical absorption corrections. It is apparent that the principal axes of motion of the fluorine atoms in XeF$_5^-$ and XeF$_4$[37] are perpendicular to the bond directions, producing the anticipated polar flattening of the thermal ellipsoids in the Xe–F bond directions. However, the thermal ellipsoids in XeF$_5^-$ are elongated in the direction of the C_5-axis and flattened in the direction perpendicular to the Xe–F bonds in the molecular plane. In contrast to the fluorine thermal ellipsoids in XeF$_5^-$, those of XeF$_4$ are essentially isotropic in the directions perpendicular to the Xe–F bonds and in the molecular plane where the fluorine atoms are apparently not contacting one another to any significant
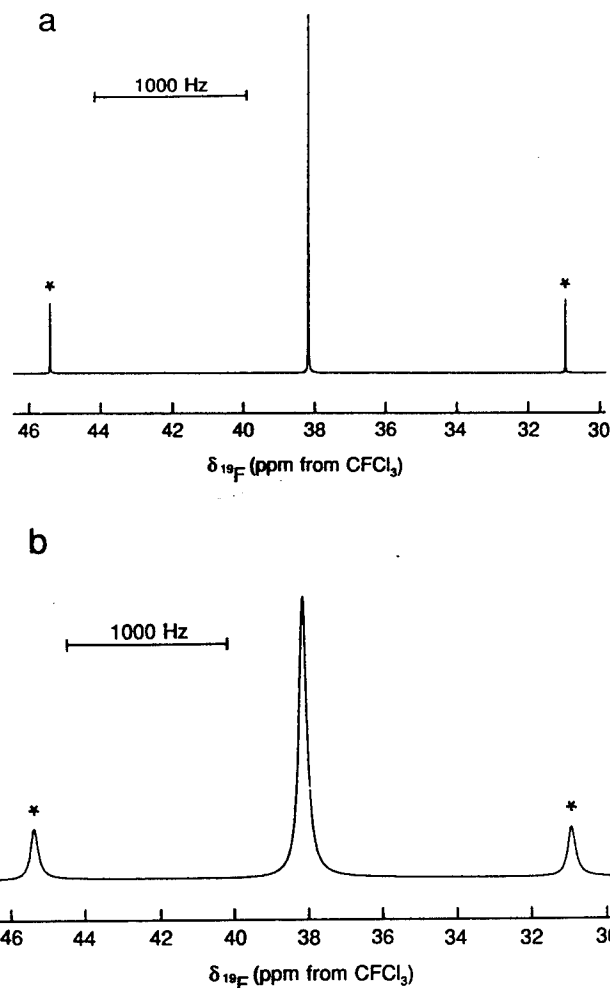
(37) Burns, J. H.; Agron, P. A.; Levy, H. A. *Science* **1963**, *139*, 1208.
(38) Adams, W. J.; Thompson, H. B.; Bartell, L. S. *J. Chem. Phys.* **1970**, *53*, 4040.

Figure 5. ^{19}F NMR spectrum (235.36 MHz) at 24 °C of (a) a saturated solution of N(CH$_3$)$_4$$^+XeF_5$$^-$ in CH$_3$CN containing a 1 M excess of N-(CH$_3$)$_4$$^+F^-$ and (b) a saturated solution of pure N(CH$_3$)$_4$$^+XeF_5$$^-$ in CH$_3$CN. Asterisks (*) denote ^{129}Xe satellites.

extent. Steric congestion in XeF$_5^-$ is additionally supported by vibrational force constant calculations (see below).

^{129}Xe and ^{19}F NMR Spectra of the XeF$_5^-$ Anion. The ^{129}Xe NMR spectrum of N(CH$_3$)$_4$$^+XeF_5$$^-$ dissolved in CH$_3$CN containing a 1 M excess of N(CH$_3$)$_4$$^+F^-$ at 24 °C (Figure 4) displays a well-resolved binomial sextet ($\Delta\nu_{1/2}$ = 15 Hz), consistent with the coupling of the ^{129}Xe nucleus to five chemically equivalent ^{19}F nuclei in the XeF$_5^-$ anion [δ(^{129}Xe), −527.0 ppm from XeOF$_4$; ^1J(^{129}Xe–^{19}F), 3400 Hz]. The ^{129}Xe chemical shift of XeF$_5^-$ is significantly more shielded (i.e., by −843.9 ppm) than that of XeF$_4$ in CH$_3$CN at 24 °C [δ(^{129}Xe), 316.9 ppm from XeOF$_4$; ^1J(^{129}Xe–^{19}F), 3895 Hz]. This behavior follows the expected trend of increased shielding that accompanies an increase in negative charge.[39] The ^{19}F NMR spectrum of a similar sample at 24 °C (Figure 5a) shows a narrow singlet ($\Delta\nu_{1/2}$ = 2.8 Hz) flanked by natural abundance (26.44%) ^{129}Xe satellites [δ(^{19}F), 38.1 ppm from CFCl$_3$; ^1J(^{129}Xe–^{19}F), 3398 Hz]. A resonance due to unreacted fluoride was observed at −75 ppm. Interestingly, the ^{19}F chemical shift of XeF$_5^-$ is deshielded by 56.8 ppm with respect to that of XeF$_4$ in CH$_3$CN at 24 °C [δ(^{19}F), −18.7 ppm from CFCl$_3$; ^1J(^{129}Xe–^{19}F), 3896 Hz]. This result is somewhat surprising in view of the increased ionic character of the Xe–F bonds (i.e., greater bond length and smaller stretching force constant) compared with those in XeF$_4$; the reason for this is not clear but may be related to the congested environment of the fluorine ligands and the rather short nearest-neighbor F···F contact distance. The ^{19}F NMR spectrum of a sample prepared from equimolar

(39) Jameson, C. J.; Mason, J. In *Multinuclear NMR*; Mason, J., Ed.; Plenum Press: New York, 1987; Chapter 3, pp 66–68.

3356 *J. Am. Chem. Soc., Vol. 113, No. 9, 1991*

Christe et al.

a

Cs⁺XeF₅⁻

TRANSMITTANCE

INTENSITY
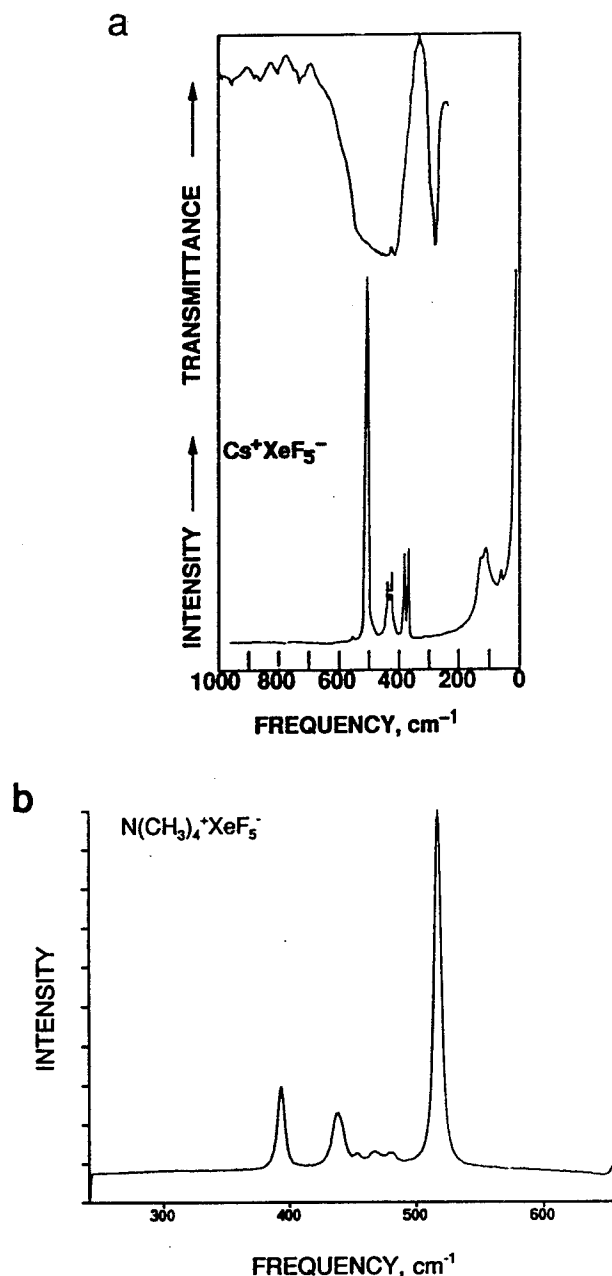
FREQUENCY, cm⁻¹

b

N(CH₃)₄⁺XeF₅⁻

INTENSITY

FREQUENCY, cm⁻¹

Figure 6. (a) Vibrational spectra of solid $Cs^+XeF_5^-$. Upper trace, infrared spectrum recorded at room temperature with an AgBr disk; lower trace; Raman spectrum recorded in a glass capillary at 25 °C with 647.1-nm excitation. (b) Single-crystal Raman spectrum of N-$(CH_3)_4^+XeF_5^-$ recorded in a glass capillary at room temperature with 514.5-nm excitation.

quantities of XeF_4 and $N(CH_3)_4^+F^-$ in CH_3CN showed a similar resonance, with accompanying ^{129}Xe satellites, at 38.1 ppm; however, the linewidth was significantly broader, $\Delta\nu_{1/2} = 53$ Hz (Figure 5b). This indicates that XeF_5^- undergoes dissociative fluorine exchange, which can be suppressed by the presence of excess fluoride. There was no evidence for the formation of XeF_6^{2-} at $XeF_4:N(CH_3)_4^+F^-$ ratios exceeding 1:1, thus casting further doubt on the previous claims[13-15] for the existence of stable salts of the XeF_6^{2-} anion.

The magnitude of the one-bond $^{129}Xe-^{19}F$ coupling constant drops from 3895 Hz in XeF_4 to 3400 Hz in XeF_5^- under the same conditions (i.e., solvent and temperature) of experimental measurement. If it is assumed that the Fermi-contact mechanism provides the dominant coupling contribution,[40] then the smaller
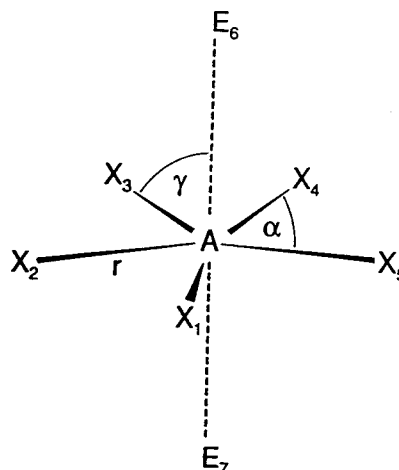
(40) (a) Jameson, C. J. In *Multinuclear NMR*; Mason, J., Ed.; Plenum Press: New York, 1987; Chapter 4, pp 97–101; Chapter 18. (b) Schrobilgen, G. J. In *NMR and the Periodic Table*; Harris, R. K., Mann, B. E., Eds.; Academic Press: New York, 1978; Chapter 14.

Figure 7. Internal coordinates for pentagonal planar AX_5.

value of $^1J(^{129}Xe-^{19}F)$ in XeF_5^- is in accord with the greater ionic character of the Xe-F bonds in the anion.

In the VSEPR notation, XeF_5^- is a seven-coordinate AX_5E_2 system, and is the first example of this geometry.[41] The solution structure proposed for the anion that is consistent with five equivalent fluorines is a pentagonal planar (D_{5h}) structure having five equivalent equatorial fluorines and two axial lone pairs of electrons. The dynamic behavior for related seven-coordinate geometries is well established in the cases of XeF_6 and IF_7. In contrast to IF_7 and XeF_5^-, the gas-phase structure of XeF_6 (AX_6E) is based upon a distorted octahedral geometry[42] in which the valence electron lone pair distorts the octahedral geometry to C_{3v} by occupying triangular faces of the octahedron, passing among adjacent faces via a transition state having intermediate C_s and C_{2v} geometries, with intramolecular exchange dynamics that are distinct from those of IF_7. The dynamic behavior of IF_7 (AX_7) is also well documented; on the basis of gas-phase electron diffraction measurements it is purported to have a puckered arrangement for the five equatorial fluorines[38] in the gas phase and it has been shown by ^{19}F NMR spectroscopy that axial and equatorial fluorine environments of IF_7 undergo rapid intramolecular exchange in solution.[43] The single fluorine environment observed in the NMR spectra of XeF_5^- could also be accounted for by assuming that the anion is fluxional. The VSEPR rules postulate that the valence shell lone pairs exert larger repulsive forces on adjacent electron pairs than do bonding pairs, so that, unlike IF_7, the transition state for exchange of axial lone pair positions with equatorial fluorine positions in XeF_5^- would presumably give rise to prohibitively large repulsive energies when a lone pair or lone pairs occupy an equatorial position, suggesting that XeF_5^- is likely to be rigid in solution.

Vibrational Spectra and Normal Coordinate Analysis of XeF_5^-. The infrared and Raman spectra of $CsXeF_5$, $RbXeF_5$, $KXeF_5$, $NaXeF_5$, and $N(CH_3)_4XeF_5$ and the Raman spectra of $NOXeF_5$ have been recorded. The observed frequencies and their assignments are summarized in Table IV. Figure 6 shows, as typical examples, the vibrational spectra of $CsXeF_5$ and $N(CH_3)_4XeF_5$.

As shown above by the NMR data and the crystal structure determination, the XeF_5^- anion is pentagonal planar and, therefore, belongs to point group D_{5h}. After the removal of translational and rotational degrees of freedom, the irreducible representation of the molecule is

$$\Gamma_{vib} = 1A_1'(R) + 1A_2''(IR) + 2E_1'(IR) + 2E_2'(R) + E_2''(ia)$$

Since XeF_5^- is the first known example of an AX_5 species of symmetry D_{5h}, it is not surprising that a normal coordinate analysis

(41) Gillespie, R. J. *Molecular Geometry*; Van Nostrand Reinhold Co.: London, 1972.
(42) (a) Bartell, L. S.; Gavin, R. M.; Thompson, H. B. *J. Chem. Phys.* **1965**, *43*, 2547. (b) Bartell, L. S.; Gavin, R. M. *J. Chem. Phys.* **1968**, *48*, 2466.
(43) Gillespie, R. J.; Quail, J. W. *Can. J. Chem.* **1964**, *42*, 2671.

The Pentafluoroxenate(IV) Anion, XeF$_5^-$

J. Am. Chem. Soc., Vol. 113, No. 9, 1991 3359

Table VIII. Internal Force Constants (mdyn/Å) and Bond Length (Å) of XeF$_5^-$ Compared with Those of XeF$_2$, XeF$_4$, and IF$_4^-$

force const	XeF$_2^a$	XeF$_4^b$	IF$_4^{-b}$	XeF$_5^{-c}$
f_r	2.83	3.055	2.221	2.096
f_{rr}	0.14	0.120	0.183	0.143
f_{rr}'		0.007	0.466	0.219
$f_\alpha\ (-f_{\alpha\alpha}')$	0.20	0.193	0.182	0.458
$f\ (-f')$		0.299	0.257	0.072
$f_{\alpha\alpha} - f_{\alpha\alpha}'$				0.045
$f_\alpha - f_{\alpha\alpha}$				0.413
$f - f'$				0.093
$f - f$				−0.021
r	1.98	1.953		2.012

^{a} Data from ref 53. ^{b} Data from ref 50. The f values in ref 49 have not been properly normalized and must be divided by two to correspond to the values from this work. ^{c} This work.

transfer of the computed frequency difference of 102 cm^{-1} for the two in-plane deformation modes from IF$_7$ to XeF$_5^-$ results in a ν_4 value of 275 cm^{-1} for XeF$_5^-$.

The only missing fundamental vibration is the ring puckering mode, $\nu_7(E_2'')$, which ideally is inactive in both the infrared and Raman spectra. Since no experimental frequency is available for this mode, the frequency of 79 cm^{-1} obtained by the ab initio calculation (see below) was used.

In addition to the fundamental vibrations, numerous Raman bands were observed in the low-frequency region, which are attributed to lattice vibrations. The infrared spectra exhibit some weak bands above 600 cm^{-1}, which can be readily assigned to different overtones or combination bands of XeF$_5^-$ (see Table IV).

In NO$^+$XeF$_5^-$ and N(CH$_3$)$_4^+$XeF$_5^-$, cation bands were also observed (see Table IV) with frequency values that are in excellent agreement with previous literature data.[4,5,7,48]

Force Constants. The symmetry force constants of XeF$_5^-$ are shown in Table VII. Except for the E$_1'$ and E$_2'$ blocks, all of the symmetry force constants are one-dimensional and well determined. In the two-dimensional E$_2'$ block, G_{56} equals zero (see Table VI), resulting in F_{56} also becoming zero. Therefore, the only remaining underdetermined problem is the two-dimensional E$_1'$ block. The range of possible solutions for this block was computed by using the extremal conditions reported by Sawodny.[49] It has previously been pointed out[49–52] that in weakly coupled (heavy central atom) systems the values of the general valence force field tend to fall within the range given by $F_{34} = 0$ as the lower and $F_{34} = \frac{1}{2}|F_{34}(\max) - F_{34}(\min)|$ as the upper limit with $F_{44} = \min$ being an excellent choice. The latter choice results in an F_{33} value of 1.830 mdyn/Å with an error limit of about 0.14 mdyn/Å and, therefore, F_{33} can be considered to be reasonably well determined.

The most important internal force constants of XeF$_5^-$, together with the known bond length, are given in Table VIII and are compared with those of the closely related XeF$_2$[53] and XeF$_4$[50] molecules and the IF$_4^-$ anion.[50] As can be seen from Table VIII, the force constants well reflect our expectations. Compared with XeF$_2$ and XeF$_4$, the increased $^{\delta+}$Xe–F$^{\delta-}$ polarity of the Xe–F bond in XeF$_5^-$, combined with the crowding effect in the equatorial plane, should decrease the Xe–F stretching (f_r), increase the in-plane deformation (f_α), and decrease the out-of-plane deformation (f_γ) force constants. Furthermore, ($f_{\alpha\alpha} - f_{\alpha\alpha}'$) and ($f_{\gamma\gamma} - f_{\gamma\gamma}'$) should exhibit positive signs as expected for adjacent angles interacting more strongly than nonadjacent angles. The excellent agreement between these expectations and the experimental values from Table VIII lends strong support to the above assignments for XeF$_5^-$.

Table IX. Calculated and Experimental Vibrational Frequencies (cm^{-1}) of XeF$_4$

assignment		calcd freq	obsd freq^a	approx mode descriptn
A$_{1g}$	ν_1	532	543	ν_{sym} (in phase)
A$_{2u}$	ν_2	271	291	δ_{sym} (out of plane)
B$_{1g}$	ν_3	498	502	ν_{sym} (out of phase)
B$_{2g}$	ν_4	182	235	δ_{sym} (in plane)
B$_{2u}$	ν_5	156	inactive	δ_{asym} (out of plane)
E$_u$	ν_6	591	586	ν_{asym}
E$_u$	ν_7	143	123	δ_{asym} (in plane)

^{a} Data from ref 55.

Table X. Calculated and Experimental Vibrational Frequencies (cm^{-1}) for XeF$_5^-$

assignment		calcd freq			obsd freq	approx mode descriptn
		a	b	c		
A$_1'$	ν_1	467	537	551	502	ν_{sym} (in plane)
A$_2''$	ν_2	270	274	275	274	δ_{sym} (out of plane)
E$_1'$	ν_3	502	574	585	400–550	ν_{asym}
E$_1'$	ν_4	248	255	254	290	δ_{asym} (in plane)
E$_2'$	ν_5	413	477	489	423	ν_{asym}
E$_2'$	ν_6	335	356	361	377	δ_{sym} (in plane)
E$_2''$	ν_7	79	21	28i		δ_{asym} (out of plane)

^{a} With the calculated Xe–F bond length of 2.077 Å. ^{b} With an assumed Xe–F bond length of 2.022 Å. ^{c} With the observed Xe–F bond length of 2.012 Å.

The data in Table VIII demonstrate that the stretching force constants f_r are mainly influenced by the polarity of the Xe–F bonds, with increasing polarity decreasing the force constant. On the other hand, steric crowding has a strong impact on the deformation constants. If this crowding is anisotropic, as in the case of XeF$_5^-$ where the crowding is concentrated in the equatorial plane, the deformation constants in the congested plane increase while the deformation constants out of the congested plane decrease significantly. The low value of the out-of-plane deformation constant f_γ, in combination with a comparable $f_{\gamma\gamma}$ value, implies a low energy barrier toward puckering of the equatorial plane. When the f_γ value approaches zero or becomes negative, spontaneous puckering should occur.

Computational Results. For a better understanding of the molecular structure of XeF$_5^-$, local density functional calculations were carried out for this ion and for XeF$_4$. The quality of these calculations for relatively large and heavy molecules was first tested for the well-characterized[54,55] and closely related XeF$_4$ molecule. The well-known square-planar (D_{4h}) symmetry and a Xe–F bond length of 1.998 Å (0.045 Å longer than that observed for the solid[54]) were obtained. The calculated vibrational frequencies are in excellent agreement with the experimental values[55] (Table IX), except for the in-plane deformation modes, where the agreement is only fair.

For XeF$_5^-$, the computations confirmed that the pentagonal planar D_{5h} structure is indeed a minimum. Again, the computed bond length (2.077 Å) is slightly longer (0.065 Å) than the observed one (2.012 Å). A comparison between the observed and calculated spectra is given in Table X. As for XeF$_4$, the agreement between computed and observed frequencies for XeF$_5^-$ is quite good, with the largest discrepancies again being found for the in-plane deformation modes. These results confirm the assignments made above for XeF$_5^-$.

The influence of the bond length on the vibrational spectrum of XeF$_5^-$ was also examined by computing the spectra for two shorter Xe–F bond distances, one at the experimental bond length and one 0.01 Å longer (Table X). As expected, the stretching frequencies are the most sensitive to changes in the bond length except for the equatorial ring puckering mode, ν_7, which is also

(48) Christe, K. O.; Wilson, W. W.; Bougon, R. A. *Inorg. Chem.* **1986**, *25*, 2163.

(49) Sawodny, W. *J. Mol. Spectrosc.* **1969**, *30*, 56.

(50) Christe, K. O.; Naumann, D. *Inorg. Chem.* **1973**, *12*, 59.

(51) Pfeiffer, M. *J. Mol. Spectrosc.* **1969**, *21*, 181.

(52) Thakur, S. N.; Rai, S. N. *J. Mol. Struct.* **1970**, *5*, 320.

(53) Siebert, H. *Anwendungen der Schwingungsspektroskopie in der Anorganischen Chemie*; Anorganische und Allgemeine Chemie in Einzeldarstellung, VII; Springer Verlag: Berlin, Germany, 1966.

(54) Burns, J. H.; Agron, P. A.; Levy, H. A. *Science* **1963**, *139*, 1208. Templeton, D. H.; Zalkin, A.; Forrester, J. D.; Williamson, S. M. *J. Am. Chem. Soc.* **1963**, *85*, 242. Ibers, J. A.; Hamilton, W. C. *Science* **1963**, *139*, 106.

(55) Claassen, H. H.; Chernick, C. L.; Malm, J. G. *J. Am. Chem. Soc.* **1963**, *85*, 1927.

Table XI. Valence Molecular Orbitals for XeF_5^-

symmetry	orbital[a]	energy, eV
A_2'	p_y anti on F	3.00
A_2''	p_z anti 0.67 Xe, 0.40 F	3.15
E_1'	p_y on F	3.71
A_1'	0.43 p_x on F, 0.57 s on Xe, anti	4.00
E_2''	p_z on F	4.06
E_1''	p_z on F some Xe d	4.69
E_2'	$p_{x,y}$ on F	4.78
E_2'	$p_{x,y}$ on F	5.72
A_2''	0.77 p_z Xe, 0.21 p_z F	7.38
E_1'	0.56 p_x, p_y Xe, 0.40 p_x on F	9.01
A_1'	0.89 Xe s	16.02

[a] x = Xe–F bond axis, y = orthogonal to Xe–F axis in plane, z = orthogonal to Xe–F axis out of plane.

very sensitive to shortening of the bond length. At the experimental distance, the degenerate deformation frequency becomes imaginary, showing that the molecule would assume a nonplanar structure. As discussed above, increasing congestion in the equatorial ring will result in spontaneous puckering and an imaginary frequency for ν_7. The calculations at the experimental geometry are far enough from the theoretical minimum that the calculated frequencies should be employed only to show the expected trends, as they do not refer to the minimum energy structure. The data in Table X also indicate that the frequency order of the Xe–F stretching modes is essentially independent of the Xe–F bond length. It should be noted that all the calculated frequencies are harmonic values and were not scaled to include anharmonicity effects, which are usually on the order of 5%.

The Mulliken charges for XeF_5^- are $+1.48e$ for the Xe atom and $-0.50e$ for the F atoms. This differs from the nominal assignments of $-1.0e$ for each F and $+4.0e$ for the Xe. The molecular orbitals (Table XI) provide some insight into the bonding in this molecule. If we consider only the valence p orbitals on F since the 2s orbitals are quite low in energy, the remaining orbitals can be qualitatively summed up as follows: There are 10 electrons in the $2p_y$ lone pairs on F orthogonal to the Xe–F bond. There are roughly 10 electrons in the $2p_z$ orbitals on F, which are orthogonal to the molecular plane. The totally symmetric group of these orbitals interacts with the out-of-plane 5p orbital on Xe in a symmetric and antisymmetric way. The $2p_x$ orbitals on fluorine along the Xe–F bond have about 10e in them. These mix with the $5p_x$ and $5p_y$ orbitals on Xe. Although the Xe 5s orbital does mix to some extent with the 2p orbitals on F, it is predominantly a lone pair. The basic description is thus a Xe with a $5s^2 5p_z^2$ occupancy surrounded by five F⁻ atoms. Delocalization of fluorine electron density into the Xe $5p_{x,y}$ orbitals with only a small participation of the d orbitals on Xe then reduces the charges on the F atoms. The HOMO is the antibonding combination of the in-plane lone pairs on the F atom orthogonal to the Xe–F axis. The NHOMO is almost degenerate in energy with the HOMO and is the antibonding out-of-plane combination of the F $2p_z$ and the Xe $5p_z$ orbitals (Figure 8).

Both the orbitals and the bonding in XeF_5^- are quite similar to those of XeF_4, which were calculated for comparison. In XeF_4, the Mulliken charges on Xe and F are $+1.65e$ and $-0.41e$, respectively. The Xe 5s orbital participates in two orbitals, with most of its density in the orbital at 22.02 eV just as in XeF_5^-. The $5p_z$ orbital of Xe and the out-of-plane $2p_z$ orbitals on the fluorines interact to give bonding and antibonding molecular orbitals. The orbital configuration at Xe is thus dominated by the $5s^2 5p_z^2$ configuration just as in the anion. The HOMO in XeF_4 is at 9.15 eV and is the $5p_y$ antibonding orbital as found in XeF_5^-. Its significantly higher value, compared with that of XeF_5^-, is in agreement with our expectations for an anion and its parent molecule.

It is important to note that the calculations provide a molecular orbital description of the bonding in XeF_5^- and XeF_4. The orbitals reported above are the canonical orbitals with molecular symmetry. Because of the molecular symmetry, the 5s and $5p_z$ orbitals cannot mix and thus give separate s^2 and p^2 occupancies. In contrast,
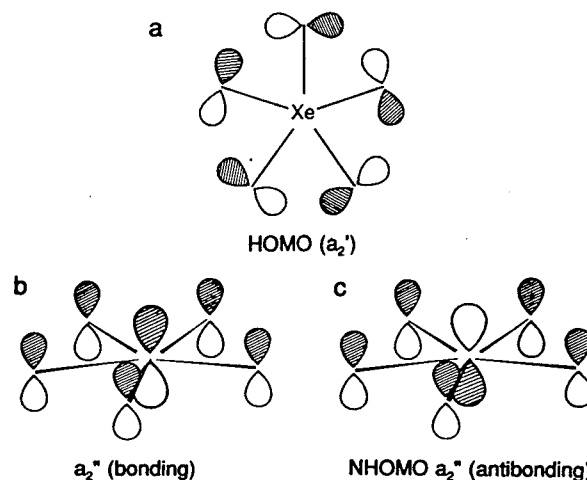

Figure 8. Selected molecular orbitals for XeF_5^-. (a) HOMO, antibonding combination of in-plane p_y's on F; (b) bonding out-of-plane orbital combination between Xe $5p_z$ and p_z's on F; (c) antibonding out-of-plane orbital combination between Xe $5p_z$ and p_z's on F.

in the VSEPR model used elsewhere in this work, the valence electron lone pairs may be described as two doubly occupied sp hybrids above and below the plane, but this is not required by the VSEPR model. The two models are equivalent, as the VSEPR model is derived from a localized orbital approach, whereas the calculations are based on a molecular orbital approach. The sum and difference of the $5s^2$ and $5p_z^2$ orbitals will lead to the two sp hybrid lone pairs. However, the total electron density, which is the invariant quantity, is independent of the choice of models used to describe it. (In a formal sense, the wave function is invariant to a unitary transformation.)

Conclusions

Xenon tetrafluoride indeed forms stable adducts with strong Lewis bases, such as tetramethylammonium fluoride and the heavier alkali-metal fluorides. However, contrary to previous reports,[13–15] these salts do not contain the XeF_6^{2-} dianion, but the XeF_5^- anion.

The XeF_5^- anion has a highly unusual pentagonal planar structure for which no other examples were previously known. It can be derived from that of a pentagonal bipyramid, such as IF_7,[38] in which the two axial fluorine ligands have been replaced by two sterically active free valence electron pairs. Compared with IF_7,
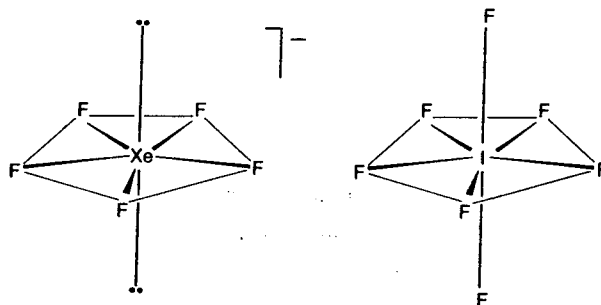
which is a fluxional molecule undergoing with relative ease a dynamic ring-puckering pseudorotation,[38,47] the equatorial XeF_5 plane of XeF_5^- appears to be considerably more rigid. The increased rigidity of the XF_5 plane in XeF_5^- is attributed to the stabilizing effect of the two free valence electron pairs on xenon. These free pairs are more diffuse and hence more repulsive than the axial I–F bond pairs in IF_7, thereby offering more resistance toward the puckering of the equatorial XeF_5 plane.

Supplementary Material Available: Tables of anisotropic thermal parameters (Table 1) and hydrogen atomic coordinates (Table 2) (2 pages); tabulation of calculated and observed structure factor amplitudes (Table 3) (13 pages). Ordering information is given on any current masthead page.

X-ray Crystal Structure and Raman Spectrum of Tribromine(1+) Hexafluoroarsenate(V), $Br_3^+AsF_6^-$, and Raman Spectrum of Pentabromine(1+) Hexafluoroarsenate(V), $Br_5^+AsF_6^-$

K. O. Christe*

Canoga Park, CA (USA), Rocketdyne Division, Rockwell International

R. Bau and D. Zhao

Los Angeles, CA (USA), University of Southern California, Department of Chemistry

Dedicated to Professor Josef Goubeau in memoriam [1])

Abstract. A single crystal of $Br_3^+AsF_6^-$ was isolated from a sample of $BrF_2^+AsF_6^-$ which had been stored for 20 years. It was characterized by x-ray diffraction and Raman spectroscopy. It is shown that $Br_3^+AsF_6^-$ (triclinic, a = 7.644(7) Å, b = 5.641(6) Å, c = 9.810(9) Å, α = 99.16(8)°, β = 86.61(6)°, γ = 100.11(7)°, space group $P\bar{1}$ R(F) = 0.0608) is isomorphous with $I_3^+AsF_6^-$. The structure consists of discrete Br_3^+ and AsF_6^- ions with some cation-anion interaction causing distortion of the AsF_6^- octahedron. The Br_3^+ cation is symmetric with a bond distance of 2.270(5) Å and a bond angle of 102.5(2)°. The three fundamental vibrations of Br_3^+ were observed at 297 (v_3), 293 (v_1), and 124 cm^{-1} (v_2). The Raman spectra of $Cl_3^+AsF_6^-$ and $I_3^+AsF_6^-$ were reinvestigated and $v_3(B_1)$ of I_3^+ was reassigned. General valence force fields are given for the series Cl_3^+, Br_3^+, and I_3^+. Reactions of excess Br_2 with either $BrF_2^+AsF_6^-$ or $O_2^+AsF_6^-$ produce mixtures of $Br_3^+AsF_6^-$ and $Br_5^+AsF_6^-$. Based on its Raman spectra, the Br_5^+ cation possesses a planar, centrosymmetric structure of C_{2h} symmetry with three semi-ionically bound, collinear, central Br atoms and two more covalently, perpendicularly bound, terminal Br atoms.

Kristallstruktur und Raman-Spektrum von Tribrom(1+) Hexafluoroarsenat(V), $Br_3^+AsF_6^-$, und Raman-Spektrum von Pentabrom(1+) Hexafluoroarsenat(V), $Br_5^+AsF_6^-$

Inhaltsübersicht. Ein Einkristall von $Br_3^+AsF_6^-$, gebildet während 20jähriger Aufbewahrung einer $BrF_2^+AsF_6^-$ Probe, wurde isoliert und mittels Röntgenstrukturanalyse und Raman-Spektren charakterisiert. Es wird gezeigt, daß $Br_3^+AsF_6^-$ (triklin, a = 7,644(7) Å, b = 5,641(6) Å, c = 9,810(9) Å, α = 99,16(8)°, β = 86,61(6)°, γ = 100,11(7)°, Raumgruppe $P\bar{1}$, R(F) = 0,0608) isomorph mit $I_3^+AsF_6^-$ ist. Die Struktur besteht aus diskreten Br_3^+- und AsF_6^--Ionen mit schwachen Anion-Kation-Wechselwirkungen, die in einer Verzerrung der AsF_6^--Oktaeder resultieren. Das Br_3^+-Kation ist symmetrisch mit einem Bindungsabstand von 2,270(5) Å und einem Bindungswinkel von 102,5(2)°. Die drei Grundschwingungen von Br_3^+ wurden bei 297 (v_3), 293 (v_1) und 124 cm^{-1} (v_2) gefunden.

---

[1]) One of us (KOC) is deeply indebted to Prof. Goubeau for the profound influence he has had on his professional and personal career. Prof. Goubeau has given him much more than a solid chemical education, he has instilled in him an everlasting love and enjoyment of chemistry.

Raman-Spektren von $Cl_3^+AsF_6^-$ und $I_3^+AsF_6^-$ wurden neu aufgenommen, und $\nu_3(B_1)$ von I_3^+ wurde neu zugeordnet. Allgemeine Valenzkraftkonstanten wurden für die Reihe Cl_3^+, Br_3^+ und I_3^+ berechnet. Umsetzungen von überschüssigem Brom mit $BrF_2^+AsF_6^-$ oder $O_2^+AsF_6^-$ resultieren in einem Gemisch von $Br_3^+AsF_6^-$ und $Br_5^+AsF_6^-$. Auf Grund der beobachteten Raman Spektren besitzt das Br_5^+-Kation eine planare, zentrosymmetrische C_{2h} Struktur mit drei halb-ionisch gebundenen, kollinearen, zentralen Bromatomen und zwei mehr kovalent und rechtwinklig gebundenen, endständigen Bromatomen.

Introduction

Homopolyatomic halogen cations are of considerable interest [1—3] because of their simplicity. They contain only one kind of atom and, contrary to transition metal cluster compounds, the absence of ligands simplifies the bonding aspects. Whereas numerous polyatomic iodine cations are known and I_2^+ [4, 5], I_3^+ [6], I_5^+ [7], I_{15}^{3+} [8], and I_4^{2+} [9] salts have been well characterized, much less is known about the lighter halogen polycations.

For bromine, the Br_2^+ cation has been well characterized in the form of its $Sb_3F_{16}^-$ salt [10, 11] and in superacid solutions [5, 12], but for Br_3^+ no structural data and only incomplete vibrational spectra [12—17] had previously been given. Furthermore, some of the vibrational frequencies attributed to Br_3^+ [17] are inconsistent with those observed for isoelectronic $SeBr_2$ [18] and the I_3^+ [1] and Cl_3^+ [19] cations. The only evidence for the existence of a polybromine cation containing more than three bromine atoms was obtained [14] when $Br_3^+[Au(SO_3F)_4]^-$ was reacted with excess Br_2 at 70 °C resulting in a solid of the composition $Br_5[Au(SO_3F)_4]$. Raman bands at 304, 295, 267, and 205 cm^{-1} were tentatively attributed [14] to the cation in this compound but are not consistent with our predictions for a centrosymmetric Hal_5^+ cation of C_{2h} symmetry (see below).

For chlorine, the only known polychlorine cation containing salt is $Cl_3^+AsF_6^-$ which is unstable and was characterized by its low-temperature Raman spectrum [19]. The Cl_2^+ ion has been observed only in the gas phase at very low pressures [20, 21]. A claim for the observation of Cl_2^+ by ESR spectroscopy in superacid solutions [22] has subsequently been disputed [2, 19, 23, 24].

In view of the scant information available on the lighter halogen homopolyatomic cations and the accidental isolation of some deeply colored single crystals from a $BrF_2^+AsF_6^-$ sample, we have undertaken a study of the bromine homopolyatomic cations.

Experimental

Materials and Apparatus

Literature methods were used for the syntheses of $BrF_2^+AsF_6^-$ [25] and $O_2^+AsF_6^-$ [26]. The Br_2 and HF were dried by storage over P_2O_5 and BiF_5 [27], respectively. Reactions involving Br_2 were carried out using a flamed out Pyrex-glass vacuum line equipped with grease-free Teflon stopcocks. Anhydrous HF was handled in a stainless steel-Teflon FEP vacuum line [28]. Nonvolatile materials were handled in the dry nitrogen atmosphere of a glove box. Raman spectra were recorded on a

Spex Model 1403 spectrophotometer using either the 647.1-nm exciting line of a Kr ion laser or the 514.5-nm line of an Ar ion laser and a previously described [29] device for obtaining the low-temperature spectra. The ^{19}F NMR spectra were recorded at 84.6 MHz on a Varian Modell EM 390 spectrometer.

Reaction of $BrF_2^+AsF_6^-$ with Br_2

A flamed out 100 ml Pyrex flask equipped with a Teflon stopcock was loaded in the dry box with $BrF_2^+AsF_6^-$ (3.94 mmol). On the vacuum line, dry Br_2 (13.49 mmol) was added at $-196\,°C$ and the resulting mixture was kept at $25\,°C$ for 2 hr. The flask was cooled to $0\,°C$ and volatile products were pumped off at $0\,°C$ for 30 min. The chocolate brown solid residue in the flask weighed 2164 mg (weight calculated for 3.94 mmol of $Br_3^+AsF_6^- = 1846$ mg and 3.94 mmol of $Br_5^+AsF_6^- = 2476$ mg). The brown solid slowly gave off bromine vapors on standing at room temperature. Pumping on the solid at room temperature for 35 min reduced the weight to 1427 mg. The resulting residue still had some dissociation pressure at ambient temperature as evidenced by the slow evolution of Br_2 vapors above the solid. Low-temperature Raman spectroscopy showed this residue to be mainly $Br_3^+AsF_6^-$ with some $Br_5^+AsF_6^-$ as a by-product.

Reaction of $O_2^+AsF_6^-$ with Br_2

$O_2^+AsF_6^-$ (5.15 mmol) and Br_2 (13.54 mmol) were combined at $-196\,°C$ in a 100 ml Pyrex flask. The mixture was warmed to $25\,°C$ for 2 hr, then cooled back to $-196\,°C$. The evolved oxygen (5.14 mmol) was pumped off at $-196\,°C$ and excess Br_2 was pumped off at $0\,°C$ for 10 min. The resulting brown residue (1871 mg, weight calculated for 5.15 mmol of $Br_3^+AsF_6^- = 2414$ mg) was somewhat inhomogeneous showing smaller patches of material ranging in color from carmine red to greyish-green. Again some Br_2 vapor evolved above the solid on standing at room temperature. Low-temperature Raman spectra of the solid taken from different patches showed mainly $Br_5^+AsF_6^-$ with varying amounts of $Br_3^+AsF_6^-$ as a by-product.

Crystal Structure Determination of $Br_3^+AsF_6^-$

During 20 years of storage of a symple of $BrF_2^+AsF_6^-$ at room temperature in a Teflon tube closed by a stainless steel fitting several single crystals of $Br_3^+AsF_6^-$ had formed. Due to their great difference in color, $BrF_2^+AsF_6^-$ is colorless and $Br_3^+AsF_6^-$ is dark brown, the crystals were easily separated in the dry box. The diffraction data were collected at room temperature, using a Siemens/Nicolet/Syntex P2$_1$ diffractometer with MoKα radiation up to a 2Θ limit of 55 deg. 1538 intensity

Table 1 Summary of Crystal Data and Refinement Results for $[Br_3]^+[AsF_6]^-$

space group	P$\bar{1}$	absorption coefficient (μ: mm^{-1})	18.6
a (Å)	7.644(7)	max. & min. transmission factors	0.55−1.66
b (Å)	5.641(6)	(scaled to an average of unity)	
c (Å)	9.810(9)	crystal dimensions (mm)	0.64×0.34×0.33
α (deg)	99.16(8)	calculated density (g cm^{-3})	3.47
β (deg)	86.61(6)	wavelength (Å) used for data collection	0.71069
γ (deg)	100.11(7)	sin Θ/λ limit (Å^{-1})	0.6497
V (Å^3)	411.3(7)	total number of reflections measured	1538
molecules/unit cell	2	number of independent reflections	1387
formula weight (g)	384.0	number of reflections used in structural analysis 1 > 3σ(I)	538
		number of variable parameters	91
		final agreement factors	R(F) = 0.0608
			R(wF) = 0.0608

values for an entire reflection sphere were collected and the two equivalent hemispheres merged to give a total of 546 unique reflections. The R factor for averaging was 2.3%. The positions of the As and three Br atoms were obtained by direct methods using the computing package SHELX-86 [30a]. The rest of the atoms were then located from a difference-Fourier map, and the entire structure was anisotropically refined by SHELX-76 [30b] to a final agreement factor of R = 6.08%, using 538 reflections with $1 > 3\sigma(I)$. At that point it was realized that the unit cell parameters were virtually identical to those of $[I_3]^+[AsF_6]^-$ [6], and the coordinates were then transformed accordingly, to be consistent with those reported for the $[I_3]^+$ analog. Crystal data and refinement results are summarized in Table 1, the final atomic coordinates and temperatures factors are given in Table 2, and the bond distances and angles are given in Table 3.

Table 2   Final Atomic Coordinates and Temperature Factors for $[Br_3]^+[AsF_6]^-$

Atom	x	y	z	$U_{11}\times10^3$	$U_{22}\times10^3$	$U_{33}\times10^3$	$U_{12}\times10^3$	$U_{13}\times10^3$	$U_{23}\times10^3$
As	0.7857(5)	0.5650(8)	0.7972(4)	46(2)	64(3)	32(2)	19(2)	−3(2)	0(2)
Br1	0.8030(5)	0.8212(8)	0.2097(3)	56(2)	79(3)	30(2)	20(2)	2(2)	5(2)
Br2	0.6162(5)	1.0790(8)	0.1780(4)	58(3)	85(3)	57(3)	20(2)	−10(2)	5(2)
Br3	0.7695(6)	0.8069(9)	0.4394(4)	68(3)	108(4)	32(2)	26(2)	0(2)	3(2)
F1	0.7800(33)	0.7883(45)	0.7066(20)	133(21)	105(20)	32(11)	43(17)	−5(12)	−7(12)
F2	0.8702(32)	0.7820(47)	0.9273(21)	106(18)	102(20)	39(12)	−12(15)	−6(12)	−15(13)
F3	0.9991(34)	0.5559(62)	0.7415(36)	74(18)	172(32)	184(31)	52(19)	52(19)	−12(24)
F4	0.5759(26)	0.5799(60)	0.8601(32)	32(13)	184(30)	169(28)	42(16)	14(15)	59(23)
F5	0.7054(37)	0.3490(52)	0.6663(25)	145(24)	117(24)	71(18)	−23(20)	−37(17)	−38(17)
F6	0.7957(36)	0.3498(56)	0.8913(32)	111(22)	112(24)	147(27)	17(19)	−16(20)	8(21)

Table 3   Bond Distances (Å) and Angles (deg) for $[Br_3]^+[AsF_6]^-$

As—F1	1.660(23)	F1—As—F2	87.4(12)
		F1—As—F3	89.9(15)
As—F2	1.693(22)	F2—As—F3	86.6(14)
		F1—As—F4	91.0(13)
As—F3	1.696(22)	F2—As—F4	90.9(15)
		F3—As—F4	177.4(17)
As—F4	1.695(20)	F1—As—F5	92.4(13)
		F2—As—F5	178.9(13)
As—F5	1.686(22)	F3—As—F5	92.3(15)
		F4—As—F5	90.2(15)
As—F6	1.652(31)	F1—As—F6	178.0(14)
		F2—As—F6	90.6(14)
Br1—Br2	2.275(5)	F3—As—F6	89.6(16)
		F4—As—F6	89.5(14)
Br1—Br3	2.266(5)	F5—As—F6	89.5(15)
		Br2—Br1—Br3	102.5(2)

Results and Discussion

Synthesis of $Br_3^+AsF_6^-$

Single crystals of $Br_3^+AsF_6^-$ were obtained from a sample of $BrF_2^+AsF_6^-$ which had been stored for 20 years at room temperature in a Teflon-stainless

steel container. Its formation can be explained by the reduction of a small amount of BrF_2^+ to Br_2 by the container material and a subsequent reaction of Br_2 with BrF_2^+ according to:

$$BrF_2^+AsF_6^- + 2\,Br_2 \rightarrow Br_3^+AsF_6^- + 2\,BrF. \tag{1}$$
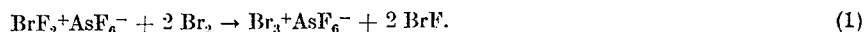
The BrF is thermally unstable and disproportionates readily [31] to BrF_3 and Br_2, with the BrF_3 most likely being reduced by the container material to additional Br_2, and the Br_2 being consumed according to (1).

To verify reaction (1) and to obtain larger amounts of $Br_3^+AsF_6^-$, a sample of $BrF_2^+AsF_6^-$ was treated at room temperature with an excess of Br_2. The colorless $BrF_2^+AsF_6^-$ was rapidly converted to a dark brown solid. After pumping off the unreacted Br_2 at 0 °C, this brown solid consisted of a mixture of $Br_3^+AsF_6^-$ and $Br_5^+AsF_6^-$ (see below). Attempts to convert the $Br_5^+AsF_6^-$ to $Br_3^+AsF_6^-$ by pumping at room temperature was only partially successful and resulted in the loss of both $Br_3^+AsF_6^-$ and $Br_5^+AsF_6^-$. This is not surprising since, at room temperature, $Br_3^+AsF_6^-$ has some dissociation pressure, as evidenced by the build up of Br_2 vapor above the brown solid. This Br_2 vapor can on standing equilibrate with $Br_3^+AsF_6^-$ to reform some $Br_5^+AsF_6^-$ thus explaining the difficulties encountered with preparing and handling samples of pure $Br_3^+AsF_6^-$. The previously reported [13] synthesis of $Br_3^+AsF_6^-$ from BrF_5, Br_2 and AsF_5 is based on the same approach, i. e. conproportionation of a higher bromine fluoride with bromine to BrF and its subsequent reaction with Br_2 and AsF_5 to form $Br_3^+AsF_6^-$ (2—4).

$$BrF_5 + 2\,Br_2 \rightleftharpoons 5\,BrF \tag{2}$$

$$5\,BrF + 5\,Br_2 + 5\,AsF_5 \rightarrow 5\,Br_3^+AsF_6^- \tag{3}$$

$$BrF_5 + 7\,Br_2 + 5\,AsF_5 \rightarrow 5\,Br_3^+AsF_6^-. \tag{4}$$

In this reaction the formation of $Br_5^+AsF_6^-$ can be suppressed by the use of excess BrF_5 and AsF_5.

We have also repeated the previously reported [13] reaction of $O_2^+AsF_6^-$ with excess Br_2. In this system, O_2 evolution is facile and quantitative, however the formed product appears inhomogenous with varying amounts of $Br_5^+AsF_6^-$ and $Br_3^+AsF_6^-$ being produced.

Crystal Structure of $Br_3^+AsF_6^-$

$Br_3^+AsF_6^-$ is isomorphous with $I_3^+AsF_6^-$ [6]. Both compounds are triclinic with similar unit cells and packing arrangements (see Figure 1). The structures are predominantly ionic containing discrete Hal_3^+ cations and AsF_6^- anions, with some cation-anion interaction (see Figure 2) resulting in a distortion of the AsF_6^- anion from O_h symmetry. As expected, the Br_3^+ cation is symmetric ($r_{Br-Br} = 2.270(5)$ Å) and bent (102.5(2)°). The Br—Br distance in Br_3^+ is similar to that for Br_2 (2.281 Å [32]) and resembles in this respect the I_3^+ (2.665(4) Å [6]) and I_2 (2.666 Å [32]) couple. The fluorine contacts to Br_3^+ are very similar to those found for I_3^+ in $I_3^+AsF_6^-$ [6], resulting in an approximately planar network

of two fluorine bridges to the central and of one fluorine bridge to each terminal bromine atom (see Figure 2). A more detailed discussion of these interactions has previously been given for $I_3^+AsF_6^-$ [6] and, therefore, does not need reiteration.
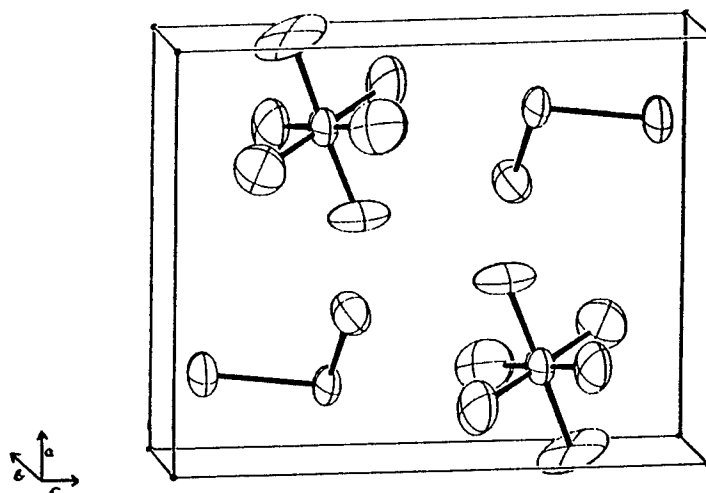
Fig. 1   Unit cell packing diagram for $Br_3^+AsF_6^-$, viewed down the b axis.
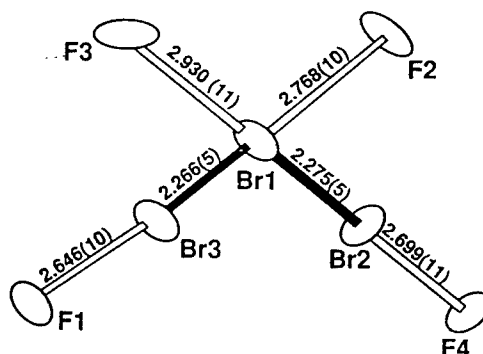
Fig. 2 Br_3^+ cation with closest anion-cation contacts.

^{19}F NMR Spectrum of $Br_3^-AsF_6^-$

The ^{19}F NMR spectrum of $Br_3^+AsF_6^-$ in anhydrous HF solution was recorded at room temperature. It consisted of a well resolved quartet of equal intensity ($\varnothing = 65$ ppm, upfield from external $CFCl_3$, with $J_{^{75}AsF} = 925$ Hz and a line width of 100 Hz), in excellent agreement with previous reports for octahedral AsF_6^- [33].

Raman Spectra of $Br_3^+AsF_6^-$, $Cl_3^+AsF_6^-$, and $I_3^+AsF_6^-$

Raman spectra of bromine polyatomic cation salts are very difficult to obtain due to the intense colors of the cations. The Raman spectrum of a randomly

oriented single crystal of $Br_3^+AsF_6^-$ at $-150\,^\circ$C is shown in Figure 3. The observed frequencies and their assignments are summarized in Table 4. The two bands at 173 and 85 cm^{-1}, respectively, are due to a small amount of Br_5^+ formed during the handling of the crystal and recording of the spectrum and are denoted in Figure 3 by an asterisk. The assignments given in Table 4 are clear cut and do not require further discussion. The fact that the observed AsF_6^- bands deviate from the O_h selection rules, i. e. $\nu_3(F_{1u})$ becomes Raman active and $\nu_2(E_g)$ is split into its degenerate components, is not surprising in view of the distortion of the AsF_6^- octahedron by fluorine bridging with the Br_3^+ cations. Raman spectra of powdered samples of $Br_3^+AsF_6^-$ were also recorded at 25 and $-150\,^\circ$C. They were of lower quality than that of the single crystal material but showed the same main features, i. e. ν_{sym} Br_3^+ at 293 cm^{-1} with a shoulder at 297 for ν_{asym} Br_3^+, δ Br_3^+ at about 120 cm^{-1}, and ν_{sym} AsF_6^- at about 675 cm^{-1}.
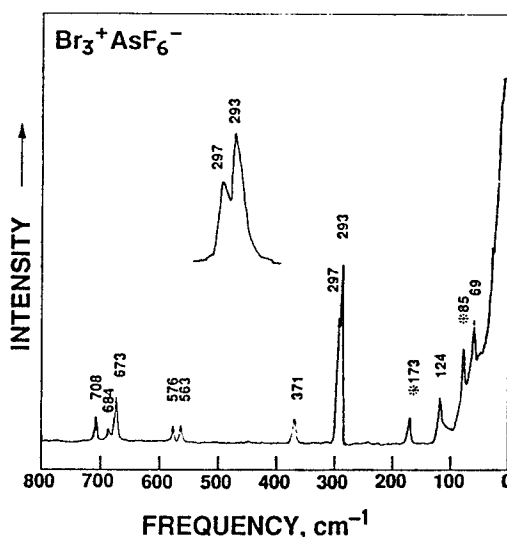
Fig. 3   Raman spectrum of a single crystal of $Br_3^+AsF_6^-$ recorded at $-150\,^\circ$C with random orientation of the crystal. The insert shows the Br_3^+ stretching bands, recorded with tenfold abscissa expansion.

Previous literature reports on the vibrational spectra of Br_3^+ suggested for $\nu_1(A_1)$ frequencies of 295 cm^{-1} in $Br_3^+[Pt(SO_3F)_6]^-$ [15], 280 cm^{-1} in $Br_3^+[Au(SO_3F)_4]^-$ [14], 290 cm^{-1} in fluorosulfuric acid solutions [12], for $\nu_3(B_1)$ a frequency of 288 cm^{-1} in $Br_3^+SO_3F^-$ [16], and for $\nu_2(A_1)$ a doublet at 227 and 238 cm^{-1} in an HBr—NO$_2$ reaction product [17]. Whereas the reported frequencies of the two stretching modes are in fair agreement with our findings for $Br_3^+AsF_6^-$, the previously reported [17] deformation mode frequency is much too high for Br_3^+, as is also obvious from a comparison with the known fundamental vibrations of I_3^+ (see below), Cl_3^+ [19], and isoelectronic $SeBr_2$ [18] which are summarized in Table 5.

Table 4   Low Temperature Raman Spectrum of a Randomly-Oriented Single Crystal of $Br_3^+AsF_6^-$

obsd. freq. (cm^{-1}) rel. int.	assignments (point group) and approximate mode descriptions	
	Br_3^- (C_{2v})	AsF_6^- (O_h)
708(15) ⎫		(O_h)
684(4) ⎭		$\nu_3(F_{1u})$, as stretch
673(25)		$\nu_1(A_{1g})$, sym in phase stretch
576(9) ⎫		
563(10) ⎭		$\nu_2(E_g)$, sym out of phase stretch
371(15)		$\nu_5(F_{2g})$, sym bend
297(60)	$\nu_3(B_1)$. asym stretch	
293(100)	$\nu_1(A_1)$. sym stretch	
124(23)	$\nu_2(A_1)$. bend	
69(25) ⎫		
39 sh ⎬		lattice vibrations
30 sh ⎭		

Table 5   Vibrational Frequencies (cm^{-1}) of Br_3^+ Compared to Those of I_3^+, Cl_3^+, and $SeBr_2$

	I_3^+		Br_3^+		Cl_3^+ [19]	$SeBr_2$ [18]
	this work	previous work [1]	this work	previous work [12—17]		
$\nu_3(B_1)$	211	233	297	288	508	290
$\nu_1(A_1)$	205	207	293	280—295	489	266
$\nu_2(A_1)$	110	114	124	227/238	225	96

The Raman spectra of $Cl_3^+AsF_6^-$ [19] and $I_3^+AsF_6^-$ [6, 34] were also recorded for comparison. The spectrum of $Cl_3^+AsF_6^-$ agreed well with that previously reported [19] with the following exceptions. The unassigned 170 cm^{-1} band was either completely absent or of variable intensity in different samples, and, therefore, does not belong to $Cl_3^+AsF_6^-$. Furthermore, two additional bands at 709 and 686 cm^{-1} were observed in the $\nu_3(F_{1u})$ region of AsF_6^- which resemble those in $Br_3^+AsF_6^-$. In the low frequency region, two lattice vibrations were observed at 132 and 101 cm^{-1}, respectively.

The Raman spectrum of $I_3^+AsF_6^-$ which was prepared from I_2 and AsF_5 in AsF_3 solution [34], was recorded for both the solid state and in anhydrous HF solutions using either 647.1, 514.5, or 488 nm excitation. Due to the intense, dark brown to black color of $I_3^+AsF_6^-$ the quality of the obtainable spectra was poor. With 647.1 nm excitation, the spectra were dominated by a very intense resonance Raman spectrum of I_2^+ [2] which was present in the sample as a minor impurity. In addition to the intense 238 cm^{-1} band of I_2^+ [1, 2], a weak band at 206 cm^{-1} was observed for $\nu_1(A_1)$ of I_3^+. With 488 nm excitation, only a weak band at 208 cm^{-1} was observed. The best spectrum was obtained with 514.5 nm excitation and is shown in Figure 4. It clearly locates $\nu_1(A_1)$ and $\nu_2(A_1)$ of I_3^+ at 205 and 110 cm^{-1}, respectively, in good agreement with the 207 and 114 cm^{-1}
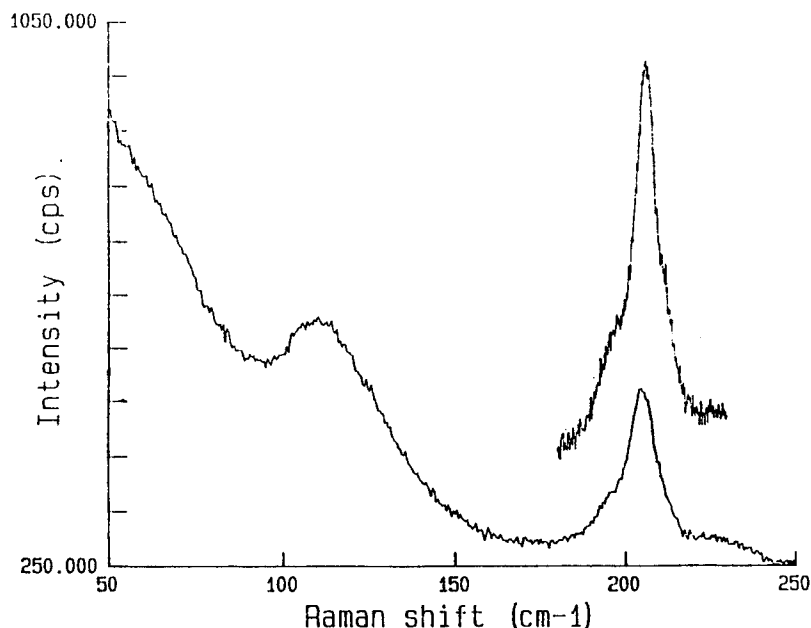
Fig. 4 Raman spectrum of an anhydrous HF solution of $I_3^+AsF_6^-$ in a Teflon-FEP tube recorded at 25°C with 514.5-nm excitation. The band shown as an insert was recorded with a smaller slit width of 2 cm^{-1} to resolve the shoulder on the high frequency side.

values previously reported [1]. However, the previously reported [1] 233 cm^{-1} band for $\nu_3(B_1)$ could not be confirmed. By analogy with Br_3^+ and based on model calculations for the frequency separation of the two stretching modes of an XY_2 group as a function of their bond angle and relative masses [35], $\nu_3(B_1)$ of I_3^+ should be about 5 cm^{-1} higher than $\nu_1(A_1)$. As shown by the insert in Figure 4, the 205 cm^{-1} Raman band of I_3^+ indeed exhibits a pronounced shoulder at 210 cm^{-1} which is assigned to $\nu_3(B_1)$. This reassignment of ν_3 is also supported by our force field calculations (see below). On the low frequency side of the 205 cm^{-1} Raman band of I_3^+ another shoulder was observed. A firm assignment cannot be given for this shoulder at the present time, but based on the arguments given in [35] it cannot represent $\nu_3(B_1)$ of I_3^+.

General Valence Force Fields for Cl_3^+, Br_3^+, and I_3^+

General valence force fields were calculated for Cl_3^+, Br_3^+, and I_3^+ using WILSONS GF method [36]. Since the A_1 block (2 frequencies, 3 force constants) is underdetermined, the complete range of possible solutions was computed using SAWODNYs method [37]. The resulting force constant ellipses are given in Figure 5. To allow a better comparison, the stretch-bend interaction constants F_{12} and bending constants F_{22} have been normalized for distance.
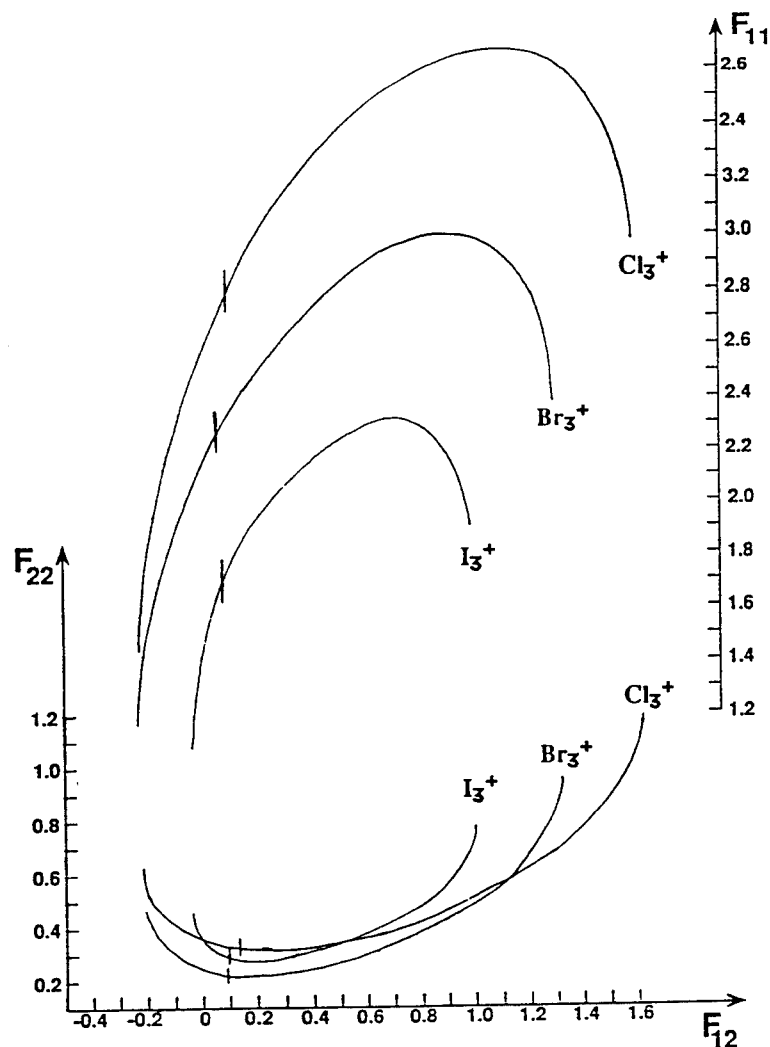
Fig. 5   Range of possible solutions for the A_1 General Valence Force Fields for Cl_3^+, Br_3^+, and I_3^+ (all values in mdyn/Å). The preferred solutions have been marked by vertical lines.

As can be seen from Figure 5, the values of the stretching force constants F_{11} strongly depend on the choice of F_{12}. In the absence of additional experimental data, assumptions about the values of F_{12} had to be made to select preferred sets of force constants. The method of Thakur {factoring the F_{12} value of the $F_{22} \equiv$ minimum solution [37] by $G_{12}/\sqrt{(G_{11} \cdot G_{22} + G_{12}^2)}$} was chosen because it best duplicates the General Valence Force Fields of molecules with similar mass ratios [38]. The internal force constants obtained in this manner for Cl_3^+, Br_3^+, and I_3^+ are summarized in Table 6 and compared to those of the related Hal_2 molecules and Hal_2^+ cations.

Table 6   Internal Force Constants (mdyn/Å) and Bond Lengths (Å) and Angles (deg) of the Hal_3^+, Hal_2, and Hal_2^+ Series

	Cl_3^+	Cl_2 [1]	Cl_2^+ [1]	Br_3^-	Br_2 [2]	Br_2^+ [1]	I_3^+ [1]	I_3^+ this work	I_2 [1]	I_2^+ [1]
fr	2.607	3.16	4.29	2.063	2.36	3.05	1.923	1.607	1.70	2.12
frr	0.184	—	—	0.192	—	—	0.156	0.097	—	—
$f\alpha$	0.314	—	—	0.216	—	—	0.294	0.273	—	—
$fr\alpha$	0.076	—	—	0.052	—	—	0.070	0.065	—	—
r	[1.98][a]	1.98	1.89	2.268	2.28	2.13	2.665		2.666	2.56
α	[103][a]	—	—	102.7	—	—	101.75		—	—

[a] estimated values

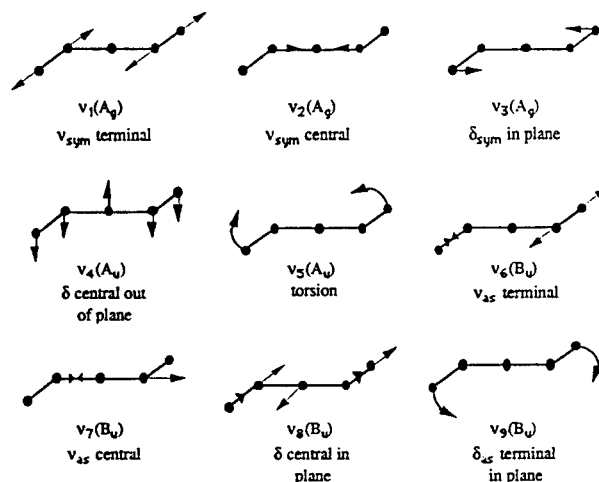As can be seen from Figure 5 and Table 6, the stretching force constants fr monotonously increase from Cl_3^+ to I_3^+, in good analogy with those of the Hal_2 molecules and Hal_2^+ cations. The finding that the stretching force constants in Hal_3^+ cations are smaller than those predicted from their bond lengths and the known force constants and bond lengths in the corresponding homonuclear diatomic molecules or ions, is not surprising. From NQR measurements on I_3^+ [39] it is known that in Hal_3^+ cations most of the positive charge resides on the central atom. This results in a significant bond polarity for the Hal_3^+ cations, while the bond polarity in the homonuclear diatomics is zero. Since polar bonding contributes strongly to the bond shortening but not to the stretching force constants, it is not surprising that the stretching force constant of a Hal_3^+ cation should be smaller than that of a Hal_2 molecule or ion possessing the same bond length. A closer inspection of the data of Table 6 reveals that for I_3^+ only our revised assignment for v_3 results in a plausible value for the stretching force constant fr.

The Raman Spectrum of $Br_5^+AsF_6^-$

In the reactions of either $Br_2^+AsF_6^-$ or $O_2^+AsF_6^-$ with an excess of Br_2 (see above) products were obtained which contained in addition to Br_3^+ a second polybromine cation salt. Its Raman spectrum is shown in Figure 6, and the observed frequencies and their assignments are summarized in Table 7. The most likely candidate for this cation is Br_5^+. In the literature, only one brief reference was made [14] to Br_5^+ and Raman bands at 304, 295, 267, and 205 cm^{-1} were tentatively attributed to Br_5^+. Otherwise, the only structural information available for a Hal_5^+ cation is a crystal structure of $I_5^+AsF_6^-$ [7]. The latter study showed that I_5^+ has a centrosymmetric, planar structure of C_{2h} symmetry $\left[_{I} \diagup ^{I-I-I} \diagup ^{I} \right]^+$. It is therefore reasonable to assume an analogous C_{2h} structure for Br_5^+.

A Br_5^+ cation of symmetry C_{2h} possesses nine fundamental vibrations which are classified as $\Gamma = 3A_g + 2A_u + 4B_u$. Of these, the A_g modes are only Raman

and the A_u and the B_u modes only infrared active. The following diagram gives an approximate description of these modes.

$\nu_1(A_g)$	$\nu_2(A_g)$	$\nu_3(A_g)$
ν_{sym} terminal	ν_{sym} central	δ_{sym} in plane
$\nu_4(A_u)$	$\nu_5(A_u)$	$\nu_6(B_u)$
δ central out of plane	torsion	ν_{as} terminal
$\nu_7(B_u)$	$\nu_8(B_u)$	$\nu_9(B_u)$
ν_{as} central	δ central in plane	δ_{as} terminal in plane

Table 7 Raman Spectra of $Br_5^+AsF_6^-$

obsd. freq. (cm⁻¹), rel. int.		assignments (point group) and approximate made descriptions	
solid, −155 °C	HF solution, 25 °C	AsF_6^- (O_h)	Br_5^+ (C_{2h})
718(0.5)			
681(0.7)		$\nu_3(F_{1u})$	
670(3.5)	685(4)	$\nu_1(A_{1g})$	
618(0.4)			
570(0.2)			
563(0.3)		$\nu_2(E_g)$	
487(0.2)			
399(0.1)		$\nu_4(F_{1u})$	
366(0.8)			
348(1)		$\nu_5(F_{2g})$	
309(9)	309(20) pol		$\nu_1(A_g)$, sym terminal stretch
190 sh			$\nu_7(B_u)$, asym central stretch
174(100)	182(100) pol		$\nu_2(A_g)$, sym central stretch
87(69)	108(68) pol		$\nu_3(A_g)$, sym term. in plane def
66(3)			
37(20)		lattice vibrations	
27(12)			

Since in I_5^+ the collinear central I—I bonds (2.895 Å) are much longer than the perpendicular terminal ones (2.645 Å) [7], the bonding in a Hal_5^+ cation is best described by a semi-ionic, three center-four electron bonding model [40—43], as in the Hal_3^- anions, for the three central halogen atoms and two essentially normal covalent bonds, as in Hal_2 and Hal_3^+, for the perpendicular terminal bonds.
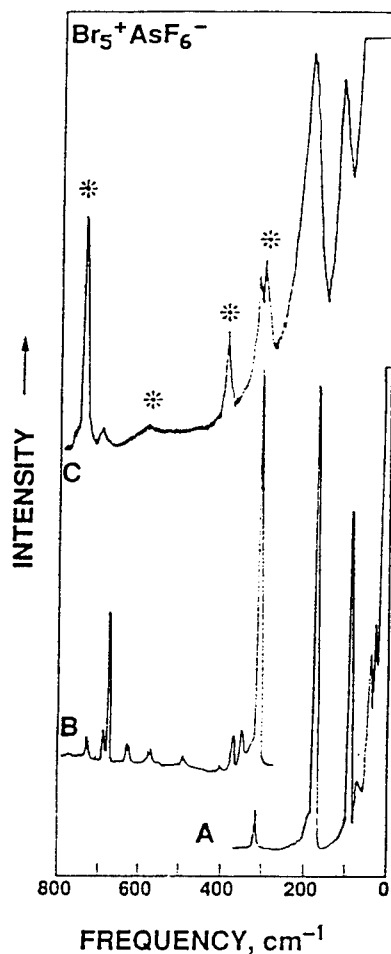
Fig. 6   Raman spectrum of $Br_5^+AsF_6^-$. Traces A and B are spectra of the solid recorded at $-155\,°C$ at two different recorder voltages; trace C is the spectrum of a saturated solution in anhydrous HF at $25\,°C$. Bands marked by an asterisk are due to the Teflon container.

Consequently, the frequencies of the three Raman active modes of Br_5^+ can be predicted as follows: $\nu_1(A_g)$ should be similar to that in Br_2 ($320\,cm^{-1}$ [2]), $\nu_2(A_g)$ to that of ν_{sym} in Br_3^- ($162\,cm^{-1}$[44]), and $\nu_3(A_g)$ to that of the bending mode in Br_3^+ ($124\,cm^{-1}$, see above).

The observed spectra (Figure 5, Table 7) are in excellent agreement with the above predictions for a Br_5^+ cation of C_{2h} symmetry. Disregarding the weak lines above $300\,cm^{-1}$ which are due to AsF_6^- and the lattice modes which disappear for the HF solution, we are left with three very intense Raman lines at 309, 174, and $84\,cm^{-1}$ in the solid and at 309, 182, and $108\,cm^{-1}$ in the HF solution which in the solution spectrum are all polarized as expected for A_g modes. The frequency differences between the solid state and solution spectra are attributed to solid

state and solvation effects. The weak shoulder observed at 190 cm^{-1} for the solid is attributed to the antisymmetric central Br_3 stretching mode $\nu_7(B_u)$, which is activated by solid state effects and occurs for $Br_3{}^-$ at 193 cm^{-1} [44].

In view of this excellent agreement the observed spectra can be attributed to a $Br_5{}^+$ cation of C_{2h} symmetry with bonding conditions similar to those in $I_5{}^+$, i. e. a semi-ionic, three center-4 electron bond for the three collinear central bromine atoms and two mainly covalent bonds for the perpendicular terminal bromine atoms. The occurrence of a semi-ionic, three center-four electron bond in $Br_5{}^+$ but not in $Br_3{}^+$ is readily understood from a simple consideration of the number of valence electrons in each cation. In $Br_3{}^+$, all three bromine atoms have an electron octet, whereas in $Br_5{}^+$ the central bromine atom is hypervalent possessing 10 valence electrons which favors the formation of semi-ionic, three center-four electron bonds [43].

Note added in proof: After submission of this paper we learned from Prof. Dr. HARTL about an x-ray crystal structure determination for $Br_5{}^+AsF_6{}^+$ wich confirms the above conclusions about the structure of $Br_5{}^+$.

References

[1] GILLESPIE, R. J.; MORTON, M. J.; SOWA, J. M.: Adv. Raman Spectrosc. 1 (1972) 539.

[2] GILLESPIE, R. J.; PASSMORE, J.: Adv. Inorg. Chem. Radiochem. 17 (1975) 49.

[3] LI, Y.; WANG, X.; JENSEN, F.; HOUK, K. N.; OLAH, G. A.: J. Amer. Chem. Soc. 112 (1990) 3922.

[4] DAVIS, C. G.; GILLESPIE, R. J.; IRELAND, P. R.; SOWA, J. M.: Canad. J. Chem. 52 (1974) 2048.

[5] WILSON, W. W.; THOMPSON, R. C.; AUBKE, F.: Inorg. Chem. 19 (1980) 1489.

[6] PASSMORE, J.; SUTHERLAND, G.; WHITE, P. S.: Inorg. Chem. 20 (1981) 2169.

[7] APBLETT, A.; GREIN, F.; JOHNSON, J. P.; PASSMORE, J.; WHITE, P. S.: Inorg. Chem. 25 (1986) 422.

[8] PASSMORE, J.; TAYLOR, P.; WHIDDEN, T.; WHITE, P. S.: Canad. J. Chem. 57 (1979) 968.

[9] GILLESPIE, R. J.; KAPOOR, R.; FAGGIANI, R.; LOCK, C. J.; MURCHIE, M.; PASSMORE, J.: J. Chem. Soc. Chem. Commun. (1983) 8.

[10] EDWARDS, A. J.; JONES, G. R.; SILLS, R. J. C.: J. Chem. Soc. Chem. Commun. (1968) 1527.

[11] EDWARDS, A. J.; JONES, G. R.: J. Chem. Soc. A, (1971) 2318.

[12] GILLESPIE, R. J.; MORTON, M. J.: Inorg. Chem. 11 (1972) 586, and J. Chem. Soc. Chem. Commun. (1968) 1565.

[13] GLEMSER, O.; SMALC, A.: Angew. Chem., Int. Ed. Engl. 8 (1969) 517.

[14] LEE, K. C.; AUBKE, F.: Inorg. Chem. 19 (1980) 119.

[15] LEE, K. C.; AUBKE, F.: Inorg. Chem. 23 (1984) 2124.

[16] WILSON, W. W.; WINFIELD, J.; AUBKE, F.: J. Fluorine Chem. 7 (1976) 245.

[17] CHEN, L. H.; NOUR, E. M.; LAANE, J. M.: J. Raman Spectrosc. 14 (1983) 232.

[18] MILNE, J.: Polyhedron 4 (1985) 65.

[19] GILLESPIE, R. J.; MORTON, M. J.: Inorg. Chem. 9 (1970) 811.

[20] HERZBERG, G.: "Molecular Spectra and Molecular Structure", Vol. 1; Van Nostrand-Reinhold, Princeton, NJ, 1960.

[21] „Gmelins Handbuch der Anorganischen Chemie", Chlor, Ergänzungsband, Teil A, p. 183; Verlag Chemie, Weinheim, Germany, 1968.

[22] OLAH, G. A.; COMISAROW, M. B.: J. Amer. Chem. Soc. 90 (1968) 5033 and 91 (1969) 2172.

[23] CHRISTE, K. O.; MUIRHEAD, J. S.: J. Amer. Chem. Soc. 91 (1969) 7777.

[24] EACHUS, R. S.; SLEIGHT, T. P.; SYMMONS, M. C. R.: Nature (London) 222 (1969) 769.

[25] CHRISTE, K. O.; SCHACK, C. J.: Inorg. Chem. 9 (1970) 2296.

[26] SHAMIR, J.; BINENBOYM, J.: Inorg. Chim. Acta 2 (1968) 37.

[27] CHRISTE, K. O.; WILSON, W. W.; SCHACK, C. J.: J. Fluorine Chem. 11 (1978) 71.

[28] CHRISTE, K. O.; WILSON, R. D.; SCHACK, C. J.: Inorg. Synth. 24 (1986) 3.

[29] MILLER, F. A.; HARNEY, B. M.: Appl. Spectrosc. 23 (1969) 8.

[30] a) SHELDRIX, G. M.: SHELX-86 System of Crystallographic Computational Programs, University of Göttingen, Germany, 1986.
   b) SHELDRIX, G. M.: SHELX-76 System of Crystallographic Computational Programs, University of Cambridge, England, 1976.

[31] NAUMANN, D.: „Fluor und Fluorverbindungen", Spezielle Anorganische Chemie, Band 2; Steinkopff, Darmstadt, Germany, 1980.

[32] HUBER, K. P.; HERZBERG, G.: "Molecular Spectra and Molecular Structure"; Vol. 4; Van Nostrand-Reinhold, New York, NY, 1979.

[33] MUETTERTIES, E. L.; PHILLIPS, W. D.: J. Amer. Chem. Soc. 81 (1959) 1084, PACKER, K. J.; Muetterties, E. L.: Proc. Chem. Soc., London 1964, 147.

[34] PASSMORE, J.; TAYLOR, P. J.: Chem. Soc., Dalton Trans. 1976, 804.

[35] WEIDLEIN, J.; MÜLLER, U.; DEHNICKE, K.: „Schwingungsspektroskopie"; G. Thieme Verlag, Stuttgart, Germany, 1982.

[36] WILSON, E. B.; DECIUS, J. C.; CROSS, P. C.: "Molecular Vibrations. The Theory of Infrared and Raman Vibrational Spectra"; McGraw Hill Book Co., New York, 1955.

[37] SAWODNY, W.: J. Mol. Spectrosc. 30 (1969) 56.

[38] THAKUR, S. N.; RAI, S. M.: J. Mol. Structure 5 (1970) 320.

[39] MERRYMAN, D. J.; CORBETT, J. D.; EDWARDS, P. A.: Inorg. Chem. 14 (1975) 428.

[40] PIMENTEL, G. C.: J. Chem. Phys. 19 (1951) 446.

[41] HACH, R. J.; RUNDLE, R. E.: J. Amer. Chem. Soc. 73 (1951) 4321.

[42] RUNDLE, R. E.: J. Amer. Chem. Soc. 85 (1963) 112.

[43] WIEBENGA, E. H.; HAVINGA, E. E.; BOSWIJK, K. H.: Adv. Inorg. Chem. Radiochem. 3 (1961) 158.

[44] PERSON, W. B.; Anderson, G. R.; FORDEMWALT, J. N.; STAMMREICH, H.; FORNERIS, R.: J. Chem. Phys. 35 (1961) 908.

Anschr. d. Verf.: Dr. K. O. CHRISTE, Rocketdyne Division, Rockwell International Corporation, Canoga Park, CA 91303, USA

High-coordination Number Fluoro- and Oxofluoro-anions; IF_6O^-, TeF_6O^{2-}, TeF_7^-, IF_8^- and TeF_8^{2-}

Karl O. Christe,*[a] Jeremy C. P. Sanders,[b] Gary J. Schrobilgen*[b] and William W. Wilson[a]

[a] *Rocketdyne, a Division of Rockwell International Corporation, Canoga Park, California 91303, USA*
[b] *The Department of Chemistry, McMaster University, Hamilton, Ontario L8S 4M1, Canada*

The novel hypervalent, highly coordinated, high-oxidation state anions IF_6O^-, TeF_6O^{2-}, TeF_7^-, IF_8^- and TeF_8^{2-} have been synthesized in anhydrous MeCN using anhydrous $N(Me)_4^+F^-$ as the fluoride ion source; the anions have been characterized by NMR and vibrational spectroscopy and represent novel examples of seven and eight-coordinate species having symmetries C_{5v} (IF_6O^-, TeF_6O^{2-}), D_{5h} (TeF_7^-) and D_{4d} (IF_8^-, TeF_8^{2-}).

The study of fluoro-anions having coordination numbers higher than six and, in particular, those involving free valence electron pairs, have recently received considerable attention.[1-6] To a large extent, these studies have been greatly facilitated by the development of a convenient preparative scale synthesis of anhydrous $N(Me)_4^+F^-$[7] and the realization that this salt is an excellent reagent for the preparation of novel, high-oxidation state complex fluoro- or oxofluoro-anions. Furthermore, the high solubilities of these $N(Me)_4^+$ salts in solvents such as MeCN or CHF_3 permit the gathering of valuable structure information through NMR and vibrational studies and the growth of single crystals suitable for X-ray structure determinations.

Our recent success with the preparation of the XeF_5^- anion,[4] the first known example of a pentagonal planar AX_5E_2 (where E stands for a free valence electron pair) species, prompted us to study some closely related iodine and tellurium compounds. In addition, there are relatively few examples of main-group species which allow the applicability of the valence shell electron pair repulsion (VSEPR) rules to coordination numbers exceeding six to be tested.[8] In this note, we report on the syntheses and structures of the novel IF_6O^- anion and on the $N(Me)_4^+$ salts of TeF_7^-, TeF_8^{2-} and IF_8^-.

The salt, $N(Me)_4^+IF_6O^-$, was prepared according to eqn. (1) by the reaction of anhydrous $N(Me)_4^+F^-$ with a threefold excess of IF_5O in dry MeCN at -31 °C for 30 min.

$$N(Me)_4^+F^- + IF_5O \xrightarrow[-31\,°C]{MeCN} N(Me)_4^+IF_6O^- \qquad (1)$$
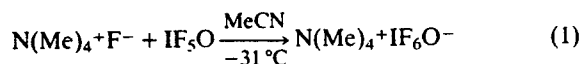
The solvent and unreacted IF_5O were pumped off at -31 °C leaving behind $N(Me)_4^+IF_6O^-$ as a colourless crystalline solid in quantitative yield. According to differential scanning calorimetry (DSC) and pyrolysis data, the compound starts to decompose at about 137 °C with formation of CF_4, COF_2 and IF_4O^- as the major products.

The ^{19}F NMR spectrum of $N(Me)_4^+IF_6O^-$ in MeCN solution recorded at -40 °C (Fig. 1) is consistent with the structure predicted by the VSEPR rules, consisting of a pentagonal bipyramidal structure of C_{5v} symmetry (structure 1) in which the oxygen atom occupies an axial position. The spectrum consists of a doublet at δ 166.0, assigned to the

equatorial fluorines, and a $1:5:10:10:5:1$ sextet at δ 111.1, assigned to the axial fluorine trans to oxygen. Both resonances are broadened by partially quadrupole-collapsed spin coupling to ^{127}I ($I = 5/2$). The fluorine–fluorine scalar coupling, $^2J(^{19}F_a\text{–}F_e)$ 205 Hz, is very similar in magnitude to those for IF_5O (271–280 Hz)[9] and cis-$IO_2F_4^-$ (204 Hz in MeCN).[10]

The vibrational spectra of IF_6O^- are also in excellent agreement with symmetry C_{5v}. The assignments were made by comparison with the related IF_7 molecule (see Table 1) and XeF_5^- anion.[4]

The reactions between TeF_6 and alkali metal fluorides have been reported previously, although definitive characterization of the products was never achieved.[11,12] The reactions of TeF_6 with CsF and RbF suspended in C_6F_6 resulted in products approaching the limiting compositions $CsF\cdot TeF_6$ and $2RbF\cdot TeF_6$, respectively.[12] Vibrational studies on these materials were tentatively interpreted as indicating D_{5h} and D_{4d} structures for TeF_7^- and TeF_8^{2-}, respectively. However, since both compounds decomposed in solution, a fuller characterization of their nature was precluded.

The preparation of $N(Me)_4^+TeF_7^-$ was similar to that for the IF_6O^- salt except that a 5% excess of TeF_6 was allowed to
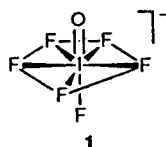
1
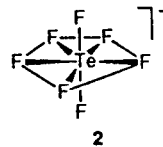
2
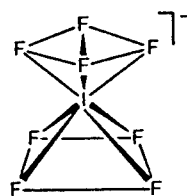
3
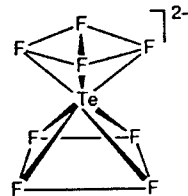
4

react with $N(Me)_4^+F^-$ according to equation (2). The solvent and an excess of TeF_6 were pumped off at room temperature leaving a white solid in quantitative yield.

$$N(Me)_4^+F^- + TeF_6 \xrightarrow[-40\,°C]{MeCN} N(Me)_4^+TeF_7^- \qquad (2)$$
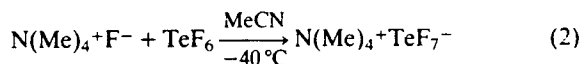
The room temperature ^{125}Te NMR spectrum of $N(Me)_4^+TeF_7^-$ in MeCN consists of a $1:7:21:35:35:21:7:1$ octet centred at δ 327.4 (Fig. 2). The octet fine structure arises from the one-bond spin–spin coupling between the central ^{125}Te and the ^{19}F ligands [$^1J(^{125}Te–^{19}F)$ 2876 Hz] and is in accord with a TeF_7^- anion structure in which all seven fluorines are rendered equivalent on the NMR time scale by a facile intramolecular exchange process. The ^{19}F NMR spectrum is also consistent with the TeF_7^- anion undergoing a fluxional process in solution, and consists of a single environment (δ 16.1) and natural abundance satellite spectra arising from $^1J(^{123}Te–^{19}F)$ 2385 and $^1J(^{125}Te–^{19}F)$ 2876 Hz. Under high resolution at an external field strength of 11.744 T, the central line displays the isotopic shift pattern arising from the natural abundance spinless tellurium isotopes corresponding to the fluorines of the ^{130}Te, ^{128}Te, ^{126}Te, ^{124}Te and ^{122}Te isotopomers, with each iso-topomer shifted successively to higher frequency of $^{130}TeF_7^-$, by 0.004 ppm. Earlier NMR studies have shown that the isoelectronic IF_7 molecule also undergoes rapid intramol-ecular exchange and gives rise to a single fluorine environ-ment in the room temperature ^{19}F NMR spectrum with partially quadrupole-collapsed fine structure arising from $^1J(^{127}I–^{19}F)$.[13]

The vibrational spectra of TeF_7^- have been assigned by analogy with those of the isoelectronic IF_7 molecule (Table 1) and are in agreement with a pentagonal bipyramidal structure of D_{5h} symmetry (structure 2). In general, the TeF_7^- frequencies are shifted to lower frequencies relative to those of IF_7, in accordance with the formal negative charge of TeF_7^-.

The syntheses of $Cs^+IF_8^-$,[14] $NO^+IF_8^-$[14.15] and $NO_2^+IF_8^-$[15] have previously been reported, and the ionic nature of these salts was established by the observation of the vibrational bands characteristic for NO^+ and NO_2^+.[14.15] Although partial Raman[14] and IR spectra[15] had been reported for IF_8^-, no conclusions could be drawn from these data about the exact structure of this interesting octacoordinated anion. To allow a
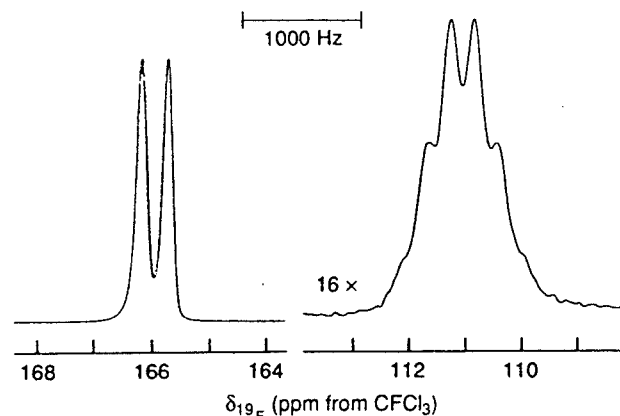
Fig. 1 The ^{19}F NMR spectrum of $N(Me)_4^+IF_6O^-$ recorded at 471.599 MHz in MeCN solvent at -40 °C
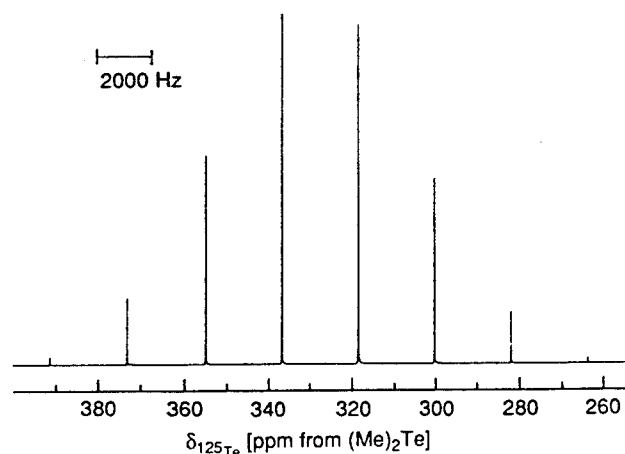
Fig. 2 The ^{125}Te NMR spectrum of $N(Me)_4^+TeF_7^-$ recorded at 157.792 MHz in MeCN solvent at 30 °C

Table 1 Vibrational frequencies (cm^{-1}) and tentative assignments for IF_6O^-, IF_7 and TeF_7^-

			$IF_6O^- (C_{5v})^a$				$IF_7 (D_{5h})^b$	$TeF_7^- (D_{5h})^a$
A_1	v_1	v I=O	873 [vs, IR: 5.3, R (p)]					
	v_2	v IF ax	649 [s, IR: 8.8 R (p)]	A_1'	v_1	v sym MF_2 ax	675 [2.0, R (p)]	597 (2.6, R)
	v_3	v sym IF_5	584 [10, R (p)]		v_2	v sym MF_5	629 [10, R (p)]	640 (10, R)
				A_2''	v_3	v asym MF_2 ax	746 (s, IR)	695 (vs, IR)
	v_4	δ umbrella IF_5	359 (s, IR)		v_4	δ umbrella MF_5	363 (s, IR)	332 (s, IR)
E_1	v_5	v asym IF_5	585 (vs, IR)	E_1'	v_5	v asym MF_5	672 (vs, IR)	625 (vs, IR)
	v_6	δ wag I=O	457 (4.9, R)		v_6	δ scissoring MF_2ax	425 (vs, IR)	384 (vs, IR)
	v_7	δ wag IF ax	405 (vs, IR)					
	v_8	δ asym IF_5 in plane	260 (s, IR; 0.2, R)		v_7	δ asym MF_5 in plane	257 (w, IR)	c
				E_1''	v_8	δ wag MF_2 ax	308 (0.6, R)	299 (0.6, R)
E_2	v_9	v asym IF_5	530 (0.4, R)	E_2'	v_9	v asym MF_5	509 (0.9, R)	458 (1.6, R)
	v_{10}	δ scissoring IF_5 in plane	341 (6.2, R)		v_{10}	δ scissoring MF_5 in plane	342 (0.6, R)	326 (0.7, R)
	v_{11}	δ pucker IF_5	d	E_2''	v_{11}	δ pucker MF_5	d	d

^{a} Spectra recorded for the $N(Me)_4^-$ salts at 25 °C. ^{b} Frequencies are taken from H. H. Eysel and K. Seppelt, *J. Chem. Phys.*, 1972, **56**, 5081. A number of modes have been reassigned so that they are consistent with the corresponding assignments for XeF_5^- (ref. 4), which have been confirmed by a force constant analysis and theoretical calculations. ^{c} Mode not observed. ^{d} Inactive in both the IR and Raman spectra.

Table 2 Vibrational frequencies (cm^{-1}) and assignments for IF_8^- in $N(Me)_4^+IF_8^-$ and TeF_8^{2-} in $[N(Me)_4^+]_2TeF_8^{2-}$ in point group D_{4d}

Raman				IR (solid 25 °C)		Assignment in D_{4d}
IF_8^-			TeF_8^{2-}	IF_8^-	TeF_8^-	
Solid		MeCN sol'n				
25 °C	−142 °C					
660 (0+)	660 (0+)			590 vs, br	558 vs	v_{12} (E$_3$) v_4 (B$_2$) v_6 (E$_1$)
587 (10)	595 (10) 588 (6.5)	590 (10) p	582 (10)			v_1 (A$_1$)
550 (0.3) 463 (1.8)	550 (0.5) 463 (1.9)	550 (0+) dp 462 (0.5) p	490 (0.2), br 408 (1.0)	410 s	375 vs	v_9 (E$_2$) v_2 (A$_1$) v_5 (B$_2$) v_8 (E$_1$)
411 (0.7)	419 (0.9) 410 (1.4)	410 sh^a	388 (1.8)			v_{10} (E$_2$)
	380 (0+)^b		325 (0.3)	314 m	265 w	v_{13} (E$_3$) v_7 (E$_1$)

^{a} Shoulder on strong MeCN solvent band. ^{b} This band could possibly be due to the $N(Me)_4^+$ cation.

better characterization of the IF_8^- anion, we have prepared the new $N(Me)_4^+IF_8^-$ salt and its isoelectronic tellurium analogue, TeF_8^{2-}, by the reaction of $N(Me)_4^+F^-$ with excess IF_7 and a stoichiometric amount of $N(Me)_4^+TeF_7^-$, respectively. For reaction (3) the solvent and unreacted IF_7 were pumped off at −22 and 0 °C, respectively, leaving behind colourless $N(Me)_4^+IF_8^-$ in quantitative yield. In the case of reaction (4), $[N(Me)_4^+]_2TeF_8^{2-}$ was isolated in admixture with ca. 20–30% $N(Me)_4^+TeF_7^-$. The $[N(Me)_4^+]_2TeF_8^-$ salt

$$N(Me)_4^+F^- + IF_7 \xrightarrow[\,-31\,°C\,]{MeCN} N(Me)_4^+IF_8^- \qquad (3)$$

$$N(Me)_4^+F^- + N(Me)_4^+TeF_7^- \xrightarrow[\,0\,°C\,]{MeCN} [N(Me)_4^+]_2TeF_8^{2-} \qquad (4)$$
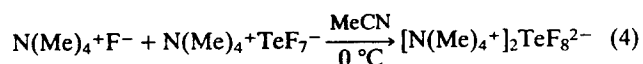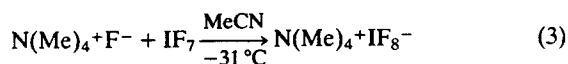
has a strong tendency to dissociate in MeCN, thus far preventing the preparation of a sample containing only the TeF_8^{2-} anion. At room temperature, dissociation of the insoluble TeF_8^{2-} anion into TeF_7^- and F^- results in rapid solvent attack by F^{-16} and formation of HF_2^- anion. Even in the presence of a fivefold excess of $N(Me)_4^+F^-$ at −5 °C, significant amounts of TeF_7^- and F^- were observed in the ^{19}F NMR spectrum, but no resonance attributable to TeF_8^{2-} could be observed. The $N(Me)_4^+IF_8^-$ salt is a crystalline solid which, according to DSC data, is stable up to ca. 110 °C where it undergoes exothermic decomposition.

The IF_8^- and TeF_8^{2-} anions possess eight fluorine ligands and no free central atom valence electron pair. Their structures could, therefore, be either a cube of symmetry O_h, which is unlikely owing to steric interactions,[8] a dodecahedron of symmetry D_{2d} or a square antiprism of symmetry D_{4d} (structures **3** and **4**).[17–20] Distinction among these three possibilities was made by vibrational spectroscopy. The dodecahedral structure is expected to give rise to two polarized stretching modes and four deformation modes (two polarized; two depolarized) exclusively in the Raman. The IR bands are mutually non-exclusive and comprise four stretching modes and five deformation modes which are all depolarized in the Raman. All Raman and IR bands observed for IF_8^- and TeF_8^{2-} are mutually exclusive, thereby eliminating D_{2d}

symmetry. For the cubic O_h structure, two stretching modes are expected (one polarized; the other depolarized) and two depolarized deformation modes in the Raman, as well as one stretching and one deformation mode in the infrared. All these modes should be mutually exclusive.[18] For the square antiprismatic D_{4d} structure, one polarized and two depolarized stretching modes are expected as well as one polarized and three depolarized deformation modes in the Raman. In the IR spectrum, two stretching and three deformation modes are expected, which again should be mutually exclusive.[17,19,20] Although the full number of fundamentals for D_{4d} was not observed (see Table 2), probably because of either low relative intensities or coincidences, the observation of a polarized Raman deformation band at 462 cm^{-1} and of at least two IR active deformation modes at 410 and 314 cm^{-1}, respectively, establish the square antiprismatic D_{4d} structure for IF_8^-. It was not possible to obtain polarization data on TeF_8^{2-} owing to the insolubility of the salt and its tendency to dissociate in MeCN. However, the vibrational spectra of TeF_8^{2-} can be assigned by their close analogy to those of IF_8^- (Table 2) and it may be concluded that TeF_8^{2-} also possesses a square antiprismatic structure.

X-Ray crystal structure determinations on these and other closely related anions are underway both in our laboratories and in an independent effort by Dr K. Seppelt and coworkers at the Freie Universität, Berlin.

Note added in proof: The TeF_6O^{2-} anion has also been synthesized by the reaction of equimolar amounts of $N(Me)_4^+F^-$ and $N(Me)_4^+TeF_5O^-$ at −9 °C in MeCN. The vibrational assignments (v/cm^{-1}) under C_{5v} establish that TeF_6O^{2-} is isostructural with IF_6O^-: v_1 829 (s, IR; s, R); v_2 613 (m, IR; vs, R); v_3 528 (m, R), v_4 330 (s, IR); v_5 525 (vs, IR); v_6 388 (m, R); v_7 365 (vs, IR); v_8 245 (not observed, beyond spectrometer limit; w, R); v_9 not observed; v_{10} 322 (s, R); v_{11} (not observed). The ^{19}F NMR spectrum of $N(Me)_4^+IF_8^-$ has been obtained at 30 °C (δ 248.6) and is a partially quadrupole collapsed multiplet (saddle-shaped with a 'doublet' separation of 3807 Hz) arising from the $^{127}I–^{19}F$ scalar coupling and is consistent with the small electric field gradient at the ^{127}I nucleus that is anticipated for a square antiprismatic AX_8 geometry.

References

1 W. W. Wilson and K. O. Christe, *Inorg. Chem.*, 1989, **28**, 4172.
2 K. O. Christe and W. W. Wilson, *Inorg. Chem.*, 1989, **28**, 3275.
3 K. O. Christe, W. W. Wilson, R. V. Chirakal, J. C. P. Sanders and G. J. Schrobilgen, *Inorg. Chem.*, 1990, **29**, 3506.
4 K. O. Christe, E. C. Curtis, D. A. Dixon, H. P. Mercier, J. C. P. Sanders and G. J. Schrobilgen, *J. Am. Chem. Soc.*, 1991, **113**, 3351.
5 A. R. Mahjoub, A. Hoser, J. Fuchs and K. Seppelt, *Angew. Chem., Int. Ed. Engl.*, 1989, **28**, 1526.
6 A. R. Mahjoub, B. Nuber and K. Seppelt, personal communication.
7 K. O. Christe, W. W. Wilson, R. D. Wilson, R. Bau and J. Feng, *J. Am. Chem. Soc.*, 1990, **112**, 7619.
8 R. J. Gillespie and I. Hargittai, *The VSEPR Model of Molecular Geometry*, Allyn and Bacon, Boston, 1991.
9 R. J. Gillespie and J. W. Quail, *Proc. Chem. Soc.*, 1963, 278; M. Brownstein, R. J. Gillespie and J. P. Krasznai, *Can. J. Chem.*, 1978, **56**, 2253.
10 K. O. Christe, R. D. Wilson and C. J. Schack, *Inorg. Chem.*, 1981, **20**, 2104.
11 E. L. Muetterties, *J. Am. Chem. Soc.*, 1957, **79**, 1004.
12 H. Selig, S. Sarig and S. Abramowitz, *Inorg. Chem.*, 1974, **13**, 1508.
13 R. J. Gillespie and J. W. Quail, *Can. J. Chem.*, 1964, **42**, 2671; E. L. Muetterties and K. J. Packer, *J. Am. Chem. Soc.*, 1964, **86**, 293.
14 C. J. Adams, *Inorg. Nucl. Chem. Lett.*, 1974, **10**, 831.
15 F. Seel and M. J. Pimpl, *J. Fluorine Chem.*, 1977, **10**, 413.
16 K. O. Christe and William W. Wilson, *J. Fluorine Chem.*, 1990, **47**, 117.
17 A. Beuter, W. Kuhlmann and A. Sawodny, *J. Fluorine Chem.*, 1975, **6**, 367.
18 C. W. F. T. Pistorius, *Bull. Soc. Chim. Belg.*, 1959, **68**, 630.
19 H. L. Schläfer and H. F. Wasgestian, *Theoret. Chim. Acta*, 1963, **1**, 369.
20 K. O. Hartman and F. A. Miller, *Spectrochim. Acta, Part A*, 1968, **24**, 669.

The N_2F^+ Cation. An Unusual Ion Containing the Shortest Presently Known Nitrogen–Fluorine Bond

Karl O. Christe,*,† Richard D. Wilson,† William W. Wilson,† Robert Bau,‡ Sunanda Sukumar,‡ and David A. Dixon§

Contribution from Rocketdyne, A Division of Rockwell International Corporation, Canoga Park, California 91303, the Department of Chemistry, University of Southern California, Los Angeles, California 90007, and the Central Research and Development Department, E.I. du Pont de Nemours and Company, Inc., Experimental Station, Wilmington, Delaware 19880. Received May 3, 1990

Abstract: The $N_2F^+AsF_6^-$ salt was prepared in high yield from *trans*-N_2F_2 by thermal trans–cis isomerization in the presence of AsF_5 at 70 °C. A displacement reaction between $N_2F^+AsF_6^-$ and FNO yields exclusively *cis*-N_2F_2. The Lewis acids BF_3 and PF_5 do not form a stable adduct with *cis*-N_2F_2 at temperatures as low as −78 °C and do not catalyze the N_2F_2 trans–cis isomerization. A semiempirical molecular orbital model is used to explain the puzzling differences in the reaction chemistry of *cis*- and *trans*-N_2F_2. The crystal structure of $N_2F^+AsF_6^-$ (monoclinic, $C2/m$, $a = 9.184$ (5) Å, $b = 5.882$ (2) Å, $c = 5.160$ (2) Å, $\beta = 90.47$ (4)°, $Z = 2$) was determined. Alternate space groups (Cm and $C2$) can be rejected on the basis of the observed vibrational spectra. Since in $C2/m$ the N_2F^+ cations are disordered, only the sum of the N–F and N–N bond distances could be determined from the X-ray data. Local density functional calculations were carried out for N_2F^+ and the well-known isoelectronic FCN molecule. The results from these calculations allowed the sum of the N_2F^+ bond lengths to be partitioned into the individual bond distances. The resulting N–F bond length of 1.217 Å is by far the shortest presently known N–F bond, while the N–N bond length of 1.099 Å is comparable to the shortest presently known N–N bond length of 1.0976 (2) Å in N_2. The surprising shortness of both bonds is attributed to the high s-character (sp hybrid) of the σ-bond orbitals on nitrogen and the formal positive charge on the cation. Thus, the shortening of the N–F bond on going from sp^3-hybridized NF_4^+ (1.30 Å) to sp-hybridized N_2F^+ (1.22 Å) parallels those found for the C–H and C–F bonds in the CH_4, $CH_2=CH_2$, $CH\equiv CH$ and CF_4, $CF_2=CF_2$, $FC\equiv N$ series, respectively. The oxidative power of N_2F^+ has also been studied. The N_2F^+ cation oxidized Xe and ClF to XeF^+ and ClF_2^+, respectively, but did not oxidize ClF_5, BrF_5, IF_5, XeF_4, NF_3, or O_2.

Introduction

The chemistry of N_2F_2 and its derivatives is fascinating and presents many mysteries.[1] Thus, N_2F_2 exists as two planar FN=NF isomers, a cis and a trans form. In spite of only a small enthalpy difference of 3.04 kcal/mol between the two isomers,[2] their properties and reaction chemistry are very different. For example, only the cis isomer reacts with strong Lewis acids to form N_2F^+ salts. Furthermore, some of the synthetic methods for N_2F_2 produce exclusively the trans isomer, and its slow and erratic isomerization to the more stable cis isomer is poorly understood, as shown by recent ab initio calculations.[3]

The N_2F^+ cation[4–9] is also of great interest. Force field[9] and ab initio calculations[10–12] suggested that this cation should possess an unusually short N–F bond. On the basis of the previously published[9] NF stretching force constant value of 8.16 mdyn/Å and N–F bond length–force constant plots,[10,13] a value of about 1.23 Å can be extrapolated for the N–F bond in N_2F^+. This surprisingly short N–F bond length value for N_2F^+ was also supported by ab initio calculations[10–12] which resulted in values of 1.28, 1.24, and 1.23 Å, respectively. Considering that in covalent main group element fluorides the bond length generally decreases with an increase in the formal oxidation state of the central atom and that the shortest previously known N–F bond was 1.30 Å in NF_4^+ (+V),[14] a value of about 1.23 Å for N_2F^+ (+I) would be unique indeed.

On the other hand, if the N–F bond length in N_2F^+ were considerably longer than the value predicted from the force field computations, the N_2F^+ cation would be an ideal test case for "Gordy's rule".[15] According to this rule, the bond stretching force constant k is related to the bond distance d by the equation

$$k_{AB} = aN(X_A X_B / d_{AB}^2)^{3/4} + b$$

where X are the Pauling electronegativities, N the bond order, and a and b empirically determined constants. Although no a priori reason dictates such a relationship since bond lengths

measure the position of the potential energy minimum whereas force constants indicate its curvature, only one exception to Gordy's rule has previously been reported.[16] Thus, a knowledge of the N–F bond distance in N_2F^+ was of significant interest since it would either confirm the existence of an unusually short N–F bond or provide a rare example of a species not obeying Gordy's rule.

Experimental Section

Materials. The following commercial materials were used without further purification: N_2F_4 (Air Products); Xe, O_2, IF_5, PF_5, and BF_3 (Matheson); ClF_5 and NF_3 (Rocketdyne); and ClF (Ozark Mahoning). Literature methods were used for the syntheses of *trans*-N_2F_2,[17] N_2F^+-AsF_6^-,[4] FNO,[18] and XeF_4,[19] the purification of BrF_5,[20] and the drying of HF.[21]

---

(1) For an exhaustive review of the properties and chemistry of N_2F_2 see: *Gmelin Handbook of Inorganic Chemistry, Fluorine*, Springer Verlag; Berlin, 1986; Suppl. Vol. 4, pp 385–403.
(2) Craig, N. C.; Piper, L. G.; Wheller, V. L. *J. Phys. Chem.* **1971**, *75*, 1453.
(3) Lee, T. J.; Rice, J. E.; Scuseria, G. E.; Schaefer, H. F., III *Theor. Chim. Acta* **1989**, *75*, 81.
(4) Moy, D.; Young, A. R. *J. Am. Chem. Soc.* **1965**, *87*, 1889.
(5) Ruff, J. K. *Inorg. Chem.* **1966**, *5*, 1791.
(6) Roesky, H. W.; Glemser, O.; Bormann, D. *Chem. Ber.* **1966**, *99*, 1589.
(7) Pankratov, A. V.; Savenkova, N. I. *Russ. J. Inorg. Chem.* **1968**, *13*, 1345.
(8) Shamir, J.; Binenboym, J. *J. Mol. Struct.* **1969**, *4*, 100.
(9) Christe, K. O.; Wilson, R. D.; Sawodny, W. *J. Mol. Struct.* **1971**, *8*, 245.
(10) Pulay, P.; Ruoff, A.; Sawodny, W. *Mol. Phys.* **1975**, *30*, 1123.
(11) Peters, N. J. S. *Chem. Phys. Lett.* **1987**, *142*, 76.
(12) Yakobson, V. V.; Zyubina, T. S.; Charkin, O. P. *Russ. J. Inorg. Chem., Engl.* **1988**, *33*, 1727.
(13) Christe, K. O. *Spectrochim. Acta, Part A* **1986**, *42A*, 939.
(14) Christe, K. O.; Lind, M. D.; Thorup, N.; Russell, D. R.; Fawcett, J.; Bau, R. *Inorg. Chem.* **1988**, *27*, 2450.
(15) Gordy, W. *J. Chem. Phys.* **1946**, *14*, 305.
(16) Mack, H. G.; Christen, D.; Oberhammer, H. *J. Mol. Struct.* **1988**, *190*, 215.
(17) Münch, V.; Selig, H. *J. Fluorine Chem.* **1980**, *15*, 235.
(18) Christe, K. O. *Inorg. Chem.* **1973**, *12*, 1580.
(19) Bartlett, N.; Sladky, F. O. *J. Am. Chem. Soc.* **1968**, *90*, 5316.
(20) Wilson, W. W.; Christe, K. O. *Inorg. Chem.* **1987**, *26*, 1573.

---

†Rocketdyne Division, Rockwell International Corp.
‡University of Southern California, Los Angeles.
§E.I. du Pont de Nemours and Company, Inc.

Table I. Summary of Crystal Data and Refinement Results for $N_2F^+AsF_6^-$

space group	$C2/m$ (No. 12)
a, Å	9.184 (5)
b, Å	5.882 (2)
c, Å	5.160 (2)
β, deg	90.47 (4)
V, Å^3	278.7 (2)
molecules per unit cell	2
formula weight, g	235.9
cryst dimens, mm	$0.32 \times 0.38 \times 1.08$
calcd density, g cm^{-3}	2.82
abs coeff, mm^{-1}	59.8
range in transmission factor (normalized to unity)	0.61–1.00
wavelength used for data collection, Å	0.71069
sin θ/λ limit, Å^{-1}	0.6497
tot no. of reflcns measd	1272
no. of independent reflcns	364
no. of reflcns used in structural analysis $I > 3\sigma(I)$	362
no. of variable params	30
final agreement factor	0.0404

Table II. Final Atomic Coordinates for $N_2F^+AsF_6^-$

atom	x	y	z	no.[a]
As1	0	0	0.5	2
F2	0.1235 (6)	0	0.2574 (9)	4
F3	−0.0948 (5)	0.2027 (9)	0.3406 (9)	8
N4	0	0.5	1	2
X5[b]	−0.1203 (7)	0.5	0.9313 (11)	4

[a] Number of times this atom appears in the unit cell. [b] X is the disordered terminal atom (50% N/50% F) of the $[N_2F]^+$ cation in space group $C2/m$.

Apparatus. Volatile materials were handled in a well-passivated (with ClF_3) stainless steel Teflon-FEP vacuum line.[22] Nonvolatile materials were manipulated under the dry nitrogen atmosphere of a glovebox. Vibrational spectra were recorded as previously described.[20]

Reaction of $N_2F^+AsF_6^-$ with FNO. A sample of $N_2F^+AsF_6^-$ (1.84 mmol) was placed inside the drybox into a prepassivated $^3/_4$ in. Teflon-FEP ampule that was closed by a stainless steel valve. On the vacuum line, FNO (4.14 mmol) was added at −196 °C, and the resulting mixture was allowed to slowly warm from −196 to −78 °C by the use of a liquid N_2–dry ice slush bath. The mixture was then allowed to slowly warm from −78 °C to room temperature over a 12-h period. The ampule was cooled to −196 °C, and the volatile material was separated during warm-up of the ampule to 25 °C by fractional condensation through traps kept at −126 and −210 °C. The −126 °C trap contained unreacted FNO (2.29 mmol) and the −210 °C trap contained cis-N_2F_2 (1.8 mmol). The white solid residue (401 mg, weight calcd for 1.84 mmol of NO$^+$-AsF$_6^-$ = 403 mg) was identified by vibrational spectroscopy as NO$^+$-AsF$_6^-$.[23]

Oxidation Reactions of $N_2F^+AsF_6^-$. All oxidation reactions of N_2F^+-AsF$_6^-$ were carried out in the same manner. About 2 mmol of N_2F^+-AsF$_6^-$ was placed in the drybox into a prepassivated 0.5 in. o.d. Teflon-FEP ampule that was closed by a stainless steel valve. On the vacuum line, about 2 mL of liquid anhydrous HF and about 5 mmol of the compound to be oxidized were added, and the resulting mixture was kept at room temperature for 24 h. The ampule was cooled to −196 °C and the amount of evolved nitrogen was measured by expansion into the vacuum line. The material volatile at room temperature was separated by fractional condensation through a series of cold traps kept at appropriate temperatures. The contents of these traps were measured by PVT and identified by infrared spectroscopy. The solid residues in the ampule were weighted and identified by infrared and Raman spectroscopy.

Crystal Structure Determination of $N_2F^+AsF_6^-$. Single crystals of $N_2F^+AsF_6^-$ were obtained by slowly cooling a saturated HF solution from 25 to 0 °C and separating the resulting crystals from the cold solution by decantation. A suitable crystal was selected under a microscope inside the glovebox and sealed in a quartz capillary.

Diffraction data were collected at room temperature using a Siemens/Nicolet/Syntex P2$_1$ diffractometer with Mo Kα radiation up to a 2θ limit of 45°. A total of 1272 intensity values for an entire reflection sphere was collected and the four equivalent quadrants merged to give 364 unique reflections. An empirical ψ-scan absorption correction was applied, based on the variation in intensity of an axial reflection.[24]

The pattern of systematic absences was consistent with any one of the following centered monoclinic space groups: $C2$ (No. 5), Cm (No. 8), or $C2/m$ (No. 12). The structure was solved for all three space groups. The positions of the atoms were obtained by direct methods with use of

the computing package SHELX-86.[25] The structures were then refined with use of 362 reflections with $I > 3\sigma(I)$. Details of the data collection parameters and other crystallographic information are given in Table I. The final atomic coordinates, thermal parameters, interatomic distances, and bond angles for the preferred (see Discussion section) $C2/m$ model are given in Tables II–IV, respectively.

Computational Methods. The geometry and vibrational frequencies of N_2F^+ and FCN were calculated in the local density functional approximation[26] by using the program system DMol.[27] The atomic basis functions are given numerically on an atom-centered, spherical-polar mesh. The radial portion of the grid is obtained from the solution of the atomic LDF equations by numerical methods. The radial functions are stored as sets of cubic spline coefficients so that the radial functions are piece-wise analytic, a necessity for the evaluation of gradients. The use of exact spherical atom results offers some advantages. The molecule will dissociate exactly to its atoms within the LDF framework, although this does not guarantee correct dissociation energies. Furthermore, because of the quality of the atomic basis sets, basis set superposition effects should be minimized and correct behavior at the nucleus is obtained.

Since the basis sets are numerical, the various integrals arising from the expression for the energy need to be evaluated over a grid. The integration points are generated in terms of angular functions and spherical harmonics. The number of radial points N_R is given as

$$N_R = 1.2 \times 14(Z - 2)^{1/3}$$

where Z is the atomic number. The maximum distance for any function is 12 au. The angular integration points N_0 are generated at the N_R radial points to form shells around each nucleus. The value of N_0 ranges from 14 to 302 depending on the behavior of the density.[28] The Coulomb potential corresponding to the electron repulsion term is determined directly from the electron density by solving Poisson's equation. In DMol, the form for the exchange-correlation energy of the uniform electron gas is that derived by von Barth and Hedin.[29]

All of the DMol calculations were done with a double numerical basis set augmented by polarization functions. This can be thought of in terms of size as a polarized double-ζ basis set. However, because of the use of exact numerical solutions for the atom, this basis set is of significantly higher quality than a normal molecular orbital double-ζ basis set. The fitting functions have angular momentum numbers one greater than that of the polarization function. Since all of the atoms have d polarization functions, the value of 1 for the fitting function is 3.

Geometries were optimized by using analytic gradient methods. There are two problems with evaluating gradients in the LDF framework which are due to the numerical methods that are used. The first is that the energy minimum does not necessarily correspond exactly to the point with a zero derivative. The second is that the sum of the gradients may not always be zero as required for translational invariance. These tend to introduce errors on the order of 0.001 Å in the calculation of the coordinates if both a reasonable grid and basis set are used. This gives bond lengths and angles with reasonable error limits. The difference of 0.001 Å is about an order of magnitude smaller than the accuracy of the LDF geometries when compared to the experimental ones. The frequencies

(21) Christe, K. O.; Wilson, W. W.; Schack, C. J. *J. Fluorine Chem.* **1978**, *11*, 71.

(22) Christe, K. O.; Wilson, R. D.; Schack, C. J. *Inorg. Synth.* **1986**, *24*, 3.

(23) Griffiths, J. E.; Sunder, W. A.; Falconer, W. E. *Spectrochim. Acta, Part A* **1975**, *31A*, 1207.

(24) For details on the ψ-scan empirical correction, see: Churchill, M. R.; Hollander, F. J. *Inorg. Chem.* **1978**, *17*, 3548.

(25) Sheldrix, G. M. SHELX System of Crystallographic Programs, University of Goettingen, West Germany, 1986.

(26) (a) Parr, R. G.; Yang, W. *Density Functional Theory of Atoms and Molecules*; Oxford University Press: New York, 1989. (b) Salahub, D. R. In *Ab Initio Methods in Quantum Methods in Quantum Chemistry-II*; Lawlwy, K. P., Ed.; J. Wiley & Sons: New York, 1987; p 447. (c) Wimmer, E.; Freeman, A. J.; Fu, C.-L.; Cao, P.-L.; Chou S.-H.; Delley, B. In *Supercomputer Research in Chemistry and Chemical Engineering*; Jensen, K. F., Truhlar, D. G., Eds.; ACS Symp. Ser.; American Chemical Society: Washington, DC, 1987; p 49. (d) Jones, R. O.; Gunnarsson, O. *Rev. Mod. Phys.* **1989**, *61*, 689.

(27) Delley, B. J. *Chem. Phys.* **1990**, *92*, 508. DMol is available commercially from BIOSYM Technologies, San Diego, CA.

(28) This grid can be obtained by using the FINE parameter in DMol.

(29) von Barth, U.; Hedin, L. *J. Phys. Chem.* **1972**, *5*, 1629.

Table III. Final Temperature Factors for $N_2F^+AsF_6^-$

atom	$10^4 U_{11}$	$10^4 U_{22}$	$10^4 U_{33}$	$10^4 U_{12}$	$10^4 U_{13}$	$10^4 U_{23}$
As1	416 (5)	331 (5)	333 (4)	0 (0)	9 (4)	0 (0)
F2	745 (16)	935 (17)	659 (16)	0 (0)	312 (15)	0 (0)
F3	1220 (16)	1407 (17)	1240 (16)	715 (16)	301 (15)	716 (16)
N4	723 (18)	440 (17)	532 (17)	0 (0)	146 (17)	0 (0)
X5[a]	655 (17)	750 (17)	809 (17)	0 (0)	7 (16)	0 (0)

[a] X is the disordered terminal atom (50% N/50% F) of the $[N_2F]^+$ cation in space group $C2/m$.

Table IV. Bond Distances (Å) and Bond Angles (deg) in $[N_2F]^+[AsF_6]^-$

As1–F2	1.696 (4)	F2′–As1–F3	90.8 (2)
As1–F3	1.686 (4)	F3–As1–F3′	180.0 (0)
N4–X5	1.158 (6)	F3–As1–F3″	90.0 (2)
		F3′–As1–F3″	90.0 (2)
F2–As1–F3	89.2 (2)	F3″–As1–F3‴	180.0 (0)
F2–As1–F2′	180.0 (0)	X5–N4–X5′	180.0 (0)

were determined by numerical differentiation of the gradient. A two-point difference formula was used and a displacement of 0.01 au.

Results and Discussion

Trans–Cis Isomerization of N₂F₂ and the Synthesis of N₂F⁺ Salts. Most of the known N_2F_2 syntheses produce exclusively the trans isomer.[1] Since the trans isomer is much less reactive than the cis isomer and, for example, does not form N_2F^+ salts, conversion of the trans to the cis isomer is often required. This trans–cis isomerization is usually quite erratic. Although it proceeds at room temperature in stainless steel, it often exhibits long and irreproducible induction periods and requires numerous months to go to completion. This isomerization can be accelerated by increasing the temperature; however, the yields of cis-N_2F_2 sharply decrease at elevated temperature due to decomposition of N_2F_2 to $N_2 + F_2$.[30] In our study, aimed at the isomerization of N_2F_2 and its subsequent conversion to $N_2F^+AsF_6^-$, it was found advantageous to combine the $trans$-N_2F_2 with an excess of AsF_5 in a prepassivated, small volume stainless steel cylinder and to carry out the isomerization at about 70 °C. In this manner, any cis-N_2F_2 formed is immediately removed from the cis–trans equilibrium by complexation and thereby protected against decomposition to N_2 and F_2. In this manner, yields of $N_2F^+AsF_6^-$ as high as 80% have been obtained from $trans$-N_2F_2 in 3 days at 70 °C.

It was also of interest to study which N_2F_2 isomer is formed in the displacement reactions of $N_2F^+AsF_6^-$ with a strong Lewis base, such as FNO. It was found that exclusively cis-N_2F_2 is formed in quantitative yield according to

$$N_2F^+AsF_6^- + FNO \rightarrow NO^+AsF_6^- + cis\text{-}N_2F_2$$
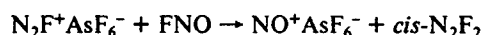
Recent ab initio calculations[3] on the transition-state structure for the N_2F_2 trans–cis isomerization resulted in the proposition of structure I. A similar transition state might be expected for a fluoride abstraction from cis-N_2F_2 (III) by a strong Lewis acid leading to the N_2F^+ cation (II).

<p style="text-align:center;">**I   II   III   IV**</p>
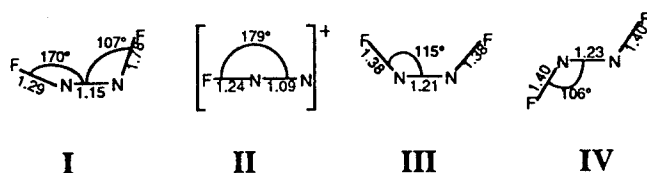
These results suggested that Lewis acids which are capable of forming N_2F^+ salts might also promote the formation of the isomerization transition state and thereby catalyze the N_2F_2 trans–cis isomerization. In order to be an effective isomerization catalyst, the strength of the Lewis acid should be such that it interacts with N_2F_2 but does not form a stable complex at the desired isomerization temperature. To test the validity of this

(30) Pankratov, A. V.; Sokolov, O. M. *Russ. J. Inorg. Chem.* **1966**, *11*, 943.

approach, we have studied the interaction of cis-N_2F_2 with BF_3 and PF_5. It was found that the resulting N_2F_2 adducts are indeed labile enough and exhibit some dissociation pressure at temperatures as low as −78 °C. However, both PF_5 and BF_3 did not catalyze the isomerization of $trans$-N_2F_2 to cis-N_2F_2 in the temperature range of −78 to 25 °C.

Thus, the chemistry of N_2F_2 raises numerous puzzling questions for which, to our best knowledge, no satisfactory answers have previously been given.[1] Among these questions are the following: (i) why does only cis-N_2F_2, but not $trans$-N_2F_2 form N_2F^+ salts, (ii) why do Lewis acids not catalyze the N_2F_2 trans–cis isomerization, and (iii) why is the cis-N_2F_2 isomer exclusively formed in the displacement reaction between N_2F^+ salts and FNO?

The great difference in reactivity between cis- and $trans$-N_2F_2 cannot be due to differences in thermodynamic properties or bond strengths because these values are very similar for both molecules.[1] Therefore, the difference in reactivity should be connected with the different spatial arrangement of the fluorine ligands and the free valence electron pairs on nitrogen. With use of a semiempirical molecular orbital model, the bonding in N_2F_2 can be described by two sp²-hybridized nitrogen atoms resulting in one N–N and two N–F σ-bonds and two sterically active, free valence electron pairs on the two nitrogens. In addition, the remaining p orbitals on the nitrogen atoms form a [p–p] π-bond perpendicular to the plane of the sp² hybrids. In linear N_2F^+, the two nitrogens form a [sp–sp] σ-bond and two perpendicular [p–p] π-bonds.

<p style="text-align:center;">**trans-N₂F₂**   **cis-N₂F₂**</p>
<p style="text-align:center;">**N₂F⁺**</p>
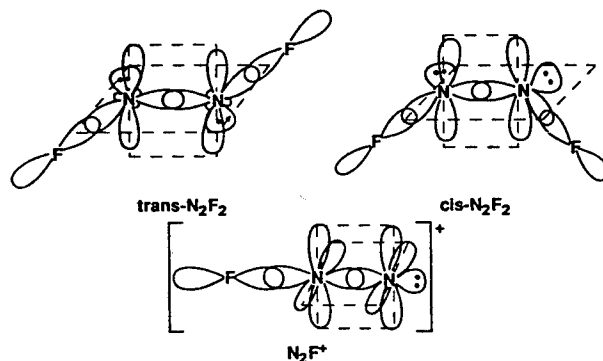
When a Lewis acid, such as AsF_5, approaches a cis-N_2F_2 molecule, one of the fluorine ligands and hereby some electron density is pulled away from the remainder of the molecule. This results in an intermediate similar to the transition state (I) of the N_2F_2 trans–cis isomerization. This removal of electron density from one of the nitrogen atoms should result in the lowering of the electron density in the antibonding orbitals of the two free valence electron pairs on the two nitrogens. This enables them to form a partial triple bond, as demonstrated by the shortening of the N–N bond from 1.21 Å in cis-N_2F_2 (III) to 1.15 Å in the postulated trans–cis isomerization transition state (I). Therefore, the energy required for the elongation of one of the N–F bonds in I can be compensated for by the simultaneous formation of a partial N≡N triple bond thereby resulting in a very low energy barrier toward N_2F^+ formation. However, the formation of such a partial N≡N triple bond should be possible only for cis-N_2F_2, i.e. when the two free valence electron pairs on the nitrogens are on the same side of the molecule and can overlap. In $trans$-N_2F_2, migration of a nitrogen free valence electron pair from one side of the molecule to the other is blocked in the N_2F_2 plane by the fluorine ligands and in the perpendicular plane by the [p–p] π-bond. Furthermore, the N≡N double bond in N_2F_2 does not

permit free rotation around the N–N axis. Therefore, N_2F^+ formation from *trans*-N_2F_2 should be a high activation energy process requiring almost complete removal of one fluoride ion from N_2F_2, before the FNN angle in the remaining FN_2 fragment becomes large enough for the nitrogen free electron pair to tunnel through to the other side and form the second π-bond.

This rationale explains not only why *trans*-N_2F_2 does not form N_2F^+ salts but also why Lewis acids do not catalyze the N_2F_2 trans–cis isomerization. As already pointed out above, the structure of the isomerization transition state closely resembles that of an expected intermediate in the N_2F^+ formation. If Lewis acids cannot abstract an F^- anion from *trans*-N_2F_2, it is then not surprising at all that they also do not promote the formation of the isomerization transition state.

The third question remaining to be answered was why in the FNO displacement reaction of $N_2F^+AsF_6^-$ exclusively the *cis*-N_2F_2 isomer is formed. In N_2F^+, the most important resonance structure is $[F—N^+\equiv N|]$ and, therefore, the formal positive charge resides mainly on the α-nitrogen atom. Furthermore, the free valence electron pair on the β-nitrogen atom is more diffuse than the N–F bond pair orbitals. Consequently, the attack of F^- on N_2F^+ should occur at the α-nitrogen atom resulting in the formation of an intermediate $F_2N=N$ molecule. The latter could easily undergo an α-fluorine migration to give FNNF.
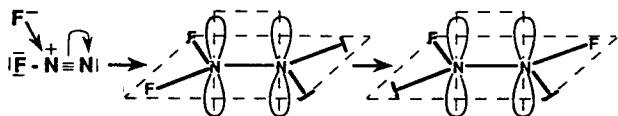
Since in all these steps a [p–p] π-bond between the two nitrogens is always retained, free rotation around the N–N axis is precluded and the rearrangement of the fluorine atoms and the nitrogen free valence electron pairs must take place in the plane perpendicular to the N–N π-bond. Therefore, the sequence of the fluorine ligands and the nitrogen free electron pairs in $F_2N=N$ (F,F,P,P) must also be retained in FNNF, resulting exclusively in the *cis*-FNNF isomer. The general ease of this type of α-migration could explain the failure to isolate the intermediate $F_2N=N$ isomer.

Structure of the N_2F^+ Cation. The crystal structure of $N_2F^+AsF_6^-$ can be solved either in the non-centrosymmetric space groups *Cm* or *C2* with ordered or disordered N_2F^+ cations, respectively, or the centrosymmetric space group *C2/m* with disordered N_2F^+ cations. All three models resulted in acceptable agreement factors (*Cm*, R = 2.96%; *C2*, R = 2.68%; *C2/m*, R = 4.04%) which to some extent are influenced by the number of variable parameters (*Cm*, 53; *C2*, 46; *C2/m*, 30). The *Cm* model resulted in an ordered almost linear N_2F^+ cation (r_{NF} = 1.221 (13) Å, r_{NN} = 1.099 (13) Å, $\angle NNF$ = 177.2 (8)°) and a strongly distorted AsF_6^- anion with angles deviating by as much as 11.5° from those of an ideal octahedron. The *C2* model resulted in a disordered bent N_2F^+ cation ($\sum r_{NF} + r_{NN}$ = 2.342 (22) Å, $\angle NNF$ = 163.6 (12)°) and again a strongly distorted AsF_6^- anion with angles deviating by as much as 13.8° from O_h symmetry. The *C2/m* model resulted in a disordered linear N_2F^+ cation ($\sum r_{NF}$ + r_{NN} = 2.316 (12) Å) and an AsF_6^- anion which within experimental error is perfectly octahedral. Since the Raman spectra of $N_2F^+AsF_6^-$ crystals are in perfect agreement with O_h symmetry (only three narrow bands at 689 (ν_1, A_{1g}), 576 (ν_2, E_g), and 376 cm^{-1} (ν_5, F_{2g}) with half widths of 10 cm^{-1} or less at 25 °C), models *Cm* and *C2* must be rejected in spite of their lower R factors. This situation closely resembles that in isotypic $NS_2^+AsF_6^-$ for which the alternate *Cm* and *C2* models could also be rejected on the basis of the observed vibrational spectra.[31] The packing diagram for $N_2F^+AsF_6^-$ is shown in Figure 1. The AsF_6^- anions occupy the corners of the cell and the centers of the *ab* faces, while the NX_2 cations occupy the remaining faces of the cell.

As pointed out already in the introduction, a knowledge of the exact N–F and N–N bond distances in N_2F^+ is of great interest.
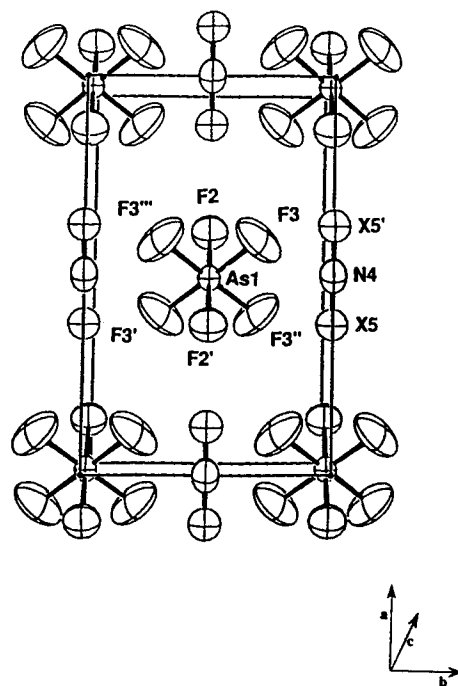
Figure 1. A unit cell plot of $N_2F^+AsF_6^-$ viewed down the *c* axis. In addition to the mirror plane, 2-fold rotational axes pass through As1 (bisecting the F3–As1–F3″ angle) and N4 (perpendicular to the X5–N4–X5′ axis). The N_2F^+ cation is required by symmetry to be disordered, with the terminal X5, X5′ positions being occupied equally by N and F atoms. This packing disorder causes the NX_2 cation to be linear and symmetric, and the central nitrogen atoms to be elongated along the molecular axis.

Table V. Calculated and Experimental Bond Distances (Å) and Vibrational Frequencies (cm^{-1}) for FCN

	expt	calcd (LDF)
$r_{C\equiv N}$	1.159	1.169
$r_{C—F}$	1.262	1.274
$C\equiv N$ stretch	2323	2355
$C—F$ stretch	1077	1081
$F—C\equiv N$ bend	451	465

Since the above crystal structure determination provides only a value for the sum of the N–F and N–N bond lengths, a reliable method was sought to partition this sum into its individual components. This partitioning was achieved by local density functional (LDF) calculations providing both the geometry and the vibrational frequencies.

The accuracy of the LDF calculations was tested for FCN which is isoelectronic with FNN$^+$ and for which both the geometry[32] and the vibrational frequencies[33] are well-known (see Table V). As expected from a number of studies,[34] the LDF method slightly overestimates the bond distances and vibrational frequencies but otherwise excellently reproduces the experimental values (see Table V). Similarly, LDF calculations for the dinitrogen molecule, N_2, resulted in a bond length value (1.113 Å) only slightly longer than the experimental one (1.098 Å).[35]

The results of the LDF calculations for N_2F^+ are summarized in Table VI. As expected, the N_2F^+ cation is linear and the bond

(31) Johnson, J. P.; Passmore, J.; White, P. S.; Banister, A. J.; Kendrick, A. G. *Acta Cryst. Part C* **1987**, *C43*, 1651.

(32) Harmony, M. D.; Laurie, V. W.; Kuczkowski, R. L.; Schwendeman, R. H.; Ramsay, D. A.; Lovas, F. J.; Lafferty, W. J.; Maki, A. G. *J. Phys. Chem. Ref. Data* **1979**, *8*, 619, see p 640.

(33) Shimanouchi, T. *J. Phys. Chem. Ref. Data* **1977**, *6*, 993.

(34) (a) Dixon, D. A.; Andzelm, A.; Fitzgerald, Wimmer, E.; Delley, B. Science and Engineering on Cray Supercomputers, Proceedings of the Fifth International Symposium, Cray Research, Minneapolis, MN, 1990. (b) Dixon, D. A.; Andzelm, A.; Fitzgerald, Wimmer, E.; Jasien, P. In *Theory and Applications of Density Functional Approaches to Chemistry*; Labanowski, J., Ed., in press.

(35) Huber, K. P.; Herzberg, G. *Constants of Diatomic Molecules*; Van Nostrand Reinhold: New York, 1979.

Table VI. Calculated and Experimental Bond Distances (Å) and Vibrational Frequencies (cm⁻¹) for FNN⁺

|	expt	calcd (LDF)				
		LDF	LDFS1	LDFS2	SCF 6-31G*[a]	MP-2 6-31G*[a]
$r_{N=N}$	(1.099)[b]	1.121	1.111	1.106	1.072	1.138
r_{N-F}	(1.217)[b]	1.248	1.236	1.225	1.240	1.256
$\sum r_{N-N} + r_{N-F}$	2.316 (12)	2.369	2.347	2.331	2.312	2.394
N≡N stretch	2373	2409				
N—F stretch	1059	1100				
F—N≡N bend	388	438				

[a] Data from ref 11. [b] Values obtained by partitioning the experimentally measured sum of $r_{N-N} + r_{N-F}$ according to their ratio in LDFS2.

lengths are, as for isoelectronic FNC, slightly too long. To obtain better estimates for the actual bond lengths, the LDF values can be scaled in the following manner. Using the scaling factors from the FCN calculations, one obtains the values labeled LDFS1. Using the N_2 results for scaling r_{N-N} and the NF_4^+ results for scaling r_{N-F} (r_{N-F}, LDF = 1.324 Å,[36] experimental = 1.297 Å[14]), one obtains the values labeled LDFS2. The sum of r_{N-N} and r_{N-F} of LDFS2 (2.331 Å) is very close to that obtained from the crystal structure determination (2.316 Å). If one partitions the experimentally determined sum of $r_{N-N} + r_{N-F}$ in the same ratio as that in LDFS2, final values of 1.217 and 1.099 Å are obtained for r_{N-F} and r_{N-N}, respectively, in N_2F^+ (see Table VI). The close agreement between these values and those ($r_{NF} = 1.221$ Å, $r_{NN} = 1.099$ Å) obtained by the rejected *Cm* model with ordered N_2F^+ cations (see above) might be fortuitous.

Of the previously calculated[10-12] N–N and N–F bond lengths for N_2F^+, the SCF 6-31G* and MP-2 6-31G* values of Peters[11] (see Table VI) come the closest to the values from this study but appear to either underestimate or overestimate the r_{N-N} value. When comparing the calculated LDF vibrational frequencies of N_2F^+ with the observed ones (see Table VI), the agreement is very satisfactory, particularly if it is kept in mind that the LDF values are unscaled, harmonic, gas-phase frequencies and the experimental values are anharmonic, solid-state frequencies.

As shown above, the N_2F^+ cation is linear. This result confirms a recent theoretical study[12] which concluded that, contrary to P_2F^+, for N_2F^+ the linear $C_{∞v}$ structure is favored by about 50–60 kcal over the symmetric, three-membered-ring structure of symmetry C_{2v}. As already pointed out in the introduction, the most interesting aspect of the N_2F^+ structure is its N–F bond distance. This distance of 1.22 Å is by far the shortest distance found to date for any N–F bond. The previously known range for N–F bonds extended from 1.512 Å in FNO to 1.30 Å in NF_4^+.[13,14] The value of 1.22 Å found for N_2F^+ is in good agreement with the value of 1.24 Å estimated from a force field calculation[9] and force constant–bond distance plot extrapolations.[11,13] The excellent agreement between our experimental value and the value extrapolated from the stretching force constant demonstrates that N_2F^+ conforms with Gordy's rule.[15]

The nitrogen–nitrogen bond distance in N_2F^+ is also of interest. Its value of 1.099 Å is comparable to those of 1.0976 (2) Å[26] in N_2 and 1.118 Å in N_2^+[38] and confirms its triple bond character. Thus the N_2F^+ cation is highly unusual. It possesses by far the shortest known N–F bond while at the same time exhibiting an N–N bond length comparable to the shortest known N–N bond. How can these unusually short bond distances be explained? It is tempting to invoke partial double bond character for the N–F bond by writing the following resonance structures:

$$[|\bar{F}-N≡N|]^+ \longleftrightarrow [\overset{/}{\underset{\backslash}{F}}=N=N\overset{\backslash}{\underset{/}{}}]^+$$
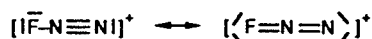
If, however, the N–F bond assumes partial double bond character, the N≡N bond must lose some of its strength and lengthen accordingly. This is not the case, as evidenced by the short N≡N bond of 1.099 Å in N_2F^+.

**Table VII.** Influence of Hybridization on Bond Lengths (Å) in Carbon and Nitrogen Compounds

	CH_4 (sp³)	$H_2C=CH_2$ (sp²)	HC≡CH (sp)
r_{C-H}	1.094[a]	1.085[a]	1.061[a]
	CF_4 (sp³)	$F_2C=CF_2$ (sp²)	FC≡N (sp)
r_{C-F}	1.323[b]	1.313[b]	1.262[a]
	NF_4^+	$[FN=NF^2]^+$	$[FN≡N]^+$
r_{N-F}	1.30[c]	?	1.22[d]

[a] Data from ref 32. [b] Data from ref 39. [c] Data from ref 14. [d] This work.

Although a formal positive charge and other highly electronegative ligands generally tend to increase the strength of an X–F bond, this effect alone is insufficient to explain the unusually short N–F and N≡N bonds in N_2F^+. For example, the N—F bond in NF_4^+ still has a value of 1.30 Å,[14] in spite of a formal positive charge and three additional fluorine ligands which should be more electronegative than the nitrogen ligand in N≡NF⁺.

The most plausible explanation for the shortening of the N–F bond in N_2F^+, compared to NF_4^+, is the change in hybridization of the nitrogen molecular orbitals. From carbon chemistry it is well-known that the C–H and C–F bond lengths significantly decrease with increasing s-character of the carbon molecular orbital. Therefore, a similar bond shortening should be expected on going from sp³-hybridized NF_4^+ to sp-hybridized N≡NF⁺ (see Table VII). To our knowledge, this is the first example of hybridization-induced, dramatic bond shortening outside of carbon chemistry.

The N₂F⁺ Cation as an Oxidative Fluorinator. In view of N_2 having a higher ionization potential than Kr, i.e. 15.576 vs 13.999 eV,[40] and KrF^+ being the most powerful presently known oxidative fluorinator,[41] it was interesting to examine the oxidative power of the N_2F^+ cation. For this purpose, the reactions of $N_2F^+AsF_6^-$, dissolved in anhydrous HF, were studied at 25 °C with the following substrates: ClF_5, BrF_5, IF_5, XeF_4, Xe, ClF, O_2, and NF_3. The KrF⁺ cation is capable of oxidizing all of these substrates under comparable reaction conditions. For example, $HalF_5$ is oxidized to $HalF_6^+$ salts, XeF_4 to XeF_5^+, O_2 to O_2^+, and NF_3 to NF_4^+.[41] In the case of N_2F^+ the only substrates oxidized were Xe and ClF according to

$$N_2F^+AsF_6^- + Xe \xrightarrow[25\ °C]{HF} XeF^+AsF_6^- + N_2$$

$$N_2F^+AsF_6^- + ClF \rightarrow ClF_2^+AsF_6^- + N_2$$
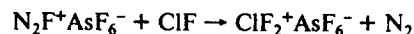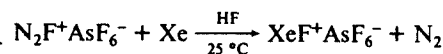
The first reaction was briefly mentioned in a previous paper,[42] but no experimental details were given.

To examine whether fluorination reactions with N_2F^+ might benefit from elevated temperatures, $N_2F^+AsF_6^-$ was heated with a large excess of either ClF_5 or BrF_5 in a small ullage stainless steel cylinder, in the absence of HF, to 70 °C for 3 days. Again, no evidence for the formation of either ClF_6^+ or BrF_6^+ was detected. In the case of ClF_5, however, a small amount of the N_2F^+ starting material was fluorinated by ClF_5 to $N_2F_3^+$. A detailed

(36) Dixon, D. A.; Christe, K. O. Unpublished work.
(37) Wilkinson, P. G. *J. Astrophys.* **1957**, *126*, 1.
(38) Wilkinson, P. G. *Can. J. Phys.* **1956**, *34*, 250.
(39) *Tables of Interatomic Distances and Configuration in Molecules and Ions*; The Chemical Society: London, *1958*; Special Publication No. 11.

(40) *CRC Handbook of Chemistry and Physics*, 60th ed.; CRC Press: Boca Raton, FL, 1979.
(41) Christe, K. O.; Wilson, W. W.; Wilson, R. D. *Inorg. Chem.* **1984**, *23*, 2058.
(42) Stein, L. *Chemistry* **1974**, *47*, 15.

analysis of the factors determining the relative strength of an oxidative fluorinator will be given in a separate paper.[43]

Supplementary Material Available: Table SI listing observed and calculated structure factors (2 pages). Ordering information is given on any current masthead page.

(43) Christe, K. O.; Wilson, W. W.; Dixon, D. A. To be published.

New Synthesis, Crystal Structure, and Vibrational Spectra of Tetramethylammonium Azide and Reactions of the Fluoride Anion with HN₃ and of the Azide Anion with HF[†]

Karl O. Christe,*,‡ William W. Wilson,‡ Robert Bau,§ and Steven W. Bunte§

Contribution from Rocketdyne. A Division of Rockwell International Corporation, Canoga Park, California 91303, and The Department of Chemistry, University of Southern California, Los Angeles, California 90007. Received October 15, 1991

Abstract: Tetramethylammonium azide, $N(CH_3)_4^+N_3^-$, was obtained in high purity and quantitative yield by the reaction of $N(CH_3)_4^+F^-$ with $Si(CH_3)_3N_3$ in CH_3CN solution. This compound is isostructural with $N(CH_3)_4^+HF_2^-$ and crystallizes in the orthorhombic system: space group, $Pmn2_1$ (No. 31); $a = 6.879$ (5) Å; $b = 5.479$ (4) Å; $c = 8.858$ (7) Å; $Z = 2$; $R(F)$ = 0.0388. Its N_3^- anion is symmetric and linear and the $N(CH_3)_4^+$ cation is somewhat distorted from tetrahedral symmetry due to crystal packing effects. The infrared and Raman spectra of $N(CH_3)_4^+N_3^-$ were also recorded. The symmetric stretching mode of N_3^- exhibits the pronounced frequency decrease expected for increasing ionicity with increasing cation size. A study of the HN_3–MF systems [M = Na, K, Rb, Cs, $N(CH_3)_4$] revealed some unexpected chemistry. Even at −80 °C, HN_3 displaces F^- from MF with formation of equimolar amounts of $M^+N_3^-$ and HF. The latter reacts with MF to give $M^+HF_2^-$. On the other hand, HF quantitatively displaces N_3^- from MN_3 with formation of HN_3 and $M^+HF_2^-$. This apparent discrepancy can be explained by the vast difference in basicity between F^- and HF_2^-. Attempts to isolate stable $F–H–N_3^-$ or $N_3–H–N_3^-$ anions from HN_3 and either MF or MN_3, respectively, were unsuccessful.

Introduction

Although tetramethylammonium azide, $N(CH_3)_4^+N_3^-$, had been known[1] since 1918, only very little information has since been reported[2-6] for this interesting compound. According to the previous reports,[1-6] the compound was prepared by either the reaction of $N(CH_3)_4I$ with AgN_3 (1) in either water[1] or anhydrous

$$N(CH_3)_4I + AgN_3 \rightarrow N(CH_3)_4N_3 + AgI\downarrow \qquad (1)$$

ethanol[4] or the neutralization[3,5,6] of $N(CH_3)_4OH$ with aqueous HN_3 (2). Both preparations involve the use of shock-sensitive

$$N(CH_3)_4OH + HN_3 \rightarrow N(CH_3)_4N_3 + H_2O\downarrow \qquad (2)$$

starting materials, i.e. AgN_3 and HN_3, and suffer from solubility and purification problems. No structural or spectroscopic data had previously been reported for $N(CH_3)_4N_3$, except for partial vibrational spectra.[6] In this paper, we report an improved synthesis for $N(CH_3)_4N_3$ and its crystal structure and vibrational spectra.

Experimental Section

Caution! *Hydrazoic acid is shock sensitive when undiluted, and appropriate shielding and safety precautions must be used when working with this compound.*

Materials. CH_3CN (Baker, Bio-analyzed, having a water content of 40 ppm) was treated with P_2O_5 and freshly distilled prior to use, thereby reducing its water content to <4 ppm. The synthesis of $N(CH_3)_4F$ has previously been described.[7] $Si(CH_3)_3N_3$ (Petrarch) was distilled prior to use. Hydrazoic acid was generated from NaN_3 and stearic acid at about 110 °C, as previously described.[8] Dry KF, RbF, and CsF were obtained by fusing these materials in a platinum crucible and transferring the resulting clinkers into a drybox while still hot. The RbF single crystal (Semi-Elements, Inc.), used for the low-temperature infrared study, was freshly cleaved with a razor blade in the drybox and then mounted in a dry N_2 atmosphere into the tip of an Air Products Model DE 202S helium refrigerator equipped with external CsI windows. The HF (Matheson) was dried by storage over BiF_5.[9]

Apparatus. Volatile materials were handled either in a flamed-out Pyrex vacuum line equipped with Kontes Teflon valves, in a stainless-steel vacuum line equipped with Teflon-FEP U-traps,[10] or in the dry nitrogen atmosphere of a glovebox. Solids were manipulated exclusively in the drybox.

Raman spectra were recorded on either a Cary Model 83 or a Spex Model 1403 spectrophotometer by use of the 488-nm exciting line of an Ar ion or the 647.1-nm line of a Kr ion laser, respectively. Baked-out Pyrex melting point capillaries were used as sample holders. Infrared spectra were recorded as KBr disks on a Perkin-Elmer Model 283

Table I. Summary of Crystal Data and Refinement Results for $N(CH_3)_4^+N_3^-$

space group	$Pmn2_1$ (No. 31)
a (Å)	6.879 (5)
b (Å)	5.479 (4)
c (Å)	8.858 (7)
V (Å³)	333.9 (7)
molecules/unit cell	2
formula weight (g/mol)	116.2
crystal dimens (mm)	0.28 × 0.34 × 0.88
calcd density (g cm⁻³)	1.156
wavelength (Å) used for data collecn	0.71069
sin (θ/λ) limit (Å⁻¹)	0.6497
total no. of reflecns measured	1469
no. of independent reflecns	762
no. of reflecns used in structural analysis, $I > 3\sigma(I)$	427
no. of variable params	77
final agreement factor	$R(F) = 0.0388$ $R_w(F) = 0.0359$

spectrophotometer. The KBr disks were pressed in a Wilks minipress and left in the press for the recording of the spectra. The spectra obtained in this manner were identical with those obtained for pressed AgCl disks, indicating that no reaction between KBr and $N(CH_3)_4N_3$ had occurred during the pressing operation. The cryostat used for the low-temperature infrared studies has previously been described.[11]

Synthesis of $N(CH_3)_4N_3$. A solution of $Si(CH_3)_3N_3$ (29.92 mmol) in 15 mL of CH_3CN was slowly added in a dry atmosphere to $N(CH_3)_4F$ (24.10 mmol) dissolved in 29 mL of CH_3CN. In a mildly exothermic reaction, a white precipitate was formed instantaneously. The mixture was agitated for about 10 min, and then all volatile material was pumped off at room temperature. The white solid residue (2.794 g; weight calculated for 24.10 mmol of $N(CH_3)_4N_3 = 2.797$ g, corresponding to a 99.9% yield) was identified by vibrational spectroscopy and a crystal

(1) Friedländer, F. *J. Am. Chem. Soc.* **1918**, *40*, 1945.
(2) Straumanis, M.; Circulis, A. *Z. Anorg. Allg. Chem.* **1943**, *252*, 17.
(3) Gutmann, V.; Hampel, G.; Leitmann, O. *Monatsh. Chem.* **1964**, *95*, 1034.
(4) Weller, F.; Dehnicke, K. *J. Organomet. Chem.* **1972**, *35*, 237.
(5) Bojes, J.; Chivers, T. *Inorg. Chem.* **1978**, *17*, 318.
(6) Glavincevski, B.; Brownstein, S. *J. Inorg. Nucl. Chem.* **1981**, *43*, 1827.
(7) Christe, K. O.; Wilson, W. W.; Wilson, R. D.; Bau, R.; Feng, J. *J. Am. Chem. Soc.* **1990**, *112*, 7619.
(8) Krakow, B.; Lord, R. C.; Neely, G. O. *J. Mol. Spectrosc.* **1968**, *27*, 198.
(9) Christe, K. O.; Wilson, W. W.; Schack, C. J. *J. Fluorine Chem.* **1978**, *11*, 71.
(10) Christe, K. O.; Wilson, R. D.; Schack, C. J. *Inorg. Synth.* **1986**, *24*, 3.
(11) Christe, K. O.; Wilson, R. D. *Inorg. Chem.* **1987**, *26*, 920.

Table II. Bond Distances (Å) for $N(CH_3)_4^+N_3^-$

N1–N2	1.155 (5)	C5–H9	0.944 (10)
N2–N3	1.176 (5)	C5–H11	0.961 (10)
N4–C5	1.496 (2)	C6–H10	1.046 (10)
N4–C6	1.470 (7)	C6–H14	0.981 (8)
N4–C7	1.529 (7)	C7–H12	1.001 (8)
C5–H8	1.030 (7)	C7–H13	0.990 (11)

Table III. Bond Angles (deg) for $N(CH_3)_4^+N_3^-$

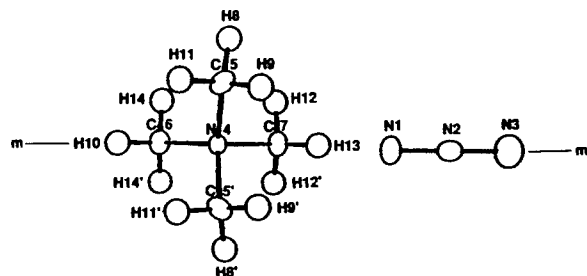| N1–N2–N3	179.0 (3)	N4–C7–H12	106.6 (7)
C5–N4–C6	111.8 (4)	N4–C7–H13	108.3 (6)
C5–N4–C7	107.3 (4)	H8–C5–H9	109.6 (9)
C5–N4–C5′	109.1 (3)	H8–C5–H11	109.6 (8)
C6–N4–C7	109.3 (2)	H9–C5–H11	112.0 (7)
N4–C5–H8	109.9 (4)	H10–C6–H14	109.2 (7)
N4–C5–H9	109.2 (6)	H14–C6–H14′	116.8 (8)
N4–C5–H11	106.5 (6)	H12–C7–H13	111.0 (7)
N4–C6–H10	107.9 (6)	H12–C7–H12′	113.1 (9)
N4–C6–H14	106.6 (7)		

Figure 1. View of the molecular $N(CH_3)_4N_3$ unit showing the positions and labeling of the hydrogen atoms and the crystallographic mirror plane.

M⁺: SMALL.   INTERMEDIATE   LARGE
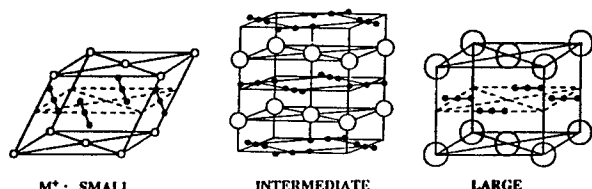
Figure 2. Packing in azides and bifluorides as a function of the cation size.

structure determination as $N(CH_3)_4N_3$. Its decomposition point was found to be 255 °C.

Crystal Structure of $N(CH_3)_4N_3$. Single crystals of $N(CH_3)_4N_3$ were grown from a hot CH_3CN solution. A suitable crystal was selected under the microscope and sealed in a glass capillary because the compound diliquesces slowly, and intensity data were collected at room temperature on a Nicolet/Syntex P2₁ automated four circle diffractometer, with Mo Kα radiation and a graphite crystal monochromator. The unit cell parameters were determined by least-squares refinement of 15 centered reflections. Data were collected with the ω-scan technique for all reflections such that $4.0° < 2\theta < 55.0°$. Throughout the data collection, three reflections were monitored periodically and no decay was observed. A set of 1469 intensity values, representing a hemisphere of data, was collected and the four equivalent octants were merged to give a total of 427 unique reflections. The R factor for averaging was 1.8%. The positions of the non-hydrogen atoms were obtained by direct methods using the computing package SHELX-86.[12] The hydrogen atoms were later located from a difference Fourier map. The structure was then refined to final agreement factors of $R(F) = 3.88\%$ and $R_w(F) = 3.59\%$, using 427 reflections with $I > 2\sigma(I)$. In the least-squares refinement, the H atoms were also varied and were assigned equal isotropic temperature factors. Details of the data collection parameters and other crystallographic information are given in Table I, and the final atomic coordinates and temperature factors are listed in Tables A and B, respectively, of supplementary material. Interatomic distances and angles are given in Tables II and III, respectively. A view of the molecular $N(CH_3)_4N_3$ unit showing the positions and labeling of the hydrogen atoms is given in Figure 1, and the packing in $N(CH_3)_4N_3$ is shown in Figure 2 for the large cation case.

Reactions of HN_3 with MF (M = Na, K, Rb, Cs, $N(CH_3)_4$). Samples of these fluorides were exposed at room temperature to about 100 Torr of HN_3 vapor for 12 h. The solid reaction products were weighed and identified by infrared and Raman spectroscopy and showed about equimolar amounts of N_3^- and HF_2^-. No evidence for the formation of any new species, such as $F–H–N_3^-$ or $N_3–H–N_3^-$, was observed.

A sample of HN_3 was condensed at 12 K onto a RbF single crystal window. The temperature of the window was steadily increased, and infrared spectra were periodically recorded. Between 12 and 100 K the spectra showed only solid HN_3, with increasing temperature causing irreversible band broadening. At 130 K the HN_3 deposit was slowly pumped away. Therefore, the pumping was interrupted and the RbF window, while kept at 190 K, was exposed to an HN_3–He mixture (1:10

mole ratio) at a total pressure of about 35 Torr. The infrared spectrum, recorded at this temperature, showed only N_3^- and HF_2^- but no unreacted HN_3. This indicates that, even at 190 K, the reaction of RbF with HN_3 to give RbN_3 and $RbHF_2$ is fast and complete.

Reactions of HF with MN_3 (M = Na, Cs, $N(CH_3)_4$). Weighed amounts of MN_3 were exposed to less than stoichiometric amounts of gaseous HF for several hours at room temperature. Essentially all of the HF was consumed, and HN_3 was liberated. The solid reaction products were identified spectroscopically as mixtures of MF-nHF and unreacted excess MN_3.

For NaN_3, a sample was treated at room temperature with a 31-fold excess of liquid anhydrous HF. After removal of the volatile products, which consisted of a mixture of HF and HN_3, the solid residue was identified as $NaHF_2$.

Results and Discussion

Synthesis and Properties of $N(CH_3)_4N_3$. The ready acess to truly anhydrous $N(CH_3)_4F^7$ combined with the commercial availability of $Si(CH_3)_3N_3$ provides a convenient and safe synthesis (3) for $N(CH_3)_4N_3$. Using a slight excess of $Si(CH_3)_3N_3$, $N(C-H_3)_4N_3$ can be prepared in quantitative yield and excellent purity.

$$N(CH_3)_4F + Si(CH_3)_3N_3 \xrightarrow[\text{room temp}]{CH_3CN}$$
$$N(CH_3)_4N_3 + Si(CH_3)_3F \quad (3)$$
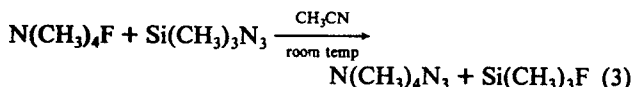
The observed decomposition point of 255 °C is in good agreement with that previously reported[4] for a sample prepared from AgN_3 and $N(CH_3)_4I$ in C_2H_5OH and recrystallized from 2-propanol but disagrees with that of 125 °C originally reported[1] by Friedländer. The compound is a white, crystallinic, nonsensitive, and slightly hygroscopic solid. It has little solubility in cold CH_3CN, moderate solubility in hot CH_3CN, and is highly soluble in alcohol and water.

Crystal Structure of $N(CH_3)_4N_3$. The structure of $N(CH_3)_4N_3$ can be derived from a primitive cubic CsCl lattice which is orthorhombically distorted by the nonspherical N_3^- anions. The packing in $N(CH_3)_4N_3$ is identical to that[13] found for $N(C-H_3)_4HF_2$, and the two compounds are isotypic. In both, the $M^+HF_2^-$ and the $M^+N_3^-$ series, the packings are governed by the ionic radii of the M^+ cations. For small M^+ (Li^+, $r = 0.60$ Å; Na^+, $r = 0.95$ Å), the anion layers are stacked perpendicular to the M^+ layers; for intermediate M^+ (K^+, $r = 1.33$ Å; Rb^+, $r = 1.48$ Å; Cs^+, $r = 1.69$ Å), the anions are oriented with their axes parallel to the M^+ layers and perpendicular to each other;[14] and for large M^+ ($N(CH_3)_4^+$, $r \approx 2.74$ Å), the anions are oriented with their axes parallel both to the M^+ layers and to each other (see Figure 2).

Both the tetramethylammonium cation and the azide anion were found to be situated on crystallographic mirror planes. The cationic mirror plane bisects the angle C5–N4–C5′ and passes through atoms N4, C6, C7, H10, and H13, while the anionic mirror plane passes through all three N atoms N1, N2, and N3. The azide ion refined to an essentially linear, symmetrical structure [N1–N2 = 1.155 (5) Å, N2–N3 = 1.176 (5) Å, N1–N2–N3 = 179.0 (3)°], even though there are no symmetry constraints that require it to be linear and symmetric. Its N–N bond length of 1.16 Å is comparable to those found for other ionic azides.[14] The

(12) Sheldrix, G. M. *SHELX System of Crystallographic Programs*; University of Goettingen: Germany, 1986.

(13) Wilson, W. W.; Christe, K. O.; Feng, J.; Bau, R. *Can. J. Chem.* **1989,** *67,* 1898.

(14) Choi, C. S. In *Energetic Materials*; Fair, H. D., Walker, R. F., Eds.; Plenum Press: New York, 1977; Vol. 1, p 97.

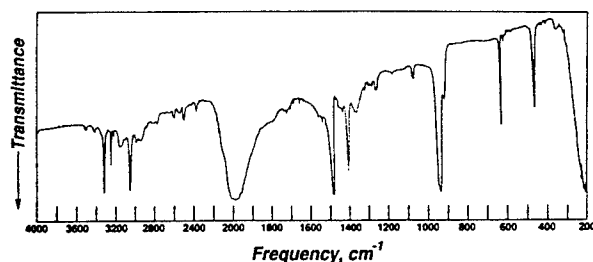Synthesis of Tetramethylammonium Azide

J. Am. Chem. Soc., Vol. 114, No. 9, 1992 3413

Figure 3. Infrared spectrum of solid $N(CH_3)_4N_3$ pressed in an AgBr disk. The absorption at 250 cm^{-1} is due to the window material.
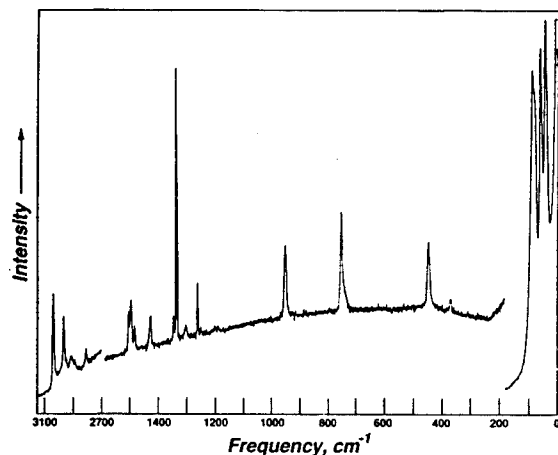

Figure 4. Raman spectrum of solid $N(CH_3)_4N_3$ recorded at ambient temperature. The region 0–200 cm^{-1} was recorded at a 10 times lower sensitivity.

tetramethylammonium cation is slightly but significantly distorted, with angles around N ranging from 107.3 (4)° to 111.8 (4)°, compared to angles ranging from 108.8 (2)° to 110.3 (2)° in isotypic $N(CH_3)_4HF_2$.[13] This increased distortion of the $N(CH_3)_4^+$ cations is attributed to packing effects caused by the slightly larger anion size on going from HF_2^- to N_3^-.

Vibrational Spectra. The infrared and Raman spectra of solid $N(CH_3)_4^+N_3^-$ are shown in Figures 3 and 4, respectively. The observed frequencies and their assignments are summarized in Table IV. The assignments and mode descriptions for $N(CH_3)_4^+$ follow those[15] published by Berg. These spectra confirm the findings from the crystal structure determination that the N-$(CH_3)_4^+$ cation in $N(CH_3)_4^+N_3^-$ is more distorted from tetrahedral symmetry than that in $N(CH_3)_4^+HF_2^-$. This is manifested by the significant difference in the relative Raman intensities of the two NC_4 deformation modes, $\nu_{19}(F_2)$ and $\nu_8(E)$, in these two compounds. In $N(CH_3)_4HF_2$, the $\nu_8:\nu_{19}$ intensity ratio equals 3.6, whereas in $N(CH_3)_4N_3$ it is only 0.29. It has previously been demonstrated[16,17] that this ratio decreases with increasing distortion of the $N(CH_3)_4^+$ cation. Additional evidence for the increased cation distortion is the frequency decrease of the antisymmetric CH_3 stretching mode, $\nu_{13}(F_2)$,[16,17] from 3036 cm^{-1} in $N(CH_3)_4HF_2$ to 3022 cm^{-1} in $N(CH_3)_4N_3$, and the infrared activity of the F_1 modes, which for strict T_d symmetry should be inactive.[15]

The bands observed for the N_3^- anion (see Table I) are in excellent agreement with those previously reported for a symmetric linear ion of symmetry $D_{\infty h}$.[18-20] The frequency of ν_1 follows a trend previously noted[20] for the alkali metal azides, i.e. a decrease in ν_1 with increasing ionic radius and ionicity of the cation (Li$^+$, 1372; Na$^+$, 1360; K$^+$, 1343; Rb$^+$, 1335; Cs$^+$, 1328; N(CH$_3$)$_4$$^+$, 1317 cm^{-1}).

Table IV. Vibrational Spectra of Solid $N(CH_3)_4^+N_3^-$

obsd frequencies, cm^{-1} (rel intens)		assignments (point group)	
IR	R	$N(CH_3)_4$ (T_d)	N_3^- ($D_{\infty h}$)
3486vw			
3400vw			
3330sh			
3297ms ⎫			$\nu_1 + \nu_3$ (Σu^+)
3225mw ⎬			
3201vw			
3130w		$\nu_{13}(F_2)\nu_{as}CH_3$	
3031ms			
3023sh	3022 (7)		
2970w		$\nu_5(E)\nu_{as}CH_3$	
	2953 (5) ⎱	$\nu_{14}(F_2)\nu_{sym}CH_3$	
2930w		$\nu_1(A_1)\nu_{sym}CH_3$	
	2900 (1)	+ combin. bands	
	2882sh		
	2802 (1) ⎭		
2790vw			
2750vw			
2579w			
2529vw			
2480w			
2358w			
1998vs			$\nu_3(\Sigma u^+)\nu_{as}$
1492s		$\nu_{15}(F_2)\delta_{as}CH_3$	
	1480 (3) ⎱	$\nu_2(A_1)\delta_{sym}CH_3$	
	1473 (5) ⎬	$\nu_6(E)\delta_{as}CH_3$	
	1460 (2) ⎭		
1439vw		$\nu_{10}(F_1)\delta_{as}CH_3$	
1414ms	1407 (3)	$\nu_{16}(F_2)\delta_{sym}CH_3$	
1365mw			
	1327 (2) ⎱		
1319vw	1317 (30) ⎭		$\nu_1(\Sigma g^+)\nu_{sym}$
1299vw ⎱			
1288vw ⎭	1287 (1)	$\nu_{17}(F_2)CH_3rock$	
1263w ⎱			
1256w			
	1245 (5) ⎭		$2\nu_2(\Sigma g^+)$
1175vw	1180 (0+)	$\nu_7(E)CH_3rock$	
1077w ⎱			
1071w ⎭		$\nu_{11}(F_1)CH_3rock$	
959sh ⎱			
950s ⎬	947 (8)	$\nu_{18}(F_2)\nu_{as}CN_4$	
922m ⎭		$2\nu_{19}(F_2)$	
	756 (11)	$\nu_3(A_1)\nu_sCN_4$	
632ms ⎱			$\nu_2(\pi_u)\delta$
614vw ⎭			
462ms	459 (7)	$\nu_{19}(F_2)\delta CN_4$	
	383 (2)	$\nu_8(E)\delta CN_4$	
347w		$\nu_{12}(F_1)\tau CH_3$	
	105 (100) ⎱		
	78 (75) ⎬	Lattice Vibrations	
	61 (75) ⎭		

A comparison of our spectra with those previously reported[6] for $N(CH_3)_4N_3$ shows significant discrepancies. Thus, ν_3 of N_3^- differs by more than 60 cm^{-1} from the previous report, and numerous other bands differ in both frequencies and relative intensities. In view of the high purity of our sample, as shown by the crystal structure and correct decomposition point, our spectra should be preferred over those previously reported.[6]

Reactions of HN_3 with the F$^-$ Anion and of HF with the Azide Anion. The N_3 group can be considered as a pseudohalogen[21] or para-halogen.[22] Since other pseudohalides, such as NO_3^- or ClO_4^-, are known to form the bihalide-type anions, $[O_2NO-H-ONO_2]^-$,[23-28] $[F-H-ONO_2]^-$,[29] and $[O_3ClO-H-OClO_3]^-$,[30] respec-

(15) Berg, R. W. *Spectrochim. Acta, Part A* **1978**, *34A*, 655.
(16) Kabisch, G.; Klose, M. *J. Raman Spectrosc.* **1978**, *7*, 311.
(17) Kabisch, G. *J. Raman Spectrosc.* **1980**, *9*, 285.
(18) Bryant, J. I. *J. Chem. Phys.* **1964**, *40*, 3195; **1966**, *45*, 689.
(19) Hathaway, C. E.; Temple, P. A. *Phys. Rev. B* **1971**, *3*, 3497.
(20) Iqbal, Z.; Prask, H. J.; Trevino, S. F. In *Energetic Materials*; Fair, H. D., Walker, R. F., Eds.; Plenum Press: New York, 1977; Vol. 1, p 131.

(21) Golub, A. M.; Köhler, H.; Skopengo, V. V. Chemistry of Pseudohalides. In *Topics in Inorganic and General Chemistry*; Clark, R. J. H., Ed.; Monograph 21; Elsevier: Amsterdam, 1986; p 28.
(22) Haas, A. *Adv. Inorg. Chem. Radiochem.* **1984**, *28*, 167.
(23) Gillard, R. D.; Mitchell, S. H. *Polyhedron* **1987**, *6*, 1885.

tively, it was interesting to study the interaction of HN_3 with both the N_3^- and the F^- anions. With $N(CH_3)_4N_3$, HN_3 did not form an adduct stable at room temperature. With MF [M = Na, K, Rb, Cs, $N(CH_3)_4$], gaseous or liquid HN_3 reacted at or below room temperature with the formation of an equimolar mixture of MN_3 and MHF_2 (4). The products of reaction 4 are best

$$2MF + HN_3 \rightarrow MN_3 + MHF_2 \qquad (4)$$

interpreted by the summation of (5) and (6), where step 5 might

$$MF + HN_3 \rightarrow MN_3 + HF \qquad (5)$$

$$MF + HF \rightarrow MHF_2 \qquad (6)$$

involve an intermediate $F-H-N_3^-$ anion which readily eliminates HF to give the final N_3^- product. Attempts were made to isolate this intermediate anion by reacting HN_3 with a RbF single crystal infrared window at low temperature. Below $-100\,°C$, no reaction occurred, and above this temperature, the only new products observable by infrared spectroscopy were RbN_3 and $RbHF_2$.

Reaction 5, i.e. the displacement of F^- from M^+F^- by HN_3, was surprising since, in aqueous solution, HN_3 ($P_k = 4.77$) is a weaker acid than HF ($P_k = 3.18$). Furthermore, molten weak organic acids such as stearic acid also displace N_3^- from NaN_3.[8] Since reaction 5 was not carried out in aqueous solution in which the acidity of HF is enhanced by the hydration energy of F^-, but between solid MF and neat gaseous or liquid HN_3, it should not

be governed by the above P_k values but by the proton affinities of F^- and N_3^-. In view of the proton affinity of F^- (371.5 kcal mol^{-1}) exceeding that of N_3^- (328.6 kcal mol^{-1}) by about 43 kcal mol^{-1}, it is then not surprising that HN_3 can displace F^- from M^+F^-.

On the other hand it was found that HF quantitatively displaces N_3^- from $M^+N_3^-$ (7). This reaction does not require the use of an excess of HF. If less than the stoichiometric amounts of HF are used, the resulting products still are MHF_2 and HN_3 and not MF and HN_3. Hence, it appears that both reactions 5 and 7 are

$$MN_3 + 2HF \rightarrow MHF_2 + HN_3 \qquad (7)$$
$$M = Na, Cs, N(CH_3)_4$$

irreversible and that the puzzling observations that HN_3 displaces F^- from MF (5) while HF displaces N_3^- from MN_3 (7) are not due to the shifting of a single chemical equilibrium (8).

$$MF + HN_3 \rightleftharpoons MN_3 + HF \qquad (8)$$

The observed reaction chemistry can be explained by the vastly different Lewis basicities of F^- and HF_2^-. Thus, the very strong Lewis base F^- is readily displaced by the weak acid HN_3 (5), but the more acidic HF_2^- anion is the final product which, once it has been formed, cannot be displaced anymore by the weak acid HN_3.

(24) Al-Zamil, N. S.; Evans, E. H. M.; Gillard, R. D.; James, D. W.; Jenkins, T. E.; Lancashire, R. J.; Williams, P. A. *Polyhedron* **1982**, *1*, 525.

(25) Rozière, J.; Lehman, M. S.; Potier, J. *Acta Crystallogr.* **1979**, *B35*, 1099.

(26) Rozière, J.; Rozière-Bories, M. T.; Williams, J. M. *Inorg. Chem.* **1976**, *15*, 2490.

(27) Williams, J. M.; Dowling, N.; Gunde, R.; Hadzi, D.; Orel, B. *J. Am. Chem. Soc.* **1976**, *98*, 1581.

(28) Rozière, J.; Berney, C. V. *J. Am. Chem. Soc.* **1976**, *98*, 1582.

(29) Al-Zamil, N.; Delf, B. W.; Gillard, R. D. *J. Inorg. Nucl. Chem.* **1980**, *42*, 1117.

(30) Karelin, A. I.; Grigorovich, Z. I.; Rosolovskii, V. Ya. *Izv. Akad. Nauk. SSSR, Ser. Khim.* **1974**, 1228.

A Quantitative Scale for the Oxidizing Strength of Oxidative Fluorinators[†,‡]

Karl O. Christe[*,§] and David A. Dixon[*,∥]

Contribution from Rocketdyne, A Division of Rockwell International Corporation, Canoga Park, California 91303, and The Central Research and Development Department, E. I. du Pont de Nemours and Company, Inc., Experimental Station, Wilmington, Delaware 19880. Received August 21, 1991

Abstract: A quantitative scale for the oxidizing strength of oxidative fluorinators has been developed for the first time. This scale is based on relative F^+ detachment energies, which were obtained by local density functional calculations, and is anchored to its F^+ zero point by an experimental value for KrF^+. The oxidizing strength of 36 oxidizers was determined in this manner and shown to be consistent with all of the previously available qualitative experiments. An analysis of the trends in the calculated data reveals some expected but also some highly unexpected features. Thus, the oxidizer strength depends not only on the number of fluorine ligands and the oxidation state and electronegativity of the central atom but also on the presence of free valence electron pairs on the central atom and the geometry of the oxidizer. The heats of formation of these oxidizers were also determined from their F^+ detachment energy values.

Introduction

The synthesis of fluorine-containing strong oxidizers generally requires powerful fluorinating agents. In this context, the question as to which agent is most powerful and which agent can oxidize a given substrate frequently arises. The ranking of these fluorinating agents according to their strength is very difficult. Direct electrochemical measurements of their oxidation potentials are not possible because the latter generally exceed the decomposition voltages of the available solvents. Therefore, no oxidizer strength scales exist at the present time, and the only data available are isolated observations[1-4] that some compounds can oxidize certain substrates while others cannot. Frequently, however, a lack of reaction is due to the choice of unfavorable reaction conditions or high activation energies and not necessarily to an insufficient oxidation potential, a thermodynamic measure.

Strong oxidizers can be separated into two main classes. The first one consists of one-electron oxidizers such as PtF_6 or UF_6, and the second one of oxidative fluorinators such as KrF^+, ClF_6^+, or N_2F^+. The case of one-electron oxidizers has previously been analyzed by Bartlett and is best exemplified by his classic example of the reaction of PtF_6 with O_2 (eq 1).[5] The reaction enthalpy,

$$O_2 + PtF_6 \rightarrow O_2^+PtF_6^- \qquad (1)$$

$\Delta H°$, of (1) can be derived from the Born–Haber cycle given in Figure 1, where IP, EA, and U_L stand for the first ionization potential of O_2, the electron affinity of PtF_6, and the lattice energy of solid $O_2^+PtF_6^-$, respectively. Neglecting entropy changes, $\Delta H°$ must be negative for the reaction to occur spontaneously. Since the ionization potentials of the substrates are usually known and the lattice energies of the solid products can be estimated quite accurately, the occurrence or lack of spontaneous reaction with different substrates was used[4] to place upper and lower limits on the electron affinity of the oxidizing species. This method allows one to estimate rough electron affinity values which in turn can be taken as a measure for the oxidizing power of these one-electron oxidizers. Since these electron-transfer reactions do not involve significant activation energies, the "go–no go" reaction approach works rather well.

The case of oxidative fluorinators, such as KrF^+ or N_2F^+, is more complex and has not been analyzed previously. The oxidizer strengths of these species is not a simple function of the electron affinity or ionization potential of the atom or molecule to which the formal "F^+" unit is attached. This was exemplified by a recent qualitative study[1] which showed that N_2F^+ (IP_{N_2} = 360.6 kcal

Figure 1. Born–Haber cycle for a typical one-electron oxidation reaction.

Figure 2. Two Born–Haber cycles which can be used for the description of a typical oxidative fluorination reaction, in this case the oxidative fluorination of Xe by N_2F^+.

mol^{-1})[6] is a weaker oxidative fluorinator than KrF^+ (IP_{Kr} = 324.2 kcal mol^{-1}).[6] Therefore, we have undertaken efforts to analyze this case and to define, if possible, a quantitative oxidizer strength scale.

Results and Discussion

Born–Haber Cycles for Oxidative Fluorination Reactions. The case of oxidative fluorination reactions is more complex than that of one-electron oxidations. In addition to the transfer of a positive charge, an existing bond must be broken and a new one must be formed. Furthermore, the bond breaking can require a substantial

---

(1) Christe, K. O.; Wilson, R. D.; Wilson, W. W.; Bau, R.; Sukumar, S.; Dixon, D. A. *J. Am. Chem. Soc.* **1991**, *113*, 3795.

(2) Christe, K. O.; Wilson, W. W.; Wilson, R. D. *Inorg. Chem.* **1984**, *23*, 2058.

(3) Sokolov, V. B.; Dobrychevskii, Yu. V.; Prusakov, V. N.; Ryzhkov, A. V.; Koroshev, S. S. *Dokl. Akad. Nauk SSSR* **1976**, *229*, 641.

(4) Bartlett, N. *Angew. Chem., Int. Ed. Engl.* **1968**, *7*, 433.

(5) Barlett, N.; Lohmann, D. H. *Proc. Chem. Soc.* **1962**, 277; *J. Chem. Soc.* **1962**, 5253.

(6) Wagman, D. D.; Evans, W. H.; Parker, V. B.; Schuman, R. H.; Halow, I.; Bailey, S. M.; Churney, K. A.; Nuttall, R. L. *J. Phys. Chem. Ref. Data* **1982**, *11*, (Suppl. 2).

[†] Dedicated to Prof. Neil Bartlett on the occasion of his sixtieth birthday.
[‡] Du Pont Contribution No. 5889.
[§] Rocketdyne.
[∥] Du Pont.

activation energy and, therefore, complicates experiments aimed at the determination of relative oxidizer strengths based on the observation or lack of observation of a reaction.

Consider the reaction between N_2F^+ and Xe in HF solution[1] as a typical example of an oxidative fluorination reaction. Assuming that the solvation energies of N_2F^+ and Xe are about the same as those of XeF^+ and N_2, this reaction can be expressed by eq 2. Figure 2 shows two Born–Haber cycles, (2a) and (2b), which can be used to describe reaction 2.

As in the case of the one-electron oxidations, $\Delta H°$ must be negative for a spontaneous reaction and, for the cycles 2a and 2b, is given by eq 3a and 3b, respectively, where FPA is the F^+ affinity

$$\Delta H° = FPA(subst) - FPA(oxid - F^+) \qquad (3a)$$

$$\Delta H° = IP(substr) - IP(oxid - F^+) + D_0(oxid) - D_0(prod) \qquad (3b)$$

($=\Delta H$ of the reaction $A + F^+ \rightarrow AF^+$), FPD is the F^+ detachment energy, IP is the first adiabatic ionization potential, D_0 is the bond dissociation energy, and EA is the electron affinity. Until now, neither cycle 2a nor 2b had been used for the determination of $\Delta H°$ values since the F^+ affinities and bond dissociation energies were generally unknown.

Calculations. If one considers reaction 2 as the transfer of F^+ from one compound to another, it is very similar to the transfer of a proton from one base to another (reaction 4). Such pro-

$$N_2H^+_{(g)} + Xe_{(g)} \rightarrow XeH^+_{(g)} + N_{2(g)} \qquad (4)$$

ton-transfer reactions can be calculated quite accurately by molecular orbital methods for both relative values and absolute values.[7] The agreement with experiment for proton-transfer processes is usually excellent if one employs good geometries and if adequate basis sets with some consideration of the correlation energy are included in the calculations. Absolute values can be obtained with somewhat larger basis sets.

Such a theoretical model could also be employed for the calculation of relative FPAs. However, most of the compounds under consideration as strong oxidants contain atoms predominantly from the right-hand side of the periodic table, and contrary to H^+, F^+ has a significant number of electrons. Thus, some method is needed which, even for describing the geometries, includes correlation effects. Since there are a significant number of compounds, all of which need to have their geometries optimized, one also requires a computationally efficient method. Rather than using traditional Hartree–Fock methods (scaling as N^4 with N as the number of basis functions) including correlation corrections (scaling as N^m, $m \geq 5$), we chose the local density functional (LDF) method (scaling as N^3).[8]

The calculation of absolute proton affinities by theoretical methods is simplified because the dissociation of BH^+ results in two closed-shell species, B and H^+, where B and BH^+ have the same number of electron pairs. However, the calculation of absolute F^+ affinities is complicated because (i) the generated F^+ is not a closed-shell singlet but a ground-state triplet[9] and (2)

the number of electron pairs is different in B and BF^+. It is also well-established that the LDF method overestimates binding energies. Thus, instead of calculating absolute FPAs, we have calculated relative FPAs.

The LDF method is based on the Hohenberg–Kohn theorem,[10] which states that the total energy E_t is a functional of the charge density ρ as follows:

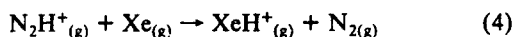$$E_t[\rho] = T[\rho] + U[\rho] + E_{xc}[\rho] \qquad (5)$$

where T is the kinetic energy of the noninteracting electrons of density ρ, U is the classical Coulomb electrostatic energy, and E_{xc} includes all of the many-body contributions to the energy. The first two terms can be evaluated using straightforward techniques. The most important contributions to E_{xc} are the exchange energy and the correlation energy, and it is in the final term where the local density approximation is introduced. A good approximation for the final term is derived from the exchange–correlation energy of the uniform electron gas by following the assumption that the charge density varies slowly on the scale of exchange and correlation effects. The form of the exchange–correlation energy employed in our calculations is that of von Barth and Hedin.[11]

The calculations were done with the program DMol[12] on a CRAY-YMP computer system. DMol employs numerical functions for the atomic basis sets. These atomic basis sets are exact spherical solutions to the density functional equations. All of the calculations were done with a double numerical basis set augmented by d ($l = 2$) polarization functions. Because exact numerical solutions are employed, the basis set is of higher quality than a normal molecular orbital basis set of the same size. Furthermore, basis set superposition errors should be minimized because of the quality of the basis set.

The various integrals required for the solution of eq 5 need to be evaluated on a grid due to our use of numerical basis functions.[13] The number of radial points is given by

$$N_R = (1.2)14(Z + 2)^{1/3} \qquad (6)$$

where Z is the atomic number and the maximum distance for any function is 12 au. The angular integration points N_O are generated at the N_R radial points to form shells around each nucleus with N_O ranging from 14 to 302 depending on the density. Fitting functions for the spherical harmonics were all done with an angular momentum number $\ell' = \ell + 1 = 3$.

Geometries were optimized by using analytic gradient methods.[14,15] Because numerical methods are used, the error in atomic coordinates determined by the optimization is on the order of 0.001 Å, which gives bond lengths and angles with errors at least 1 order of magnitude smaller than the differences between calculated and experimental values. The spin state of each structure is a singlet except for those of O_2 and F^+, which are triplets.

Oxidizer Strength Scale. Although a knowledge of the relative FPAs allows the prediction of whether a certain reaction is thermodynamically feasible and which oxidizer is stronger with respect to another one, it provides only a relative oxidizer strength scale. To obtain an absolute scale, one must identify the thermodynamic property governing the oxidizer strength, define a zero point for the scale, and then anchor the relative oxidizer strength values derived from the LDF calculations to the chosen zero point by an experimentally known number since LDF theory overes-

(7) Dixon, D. A.; Lias, S. G. In *Molecular Structures and Energies*; Liebman, J. F., Greenberg, A., Eds.; VCH Publishers: Deerfield Beach, FL, 1987; Vol. 2, Chapter 7, p 269.

(8) (a) Parr, R. G.; Yang, W. *Density Functional Theory of Atoms and Molecules*; Oxford University Press: New York, 1989. (b) Salahub, D. R. In *Ab Initio Methods in Quantum Chemistry*; Lawlwy, K. P., Ed.; J. Wiley and Sons: New York, 1987; Vol. II. (c) Wimmer, E.; Freeman, A. J.; Fu, C. L.; Cao, P. L.; Chou, S. H.; Delley, B. In *Supercomputer Research in Chemistry and Chemical Engineering*; Jensen, K. F., Truhlar, D. G., Eds.; ACS Symposium Series 353; American Chemical Society: Washington, DC, 1987; p 49. (d) Jones, R. O.; Gunnarsson, O. *Rev. Mod. Phys.* **1989**, *61*, 689. (e) Dixon, D. A.; Andzelm, J.; Fitzgerald, G.; Wimmer, E.; Delley, B. *Science and Engineering on Supercomputers*; Pitcher, E. J., Ed.; Computational Mechanics Publications: Southampton, England, 1990; p 285. (f) Dixon, D. A.; Andzelm, J.; Fitzgerald, G.; Wimmer, E.; Jasien, P. In *Density Functional Methods in Chemistry*; Labanowski, J. K., Andzelm, J., Eds.; Springer-Verlag: New York, 1991; Chapter 3, p 33.

(9) Calculations of the F^+ cation affinities of some simple organic bases have recently been reported. These ab initio molecular orbital calculations were done at the STO-3G(*PS) level and the reported affinities are for an excited state of $F^+(^1S)$: Alcami, O.; Yáñez, M.; Abboud, J.-L. M. *J. Phys. Org. Chem.* **1991**, *4*, 177.

(10) Hohenberg, P.; Kohn, W. *Phys. Rev. B* **1964**, *136*, 184.

(11) von Barth, U.; Hedin, L. *Physica C* **1972**, *5*, 1629.

(12) Delley, B. *J. Chem. Phys.* **1990**, *92*, 508. Dmol is available commercially from Biosym Technologies, San Diego, CA.

(13) This grid can be obtained by using the FINE parameter in DMol.

(14) For a discussion of Hartree–Fock methods, see: (a) Komornicki, A.; Ishida, K.; Morokuma, K.; Ditchfield, R.; Conrad, M. *Chem. Phys. Lett.* **1977**, *45*, 595. (b) Pulay, P. In *Applications of Electronic Structure Theory*; Schaefer, H. F., III, Ed.; Plenum Press: New York, 1977; p 153. (c) Jorgensen, P.; Simons, J., Eds. *Geometrical Derivatives of Energy Surfaces and Molecular Properties*; *NATO ASI Ser. C* **1986**, *166*, 207.

(15) (a) Delley, B. In *Density Functional Methods in Chemistry*; Labanowski, J. K., Andzelm, J. W., Eds.; Springer-Verlag: New York, 1991; Chapter 11, p 101. (b) Fournier, R.; Andzelm, J.; Salahub, D. R. *J. Chem. Phys.* **1989**, *90*, 6371. (c) Versluis, I.; Ziegler, T. *J. Chem. Phys.* **1988**, *88*, 3322.
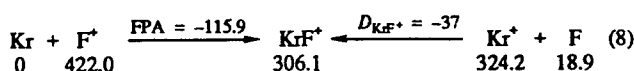
timates absolute binding energies.

According to the Born–Haber cycle 2a and eq 3a, the reaction enthalpy $\Delta H°$ equals the difference between the F^+ affinities of the substrate and of the oxidizer minus F^+. Hence, F^+ affinities are a useful criterion for an oxidizer strength scale. Since the F^+ affinity (FPA) of a substrate equals the negative value of the F^+ detachment energy (FPD) of the corresponding product, eq 3a can be rewritten as eq 7, and an oxidative fluorination reaction

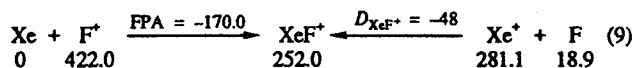$$\Delta H° = \text{FPD(oxid)} - \text{FPD(prod)} \qquad (7)$$

can be considered as the formal transfer of an F^+ cation from an oxidizer to a substrate. Since the F^+ detachment energy for F^+ itself obviously is zero, F^+ is the ideal zero point for an oxidizer strength scale based on F^+ detachment energies. On this scale, then, increasing FPD values signify decreasing oxidizer strength.

The third objective, i.e., the anchoring of the relative FPD values to the F^+ zero point, was accomplished by calculating the F^+ affinity of Kr from experimental data. From the known heat of formation of KrF_2, the appearance potential of KrF^+ from KrF_2, and the first adiabatic ionization potential of Kr, the bond energy and heat of formation of gaseous KrF^+ have been estimated[16] to be 37 and 306.1 kcal mol^{-1}, respectively, as shown by the right half of eq 8. [Numbers beneath the equations are $\Delta H_f°$ (kcal
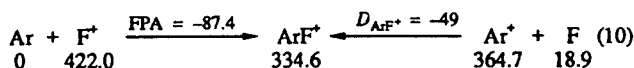
$$\begin{array}{ccccc}
\text{Kr} & + & \text{F}^+ & \xrightarrow{\text{FPA} = -115.9} & \text{KrF}^+ & \xleftarrow{D_{\text{KrF}^+} = -37} & \text{Kr}^+ & + & \text{F} \qquad (8) \\
0 & & 422.0 & & 306.1 & & 324.2 & & 18.9
\end{array}$$

mol^{-1}).] From the known heats of formation of gaseous KrF^+ and F^+,[6] the F^+ affinity of Kr can then be estimated as -115.9 kcal mol^{-1}, as shown by the left half of (8). The combination of this experimentally derived value with the F^+ affinity differences obtained by our LDF calculations permits the construction of the absolute oxidizer strength scale given in Table I.

The quality of the values in Table I was cross-checked for XeF^+. Using the previously published experimental data,[16] the FPD of XeF^+ was estimated (9) as 170.0 kcal mol^{-1}, in fair agreement with our computed value of 164.8 kcal mol^{-1} given in Table I.

$$\begin{array}{ccccc}
\text{Xe} & + & \text{F}^+ & \xrightarrow{\text{FPA} = -170.0} & \text{XeF}^+ & \xleftarrow{D_{\text{XeF}^+} = -48} & \text{Xe}^+ & + & \text{F} \qquad (9) \\
0 & & 422.0 & & 252.0 & & 281.1 & & 18.9
\end{array}$$

An additional cross-check was made for the yet unknown ArF^+ cation for which recent ab initio calculations[17] have yielded an Ar–F bond energy value of 49 ± 3 kcal mol^{-1}. Using this value, the F^+ affinity of Ar can be estimated as -87.4 kcal mol^{-1} (10) which is in good agreement with our FPD value of 84.3 kcal mol^{-1} from Table I.

$$\begin{array}{ccccc}
\text{Ar} & + & \text{F}^+ & \xrightarrow{\text{FPA} = -87.4} & \text{ArF}^+ & \xleftarrow{D_{\text{ArF}^+} = -49} & \text{Ar}^+ & + & \text{F} \qquad (10) \\
0 & & 422.0 & & 334.6 & & 364.7 & & 18.9
\end{array}$$

Heats of Formation of the Oxidizers. The knowledge of the F^+ detachment energies of the oxidizers (see Table I) also provides a convenient source for their heats of formation $\Delta H_f°$. The latter are given by eq 11, where $\Delta H_f°_{(F^+_g)}$ equals 422.0 kcal mol^{-1};

$$\Delta H_f°_{(XF^+_g)} = \Delta H_f°_{(X_g)} + \Delta H_f°_{(F^+_g)} - \text{FPD}_{(XF^+_g)} \qquad (11)$$

$\Delta H_f°_{(X_g)}$, the heat of formation of the parent molecule, is usually known, and the FPD values are taken from Table I. The resulting $\Delta H_f°_{(XF^+_g)}$ values have been included in Table I. Only few experimental estimates are available for these formation enthalpies. For example, the value of 204 kcal mol^{-1} previously reported[18] for $\Delta H_f°_{(NF_4^+_g)}$ is in fair agreement with our value of 210 kcal mol^{-1} given in Table I.

Characteristics of the Oxidizer Strength Scale. The following comments can be made about the data given in Table I.

(16) Bartlett, N.; Sladky, F. In *Comprehensive Inorganic Chemistry*; Pergamon Press: Oxford, UK, 1973; Vol. 1, pp 213–330. The appearance potentials are from J. Berkowitz, unpublished work.
(17) Frenking, G.; Koch, W.; Deakyne, C. A.; Liebman, J. F.; Bartlett, N. *J. Am. Chem. Soc.* 1989, *111*, 31.
(18) Goetschel, C. J.; Campanile, V. A.; Curtis, R. M.; Loos, K. R.; Wagner, D. C.; Wilson, J. N. *Inorg. Chem.* 1972, *11*, 1696.

Table I. Absolute Oxidizer Strength Scale and Formation Enthalpies for Oxidative Fluorinators

oxidative fluorinator[a] XF^+	F^+ detachment energy (kcal mol^{-1})[b] FPD(XF_g^+)	formation enthalpy[c] (kcal mol^{-1}) $\Delta H_f°(XF_g^+)$	ref for $\Delta H_f°(X)$
(HeF^+) $(^3\pi)$	-1.6	423.6	6
(HeF^+) $(^1\Sigma^+)$	(-16.2)	(438.2)	6
(F^+)	0	422.0	6
(NeF^+) $(^3\pi)$	0.6	421.4	6
(NeF^+) $(^1\Sigma^-)$	(-19.6)	(441.6)	6
(F_3^+)	60.0	362.0	6
(ArF^+)	84.3	337.7	6
KrF^+	115.9	306.1	6
(XeF_7^+)	116.7	222.2	15
(OF_3^+)	122.2	305.7	6
(BrF_4O^+)	131.1		
(O_2F^+)[f]	133.8	288.2	6
(ClF_4O^+)	135.6	251.0	d
N_2F^+	139.3	282.7	6
(XeF_5O^+)	139.8	276.2	e
BrF_6^+	140.8	178.7	6
$(XeF_3O_2^+)$	141.7	336.3	16
ClF_6^+	147.3	215.5	d
XeF_3^+	152.4	243.7	15
ClF_4^+	158.7	224.3	6
XeF_5^+	158.9	200.6	6
$ClF_2O_2^+$	161.0	228.4	d
(IF_4O^+)	164.0		
XeF^+	164.8	257.2	6
ClF_2^+	167.1	241.9	6
XeF_3O^+	173.1		
BrF_4^+	174.0	187.0	6
IF_6^+	175.0	40.4	6
NF_2O^+	175.3	230.8	6
Cl_2F^+	179.1	242.9	6
NF_4^+	180.1	210.5	6
$(XeFO^+)$	182.4	290.1	16
BrF_2^+	182.4	217.2	6
ClF_2O^+	193.0		
$XeFO_2^+$	195.3		
BrF_2O^+	200.5		
IF_4^+	212.1	93.9	15
IF_2^+	213.5	185.7	6
(IF_2O^+)	230.0		

[a] The cations listed in parentheses have so far not been isolated in the form of stable salts. [b] All FPD values were computed for XF^+ and X being singlet ground states and F^+ being a triplet ground state, except for HeF^+ and NeF^+, which have triplet ground states (see text) and O_2F^+ (see footnote f). [c] Calculated by eq 7, using $\Delta H_f°(X)$ values from refs 6 and 15c,d. [d] Barberi, P.; Carre, J.; Rigny, P. *J. Fluorine Chem.* 1976, *7*, 511. [e] Gunn, S. R. *J. Am. Chem. Soc.* 1965, *87*, 2290. [f] Calculated for the singlet state of O_2F^+ going to the triplet state of O_2.

(i) F^+ detachment energies are a good measure for the oxidizing power of an oxidative fluorinator. The oxidizing power of a compound decreases with an increase in its F^+ detachment energy.

(ii) A negative value for the F^+ detachment energy of an XF^+ species signifies a species that is unstable with respect to decomposition to ground-state $X(^1S)$ and $F^+(^3P)$. The negative F^+ detachment energy values for NeF^+ and HeF^+, listed in parentheses in Table I, are due to the fact that for all of our calculations the following spin states were used (12).

$$XeF^+(^1\Sigma^+) \xrightarrow{\text{FPD}} X(^1S) + F^+(^3P) \qquad (12)$$

Whereas for XeF^+, KrF^+, and ArF^+ a $^1\Sigma^+$ state is the ground state; NeF^+ and HeF^+ have a $^3\pi$ ground state. Their $^1\Sigma^+$ states are excited states which are calculated to lie 30.3 and 23.8 kcal mol^{-1}, respectively, above their ground states.[17] If for NeF^+ and HeF^+ the FPDs are computed for their $^3\pi$ ground states (13)

$$XF^+(^3\pi) \rightarrow X(^1S) + F^+(^3P) \qquad (13)$$

slightly positive values of about 4.0 and 1.2 kcal mol^{-1}, respectively, are obtained. This was shown by recent high-level ab initio

Table II. Relative Oxidizer Strengths (FPD Values)[a] of the Electronically Isovalent Series of Tetrahedral and Pseudotetrahedral Binary Fluoride Cations

group in periodic system	V A	VI A	VII A	VIII A
formal oxidation state of central atom	+V	+IV	+III	+II

[a] Numbers below each structure are calculated values (kcal mol⁻¹).

calculations[17,19] which suggest that in their ground states these cations are only weakly bound.

(iii) Except for NeF⁺ and HeF⁺, the F⁺ detachment energies listed in Table I do not represent the X–F bond dissociation energies, D_0. Since usually the first ionization potential of X is lower than that of the F atom (422 kcal mol⁻¹),[6] the lowest energy bond dissociation process becomes the one which yields X⁺ and F atoms (14).

$$XF^+(^1\Sigma^+) \xrightarrow{\ D_0\ } X^+(^2P) + F(^2P) \qquad (14)$$
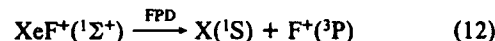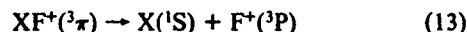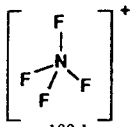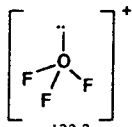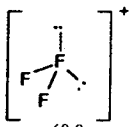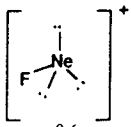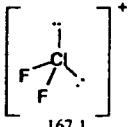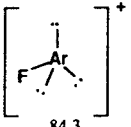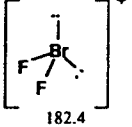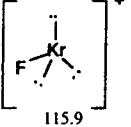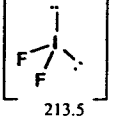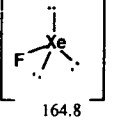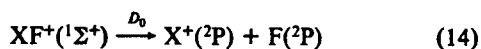
(iv) The previously reached[2] conclusion that KrF⁺ is the strongest presently known oxidative fluorinator was confirmed.

(v) The oxidative fluorination reactions can be considered as a formal transfer of F⁺ from the oxidizer to a substrate and involve the breaking of an existing and the formation of a new bond. Even when proceeding through a probable intermediate activated complex, as shown by eq 15 for the Xe + N₂F⁺ reaction, such
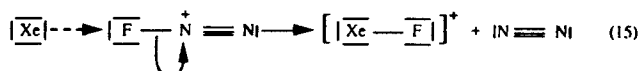
a reaction could require a substantial activation energy. Hence, it is not surprising that some of the reactions, deemed possible from the rankings in Table I, have so far experimentally not been observed. Of the previously observed oxidative fluorination reactions,[1-3,20-27] none violates the rankings given in Table I, thus supporting our results. The only somewhat ambiguous case is a previous report[27] which indicated that Cl₂F⁺AsF₆⁻ oxidized Xe

to Xe₂F₃⁺. Although Table I implies that Cl₂F⁺ is not capable of oxidizing Xe to XeF⁺, this does not allow any conclusions concerning the oxidation of Xe to Xe₂F₃⁺. Because Xe₂F₃⁺ contains an extra XeF₂ molecule and, generally, the oxidizing power of a species decreases with decreasing positive charge, Xe₂F₃⁺ is a weaker oxidizer than XeF⁺ and probably also Cl₂F⁺.

(vi) Among the yet unknown oxidizers which are listed in Table I and rank in oxidizing power below KrF⁺ are XeF₅O⁺ and ClF₄O⁺. Previous attempts to oxidatively fluorinate XeF₄O[24,25,28] or ClF₃O[29] have always resulted in oxidation of the oxygen ligand, i.e., O₂ evolution, instead of XeF₅O⁺ or ClF₄O⁺ formation, respectively. These results indicate that in the case of high-oxidation-state oxyfluorides, the oxygen ligand might become easier to oxidize than the central atom, thus foiling attempts aimed at their oxidative fluorination.

General Trends of Oxidizer Strength within the Periodic System. A systematic analysis of the data of Table I indicates the following general trends, some of which are quite obvious and fully expected but others are rather surprising.

I. Binary Fluorides. (i) Within a group of electronically isovalent[30] species, such as the series of tetrahedral and pseudotetrahedral cations shown in Table II, the oxidizing power increases on going from the left to the right and from the bottom to the top of the periodic table. Thus, NeF⁺ is the strongest oxidative fluorinator within this group, and the electronegativity of the central atom appears to be more important than its formal oxidation state, i.e., the number of fluorine ligands. The only minor exception to the above rule is BrF₆⁺ which, by analogy with the known BrO₄⁻–ClO₄⁻ case,[31] is a slightly stronger oxidative fluorinator than ClF₆⁺.

(ii) For a given central atom, the oxidizing power generally increases with an increase in its formal oxidation state, as shown in Tables III and IV. For chlorine as a central atom, the oxidizing power increases from ClF₂⁺ to ClF₄⁺ to ClF₆⁺ by roughly equal amounts. Going to the heavier central atoms, bromine and iodine, the oxidizer strength gaps between XF₂⁺ and XF₄⁺ become increasingly smaller and those from XF₄⁺ to XF₆⁺ become increasing

(19) (a) Frenking, G.; Koch, W.; Cremer, D.; Gauss, J.; Liebman, J. F. *J. Phys. Chem.* **1989**, *93*, 3397, 3410. (b) Deakyne, C. A.; Liebman, J. F.; Frenking, G.; Koch, W. *J. Phys. Chem.* **1990**, *94*, 2306.

(20) Gillespie, R. J.; Schrobilgen, G. J. *J. Chem. Soc.* **1974**, *13*, 1230.

(21) Artyukhov, A. A.; Khoroshev, S. S. *Koord. Khim.* **1977**, *3*, 1478.

(22) Christe, K. O.; Wilson, W. W.; Curtis, E. C. *Inorg. Chem.* **1983**, *22*, 3056.

(23) Stein, L. *Chemistry* **1974**, *47*, 15.

(24) McKee, D. E.; Adams, C. J.; Zalkin, A.; Bartlett, N. *J. Chem. Soc., Chem. Commun.* **1973**, 26.

(25) Holloway, J. H.; Schrobilgen, G. J. *J. Chem. Soc., Chem. Commun.* **1975**, 623.

(26) Meinert, H.; Gross, U. *Z. Chem.* **1968**, *8*, 345.

(27) Christe, K. O.; Wilson, R. D. *Inorg. Nucl. Chem. Lett.* **1973**, *9*, 845.

(28) Christe, K. O.; Wilson, R. D. *J. Fluorine Chem.* **1976**, *7*, 356.

(29) Christe, K. O.; Wilson, W. W.; Wilson, R. D., unpublished results.

(30) Haas, A. *Adv. Inorg. Chem. Radiochem.* **1984**, *28*, 167.

(31) Greenwood, N. N.; Earnshaw, A. In *Chemistry of the Elements*; Pergamon Press: Oxford, UK, 1984; p 1020.

Table III. Relative Oxidizer Strengths (FPD Values) of the Binary Halogen Fluoride Cations as a Function of the Formal Oxidation State of the Central Atom

formal oxidn state of central atom	structure of cation	calcd FPD values (kcal/mol)		
+VII	$[F_5X{\cdot}F]^+$	ClF_6^+ 147.3	BrF_6^+ 141.7	IF_6^+ 175.0
+V	$[XF_4]^+$	ClF_4^+ 158.7	BrF_4^+ 174.0	IF_4^+ 212.1
+III	$[XF_2]^+$	ClF_2^+ 167.1	BrF_2^+ 182.4	IF_2^+ 213.5

Table IV. Relative Oxidizer Strengths (FPD Values) of the Binary Xenon Fluoride Cations as a Function of the Formal Oxidation State of the Xenon Central Atom

formal oxidn state of Xe	structure of the cation	calcd FPD value (kcal/mol)
+VIII	$[XeF_7]^+$	116.7
+VI	$[XeF_5]^+$	158.9
+IV	$[XeF_3]^+$	152.4
+II	$[XeF]^+$	164.8
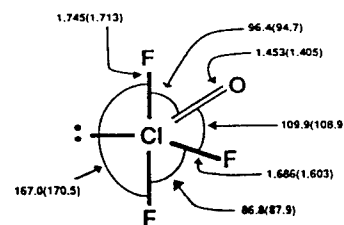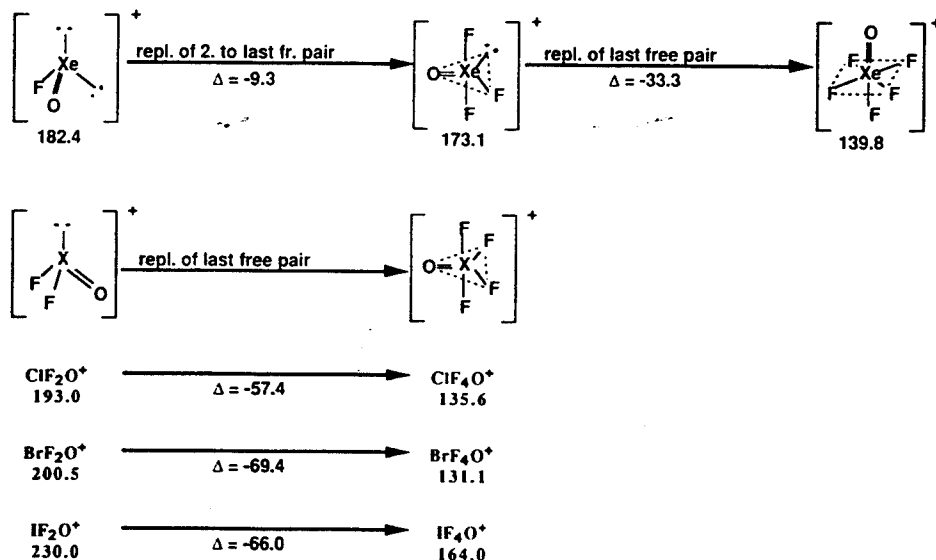
Figure 3. Geometry of ClF_3O (bond lengths in angstroms, angles in degrees) as calculated by the LDF method. The experimentally observed[32] values are given in parentheses.

Bond lengths: 1.745(1.713), 1.453(1.405), 1.686(1.603). Angles: 96.4(94.7), 109.9(108.9), 86.3(87.9), 167.0(170.5).

larger (see Table III). For the xenon fluorides (see Table IV), a similar trend is observed. The FPD gap between XeF^+ and XeF_5^+ is only 5.9 kcal mol^{-1} whereas that between XeF_5^+ and XeF_7^+ is 42.3 kcal mol^{-1}.

These features are best explained by the increased mobility of the free valence electron pair on the central atom with increasing atomic weight and by the replacement of the last free valence electron pair by two fluorine ligands, which causes a large decrease in the fluorine plus detachment (FPD) energy values. It is very plausible that the availability of a highly mobile free valence electron pair should counteract the removal of an electron-deficient F^+ cation from these species, thereby increasing the FPD values.

There appears to be a considerably weaker secondary effect, which is also apparent from the oxyfluoride cations (see below). Trigonal-bipyramidal species seem to exhibit slightly lower FPD values than the energetically more favored pseudotetrahedral or pseudooctahedral species. This causes the FPD value of XeF_3^+ to be slightly lower than those of XeF^+ and XeF_5^+ (see Table IV) and also accounts for the very small difference of 1.4 kcal mol^{-1} between IF_2^+ and IF_4^+.

The low FPD value of XeF_7^+, which is almost identical to that of KrF^+ (see Table I), also explains the failure of our previous attempts[29] to prepare the yet unknown XeF_7^+ cation from XeF_6 and KrF^+.

II. Oxyfluorides. The case of oxyfluorides is not quite as transparent as that of the binary fluorides. A priori, one might have predicted that the replacement of one free valence electron pair on a central atom by one doubly bonded oxygen ligand should increase the oxidizing power and decrease the FPD value of an oxidizer, albeit not by as much as that observed for the replacement of one free pair by two fluorine ligands. Inspection of Table I clearly shows that this is not the case. For example, the oxidizing strength of ClF_2O^+ is 25.9 kcal mol^{-1} lower than that of ClF_2^+ while that of ClF_4O^+ is 23.1 kcal mol^{-1} higher than that of ClF_4^+.

Table V. Relative Oxidizer Strengths (FPD Values) of Oxyfluorides Resulting from the Stepwise Replacement of Free Valence Electron Pairs by Two Fluorine Atoms (i.e., Oxidative Fluorination Reactions)

$[XeF_2O]^+$ 182.4 → (repl. of 2. to last fr. pair, $\Delta = -9.3$) → $[XeF_3O]^+$ 173.1 → (repl. of last free pair, $\Delta = -33.3$) → $[XeF_4O]^+$ 139.8

$[XF_2O]^+$ → (repl. of last free pair) → $[XF_4O]^+$

ClF_2O^+ 193.0	$\Delta = -57.4$	ClF_4O^+ 135.6
BrF_2O^+ 200.5	$\Delta = -69.4$	BrF_4O^+ 131.1
IF_2O^+ 230.0	$\Delta = -66.0$	IF_4O^+ 164.0

Oxidizing Strength of Oxidative Fluorinators

J. Am. Chem. Soc., Vol. 114, No. 8, 1992 2983

Table VI. Relative Oxidizer Strengths (FPD Values) of Oxyfluorides Resulting from the Stepwise Replacement of Free Valence Electron Pairs by One Doubly Bonded Oxygen Atom (i.e., Oxidative Oxygenation Reactions)
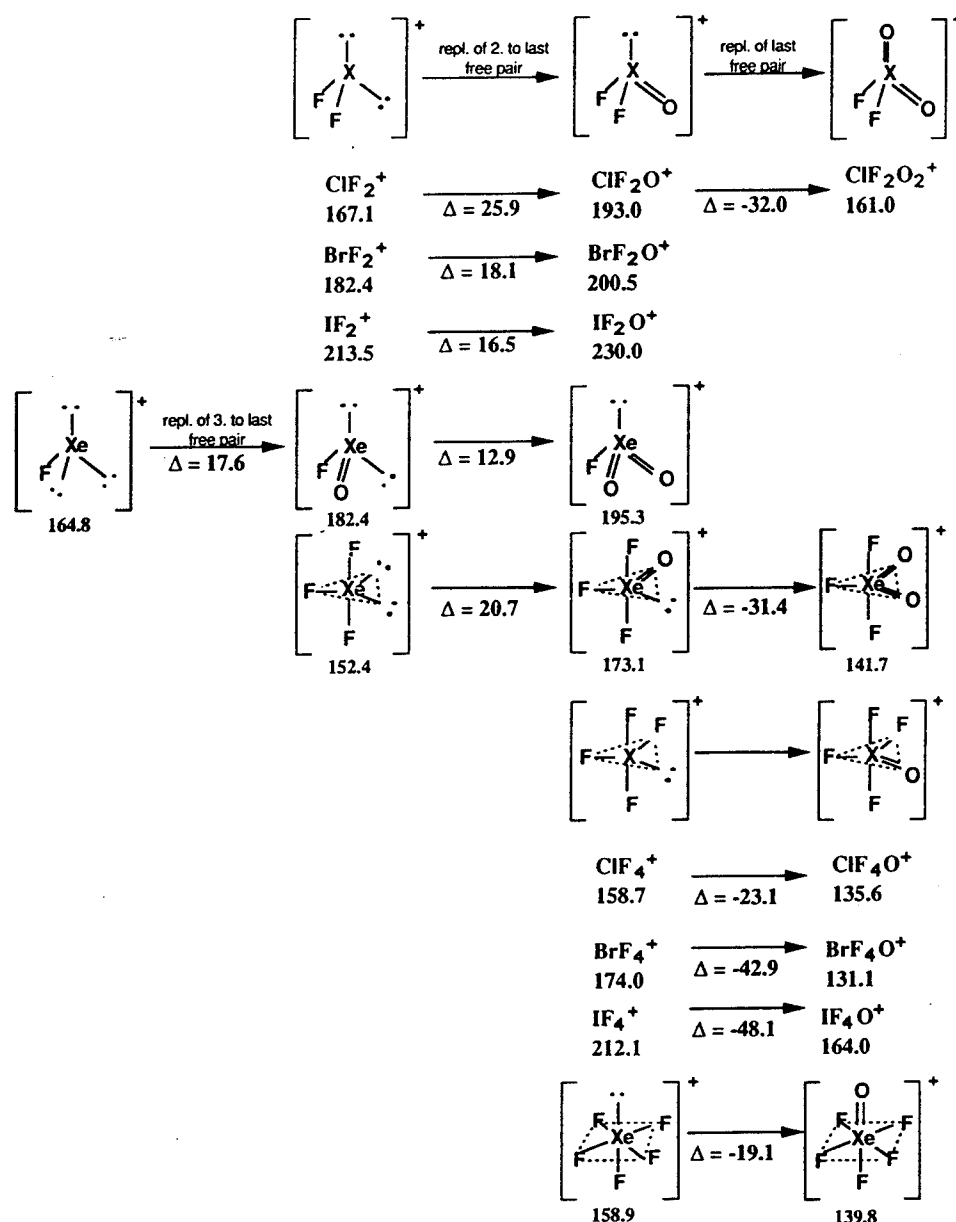
To verify that these results were not caused by computational problems, the geometry of the ClF_3O molecule was computed and compared to that experimentally determined.[32] As can be seen from Figure 3, the agreement between the calculated and experimental geometry was good, particularly when one remembers that the bond lengths calculated by the LDF method are generally about 0.05 Å longer than the observed valued for these types of compounds.[33] Similarly, the geometry calculated for ClF_4O^+ is very similar to that previously determined[34] for isoelectronic SF_4O (see Figure 4). Therefore, the LDF method results are deemed reliable for this type of compounds.
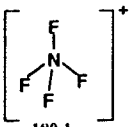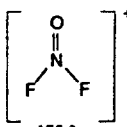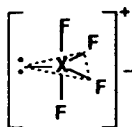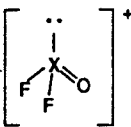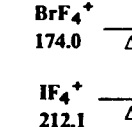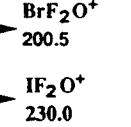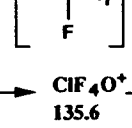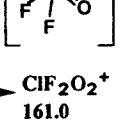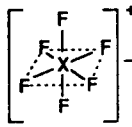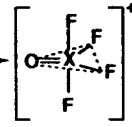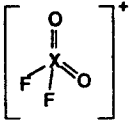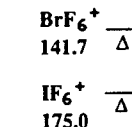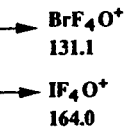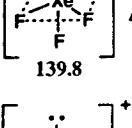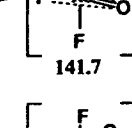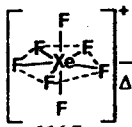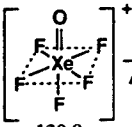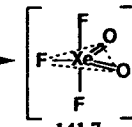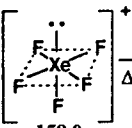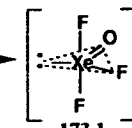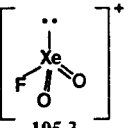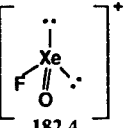
In spite of the seeming lack of an obvious general trend to the FPD values of the oxyfluorides of Table I, a closer inspection reveals that the data are indeed self-consistent and exhibit systematic trends. These become obvious from an analysis of how the FPD values vary with the following three processes.

(32) Oberhammer, H.; Christe, K. O. *Inorg. Chem.* **1982**, *21*, 273.

(33) Christe, K. O.; Curtis, E. C.; Dixon, D. A.; Mercier, H. P.; Sanders, J. C. P.; Schrobilgen, G. J. *J. Am. Chem. Soc.* **1991**, *113*, 3351.

(34) (a) Gundersen, G.; Hedberg, K. *J. Chem. Phys.* **1969**, *51*, 2500. (b) Hargittai, I. *J. Mol. Struct.* **1979**, *56*, 301. (c) Oberhammer, H.; Boggs, J. E. *J. Mol. Struct.* **1979**, *56*, 107.
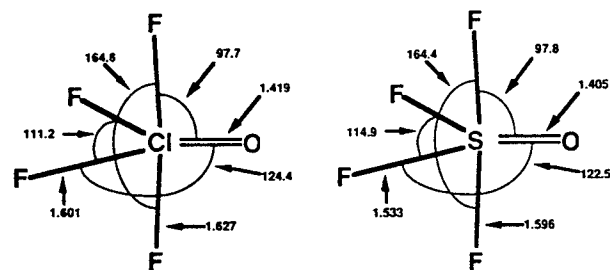
Figure 4. Calculated geometry of ClF_4O^+ compared to that experimentally determined[34] for isoelectronic SF_4O.

(i) Stepwise Replacement of Free Valence Electron Pairs on the Central Atom by Fluorine Ligands (i.e., Oxidative Fluorination Reactions). When a sterically active free valence electron pair is replaced by two fluorine ligands, the coordination number and the formal oxidation state of the central atom are increased by one and two units, respectively; i.e., we are dealing with an oxidative fluorination reaction. As can be seen from the examples given in Table V, and also from those given for oxidative oxygenation reactions (Table VI), the replacement of the last free valence electron pair results in a much larger increase in the

Table VII. Relative Oxidizer Strengths (FPD Values) of Oxyfluorides Resulting from the Stepwise Replacement of Two Fluorine Ligands by a Doubly Bonded Oxygen Ligand (i.e., Fluorine–Oxygen Exchange Reactions)

pentagonal bipyramid	octahedron	trigonal bipyramid	tetrahedron	trigonal plane

NF_4^+ 180.1 $\xrightarrow{\Delta = -4.8}$ NOF_2^+ 175.3

ClF_4^+ 158.7 $\xrightarrow{\Delta = 34.3}$ ClF_2O^+ 193.0

BrF_4^+ 174.0 $\xrightarrow{\Delta = 26.5}$ BrF_2O^+ 200.5

IF_4^+ 212.1 $\xrightarrow{\Delta = 17.9}$ IF_2O^+ 230.0

ClF_6^+ 147.3 $\xrightarrow{\Delta = -11.7}$ ClF_4O^+ 135.6 $\xrightarrow{\Delta = 25.4}$ $ClF_2O_2^+$ 161.0

BrF_6^+ 141.7 $\xrightarrow{\Delta = -10.6}$ BrF_4O^+ 131.1

IF_6^+ 175.0 $\xrightarrow{\Delta = -11.0}$ IF_4O^+ 164.0

116.7 $\xrightarrow{\Delta = 23.1}$ 139.8 $\xrightarrow{\Delta = 1.9}$ 141.7

158.9 $\xrightarrow{\Delta = 14.2}$ 173.1 $\xrightarrow{\Delta = 22.2}$ 195.3

152.4 $\xrightarrow{\Delta = 30.0}$ 182.4

oxidizer strength of the product than the replacement of any of the other free pairs. As for the binary fluoride cations (see above), the FPD values increase for isotypic cations with increasing atomic weight of the central atom. Again, the only exception is Br(+VII), which is a slightly stronger oxidizer than Cl(+VII).[31]

(ii) **Stepwise Replacement of Free Valence Electron Pairs on the Central Atom by Oxygen Ligands (i.e., Oxidative Oxygenation Reactions).** Although, in oxidative oxygenation reactions, the replacement of a free valence electron pair by a doubly bonded oxygen ligand increases again the formal oxidation state of the central atom by two, its coordination number remains unchanged. As observed above for the oxidative fluorination reactions, the most salient feature is again the large decrease in the FPD value on replacement of the last free valence electron pair. For the replacement of any of the other pairs, the FPD values of all our examples actually increase; i.e., in these cases oxidative oxygen-

ation results in a weaker oxidizer. This is a highly remarkable and unexpected result. The only previous indication for the existence of such an effect was based on normal coordinate analyses for some of these ions, which showed that, for XF_nO_m-type compounds, frequently the X–F force constants decreased with oxidative oxygenation.[35] In these compounds, a weakening of the force constant implies an increase of the $X^{(\delta+)} - F^{(\delta-)}$ polarity of the X–F bond which counteracts the F-plus dissociation (FPD), thereby increasing the FPD value and decreasing the oxidizer strength of the species.

(iii) **Stepwise Replacement of Two Fluorine Ligands by a Doubly Bonded Oxygen Ligand (i.e., Fluorine–Oxygen Exchange Reactions).** In fluorine–oxygen exchange reactions, two singly bonded

(35) Christe, K. O.; Schack, C. J. *Adv. Inorg. Chem. Radiochem.* **1976**, *18*, 331.

Table VIII. Comparison between Intuitively Predicted Qualitative and Calculated Oxidizer Strengths for Fluorides and Oxyfluorides of Chlorine and Xenon

predicted order		calculated order		
oxidation state	species	oxidation state	species	FPD value (kcal/mol)
+VII	ClF_6^+	+VII	ClF_4O^+	135.6
+VII	ClF_4O^+	+VII	ClF_6^+	147.3
+VII, +V	$ClF_2O_2^+$, ClF_4^+	+V	ClF_4^+	158.7
+V	ClF_2O^+	+VII	$ClF_2O_2^+$	161.0
+III	ClF_2^+	+III	ClF_2^+	167.1
+I	Cl_2F^+	+I	Cl_2F^+	179.1
		+V	ClF_2O^+	193.0
+VIII	XeF_7^+	+VIII	XeF_7^+	116.7
+VIII	XeF_5O^+	+VIII	XeF_5O^+	139.8
+VIII, +VI	$XeF_3O_2^+$, XeF_5^+	+VIII	$XeF_3O_2^+$	141.7
+VI	XeF_3O^+	+IV	XeF_3^+	152.4
+VI, +IV	$XeFO_2^+$, XeF_3^+	+VI	XeF_5^+	158.9
+IV	$XeFO^+$	+II	XeF^+	164.8
+II	XeF^+	+VI	XeF_3O^+	173.1
		+IV	$XeFO^+$	182.4
		+VI	$XeFO_2^+$	195.3

fluorine ligands are replaced by one doubly bonded oxygen ligand. Therefore, the formal oxidation state of the central atom remains the same but its coordination number is decreased by one. Since the formal oxidation state does not change, the number of free valence electron pairs on the central atom also remains constant. Hence, a study of the trends of the FPD values in fluorine–oxygen exchange reactions is ideally suited for the elimination of the strong effect exercised by a change in the number of free valence electron pairs (see above) and for an analysis of the influence caused by a change in the coordination numbers, i.e., of steric effects. In the absence of any steric effects, the oxidizing strength should monotonically decrease (i.e., the FPD values increase) with the stepwise replacement of two fluorines by one oxygen. Inspection of Table VII, however, clearly shows that the FPD values do not change monotonically, and that pseudooctahedral and pseudo-tetrahedral species are considerably weaker oxidizers than pseudo-pentagonal-bipyramidal, pseudo-trigonal-bipyramidal, and pseudo-trigonal-planar species. This effect is most pronounced for the transitions from the $HalF_6^+$ to the $HalF_4O^+$ cations. Instead of increasing FPD values, they exhibit a systematic decrease by about 11 kcal mol^{-1}. The surprising implication that $HalF_4O^+$ cations are significantly stronger oxidizers than the corresponding $HalF_6^+$ cations is in accord with our past experimental failures to synthesize these $HalF_4O^+$ cations.

Conclusions

Local density functional calculations are well-suited for the calculation of the geometries and relative energies of oxidative fluorinators. The oxidizing strength of oxidative fluorinators is determined by their F^+ detachment energies. A relative scale of FPD values can be obtained from the LDF calculations and can be converted to an absolute scale by the choice of a suitable zero point (FPD of $F^+ \equiv 0$) and an experimentally known FPD value (KrF^+ in this study).

An analysis of the oxidizer strengths, calculated in the above manner for 36 oxidative fluorinators, shows that the results are self-consistent and exhibit some expected, but also some highly unexpected features. Obviously, the oxidizing strength is governed to a large extent by the oxidation state and electronegativity of the central atom and the fact that the contribution of one doubly bonded oxygen is less than that of two singly bonded fluorine ligands. Among the less expected features are the following: (i) the presence of one or more free valence electron pairs on the central atom strongly decreases the oxidizing strength of a species, and (ii) the oxidizer strengths of pseudooctahedral and -tetrahedral species are depressed relative to those of pseudopentagonal or -trigonal-bipyramidal and -trigonal-planar ions. Thus, a simplistic picture is inadequate, that is, that the oxidizer strength should be governed exclusively by the oxidation state of the central atom and that, in case of similar values between a binary fluorine and oxyfluorides, the species with the larger number of fluorine ligands will be the stronger oxidizer. This is demonstrated by Table VIII, which shows a comparison between intuitive qualitative predictions and the quantitative results from our calculations for the fluorides and oxyfluorides of chlorine and xenon. For the chlorine compounds, the top placement of ClF_4O^+ and last placement of ClF_2O^+ are highly unexpected. Similarly, the last rank of $XeFO_2^+$ and the position of XeF_5^+ below XeF_3^+ and the high ranking of XeF^+ are a total surprise, but can be understood on the basis of the above analysis.

The availability of a quantitative oxidizer strength scale is expected to significantly contribute to our understanding of oxidizer chemistry and to the future syntheses of novel and known oxidative fluorinators. It also stresses the importance of employing high activation energy sources such as discharges or plasmas to generate intermediate F^+ cations, if novel oxidizers are desired which are more powerful than KrF^+.

■■■■ **CHAPTER 2**

Controlled Replacement of Fluorine by Oxygen in Fluorides and Oxyfluorides

KARL O. CHRISTE, WILLIAM W. WILSON, and CARL J. SCHACK

2.1. INTRODUCTION

Fluorine–oxygen exchange reactions play an important role in synthetic chemistry. Although numerous methods and reagents have been described for these exchange reactions, the emphasis of these studies has been almost exclusively on the selective replacement of oxygen by fluorine. For example, SF_4[1] and its derivatives, such as $SF_3N(CH_3)_2$,[2] have been widely used to convert carbonyl groups to CF_2 groups, and inorganic oxides can be transformed into fluorides by reagents such as HF, F_2, or halogen fluorides.[3] However, much less attention has been paid to the opposite reaction, that is, the conversion of fluorides to oxyfluorides. This is not surprising because generally

oxides are more readily preparable than fluorides, and many fluorides undergo facile hydrolysis to the corresponding oxyfluorides and oxides.

For the replacement of fluorine by oxygen, hydrolysis is the most frequently used method. For highly fluorinated compounds of the more electronegative elements, however, these hydrolysis reactions often present significant experimental difficulties, particularly when a controlled and stepwise replacement of fluorine by oxygen is desired. The hydrolysis reactions of these compounds are often violent, as found for XeF_6[4,5] or ClF_3,[6] and require careful moderation. Thus, SiO_2 combined with a trace of HF can be used for the slow formation of water (Eq. 2.1), followed by a continuous regeneration of the HF during the hydrolysis of the fluoride starting material (Eq. 2.2). This approach has been demonstrated previously for compounds such as IF_7.[7-10]

$$SiO_2 + 4HF \rightarrow SiF_4 + 2H_2O \tag{2.1}$$

$$IF_7 + H_2O \rightarrow IOF_5 + 2HF \tag{2.2}$$
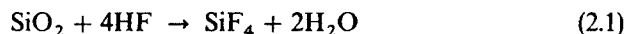
Another approach to moderate otherwise violent or uncontrollable hydrolysis reactions involves the use of suitable solvents, such as HF, and of stoichiometric amounts of water, as reported for XeF_6 [5](Eq. 2.3).

$$XeF_6 + H_2O \xrightarrow{\text{HF}} XeOF_4 + 2HF \tag{2.3}$$
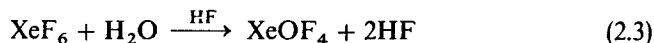
In spite of the above improvements in the techniques of hydrolyzing highly reactive fluorides, these reactions remain experimentally challenging and often are dangerous[5] and difficult to scale up. Consequently, alternate reagents that allow the safe, easily controllable, and stepwise replacement of fluorine by oxygen, are highly desirable.

Previously investigated examples for such alternate reagents include SiF_3OSiF_3, SeO_2F_2, POF_3, and several oxides. Most of these alternate reagents exhibit drawbacks. Thus, SiF_3OSiF_3 reacted with XeF_6 (Eq. 2.4),

$$XeF_6 + SiF_3OSiF_3 \rightarrow XeOF_4 + 2SiF_4 \tag{2.4}$$

but did not work for IF_7, BrF_5, and so on.[11] Similarly, the highly toxic SeO_2F_2 was demonstrated only for XeF_6 (Eq. 2.5).[12]

$$XeF_6 + SeO_2F_2 \rightarrow XeOF_4 + SeOF_4 \tag{2.5}$$
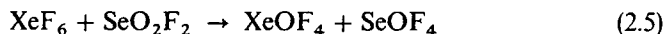
The most versatile of these alternate reagents appears to be POF_3, which reacted with XeF_6 (Eq. 2.6),[13] UF_6 (Eq. 2.7),[14] ClF_5,[14] and IF_7 (Eq. 2.8).[15]

$$XeF_6 + POF_3 \rightarrow XeOF_4 + PF_5 \tag{2.6}$$

$$UF_6 + POF_3 \rightarrow UOF_4 + PF_5 \tag{2.7}$$

$$IF_7 + POF_3 \rightarrow IOF_5 + PF_5 \tag{2.8}$$
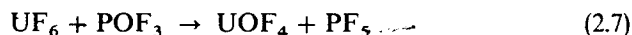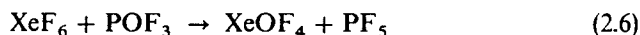
Most of the previously reported, oxide based fluorine–oxygen exchange reactions, such as (Eqs. 2.9,[10] 2.10,[16] or 2.11[17]

$$IF_7 + I_2O_5 \rightarrow IOF_5 + 2IO_2F \qquad (2.9)$$

$$4ClF_3 + 6NaClO_3 \rightarrow 6ClO_2F + 6NaF + 2Cl_2 + 3O_2 \quad (2.10)$$

$$2BrF_5 + CsIO_4 \rightarrow 2BrOF_3 + CsIO_2F_4 \qquad (2.11)$$
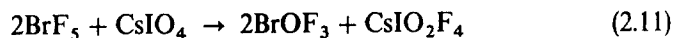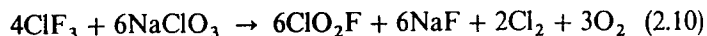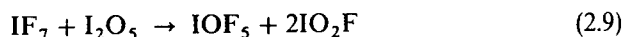
represent useful syntheses for specific compounds, but the exchange reagents have not been studied systematically.

Several years ago, while studying the compatibility of the nitrate and sulfate anions with various halogen fluorides,[18] we surprisingly found that these anions are excellent, general reagents for fluorine–oxygen exchange. Since then, we have systematically investigated the scope of these reactions and we present a summary of our results in this chapter.

2.2. REACTIONS OF THE NITRATE ANION

2.2.1. Xenon(VI) Fluoride and Oxyfluorides

Xenon hexafluoride is an ideal test case for the general usefulness of a fluorine–oxygen exchange reagent since it can undergo stepwise fluorine replacement (Eq. 2.12). When preparing $XeOF_4$ and XeO_2F_2,

$$XeF_6 \rightarrow XeOF_4 \rightarrow XeO_2F_2 \rightarrow XeO_3 \qquad (2.12)$$
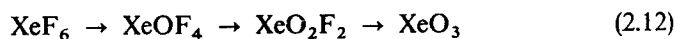
precise control of the stepwise exchange is of utmost importance because of the shock sensitivity of the potential by-product XeO_3. Other important aspects, besides high yields and ready availability of the exchange reagent, are the ease of product separation and mild reaction conditions to avoid product decomposition.

In our studies[19] it was found that $NaNO_3$ is best suited for the conversion of XeF_6 to $XeOF_4$ (Eq. 2.13).

$$XeF_6 + NaNO_3 \xrightarrow[10h]{70°C} XeOF_4 + NaF + NO_2F \qquad (2.13)$$
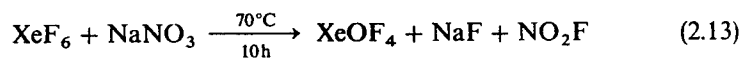
The formation of XeO_2F_2 can be suppressed by the use of a moderate excess of XeF_6. The excess of XeF_6 is readily separable from the desired $XeOF_4$ because at the reaction temperature it forms stable $NaXeF_7$ and Na_2XeF_8 salts with the NaF by-product. The only other volatile by-product is NO_2F, which is much more volatile than $XeOF_4$ and can be separated easily from the $XeOF_4$ by fractional condensation through traps kept at -78 and $-196°C$. The yields of $XeOF_4$ are about 80% based on the limiting reagent $NaNO_3$. The use of other alkali metal nitrates is less desirable. In the case of $CsNO_3$ the resulting CsF

complexes $XeOF_4$ with formation of $CsXeOF_5$[20-22] and for $LiNO_3$ the resulting LiF does not complex any unreacted XeF_6 starting material.

For the conversion of $XeOF_4$ to XeO_2F_2, the use of alkali metal nitrates is possible but, due to the relative involatility of XeO_2F_2 and its ease of forming stable $XeO_2F_3^-$ salts, N_2O_5 is the preferred reagent.[23] In the solid state, N_2O_5 has the ionic structure $NO_2^+NO_3^-$ [24,25] and reacts with $XeOF_4$ according to (Eq. 2.14).

$$XeOF_4 + NO_2^+NO_3^- \xrightarrow[15h]{25°C} XeO_2F_2 + 2NO_2F \qquad (2.14)$$
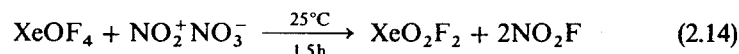
In this manner and by the use of an excess of $XeOF_4$, the only product of low volatility is XeO_2F_2, thus allowing for an efficient product separation. Again, the formation of XeO_3 was suppressed by the use of a slight excess of $XeOF_4$ starting material, and the yield of XeO_2F_2 was essentially quantitative. The only minor complication in this XeO_2F_2 synthesis is the formation of an unstable $NO_2^+[XeO_2F_3 \cdot nXeO_2F_2]^-$ type adduct between NO_2F and XeO_2F_2, which requires prolonged pumping on the product at room temperature to ensure complete NO_2F removal from the XeO_2F_2.[23]

Conversion of either XeF_6, $XeOF_4$, or XeO_2F_2 to the highly explosive XeO_3 can be achieved by their reactions with excess N_2O_5.[23] However, no detailed studies were carried out on these systems due to the sensitivity of XeO_3.

2.2.2. Chlorine Fluorides and Oxyfluorides

Excess $NaNO_3$ readily reacts with ClF at subambient temperatures to give NaF and $ClONO_2$ (Eq. 2.15).[26]

$$ClF + NaNO_3 \rightarrow NaF + ClONO_2 \qquad (2.15)$$
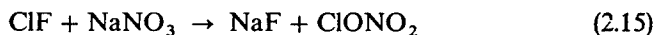
The yield of $ClONO_2$, however, was only about 75% because of the competing reaction (Eq. 2.16) which is favored by an excess of ClF.

$$ClF + ClONO_2 \rightarrow Cl_2O + NO_2F \qquad (2.16)$$
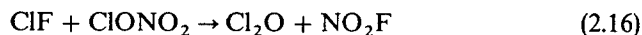
With a sufficiently large excess of ClF, the overall reaction then becomes (Eq. 2.17).

$$2ClF + NaNO_3 \rightarrow Cl_2O + NaF + NO_2F \qquad (2.17)$$
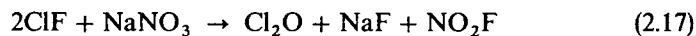
In addition to the NaF, $ClONO_2$, and NO_2F products, smaller amounts of Cl_2 and ClO_2F were also observed as by-products due to the side reactions (Eqs. 2.18 and 2.19), which result in the following net reaction (Eq. 2.20).

$$2ClF + 2Cl_2O \rightarrow 2[FClO] + 2Cl_2 \qquad (2.18)$$

$$2[FClO] \rightarrow ClF + ClO_2F \qquad (2.19)$$

$$ClF + 2Cl_2O \rightarrow ClO_2F + 2Cl_2 \qquad (2.20)$$
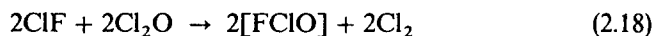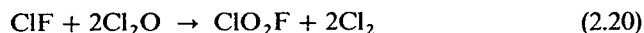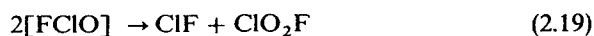
Thus, ClF readily undergoes fluorine–oxygen exchange with the NO_3^- anion with the ratio of the major products, $ClONO_2$ and Cl_2O, depending on the stoichiometry of the reactants. Smaller amounts of Cl_2 and ClO_2F formed in this system are due to side reactions.

In the case of ClF_3, the main reaction with the NO_3^- anion is again a facile fluorine–oxygen exchange (Cl. 2.21)[26]

$$ClF_3 + NaNO_3 \xrightarrow{25°C} [FClO] + NaF + NO_2F \qquad (2.21)$$

with the thermally unstable FClO either undergoing disproportionation (Eq. 2.22) or decomposition (Eq. 2.23).

$$2[FClO] \rightarrow ClF + ClO_2F \qquad (2.22)$$

$$2[FClO] \rightarrow 2ClF + O_2 \qquad (2.23)$$
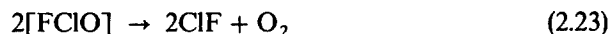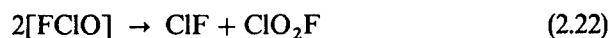
The formation of ClF, ClO_2F, O_2, and NO_2F is favored by the use of an excess of ClF_3. If, however, a large excess of $NaNO_3$ is used, side reactions (Eqs. 2.15, 2.24, 2.25) are also observed.

$$NO_2F + NaNO_3 \rightarrow N_2O_5 + NaF \qquad (2.24)$$

$$ClO_2F + NaNO_3 \rightarrow ClONO_2 + O_2 + NaF \qquad (2.25)$$
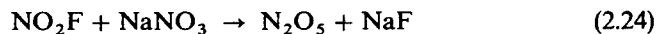
The compound ClF_5 also reacts readily at room temperature with nitrates.[26] Even in the presence of a large excess of ClF_5, the fluorine–oxygen exchange cannot be stopped at the $ClOF_3$ stage but proceeds all the way to ClO_2F (Eq. 2.26).

$$ClF_5 + 2MNO_3 \xrightarrow{25°C} ClO_2F + 2NO_2F + 2MF \qquad (2.26)$$
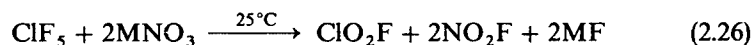
(M = Li, Na, K, Rb, and Cs)

This is in marked contrast to BrF_5 and IF_5 (see below) and is due to the extraordinary reactivity of $ClOF_3$, which is much more reactive than ClF_5.[27] Attempts to trap the intermediately formed $ClOF_3$ as $M^+ClOF_4^-$ salts were also unsuccessful indicating that the complexation of $ClOF_3$ with MF is slower than its fluorine–oxygen exchange with the nitrate anion.

When a large excess of nitrate is used in the reaction of ClF_5 with MNO_3 (Eq. 2.26), the ClO_2F product can undergo further fluorine–oxygen exchange with NO_3^- (Eq. 2.25). This was confirmed by separate experiments between ClO_2F and either $LiNO_3$ or $NO_2^+NO_3^-$.[26]

Thus, all the chlorine fluorides and oxyfluorides, except for the highly unreactive ClO_3F,[27] undergo rapid fluorine–oxygen exchange with the nitrate anion. Due to the high reactivity of $ClOF_3$ and in contrast to BrF_5 and IF_5, a controlled single step fluorine–oxygen exchange in ClF_5 could not be realized (see note added in proof).

2.2.3. Bromine Pentafluoride

The reactions of BrF_5 with $M^+NO_3^-$ serve as excellent examples of how the nature of the products can be influenced by the appropriate choices of the M^+ cation and the reaction stoichiometries.[18,28] With an excess of BrF_5 and M being either Na, K, Rb, or Cs, the corresponding $M^+BrOF_4^-$ salts can be prepared in 70–100% yield under very mild (-30 to $25\,^\circ C$) conditions (Eq. 2.27).

$$BrF_5 + MNO_3 \xrightarrow[\text{excess BrF}_5]{-30 \text{ to } 25\,^\circ C} MBrOF_4 + NO_2F \qquad (2.27)$$
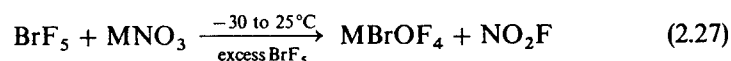
(M = Na, K, Rb, and Cs)

Since lithium does not form a stable $LiBrOF_4$ salt, the reaction of $LiNO_3$ with excess BrF_5 (Eq. 2.28) can be used for a convenient synthesis of free $BrOF_3$.

$$BrF_5 + LiNO_3 \xrightarrow[\text{excess BrF}_5]{0\,^\circ C} BrOF_3 + LiF + NO_2F \qquad (2.28)$$
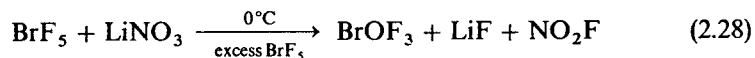
Since $BrOF_3$ is considerably less volatile than BrF_5, the two can be separated readily by fractional condensation or distillation.

While the use of an excess of BrF_5 results in the single-step replacement of two fluorines by one oxygen, the application of a 1:3 mol ratio of $BrF_5:LiNO_3$ causes complete fluorine–oxygen exchange with $BrONO_2$ formation (Eq. 2.29).[28]

$$BrF_5 + 3LiNO_3 \xrightarrow[\text{excess LiNO}_3]{0\,^\circ C} BrONO_2 + 3LiF + O_2 + 2NO_2F \qquad (2.29)$$
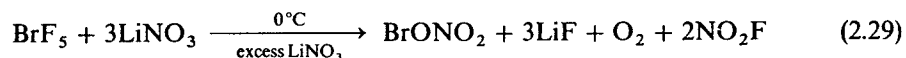
If the $BrF_5:LiNO_3$ mole ratio is further changed to 1:5 or greater, N_2O_5 is produced (Eq. 2.30)

$$2NO_2F + 2LiNO_3 \rightarrow NO_2^+NO_3^- + 2LiF \qquad (2.30)$$

which can react with $BrONO_2$ (Eq. 2.31).[28]

$$NO_2^+NO_3^- + BrONO_2 \geqq NO_2^+[Br(ONO_2)_2]^- \qquad (2.31)$$
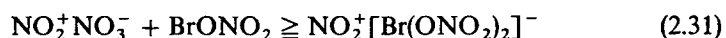
2.2.4. Iodine Fluorides and Oxyfluorides

The reactions of IF and IF_3 with nitrates were not studied since IF and IF_3 are relatively unstable and easily disproportionate to I_2 and IF_5. With excess IF_5, the alkali metal nitrates undergo a controlled, single-step fluorine–oxygen exchange to form the corresponding $MIOF_4$ salts (Eq. 2.32).[29]

$$IF_5 + MNO_3 \rightarrow MIOF_4 + NO_2F \qquad (2.32)$$
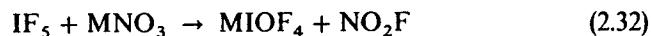
(M = Li, K, Cs)

However, these reactions are more sluggish than the corresponding BrF_5 reactions. As a consequence, the side reaction (Eq. 2.33)

$$NO_2F + MNO_3 \rightarrow N_2O_5 + MF \qquad (2.33)$$
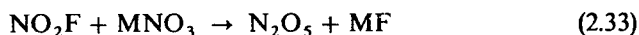
becomes faster than the previous reaction (Eq. 2.32) resulting in an equal consumption of MNO_3 by its reactions with IF_5 and NO_2F (Eqs. 2.32 and 2.33). Furthermore, the following reactions (Eqs. 2.34 and 2.35) also become competitive,

$$KF + IF_5 \rightarrow KIF_6 \qquad (2.34)$$

$$CsF + 3IF_5 \rightarrow CsI_3F_{16} \qquad (2.35)$$
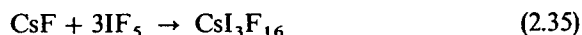
and some of the N_2O_5 decomposes to $N_2O_4 + O_2$ under these conditions. Consequently, the $MIOF_4$ salts prepared in this manner, usually contain substantial amounts of IF_6^- and $I_3F_{16}^-$ salts as by-products.

From the reaction of excess IF_7 with either $LiNO_3$ or $NaNO_3$, no IOF_5 is isolated. Instead, IF_5 and O_2 are obtained (Eq. 2.36),

$$IF_7 + MNO_3 \xrightarrow{60°C} IF_5 + \tfrac{1}{2}O_2 + MF + NO_2F \qquad (2.36)$$
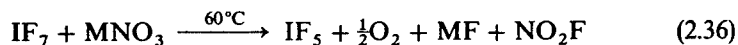
indicative of a competing deoxygenation reaction.[29] In the case of $CsNO_3$, the same deoxygenation occurs but the CsF product reacts with IF_5 and IF_7 to give CsI_3F_{16} and $CsIF_8$, respectively. If an excess of MNO_3 is used, the IF_5 product can react further with MNO_3 and form $MIOF_4$ salts (Eq. 2.32). It was further experimentally confirmed that IOF_5 does not undergo fluorine–oxygen exchange giving IO_2F_3, but loses oxygen giving IF_5, which then undergoes fluorine–oxygen exchange with formation of IOF_4^- salts (Eq. 2.32).[29]

The fact that IF_7 readily undergoes fluorine–oxygen exchange either during controlled hydrolysis[7-10] or with POF_3,[15] but not with the NO_3^- anion remains somewhat a puzzle. It has previously been speculated[29] that this lack of fluorine–oxygen exchange in the IF_7–nitrate system might be due to either the instability of an intermediate IOF_6^- anion or the lack of a free valence electron

pair on the iodine central atom of IF_7. Since then, however, we have synthesized and characterized stable IOF_6^- salts[30]; thus, the first explanation can be ruled out.

2.2.5. Carbonyl Fluoride

The nitrate anion can also exchange carbon bonded fluorine for oxygen. This was demonstrated[31] for carbonyl fluoride, COF_2 (Eq. 2.37).

$$COF_2 + MNO_3 \xrightarrow[\text{CsF}]{85°C} CO_2 + MF + NO_2F \qquad (2.37)$$
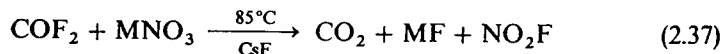
(M = Li and Na)

The reactions were carried out in a steel cylinder and, in this manner, essentially quantitative yields of NO_2F are obtainable. This reaction is remarkable because it is a very rare example for the formation of a nitrogen–fluorine bond using a fluorinating agent as mild as COF_2. Furthermore, it is interesting that the heavier alkali metal nitrates, such as $CsNO_3$, do not react under these conditions with COF_2. This was explained[31] by thermochemical calculations, which show that for Li and Na the ΔH values are still favorable but become increasingly more positive for the heavier alkali metals. It should be noted that all the ΔH values given in Ref. 31 are slightly in error[32] by -11 kcal mol^{-1}, but that the general trend remains the same for the different alkali metals.

2.2.6. Mechanism of the Fluorine–Oxygen Exchange Involving Nitrates

Of the nitrate based fluorine–oxygen exchange reactions studied so far, the simplest case is that of MNO_3 and ClF, which yields MF and $ClONO_2$ (Eq. 2.15).[26] Assuming for the more highly fluorinated starting materials an analogous first reaction step (Eq. 2.38),

$$XF_n + MNO_3 \rightarrow F_{(n-1)}XONO_2 + MF \qquad (2.38)$$

the formation of an intermediate $F_{(n-1)}XONO_2$ is expected. This intermediate could easily undergo an internal nucleophilic substitution (S_{Ni}) reaction,[18] accompanied by NO_2F elimination (Eq. 2.39).

$$(2.39)$$
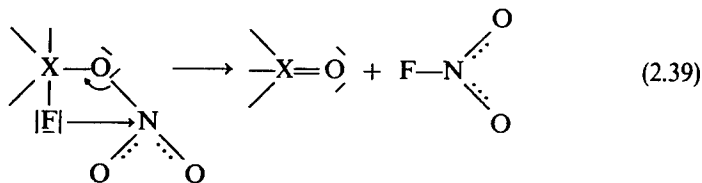
Such a mechanism could account for the generally observed reaction products, MF, NO_2F, and the corresponding oxyfluoride. If the oxyfluoride end product is amphoteric and can form a stable salt with the cogenerated alkali metal fluoride, then this salt is observed as the final product (Eq. 2.40).

$$XOF_{(n-2)} + MF \rightarrow M^+[XOF_{(n-1)}]^- \qquad (2.40)$$

If, as for the $ClF + NO_3^-$ reaction (Eq. 2.15), the resulting nitrate intermediate no longer contains a fluoride ligand, NO_2F elimination becomes impossible, and the halogen nitrate becomes the final product.

All the nitrate reactions studied so far seem to follow this pattern, except for the IF_7 case where deoxygenation of the expected IOF_5 product occurred (Eq. 2.36). Since the $IF_7 + MNO_3$ reactions require elevated temperatures and conditions under which IOF_5 can undergo deoxygenation,[29] the latter might be a secondary reaction, and the $IF_7 + MNO_3$ reaction might involve the same primary steps as all the other nitrate reactions.

2.3. REACTIONS OF THE SULFATE ANION

The reactions of the sulfate anion with highly fluorinated compounds of the more electronegative elements resemble those of the nitrate anion. Again, fluorine–oxygen exchange occurs but this exchange generally stops at the SO_3F^- level (Eq. 2.41),

$$XF_n + M_2SO_4 \rightarrow XOF_{(n-2)} + MSO_3F + MF \qquad (2.41)$$
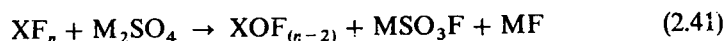
and does not proceed further to the SO_2F_2 stage (Eq. 2.42).[33]

$$XF_n + MSO_3F \rightarrow XOF_{(n-2)} + SO_2F_2 + MF \qquad (2.42)$$
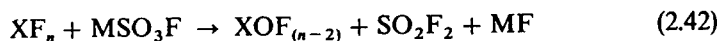
Since MSO_3F is a nonvolatile solid, whereas NO_2F is a volatile gas, the use of M_2SO_4 may be more convenient than that of MNO_3 if the desired product is volatile but either complexes with NO_2F or is difficult to separate from it. Compared to the nitrate anion, the sulfate anion is less reactive and requires longer reaction times and/or higher temperatures. Consequently, the reactions of the sulfate anion were not studied as extensively as those of the nitrate anion and were limited to the following examples.

2.3.1. Bromine Pentafluoride

At room temperature Cs_2SO_4 readily undergoes fluorine–oxygen exchange with BrF_5 (Eq. 2.43).[33]

$$BrF_5 + Cs_2SO_4 \xrightarrow[1\,day]{25\,°C} CsBrOF_4 + CsSO_3F \qquad (2.43)$$
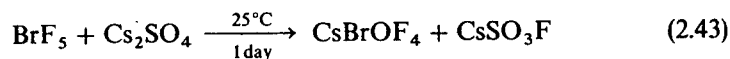
Even with an 80-fold excess of BrF_5, the fluorine–oxygen exchange did not proceed past the $CsSO_3F$ stage. Attempts were made to use this reaction for the synthesis of free $BrOF_3$ by the replacement of Cs_2SO_4 with Li_2SO_4 since lithium does not form a stable $BrOF_4^-$ salt. Under conditions (0 °C, 1 day), which worked well for $LiNO_3$[28], no reaction was observed for Li_2SO_4. This shows that the SO_4^{2-} anion is less reactive than NO_3^-.

2.3.2. Iodine Fluorides

Reaction temperatures in excess of 70 °C were required to initiate a slow reaction between IF_7 and Li_2SO_4. Even at this temperature, the conversion of the Li_2SO_4 was only about 6–7%. As in the case of NO_3^-, deoxygenation of the IOF_5 occurred and IF_5 and O_2 were the observed products (Eq. 2.44).[34]

$$IF_7 + Li_2SO_4 \xrightarrow{70\,°C} IF_5 + 0.5O_2 + LiSO_3F + LiF \qquad (2.44)$$
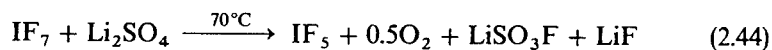
Attempts to convert IOF_5 with Li_2SO_4 to IO_2F_3 at 75 °C were, as in the case of NO_3^-, also unsuccessful.[34]

2.3.3. Xenon Fluorides

At room temperature, excess XeF_6 reacts with Li_2SO_4 to give the expected $XeOF_4$ in high yield (Eq. 2.45).[34]

$$XeF_6 + Li_2SO_4 \xrightarrow{25\,°C} XeOF_4 + LiSO_3F + LiF \qquad (2.45)$$
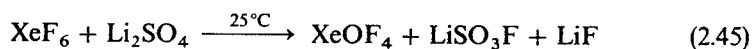
The $XeOF_4$ can be reacted further with Li_2SO_4 to give XeO_2F_2 in modest yield (Eq. 2.46).[34]

$$XeOF_4 + Li_2SO_4 \xrightarrow{25\,°C} XeO_2F_2 + LiSO_3F + LiF \qquad (2.46)$$
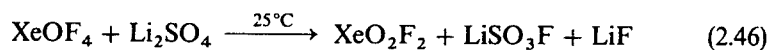
As in the case of NO_3^-, care must be taken to use excess $XeOF_4$ to avoid the formation of explosive XeO_3.

2.4. SUMMARY

Oxoanions, such as NO_3^- or SO_4^{2-}, are effective, readily available, nontoxic, and low cost reagents for controlled, stepwise fluorine–oxygen exchange in highly fluorinated compounds of the more electronegative elements. Product separations can be facilitated greatly by appropriate choices of the anion, the countercations and the mole ratios of the reagents. The reactions appear to be quite general, controllable, safe, and scalable.

ACKNOWLEDGMENTS

REFERENCES

1. Burmakov, A. I., Kunshenko, B. V., Alekseeva, L. A., and Yagupolskii, L. M., in *New Fluorinating Agents in Organic Synthesis* (L. German and S. Zemskov, Eds.), Springer-Verlag, Berlin, 1989, pp. 197–253.
2. Hudlicky, M., in *Organic Reactions*, Wiley, New York, 1988, pp. 513–637.
3. Many examples for these types of reactions can be found in Vols. 3 and 4 of *Inorganic Reactions and Methods* (J. J. Zuckerman and A. P. Hagen, Eds.), VCH Publishers, New York, 1989.
4. Chernik, C. L., Claassen, H. H., Malm, J. G., and Plurien, P. L., in *Noble-Gas Compounds* (H. H. Hyman, Ed.), University of Chicago Press, 1963, p. 106.
5. Schumacher, G. A. and Schrobilgen, G. J., *Inorg. Chem.*, **23**, 2923 (1984).
6. Bougon, R., Carles, M., and Aubert, J., *C. R. Acad. Sci. Ser. C*, **265**, 179 (1967).
7. Gillespie, R. J. and Quail, J. W., *Proc. Chem. Soc.*, 278, (1963).
8. Schack, C. J., Pilipovich, D., Cohz, S. N., and Sheehan, D. F., *J. Phys. Chem.*, **72**, 4697 (1968).
9. Alexakos, L. G., Cornwell, C. D., and Pierce, S. B., *Proc. Chem. Soc.*, 341 (1963).
10. Bartlett, N. and Levchuck, L. E. *Proc. Chem. Soc.*, 342 (1963).
11. Jacob, E., *Z. Naturforsch.*, **35b**, 1095 (1980).
12. Seppelt, K. and Rupp, H. H., *Z. Anorg. Allg. Chem.*, **409**, 331 (1974).
13. Nielsen, J. B., Kinkead, S. A., and Eller, P. G., *Inorg. Chem.*, **29**, 3621 (1990).
14. Kinkead, S. A. and Nielsen, J. B., paper 47 presented at the ACS Ninth Winter Fluorine Conference, St. Petersburg, FL (February, 1989).
15. Schack, C. J. and Christe, K. O., *J. Fluorine Chem.*, **49**, 167 (1990).
16. Christe, K. O., Wilson, R. D., and Schack, C. J., *Inorg. Nucl. Chem. Lett.*, **11**, 161 (1975).
17. Christe, K. O., Wilson, R. D., and Schack, C. J., *Inorg. Nucl. Chem. Lett.*, **20**, 2104 (1981).
18. Wilson, W. W. and Christe, K. O., *Inorg. Chem.*, **26**, 916 (1987).
19. Christe, K. O. and Wilson, W. W., *Inorg. Chem.*, **27**, 1296 (1988).
20. Selig, H., *Inorg. Chem.*, **5**, 183 (1966).
21. Waldman, M. C. and Selig, H., *J. Inorg. Nucl. Chem.*, **35**, 2173 (1973).
22. Schrobilgen, G. J., Martin-Rovet, D., Charpin, P., and Lance, M., *J. Chem. Soc. Chem. Commun.*, 894 (1980).
23. Christe, K. O. and Wilson, W. W., *Inorg. Chem.*, **27**, 3763 (1988).
24. Grison, E., Eriks, K., and De Vries, J. L., *Acta Crystallogr.*, **3**, 290 (1950).
25. Wilson, W. W. and Christe, K. O., *Inorg. Chem.*, **26**, 1631 (1987).

26. Christe, K. O., Wilson, W. W., and Wilson, R. D., *Inorg. Chem.*, **28**, 675 (1989).
27. Christe, K. O. and Schack, C. J., *Adv. Inorg. Chem. Radiochem.*, **18**, 319 (1976).
28. Wilson, W. W. and Christe, K. O., *Inorg. Chem.*, **26**, 1573 (1987).
29. Christe, K. O., Wilson, W. W., and Wilson, R. D., *Inorg. Chem.*, **28**, 904 (1989).
30. Christe, K. O., Sanders, J. C. P., Schrobilgen, G. J., and Wilson, W. W., *J. Chem. Soc. Chem. Commun.*, 837 (1991).
31. Schack, C. J. and Christe, K. O., *Inorg. Chem.*, **27**, 4771 (1988).
32. The authors are grateful to Dr. W. Jolly for bringing the error to their attention.
33. Christe, K. O., Wilson, W. W., and Schack, C. J., *J. Fluorine Chem.*, **43**, 125 (1989).
34. Wilson, W. W. and Christe, K. O., unpublished results.

Note added in proof: The controlled replacement of two fluorines by one oxygen atom in ClF_5 has recently been achieved by B. B. Chaivanov, Y. B. Sokolov and S. N. Spirin, "Researchers in the Field of Inorganic Fluorine Chemistry," Preprint IAE-4936/13, Moscow, 1989, by the reaction of ClF_5 with $H_3O^+BF_4^-$ according to

$$ClF_5 + H_3O^+BF_4^- \rightarrow ClOF_2^+BF_4^- + 3HF.$$
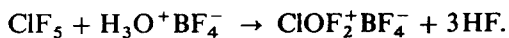
Osmium Tetrafluoride Dioxide, OsF_4O_2: a New Osmium(VIII) Oxide Fluoride

Karl O. Christe*[a] and Roland Bougon[b]

[a] *Rocketdyne, A Division of Rockwell International Corporation, Canoga Park, California 91303, USA*
[b] *SCM-URA CNRS 331, CEA—Centre d'Etudes Nucléaires de Saclay, 91191 Gif-sur-Yvette, France*

The reaction of OsO_4 with KrF_2 in anhydrous HF produces *cis*-OsF_4O_2 and not OsF_6O as previously reported.

Of the three possible mononuclear oxide fluorides of osmium in its +VIII oxidation state, OsF_6O, OsF_4O_2 and OsF_2O_3, only the latter had been well known and characterized.[1-3] Attempts to prepare the other two oxide fluorides had not only failed, but also suggested that such compounds will disproportionate readily.[2,4,5] Very recently, a new osmium(VIII) oxide fluoride was prepared at Saclay and identified as OsF_6O by elemental analysis, X-ray powder data and vibrational spectroscopy.[6]

During an ongoing effort at Rocketdyne on highly coordinated, high oxidation state compounds, including several XF_6O type ions,[7] a poor agreement between the vibrational spectra of the alleged OsF_6O and the other XF_6O ions was noticed, and the Saclay experiments were repeated at Rocketdyne. The following results establish that the new osmium(VIII) oxide fluoride, discovered at Saclay, is not OsF_6O but *cis*-OsF_4O_2. Further characterization of the material carried out independently at Saclay also led to this conclusion.

The synthesis of the new osmium(VIII) oxide fluoride was carried out from OsO_4 and an excess of KrF_2 in anhydrous HF solution, as previously described.[6] A careful separation, measurement and identification of all reactants and reaction products by both pressure–volume–temperature measurements for the volatile species and weights for all of them established the following quantitative 1:2 reaction (1). The excess of KrF_2 used was recovered unchanged.

$$OsO_4 + 2KrF_2 \rightarrow OsF_4O_2 + 2Kr + O_2 \qquad (1)$$
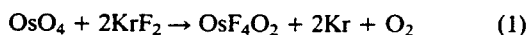
The physical properties of the osmium oxide fluoride prepared in this manner (burgundy-red solid, m.p. 90 °C, vapour pressure ~ 1 Torr at room temperature), its X-ray powder diffraction pattern and vibrational spectra were within

experimental error identical to those previously reported[6] and leave no doubt that the two compounds are the same.†

One of the authors (K. O. C.) thanks the US Air Force Phillips Laboratory and the US Army Research Office for financial support.

References

1 M. A. Hepworth and P. L. Robinson, *J. Inorg. Nucl. Chem.*, 1957, **4**, 24.
2 Nguyen-Nghi and N. Bartlett, *C. R. Acad. Sci. Paris Sec. C*, 1969, **269**, 756.
3 E. G. Hope, W. Levason and J. S. Ogden, *J. Chem. Soc., Dalton Trans.*, 1988, 61 and 997.
4 W. E. Falconer, F. J. Dissalvo, J. E. Griffiths, F. A. Stevie, W. A. Sunder and M. J. Vasile, *J. Fluorine Chem.*, 1975, **6**, 499.
5 J. H. Holloway and D. Laycock, *Adv. Inorg. Chem. Radiochem.*, 1984, **28**, 85.
6 R. Bougon, *J. Fluorine Chem.*, 1991, **53**, 419.
7 K. O. Christe, J. C. P. Sanders, G. J. Schrobilgen and W. W. Wilson, *J. Chem. Soc., Chem. Commun.*, 1991, 837.
8 K. O. Christe, R. D. Wilson and C. J. Schack, *Inorg. Chem.*, 1985, **20**, 2104.

† Vibrational spectra: The IR and Raman spectra of the solid and the Raman spectrum of an HF solution were recorded. The general pattern of these spectra resembles that[8] of *cis*-$IF_4O_2^-$ more closely than those[7] of IF_6O^- and TeF_6O^{2-}. Furthermore, two Raman bands at 942 and 932 cm^{-1} are observed for the solid in the Os=O stretching region that had previously been interpreted[6] as being due to a crystal field splitting of an Os=O group containing a single oxygen atom. The present study, however, shows that in HF solution this splitting is retained and suggests the presence of more than one oxygen atom in the molecule.

^{19}F NMR spectrum: The ^{19}F NMR spectrum of the new osmium oxide fluoride in HF solution was recorded and exhibits an A_2B_2 pattern, *i.e.* two almost identical 1:2:1 triplets at δ 61.3 and 14.7 downfield from external $CFCl_3$ with J_{FF} 136 Hz. No other signals were observed. This clearly establishes that the new osmium oxide fluoride contains only four and not five fluorine atoms and must be OsF_4O_2 and not OsF_6O. Furthermore, the observation of two nonequivalent sets of two fluorine atoms each shows that the OsF_4O_2 is present exclusively as the *cis*- and not as the *trans*-isomer. For *trans*-OsF_4O_2, only a single resonance should be observed with no signs of splittings due to F–F coupling.
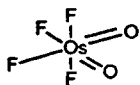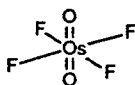
cis-OsF_4O_2 *trans*-OsF_4O_2

The Pentabromine(1+) Cation, Br_5^+. Local Density Functional Calculations and Vibrational Spectra

K. O. Christe

Canoga Park, CA (USA), Rocketdyne Division, Rockwell International

D. A. Dixon

Wilmington, DE (USA), Central Research and Development, Du Pont[1])

R. Minkwitz

Dortmund, Institut für Anorganische Chemie der Universität

Abstract. The geometry, vibrational spectra and charge distribution of Br_5^+ were calculated by the use of the local density functional (LDF) method. The results show that for free Br_5^+ the lowest energy configuration is a skew structure with the three central Br atoms forming an angle of 168.6° und the two terminal Br atoms exhibiting a dihedral angle of 82°. This skew configuration is in contrast to the planar trans configuration of C_{2h} symmetry found for Br_5^+ in solid $Br_5^+MF_6^-$ (M = As, Sb). The small energy difference of 1.2 kcal mol^{-1} between the skew and the trans configurations, combined with crystal packing effects, can account for the planar trans configuration of Br_5^+ in solid $Br_5^+MF_6^-$. The computed vibrational spectra were used to select the most likely set from three sets of previously published and widely diverging spectra. Contrary to previous STO-3G calculations for Cl_5^+, the present LDF calculations for Br_5^+ and Cl_5^+ result in charge distribution which agree with a previously proposed simple valence bond model for pentahalogen(1+)cations.

Key words: Pentabromine(1+) cation; local density functional calculations; Vibrational spectra

Das Pentabrom(1+)-Kation, Br_5^+. Berechnungen mit der Dichtefunktional-Methode und Schwingungsspektren

Inhaltsübersicht. Für das Br_5^+-Kation werden mit der Dichtefunktional-Methode Geometrie, Schwingungsspektren und Landungsverteilung berechnet. Das freie Ion hat in der gauche-Konfiguration die niedrigste Energie. Die drei mittleren Br-tome bilden danach einen Winkel von 168,8° und der Diederwinkel der beiden terminalen Br-tome beträgt 82°. Diese Konfiguration steht damit im Gegensatz zu der planaren trans-Konfiguration mit C_{2h}-Symmetrie, die für Br_5^+ im $Br_5^+MF_6^-$ (M = As, Sb) durch Röntgenbeugung gefunden wurden. Die geringe Energiedifferenz von 1,2 kcal mol^{-1} zwischen der gauche- und trans-Konfiguration, verbunden mit Kristallpackungseffekten, könnten für die trans-Konfiguration von Br_5^+ im festen $Br_5^+MF_6^-$ verantwortlich sein.

Um den Wahrscheinlichsten, der bereits publizierten sich stark unterscheidenden Frequenzsätze, zu bestimmen, wurden die berechneten Schwingungsspektren herangezogen.

Im Gegensatz zu früheren STO-3G-Rechnungen für Cl_5^+, können mit diesen LDF-Rechnungen für Br_5^+ und Cl_5^+ Ladungsverteilungen wiedergegeben werden, die mit einem früher vorgeschlagenen einfachen „valence-bond-model" für Pentahalogen(1+)-Kationen übereinstimmen.

Introduction

The first report on the existence of the Br_5^+ cation was published in 1980 by *Lee* and *Aubke* who prepared its $Au(SO_3F)_4^-$ salt and published its vibrational spectra [1]. The only other reports on Br_5^+ are two recent papers by *Hartl, Nowicki* and *Minkwitz* on the crystal structures and vibrational spectra of $Br_5^+MF_6^-$ (M = As, Sb) [2] and by *Christe, Bau* and *Zao* on the Raman spectrum of $Br_5^+AsF_6^-$ [3]. Although the existence and structure of Br_5^+ are firmly established, the three sets of vibrational spectra published [1−3] for Br_5^+ diverge strongly. This is not surprising because the recording of vibrational spectra for these compounds is very difficult. The compounds are of marginal stability, difficult to handle, intensely colored, photolytically unstable, and often contain impurities which can give rise to very intense resonance Raman spectra. Since local density functional (LDF) calculations are well suited for computations involving large molecules and heavy atoms [4], we performed LDF calculations for the Br_5^+ cation to resolve some of the problems surrounding this interesting cation.

Computational Method

The calculations described below were done in the local density functional approximation [4−11] by uising the program system DMol [12, 13]. The atomic basis functions are given numerically on an atom-centered, spherical-polar mesh. The radial portion of the grid is obtained from the solution of the atomic LDF equations by numerical methods. Since the basis sets are numerical, the various integrals arising from the expression for the energy need to be evaluated over a grid. The integration points are generated in terms of angular functions and spherical harmonics. The number of radial points N_R is given as

$$N_R = 1.2 \times 14 (Z + 2)^{1/3}$$

where Z is the atomic number. The maximum distance for any function is 12 a.u. The angular integration points N_0 are generated at the N_R radial points to form shells around each nucleus. The value of N_0 ranges from 14 to 302 depending on the behavior of the density [14]. The Coulomb potential corresponding to the electron repulsion term is determined directly from the electron density by solving Poisson's equation. In DMol, the form for the exchange-correlation energy of the uniform electron gas is that derived by *von Barth* and *Hedin* [15].

All of the DMol calculations were done with a double numerical basis set augmented by polarization functions. This can be considered in terms of size, for comparison to traditional molecular orbital calculations, as a polarized double zeta basis set. However because of the use of exact numerical solutions for the atom, this basis set is of significantly higher quality than a normal molecular orbital polarized double zeta basis set. The fitting functions have angular momentum numbers, l, one greater than that of the polarization function. Since all of the atoms have d polarization functions, the value of l for the fitting function is 3.

Geometries were optimized by using analytic gradient methods [16]. There are two problems with evaluating gradients in the LDF framework which are due to the numerical methods that are used. The first is that the energy minimum does not necessarily correspond exactly to the point with a zero derivative. The second is that the sum of the gradients may not always be zero as required for translational invariance. These tend to introduce errors on the order of 0.001 Å in the calculation of the coordinates if both a reasonable grid and basis set are used. This gives bond lengths and angles with reasonable error limits. The difference of 0.001 Å is about an order of magnitude smaller than the accuracy of the LDF geometries as compared to experiment. The frequencies were determined by numerical differentiation of the gradient. A two point difference formula was used and a displacement of 0.01 a.u.

Results and Discussion

Structure of Br_5^+

The geometries and vibrational spectra of Br_5^+ were computed by the LDF method for two symmetries (see Tables 1 and 2). The first one is C_{2h}, as found [2] by the crystal structure determination, and is shown in Figure 1.
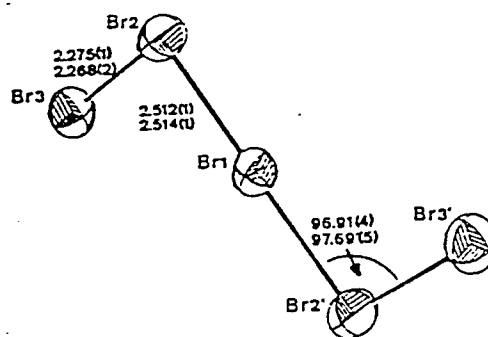
Fig. 1 ORTEP plot of Br_5^+ according to ref. [2]

In C_{2h} symmetry, Br_5^+ is planar, i.e. the terminal Br3 atoms are in trans position, and the three central bromine atoms are linear. The second structure (see Figure 2) which is the energy minimum at the LDF level, has no symmetry and is 1.2 kcal mol^{-1} more stable than the C_{2h} structure.

In this optimized structure, the three central Br atoms slightly deviate from linearity by 11.4°, and the terminal Br atoms form a dihedral angle of 82° about the Br2—Br2' axis, similar to the angles found for *Foof* and *Hooh* [17]. This skewing is caused by the repulsive interactions between the bonded atoms and the sterically active free valence electron pairs on the central atoms and of
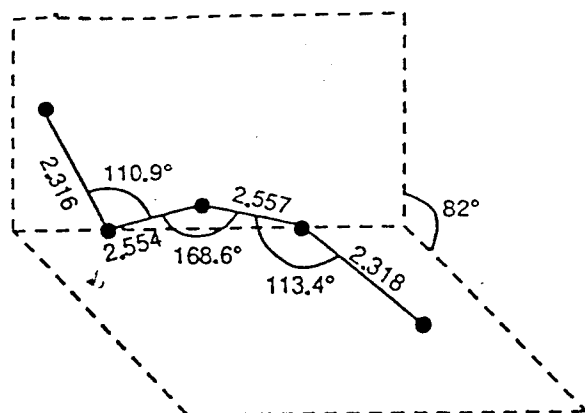
Fig. 2 Optimizing Structure of the Free Br_5^+ Cation

Table 1 Computed and Experimental Bond Distances (Å) and Bond Angles (deg) for Br_5^+ and Cl_5^{-*})

Bond Lengths

	Expt [2]	Br_5^+ LDF C_{2h}	LDF opt	Cl_5^+ LDF C_{2h}
X1—X2	2.512(1)	2.572	2.554	2.295
X1—X2′	2.514(1)	2.572	2.557	2.295
X2—X3	2.275(1)	2.310	2.316	1.991
X2′—X3′	2.268(2)	2.310	2.318	1.991

Bond Angles

	Br_5^+			Cl_5^+
X2—X1—X2′	180	180	168.6	180
X1—X2—X3	96.9i(4)	108.9	110.9	108.4
X1—X2′—X3′	97.69(5)	108.9	113.4	108.4

*) For Cl_5^+ no experimental values are known. The C_{2h} geometry was chosen to match that used in [22]

ten can vary over a wide range. For example, in various solid phases containing *Hooh*, the dihedral angle can span a complete range from 90° to 180° [18]. In view of these analogies and the small energy difference of only 1.2 kcal mol^{-1} between the trans and the optimized skew

configurations of Br_5^+, the existence of trans $-Br_5^+$ in its $Br_5^+MF_6^-$ salts is not surprising and can be explained by crystal packing effects. Evidence for such an effect is also provided by the frequency shifts observed for the Raman bands of $Br_5^+AsF_6^-$ on going from the solid state to the HF solution [3].

As can be seen from Table 1, the geometry computed for Br_5^+ of C_{2h} symmetry agrees well with the experimentally observed one [2], particularly if it is kept in mind that for similar molecules and ions, such as XeF_4, XeF_5^- [19], Br_3^+, and Br_3^- (see below), the computed bond lengths are also about 0.05 Å longer than the experimentally observed ones.

Vibrational Spectra

The computed vibrational frequencies are summized in Table 2. Since the C_{2h} configuration is not an energy minimum, it has two negative directions of curvature which result in imaginary frequencies of 24 and 49 cm^{-1}. Rotation about the Br2—Br2′ axis leads to a structure with

Table 3 Computed and Experimental Geometries and Vibrational Frequencies for Br_3^+ and Br_3^-

	Br_3^+ experim [3]	computed*)	Br_3^- experim [20−22]	computed
r (Å)	2.270(5)	2.322	2.536(2)	2.593
⌀ (deg)	102.5(2)	110.8	180	180
asym.stretch	297	295	203	216
sym.stretch	293	280	163	158
deformation	124	75	80	81

*) The vibrational frequencies of Br_3^+ were also computed using the experimental geometry of 2.27 Å and 102.5°. As expected, the frequencies of the two stretching modes increased somewhat to 328 and 325 cm^{-1}, respectively, but that of the bending mode remained essentially unchanged at 76 cm^{-1}. Hence the discrepancy between the observed and the computed deformation frequencies is not caused by the slightly different geometries

Table 2 Computed and Experimental Vibrational Frequencies (cm^{-1}) for Br_5^+

assignment in point group C_{2h}	experimental $Br_5^+Au(SO_3F)_4^-$ solid [1]	$Br_5^+AsF_6^-$ solid [2]	$Br_5^+AsF_6^-$ [3] solid	HF solut.	computed LDF C_{2h}	LDF opt*)
A_g $\nu_1\nu$sym term	304.295[b])	272	309	309	307	303*
$\nu_2\nu$sym centr	267	220	174	182	139	161
$\nu_3\delta$sym in plane	205	170	84	108	24	45**
A_u $\nu_4\delta$centr out of plane					63	94
ν_5 torsion					24i	26
B_u $\nu_6\nu$ as term	305.295[b])	290.275[b])			307	300*
$\nu_7\nu$ as centr	260	185			172	180
$\nu_8\delta$centr in plane					129	105
$\nu_9\delta$ as term in plane					49i	33**

*) The LDF opt configuration has no symmetry, and the motions marked by asterisks and double asterisks mix
[b]) Assuming a splitting of these bands due to solid state effects

lower energy and to all positive directions of curvature. The resulting structure [LDF opt] is a true minimum of the LDF potential energy surface and has all real frequencies. Since this configuration has no symmetry, the C_{2h} selection rules no longer apply and all fundamentals can be active in both the infrared and the Raman spectra.

A comparison of the computed vibrational frequencies with the observed ones [1−3] is given in Table 2. To test how well these LDF computations for a free ion can duplicate the observed frequencies in similar, closely related solids, the vibrational spectra of the known Br_3^+ [3] and Br_3^- [20−22] ions were also calculated. As can be seen from Table 3, the agreement is very good for all the modes, except for the deformation mode of Br_3^+ for which the calculated frequency is considerably lower than the observed one. Since in Br_5^+ the three central atoms mimic the Br_3^- anion and the two terminal ones resemble those in Br_3^+ [3], their computed and observed stretching frequencies should also be in good agreement. As can be seen from Table 2, only the Raman spectrum given in [3] satisfies the computed stretching frequencies and, therefore, is the preferred choice.

The exact reasons for the large discrepancies among the three observed data sets [1−3] are not clear at the present time, but should caution future investigators against relying too heavily on vibrational spectra for the identification of these polybromine cations.

The frequency changes observed in [3] on going from solid $Br_5^+AsF_6^-$ to its HF solution, might be due to Br_5^+ having C_{2h} symmetry in the solid and a skew conformation in HF solution. This could also cause the 108 cm^{-1} Raman band observed [3] for the HF solution being possibly due to one of the other modes, (ν_4 or ν_8), which are Raman inactive under C_{2h} symmetry. When judging the quality of the agreement, it must be also kept in mind that the computed values are harmonic frequencies for the free gaseous species, whereas the observed values are anharmonic frequencies recorded for either ionic solids or solvated ions.

Charge Distribution

The charge distribution in Br_5^+ has also been calculated and is given in Table 4. As has been pointed out previously [23] in a study of I_5^+, the structure and bonding in pentahalogen (1+) cations can be simply rationalized in terms of the following valence bond structures,

```
    X                 X
    |          ↔      |
⁺X—X   X         X   X—X⁺
     ·|               |
     X                X
```
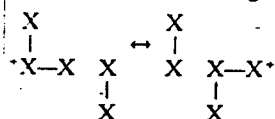
resulting in weak three-centered four-electron bonds for the three central halogen atoms and "normal" terminal halogen-halogen bonds with a bond order of about one. According to this model, the halogen atoms 2 and 2' should carry most of the positive charge. In the previous

Table 4 Computed Charge Distributions for Br_5^+ and Cl_5^+

| | atomic charge (e) | | |
atom	Br_5^+ LDF C_{2h}	LDF opt	Cl_5^+ LDF C_{2h}
X1	0.09	0.11	0.08
X2	0.25	0.25	0.26
X2'	0.25	0.25	0.26
X3	0.20	0.20	0.20
X3'	0.20	0.19	0.20

paper [23] on I_5^+, a charge distribution could be calculated only for Cl_5^+ due to computational limitations. Surprisingly, the central Cl atom in Cl_5^+ was found to carry most of the positive charge (+0.3 e) with Cl2 and Cl2' carrying each only +0.15 e charges. This result was in contrast to the findings for the crystal structure of I_5^+ in its AsF_6^- salt where the absence of iodine-fluorine contacts for the central iodine atom indicated that it carried little positive charge [23]. Our results for Br_5^+ with Br1 carrying only a +0.10 e charge and the two Br2 atoms carrying a total charge of +0.50 e is in good agreement with the findings for I_5^+ and the above valence bond model. To test whether the charge distribution and bonding in Cl_5^+ and Br_5^+ are indeed different, we have also computed Cl_5^+ by the LDF method. The results from this computation (see Tables 1 and 4) show that the charge distribution and hence the bonding in Cl_5^+ and Br_5^+ are very similar. These results suggest that the previous calculations of the charges [23] did not give an appropriate charge distribution, probably due to the use of a basis set that was too small.

References

[1] K. C. Lee, F. Aubke, Inorg. Chem. 19 (1980) 119

[2] H. Hartl, J. Nowicki, R. Minkwitz, Angew. Chem. Int. Ed. Engl.. 30 (1991) 328

[3] K. O. Christe, R. Bau, D. Zhao, Z. anorg. allg. Chem. 593 (1991) 46

[4] R. O. Jones, Angew. Chem. Int. Ed. Engl., 30 (1991) 630

[5] R. G. Parr, W. Yang, Density Functional Theory of Atoms and Molecules, Oxford University Press, New York 1989

[6] D. R. Salahub, Ab Initio Methods in Quantum Chemistry-II, ed. K. P. Lawlwy, J. Wiley & Sons, New York 1987, p. 447

[7] E. Wimmer, A. J. Freeman, C.-L. Fu, P.-L. Cou, S.-H. Chou, B. Delley, "Supercomputer Research in Chemistry and Chemical Engineering", K. F. Jensen, D. G. Truhlar, Eds., ACS Symposium Series, American Chemical Society, Washington, D.C., 1987, p. 49

[8] R. O. Jones, O. Gunnarsson, Rev. Mod. Phys. 61 (1989) 689

[9] T. Zeigler, Chem. Rev. 91 (1991) 651

[10] *D. A. Dixon, A. Andzelm, G. Fitzgerald, E. Wimmer, B. Delley*, "Science and Engineering on Supercomputers", Ed. E. J. Pitscher, Computational Science Publications, Southhampton/England 1990, p. 285

[11] *D. A. Dixon, J. Andzelm, G. Fitzgerald, E. Wimmer, P. Jasien*, "Density Functional Methods in Chemistry", Ed. J. Labanowski, J. Andzelm, Springer-Verlag, New York 1991, p. 33

[12] *B. Delley*, J. Chem. Phys. 92 (1990) 508. Dmol is available commercially from BIOSYM Technologies, San Diego, CA

[13] *B. Delley*, "Density Functional Methods in Chemistry", Ed. J. Labanowski, J. Andzelm; Springer-Verlag: New York 1991, p. 101

[14] This grid can be obtained using the FINE parameter in DMol

[15] *U. von Barth, L. Hedin*, J. Phys. C 5 (1972) 1629

[16] (a) *I. Versiuis, T. Ziegler*, J. Chem. Phys. 88 (1988) 3322; (b) *J. Andzelm, E. Wimmer, D. R. Salahub*, "The Challenge of d and f Electrons, Theory and Computation"; *D. R. Salahub, M. C. Zerner*, Eds., ACS Symposium Series 394, American Chemical Society; Washington, DC 1989, p. 228; (c) *R. Fournier, J. Andzelm, D. R. Salahub*, J. Chem. Phys. 90 (1989) 6371

[17] *M. D. Harmony, V. W. Laurie, R. L. Kuczkowski, R. M. Schwendeman, D. A. Ramsay, F. J. Lovas, W. J. Lafferty, A. G. Maki*, J. Phys. Chem. Ref. Data 8 (1979) 619

[18] *N. N. Greenwood, A. Earnshaw*, "Chemistry of the Elements", Pergamon Press, Oxford 1984, p. 744

[19] *K. O. Christe, E. C. Curtis, D. A. Dixon, H. P. Mercier, J. C. P. Sanders, G. J. Schrobilgen*, J. Amer. Chem. Soc. 113 (1991) 3351

[20] *A. W. Coleman, C. M. Means, S. G. Bott, J. L. Atwood*, J. Cryst. Spectr. Res. 20 (1990) 199

[21] *W. B. Person, G. R. Anderson, J. N. Fordemwalt, H. Stammreich, R. Forneris*, J. Chem. Phys. 35 (1961) 908

[22] *G. R. Burns, R. M. Renner*, Spectrochim. Acta 47 A (1991) 991

[23] *A. Apblett, F. Grein, J. P. Johnson, J. Passmore, P. S. White*, Inorg. Chem. 25 (1986) 422

Korrespondenzanschrift:

Dr. O. Christe
Rocketdyne Division, Rockwell Intern. Corpor.,
6633 Canoga Avenue,
Canoga Park, CA 91303/U.S.A.

9934

Nitrogen Pentafluoride: Covalent NF$_5$ versus Ionic NF$_4^+$F$^-$ and Studies on the Instability of the Latter

Karl O. Christe* and William W. Wilson

Contribution from Rocketdyne, A Division of Rockwell International Corporation, Canoga Park, California 91039-7922. Received June 9, 1992

Abstract: Recent ab initio calculations suggesting that covalent NF$_5$ and even NF$_6^-$ are vibrationally stable and might be experimentally accessible prompted us to critically evaluate the presently available theoretical and experimental data for NF$_5$ and to carry out experiments on the stability of ionic NF$_4^+$F$^-$. It is shown that covalent NF$_5$ of D_{3h} symmetry and crystalline NF$_4^+$F$^-$ should be of comparable energy but that covalent NF$_5$ should suffer from severe ligand-crowding effects that would make its synthesis experimentally very difficult. On the other hand, crystalline NF$_4^+$F$^-$ should be readily accessible from the well-known solvated NF$_4^+$ and F$^-$ ions. The recent discoveries of a convenient synthesis of truly anhydrous N(CH$_3$)$_4$F as a source of soluble "naked" fluoride ions and of solvents which possess sufficient kinetic stability toward strong oxidizers allowed us to carry out experiments on the thermal stability of NF$_4^+$F$^-$. It is shown that at temperatures as low as -142 °C crystalline NF$_4^+$F$^-$ is unstable toward decomposition to NF$_3$ and F$_2$, a process which is calculated to be exothermic by about 32 kcal mol^{-1}.

Introduction

Ever since the first successful synthesis of the NF$_4^+$ cation in 1966,[1] the possible existence of its parent molecule, NF$_5$, has been a challenge to both experimental chemists[2-10] and theoreticians.[11-14] Although the experimentalists have so far failed to isolate NF$_5$, interest in its synthesis was renewed by recent ab initio calculations which suggested that NF$_5$ is a vibrationally stable molecule[13,14] and that even NF$_6^-$ might be structurally stable.[15] Since NF$_5$ could exist either as a covalent, trigonal pyramidal molecule of D_{3h} symmetry
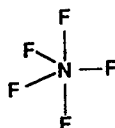
or as an ionic NF$_4^+$F$^-$ salt, it was necessary to evaluate the relative energies of the two forms and their synthetic accessibility in view of previously published[2-14] and new experimental data.

Results and Discussion

The relative energies of covalent NF$_5$ and ionic NF$_4^+$F$^-$ with respect to each other and to NF$_3$ and F$_2$ can be estimated from a Born–Haber cycle using the following data:

Taking the average of two values of 30.1 and 35.5 kcal mol^{-1} calculated[13,14] for ΔH_1 at the MP2/6-31++G** and MP2/6-311+G* levels of theory, respectively, the formation of covalent NF$_5$ from NF$_3$ and F$_2$ is endothermic by about 32.8 kcal mol^{-1}. Furthermore, the enthalpy of formation, ΔH_2, of the free gaseous NF$_4^+$ and F$^-$ ions from NF$_3$ and F$_2$ can be estimated as $+182.4$ kcal mol^{-1} by taking the average between the values of 183.7 and 181.1 kcal mol^{-1} obtained by the MP2/6-31G* calculation and from a combination of the experimental values for the dissociation energy of F$_2$ and the first ionization potential and electron affinity of the F atom[16,17] and the calculated F$^+$ affinity of NF$_3$,[18] respectively. From $\Delta H_1 - \Delta H_2$, the enthalpy of formation of covalent NF$_5$ from gaseous free NF$_4^+$ and F$^-$ ions becomes $\Delta H_3 = -149.6$ kcal mol^{-1}. The value of ΔH_4, the enthalpy of formation of crystalline NF$_4^+$F$^-$ from NF$_3$ and F$_2$, is given by the sum of ΔH_2 and the lattice energy U_L of NF$_4^+$F$^-$(cr). The value of U_L is the average of two previous estimates (-150.6 and -147.0 kcal mol^{-1})[9,19] and a value of -154.1 kcal mol^{-1} obtained by Bartlett's empirical equation,[20] U_L (kcal/mol) = 556.3(V_m)$^{-1/3}$ + 26.3, where V_m is the sum of the molar volumes of NF$_4^+$ and F$^-$ that were estimated as 64.9 and 17.5 Å^3, respectively, from known crystal structures.[21,22] From $\Delta H_1 - \Delta H_4$, the energy difference between crystalline NF$_4^+$F$^-$ and covalent NF$_5$ can then be estimated to be rather small and be of the order of about 1 ± 6 kcal mol^{-1},

(1) Christe, K. O.; Guertin, J. P.; Pavlath, A. E. *Inorg. Nucl. Chem. Lett.* **1966**, *2*, 83; U.S. Patent 3503719, 1970.

(2) Miller, A. R.; Tsukimura, R. R.; Velten, R. *Science (Washington, D.C.)* **1967**, 688.

(3) Goetschel, C. T.; Campanile, V. A.; Curtis, R. M.; Loos, K. R.; Wagner, C. D.; Wilson, J. N. *Inorg. Chem.* **1972**, *11*, 1696.

(4) Solomon, I. J.; Keith, J. N.; Snelson, A. *J. Fluorine Chem.* **1972/73**, *2*, 129.

(5) Olah, G. A.; Donovan, D. J.; Shen, J.; Klopman, G. *J. Am. Chem. Soc.* **1975**, *97*, 3559.

(6) Christe, K. O.; Schack, C. J.; Wilson, R. D. *Inorg. Chem.* **1976**, *15*, 1275.

(7) Keith, J. N.; Solomon, I. J.; Sheft, I.; Hyman, H. *Inorg. Nucl. Chem.—Herbert H. Hyman Mem. Vol.* **1976**, 143.

(8) Christe, K. O.; Wilson, R. D.; Goldberg, I. B. *Inorg. Chem.* **1979**, *18*, 2572.

(9) Bougon, R.; Bui Huy, T.; Burgess, J.; Christe, K. O.; Peacock, R. D. *J. Fluorine Chem.* **1982**, *19*, 263.

(10) Christe, K. O.; Wilson, W. W.; Schrobilgen, G. J.; Chirakal, R. V.; Olah, G. A. *Inorg. Chem.* **1988**, *27*, 789.

(11) Murrell, J. N.; Scollary, C. E. *J. Chem. Soc., Dalton Trans.* **1976**, 818.

(12) Peters, N. J. S. Dissertation, Princeton University, 1982. Peters, N. J. S.; Allen, L. C. In *Fluorine Containing Molecules*; Liebman, J. F., Greenberg, A., Dolbier, W. R., Eds.; VCH Publishers: Weinheim, Germany, 1988; pp 252–4.

(13) Ewig, C. S.; Van Wazer, J. R. *J. Am. Chem. Soc.* **1989**, *111*, 4172.

(14) Michels, H. H.; Montgomery, J. A., Jr. *J. Chem. Phys.* **1990**, *93*, 1805.

(15) Ewig, C. S.; Van Wazer, J. R. *J. Am. Chem. Soc.* **1990**, *112*, 109.

(16) Berkowitz, J.; Wahl, A. C. *Adv. Fluorine Chem.* **1973**, *7*, 147.

(17) Chase, M. W.; Davies, C. A.; Downey, J. R.; Frurip, D. J.; McDonald, R. A.; Syverud, A. N. *J. Phys. Chem. Ref. Data, Suppl.* **1985**, *14*, 1011–3.

(18) Christe, K. O.; Dixon, D. A. *J. Am. Chem. Soc.* **1992**, *114*, 2978.

(19) Wilson, J. N. *Adv. Chem. Ser.* **1966**, *54*, 30.

(20) Richardson, T. J.; Tanzella, F. L.; Bartlett, N. *J. Am. Chem. Soc.* **1986**, *108*, 4937.

(21) Christe, K. O.; Lind, M. D.; Thorup, N.; Russell, D. R.; Fawcett, J.; Bau, R. *Inorg. Chem.* **1988**, *27*, 2450.

(22) Christe, K. O.; Wilson, W. W.; Wilson, R. D.; Bau, R.; Feng, J. *J. Am. Chem. Soc.* **1990**, *112*, 7619.

Integrating eq 3, with the aid of the integral $Ei(-x) = -\int_{-x}^{\infty}(e^{-x}/x)$ $\approx e^{-x}(x^{-2} - x^{-1})$ for $x \gg 1$, yields

$$\chi = \frac{K}{\alpha}\left(\frac{RT}{\Delta H_s}\right)\exp\left[-\frac{\Delta H_s}{RT}\right]\cdots \qquad (5)$$

The heat of sublimation ΔH_s is determined by plotting the TGA data as shown in Figure 4. From the slopes of $\ln(\chi/T)$ versus $1/T$ curves, we obtain $\Delta H_s = 30$, 35, and 39 kcal/mol for $\alpha = 0.3$, 1.2, and 5 °C/min, respectively. Also from $\ln(\alpha/T)$ vs $1/T$ plots for a given χ, e.g., 0.1, we obtain $\Delta H_s = 40$ kcal/mol.

The heat of sublimation of C_{60} powders has been reported previously to be 40 kcal/mol.[14] Our result of $\Delta H_s = 39$ kcal/mol, determined at a scan rate of 5.0 °C/min, is in a good agreement with the reported data. The cause of the lower values, e.g., 30 and 35 kcal/mol obtained at lower rates of 0.3 and 1.2 °C/min, is not clear. Haufler et al.[1] reported a much lower value of ΔH_s ~22 kcal/mol. It has been suggested[14] that the low values of ΔH_s observed may be due to the less structurally ordered C_{60} powders which undergo a change during the experiment. Alternatively, we proposed here that the presence of nonuniform defective microstructure, such as stacking fault and grain boundary, is responsible for the lower heats of sublimation derived from TGA measurements. C_{60} molecules at such defective structures sublime at lower temperature than does those in bulk crystal grain, and in TGA scan it contributes to the weight loss in the low-temperature regime. This results in the drastic reduction in the slope of χ/T vs $1/T$ curve and thus in the apparent heat of sublimation determined. To test this viewpoint, we prepared a new batch of C_{60} powders sublimed from a purified C_{60} extract at a slower rate. The new sample showed sharp X-ray diffraction lines, indicating a good crystallinity. The new sample shows no detectable structural relaxation in TGA scan up to 450 °C. The TGA curve at 0.3 °C/min of this new sample diverges starting ≤400 °C and merges again ~620 °C with that of the less ordered structural sample (see Figure 4). Although the deviation is small, the heat of sublimation of the new sample, ~35 kcal/mol, is higher by 5 kcal/mol. We may conclude that the heats of sublimation obtained are of the lower limiting values. The $\Delta H_s \sim 40$ kcal/mol of C_{60} powders is low as compared with that of graphite's ($\Delta H_s \sim 170$ kcal/mol). This reflects the weak van der Waals bonding among C_{60} molecules in the fcc structure.[15,16]

(14) Pan, C.; Sampson, M. P.; Chai, Y.; Hauge, R. H.; Margrave, J. L. *J. Phys. Chem.* **1991**, *95*, 2944.

(15) Fischer, J. E.; Heiney, P. A.; McGhie, A. R. *Science* **1991**, *252*, 1288.
(16) Fleming, R. M.; Hessen, B.; Kortan, A. R.; Siegriest, T.; Marsh, P.; Murphy, D. W.; Haddon, R. C.; Tycho, R.; Dabbagh, G.; Mujsce, A. M.; Kaplan, M. L.; Zahurak, S. M. *Mater. Res. Soc. Symp. Proc.* **1991**, *206*, 691.

Nitrosyl Hypofluorite: Local Density Functional Study of a Problem Case for Theoretical Methods[†]

David A. Dixon*,‡ and Karl O. Christe§

Central Research and Development Department, E. I. du Pont de Nemours and Company, Inc., Experimental Station, Wilmington, Delaware 19880, and Rocketdyne, A Division of Rockwell International Corporation, Canoga Park, California 91303 (Received: October 21, 1991; In Final Form: December 17, 1991)

Local density functional (LDF) theory can successfully reproduce the previously published vibrational spectra and the salient geometrical parameters derived from them for FONO for which conventional ab initio methods (CISD/6-31G*) fail. LDF theory was used to calculate the geometries, vibrational spectra, force fields, and charge distributions for the three isomers *cis*-FONO, *trans*-FONO, and FNO₂. It is shown that FNO₂ is 40.8 kcal mol⁻¹ more stable than *cis*-FONO, which in turn is favored by 25.2 kcal mol⁻¹ over the trans isomer. It is shown that the previously published approximate mode descriptions for FONO are correct but that the observed spectra must be due to *cis*-FONO and not to the trans isomer as previously proposed. The bonding in *cis*-FONO is best rationalized in terms of an F atom loosely bonded through an oxygen atom to an NO₂ molecule, resulting in the following structural parameters: $r_{F-O} = 1.673$ Å, $r_{FO-N} = 1.216$ Å, $r_{N-O} = 1.190$ Å, $\angle FON = 118.0°$, and $\angle ONO = 135.2°$.

Introduction

Although much progress has been made during the past 20 years in the field of ab initio calculations of the geometries and energetics of molecules, there have been a number of cases which have been extremely difficult to compute with conventional methods. A classic example for such a "problem" molecule is FOOF, for which very high level calculations (CAS/CCI or CCSD(T)) with a large basis set were required to duplicate the experimental geometry.[1a] An even more difficult test is the duplication of the observed vibrational spectra. In a recent study,[1b] it has been shown that density functional theory (which is an ab initio method) in the local density approximation (LDF)[2] can predict both the structure and harmonic frequencies of FOOF.

TABLE I: Geometry Parameters for FNO₂[a]

param	LDF	expt[13]
N–F	1.487	1.467
N–O	1.190	1.180
$\angle$(F–N–O)	111.8	112
$\angle$(O–N–O)	136.4	136

[a] Bond distances in angstroms, bond angles in degrees.

Noble has recently called attention[3] to another similar "problem" molecule, FONO, or nitrosyl hypofluorite. This

[†] Contribution No. 6018.
‡ E. I. du Pont de Nemours and Co., Inc.
§ Rocketdyne Division, Rockwell International Corp.

(1) (a) See: Scuseria, G. E. *J. Chem. Phys.* **1991**, *94*, 442, for the most recent ab initio molecular orbital calculations. (b) See: Dixon, D. A.; Andzelm, J.; Fitzgerald, G.; Wimmer, E. *J. Phys. Chem.* **1991**, *95*, 9197, for the LDF calculations on FOOF and a discussion of previous calculations.

TABLE II: Vibrational Frequencies, Potential Energy Distribution, and Assignments for FNO_2

mode designation in point group C_{2v}	approx description of mode	frequency, cm^{-1}		potential energy distribution LDF
		expt[11,12]	LDF	
$A_1\ \nu_1$	ν sym NO_2	1310	1361	−0.730 (1)−0.347 (2)−0.589 (3)
$A_1\ \nu_2$	ν NF	568	590	0.042 (1)−0.816 (2)+0.577 (3)
$A_1\ \nu_3$	δ sciss NO_2	822	821	−0.027 (1)−0.504 (2)−0.864 (3)
$B_1\ \nu_4$	ν asym NO_2	1792	1892	−0.808 (4)+0.590 (5)
$B_1\ \nu_5$	$\delta\ FNO_2$ in plane	560	541	0.037 (4)+0.999 (5)
$B_2\ \nu_6$	$\delta\ FNO_2$ out of plane	742	740	−1.0 (6)

*The following symmetry coordinates were used for the PED: (1) N−O1 + N−O2; (2) N−F; (3) O1−N−O2; (4) N−O1 − N−O2; (5) F−N−O1 − F−N−O2; (6) F−NO_2.

molecule has been observed only in a matrix by infrared spectroscopy.[4] A force constant analysis of these spectra suggested a planar trans configuration with a weak F−O bond[5] which could not be duplicated by traditional ab initio molecular orbital methods.[3] In view of the excellent results[1b] of LDF theory for FOOF, which has a structure similar to that of FONO, it was interesting to examine whether this theory can also master the FONO problem.

Computational Methods

The calculations described below were done in the local density functional approximation[2] by using the program system DMOL.[6,7] The atomic basis functions are given numerically on an atom-centered, spherical-polar mesh. The radial portion of the grid is obtained from the solution of the atomic LDF equations by numerical methods. The use of exact spherical atom results offers some advantages. The molecule will dissociate exactly to its atoms within the LDF framework, although this does not guarantee correct dissociation energies. Furthermore, because of the quality of the atomic basis sets, basis set superposition effects should be minimized and correct behavior at the nucleus is obtained.

Since the basis sets are numerical, the various integrals arising from the expression for the energy need to be evaluated over a grid. The integration points are generated in terms of radial functions and spherical harmonics. The number of radial points N_R is given as

$$N_R = 1.2 \times 14(Z + 2)^{1/3}$$

where Z is the atomic number. The maximum distance for any function is 12 au. The angular integration points N_θ are generated at the N_R radial points to form shells around each nucleus. The value of N_θ ranges from 14 to 302 depending on the behavior of the density.[8] The Coulomb potential corresponding to the electron repulsion term is determined directly from the electron density by solving Poisson's equation. In DMOL, the form for the exchange-correlation energy of the uniform electron gas is that derived by von Barth and Hedin.[9]

(2) (a) Parr, R. G.; Yang, W. *Density Functional Theory of Atoms and Molecules*; Oxford University Press: New York, 1989. (b) Salahub, D. R. In *Ab Initio Methods in Quantum Chemistry-II*; Lawley, K. P., Ed.; Wiley: New York, 1987; p 447. (c) Wimmer, E.; Freeman, A. J.; Fu, C.-L.; Cao, P.-L.; Chou, S.-H.; Delley, B. In *Supercomputer Research in Chemistry and Chemical Engineering*; Jensen, K. F., Truhlar, D. G., Eds.; ACS Symposium Series; American Chemical Society: Washington, D.C., 1987; p 49. (d) Jones, R. O.; Gunnarsson, O. *Rev. Mod. Phys.* **1989**, *61*, 689. (e) Zeigler, T. *Chem. Rev.* **1991**, *91*, 651. (f) Dixon, D. A.; Andzelm, A.; Fitzgerald, Wimmer, E.; Delley, B. In *Science and Engineering on Supercomputers*; Pitcher, E. J., Ed.; Computational Science Publications: Southhampton, England, 1990; p 285. (g) Dixon, D. A.; Andzelm, J.; Fitzgerald, G.; Wimmer, E.; Jasien, P. In *Density Functional Methods in Chemistry*; Labanowski, J., Andzelm, J., Eds.; Springer-Verlag: New York, 1991; p 33.
(3) Noble, P. N. *J. Phys. Chem.* **1991**, *95*, 4695.
(4) Smardzewski, R. R.; Fox, W. B. *J. Chem. Phys.* **1974**, *60*, 2980.
(5) Sorenson, S. A.; Noble, P. N. *J. Chem. Phys.* **1982**, *77*, 2483.
(6) Delley, B. *J. Chem. Phys.* **1990**, *92*, 508. DMOL is available commercially from BIOSYM Technologies, San Diego, CA.
(7) Delley, B. In *Density Functional Methods in Chemistry*; Labanowski, J., Andzelm, J., Eds.; Springer-Verlag: New York, 1991; p 101.
(8) This grid can be obtained by using the FINE parameter in DMOL.
(9) von Barth, U.; Hedin, L. *J. Phys. C* **1972**, *5*, 1629.

TABLE III: Symmetry Force Constants (mdyn/Å) of FNO_2

	1	2	3	4	5	6
1	13.97					
2	1.13	3.03				
3	0.56	−0.71	1.82			
4				11.44		
5				0.51	1.26	
6						0.40

All of the DMOL calculations were done with a double numerical basis set augmented by polarization functions. This can be considered in terms of size, for comparison to traditional molecular orbital calculations, as a polarized double-ζ basis set. However, because of the use of exact numerical solutions for the atom, this basis set is of significantly higher quality than a normal molecular orbital polarized double-ζ basis set. The multipolar fitting functions for the model density used to evaluate the effective potential have angular momentum numbers, l, one greater than that of the polarization function. Since all of the atoms have d polarization functions, the value of l for the fitting function is 3.

Geometries were optimized by using analytic gradient methods. There are two problems with evaluating gradients in the LDF framework which are due to the numerical methods that are used. The first is that the energy minimum does not necessarily correspond exactly to the point with a zero derivative. The second is that the sum of the gradients may not always be zero as required for translational invariance. These tend to introduce errors on the order of 0.001 Å in the calculation of the coordinates if both a reasonable grid and basis set are used. This gives bond lengths and angles with reasonable error limits. The difference of 0.001 Å is about an order of magnitude smaller than the accuracy of the LDF geometries as compared to experiment. The frequencies were determined by numerical differentiation of the gradient. A two point difference formula was used and a displacement of 0.01 au. The force constant analysis was done with the BMATRIX program of Komornicki.[10]

Results and Discussion

Nitryl Fluoride, FNO_2. Since nitryl fluoride, FNO_2, is isomeric with FONO and well characterized,[11-13] the quality of the LDF calculation was first examined for this molecule. As shown in Table I, the agreement between the calculated and experimental structures[13] is very good, with the LDF bond distances being 0.01–0.02 Å longer than the experimental values as found for other similar compounds.[2f,g] The vibrational spectrum and the assignments in terms of internal coordinates are given in Table II and the symmetry force constants in Table III. The agreement between theory and experiment[11,12] is also quite good considering that the calculated values correspond to harmonic values and the experimental ones include the effects of anharmonicity.

(10) Komornicki, A. Private communication. This program was developed to help in analyzing the results from the GRADSCF program system.
(11) Christe, K. O.; Schack, C. J.; Wilson, R. D. *Inorg. Chem.* **1974**, *13*, 2811.
(12) Bernitt, D. L.; Miller, R. H.; Hisatsune, I. C. *Spectrochim. Acta, Part A* **1967**, *23*, 237.
(13) Harmony, M. D.; Laurie, V. W.; Kuczkowski, R. L.; Schwendeman, R. H.; Ramsay, D. A.; Lovas, F. J.; Lafferty, W. J.; Maki, A. G. *J. Phys. Chem. Ref. Data* **1979**, *8*, 619.

TABLE IV: Geometry Parameters[a] Computed by Different Methods for FONO

| | LDF | | force field | HF/6-31+G*[3] | | CISD/6-31+G*[3] | |
param	cis	trans	analysis[5] trans	cis	trans	cis	trans
F–O1	1.673	1.888	1.57	1.365	1.360	1.405	1.398
N–O1	1.216	1.163	1.27	1.366	1.381	1.399	1.425
N–O2	1.190	1.193	1.18	1.141	1.143	1.159	1.161
∠F–O1–N	118.0	106.5	110	111.3	104.7	110.6	104.0
∠O1–N–O2	135.2	152.1	160	116.0	108.9	115.9	108.0

[a] Bond distances in angstroms, bond angles in degrees.

TABLE V: Mulliken Charges (e) for FONO

atom	cis	trans	atom	cis	trans
O1	0.08	0.06	F	–0.30	–0.41
N	0.29	0.42	O2	–0.07	–0.07

Nitrosyl Hypofluorite, FONO. Whereas the FNO_2 molecule is not particularly difficult to calculate by conventional ab initio methods, its FONO isomer is a real "problem" molecule[3] and a challenge to almost any computational method. The FONO molecule could exist either as a cis, a skew, or a trans isomer:
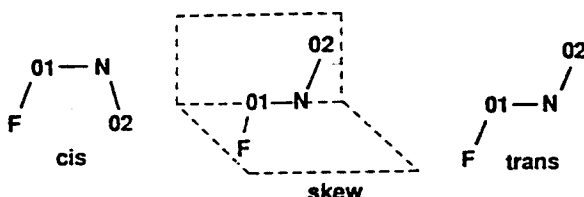
LDF calculations starting with a skew structure and a dihedral angle of 90° led to the cis configuration. The cis isomer was found to be 25.2 kcal mol⁻¹ more stable than the trans and 40.8 kcal mol⁻¹ less stable than FNO_2. The geometry parameters calculated by the LDF method for cis- and trans-FONO are shown in Table IV and are compared to those either derived from the force field analysis[5] of the observed vibrational spectra[4] or calculated by conventional ab initio methods.[3] As can be seen, only the LDF values approximate the "experimental" bonding parameters derived from the force-field analysis[5] with the cis isomer resulting in a better agreement. The latter fact is no surprise as the cis isomer is energetically favored over the trans isomer by 25.2 kcal mol⁻¹. For the LDF computed trans isomer, the F–O bond is very long and also the N–O1 bond is shorter than the terminal N–O bond, which is not expected as two atoms are bonded to this oxygen (O1) as compared to a single atom bonded to the terminal oxygen. Unfortunately, the previous force-field analysis[5] has been carried out only for the trans isomer using vibrational frequencies which belong to the cis isomer (see below). If the force-field analysis[5] had been carried out with the more likely cis geometry, the agreement with the cis isomer LDF values would certainly have been better.

The geometry calculated by the LDF method for cis-FONO is very plausible. The F–O bond length is 0.1 Å longer than that in FOOF (1.575 Å experimental[13] and 1.563 Å calculated[1]), as expected from the lower thermal stability of FONO. The two N–O bond distances are quite similar with oxygen bonded to the F having an N–O bond distance 0.026 Å longer than the terminal N–O distance. The structure of the NO_2 fragment is very similar

to that of the free NO_2 radical which has an N–O distance of 1.197 Å and an O–N–O bond angle of 133.8°.[13] The F–O1–N bond angle is near 120° and is somewhat larger than the tetrahedral OOF bond angle in FOOF. These results show that the FONO structure is significantly different from that of cis-nitrous acid[13] and more closely resembles that of FOOF. Furthermore, the data in Table IV demonstrate that in agreement with the findings[1] for FOOF, the molecular orbital CISD/6-31G* calculations based on a single configuration[3] fail to predict the correct structure for FONO.

The main differences between the cis and the trans configurations of FONO are the following. In trans-FONO, the F–O bond length has increased by 0.2 Å. At the same time the average N–O bond length has shortened by about 0.02 Å and the O–N–O bond angle has significantly increased by 17°. These changes demonstrate that in trans-FONO the contributions from the ionic $[O=N=O]^+F^-$ structure have significantly increased. This interpretation is confirmed by the Mulliken populations given in Table V, which show that the ionic character increases from cis-FONO to trans-FONO.

The vibrational frequencies were calculated for both cis- and trans-FONO and, together with their assignments and potential energy distributions, are summarized in Table VI. As can be seen from this table, the experimentally observed[4] frequencies must belong to the energetically favored cis isomer and not, as previously assumed,[5] to the trans isomer. The agreement between the computed and experimental frequencies is quite good considering the difficulty of this problem. As for FNO_2 (see above), most of the fundamental vibrations of FONO are not pure vibrations but strong mixtures of several symmetry coordinates. The present analysis confirms the approximate mode descriptions previously proposed[5] on the basis of the observed[4] isotopic shifts. Thus, the 1716-cm⁻¹ transition is mainly an antisymmetric combination of the two N–O stretching coordinates with a larger contribution from the terminal N–O2 stretch. The 1200-cm⁻¹ transition is mainly a symmetric combination of the two N–O stretching coordinates with a larger contribution from the internal N–O1 stretch. The two bending motions, ν_4 and ν_5, also contribute significantly to these two transitions. The 412-cm⁻¹ transition involves mainly the stretching of the O–F bond and therefore is properly assigned as the O–F stretching mode, whereas the 702-cm⁻¹ transition is mainly due to the ONO scissoring mode. The fact that for FONO the computed O–F stretching frequency is 115 cm⁻¹ higher than the observed one is consistent with the previous findings[1] for FOOF, where the calculated stretches (749 and 715 cm⁻¹) were also about 110 cm⁻¹ higher than the observed ones (630 and 615 cm⁻¹).[14] The lowest frequency vibration

TABLE VI: Vibrational Frequencies, Potential Energy Distribution,[a] and Assignments for FONO

mode in designation C_s	approx description of mode	expt[4]	LDF cis		LDF trans	
A′ ν_1	ν NO_2	1716	1810	0.75 (1)–0.52 (2)–0.21 (4)+0.34 (5)	2090	0.67 (1)–0.72 (2)
A′ ν_2	ν NO1	1200	1217	–0.38 (1)–0.83 (2)+0.25 (4)+0.32 (5)	1264	–0.63 (1)–0.54 (2)+0.16 (3)+0.30 (4)+0.43 (5)
A′ ν_3	ν OF	412	527	–0.16 (2)+0.76 (3)+0.44 (4)–0.45 (5)	470	–0.66 (3)+0.58 (4)+0.48 (5)
A′ ν_4	δ ONO in plane	702	721	–0.14 (2)–0.10 (3)+0.85 (4)–0.48 (5)	148	0.13 (3)+0.97 (4)–0.17 (5)
A′ ν_5	δ FNO in plane		166	0.13 (3)+0.50 (4)+0.86 (5)	254	0.17 (3)+0.77 (4)+0.61 (5)
A″ ν_6	torsion		522	1.0 (6)	380	1.0 (6)

[a] The following symmetry coordinates were used for the PED: (1) N–O2; (2) N–O1; (3) O1–F; (4) O1–N–O2; (5) F–O1–N; (6) F–O1–N–O2.

TABLE VII: Symmetry Force Constants (mdyn/Å) for FONO

	1	2	3	4	5	6
			LDF Cis			
1	13.02					
2	1.38	9.29				
3	0.23	1.03	1.95			
4	0.46	1.14	−0.53	1.12		
5	−0.09	−0.48	0.16	−0.25	0.57	
6						0.23
			LDF Trans			
1	12.78					
2	0.55	14.34				
3	0.40	0.14	1.08			
4	0.51	0.85	−0.09	0.19		
5	−0.16	0.11	0.16	−0.09	0.48	
6						0.09
		Experimental, Using Cis Frequencies and Trans Configuration and Assuming $\nu_5 = 205$ cm^{-1} (refs 4, 5)[a]				
1	13.06					
2	2.52	8.48				
3	0	0	1.01			
4	0.90	−0.27	0.43	1.32		
5	0	0	0	0	0.30	

[a] In the "experimental" force field, the deformation and stretch–bend interaction constants have been normalized for distance and have dimensions of mdyn Å rad^{-2} and mdyn rad^{-1}, respectively.

predicted (166 cm^{-1}) is below the spectrometer cutoff of the previous experimental study[4] and, therefore, would not have been observed. Thus, the calculations for cis-FONO can account for all the observed features, and the approximate mode descriptions previously given[5] by Sorenson and Noble are correct, although made for the incorrect trans isomer. In view of the ab initio CISD/6-31G* calculations failing to yield a correct geometry for FONO (see above), it is also not surprising that they could not reproduce[3] the experimentally observed frequencies.

The force constants calculated by the LDF method for cis- and trans-FONO are given in Table VII and are compared to the force

(14) Kim, K. C.; Campbell, G. M. *J. Mol. Struct.* **1985**, *129*, 263.

field previously reported[5] for trans-FONO using the experimental[4] cis-FONO frequencies and isotopic shifts for $\nu_1-\nu_4$ and assuming a frequency of 205 cm^{-1} for ν_5. In spite of the obvious shortcomings of this "experimental" force field, it can be seen that it agrees much better with the LDF cis-isomer force field than with the trans-isomer one. This lends further support to our conviction that the previously reported infrared spectrum must be due to the cis and not to the trans isomer of FONO.

The force field of cis-FONO (see Table VII) is in good agreement with our expectations[1] for such a molecule. It shows significant coupling between the two NO stretches and between the internal N–O1 stretch and the O–F stretch and ONO scissoring mode. The suggested large difference of 3.73 mdyn/Å between the two N–O stretching force constants is somewhat surprising in view of their relatively small difference in bond lengths of only 0.026 Å. This force constant difference strongly depends on the values of the interaction force constants which are quite large in FONO. The calculated LDF force field and geometry, together with the available experimental isotopic shifts,[4] could be used to fine tune the force field and to verify the large difference in the N–O stretching force constants. This large difference could be caused by strong perturbations in the electronic structure of the ONO fragment of FONO due to the weakly bonded fluorine atom.

Conclusion

The LDF method is well suited for the prediction of the structures and vibrational spectra of "problem" compounds such as FOOF and FONO for which conventional ab initio molecular orbital methods at the CISD/6-31G* level fail. Furthermore, the vibrational spectra previously reported[4] for FONO and attributed to its trans isomer are compatible only with the cis isomer. The bonding in cis-FONO resembles that in FOOF and consists of a fluoride ligand loosely coupled through an oxygen atom to the NO$_2$ molecule, thus resulting in weak F–O and strong NO$_2$ bonds.

Forced Electrochemical Nonlinear Oscillator Assembled on Rotating Ring–Disk Electrodes

Seiichiro Nakabayashi and Akira Kira*

The Institute of Physical and Chemical Research (RIKEN), Wako-shi, Saitama 351, Japan
(Received: November 12, 1991)

Self-sustained potential oscillation was observed on a polycrystalline platinum ring electrode under the galvanostatic (constant current) electrochemical oxidation of formaldehyde in a rotating ring–disk electrode cell. When a pulsed stream of hydrogen was supplied to the ring electrode from the disk electrode, the self-sustained oscillation changed to the forced oscillation under certain conditions.

Introduction

Some chemical reactions oscillate. The Belousov–Zhabotinski reaction is famous along oscillating homogeneous reactions.[1] In heterogeneous reactions, the catalytic oxidation of carbon mon-

oxide on the platinum surface is an established oscillating reaction.[2,3] Recently, instabilities in electrochemical systems have attracted great interest.[4–9] Some of them show transition into

(1) Scott, S. K. *Chemical Chaos*; Clarendon Press: Oxford, U.K., 1991; and references cited therein.

(2) Fink, T.; Imbihl, R.; Ertl, G. *J. Chem. Phys.* **1989**, *91*, 5002.
(3) Rotermund, H. H.; Jakubith, S.; von Oertzen, A.; Ertl, G. *J. Chem. Phys.* **1989**, *91*, 4942.
(4) Basset, M. R.; Hudson, J. L. *J. Phys. Chem.* **1988**, *92*, 6963.

Tetrafluorosulfate(1-) and Tetrafluorooxosulfate(1-) Radical Anions (SF$_4^-$ and SF$_4$O$^-$)[†,‡]

K. O. Christe,*[,4] D. A. Dixon,[3] I. B. Goldberg,[2] C. J. Schack,[4] B. W. Walther,[1,§]
J. T. Wang,[1] and F. Williams*[,1]

*Contribution from the Department of Chemistry, University of Tennessee,
Knoxville, Tennessee 37996-1600, Science Center, Rockwell International Corporation,
Thousand Oaks, California 91360, Central Research Department, Experimental Station, E.I.
DuPont de Nemours and Company, Wilmington, Delaware 19880-0328, and Rocketdyne Division,
Rockwell International, Canoga Park, California 91309-7922. Received August 10, 1992*

Abstract: The novel radical anions SF$_4^-$ and *trans*-SF$_4$O$^-$ were generated by γ-irradiation of CsSF$_5$ and CsSF$_5$O, respectively, at -196 °C and characterized by their isotropic EPR spectra at $+27$ °C. The SF$_4^-$ anion ($g = 2.0045$, $a_{^{33}S} = 12.85$ mT, $a_{^{19}F}$ = 9.75 mT) has a square-planar structure close to D_{4h} symmetry derived from a pseudo-octahedron in which the two axial positions are equally occupied by a total of three sterically active valence electrons. Accordingly, the greatest portion of the unpaired electron spin is localized in a sulfur p$_z$ orbital. The *trans*-SF$_4$O$^-$ anion ($g = 2.0027$, $a_{^{33}S} = 36.26$ mT, $a_{^{19}F} = 18.95$ mT) has a closely related, pseudo-octahedral structure of C_{4v} symmetry in which the equatorial positions are occupied by four equivalent fluorines, one axial position is occupied by a doubly bonded oxygen, and the second axial position is occupied by the sterically active free valence electron. Accordingly, the greatest portion of the unpaired electron spin is localized in an axial sp-hybrid orbital of sulfur. The structures and electron spin density distributions of SF$_4^-$ and *cis*- and *trans*-SF$_4$O$^-$ were analyzed by a local density functional study which also provided vibrational frequencies and charge distributions for these radical anions. For comparison, the closely related SF$_5$ radical, the *cis*- and *trans*-PF$_4$O^{2-} radical anions, and the SF$_4$, SF$_4$O, and SF$_6$ molecules were also calculated by this method. These calculations show that the exclusive formation of *trans*-SF$_4$O$^-$ under our experimental conditions is probably due to both energetic and reaction mechanistic reasons and that the agreement between the LDF calculations and the experimental data is good.

Introduction

Previous studies have demonstrated that γ-irradiation of salts containing complex fluoro ions can result in the loss of one fluorine atom and in the formation of new complex fluoro radical ions that contain one fluorine atom less than the parent ion. Thus, the radical ions PF$_5^-$,[5-8] AsF$_5^-$,[8,9] and NF$_3^+$ [10,11] have been obtained from PF$_6^-$, AsF$_6^-$, and NF$_4^+$ containing salts, respectively, and

(1) University of Tennessee.
(2) The Science Center, Rockwell International Corp.
(3) E.I. DuPont de Nemours and Co.
(4) The Rocketdyne Division, Rockwell International Corp.
(5) (a) Morton, J. R. *Can. J. Phys.* 1963, *41*, 706. (b) Atkins, P. W.; Symons, M. C. R. *J. Chem. Soc.* 1964, 4363.
(6) Morton, J. R.; Preston, K. F. In *Fluorine-Containing Free Radicals*; Root, J. W., Ed.; ACS Symposium Series 66, American Chemical Society: Washington, D.C., 1978; p 386.
(7) Mishra, S. P.; Symons, M. C. R. *J. Chem. Soc., Chem. Commun.* 1974, 279.

characterized by electron paramagnetic resonance (EPR) spectroscopy.

Characterization by EPR is not always unambiguous. For example, the pseudo-octahedral XF_5 radicals PF_5^-[7] and SF_5[12]

$$\text{F} \underset{\underset{\text{F}}{\underset{|}{\overset{|}{\diagup}}}}{\overset{\overset{|}{\cdot}}{\underset{\text{F}}{\diagdown}}}\text{F} \qquad \text{I}$$
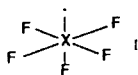
exhibited detectable hyperfine splittings (hfs) only for the four equatorial fluorine atoms but, surprisingly, not for the axial fluorine atom. For PF_5^- this led originally to an incorrect identification as PF_4.[5] In this respect, it seemed interesting to prepare the yet unknown SF_4^- radical. By comparison with the known isoelectronic ClF_4 radical,[13–15] a pseudo-octahedral structure with a square-planar XF_4 moiety

$$\text{F} \underset{\underset{\text{F}}{\underset{|}{\overset{|}{\diagup}}}}{\overset{\overset{|}{\cdot}}{\underset{\text{F}}{\diagdown}}}\text{F} \qquad \text{II}$$
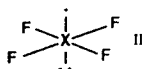
can be expected for SF_4^-. Therefore, the EPR spectrum of SF_4^- should, in general appearance, resemble that of the SF_5 radical,[12] but the g-factor and ^{19}F and ^{33}S hyperfine splittings should be significantly different.

After completion of this work, the results of a theoretical investigation on the molecular and electronic structure of the SF_n (n = 1–5) and their singly charged negative ions using density functional theory was published which also predicted an approximately square-planar structure for SF_4^-.[16]

Similarly, the preparation of the yet unknown SF_4O^- radical anion should be interesting. Its structure is expected to be similar to that of SF_4^-, except for the replacement of the axial free valence electron pair by an oxygen ligand.

$$trans \quad \text{F} \underset{\underset{\text{O}}{\underset{||}{\overset{|}{\diagup}}}}{\overset{\overset{|}{\cdot}}{\underset{\text{F}}{\diagdown}}}\text{F} \qquad \text{III}$$
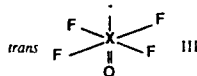
Since ^{16}O does not possess a nuclear spin, the EPR pattern of SF_4O^- should again resemble those of SF_5 and SF_4^- in general appearance, but with a different g-factor and hyperfine splittings.

For SF_4O^-, additional interest comes from the fact that the isoelectronic PF_4O^{2-} and AsF_4O^{2-} radical anions[8] exhibit two stereoisomers (III and IV). Isomer III, labeled trans, has one axial oxygen ligand opposite to the orbital containing the unpaired electron. Isomer IV has one equatorial oxygen ligand adjacent to the orbital containing the unpaired electron. It would be interesting to examine whether such isomerism is also observable for SF_4O^-.

$$cis \quad \text{F} \underset{\underset{\text{F}}{\underset{|}{\overset{|}{\diagup}}}}{\overset{\overset{|}{\cdot}}{\underset{\text{F}}{\diagdown}}}\text{O} \qquad \text{IV}$$
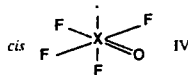
Experimental Section

The samples of $CsSF_5$ and $CsSF_5O$ were prepared as previously described,[17,18] from dry CsF and SF_4 or SF_4O. On the basis of the observed
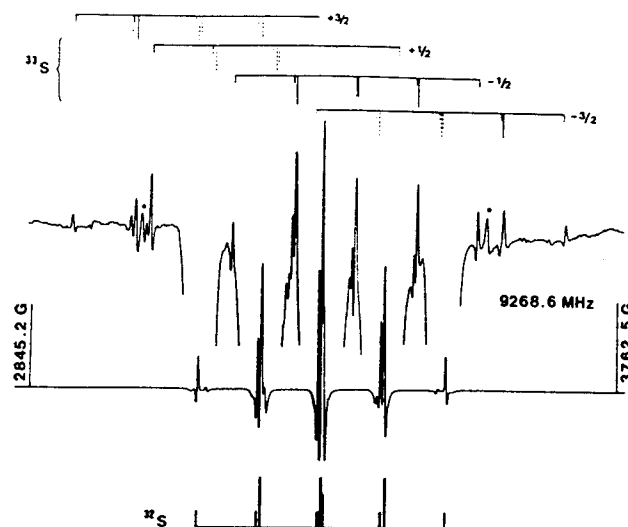
Figure 1. EPR spectrum and spectral analysis of the SF_4^- anion radical. The upper trace was obtained by signal averaging from 30 scans and recorded at 500 times the gain of the lower trace. The lines marked by an asterisk do not belong to the pattern of SF_4^-.
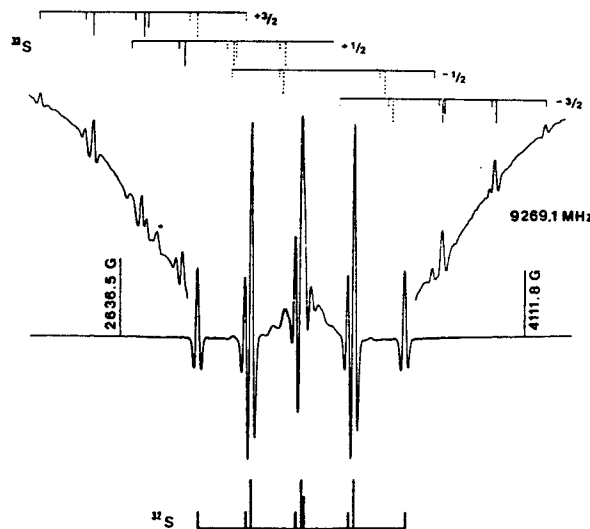
Figure 2. EPR spectrum and spectral analysis of the SF_4O^- anion radical. The upper trace was obtained by signal averaging from 30 scans and recorded at 500 times the gain of the lower trace. The line marked by an asterisk does not belong to the pattern of SF_4O^-.

material balances, the conversion of CsF was 50% for $CsSF_5$ and 85% for $CsSF_5O$. The purity of the compounds was verified by Raman spectroscopy, which showed only the bands characteristic[17,18] of SF_5^- and SF_5O^-, respectively. In the dry nitrogen atmosphere of a glovebox, the samples were loaded into flamed-out 4-mm o.d. Suprasil EPR sample tubes (Wilmad Glass Co.) that were flame-sealed under vacuum. These tubes were then irradiated in a ^{60}Co γ-radiation source (Gammacel 200, Nordion International, Inc., Kanata, Ontario, Canada) at a dose rate of 1.03×10^5 rad/h for a total dose of 4 Mrad (4×10^4 J/kg). The EPR spectra were recorded at sample temperatures ranging from –190 to 90 °C. Since the spectral features did not sharpen up any further above room temperature and a slight amount of decay was observed above 60 °C, the reported spectra were recorded at ambient temperature. Preliminary work with a Varian V4302-15 EPR spectrometer led to the detection of the main ^{32}S spectra of the subject radicals while the ^{33}S satellite lines in natural abundances were only revealed by optimization of microwave power (4 dB ≡ 79 mW) and modulation amplitude (1.25–2.5 mT) using a more sensitive Bruker ER 200D SRC instrument.

Computations were carried out in the local density functional (LDF) approximation[19] by using the program system DMol,[20,21] as previously

(8) Morton, J. R.; Preston, K. F.; Strach, S. J. *J. Magn. Reson.* **1980**, *37*, 321.

(9) Symons, M. C. R. *Int. J. Radiat. Phys. Chem.* **1976**, *8*, 643.

(10) Mishra, S. P.; Symons, M. C. R.; Christe, K. O.; Wilson, R. D.; Wagner, R. I. *Inorg. Chem.* **1975**, *14*, 1103.

(11) Goldberg, I. B.; Crowe, H. R.; Christe, K. O. *Inorg. Chem.* **1978**, *17*, 3189.

(12) (a) Morton, J. R.; Preston, K. F. *Chem. Phys. Lett.* **1973**, *18*, 98. (b) Hasegawa, A.; Williams, F. *Chem. Phys. Lett.* **1977**, *45*, 275.

(13) (a) Morton, J. R.; Preston, K. F. *J. Chem. Phys.* **1973**, *58*, 3112. (b) Nishikida, K.; Williams, F.; Mamantov, G.; Smyrl, N. *J. Am. Chem. Soc.* **1975**, *97*, 3526.

(14) Gregory, A. R. *J. Chem. Phys.* **1974**, *60*, 3713.

(15) (a) Ungemach, S. R.; Schaefer, H. F. *J. Am. Chem. Soc.* **1976**, *98*, 1658. (b) So, S. P.; Richards, W. G. *J. Chem. Soc., Faraday Trans. II* **1979**, *75*, 55.

(16) Ziegler, T.; Gutsev, G. L. *J. Chem. Phys.* **1992**, *96*, 7623.

(17) Christe, K. O.; Curtis, E. C.; Schack, C. J.; Pilipovich, D. *Inorg. Chem.* **1972**, *11*, 1679.

(18) Christe, K. O.; Schack, C. J.; Pilipovich, D.; Curtis, E. C.; Sawodny, W. *Inorg. Chem.* **1973**, *12*, 620.

Table I. Hyperfine Splittings, g-Factors, and s-Orbital Electron Spin Densities of SF_4^- and SF_4O^- and Related Radicals Calculated from the Observed Hyperfine Splittings

radical	a_X (mT)	$n_F{}^b$	a_F (mT)	g-factor	$\rho_s{}^{X\,c}$	$\rho_s{}^{F\,c}$	ref
$^{33}SF_4^-$	12.85	4	9.75	2.0045	0.104	0.0052	a
$^{35}ClF_4$	28.82	4	7.87	2.0117	0.141	0.0042	13
$^{33}SF_4O^-$	36.26	4	18.95	2.00274	0.293	0.0105	a
$^{33}SF_5$	30.68	4	14.30	2.0044	0.248	0.0076	12, 23, 24a
$^{75}SeF_5$	187.7	4	11.80	2.0072	0.261	0.0063	24a
$^{31}PF_5^-$	135.6	4	19.8	2.0017	0.286	0.0105	7, 8
			0.3			0.0002	
$^{75}AsF_5^-$	182.9	4	18.3	1.9996	0.350	0.0097	8
			0.5			0.0003	
$^{31}PF_4O^{2-}$							8
trans	139.0	4	21.2	2.0019	0.293	0.0112	
cis^d	124.3	2	22.4	2.0025	0.261	0.0119	
		1	17.6			0.0093	
$^{75}AsF_4O^{2-}$							8
trans	185.0	4	19.3	1.9998	0.354	0.0102	
cis^d	165.1	2	21.9	2.0011	0.316	0.0116	
		1	15.4			0.0082	

^{a} This work. ^{b} Number of equivalent fluorine atoms. ^{c} Calculated based on parameters given in ref 24b. ^{d} No splittings due to interactions with the apical fluorine ligand were observed.

described in more detail.[22]

The SCF equations for the triplet states were solved by spin unrestricted methods similar to those employed in unrestricted Hartree–Fock (UHF) calculations. Geometries were optimized by using analytic gradient methods.[21] There are two problems with evaluating gradients in the LDF framework which are due to the numerical methods that are used. The first is that the energy minimum does not necessarily correspond exactly to the point with a zero derivative. The second is that the sum of the gradients may not always be zero, as required for translational invariance. These tend to introduce errors on the order of 0.001 Å in the calculation of the coordinates if both a reasonable grid and basis set are used. This gives bond lengths and angles with reasonable error limits. The difference of 0.001 Å is about an order of magnitude smaller than the accuracy of the LDF geometries as compared to experiment. The frequencies were determined by numerical differentiation of the gradient. A two-point difference formula was used with a displacement of 0.01 au.

Results and Discussion

EPR Spectra. The second-derivative isotropic EPR spectra of the SF_4^- and SF_4O^- radical ions are shown in Figures 1 and 2, respectively. Each spectrum shows the satellite lines due to naturally abundant ^{33}S. At sample temperatures from -50 to 90 °C, the spectra gave only slight indications of residual anisotropy, suggesting that, in this range, the radicals rotate freely at their lattice positions. Because the hyperfine splittings are large, the azimuthal nuclear spin quantum number, M_I, lines for ^{19}F exhibit "second-order" splittings[23,24] and the M_I lines for ^{33}S exhibit shifts, making the separation between lines nonlinear in M_I. The analyses of the spectra of the ^{32}S-centered radicals, including the higher

(19) (a) Parr, R. G.; Yang, W. *Density Functional Theory of Atoms and Molecules*; Oxford University Press: New York, 1989. (b) Salahub, D. R. In *Ab Initio Methods in Quantum Chemistry*; Lawley, K. P., Ed.; J. Wiley & Sons: New York, 1987; Vol. II, p 447. (c) Wimmer, E.; Freeman, A. J.; Fu, C.-L.; Cao, P.-L.; Chou, S.-H.; Delley, B. In *Supercomputer Research in Chemistry and Chemical Engineering*; Jensen, K. F., Truhlar, D. G., Eds.; ACS Symposium Series, American Chemical Society: Washington, D.C., 1987; p 49. (d) Jones, R. O.; Gunnarsson, O. *Rev. Mod. Phys.* **1989**, *61*, 689. (e) Zeigler, T. *Chem. Rev.* **1991**, *91*, 651. (f) Dixon, D. A.; Andzelm, A.; Fitzgerald, G.; Wimmer, E.; Delley, B. In *Science and Engineering on Supercomputers*; Pitcher, E. J., Ed.; Computational Science Publications: Southhampton, England, 1990; p 285. (g) Dixon, D. A.; Andzelm, J.; Fitzgerald, G.; Wimmer, E.; Jasien, P. In *Density Functional Methods in Chemistry*; Labanowski, J., Andzelm, J., Eds.; Springer-Verlag: New York, 1991; p 33.
(20) Delley, B. *J. Chem. Phys.* **1990**, *92*, 508. DMol is available commercially from BIOSYM Technologies, San Diego, CA.
(21) Delley, B. In *Density Functional Methods in Chemistry*; Labanowski, J., Andzelm, J., Eds.; Springer Verlag: New York, 1991; p 101.
(22) Christe, K. O.; Curtis, E. C.; Dixon, D. A.; Mercier, H. P.; Sanders, J. C. P.; Schrobilgen, G. J. *J. Am. Chem. Soc.* **1991**, *113*, 3351.
(23) Fessenden, R. W. *J. Magn. Reson.* **1969**, *1*, 277.
(24) (a) Morton, J. R.; Preston, K. F.; Tait, J. C. *J. Chem. Phys.* **1975**, *62*, 2029. (b) Morton, J. R.; Preston, K. F. *J. Magn. Reson.* **1978**, *30*, 577.

Table II. Geometry, Unscaled Vibrational Spectrum, Spin Populations, and Atomic Charges Calculated for SF_4^- by the LDF Method

Geometry		C_{4v}	D_{4h}
r S–F (Å)		1.793	1.803
∢ FSF (deg)		89.2	90
∢ FS–C_{4v} axis (deg)		83.3	90

Vibrational Frequencies (cm⁻¹)

approx. mode description					
ν sym SF4 in phase	A_1	ν_1	547	A_{1g} ν_1	516
δ sym SF4 out of plane, in ph.		ν_2	299	A_{1u} ν_2	245i
ν sym SF4 out of phase	B_1	ν_3	425	B_{1g} ν_3	406
δ sym SF4 out of plane, out of ph.		ν_4	130	B_{1u} ν_4	121
δ sciss SF4	B_2	ν_5	274	B_{2g} ν_5	258
ν as SF4	E	ν_6	612	E_u ν_6	604
δ as SF4 in plane		ν_7	227	ν_7	210

Spin Populations

atom	orbital			
S	3s		0.033	-0.014
S	3px,y } 3p	0.013 } 0.627	0.710	
S	3pz	0.602		
S	3dxy,x²-y²	0.001		
S	3dxz,yz } 3d	0.003 } 0.026	0.021	
S	3dz²	0.019		
F	2px,y } 2p	0.016 } 0.078	0.069	
F	2pz	0.045		

Atomic Charges

S		0.725
F		-0.431

Table III. Geometries, Unscaled Vibrational Spectra, Spin Populations, and Atomic Charges Calculated for the *trans*-PF_4O^{2-}, SF_4O^-, and SF_5 Radicals and the Observed Vibrational Spectrum of ClF_4O^-

Geometry		C_{4v}	C_{4v}	C_{4v}	C_{4v}
r X–Y (Å)		1.530	1.464		1.587
r X–F (Å)		1.841	1.770		1.645
∢ YXF (deg)		100.3	101.6		91.7

Vibrational Frequencies (cm⁻¹)

approx. mode description					
A_1 ν_1 vX–Y	1096	1211	1203	837
ν_2 v sym XF4	422	503	456	605
ν_3 δ sym in phase XF4 out of plane	354	361	339	461
B_1 ν_4 sym XF4 out of phase	333	421	345	563
ν_5 δ sym out of phase XF4 out of plane	159	148		201
B_2 ν_6 δ sciss XF4	267	315	283	403
E ν_7 v as XF4	538	635	578	809
ν_8 δ YXF4	329	375	406	453
ν_9 δ as XF4 in plane	203	250	204	311

Spin Populations

atom	orbital				
X	3s	0.412	0.258		0.258
X	3px,y } 3p	0.227 } 0.239	0.001 } 0.169	0.166 }	0.201 } 0.202
X	3pz		0.166		0.201
X	3dxy,x²-y²	0.001	-0.002		
X	3dxz,yz } 3d	0.030 } 0.039	0.002 } 0.027		0.069 } 0.075
X	3dz²		0.024		0.069
F	2s	-0.004	-0.002		-0.001
F	2px,y } 2p	0.037 } 0.007	0.067 } 0.136		0.046 } 0.119
F	2pz	0.002	0.004		0.026
Y	2s	-0.005	-0.003		-0.004
Y	2px,y } 2p	0.027 } 0.023	-0.005 } 0.016		-0.001 } -0.002
Y	2pz		0.025		-0.002

Atomic Charges

X	0.610	0.864		0.996
F	-0.504	-0.376		-0.212
Y	-0.593	-0.360		-0.148

^{a} X = P, S, or Cl; Y = O or the unique F.

order effects for the fluorine hyperfine lines, are given below the spectra, and those for the ^{33}S-centered radicals are given above the spectra. The EPR parameters were determined using a least-squares matrix diagonalization program,[25] and the isotropic hyperfine splittings and g-factors of these radicals and other analogous species[7,8,12,13,23,24] are given in Table I. Spin densities in the s orbitals of the central atoms or fluorine, X, were calculated according to

$$\rho_s{}^X = a_X / a_X{}^o$$

(25) Hasegawa, A.; Hayashi, M.; Kerr, C. M. L.; Williams, F. *J. Magn. Reson.* **1982**, *48*, 192.

where a_X and $a_X°$ are respectively the isotropic hyperfine splitting of atom X in the radical and the hyperfine splitting of the atom assuming that there was one unpaired electron in the outermost s orbital of that atom.[25]

EPR spectra showing varying degrees of ^{19}F hyperfine anisotropy were obtained in each case with sample temperatures below −50 °C. In particular, the spectrum of SF_4^- between −190 and −170 °C consisted of a strong central absorption at $g = 2.005$ flanked by three pairs of broad features separated by ca. 40.0, 47.0, and 55.0 mT. The two outer pairs of wing features must be anisotropic components, since the total width of the $^{32}SF_4^-$ anisotropic spectrum is only 29.0 mT. Between −170 and −80 °C, these outer features gradually weakened while an additional pair of lines, separated by ca. 20 mT and destined to become the $M_1 = \pm 1$ lines of the isotropic spectrum at higher temperatures, developed considerable intensity. The low-temperature spectra of SF_4O^- recorded below −70 °C revealed a pair of anisotropic features, separated by ca. 90.1 mT, in addition to broad resonances at the isotropic positions, but otherwise the spectra were not very informative in this low-temperature region.
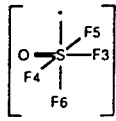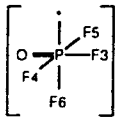
Local Density Functional Calculations. The geometries, vibrational spectra, spin populations, and atomic charges for the SF_4^-, cis- and trans-SF_4O^-, cis- and trans-PF_4O^{2-}, and SF_5 radicals were calculated using local density functional theory. The results are summarized in Tables II–IV.

For SF_4^-, a C_{4v} structure, which deviates from the planar configuration by 6.7° and has an FSF bond angle of 89.2°, was found to be the energy minimum on the potential energy surface, in excellent agreement with the results from an independent LDF calculation.[16] The planar D_{4h} structure is 1.51 kcal mol^{-1} higher in energy and is a transition state characterized by an imaginary frequency (ν_2 in Table II). Since the axial positions in SF_4^- are occupied by free valence electrons which can rapidly move from one side of the SF_4 plane to the other, thereby creating the possibility for inversion, the potential energy curve of the C_{4v} model of SF_4^- has two minima, one at 6.7° above and one at 6.7° below the plane. The planar D_{4h} structure represents the inversion barrier, and the energy difference of 1.51 kcal mol^{-1} between the C_{4v} and the D_{4h} structures is the barrier height. The inversion mode is the symmetric out of plane deformation, $\nu_2(A_1)$, with a zero-point energy of one half of 299 cm^{-1} or 0.43 kcal mol^{-1}. In view of the small energy required for inversion, the assumption of a D_{4h} ground-state symmetry for SF_4^- under normal conditions is not unreasonable. As can be seen from Table II, the properties of SF_4^- do not change much between the C_{4v} and the D_{4h} configurations. As expected, the largest change involves the inversion mode, i.e. the symmetric out of plane deformation mode, ν_2.

For SF_4O^- and isoelectronic PF_4O^{2-}, the lowest energy structures are configuration III of symmetry C_{4v} (see Introduction), in which the sterically active unpaired electron is trans to the oxygen ligand. According to our calculations, the trans isomers of SF_4O^- and PF_4O^{2-} are 8.6 and 5.6 kcal mol^{-1}, respectively, lower in energy than their cis isomers (IV), and both isomers are minima on the potential energy surfaces. The exclusive formation of trans-SF_4O^- in our study is favored from energetic considerations. From reaction mechanistic arguments both isomers are about equally favored. Although the exact lengths of the axial and the equatorial fluorine bonds in SOF_5^- are unknown,[26a] those in closely related $TeOF_5^-$ and IOF_5[26b] are about equal. Therefore, breakage of either fluorine bond should be about equally likely. In the previous study on PF_4O^{2-}, in which both isomers were observed,[8] these radical anions were generated from unidentified hydrolysis products of PF_6^- and, therefore, may have involved intramolecular HF elimination from hydroxy-substituted phosphorus fluoride anions. Since such an HF elimination would involve neighboring cis ligands, the formation of some cis-PF_4O^{2-} could be readily explained.

The fact that, in the trans-XF_4O radical anions, the F–X–O angles are about 101° and are significantly larger than 90° demonstrates that a doubly bonded oxygen ligand is more repulsive than a sterically active unpaired valence electron. As expected, a singly bonded fluorine ligand is much less repulsive than a doubly

Table IV. Calculated Geometries, Unscaled Vibrational Spectra, Spin Populations, and Atomic Charges for the cis-SF_4O^- and cis-PF_4O^{2-} Radical Anions

Geometry		cis-SF_4O^-	cis-PF_4O^{2-}
rX-O (Å)		1.490	1.558
rX-F3		1.860	1.945
rX-F4, rX-F5		1.753	1.822
rX-F6		1.656	1.704
∢ F3-X-O (deg)		169.0	174.1
∢ F4-X-O		96.0	96.8
∢ F6-X-O		103.1	101.1
∢ F4-X-F6		88.2	88.7
∢ F4-X-F5		168.0	166.5
∢ F3-X-F4		84.2	83.3
∢ F3-X-F6		87.9	84.8

Spin Populations[a] atom	orbital				
X	3s	0.238		0.387	
X	3py	0.042		0.055	
X	3pz }3p	0.082	0.131	0.078	0.211
X	3px	0.007		0.078	
X	3dxy	0.010		0.008	
X	3dyz	0.008		0.008	
X	3dz² }3d	0.029	0.046	0.008	0.068
X	3dxz	0.007		0.028	
X	3dx²-y²			0.016	
O	2s	0.002		-0.004	
O	2py	0.106		0.080	
O	2pz }2p	0.070	0.182	0.028	0.136
O	2px	0.004		0.028	
F3	2s			-0.002	
F3	2py	0.215		0.103	
F3	2pz }2p	0.011	0.227	0.004	0.110
F3	2px			0.004	
F4	2s	-0.001		-0.004	
F4	2pz }2p	-0.001	0.085	0.007	0.050
F4	2px	0.086		0.044	
F5	2s	-0.001		-0.004	
F5	2pz }2p	0.086	0.085	0.044	0.050
F5	2px	-0.001		0.007	
F6	2s	-0.003		-0.005	
F6	2pz }2p	0.013	0.013	0.003	0.005
F6	2px	0.001		0.003	

Vibrational Frequencies (cm^{-1})		
	1101	991
	708	655
	644	545
	498	434
	451	405
	427	366
	399	334
	367	316
	318	279
	283	242
	270	239
	158	152

Atomic charges		
X	0.80	0.54
O	-0.37	-0.59
F3	-0.41	-0.55
F4	-0.37	-0.49
F5	-0.37	-0.49
F6	-0.28	-0.41

[a] The X–O axis is approximately the y axis, and F4, F5, and F6 are approximately in the x,z plane.

bonded oxygen but still slightly more so than an unpaired valence electron. This is shown by the F_{ax}–S–F_{eq} bond angle of 91.7° calculated for the SF_5 radical (see Table III).

Since no experimental geometries nor vibrational frequencies are known for these radicals, with the exception of two infrared bands attributed[27] to SF_5 in a matrix, it was important to test the accuracy of our LDF calculations for closely related, well-known molecules. For this purpose, the geometries and vibrational spectra of SF_4,[28-32] SF_4O,[29,30,33-36] and SF_6[37,38] were calculated by the LDF method and, in Table V, are compared to the experimental data. As can be seen from this table, LDF theory duplicates well the observed geometries and vibrational frequencies, particularly if it is kept in mind that, for these types of fluorides,[22] LDF theory generally predicts bond lengths which are about 0.04-Å longer than the observed ones. Therefore, the values calculated for the radicals of this study are also deemed to be good approximations to the true values, particularly if the calculated bond lengths are corrected (shortened) by about 0.04 Å. Of the two infrared bands previously reported for SF_5 in an Ar matrix,[27] the very intense

SF_4^- and SF_4O^- Radical Anions

J. Am. Chem. Soc., Vol. 115, No. 3, 1993 1133

Table V. Calculated and Experimental Geometries and Unscaled Vibrational Spectra of SF_4, SF_4O, and SF_6

	calcd	obsd [29,31]	calcd	obsd [29,33,34,36]	calcd	obsd [37,38]
Geometry	C_{2v}		C_{2v}		O_h	
r S–F ax (Å)	1.679	1.646	1.628	1.593	1.593	1.564
r S–F eq	1.607	1.545	1.590	1.535		
r S–O	--	--	1.437	1.406		
∢F_{ax}-S-F_{ax} (deg)	172.9	173.1	163.3	164.4	180	180
∢F_{eq}-S-F_{eq}	100.6	101.6	112.3	114.9	90	90
Vibrational Frequencies (cm⁻¹)						
A_1 v_1	826	892	A_1 v_1 1340	1380	A_{1g} v_1 713	774
v_2	560	558	v_2 730	796	E_g v_2 627	642
v_3	453	532	v_3 582	588	F_{1u} v_3 934	948
v_4	193	228	v_4 511	566	v_4 556	616
A_2 v_5	402	[437]	v_5 136	174	F_{2g} v_5 472	525
B_1 v_6	811	867	A_2 v_6 505	--	F_{2u} v_6 309	347
v_7	305	353	B_1 v_7 870	924		
B_2 v_8	782	730	v_8 508	566		
v_9	464	475	v_9 232	265		
			B_2 v_{10} 837	815		
			v_{11} 574	640		
			v_{12} 497	447		

one at 812 cm⁻¹ is in excellent agreement with our calculated value of 809 cm⁻¹ for v_7(E), but the frequency of the weak band observed at 552 cm⁻¹ appears somewhat high when compared to the value of 453 cm⁻¹ calculated for v_7(E). This raises a question as to whether the 552-cm⁻¹ band belongs to SF_5.

SF_4^- Radical Anion. The paramagnetic species generated by γ-irradiation of $Cs^+SF_5^-$ is attributed to the novel SF_4^- radical anion for the following reasons. Its EPR spectrum shows the presence of four equivalent nuclei with spin $I = {}^1/_2$ attributed to ¹⁹F, and the satellite lines reveal the presence of a nucleus of spin $I = {}^3/_2$ at the 0.2% intensity expected for naturally abundant ³³S. Furthermore, the s-orbital spin densities on sulfur, $ρ_s s$, and on fluorine, $ρ_s F$, derived from the hyperfine splittings, and the g-factor are similar to those of the known,[13] isoelectronic ClF_4 radical (see Table I). As shown by the LDF calculations for SF_4^- (see Table II) and the CNDO and INDO calculations for ClF_4,[14] the most stable geometry for these two XF_4 radicals is a near-square-planar structure of approximate D_{4h} symmetry in which the electron densities above and below the plane are about equal, as depicted by the two mesomeric structures.

The small C_{4v} distortions, suggested for SF_4^- and ClF_4 by the LDF

and INDO calculations, respectively, for the minimum energy structures, are insignificant and result in inversion energy barriers which are comparable to the zero-point energies of the inversion modes in the ground states.

A comparison between the observed (see Table I) and calculated (see Table II) s-orbital spin densities of SF_4^- shows qualitative agreement. Although the value of 0.033 calculated for the sulfur 3s-orbital spin density of the C_{4v} structure of SF_4^- is smaller than that of 0.103 derived from the observed ³³S hyperfine splitting, it should be noted that the former is very sensitive to small changes in the bond angle (see Table II). A slightly larger distortion of SF_4^- from D_{4h} symmetry could significantly increase the calculated 3s-orbital spin density on sulfur. In view of the relatively small energy difference between the C_{4v} and the D_{4h} structures (see above), the C_{4v} distortion and hence the hfs and spin densities could, in theory, be strongly temperature dependent. However, the experimental ³³S hyperfine splitting showed virtually no difference between 20 and 70 °C. Unfortunately, precise measurements at lower temperatures were precluded by anisotropic line broadening.

Comparison of SF_4^- with isoelectronic ClF_4 (see Table I) shows that SF_4^- has a slightly smaller g-factor than ClF_4, as expected from the smaller spin–orbit coupling of sulfur. Comparison of SF_4^- with SF_5[12] shows a marked difference (see Tables I–III). In SF_4^- the unpaired electron is concentrated mainly in the sulfur p_z orbital, whereas in SF_5 it is mainly located in an sp-hybrid orbital, which accounts for the much larger ³³S hfs of the latter.

SF_4O^- Radical Anion. By analogy to the generation of the SF_4^- radical anion by γ-irradiation of $Cs^+SF_5^-$ (see above), the novel SF_4O^- radical anion was generated by γ-irradiation of $Cs^+SF_5O^-$. In both cases, the probable reaction mechanism involves the loss of a fluorine ligand due to secondary electron capture.[39]

$$SF_5O^- + e^- \rightarrow SF_4O^- + F^-$$
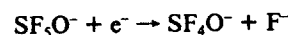
The observed EPR spectrum exhibits hyperfine splittings due to four equivalent fluorine atoms, with weak satellite lines of 0.2% intensity due to the naturally occurring ³³S isotope. The fact that four equivalent fluorine atoms are present in the radical leaves no doubt that the observed radical is the trans isomer (III) rather than the cis isomer (IV). By analogy with cis-PF_4O^{2-} (see Table I), cis-SF_4O^- would be expected to exhibit three fluorine atoms, not necessarily equivalent, with large hfs and one fluorine atom with a very small hfs. As discussed above, the exclusive formation of the $trans$-SF_4O^- isomer is probably due to both energetic and reaction mechanistic reasons. If the fluorine atom were eliminated from the SF_5O^- precursor by random electron capture, the cis isomer would be four times more likely to form than the trans isomer.

As can be seen from Tables I and III, the orbital spin densities in isoelectronic $trans$-SF_4O^- and $trans$-PF_4O^{2-} are similar to those in SF_5 but deviate significantly from those in SF_4^-. This indicates that in $trans$-SF_4O^- and SF_5 the unpaired electron is concentrated mainly in an axial sulfur sp-hybrid orbital, which accounts for their large ³³S hfs (see Table I). The experimentally found, high values of the 3s-orbital spin densities on sulfur in $trans$-SF_4O^- and SF_5 are also supported by the results from the LDF calculations (see Table III). However, the relatively large changes in the spin densities between isoelectronic $trans$-SF_4O^- and $trans$-PF_4O^{2-}, predicted by the LDF calculations (see Table III), are not substantiated by the experimental data given in Table I. As indicated by the LDF calculations (see Table III), the axial oxygen or fluorine ligands in $trans$-SF_4O^- or SF_5 have little spin density, contrary to the case of cis-SF_4O^-, for which the calculated total spin density on oxygen is 0.184 (see Table IV).

Bonding in SF_4^- and SF_4O^-. For SF_4^-, the LDF calculated and corrected (−0.04 Å) S–F bond length of about 1.75 Å suggests

(26) (a) Although the crystal structure of $(Me_2N)_3S^+SF_5O^-$ has recently been published (Heilemann, W.; Mews, R.; Pohl, S.; Saak, W. *Chem. Ber.* **1989**, *122*, 427), no reliable individual bond lengths were obtained for SF_5O^- due to disorder of the anion. (b) In $TeOF_5^-$, the axial and the equatorial fluorine bonds are of almost equal length (see: Miller, P. K.; Abney, K. D.; Rappé, A. K.; Anderson, O. P.; Strauss, S. H. *Inorg. Chem.* **1988**, *27*, 2255), and a recent study of IOF_5 (Christe, K. O.; Curtis, E. C.; Dixon, D. A. *J. Fluorine Chem.*, in press) has shown that the same applies to this molecule and that the previously reported (Bartell, L. S.; Clippard, F. B.; Jacob, E. *J. Inorg. Chem.* **1976**, *15*, 3009) structure should be revised.
(27) Smardzewski, R. R.; Fox, W. B. *J. Chem. Phys.* **1977**, *67*, 2309.
(28) Sawodny, W.; Birk, K.; Fogarasi, G.; Christe, K. O. *Z. Naturforsch.*, B **1980**, *35B*, 1137.
(29) Christe, K. O.; Willner, H.; Sawodny, W. *Spectrochim. Acta, Part A* **1979**, *35A*, 1351.
(30) Kimura, K.; Bauer, S. H. *J. Chem. Phys.* **1963**, *39*, 3172.
(31) Tolles, W. M.; Gwinn, W. D. *J. Chem. Phys.* **1962**, *36*, 1119.
(32) Inoue, H.; Naruse, A.; Hirota, E. *Bull. Chem. Soc. Jpn.* **1976**, *49*, 1260.
(33) Oberhammer, H.; Boggs, J. E. *J. Mol. Struct.* **1979**, *56*, 107.
(34) Gundersen, G.; Hedberg, K. *J. Chem. Phys.* **1969**, *51*, 2500.
(35) Hencher, J. L.; Cruickshank, D. W. J.; Bauer, S. H. *J. Chem. Phys.* **1968**, *48*, 518.
(36) Christe, K. O.; Schack, C. J.; Curtis, E. C. *Spectrochim. Acta, Part A* **1977**, *33A*, 323.
(37) Shimanouchi, T. *Natl. Stand. Ref. Data Ser. (U.S. Natl. Bur. Stand.)* **1972**, *39*, 33.
(38) McDowell, R. S.; Aldridge, J. P.; Holland, R. F. *J. Phys. Chem.* **1976**, *80*, 1203.

(39) This mechanism has been demonstrated for electron capture by F_3NO and $FClO_3$, since their radical anions were observed by EPR to dissociate into F_2NO and ClO_3, respectively, on annealing to higher temperature. Nishikida, K.; Williams, F. *J. Am. Chem. Soc.* **1975**, *97*, 7166. Hasegawa, A.; Hudson, R. L.; Kikuchi, O.; Nishikida, K.; Williams, F. *J. Am. Chem. soc.* **1981**, *103*, 3436. Hasegawa, A.; Williams, F. *J. Am. Chem. Soc.* **1981**, *103*, 7051.

1134

long and weak bonds, when compared to normal S–F single bonds, which have values ranging from about 1.53 to 1.56 Å (see Table V). These long S–F bonds in SF_4^-, combined with the above analysis of the electron spin density distribution, suggest the following idealized bonding scheme for SF_4^-. The four equatorial fluorines are bound to sulfur by two semi-ionic, three-center-four-electron bond pairs[40-43] involving the p_x and p_y orbitals of sulfur. The third p orbital of sulfur, the p_z orbital, accommodates primarily the unpaired free electron, while the remaining sulfur free valence electron pair is localized mainly in its s orbital.

For trans-SF_4O^-, the bonding of the four equatorial fluorines (calculated bond length = 1.77 – 0.04 = 1.73 Å) is similar to that proposed above for SF_4^-, i.e. weak, semi-ionic, three-center-four-electron bonds involving the sulfur p_x and p_y orbitals. The LDF calculated S—O bond length (1.464 – 0.04 = 1.42 Å) is comparable to normal S=O double bonds (r_{SO} in SF_4O = 1.406 Å),[34] supporting, for oxygen, a predominantly covalent bonding scheme through a sulfur sp_z hybrid, which also accommodates, to a large extent, the unpaired free electron. The bonding scheme in SF_4O^- is completed by the formation of an additional double bond between sulfur and oxygen.

In SF_5, the basic bonding scheme somewhat resembles that in trans-SF_4O^-, but the ionic character of the four equatorial bonds is less pronounced. This is not surprising in view of the lack of a formal negative charge (neutral radical versus radical anion) which strongly enhances semi-ionic bonding. This interpretation

is nicely supported by the atomic charges calculated by the LDF method for these radicals. As predicted from the above analysis, the negative charges on the four equatorial fluorine ligands decrease from –0.431 in SF_4^- to –0.376 in trans-SF_4O^- to –0.212 in SF_5.

Conclusions

The novel SF_4^- and trans-SF_4O^- radical anions[44] were prepared by γ-irradiation of SF_5^- and SF_5O^- containing salts, respectively, and were characterized by their isotropic EPR spectra, which permitted the determination of the s-orbital electron spin densities. Although anisotropic EPR data were not available for a complete electron spin density analysis, the nature and bonding of these interesting radical anions were elucidated using local density functional calculations. LDF theory was also used to predict the geometries and vibrational spectra of these and other closely related radicals. The reliability of these calculations was confirmed by comparison with experimental data from several well-known sulfur fluorides and oxyfluorides.

(40) Pimentel, G. C. *J. Chem. Phys.* **1951**, *19*, 446.
(41) Hach, R. J.; Rundle, R. E. *J. Am. Chem. Soc.* **1951**, *73*, 4321.
(42) Rundle, R. E. *J. Am. Chem. Soc.* **1963**, *85*, 112.
(43) Wiebenga, E. H.; Havinga, E. E.; Boswijk, K. H. *Adv. Inorg. Chem. Radiochem.* **1961**, *3*, 158.

(44) Morton and Preston have noted in ref 6 that for isoelectronic pairs of radicals the F^{19} hyperfine interaction is always larger in the radical anion than in the neutral species. The results of the present study are in accord with this generalization, since the F^{19} splittings for SF_4^- and SF_4O^- are greater than those for ClF_4 and SF_5, respectively (see Table I).

On the Problem of Heptacoordination: Vibrational Spectra, Structure, and Fluxionality of Iodine Heptafluoride

Karl O. Christe,*,[1] E. C. Curtis,[1] and David A. Dixon[2]

Contribution from Rocketdyne, A Division of Rockwell International Corporation, Canoga Park, California 91309, and the Central Research and Development Department, E. I. du Pont de Nemours and Company, Inc., Experimental Station, Wilmington, Delaware 19880-0328. Received August 17, 1992

Abstract: Iodine heptafluoride, the most studied prototype of a heptacoordinated molecule, had presented many mysteries concerning its spectroscopic and structural properties. It is shown by ab initio calculations and a reexamination of the vibrational spectra and their normal coordinate analysis that most of the previously implied abnormalities were due to incorrect assignments. All the available structural data for IF_7 are consistent with a highly fluxional, dynamically distorted pentagonal-bipyramidal molecule possessing D_{5h} symmetry in the ground state. The fluxionality of IF_7 can be attributed to (i) a rapid dynamic puckering of the highly congested pentagonal equatorial plane involving a very low frequency, large amplitude puckering mode which induces a small axial bend and (ii) a much slower intramolecular exchange of the axial and equatorial fluorines resulting in their equivalence on the NMR time scale. The high degree of ligand congestion in the equatorial plane of the pentagonal bipyramid, combined with a semi-ionic, 6-center 10-electron bonding scheme, results in the equatorial I–F bonds being significantly longer than the axial ones and the equatorial in-plane deformation force constants being much larger than the out-of-plane ones. It is shown that the VSEPR model of repelling points on a sphere cannot account for either the pentagonal-bipyramidal structure of heptacoordinated molecules or the planarity of their equatorial fluorine belts. These features can be explained, however, by a bonding scheme involving a planar, delocalized $p_{x,y}$ hybrid on the central atom for the formation of five equatorial, semi-ionic, 6-center 10-electron bonds and an sp_z hybrid for the formation of two mainly covalent axial bonds.

Introduction

Inorganic fluorides offer a unique opportunity to study unusually high coordination numbers and problems associated with them, such as steric activity of free valence electron pairs, steric crowding of the ligands, and fluxionality.[3] Of particular interest in this respect are structures involving five-fold symmetry, i.e. structures in which a central atom possesses five equatorial ligands. Whereas four equatorial ligands can generally be accommodated in a plane around a central atom without difficulty, five of them at reasonably short bond distances are usually subject to severe steric crowding.[4] The steric crowding and the resulting mutual repulsion between these ligands can be relieved by puckering. In the case of five-fold symmetry, however, this puckering presents a special problem. The odd number of ligands does not allow for a highly symmetric rigid arrangement in which all five equatorial ligands can be placed in equivalent positions, with identical displacements alternately above and below the equatorial plane. This poses several interesting questions, such as (i) are the five equatorial ligands equivalent and, if so, how is this equivalency achieved; (ii) are these molecules rigid or fluxional and, if they are fluxional, on what time scale; and (iii) what causes heptacoordinated molecules to adopt, contrary to the "repelling points on a sphere" VSEPR concepts, pentagonal-bipyramidal structures with either planar or only slightly puckered equatorial fluorine belts?

Until now, only a very few simple molecules with five-fold symmetry had been known. The simplest and most thoroughly studied example of a molecule of five-fold symmetry is IF_7. During an ongoing study of the closely related TeF_7^-, IF_6O^-, TeF_6O^{2-}, and XeF_5^- anions,[3,4] however, it became apparent that the vibrational assignments and some of the structural features proposed[5,6] for IF_7 were seemingly incompatible with our results for these anions. Therefore, we decided to reinvestigate IF_7.

IF_7 has been known for 61 years,[7] and many papers dealing with its properties and structure have been published. The following paragraph summarizes the salient features and conclusions from the previous studies: (i) Crystal structure determinations of solid IF_7 were inconclusive due to disorder problems.[8-13] (ii) In the liquid and gas phases, all seven fluorine ligands were shown to be magnetically equivalent on the time scale of NMR spectroscopy due to an intramolecular exchange of equatorial and axial fluorines.[14-18] (iii) Gaseous IF_7 at room temperature does not possess a permanent dipole moment, as shown by the absence of microwave transitions[19] and of deflections in inhomogenous electric fields.[20] (iv) Gas-phase electron diffraction data[5,21,22] show that IF_7 closely approaches D_{5h} symmetry with a misfit in the 2.1–2.7 Å region which is not much larger than common amplitudes of vibration. The breadth and skewing of the 2.5-Å nonbonded F_{ax}–F_{eq} radial distribution peak were explained by an asymmetric molecule involving fluxionality and a dynamic pseudorotational ring puckering which resulted in average displacements of 7.5° for the equatorial fluorines and of 4.5° for the axial fluorines.[5] (v) At least nine studies of the vibrational spectra of IF_7 have previously been reported,[23-32] and although all nine studies ana-

(1) Rockwell International, Rocketdyne Division.
(2) E. I. du Pont de Nemours and Company, Inc.
(3) See for example: Christe, K. O.; Sanders, J. C. P.; Schrobilgen, G. J.; Wilson, W. W. *J. Chem. Soc., Chem. Commun.* **1991**, 837 and references cited therein.
(4) Christe, K. O.; Curtis, E. C.; Dixon, D. A.; Mercier, H. P.; Sanders, J. C. P.; Schrobilgen, G. J. *J. Am. Chem. Soc.* **1991**, *113*, 3351.
(5) Adams, W. J.; Thompson, B. H.; Bartell, L. S. *J. Chem. Phys.* **1970**, *53*, 4040.
(6) Bartell, L. S.; Rothman, M. J.; Gavezzotti, A. *J. Chem. Phys.* **1982**, *76*, 4136.

(7) Ruff, O.; Keim, R. *Z. Anorg. Chem.* **1931**, *201*, 245.
(8) Burbank, R. D.; Bensey, F. N., Jr. *J. Chem. Phys.* **1957**, *27*, 981.
(9) Donohue, J. *J. Chem. Phys.* **1959**, *30*, 1618.
(10) Burbank, R. D. *J. Chem. Phys.* **1959**, *30*, 1619.
(11) Lohr, L. L., Jr.; Lipscomb, W. N. *J. Chem. Phys.* **1962**, *36*, 2225.
(12) Burbank, R. D. *Acta Crystallogr.* **1962**, *15*, 1207.
(13) Donohue, J. *Acta Crystallogr.* **1965**, *18*, 1018.
(14) Gutowski, H. S.; Hoffmann, C. J. *J. Chem. Phys.* **1951**, *19*, 1259.
(15) Muetterties, E. L.; Packer, K. J. *J. Am. Chem. Soc.* **1964**, *86*, 293.
(16) Alexakos, L. G.; Cornwell, C. D.; Pierce, St. B. *Proc. Chem. Soc., London* **1963**, 341.
(17) Bartlett, N.; Beaton, S.; Reeves, L. W.; Wells, E. J. *Can. J. Chem.* **1964**, *42*, 2531.
(18) Gillespie, R. J.; Quail, J. W. *Can. J. Chem.* **1964**, *42*, 2671.
(19) Kukolich, S. G. Private communication, 1991.
(20) Kaiser, E. W.; Muenter, J. S.; Klemperer, W.; Falconer, W. E. *J. Chem. Phys.* **1970**, *53*, 53.
(21) Thompson, H. B.; Bartell, L. S. *Trans. Am. Crystallogr. Assoc.* **1966**, *2*, 190.
(22) La Villa, R. E.; Bauer, S. H. *J. Chem. Phys.* **1960**, *33*, 182.
(23) Lord, R. C.; Lynch, M. A.; Schumb, W. C.; Slowinski, E. J. *J. Am. Chem. Soc.* **1950**, *72*, 522.

Table I. Mesh Parameters Used for the LDF Calculations

parameter	FINE[a]	XFINE[a]
A	1.2	1.5
R_{max}	12.0	15.0
threshold[b]	0.00001	0.000001
max l	29	35
N points	302	434

[a] Mesh parameter in DMol. [b] Angular sampling threshold.

lyzed the observed spectra in point group D_{5h}, all sets of assignments were different and none was able either to duplicate the experimental mean square amplitudes of vibration[5] or to assign the observed infrared combination bands without violations of the D_{5h} selection rules. (vi) Results from a pseudopotential SCF-MO study[6] yielded a minimum-energy structure with D_{5h} symmetry and an alternative assignment for the vibrational spectra; however, the agreement between calculated and observed frequencies was poor, and a complete vibrational spectrum was not calculated at that time due to the lack of analytic second-derivative methods for pseudopotentials.

Experimental Section

Materials and Apparatus. The preparation and purification of IF_7 have previously been described.[33] For its handling, a well-passivated (with ClF_3) stainless-steel vacuum line,[34] equipped with Teflon-FEP U-traps, was used. Raman spectra were recorded on a Spex Model 1403 spectrophotometer using the 647.1-nm line of a Kr ion laser for excitation and a Miller–Harney-type[35] cooling device. Flamed-out quartz tubes were used as sample containers in the transverse-viewing–transverse-excitation mode. Infrared spectra of the gas were recorded on a Perkin-Elmer Model 283 spectrophotometer using a 5 cm path length Teflon cell equipped with AgCl windows. The ^{19}F NMR spectra of IF_7 in $CFCl_3$ solution either with or without NaF as an HF getter were recorded at 84.6 MHz on a Varian Model EM390 spectrometer equipped with a variable-temperature probe.

Computational Methods. The electronic structure calculations were done at the ab initio molecular orbital (MO) and local density functional (LDF) levels. The ab initio MO calculations were done both with all electrons and with an effective core potential (ECP) replacing all of the core electrons on the iodine. In both cases, the valence basis set was of polarized double ζ quality. The fluorine basis set for both calculations is from Dunning and Hay.[36] The all-electron basis set for iodine is from Huzinaga et al.,[37] and the ECP calculations were done with the ECP of Hay and Wadt[38] including relativistic corrections. The geometries were optimized by using gradient techniques,[39] and the force fields were calculated analytically.[40,41] The ab initio MO calculations were done with

the program GRADSCF[42] as implemented on a Cray YMP computer system.

The LDF calculations[43] were done with the program system DMol[44] on a Cray YMP computer. A polarized double numerical basis set was used for the calculations; the atomic basis functions are given numerically on an atom-centered, spherical-polar mesh. Since the basis sets are numerical, the various integrals arising from the expression for the energy need to be evaluated over a grid. The radial portion of the grid is obtained from the solution of the atomic LDF equations by numerical methods. The number of radial points N_R is given as

$$N_R = 14A(Z + 2)^{1/3} \qquad (1)$$

where Z is the atomic number. The maximum distance for any function is R_{max}. The angular integration points N_f are generated at the N_R radial points to form shells around each nucleus. The value of N_f ranges from 14 to N_{max} depending on the behavior of the density and the maximum l value for the spherical harmonics, L_{max}. These quantities for the two meshes used in this study are given in Table I.

The conversion of the Cartesian second derivatives to symmetry-adapted internal coordinates was done with the BMATRIX program[45] using Khanna's symmetry coordinates. The axial and equatorial bond lengths used were 1.76 and 1.86 Å,[21] respectively. The mean amplitudes of vibration were calculated by using the NORCORL program,[46] which follows the definitions given by Cyvin.[47]

Results and Discussion

Ab Initio Calculations. As our recent results on the vibrational spectra and structures of the pentagonal-planar XeF_5^- and pentagonal-bipyramidal IF_6O^- anions[3,4] substantially differed from those[5,6,23–32] previously reported for pentagonal-bipyramidal IF_7, ab initio calculations were carried out for IF_7 at the following levels of theory: (i) local density functional (LDF) theory with numerical functions; (ii) all-electron MO calculations; and (3) MO calculations with an effective core potential (ECP) on iodine. All three calculations resulted in a pentagonal bipyramid of D_{5h} symmetry as the lowest energy structure. The calculated geometries and vibrational frequencies are summarized in Table II and compared to the revised (see below) experimental values. The IF_7 structure obtained by the LDF method with a FINE grid had a degenerate imaginary frequency of $50i$ cm^{-1} for the equatorial puckering mode. Very low frequency, degenerate modes in highly symmetrical structures are very sensitive to the nature of the grid in numerical basis set LDF calculations, as shown previously for $Ni(CO)_4$.[48] Improving the mesh quality (XFINE in Table I) did not change the structure or change the frequencies except to reduce the magnitude of the imaginary E_2'' mode to $40i$ cm^{-1}. Reducing the symmetry to C_2 or C_1 resulted in structures with only one component of the E_2'' mode being imaginary and having smaller values but led to structures that were higher in energy by <0.05 kcal/mol and with the remaining frequencies, excluding the E_2'' mode, within 10 cm^{-1} of those for the LDF D_{5h} structure. As can be seen from Table II, the resulting changes in the frequencies and geometries for the C_2 and C_1 structures from the D_{5h} structure are rather small and demonstrate the great similarities between the ideal D_{5h} structure and the other structures which are somewhat deformed by equatorial puckering and slight axial bending. This is in accord with the previous conclusion that the potential energy well for IF_7 at D_{5h} is very flat and shallow

(24) Nagarajan, G. *Curr. Sci.* **1961**, *30*, 413; *Bull. Soc. Chim. Belg.* **1962**, *71*, 82.

(25) Khanna, R. K. *J. Mol. Spectrosc.* **1962**, *8*, 134.

(26) Arighi, L. S. Ph.D. Thesis, University of Wisconsin, 1965.

(27) Claassen, H. H.; Gasner, E. L.; Selig, H. *J. Chem. Phys.* **1968**, *49*, 1803.

(28) Ramaswamy, K.; Muthusubramanian. *J. Mol. Struct.* **1970**, *6*, 205.

(29) Wendling, E.; Mahmoudi, S. *Bull. Soc. Chim. Fr.* **1972**, 33.

(30) Eysel, H. H.; Seppelt, K. *J. Chem. Phys.* **1972**, *56*, 5081.

(31) Mohan, S. *Acta Cienc. Indica* **1978**, *1*, 31.

(32) Bernstein, L. S. Ph.D. Thesis, University of California, Berkeley, 1974.

(33) Schack, C. J.; Pilipovich, D.; Cohz, S. N.; Sheehan, D. F. *J. Phys. Chem.* **1968**, *72*, 4697.

(34) Christe, K. O.; Wilson, R. D.; Schack, C. J. *Inorg. Synth.* **1986**, *24*, 5.

(35) Miller, F. A.; Harney, B. M. *Appl. Spectrosc.* **1969**, *23*, 8.

(36) Dunning, T. H., Jr.; Hay, P. J. In *Methods of Electronic Structure Theory*; Schaefer, H. F., III, Ed.; Plenum Press: New York, 1977; Chapter 1.

(37) Huzinaga, S.; Andzelm, J.; Klobukowski, M.; Radzio, E.; Sakai, Y.; Tatasaki, H. *Gaussian Basis Sets for Molecular Calculations*; Elsevier: Amsterdam, 1984.

(38) Hay, P. J.; Wadt, W. R. *J. Chem. Phys.* **1985**, *82*, 299.

(39) (a) Komornicki, A.; Ishida, K.; Morokuma, K.; Ditchfield, R.; Conrad, M. *Chem. Phys. Lett.* **1977**, *45*, 595. (b) McIver, J. W., Jr.; Komornicki, A. *Chem. Phys. Lett.* **1971**, *10*, 202. (c) Pulay, P. In *Applications of Electronic Structure Theory*; Schaefer, H. F., III, Ed.; Plenum Press: New York, 1977; p 153.

(40) (a) King, H. F.; Komornicki, A. *J. Chem. Phys.* **1986**, *84*, 5465. (b) King, H. F.; Komornicki, A. In *Geometrical Derivatives of Energy Surfaces and Molecular Properties*; Jorgenson, P., Simons, J., Eds.; NATO ASI Series C, Vol. 166, D. Reidel: Dordrecht, The Netherlands, 1986; p 207.

(41) Breidung, J.; Thiel, W.; Komornicki, A. *Chem. Phys. Lett.* **1988**, *153*, 76.

(42) GRADSCF is an ab initio program system designed and written by Komornicki, A. at Polyatomics Research.

(43) Dixon, D. A.; Andzelm, J.; Fitzgerald, G.; Wimmer, E.; Jasien, P. In *Density Functional Methods in Chemistry*; Labanowski, J., Andzelm, J., Eds.; Springer-Verlag: New York, 1991; p 33.

(44) Delley, B. J. *Chem. Phys.* **1990**, *92*, 508. DMol is available commercially from BIOSYM Technologies, San Diego, CA. The multipolar fitting functions for the model density used to evaluate the effective potential have angular momentum numbers of 3 for F and I.

(45) Komornicki, A. Private communication. This program was developed to help in analyzing the results from the GRADSCF program system.

(46) Christen, D.; Oberhammer, H. Private communication.

(47) Cyvin, S. J. *J. Mol. Struct.* **1978**, *15*, 189.

(48) Sosa, C.; Andzelm, J.; Wimmer, E.; Elkin, B.; Dobbs, K. D.; Dixon, D. A. *J. Phys. Chem.*, in press.

Table II. Observed and Calculated Vibrational Frequencies and Geometries for IF₇

assignments and approximate mode descriptions in point group D_{5h}		obsd frequencies (cm⁻¹)		calculated frequencies (cm⁻¹)				
				ECP[a]	SCF	LDF		
		IR	R	D_{5h}	D_{5h}	D_{5h}	C_2	C_1
A_1'	ν_1	ν sym XF₂ ax		676 (2) p	673	743	630	629	625
	ν_2	ν sym XF₅ eq		635 (10) p	644	704	598	596	596
A_2''	ν_3	ν as XF₂ ax	746 s		753	834	710	708	703
	ν_4	δ umbrella XF₅ eq	365 s		368	366	304	310	305
E_1'	ν_5	ν as XF₅ eq	670 vs		681	761	647	644	646
	ν_6	δ as XF₅ in plane	425 vs		441	454	377	375	376
	ν_7	δ sciss XF₂ ax	257 w		265	261	213	211	212
E_1''	ν_8	δ rock XF₂ ax		319 (0.6)[b]	320	321	259	268	282
E_2'	ν_9	mixture of δ sciss XF₅ in plane		596 (0.2)	605	651	561	559	560
	ν_{10}	and ν as XF₅ eq		510 (1.7)	515	555	467	464	458
E_2''	ν_{11}	δ pucker XF₅ eq		[68][c]	59	39	50i	4133i	4223i

	obsd⁵		calculated			
			ECP[a]	SCF	LDF	
geometry values	$C_2\text{-}C_s$	D_{5h}	D_{5h}	D_{5h}	D_{5h}	C_1
$r(\text{I–F}_{ax})$ (Å)	1.786 (7)	1.781	1.7705	1.807	1.870	1.874
$r(\text{I–F}_{eq})$ (Å)	1.858 (4)	1.857	1.8333	1.862	1.918	1.917
average eq puckering angle (deg)	7.5	0	0[d]	0[d]	0[d]	4.0[e]
deviation of ax bonds from 180°	4.5	0	0	0	0	1.7[e]

[a] The ECP frequencies were scaled by a factor of 0.932. [b] This frequency value was derived from the two Raman bands at 310 (0.6) and 352 (0.6) cm⁻¹ by correction for Fermi resonance (see text). [c] Estimated from the $(\nu_7 + \nu_{11})$ combination band (see text). [d] Although D_{5h} symmetry requires the equatorial plane in the average to be planar, the low frequency of ν_{11} combined with the large $F_{ax}\cdots F_{eq}$ amplitude of vibration makes the effective equatorial puckering comparable to that found for the lower symmetries (see text). [e] The actual displacements of the five equatorial fluorines from the ideal plane in a clockwise sense were +0.35°, –3.15°, +6.65°, –6.65°, and +3.25° with the axial fluorines being bent toward the equatorial fluorine with the smallest (0.35°) equatorial displacement.

and has a nearly quartic contour for buckling along either a C_2 or a C_s symmetry coordinate.[49] It seems likely that the out-of-plane potential would be quadratic when the repulsion of the fluorine atoms is neglected. Including the fluorine repulsions adds a double minimum term which adds up to a quartic well near the minimum and undoubtably has a complex shape. Table II shows that the effective core potential data set, after scaling by a factor of 0.932, duplicates best the experimental frequencies[27,30] with an average frequency deviation of only 7 cm⁻¹. This small deviation is excellent considering that the calculated values are harmonic, gas-phase frequencies, while the observed values are anharmonic frequencies measured in some cases even in liquid or solid phases.

Raman Spectrum of Solid IF₇. A comparison between the calculated (see Table II) and previously reported[23–32] vibrational frequencies, irrespective of their detailed assignments, revealed the following general problems: (i) a Raman active mode having a predicted frequency of about 605 cm⁻¹ was missing; (ii) there was one excess fundamental vibration in the 300–400-cm⁻¹ region; and (iii) the puckering mode of the equatorial plane, which should be inactive in both the Raman and infrared spectra, should have a very low frequency of about 60 cm⁻¹ and be observable only indirectly in the form of combination bands.

For these reasons, the Raman spectrum of solid IF₇ was reinvestigated at different temperatures. As can be seen from Figure 1, at –142 °C a distinct Raman band is observed at 596 cm⁻¹, exhibiting about the right intensity for the missing equatorial IF₅ antisymmetric stretching or in-plane scissoring modes. At higher temperature, this band becomes hidden in the foot of the intense 635-cm⁻¹ band due to the increased line widths. In the 300–360-cm⁻¹ region, two fundamental vibrations had previously been identified[27] at 310 and 352 cm⁻¹. Figure 1 shows that, on cooling from –13 to –142 °C, the frequency separation of these two bands decreases from 42 to 29 cm⁻¹ while at the same time the relative intensity of the higher frequency band decreases markedly. This behavior is characteristic for a Fermi resonance between a fundamental vibration and a combination band where the population of the combination band decreases with decreasing temperature. Therefore, the 352-cm⁻¹ Raman band does not represent a fundamental vibration. It is due (see below) to a combination band

(49) Thompson, H. B.; Bartell, L. S. *Inorg. Chem.* **1968**, *7*, 488.

$348 = \nu_7 (E_1') + \nu_{11} (E_2'') = (E_1'' + E_2'')$
$319 = \nu_8 (E_1'')$
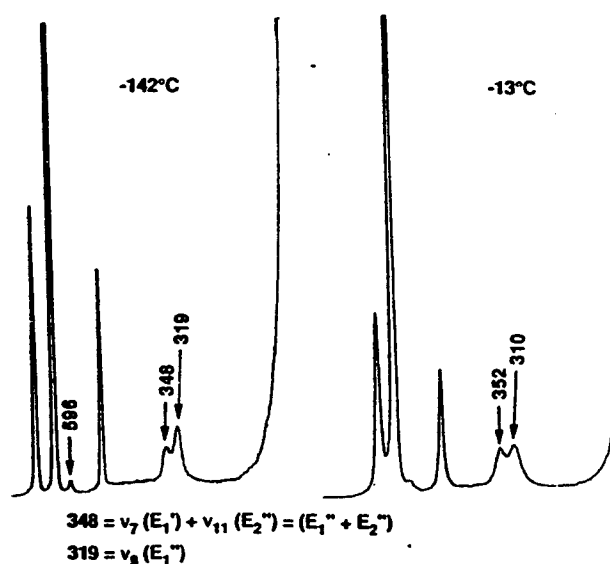
Figure 1. Raman spectra of solid IF₇ recorded at –142 and –13 °C.

which involves the inactive equatorial ring-puckering mode and confirms the predicted low-frequency value of the latter.

Vibrational Assignments. In view of the above findings, the vibrational assignments for IF₇ (see Table II) can now be easily made by comparison with the calculated ECP frequencies. All bands strictly follow the selection rules for D_{5h} symmetry, $2A_1'(\text{Ra}) + 2A_2''(\text{IR}) + 3E_1'(\text{IR}) + 1E_1''(\text{R}) + 2E_2'(\text{R}) + 1E_2''(\text{ia})$, and exhibit the expected relative intensities, infrared gas-phase band contours, and Raman polarization. The agreement between calculated and observed frequencies (average $\Delta\nu = 7$ cm⁻¹) is excellent and supports the present assignments.

The difficulty of assigning the vibrational spectra of IF₇ without the help of reliable ab initio calculations is best reflected by the failures of the previous vibrational analyses,[23–32] in which no more than four out of the eleven fundamental vibrations had been correctly assigned, a disappointing result if one considers the large number of studies and the expertise of the previous investigators. The only significant improvement over these poor results had previously been achieved by Bartell and co-workers, who, with the aid of pseudopotential SCF-MO calculations, correctly located

Table III. Combination Bands Observed in the Infrared Spectrum of Gaseous IF$_7$ and Their Assignment

frequency (cm^{-1}), rel int	assignment
1417 m	676 (A$_1'$) + 746 (A$_2''$) = 1422 (A$_2''$)
1380 sh	635 (A$_1'$) + 746 (A$_2''$) = 1381 (A$_2''$)
1345 vw	676 (A$_1'$) + 670 (E$_1'$) = 1346 (E$_1'$)
1302 m	635 (A$_1'$) + 670 (E$_1'$) = 1305 (E$_1'$)
1258 mw	596 (E$_2'$) + 670 (E$_1'$) = 1266 (E$_1'$ + E$_2'$)
1177 mw	670 (E$_1'$) + 510 (E$_2'$) = 1180 (E$_1'$ + E$_2'$)
1100 w	676 (A$_1'$) + 425 (E$_1'$) = 1100 (E$_1'$)
1058 w	635 (A$_1'$) + 425 (E$_1'$) = 1060 (E$_1'$)
1000 sh	635 (A$_1'$) + 365 (A$_2''$) = 1000 (A$_2''$)
934 vw	676 (A$_1'$) + 257 (E$_1'$) = 933 (E$_1'$)
886 vw	635 (A$_1'$) + 257 (E$_1'$) = 892 (E$_1'$)
839 w	510 (E$_2'$) + 331 (E$_1''$ + E$_2''$) = 841 (A$_1''$ + A$_2''$ + E$_1''$ + E$_2''$)
518 vw	596 (E$_2'$) − 74 (E$_2''$) = 522 (A$_1''$ + A$_2''$ + E$_1''$)

seven of the eleven fundamental vibrations and predicted the right frequency range for two additional ones.[6] Most of these difficulties can be attributed to the fact that the previous investigators did not realize that the equatorial in-plane bending modes of IF$_7$ have such unusually high frequencies.

In several of the previous studies, the inability to assign the observed infrared combination bands of IF$_7$ without violations of the D_{5h} selection rules had been explained by a strong coupling between the E$_2''$ and E$_1'$ modes which should make the E$_2''$ overtones and the pseudoradial, pseudoangular combination bands slightly infrared active, with intensity borrowed from the induced E$_1'$ displacements.[5,30,50] As can be seen from Table III, the revised assignments for IF$_7$ given in Table II permit the assignment of all the observed infrared overtones and combination bands without any violations of the D_{5h} selection rules, thus eliminating one of the arguments previously advanced[6,30] against IF$_7$ having an average symmetry of D_{5h}.

The above mentioned, Raman active combination band at 352 cm^{-1}, which is in Fermi resonance with ν_8 (E$_1''$) requires some special comment. First of all, Fermi resonance requires this band to have the same E$_1''$ symmetry as ν_8; secondly, the band cannot be assigned using any of the remaining fundamental vibrations of IF$_7$; and thirdly, there are only two fundamental vibrations, ν_7 (E$_1'$) and ν_{11} (E$_2''$), that have frequencies lower than that of ν_8. Therefore, the 352-cm^{-1} band can only be due to a combination of ν_7 (E$_1'$) with the inactive equatorial ring-puckering mode, ν_{11} (E$_2''$), which results in the required E$_1''$ symmetry for the ensuing combination band. After a correction for the Fermi resonance induced frequency shift,[51] a frequency of about 68 cm^{-1} is obtained for the ring-puckering mode, ν_{11}, which is in good agreement with the value of 59 cm^{-1} predicted by our ECP calculations. Furthermore, this [ν_7 (E$_1'$) + ν_{11} (E$_2''$)] combination band represents the mode proposed[5,6] by Bartell for the pseudorotation in IF$_7$.

Force Constants and Mean Square Amplitudes of Vibration. Another problem in the previous IF$_7$ studies[22–32] was the discrepancy between the mean square amplitudes of vibration from the electron diffraction study[5] and those derived from normal coordinate analyses of the vibrational spectra. Since all the previous normal coordinate analyses for IF$_7$ had been carried out with partially incorrect assignments, such an analysis was repeated using our ab initio (ECP) force field. The resulting symmetry force constants, the explicit F matrix, and the potential energy distribution (PED) are summarized in Table IV. The listed frequencies and force constants were scaled by factors of 0.932 and 0.932^2 = 0.8686, respectively, to maximize the frequency fit with the observed spectra. As can be seen from the PED in Table IV, most of the fundamental vibrations are highly characteristic and well described by the approximate mode descriptions given in Table II. The only exceptions are (i) the equatorial, antisym-

metric in-plane bending vibration, ν_6 (E$_1'$), which contains a strong contribution from axial bending and (ii) the two E$_2'$ modes, ν_9 and ν_{10}, which have similar frequencies and, therefore, are almost equal mixes of equatorial stretching and in-plane bending.

Inspection of the internal force constants of IF$_7$ (see Table V) reveals several interesting features: (i) The stretching force constant of the axial bonds, f_D, is considerably larger than that of the equatorial bonds, as expected from the observed bond lengths[5] and general valence shell electron pair repulsion (VSEPR)[52] arguments which attribute the longer equatorial bonds to the congestion and increased mutual repulsion of the ligands in the equatorial plane. The absolute value of f_D, 5.01 mdyn/Å, is lower than that of 5.42 mdyn/Å previously found for the IF$_6^+$ cation,[53] as expected for going from a fluorocation to its parent molecule, and (ii) the values of the equatorial angle deformation constants, f_α and f_β, exhibit a huge difference. As expected, the in-plane deformation, f_α, is very large (0.84 mdyn/Å) due to the severe crowding in the equatorial plane, while the out-of-plane deformation, f_β, is very small (0.16 mdyn/Å) because of the ease of equatorial ring puckering. These force constants lend strong support to our model of the bonding and fluxionality in IF$_7$ (see below).

For our calculation of the mean square amplitudes of vibration from the force field, internal force constants were required. For this purpose, the explicit F matrix (see Table IV) and a set of internal force constants (see Table V) were derived for IF$_7$. Since there are more internal force constants than symmetry force constants, additional relations, such as the procedures of the pure vibrational force field by Kuczera[54–58] and molecular-orbital-following arguments, were used for the estimation of the internal force constants.

The previous electron diffraction study[5] had resulted in two different sets of mean square amplitudes of vibration which, depending on the choice of the structural model, strongly differed in their value for the nonbonded ℓ(F$_{ax}$···F$_{eq}$) amplitude. For a static D_{5h} model, this amplitude had a value of 0.169 Å, whereas for the statically or dynamically distorted C_2 (50% C_2 + 50% C_s) or C_s models, values ranging from 0.104 to 0.107 Å were obtained. Since the analysis of the vibrational spectra provides an independent experimental set of mean square amplitudes for IF$_7$, this set can be used to distinguish between the two structural models which were proposed[5] on the basis of the electron diffraction data. As can be seen from Table VI, the mean square amplitudes from the vibrational spectra are in good agreement with the D_{5h} but not the other models. It must be kept in mind, however, that the unusually large vibrational amplitude of 0.16 Å for ℓ(F$_{ax}$···F$_{eq}$) in the D_{5h} model corresponds to a 6.9° displacement of a fluorine ligand from the equatorial plane and is very close to the average equatorial puckering angle of 7.5° deduced from the electron diffraction data for the distorted models.[5] The good agreement between the mean square amplitudes of vibration derived from our force field and those deduced for the D_{5h} model from the electron diffraction data,[5] is very gratifying and attests to the correctness of our revised assignments.

Axial–Equatorial Ligand Exchange. In addition to the above described, very fast dynamic puckering of the pentagonal equatorial fluorine plane which requires very little energy (ν_{11} = 59 cm^{-1} = 0.17 kcal mol^{-1}) and hence is thermally populated at higher vibrational levels even at low temperatures,[59] a second type of

(50) Jacob, E. J.; Bartell, L. S. *J. Chem. Phys.* **1970**, *53*, 2235.

(51) Weidlein, J.; Müller, U.; Dehnicke, K. *Schwingungsspektroskopie*; Georg Thieme Verlag: Stuttgart, Germany, 1982; p 37.

(52) Gillespie, R. J. *Molecular Geometry*; Van Nostrand Reinhold Co.: London, 1972.

(53) Christe, K. O.; Wilson, R. D. *Inorg. Chem.* **1975**, *14*, 694.

(54) Kuczera, K.; Czerminski, R. *J. Mol. Struct.* **1983**, *105*, 269.

(55) Kuczera, K. *J. Mol. Struct.* **1987**, *160*, 159.

(56) Lopez Gonzalez, J. J.; Fernandez Gomez, M.; Martinez Torres, E. *J. Mol. Struct.* **1992**, *265*, 397.

(57) Fernandez Gomez, M.; Lopez Gonzalez, J. J. *J. Mol. Struct.* **1990**, *220*, 287.

(58) Lopez Gonzalez, J. J.; Fernandez Gomez, M. *J. Mol. Struct.* **1990**, *216*, 297.

(59) The vibrational partition function terms for ν_{11} are 3.6 and 1.9 at 20 and −142 °C, respectively, which means that, at these temperatures, only 21% and 34% of the molecules are in the ground state.

Table IV. F Matrix and Scaled ab Initio Effective Core Potential Force Field and Potential Energy Distribution for IF_7 of Symmetry D_{5h}

assignment	freq (cm^{-1})	symmetry force constants[a]		potential energy distribution (%)[b]
A_1' ν_1	673	$F_{11} = f_D + f_{DD}$	5.063	100 (1)
		$F_{12} = \sqrt{10} f_{Dd}$	−0.0058	
	ν_2	644	$F_{22} = f_d + 2f_{dd} + 2f_{dd'}$	4.651	100 (2)
A_2'' ν_3	753	$F_{33} = f_D - f_{DD}$	4.947	92 (3) + 8 (4)
		$f_{34} = \sqrt{5}(f_{D\beta} - f_{D\beta'})$	0.342	
	ν_4	368	$F_{44} = f_\beta + 2f_{\beta\beta} - f_{\beta\beta'} + 2f_{\beta\beta''} - 2f_{\beta\beta'''} - 2f_{\beta\beta''''}$	1.624	100 (4)
E_1' ν_5	681	$F_{55} = f_d + 2f_{dd} \cos\alpha + 2f_{dd'} \cos 2\alpha$	4.105	97 (5) + 3 (7)
		$F_{56} = f_{d\alpha} + 2f_{d\alpha'} \cos\alpha + 2f_{d\alpha''} \cos 2\alpha$	−1.427	
		$F_{57} = \sqrt{2}(f_{d\beta} + 2f_{d\beta'} \cos\alpha + 2f_{d\beta''} \cos 2\alpha)$	0.231	
	ν_6	441	$F_{66} = f_\alpha + 2f_{\alpha\alpha} \cos\alpha + 2f_{\alpha\alpha'} \cos 2\alpha$	3.879	62 (6) + 33 (7) + 5 (5)
		$F_{67} = \sqrt{2}(f_{\alpha\beta} + 2f_{\alpha\beta'} \cos\alpha + 2f_{\alpha\beta''} \cos 2\alpha)$	−0.318	
	ν_7	265	$F_{77} = f_\beta + 2f_{\beta\beta} \cos\alpha + f_{\beta\beta'} + 2f_{\beta\beta''} \cos 2\alpha + 2f_{\beta\beta'''} \cos\alpha + 2f_{\beta\beta''''} \cos 2\alpha$	0.980	93 (7) + 7 (6)
E_1'' ν_8	320	$F_{88} = f_\beta + 2f_{\beta\beta} \cos\alpha - f_{\beta\beta'} + 2f_{\beta\beta''} \cos 2\alpha - 2f_{\beta\beta'''} \cos\alpha - 2f_{\beta\beta''''} \cos 2\alpha$	0.823	100 (8)
E_2' ν_9	605	$F_{99} = f_d + 2f_{dd} \cos 2\alpha + 2f_{dd'} \cos\alpha$	3.436	57 (10) + 43 (9)
		$F_{9,10} = f_{d\alpha} + 2f_{d\alpha'} \cos 2\alpha + 2f_{d\alpha''} \cos\alpha$	0.531	
	ν_{10}	515	$F_{10,10} = f_\alpha + 2f_{\alpha\alpha} \cos 2\alpha + 2f_{\alpha\alpha'} \cos\alpha$	3.375	61 (9) + 39 (10)
E_2'' ν_{11}	59	$F_{11,11} = f_\beta + 2f_{\beta\beta} \cos 2\alpha - f_{\beta\beta'} + 2f_{\beta\beta''} \cos\alpha - 2f_{\beta\beta'''} \cos 2\alpha - 2f_{\beta\beta''''} \cos\alpha$	0.0647	100 (11)

[a] Stretching constants in mdyn/Å, deformation constants in mdyn Å/rad^2, and stretch–bend interaction constants in mdyn/rad. [b] The symmetry coordinates used for our normal coordinate analysis of IF_7 were taken from ref 25, but the sequence of S_1 and S_2 was interchanged and the E_1'' coordinate was placed ahead of the E_2' block.

Table V. Internal Force Constants[a] (mdyn/Å)[b] of IF_7

$f_D = 5.005$	$f_\beta = 0.163$
$f_{DD} = 0.058$	$f_{\beta\beta} = 0.078$
$f_{Dd} = -0.0018$	$f_{\beta\beta'} = -0.042$
$f_d = 3.947$	$f_{\beta\beta''} = -0.038$
$f_{dd} = 0.326$	$f_{\beta\beta'''} = -0.044$
$f_{dd'} = 0.0265$	$f_{\beta\beta''''} = -0.058$
$f_\alpha = 0.841$	$f_{d\beta} = 0.090$
$f_{\alpha\alpha} = -0.187$	$f_{d\beta'} \equiv f_{d\beta''} \equiv 0$
$f_{\alpha\alpha'} = -0.243$	$f_{\alpha\beta} \equiv f_{\alpha\beta'} \equiv -f_{\alpha\beta''} = -0.021$
$f_{d\alpha} \equiv f_{d\alpha'} \equiv -f_{d\alpha''} = -0.238$	$f_{D\beta} = -f_{D\beta'} = 0.042$

[a] $D = I-F_{ax}$, $d = I-F_{eq}$, $\alpha = \angle F_{eq}-I-F_{eq}$, $\beta = \angle F_{ax}-I-F_{eq}$, dd = coupling to adjacent d, dd' = coupling to opposite d, $\alpha\alpha$ = adjacent α, $\alpha\alpha'$ = opposite α, $d\alpha$ = α opposite to d, $d\alpha'$ = remote α, $d\alpha''$ = adjoining α, $\beta\beta$ = common D and adjoining d, $\beta\beta'$ = noncommon D and common d, $\beta\beta''$ = common D and remote d, $\beta\beta'''$ = noncommon D and adjoining d, $\beta\beta''''$ = noncommon D and remote d, $d\beta$ = common d, $d\beta'$ = adjoining d, $d\beta''$ = remote d, $\alpha\beta$ = opposite d, $\alpha\beta'$ = adjoining d, $\alpha\beta''$ = common d, $D\beta$ = common D, $D\beta'$ = opposite D. [b] The internal force constants have been normalized for distance assuming $D = 1.781$ Å and $d = 1.857$ Å.

Table VI. Comparison of the Mean Square Amplitudes (Å) of Vibration of IF_7 Obtained from the Vibrational Spectra with Those Derived from the Electron Diffraction Study under the Assumption of Different Structural Models

	vibrational spectra (D_{5h})	electron diffraction[5]	
		D_{5h}	50% C_2–50% C_s
$\ell(I\cdots F_{ax})$	0.039	0.042[a]	0.043 ± 0.003
$\ell(I\cdots F_{eq})$	0.043	0.044	0.045 ± 0.003
$\ell(F_{eq}\cdots F_{eq})$ short	0.061	0.061	0.061 ± 0.005
$\ell(F_{eq}\cdots F_{eq})$ long	0.060		
$\ell(F_{ax}\cdots F_{ax})$	0.053	0.093[b]	0.091 ± 0.006[b]
$\ell(F_{eq}\cdots F_{ax})$	0.163	0.169	0.106 ± 0.008

[a] Obtained from constraint $\ell(I\cdots F_{ax}) = \ell(I\cdots F_{eq}) - 0.002$ Å. [b] Overlapping peak which could not be resolved into its two components.

fluxionality is possible for IF_7. This second type of fluxionality involves an intramolecular exchange of axial and equatorial fluorines. This was shown by the magnetic equivalence of all seven fluorine ligands of IF_7[14–18] or the isoelectronic TeF_7^- anion[4] on the NMR time scale. This exchange process, with an estimated[17] lifetime of a given configuration of $\sim 2.5 \times 10^{-3}$ s, is considerably slower than that for ring puckering and involves higher vibrational levels of ν_7 (E_1'). This motion can best be described as an antisymmetric combination of the axial and equatorial bending symmetry coordinates, S_6 and S_7, which is accompanied by an

out-of-plane twisting motion of the three remote equatorial fluorine ligands.

ν_7 (E_1') = 265 cm^{-1}
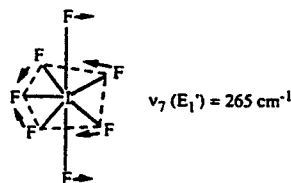
This axial-equatorial exchange mechanism is analogous to that previously proposed by Berry[60] for trigonal-bipyramidal molecules, such as PF_5 or SF_4, and involves a substantial energy barrier of several vibrational levels of ν_7.

The previous reports[14–18] for the ^{19}F NMR spectra of IF_7 were confirmed by our study. Spectra of IF_7 in $CFCl_3$ solution, in the presence or absence of NaF, showed at −110 °C only one broad line at $\Phi = 173.5$ with a line width of ~ 1150 Hz, which at higher temperatures became extremely broad, as expected from the large $^{127}I-^{19}F$ spin–spin coupling of about 2100 Hz,[18] the $^5/_2$ spin of iodine, and a quadrupolar mechanism.[17]

Structure of IF_7. Whereas the results of the ab initio calculations, the microwave study, and the normal coordinate analysis are best interpreted in terms of a structural model of average D_{5h} symmetry that undergoes a rapid dynamic puckering of the equatorial plane with very large vibrational amplitudes, the previous electron diffraction data[5] favored a pseudorotational C_2–C_s model with an equilibrium structure that is distorted from D_{5h} symmetry. The question then arises whether one of these seemingly different models is incorrect or if the differences are only due to semantics of how to best describe a highly fluxional and dynamically distorted molecule.

First of all, one must understand what type of information can be gained from the different methods of investigation. Electron diffraction results generally describe the average structure of vibrating molecules and not the minimum-energy geometries.[61] If a highly fluxional molecule, such as IF_7, undergoes a large dynamic distortion at low energy, then electron diffraction will only see a distorted molecule. A classic example for such a case is the linear CO_2 molecule, which, according to its electron diffraction data, would be bent because in the vibrating molecule the average nonbonded O–O distance becomes shorter than twice

(60) Berry, R. S. *J. Chem. Phys.* **1960**, *32*, 933.
(61) Bartell, L. S. In *Physical Methods of Chemistry*; Weissberger, A., Rossiter, B. A., Eds.; Wiley Interscience: New York, 1972; Vol. I, Part IIID, p 125.

the bonded C–O distance.[61] Returning to the electron diffraction data for IF₇, the conclusions[5,6] reached by Bartell and co-workers are compelling by their logic and thoroughness: The plane of the five equatorial fluorines of IF₇ is highly congested. This congestion can be relieved by a large-amplitude, dynamic puckering. For a five-fold symmetry, the five ligands cannot be displaced from the equatorial plane in a manner which renders them at any given time equivalent and equidistant from the ideal equatorial plane as shown by the previously published[5] geometries of the C_2 or C_s models of IF₇. As a consequence of these uneven equatorial ligand displacements, the axial ligands experience an uneven repulsion from the equatorial plane and will bend away from those ligands which exhibit the largest displacements from the equatorial plane.[52] Since the experimental evidence overwhelmingly suggests that all the equatorial ligands are equivalent, a rapid dynamic pseudo-rotation of the puckering motion must be invoked which is phase-coupled to a precession of the slightly bent axial FIF group (i.e. Bartell's pseudorotational model).[5] Due to the short time scale of the electron diffraction technique, it detects at all times a distorted IF₇ molecule that exhibits a strong and uneven equatorial puckering and, as a consequence, also an axial bend which results in an equilibrium symmetry lower than D_{5h}.

On the other hand, ab initio calculations and vibrational spectroscopy generally describe the symmetry of the minimum-energy geometry, which for IF₇ would be D_{5h} if the distortions are only dynamic in nature and not static. Although the knowledge of the exact potential energy curve of IF₇ would be desirable to distinguish between a distorted and an undistorted ground-state configuration, the absence of a permanent dipole moment[20] and microwave transitions[19] and the results from this study strongly favor an undistorted D_{5h} ground state which undergoes facile dynamic distortion, most likely by Bartell's pseudorotation mechanism.[5] This signifies that *both* the D_{5h} and the dynamically distorted model descriptions for IF₇ are, in principle, correct because they describe different time domains. The undistorted D_{5h} model describes the nonvibrating ground state whereas the distorted, dynamically puckered, pseudorotational model depicts the vibrating molecule.

Corroborating evidence that heptacoordinated molecules, with either fluorine, oxygen, or free valence electron pairs as ligands, possess in their ground states pentagonal-bipyramidal structures with an unpuckered equatorial plane comes from ongoing ab initio calculations and two recent X-ray crystal structure determinations. It has experimentally been shown that in XeF₅⁻, in which the longer Xe–F bond distances of 1.979 (2)–2.034 (2) Å lessen the equatorial ligand–ligand repulsions (f_α = 0.364 mdyn/Å), the equatorial fluorines are essentially coplanar.[4] It has also been shown that in IF₆O⁻ (f_α = 0.690 mdyn/Å), which has considerably shorter (1.88 Å) equatorial bonds than XeF₅⁻, the equatorial fluorines are puckered, but that with decreasing temperature the degree of puckering strongly decreases.[62]

The fact that heptacoordinated species in their ground states exhibit pentagonal-bipyramidal structures with an unpuckered equatorial plane cannot be rationalized by VSEPR theory[63] in terms of a "repelling points on a sphere" (POS) model which should result in either a monocapped octahedron or a monocapped trigonal prism. Furthermore, it cannot be explained by conventional bonding schemes involving localized electron orbitals of the central atom to enforce the coplanarity of a central atom and five equatorial ligands. The best explanation to account for this planarity is the bonding scheme first proposed[4] for XeF₅⁻ based on an ab initio calculation of the molecular orbital population. In this scheme, the structure and bonding of XeF₅⁻ are explained by a simple model derived from XeF₄. The bonding in the square-planar XeF₄ can be described by two semi-ionic, 3-center 4-electron (3c-4e) bonds[64] for the four Xe–F bonds and two lone

Table VII. Atomic Populations (e) in the Valence Electron Orbitals and Total Charge Distributions for XeF₅⁻ and IF₇

	XeF₅⁻	IF₇
Central Atom		
s	2.22	1.35
$p_x = p_y$	0.61	0.64
p_z	2.02	0.60
d_{z^2}	0.03	0.11
$d_{x^2} = d_{y^2}$	0.06	0.12
d_{xy}	0.14	0.20
$d_{xz} = d_{yz}$	0.04	0.14
d total	0.37	0.83
Equatorial Fluorines		
s	1.98	1.93
p bond	1.70	1.57
p in plane	1.98	1.96
p_z	1.97	1.94
d	0	0.03
Axial Fluorines		
s		1.92
p_z		1.54
$p_x = p_y$		1.94
d		0.04
Total Charges		
central atom	2.25	2.94
F_{eq}	−0.63	−0.43
F_{ax}		−0.39

valence electron pairs on Xe ($s^2 p_z^2$ hybrids). The 3c-4e bonds involve the p_x^2 and p_y^2 orbitals of xenon. Addition of an F⁻ ion to the equatorial plane in XeF₄ results in pentagonal-planar XeF₅⁻ and the formation of a semi-ionic, 6-center 10-electron (6c-10e) bond involving the delocalized $p_x^2 p_y^2$ hybrid orbitals of Xe and six electrons on the five F ligands.[4] The two lone valence electron pairs on Xe in XeF₅⁻ are analogous to those in XeF₄.

The planar IF₅ fragment of IF₇ has essentially the same bonding as XeF₅⁻, as shown by the atomic population calculations given in Table VII. As expected for the replacement of two free valence electron pairs on the central atom by two bonded ligands, each of which contributes one electron to its bond, the population of the s^2 and p_z^2 orbitals of I in IF₇ has decreased by about two electrons, compared to those in XeF₄ and XeF₅⁻. The higher oxidation state of the central atom in IF₇ (+VII) results in I having a higher positive charge than Xe (+IV) in XeF₅⁻. This causes the effective electronegativity difference between the central atom and the ligands in IF₇ to be smaller than those in XeF₄ and XeF₅⁻ and results in an increased covalency and a shortening of the central atom–fluorine bonds. Furthermore, the axial fluorine ligands in IF₇ carry less of a negative charge than the equatorial ones and their bonds have higher s-character, which accounts for the axial I–F bonds to be more covalent and, hence, shorter than the equatorial ones.

Of course, the above model does not account for the fact that the electrons will try to minimize their mutual repulsions and occupy all of the available orbitals to do so. This results in the participation of some d functions. Although we are not proposing a d hybridization model, the population in the d orbitals does suggest a redistribution into these orbitals beyond that expected if the d orbitals were to act solely as polarization functions.

The above atomic population and total charge distribution analysis qualitatively confirms our simple bonding model for pentagonal-bipyramidal molecules. This model involves the use of delocalized p_x^2 and p_y^2 hybrid orbitals of the cental atom for the formation of a semi-ionic, 6c-10e bond with the five equatorial ligands and of an sp_z hybrid orbital for the formation of two, more covalent, axial bonds. This bonding scheme can account for all the observed structural features and also the observed bond length differences. The planarity of the p_x^2 and p_y^2 hybrid orbitals of

(62) Christe, K. O.; Dixon, D. A.; Mahjoub, A. R.; Mercier, H. P.; Sanders, J. C. P.; Seppelt, K.; Schrobilgen, G. J.; Wilson, W. W. *J. Am. Chem. Soc.*, in press.

(63) Gillespie, R. J.; Hargittai, I!. In *The VSEPR Model of Molecular Geometry*; Allyn and Bacon, A Division of Simon & Schuster, Inc.: Needham Heights, MA, 1991; p 58.

(64) Pimentel, G. C. *J. Chem. Phys.* **1951**, *10*, 446. Hach, R. J.; Rundle, R. E. *J. Am. Chem. Soc.* **1951**, *73*, 4321. Rundle, R. E. *J. Am. Chem. Soc.* **1963**, *85*, 112.

the central atom also provides the explanation of why the heptacoordinated main group fluorides prefer pentagonal-bipyramidal structures and not the monocapped octahedral or trigonal prismatic ones expected from VSEPR arguments.[63]

The possible puckering of the equatorial plane in pentagonal-bipyramidal molecules is due to the high degree of congestion in this plane. While in XeF_5^- ($r(Xe–F) \approx 2.00$ Å)[4] the congestion is relatively low and, therefore, the anion is still planar, the considerably shorter equatorial I–F bonds ($r = 1.857$ Å)[5] in IF_7 result in increased repulsion and significant puckering.

Conclusion

The problems previously encountered with the vibrational spectra and normal coordinate analyses of IF_7 have been resolved and were caused by partially incorrect assignments. It is shown that the lowest energy structure of IF_7 is a pentagonal bipyramid of D_{5h} symmetry that can undergo a facile, rapid, dynamic, low-frequency equatorial ring puckering with very large vibrational amplitudes. Equivalence of the five equatorial ligands in species of five-fold symmetry is most likely achieved by Bartell's pseudorotational mechanism,[5] which can also account for the deviations from D_{5h} symmetry observed by electron diffraction studies of the molecules at room temperature in the gas phase. The pentagonal-bipyramidal structures of heptacoordinated fluoride or oxy-fluoride complexes, the planarity of their equatorial ligands in their minimum-energy structures, and the large differences in their equatorial and axial bond lengths are attributed to a bonding scheme which involves a planar, delocalized $P_{x,y}$ hybrid orbital of the central atom for the formation of five equatorial, semi-ionic, 6-center 10-electron bonds and an sp_z hybrid for the formation of two mainly covalent axial bonds. The apparent puckering of the fluorine ligands in the equatorial plane is due to their wide vibrational amplitudes involving large vibrational quantum numbers. This effect depends strongly on the relative sizes of the central atom and its ligands and the temperature. Thus, XeF_5^-, which is least congested, is, within experimental error, planar,[4] while IF_6O^- is strongly puckered, but its degree of puckering significantly decreases with decreasing temperature.[62] In IF_7, the I–F bonds are the shortest and, hence, the puckering is most pronounced. These data suggest that a wide spectrum of structures should exist for pentagonal-bipyramidal molecules which range from complete planarity to a strong puckering of the equatorial ligands.

Note Added in Proof: The Coriolis ζ constants of the E_1' block of IF_7 were calculated from the force field and have the following values: $\zeta_{55} = -0.113$, $\zeta_{66} = 0.201$, $\zeta_{77} = 0.913$. Using these values, Dr. L. Bernstein has calculated the infrared band contour of ν_5. It exhibits a PQR structure similar to that observed for the 670 cm^{-1} band. The absence of pronounced PQR structure for the 746-cm^{-1} band is attributed to interference from hot bands. A high resolution study would be required to better understand the details of the observed band contours.

The Aminodiazonium Cation, $H_2N_3^+$ [†]

**Karl O. Christe,*,[1] William W. Wilson,[1] David A. Dixon,[2] Saeed I. Khan,[3] Robert Bau,[4]
Tobias Metzenthin,[4] and Roy Lu[4]**

*Contribution from Rocketdyne, A Division of Rockwell International Corporation, Canoga Park,
California 91309, Central Research and Development Department, E. I. du Pont de Nemours and
Company, Inc., Experimental Station, Wilmington, Delaware 19880-0328, J. D. McCullough
X-ray Crystallography Laboratory, Department of Chemistry and Biochemistry, University of
California, Los Angeles, California 90024, and Department of Chemistry, University of Southern
California, Los Angeles, California 90089. Received August 13, 1992*

Abstract: The $H_2N_3^+$ salts of SbF_6^-, AsF_6^-, and BF_4^- have been prepared and, for the first time, been isolated from HF solutions of HN_3 and the corresponding Lewis acids. They are hygroscopic white solids which are stable at room temperature. The crystal structure of $H_2N_3^+SbF_6^-$ was determined at 20 K. This compound crystallizes in the orthorhombic system, space group $Pmc2_1$, with two molecules in a unit cell of dimensions $a = 5.794$ (3) Å, $b = 5.113$ (2) Å, and $c = 9.919$ (5) Å with $R = 0.015$, $R_w = 0.022$, for 587 observed $[I > 3\sigma(I)]$ reflections. In addition to two almost perfectly octahedral SbF_6^- anions, the unit cell contains two asymmetric $H_2N_3^+$ cations with N(1)–N(2) = 1.295 (5) Å, N(2)–N(3) = 1.101 (6) Å, and N(1)–N(2)–N(3) = 175.3 (5)° and both hydrogens bonded to the same nitrogen atom, N(1). The infrared and Raman spectra of these salts were also recorded. Local density functional calculations were carried out for $H_2N_3^+$ and isoelectronic H_2NCN and used for the assignment of the observed vibrational spectra and the determination of their force fields. The general agreement between the calculated and observed geometries and frequencies is very good. The results from the LDF calculations indicate that the $H_2\bar{N}$ group in $H_2N_3^+$ is less pyramidal than that in H_2NCN and, therefore, possesses a lower inversion energy barrier.

Introduction

During our attempted fluorination of HN_3 in anhydrous HF solutions using either $XeF^+AsF_6^-$ or F_2 and the Lewis acids SbF_5, AsF_5, and BF_3, stable white solids were isolated which were identified as $H_2N_3^+$ salts of the corresponding Lewis acids. Relatively little had been known about salts derived from protonated hydrazoic acid. In 1966, Schmidt reported[5] the preparation of $H_2N_3^+SbCl_6^-$ from the reaction of HN_3 with $SbCl_5$ and HCl in CH_2Cl_2 at −78 °C. On the basis of the observation of an infrared band at 1522 cm^{-1}, which on deuteration was shifted to 1163 cm^{-1}, he proposed that $H_2N_3^+$ has the asymmetric aminodiazonium structure, $H_2N-N_2^+$, and not the symmetric diazenium structure, $[HN=N=NH]^+$. However, out of the nine fundamental vibrations expected for $H_2N-N_2^+$, only four were experimentally observed, and no explanation was offered for the absence of the other five bands. In 1983, Olah and co-workers studied the protonation of HN_3 in HF/SbF_5, HF/BF_3, and HSO_3F/SbF_5 solutions.[6] By ^{1}H and ^{15}N NMR spectroscopy, they unequivocally established that $H_2N_3^+$ has indeed the asymmetric aminodiazonium structure but did not isolate or further characterize these salts. On the basis of ab initio molecular orbital calculations at the 3-21G level of theory, they furthermore concluded that the aminodiazonium structure, $H_2N-N_2^+$, is favored by 49.8 kcal mol^{-1} over the symmetric diazenium structure, $[HN=N=NH]^+$ and that the optimized $H_2N-N_2^+$ structure has the following planar configuration of symmetry C_{2v}:
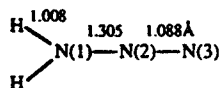
To our knowledge, no other studies on aminodiazonium salts have been published.

Experimental Section

Caution! Neat hydrazoic acid is shock sensitive, and proper safety precautions, such as working on a small scale and using safety shields, should be taken when handling the material.

Materials. HN_3 was prepared from NaN_3 and stearic acid at 110–130 °C.[7] HF (Matheson) was dried by storage over BiF_5.[8] AsF_5, SbF_5 (Ozark Mahoning), and BF_3 (Matheson) were purified by fractional condensation prior to use.

Apparatus. HN_3 was generated and handled on a Pyrex vacuum line equipped with Kontes Teflon valves. HF and the Lewis acids were

handled in a stainless steel–Teflon–FEP vacuum system,[9] and solids, in the dry N_2 atmosphere of a glovebox. Vibrational spectra were recorded as previously described.[10]

Preparation of $H_2N_3^+AsF_6^-$. A prepassivated (with ClF_3 and HF) Teflon–FEP ampule that was closed by a stainless steel valve was loaded on the metal vacuum line with HF (4.6 g). On the Pyrex line, HN_3 (2.73 mmol) was added at −196 °C, and the mixture was homogenized at room temperature. AsF_5 (2.86 mmol) was added on the metal line at −196 °C, and the mixture was warmed to −78 °C for 1.5 h. The HF solvent and the unreacted starting material were pumped off while the ampule was warmed slowly to ambient temperature. Pumping was continued for 1 h at 20 °C. The ampule contained 633 mg of a white solid (weight calculated for 2.73 mmol of $H_2N_3^+AsF_6^-$ = 636 mg) which was identified by vibrational spectroscopy and X-ray diffraction as $H_2N_3^+AsF_6^-$.

Preparation of $H_2N_3^+SbF_6^-$. Antimony pentafluoride (2.74 mmol) was transferred on the metal line in a dynamic vacuum into a prepassivated Teflon–FEP U-tube that was kept at −78 °C and closed by two stainless steel valves. Anhydrous HF (1.6 g) was added at −196 °C, and the mixture was briefly warmed to room temperature. Hydrazoic acid (3.23 mmol) was added at −196 °C on the Pyrex line, and the mixture was warmed to room temperature. All material, volatile at room temperature, was pumped off for 30 min, resulting in a white, stable solid (760 mg; weight calculated for 2.74 mmol of $H_2N_3^+SbF_6^-$ = 766 mg) which was identified by vibrational spectroscopy and a crystal structure determination as $H_2N_3^+SbF_6^-$.

Preparation of $H_2N_3^+BF_4^-$. According to the procedure described above for $H_2N_3^+AsF_6^-$, HN_3 (2.88 mmol) was combined with BF_3 (3.23 mmol) in HF (5.66 g). Warming of the resulting mixture from −196 to −78 °C produced a gel-type product which on further warming to −22 °C formed a clear solution. Volatile products were pumped off at −22 °C for 2 h and at 20 °C for 10 min, leaving behind 379 mg of a white, somewhat tacky, solid (weight calculated for 2.88 mmol of $H_2N_3^+BF_4^-$ = 377 mg) which was identified by vibrational spectroscopy as $H_2N_3^+$-BF_4^-.

---

(1) Rocketdyne.
(2) E. I. du Pont de Nemours and Company, Inc.
(3) University of California, Los Angeles.
(4) University of Southern California.
(5) Schmidt, A. *Chem. Ber.* 1966, *99*, 2976.
(6) Mertens, A.; Lammertsma, K.; Arvanaghi, M.; Olah, G. A. *J. Am. Chem. Soc.* 1983, *105*, 5657.
(7) Krakow, B.; Lord, R. C.; Neely, G. O. *J. Mol. Spectrosc.* 1968, *27*, 198.
(8) Christe, K. O.; Wilson, W. W.; Schack, C. J. *J. Fluorine Chem.* 1978, *11*, 71.
(9) Christe, K. O.; Wilson, R. D.; Schack, C. J. *Inorg. Synth.* 1986, *24*, 3.
(10) Wilson, W. W.; Christe, K. O. *Inorg. Chem.* 1987, *26*, 1573.

[†] Dedicated to Professor G. Olah on the occasion of his 65th birthday.

Table I. Details of the Data Collection and Structure Refinement for $H_2N_3{}^+SbF_6{}^-$ at 20 K

formula	$H_2N_3SbF_6$
fw	279.78
cryst system	orthorhombic
space group	*Pmc2₁*
cryst dimens, mm	0.15 × 0.30 × 0.50
cryst color	colorless
cryst habit	irregular
a, Å	5.794 (3)
b, Å	5.113 (2)
c, Å	9.919 (5)
Z	2
V, Å³	293.88
ρ(calcd), g/cm³	1.79
radiation (λ, Å)	Mo Kα (0.7107)
abs coeff (μ), cm⁻¹	2.42
abs cor type	empirical
abs factor range (intensity)	1.14–1.00
$F(000)$, e	154
temp, K	20
diffractometer	Huber (Crystal Logic)
scan mode; speed, deg/min	θ–2θ; 12.0
2θ range, deg	1–65
total no. of reflns measd	2095 ($+h,\pm k,\pm l$)
no. of unique reflns	649
R_{int}	0.024
no. of reflns used in refinement	587 ($I > 3\sigma(I)$)
no. of params refined	58
final shift/error: max, av	0.021, 0.002
max residual density, e/Å³	1.55 (0.75 Å from Sb)
$R = \sum\|\|F_o\| - \|F_c\|\|/\sum\|F_o\|$	0.015
$R_w = (\sum w(\|F_o\| - \|F_c\|)^2/\sum w(\|F_o\|)^2)^{1/2}$	0.022
GOF $= (\sum w(\|F_o\| - \|F_c\|)^2/(N_o - N_v))^{1/2}$	1.024
isotropic extinction param ($\times 10^5$)	1.883

Crystal Structure Determination of $H_2N_3{}^+SbF_6{}^-$. Single crystals of $H_2N_3{}^+SbF_6{}^-$ were obtained by recrystallization from anhydrous HF solution. Suitable crystals were selected under a microscope inside the glovebox and sealed in quartz capillaries. Initial data collection was carried out at room temperature on a Siemens P2₁ diffractometer. The structure was solved and refined to an agreement factor of $R = 0.049$ for 409 reflections. This structure revealed an asymmetric $H_2N_3{}^+$ cation with two poorly-defined H atoms attached to one of the terminal N atoms. Since the hydrogen positions in this room-temperature X-ray analysis were not entirely satisfactory, it was decided to re-collect data at low temperature.

Low-temperature diffraction data were collected on a four-circle Huber diffractometer equipped with a closed-cycle helium refrigerator.[11] The crystal was slowly cooled, over a period of 4 h, to 20 (5) K. Accurate unit cell parameters at this temperature were obtained by least-squares refinement of 15 centered reflections and are listed in Table I together with other details of data collection and structure refinement. Intensity data at 20 K were collected with the θ–2θ step scan technique, up to a maximum 2θ of 65°. Three standard reflections measured after every 97 reflections showed no decay. A total of 2095 reflections were measured over one hemisphere of reciprocal space and were then averaged for multiple observations to give a set of 649 unique reflections. R(av) was 0.024. Corrections for Lorentz and polarization effects were made, and an empirical absorption correction was applied using the ψ-scan procedure.

The position of antimony was determined from a Patterson map, and the remaining non-hydrogen atom positions were obtained from the initial difference Fourier map. The structure was then refined using 587 reflections with $I > 3\sigma(I)$, first with isotropic and later with anisotropic thermal parameters. At this point, a difference electron density map revealed the positions of the hydrogen atoms at a distance of 0.85 Å from N(1). In the final cycles of least-squares refinement, the hydrogen atom positions were also refined with a fixed isotropic temperature factor. The assigned thermal parameter for the hydrogen atoms was 30% higher than the average isotropic thermal parameters of the rest of the atoms, excluding Sb. Refinement converged with final agreement factors of $R(F) = 0.015$ and $R_w(F) = 0.022$ and GOF = 1.024. In the final difference map, except for two ripples associated with Sb (1.55 and 1.51 e/Å³ about 0.68 and 0.75 Å away, respectively), the maximum residual electron

(11) Strouse, C. E. *Rev. Sci. Instrum.* **1976**, *47*, 871–876.

Table II. Fractional Atomic Coordinates and Equivalent Isotropic Thermal Parameters (Å²) with Esd's of the Refined Parameters in Parentheses for $H_2N_3{}^+SbF_6{}^-$ at 20 K

atom	x	y	z	$10^4 U_{eq}{}^a$
Sb	0.0000	0.13576 (3)	0.1873^b	40 (1)
F(1)	−0.2303 (3)	−0.0176 (3)	0.0790 (2)	85 (6)
F(2)	0.2311 (3)	0.2909 (3)	0.2946 (2)	88 (6)
F(3)	0.0000	0.4289 (5)	0.0720 (3)	84 (10)
F(4)	0.0000	−0.1618 (5)	0.2993 (4)	83 (11)
N(1)	0.5000	−1.4511 (7)	1.0250 (4)	83 (14)
N(2)	0.5000	−1.6211 (6)	0.9282 (5)	85 (18)
N(3)	0.5000	−1.7781 (7)	0.8523 (4)	111 (15)
H(1)	0.388 (13)	−1.3753 (65)	1.020 (11)	127^c

$^a U_{eq} = [1/(6\pi^2)]\sum_i\sum_j\beta_{ij}\mathbf{a}_i\cdot\mathbf{a}_j$. $^b z$ coordinate held constant to define origin. ^{c} Assigned isotropic temperature factor held constant.

Table III. Interatomic Distances (Å) and Angles (deg) with Esd's in Parentheses for $H_2N_3{}^+SbF_6{}^-$ at 20 K^a

$H_2N_3{}^+$			
N(1)–N(2)	1.295 (5)	N(1)–H(1)	0.76 (7)
N(2)–N(3)	1.101 (6)	H(1)–H(1')	1.30 (16)
N(1)–N(2)–N(3)	175.3 (5)	H(1)–N(1)–N(2)	107 (6)
H(1)–N(1)–H(1')	118 (8)		

$SbF_6{}^-$			
Sb–F(1)	1.884 (2)	Sb–F(3)	1.885 (3)
Sb–F(2)	1.885 (2)	Sb–F(4)	1.884 (3)
F(1)–Sb–F(1')	90.20 (1)	F(2)–Sb–F(2')	90.5 (1)
F(1)–Sb–F(2)	89.65 (8)	F(2)–Sb–F(3)	90.46 (8)
F(1)–Sb–F(2')	179.58 (9)	F(2)–Sb–F(4)	90.4 (1)
F(1)–Sb–F(3)	89.15 (9)	F(3)–Sb–F(4)	178.8 (1)
F(1)–Sb–F(4)	90.00 (9)		

^{a} Room-temperature parameters: N(1)–N(2) = 1.36 (5) Å, N(2)–N(3) = 1.06 (5) Å, N(1)–N(2)–N(3) = 173 (5)°.
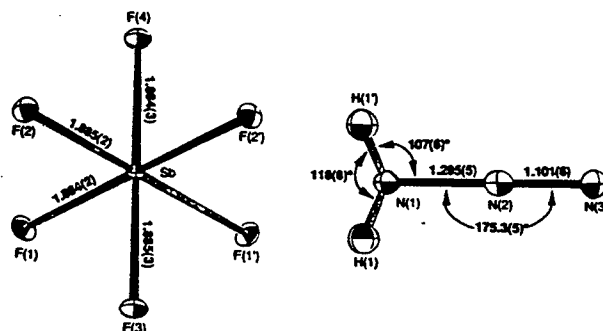
Figure 1. Atom numbering schemes, bond lengths (Å), and bond angles (deg) for $H_2N_3{}^+$ and $SbF_6{}^-$ at 20 K.
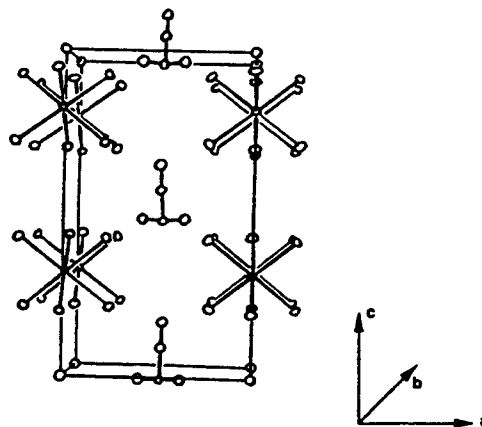
Figure 2. Packing diagram of $H_2N_3{}^+SbF_6{}^-$ viewed along the *b* axis.

density was less than 0.75 e/Å³. No significant correlations were observed. All data reduction, structure solution and refinement, and graphics were executed using the UCLA crystallographic package.[12]

Figure 3. Vibrational spectra of solid $H_2N_3^+SbF_6^-$: trace A, infrared spectrum of a sample pressed between AgBr windows; traces B and C, Raman spectra recorded at 25 and −145 °C, respectively.

Final atomic coordinates with equivalent isotropic thermal parameters are listed in Table II. Interatomic distances and angles are given in Table III, and the anisotropic temperature factors are listed in Table 1S in the supplementary material. An Ortep plot of the molecule is shown in Figure 1, and unit cell packings along the *b* and *a* axes are shown in Figures 2 and 3, respectively.

Crystal Structure Determination of $H_2N_3^+AsF_6^-$. This compound crystallizes in the orthorhombic space group *Pma*2 (No. 28), with *a* = 20.056 Å, *b* = 5.468 Å, *c* = 5.523 Å, *V* = 604.7 Å³, and *Z* = 4. Data were collected at room temperature, and the structure was refined to an agreement factor of *R* = 0.057 for 387 nonzero reflections. The structure shows a linear and apparently almost symmetric $H_2N_3^+$ cation [N–N = 1.16 (2) and 1.19 (2) Å; N–N–N = 177 (2)°]. However, the structure analysis was marred by extensive disordering of the AsF_6^- anion, and it is quite possible that the $H_2N_3^+$ cation suffers from a 2-fold packing disorder as well. The H atoms in $H_2N_3^+AsF_6^-$ could not be located.

Computational Methods. The geometry, vibrational frequencies, and force field of $H_2N_3^+$ were calculated, as previously described,[13] in the local density functional (LDF) approximation by using the program system DMol with a polarized double numerical basis set.

Results and Discussion

Syntheses and Properties of $H_2N_3^+$ Salts. Protonation of HN_3 by mixtures of HF and the strong Lewis acids SbF_5, AsF_5, and BF_3, followed by removal of solvent and unreacted starting ma-

(12) The programs used in this work included modified versions of the following programs: REDUCE (Broach, Coppens, Becker, and Blessing), peak profile analysis, Lorentz and polarization corrections; ORFLS (Busing, Martin, and Levy), structure factor calculation, full-matrix least-squares refinement; ORFEE (Busing, Martin, and Levy), distance, angle, and error calculations; ORTEP (Johnson), figure plotting. Scattering factors and corrections for anomalous dispersion were taken from: *International Tables for X-ray Crystallography*; Kynoch Press; Birmingham, England, 1974; Vol. IV. All calculations were performed on a DEC VAX 3100 cluster.

(13) (a) Christe, K. O.; Wilson, R. D.; Wilson, W. W.; Bau, R.; Sukumar, S.; Dixon, D. A. *J. Am. Chem. Soc.* **1991**, *113*, 3795. (b) Dixon, D. A.; Andzelm, J.; Fitzgerald, G.; Wimmer, E.; Jasien, P. In *Density Functional Methods in Chemistry*; Labanowski, J., Andzelm, J., Eds.; Springer Verlag: New York, 1991; p 33. (c) Dixon, D. A.; Christe, K. O. *J. Phys. Chem.* **1992**, *96*, 1018. (d) Delley, B. *J. Chem. Phys.* **1990**, *92*, 508. Dmol is available commercially from BIOSYM Technologies, San Diego, CA. A FINE grid was used. The multipolar fitting functions for the model density used to evaluate the effective potential have angular momentum numbers of 3 for N and 2 for H.

terial at room temperature, produces the $H_2N_3^+$ salts of SbF_6^-, AsF_6^-, and BF_4^-, respectively.

$$HN_3 + HF + XF_n \xrightarrow{HF} H_2N_3^+XF_{n+1}^-$$
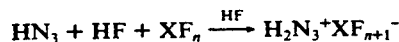
Although the existence of the $H_2N_3^+$ cation in these solutions had previously been established by multinuclear NMR spectroscopy,[6] the actual salts had not been isolated and characterized. All salts are white, crystallinic solids that are stable at room temperature. They are strongly hygroscopic and, when exposed to moisture, form the corresponding H_3O^+ salts[14]

$$H_2N_3^+SbF_6^- + H_2O \rightarrow H_3O^+SbF_6^- + HN_3$$
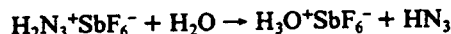
as expected from H_2O being a stronger base than HN_3 and, therefore, being able to displace HN_3 from its salts.

X-ray Crystal Structure of $H_2N_3^+SbF_6^-$. The crystal structure of $H_2N_3^+SbF_6^-$ was determined both at room temperature and at 20 K. The structures were almost identical at both temperatures (see Table III and footnote), but the low-temperature data were of much better quality. The structure consists of well-separated $H_2N_3^+$ and SbF_6^- ions (see Figure 1). The SbF_6^- anion is a nearly perfect octahedron with angles ranging from 89.15 (9) to 90.5 (1)° and identical Sb–F bond lengths of 1.885 (3) Å. The $H_2N_3^+$ cation is asymmetric, with both hydrogens attached to the same nitrogen. Furthermore, the two N–N bond distances are very different, the N–N–N group is slightly distorted from linearity (N(1)–N(2)–N(3) = 175.3°), and the NH₂ group is pyramidal. These findings demonstrate that the structure of $H_2N_3^+$ is best described by I, with little contribution from resonance structure

II. The fact that the repulsion from the free valence electron pair on N(1) is larger than those from the two hydrogen ligands can account for N(2) being slightly bent away from this free pair. The observed N—N bond lengths are in good agreement with our expectations for an N—N single and an N≡N triple bond, and their differences are more pronounced than those found for other covalent azides such as CF_3N_3 (N(1)–N(2) = 1.252 (5) Å, N-(2)–N(3) = 1.118 (3) Å)[15] or FN_3 (N(1)–N(2) = 1.253 (10) Å, N(2)–N(3) = 1.132 (10) Å).[16] The observed N–H bond length of 0.76 (7) Å is unrealistically short due to the fact that hydrogen does not possess any core electrons, and therefore, the X-rays are being diffracted by the binding electrons. This results in an artificially short N–H bond length, which is no surprise in view of the well-known difficulties of obtaining reliable hydrogen bond lengths by X-ray diffraction. On the basis of the ab initio calculation (see below), a realistic N–H bond distance in $H_2N_3^+$ is about 1.01 Å. The H–N–H and H–N–N bond angles, on the other hand, should not be affected, as the binding electrons are located along the N–H bond axes, and, therefore, are considered more reliable.

A packing diagram of $H_2N_3^+SbF_6^-$ is shown in Figure 2. The anion and the cation are located on crystallographic mirror planes. The anionic mirror plane passes through the atoms F(3)–Sb–F(4) whereas the cationic mirror plane passes through all three nitrogen atoms and bisects the H–N–H angle. The cations are stacked parallel to each other down the crystallographic *b* axis (see Figure 2) but are oriented perpendicular to each other in the *b–c* plane, causing a doubling of the repeat distance along the *c* axis. The nearest anion–cation interactions are N(1)—F(1) at 2.765 Å and H(1)—F(1) at 2.127 Å, which are significantly shorter than the

(14) Christe, K. O.; Schack, C. J.; Wilson, R. D. *Inorg. Chem.* **1975**, *14*, 2224.

(15) Christe, K. O.; Christen, D.; Oberhammer, H.; Schack, C. J. *Inorg. Chem.* **1984**, *23*, 4283.

(16) Christen, D.; Mack, H. G.; Schatte, G.; Willner, H. *J. Am. Chem. Soc.* **1988**, *110*, 707.

Table IV. Calculated and Observed Geometries of Isoelectronic $H_2N_3^+$ and H_2NCN

	[H_2N—$N\equiv N$]$^+$			H_2N—$C\equiv N$			
	expt[a]	LDF	3-21G[b]	expt[c]	LDF	6-31G*[d]	STO-3G[d]
Bond Distances, Å							
r_1, r_2 (N—H)	e	1.043	1.008	1.001	1.031	0.998	1.031
r_3 (N—X)	1.295 (5)	1.276	1.305	1.346	1.341	1.344	1.399
r_4 (X≡N)	1.101 (6)	1.126	1.088	1.160	1.172	1.138	1.158
Bond Angles, deg							
α (H—N—H)	118 (8)	117.9	f	113.5	110.5	113.2	108.8
β_1, β_2 (H—N—X)	107 (6)	114.5	f	115.6	113.6	114.5	110.4
$\sum(\alpha + \beta_1 + \beta_2)^g$	332 (20)	346.9	360[f]	344.7	337.7	342.2	329.6
N—X≡N	175.3 (5)	175.2	f	[180][h]	176.1	178.2	176.7

[a] Data from crystal structure of $H_2N_3^+SbF_6^-$ at 20 K. [b] Data from ref 6. [c] Data from refs 24 and 30. [d] Data from ref 22. [e] The value of 0.76 (7) from Table III is much too short because of the shortcomings of X-ray diffraction methods for the determination of exact hydrogen bond distances and should not be used. [f] No angles were given in ref 6; however, from the stated planarity and C_{2v} symmetry of $H_2N_3^+$ $\sum(\alpha + \beta_1 + \beta_2)$ must equal 360°. [g] This sum of the angles is a measure for the planarity of the NH_2 group, with 360° being planar and 328.5° being an ideal trigonal pyramid. [h] Assumed value.

Table V. Calculated and Observed Vibrational Frequencies (cm^{-1}) of Isoelectronic $H_2N_3^+$ and H_2NCN

Approx description of mode in point group C_s	Symmetry coordinates	[H_2N-N≡N]$^+$			H_2N-C≡N					
		obsd	calcd LDF	PED[a] LDF	obsd	calcd LDF	calcd 6-31G*[d]	calcd 4-31G*[g]	PED LDF	PED 4-31G*[g]
A' v_1 v sym NH_2	$S_1 = \frac{1}{\sqrt{2}}(\Delta r_1 + \Delta r_2)$	3170	3248	$98S_1 + 1S_3$	3420[b]	3375	3787	3722	$100S_1$	$100S_1$
v_2 v X≡N	$S_2 = \Delta r_4$	2318	2350	$69S_2 + 31S_4$	2270[b]	2301		2611	$66S_2 + 34S_4$	$90S_2 + 14S_4$
v_3 δ sciss NH_2	$S_3 = \frac{1}{\sqrt{6}}(2\Delta\alpha - \Delta\beta_1 - \Delta\beta_2)$	1547	1526	$100S_3$	1595[b]	1556	1804	1818	$100S_3$	$102S_2$
v_4 vN-X	$S_4 = \Delta r_3$	1129	1190	$88S_4 + 8S_2 + 4S_6$	1055[b]	1092	1159	1170	$85S_4 + 8S_2 + 5S_3 + 2S_6$	$79S_4 + 10S_2$
v_5 δNXN in plane	$S_5 = N(-),X(+),N(-)$ in plane	530	516	$79S_5 + 20S_6$	(538)[d]	477	531	554	$85S_5 + 15S_6$	$74S_5 + 23S_6$
v_6 δNH_2 wag (inversion at N)	$S_6 = \frac{1}{\sqrt{3}}(\Delta\alpha + \Delta\beta_1 + \Delta\beta_2)$	489	479	$72S_6 + 24S_5 + 3S_3$	$\binom{714,670}{414,364}$[e]	622	691	688	$86S_6 + 13S_5 + 1S_4$	$96S_6 + 27S_5 + 21S_4$
A" v_7 vas NH_2	$S_7 = \frac{1}{\sqrt{2}}(\Delta r_1 - \Delta r_2)$	3280	3372	$98S_7 + 2S_8$	3480[b]	3469	3890	3829	$98S_7 + 1S_8$	$100S_7$
v_8 δas NH_2	$S_8 = \frac{1}{\sqrt{2}}(\Delta\beta_1 - \Delta\beta_2)$	1259	1232	$99S_8 + 1S_9$	$\binom{1055}{\text{or }1150}$[c]	1151	1323	1343	$98S_8 + 2S_9$	$93S_8$
v_9 δNXN out of plane	$S_9 = t_1 + t_2$[h]	418	429	$85S_9 + 14S_8$	(437)[d]	408	463	485	$85S_9 + 15S_8$	$99S_9$

(a) in percent; (b) infrared gas phase frequencies from ref. 21; (c) see text; (d) Raman of the liquid (ref. 28) and solid (ref. 32); (e) components of the inversion splitting (see refs. 21,24,27); (f) data from ref. 22; (g) data from ref 24; (h) t_1 = angle of C(2)–N(3) with respect to the plane H(1)–C(2)–N(1); t_2 = angle of C(2)–N(3) with respect to the plane H(2)–C(2)–N(1); see also comments made in the discussion of the results of the normal coordinate analysis.

sums of their Pauling van der Waals radii.[17] Although these short distances suggest appreciable hydrogen–fluorine bridging, they do not result in a significant distortion of the SbF_6^- octahedron (see above).

The above crystal structure demonstrates that $H_2N_3^+$ has indeed the asymmetric aminodiazonium structure. This is not surprising in view of a previous ab initio calculation which indicated that the aminodiazonium structure is 49.8 kcal mol^{-1} more favorable than the symmetric diazenium structure.[6] It must be pointed out, however, that, in spite of the good agreement between the predicted[6] and our observed N–N bond lengths (1.305 and 1.088 Å versus 1.295 (5) and 1.101 (6) Å), the previous calculation[6] predicted a planar NH_2 group whereas the crystal structure and our LDF calculations (see below) show that the NH_2 group in $H_2N_3^+$ is pyramidal. This was due to the lack of polarization functions on the nitrogens at the 3-21G level.

Computational Results. To support our analysis of the vibrational spectra of the $H_2N_3^+$ cation, the structure, vibrational frequencies, and force field of the free $H_2N_3^+$ cation in the gas phase were calculated using local density functional (LDF) theory. To test the quality of these computations, the electronic structure of the known,[18-32] isoelectronic cyanamide molecule, H_2NCN, was

Table VI. Symmetry Force Constants (mdyn/Å) of $H_2N_3^+$ and H_2NCN Calculated by the LDF Method

$H_2N_3^+$										
A'	1	2	3	4	5	6	A"	7	8	9
1	6.04	-0.20	0.01	0.24	0.02	0.25	7	6.11	0.06	0.04
2		20.17	0.01	0.57	0.06	-0.20	8		0.74	-0.11
3			0.54	-0.47	-0.03	-0.14	9			1.94
4				9.53	0.18	0.99				
5					0.56	-0.14				
6						0.54				
H_2NCN										
A'	1	2	3	4	5	6	A"	7	8	9
1	6.48	-0.14	0.07	0.18	0.04	0.32	7	6.53	0.17	-0.02
2		17.58	-0.01	0.39	0.04	-0.11	8		0.64	-0.13
3			0.57	-0.33	-0.03	-0.03	9			1.04
4				7.98	0.09	0.65				
5					0.51	-0.03				
6						0.45				

also calculated. The results are summarized in Tables IV–VI and demonstrate that, for this type of molecule, LDF theory duplicates

(18) Brown, R. D.; Godfrey, P. D.; Head-Gordon, M.; Wiedenmann, K. H.; Kleibömer, B. *J. Mol. Spectrosc.* **1988**, *130*, 213.

(19) Hunt, R. D.; Andrews, L. *J. Phys. Chem.* **1987**, *91*, 2751.

(20) Read, W. G.; Cohen, E. A.; Picket, H. M. *J. Mol. Spectrosc.* **1986**, *115*, 316.

(17) Pauling, L. *The Nature of the Chemical Bond*, 3rd ed.; Cornell University Press: Ithaca, NY, **1960**; p 260.

1840   *J. Am. Chem. Soc., Vol. 115, No. 5, 1993*

Christe et al.

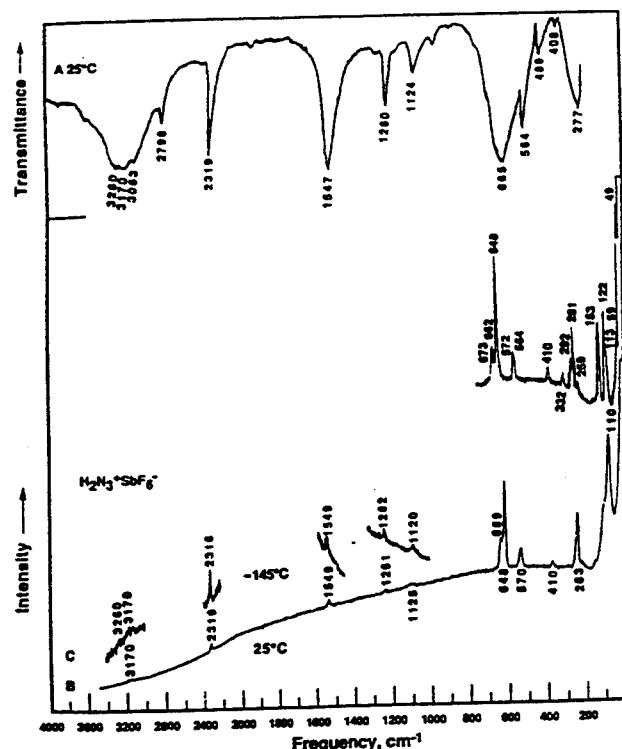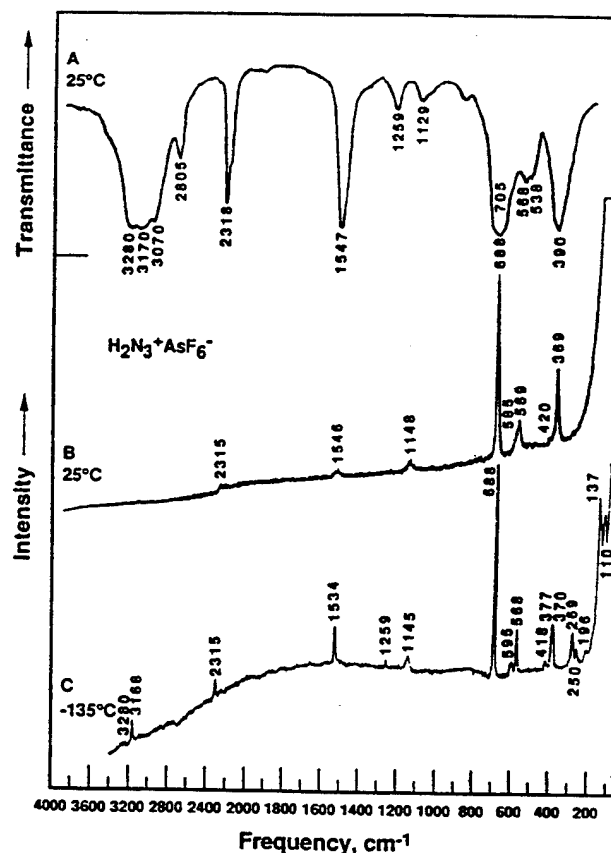**Figure 4.** Vibrational spectra of solid $H_2N_3^+AsF_6^-$: trace A, infrared spectrum of a sample pressed between AgBr windows; traces B and C, Raman spectra recorded at 25 and −135 °C, respectively.

Figure 5. Vibrational spectra of solid $H_2N_3^+BF_4^-$: trace A, infrared spectrum of a sample pressed between AgBr windows; trace B, Raman spectra recorded at −130 °C.

the experimental frequency values better than calculations at either the 4-31G*[24] or 6-31G*[22] level. In agreement with previous calculations at the 4-31G[24] or higher levels[22] for H_2NCN, the lowest energy structure found for $H_2N_3^+$ by using LDF theory is nonplanar (C_s symmetry) with a pyramidal amino group. The planar C_{2v} structure previously calculated for $H_2N_3^+$ at the 3-21G level[6] is due to the lower level of theory used and, for isoelectronic H_2NCN, represents a saddle point on the potential energy surface.[22] It should also be pointed out that LDF theory predicts the $H_2N–N$ group in $H_2N_3^+$ to be considerably flatter than the $H_2N–C$ group in H_2NCN. This should result in a lower inversion barrier for the NH_2 group in $H_2N_3^+$, which is also apparent from the lowering of the frequency of the NH_2 wagging mode, $\nu_6(A')$, which, on the basis of its symmetry coordinate and potential energy distribution, represents the inversion motion (see below).

Vibrational Spectra. Infrared and Raman spectra were recorded for $H_2N_3^+SbF_6^-$, $H_2N_3^+AsF_6^-$, and $H_2N_3^+BF_4^-$ (see Figures 3–5). Table VII shows the observed frequencies and their assignments.

Approximate mode descriptions, symmetry coordinates, and potential energy distributions for $H_2N_3^+$ and isoelectronic H_2NCN are included in Table V. The LDF force fields for $H_2N_3^+$ and H_2NCN were analyzed in terms of internal coordinates and are given in Table VI.

Although cyanamide, H_2NCN, is a simple molecule of great industrial importance and its structure is well-known from microwave spectroscopy,[20,30,31] its vibrational analysis is still incomplete. This is partially due to experimental difficulties, i.e. its low vapor pressure and tendency to polymerize, and to complications caused by its low inversion barrier at the nitrogen atom.

The H_2NCN molecule and the isoelectronic $H_2N_3^+$ cation possess symmetry C_s, and their nine fundamental vibrations are classified as $\Gamma = 6A' + 3A''$ (see Table V). Of the nine fundamental vibrations of H_2NCN, the antisymmetric NH_2 deformation, $\nu_8(A'')$, has not been experimentally observed, the two NCN bending modes, $\nu_5(A')$ and $\nu_9(A'')$, have been observed only in the liquid phase[28] or solution,[24] and the NH_2 wagging mode, $\nu_6(A')$, is complicated by inversion splittings.[21] Nevertheless, H_2NCN served as a good case for testing the accuracy of the LDF calculations. As can be seen from Table V, our LDF results for H_2NCN are in good agreement with the experimental frequencies. Consequently, the LDF values for $H_2N_3^+$ should be equally good and were used as a guide for the following assignments for $H_2N_3^+$.

The assignment of the two NH_2 stretching modes, $\nu_1(A')$ and $\nu_7(A'')$, the N≡N stretching mode, $\nu_2(A')$, and the NH_2 scissoring mode, $\nu_3(A')$, to the bands at about 3170, 3280, 2318, and 1547 cm^{-1}, respectively, is unambiguous. In the 1100–1300-cm^{-1} region, two bands are observed at about 1129 and 1259 cm^{-1}, respectively, which, on the basis of the LDF predictions, should represent the N–N stretching mode, $\nu_4(A')$, and the antisymmetric NH_2 deformation, $\nu_8(A'')$, respectively. This choice of assignments is also supported by the observations that the 1259-cm^{-1} mode is more intense in the infrared and less intense in the Raman spectra and that, in the room-temperature Raman spectrum of $H_2N_3^+SbF_6^-$, it is broadened so much that it is no longer observable. A similar broadening of the Raman bands at ambient temperature has also been observed for the remaining NH_2-group modes in the $H_2N_3^+SbF_6^-$ spectrum. This positive identification of the antisymmetric NH_2 deformation vibration for $H_2N_3^+$ suggests that, in H_2NCN, this mode should occur in a similar frequency range and might either by assigned to the broad band at about 1150 cm^{-1} in the infrared spectrum of liquid H_2NCN,[27] or, in the gas phase, coincide with the N–C stretching mode at 1055 cm^{-1}.

The remaining three, yet unassigned, fundamental vibrations are the NH_2 wagging mode, $\nu_6(A')$, and the two N_3 skeletal deformation modes, $\nu_5(A')$ and $\nu_9(A'')$. On the basis of the LDF calculations, these three modes are expected to occur in the

(21) Birk, M.; Winnewisser, M. *Chem. Phys. Lett.* **1986**, *123*, 382.
(22) Saebo, S.; Farnell, L.; Riggs, N. V.; Radom, L. *J. Am. Chem. Soc.* **1984**, *106*, 5047.
(23) Khaikin, L. S.; Mochalov, V. I.; Grikina, O. E.; Pentin, Yu. A. *Vestn. Mosk. Univ., Ser. 2: Khim.* **1983**, *24*, 536.
(24) Ichikawa, K.; Hamada, Y.; Sugawara, Y.; Tsuboi, M.; Kato, S.; Morokuma, K. *Chem. Phys.* **1982**, *72*, 301.
(25) Daoudi, A.; Pouchan, C.; Sauvaitre, H. *J. Mol. Struct.* **1982**, *89*, 103.
(26) King, S. T.; Strope, J. H. *J. Chem. Phys.* **1971**, *54*, 1289.
(27) Jones, T. R.; Sheppard, N. *J. Chem. Soc. D* **1970**, 715.
(28) Fletcher, W. H.; Brown, F. B. *J. Chem. Phys.* **1963**, *39*, 2478.
(29) Wagner, G. D.; Wagner, E. L. *J. Chem. Phys.* **1960**, *34*, 1480.
(30) Tyler, J. K.; Sheridan, J.; Costain, C. C. *J. Mol. Spectrosc.* **1972**, *43*, 248.
(31) Johnson, D. R.; Suenram, R. D.; Lafferty, W. J. *Astrophys. J.* **1976**, *208*, 245.
(32) Durig, J. R.; Walker, M.; Baglin, F. G. *J. Chem. Phys.* **1968**, *48*, 4675.

The Aminodiazonium Cation

J. Am. Chem. Soc., Vol. 115, No. 5, 1993 1841

Table VII. Vibrational Spectra for Solid $H_2N_3^+SbF_6^-$, $H_2N_3^+AsF_6^-$, and $H_2N_3^+BF_4^-$ and Their Assignments

			obsd freq, cm⁻¹ (rel intens)							
$H_2N_3^+SbF_6^-$			$H_2N_3^+AsF_6^-$			$H_2N_3^+BF_4^-$		assignt (point group)		
IR	Raman		IR	Raman		IR	Raman			
25 °C	25 °C	−144 °C	25 °C	25 °C	−135 °C	25 °C	−130 °C	$H_2N_3^+$ (C_s)	XF_6^- (O_h)	BF_4^- (T_d)
3260 vs		3260 (0+)	3280 vs		3280 (0+)	3160 vs		$\nu_7(A'')$		
3170 vs	3170 (0+)	3170 (0.5)	3170 vs		3168 (0.9)	3020 vs	3110 (0.2)	$\nu_1(A')$		
3063 m			3070 m					$2\nu_3(A')$		
2798 m			2805 m			2850 sh		$(\nu_3 + \nu_8)(A'')$		
2319 s	2319 (0.7)	2316 (2)	2318 s	2315 (0.3)	2315 (0.7)	2304 s	2319 (0.7)	$\nu_2(A')$		
1958 vw			1960 vw			1995 vw		$(\nu_3 + \nu_9)(A'')$		
1547 vs	1549 (0.8)	1549 (0.6)	1547 vs	1546 (0.4)	1534 (1.6)	1555 vs	1580 (1.5)	$\nu_3(A')$		
1310 vw			1400 vw						$(\nu_1 + \nu_3)(F_{1u})$	
1260 m	1261 (0.4)	1262 (0.4)	1259 m		1259 (0.4)	1297 m	1288 (1)	$\nu_8(A'')$		$(\nu_1 + \nu_4)(F_2)$
1220 vw									$(\nu_2 + \nu_3)(F_{1u} + F_{2u})$	
1124 mw	1125 (0.5)	1120 (0.5)	1129 mw	1148 (0.5)	1145 (0.7)		1163 (0.5)	$\nu_4(A')$		$\nu_3(F_2)$
						1030 vs	1023 (0.2)			
1025 vw								$(\nu_5 + \nu_6)(A')$		
						770 mw	771 (4.8)			$\nu_1(A_1)$
665 vs	669 (3)	673 (2) / 662 (1)	705 vs						$\nu_3(F_{1u})$	
	648 (10)	648 (10)		688 (10)	688 (10)				$\nu_1(A_{1g})$	
	570 (2.3)	572 (2.4)		585 sh	595 (0.5)				$\nu_2(E_g)$	
564 m		564 (1)	568 m	569 (1.6)	568 (2)					$\nu_4(F_2)$
530 sh			538 m			530 mw	536 (0.5) / 525 (0.5)	$\nu_5(A')$		
489 mw								$\nu_6(A')$		
408 vw	410 (0.8)	410 (1.0)	420 sh	418 (0.3)		420 m		$\nu_9(A'')$		
277 s			390 s						$\nu_4(F_{1u})$	
		332 (0.8)			377 (1.9) / 370 (1.7)			F—H bridge		
	283 (6.2)	292 (2) / 281 (5.8)		369 (4)					$\nu_5(F_{2g})$	
		259 (0.5)				351 w	358 (1.9)	F—H bridge		$\nu_2(E)$
					269 (1.5) / 250 (0.5)				$\nu_6(F_{2u})$	
150 sh	153 (8)			196 (0.2) / 137 (4) / 110 (3.5)			221 (0.5) / 200 (2) / 163 (10) / 135 (8)		lattice vibrations	
110 (10)	122 (8.5) / 113 (2) / 59 (2) / 49 (8)									

400–500-cm⁻¹ frequency range, which is complicated by bands due to the anions. Futhermore, the A″ skeletal bending mode, ν_9, is expected to be of very low infrared intensity,[23] and the NH₂ wagging mode, $\nu_6(A')$, should not exhibit any inversion splittings since in the crystallinic salts the hydrogens are locked into fixed positions by fluorine bridges (see X-ray crystal structure section).

Inspection of the low-temperature Raman spectra of $H_2N_3^+$-SbF_6^- and $H_2N_3^+AsF_6^-$ reveals a reasonably intense band at 410–420 cm⁻¹, which has a very weak counterpart in the infrared spectra and is only slightly broadened at room temperature. Hence, this vibration should belong to one of two skeletal bending modes of $H_2N_3^+$. Since, in the Raman spectra of liquid[24,28] or dissolved[24] H₂NCN, the out-of-plane NCN deformation mode has by far the highest intensity of the three modes in question and the 410–420-cm⁻¹ frequency value is very close to that of 429 cm⁻¹ calculated by us for the out-of-plane N₃ deformation mode of $H_2N_3^+$, this 410–420-cm⁻¹ band can be assigned with confidence to the $\nu_9(A'')$ mode of $H_2N_3^+$.

The two remaining A′ modes, ν_5 and ν_6, are more difficult to assign. In view of their similar predicted frequencies (530 and 489 cm⁻¹) and related motions, we expect their symmetry coordinates to be strongly mixed (see PED of Table V), i.e. to be symmetric and antisymmetric combinations of S_5 and S_6. Both modes are expected to be of low Raman[32] but significant infrared intensity[24] and, therefore, should be detectable in the infrared spectra. The infrared spectrum of $H_2N_3^+SbF_6^-$ shows a shoulder at 530 cm⁻¹ and a medium weak band at 489 cm⁻¹, and that of $H_2N_3^+AsF_6^-$ shows a medium band at 538 cm⁻¹. In $H_2N_3^+BF_4^-$, the 530-cm⁻¹ region is obscured by the antisymmetric BF₄⁻ deformation, $\nu_4(F_2)$. Consequently, the ν_5 and ν_6 modes of $H_2N_3^+$ are tentatively assigned to the bands at about 530 and 489 cm⁻¹, respectively.

The above assignments can account for all the observed features in the vibrational spectra of the $H_2N_3^+$ salts, except for a medium weak band at 900 cm⁻¹ and a shoulder at 820 cm⁻¹ in the infrared spectrum of $H_2N_3^+AsF_6^-$. These two features are of variable intensity and show no counterparts in the IR spectrum of $H_2N_3^+SbF_6^-$. Therefore, they are judged to be due to an unknown impurity.

In the low-temperature Raman spectra of $H_2N_3^+SbF_6^-$ and $H_2N_3^+AsF_6^-$, the anion bands become much more complex than those in the room-temperature spectra. This is attributed to the freezing out of ion rotation, which for the anions causes splittings into degenerate components and violations of the O_h selection rules, as shown by the observation of the ν_6 mode for AsF₆⁻. In addition, the low-temperature Raman spectrum of $H_2N_3^+SbF_6^-$ shows two bands at 332 and 259 cm⁻¹, which probably are not due to the SbF₆⁻ anion but represent H—F bridge bonds. This temperature effect on the vibrational spectra might also cause a significant broadening of the NH₂ wagging band, ν_6, at room temperature and, thereby, contribute to the difficulty of observing this mode in our infrared spectra.

In summary, the nine fundamental vibrations of $H_2N_3^+$ have been observed with frequencies which are in very good agreement with our LDF calculations. This confirms the asymmetric nonplanar aminodiazonium structure of $H_2N_3^+$, found by the X-ray crystal structure determination. The previous failure[5] to observe most of these bands for $H_2N_3^+SbCl_6^-$ is attributed to their relatively low infrared intensities and relative broadness at room temperature.

Normal-Coordinate Analysis. To support our vibrational assignments for $H_2N_3^+$, normal-coordinate analyses were carried out for $H_2N_3^+$ and isoelectronic H₂NCN (see Tables V and VI) with the LDF force fields. The corresponding frequencies and

symmetry coordinates are listed in Table V. Our LDF force field for H_2NCN is in good general agreement with that previously published[24] by Ichikawa et al. at the 4-31G* level of theory, if it is kept in mind that the frequencies at the 4-31G* level are on average about 10% higher than the experimental ones. The potential energy distributions are given in Table V and support the given mode descriptions.

A special comment is required on the magnitudes of F_{99} in our force fields, which are given in Table VI. The listed F_{99} values are clearly too high and should be comparable to those of F_{55}. The $\nu_5(A')$ and $\nu_9(A'')$ modes represent the in-plane and out-of-plane deformations of the nearly linear NXN groups, which, therefore, should be almost degenerate and exhibit similar frequencies and force constants. Whereas the frequencies of ν_9 are comparable to those of ν_5, the F_{99} values in Table VI are about 2–4 times larger than those of F_{55}. This is an artifact caused by the inability to exactly describe with our computer input code the S_9 symmetry coordinate of the out-of-plane NXN deformation for these molecules when they possess a slightly bent NXN group. Our program to convert the Cartesian second derivatives to symmetry-adapted internal coordinates allows for only four kinds of internal motions: bond stretching, angle bending, a dihedral angle between two planes, and the minimum angle that a bond forms with a plane. Thus, the $\nu_9(A'')$ mode had to be defined as the sum of the angles formed between the X–N(2) bond and the two planes defined by H(1)N(1)X and H(2)N(1)X. By making the NXN bonds linear, we were able to properly describe S_9 with this code and obtain values for F_{99} ($H_2N_3^+$, 0.47 mdyn/Å; H_2N-CN, 0.44 mdyn/Å) that are in excellent agreement with our expectations (see above) and those previously reported.[24] The PED ($94S_9 + 6S_8$) for the revised F_{99} values was similar to those given in Table V, while the remainder of the A'' force field remained practically unchanged.

Supplementary Material Available: Table 1S, listing anisotropic temperature factors (1 page); Table 2S, listing observed and calculated structure factors (3 pages). Ordering information is given on any current masthead page.

2696

The IOF6- Anion: The First Example of a Pentagonal Bipyramidal AX5YZ Species[†]

K. O. Christe,[*,1] D. A. Dixon,[2] A. R. Mahjoub,[3] H. P. A. Mercier,[4] J. C. P. Sanders,[4]
K. Seppelt,[*,3] G. J. Schrobilgen,[*,4] and W. W. Wilson[1]

*Contribution from Rocketdyne, A Division of Rockwell International,
Canoga Park, California 91309, the Department of Chemistry, McMaster University,
Hamilton, Ontario L8S 4M1, Canada, the Central Research and Development Department,
E.I. du Pont de Nemours and Company, Inc., Experimental Station,
Wilmington, Delaware 19880-0328, and the Institut für Anorganische und
Analytische Chemie der Freien Universität, Berlin, Germany*

Received October 16, 1992

Abstract: The IOF6- anion, which is the first example of a pentagonal bipyramidal AX5YZ type species, was prepared in the form of its stable $N(CH_3)_4^+$ salt. Its X-ray crystal structure was determined at –93 ° and –155 °C (tetragonal, space group $P4/nmm$, $Z = 2$, $a = 8.8590$ (10) and 8.8151 (10) Å, $c = 6.3690$ (10) and 6.3213 (10) Å, $R = 0.0373$ and 0.0291 for 876 $[I > 3\sigma(I)]$ and 885 $[I > 3\sigma(I)]$ reflections, respectively). In addition to two perfectly ordered $N(CH_3)_4^+$ cations, the structure contains two IOF6- anions of approximate C_{5v} symmetry which are subject to a positional 4-fold disorder for the equatorial plane. The O–I–F_{ax} angle is constrained by symmetry to be 180°, whereas there are no constraints on the positions of the equatorial fluorines. The I–O bond length indicates substantial double bond character, and the axial I–F bond length is significantly shorter than the five equatorial I–F bond lengths. The mean O–I–F_{eq} bond angle is slightly larger than 90°, due to the doubly bonded oxygen atom being more repulsive than the singly bonded axial fluorine ligand. The equatorial IF5 plane is puckered to alleviate its congestion. In contrast to the highly fluxional, free IF7 molecule, in which the equatorial fluorines undergo a very rapid, dynamic, pseudorotational ring puckering and a slower intramolecular equatorial–axial ligand exchange, the puckering of the IOF6- anion in its $N(CH_3)_4^+$ salt is frozen out due to anion–cation interactions, and the equatorial–axial ligand exchange is precluded by the more repulsive oxygen ligand which occupies exclusively axial positions. Therefore, the IOF6- anion is ideally suited for studying the nature of the equatorial puckering in species of 5-fold symmetry. The puckering in IOF6- is of the C_s symmetry type, and the deviations from the ideal equatorial plane are relatively small and decrease with decreasing temperature. Furthermore, the axial I–O bond length decreases and the mean O–I–F_{eq} bond angle increases with decreasing temperature. These findings demonstrate that in agreement with our results from ab initio calculations and contrary to the VSEPR concept of repelling points on a sphere, the minimum energy structures of these main group heptacoordinated fluorides or oxyfluorides are those of pentagonal bipyramids with an unpuckered equatorial plane and not those of either monocapped octahedra or monocapped trigonal prisms. Whereas in solid $N(CH_3)_4^+IOF_6^-$ the equatorial ring puckering of IOF6- is frozen out, in the dissolved free ion this puckering becomes dynamic, as demonstrated by 19F NMR spectroscopy which shows five equivalent equatorial fluorine ligands. Contrary to IF7 and TeF7-, the IOF6- anion does not undergo an intramolecular equatorial–axial ligand exchange on the NMR time scale because of the more repulsive, doubly bonded oxygen. The vibrational spectra of $N(CH_3)_4^+IOF_6^-$ in both the solid state and CH_3CN solution were recorded and assigned with the help of ab initio calculations on IOF6- using effective core potentials and local density functional theory. Normal coordinate analyses were carried out for the pentagonal bipyramidal series IF7, IOF6-, XeF5- which show that the equatorial, in-plane deformation force constants (f_α) are a good measure for the degree of congestion in the equatorial plane. Puckering increases with decreasing bond lengths, increasing ligand and decreasing central atom sizes, and increasing temperature. The pentagonal bipyramidal structures of these molecules and the coplanarity of their equatorial ligands, which are found for their minimum energy structures, are explained by a bonding scheme involving delocalized p_{xy} hybrid orbitals of the central atom for the formation of a coplanar, semi-ionic, 6-center 10-electron bond system for the five equatorial bonds and of an sp_z hybrid orbital for the formation of two, more covalent, colinear, axial bonds. This bonding scheme can account for all the observed structural features and also the bond length differences.

Introduction

In main group element chemistry, coordination numbers in excess of six are relatively rare, but they are of considerable interest due to special features caused by steric crowding of the ligands, free valence electron pairs being sterically either active or inactive, and the propensity of the molecules to exhibit fluxionality. Of particular interest are heptacoordinated species which could exist either as a monocapped octahedron, a mono-

capped trigonal prism, or a pentagonal bipyramid.[5] According to the VSEPR model of "repelling points on a sphere",[5] the preferred structures should be the monocapped octahedron or trigonal prism. However, for main group elements and relatively low repulsive forces, the pentagonal bipyramid is favored[6] and has been found for species such as IF7[7,8] or TeF7-.[9-11] In pentagonal bipyramidal structures, the pentagonal equatorial plane is highly congested which results in increased repulsion

* Dedicated to Professor Jean'ne Shreeve on the occasion of her 60th birthday.
(1) Rockwell International, Rocketdyne Division.
(2) E.I. du Pont de Nemours and Company, Inc.
(3) Freie Universität, Berlin.
(4) McMaster University.

(5) Gillespie, R. J.; Hargittai, I. In *The VSEPR Model of Molecular Geometry*; Allyn and Bacon, A Division of Simon & Schuster, Inc.: Needham Heights, MA, 1991; p 58.
(6) Thompson, H. B.; Bartell, L. S. *Inorg. Chem.* **1968**, *7*, 488.
(7) Adams, W. J.; Thompson, H. B.; Bartell, L. S. *J. Chem. Phys.* **1970**, *53*, 4040.

The IOF$_6^-$ Anion

J. Am. Chem. Soc., Vol. 115, No. 7, 1993 2697

among the equatorial ligands and, as a result, in increased bond lengths and usually some kind of puckering.[5-8] In the case of 5-fold symmetry, this puckering presents a special problem. The odd number of ligands does not allow for a highly symmetric arrangement in which all five equatorial ligands can be placed into equivalent positions, i.e. with identical displacements alternately above and below the equatorial plane. One way to achieve equivalency of the equatorial ligands is a fast, dynamic, pseudorotational ring puckering, as found for IF$_7$,[7,8] which results in a highly fluxional molecule. In addition, the pentagonal bipyramidal XF$_7$ molecules generally exhibit a second kind of fluxionality, i.e. a slower, intramolecular, axial–equatorial ligand exchange.[8] The combination of these two types of fluxionality makes it experimentally very difficult to characterize and describe the structures of these molecules. Many of the difficulties with the fluxionality of the XF$_7$ species might be overcome by studying ionic XOF$_6^{n-}$ salts. The presence of one doubly bonded oxygen which is more repulsive than the fluorine ligands should preempt a facile axial–equatorial ligand exchange, and the dynamic puckering of the equatorial plane could be frozen out by anion–cation interactions. Therefore, an effort was undertaken to prepare and characterize a salt containing an XOF$_6^-$ anion. Examples of pentagonal bipyramidal XOF$_6$ species had previously been unknown and only recently been reported[10,11] in two separate preliminary notes from our laboratories. In this paper, a full account and analysis of our work on the IOF$_6^-$ anion is given.

Experimental Section

Caution: IOF$_5$ is a strong oxidizer, and its combination with organic materials, such as CH$_3$CN or N(CH$_3$)$_4^+$ salts, could be potentially hazardous. Although no difficulties were encountered in the present study, appropriate safety precautions and shielding should be used, particularly when working on a larger scale with these materials.

Materials. The CH$_3$CN (Baker, Bio-analyzed, having a water content of 40 ppm) was treated with P$_2$O$_5$ and freshly distilled prior to use, thereby reducing its water content to <4 ppm. Literature methods were used for the syntheses of IOF$_5$[12-14] and anhydrous N(CH$_3$)$_4^+$F$^-$.[15]

Synthesis of N(CH$_3$)$_4^+$IOF$_6^-$. The salt N(CH$_3$)$_4^+$IOF$_6^-$ was prepared by condensing gaseous IOF$_5$ (6.40 mmol) from the calibrated volume of a nickel and stainless steel vacuum line at room temperature onto anhydrous N(CH$_3$)$_4^+$F$^-$ (0.4473 g, 5.779 mmol) in 8 mL of dry CH$_3$CN at –196 °C. The mixture was warmed and allowed to react, with frequent agitation, at –35 °C for 30 min. The solvent and unreacted IOF$_5$ were pumped off at –35 °C leaving behind N(CH$_3$)$_4^+$IOF$_6^-$ as a very pale yellow crystalline solid in essentially quantitative yield (1.8298 g, 5.772 mmol). Anal. Calcd for C$_4$H$_{12}$F$_6$IO: C, 14.50; H, 3.63; F, 33.00; I, 38.35; N, 4.23. Found: C, 14.62; H, 3.66; F, 32.4; I, 38.51; N, 4.33.

Vibrational Spectroscopy. Raman spectra were recorded on either a Cary Model 83 or a Spex Model 1403 spectrophotometer using the 488-nm exciting line of an Ar ion or the 647.1-nm line of a Kr ion laser, respectively. Baked-out Pyrex melting point capillaries or thin-walled Kel-F tubes were used as sample containers. A previously described[16] device was used for recording the low-temperature spectra.

Infrared spectra were recorded by using either AgCl or AgBr disks on a Perkin-Elmer Model 283 spectrophotometer. The finely powdered samples were sandwiched between two thin disks and pressed together in a Wilks minipress inside the drybox.

Nuclear Magnetic Resonance Spectroscopy. The ^{19}F NMR spectra were recorded at McMaster University unlocked (field drift < 0.1 Hz

h^{-1}) on a Bruker AM-500 spectrometer equipped with an 11.744 T cryomagnet and an Aspect 3000 computer. The spectra were obtained using a 5-mm combination ^{1}H/^{19}F probe operating at 470.599 MHz. The spectra were recorded in a 32K memory. A spectral width setting of 62 500 Hz was employed, yielding a data point resolution of 3.8 Hz/data point and an acquisition time of 0.262 s. No relaxation delays were applied. Typically, 40 000 transients were accumulated. The pulse width corresponding to a bulk magnetization tip angle, θ, of approximately 90° was equal to 1 μs. Line broadening parameters used in the exponential multiplication of the free induction decays were 3–4 Hz.

The low-temperature study was carried out by the use of a Bruker temperature controller. The temperature was measured with a copper–constantan thermocouple inserted directly into the sample region of the probe and was accurate to ±1 °C.

The spectra were referenced to a neat external sample of CFCl$_3$. The chemical shift convention used is that a positive (negative) sign signifies a chemical shift to high (low) frequency of the reference compound.[17]

Computational Methods. The electronic structure calculations were done at the ab initio molecular orbital level using either local density function (LDF) theory[18-21] or effective core potentials (ECP). The LDF calculations were carried out with the program system DMol,[22] as previously described,[8] with a double-numerical basis set augmented by d polarization functions. This can be considered in terms of size as a polarized double-ζ basis set. However, because exact numerical solutions are employed for the atom, this basis set is of significantly higher quality than a normal molecular orbital polarized double-ζ basis set. The fitting functions have an angular momentum number one greater than that of the polarization function, resulting in a value of $l = 3$ for the fitting functions.

The ECP calculations were done with all electrons on the F and O and with an effective core potential replacing all of the *core electrons* on the I. The valence basis set is of polarized double-ζ quality. The fluorine and oxygen basis set is from Dunning and Hay,[23] and the ECP from Hay and Wadt[24] including relativistic corrections. The valence basis set of Hay and Wadt[24] was used augmented by a d function on I with an exponent of 0.266.[25] The geometries were optimized by using gradient techniques,[26] and the force fields were calculated analytically.[27,28] The ab initio MO calculations were done with the program GRADSCF,[29] as implemented on a Cray YMP computer system.

Crystal Structure Determinations of N(CH$_3$)$_4^+$IOF$_6^-$. Two independent crystal structure determinations were carried out for this compound at McMaster University and the Freie Universität Berlin.

(8) Christe, K. O.; Curtis, E. C.; Dixon, D. A. *J. Am. Chem. Soc.* 1993, *115*, 1520.

(9) Selig, H.; Sarig, S.; Abramowitz, S. *Inorg. Chem.* 1974, *13*, 1508.

(10) Christe, K. O.; Sanders, J. C. P.; Schrobilgen, G. J.; Wilson, W. W. *J. Chem. Soc., Chem. Commun.* 1991, 837.

(11) Mahjoub, A. R.; Seppelt, K. *J. Chem. Soc., Chem. Commun.* 1991, 840.

(12) Holloway, J. H.; Selig, H.; Claassen, H. H. *J. Chem. Phys.* 1971, *54*, 4305.

(13) Schack, C. J.; Pilipovich, D.; Cohz, S. N.; Sheehan, D. F. *J. Phys. Chem.* 1968, *72*, 4697.

(14) Schack, C. J.; Christe, K. O. *J. Fluorine Chem.* 1990, *49*, 167.

(15) Christe, K. O.; Wilson, W. W.; Wilson. R. D.; Bau, R.; Feng, J. *J. Am. Chem. Soc.* 1990, *112*, 7619.

(16) Miller, F. A.; Harney, B. M. *Appl. Spectrosc.* 1969, *23*, 8.

(17) *Pure Appl. Chem.* 1972, *29*, 627; 1976, *45*, 217.

(18) Parr, R. G.; Yang, W. *Density Functional Theory of Atoms and Molecules*; Oxford University Press: New York, 1989.

(19) Salahub, D. R. In *Ab Initio Methods in Quantum Methods in Quantum Chemistry*, 2nd ed.; Lawley, K. P., Ed.; J. Wiley & Sons: New York, 1987; p 447.

(20) (a) Wimmer, E.; Freeman, A. J.; Fu, C.-L.; Cao, P.-L.; Chou, S.-H.; Delley, B. In *Supercomputer Research in Chemistry and Chemical Engineering*; Jensen, K. F., Truhlar, D. G., Eds.; ACS Symp. Ser.; American Chemical Society: Washington, DC, 1987; p 49. (b) Dixon, D. A.; Andzelm, J.; Fitzgerald, G.; Wimmer, E.; Delley, B. In *Science and Engineering on Cray Supercomputers. Proceedings of the Fifth International Symposium*; Cray Research: Minneapolis, MN, 1990; p 285.

(21) Jones, R. O.; Gunnarsson, O. *Rev. Mod. Phys.* 1989, *61*, 689.

(22) Delley, B. *J. Chem. Phys.* 1990, *92*, 508. DMol is available commercially from BIOSYM Technologies, San Diego, CA.

(23) Dunning, T. H., Jr.; Hay, P. J. In *Methods of Electronic Structure Theory*; Schaefer, H. F., III, Ed.; Plenum Press: New York, 1977; Chapter 1.

(24) Hay, P. J.; Wadt, W. R. *J. Chem. Phys.* 1985, *82*, 299.

(25) Huzinaga, S.; Andzelm, J.; Klobukowski, M.; Radzio, E.; Sakai, Y.; Tatasaki, H. *Gaussian Basis Sets of Molecular Calculations*; Elsevier: Amsterdam, 1984.

(26) (a) Kormonicki, A.; Ishida, K.; Morokuma, K.; Ditchfield, R.; Conrad, M. *Chem. Phys. Lett.* 1977, *45*, 595. (b) McIver, J. W., Jr.; Komornicki, A. *Chem. Phys. Lett.* 1971, *10*, 202. (c) Pulay, P. In *Applications of Electronic Structure Theory*; Schaefer, H. F., III, Ed.; Plenum Press: New York, 1977; p 153.

(27) (a) King, H. F.; Komornicki, A. *J. Chem. Phys.* 1986, *84*, 5465. (b) King, H. F.; Komornicki, A. In *Geometrical Derivatives of Energy Surfaces and Molecular Properties*; Jorgenson, P., Simons, J., Eds.; NATO ASI Series C; D. Reidel: Dordrecht, 1986; Vol. 166, p 207.

(28) Breidung, J.; Thiel, W.; Komornicki, A. *Chem. Phys. Lett.* 1988, *153*, 76.

(29) GRADSCF is an ab initio program system designed and written by A. Komornicki at Polyatomics Research.

2698 J. Am. Chem. Soc., Vol. 115, No. 7, 1993

Christe et al.

At McMaster, only one type of crystal was observed, tetragonal P4/nmm crystals which have IOF_6^- with a positional 4-fold disorder for the puckered equatorial plane. The structure of one of these crystals was determined at –93 °C and is given in this paper.

At Berlin, originally a very similar, orthorhombic crystal was studied at –163 °C, and the data were refined either in P4/nmm with 4-fold disorder or Pmmn with systematic twinning; however, no puckering of the equatorial plane was observed.[11] In repeat experiments, exclusively crystals identical to those found at McMaster were obtained. The structure of one of these crystals was determined at –155 °C and is given in this paper.

Single crystals of $N(CH_3)_4^+IOF_6^-$ were grown at McMaster by making a saturated solution of $N(CH_3)_4^+IOF_6^-$ in CH_3CN in a Teflon-FEP tube at room temperature and warming it to 45 °C whereupon it completely dissolved to give a pale yellow solution. The sample tube was then positioned horizontally above a dewar containing water at 60 °C, covered with aluminum foil, and slowly allowed to cool overnight. This resulted in the growth of transparent crystals which could be described as tetragonal prisms. At McMaster, the crystals were sealed in Lindemann quartz capillaries and centered on a Siemens R3m/v diffractometer. Accurate cell dimensions were determined at $T = –93$ °C from a least-squares refinement of the setting angles (χ, ϕ, and 2θ) obtained from 25 accurately centered reflections (with $34.71° \leq 2\theta \leq 38.05°$) chosen from a variety of points in reciprocal space. Examination of the peak profiles revealed that they were single.[30] Integrated diffraction intensities were collected using a θ–2θ scan technique with scan rates varying from 1.5 to 14.65°/min (in 2θ) and a scan range of $\pm 0.6°$, so that the weaker reflections were examined slowly to minimize counting errors. Data were collected in four steps since the crystal was diffracting very strongly. In the first step, the data were collected with $-15 \leq h \leq 15$, $0 \leq k \leq 15$, and $0 \leq l \leq 11$ and with $3° \leq 2\theta \leq 45°$, using silver radiation monochromatized with a graphite crystal ($\lambda = 0.56087$ Å). During data collection, the intensities of three standard reflections were monitored every 97 reflections to check for crystal stability and alignment. A total of 1583 reflections were collected out of which 16 were standard reflections. At this stage, the distribution of the reflections in the reciprocal space indicated that the crystal was diffracting at relatively high angles, consequently a second data set was recorded with $45° \leq 2\theta \leq 55°$. This time a total of 1163 reflections were collected out of which 12 were standard reflections. Finally, a third data set was recorded with $55° \leq 2\theta \leq 60°$ giving rise to 712 reflections out of which 8 were standard reflections. These data sets were recorded with the maximum intensity (i.e. 1.5 kW Ag X-rays), without attenuation, and as a consequence, the strongest reflections at very low angles were not recorded. In order to record these missing reflections, the power had to be decreased to 750 W. Another set of data was collected with $-3 \leq h \leq 3$, $0 \leq k \leq 3$, and $0 \leq l \leq 2$. A total of 31 reflections were collected, out of which 6 were standard reflections. No crystal decay was observed. In total, 3136 reflections were collected and 876 unique reflections remained after averaging of equivalent reflections. A total of 780 reflections, satisfying the condition $I \geq 3\sigma(I)$, were used for the structure solution. These reflections exhibited systematic absences for $hk0$: $h + k = 2n$ and $h00$: $h = 2n$. Corrections were made for Lorentz and polarization effects. Absorption corrections were applied by using the program DIFABS.[31] The transmission factors ranged from 0.728 to 1.117.

The XPREP program[32] was used to determine the correct cell and space group. It confirmed that the original cell was correct and that the lattice was tetragonal primitive ($R_{int} = 0.028$). The structure was shown to be centrosymmetric by an examination of the E-statistics (calculated, 0.616; theoretical, 0.736). The two space groups which were consistent with the systematic absences (n-glide and C_2) were the centrosymmetric P4/n and P4/nmm space groups.

A first solution was obtained without absorption corrections; it was achieved in the space group P4/nmm (129) by conventional heavy-atom Patterson methods which located the positions of the iodine, nitrogen, and carbon atoms on special positions (i.e. 4mm, –4m2, .m.). The full-matrix least-squares refinement of their positions and isotropic thermal parameters gave a conventional agreement index $R = (\Sigma|F_o| – |F_c|/\Sigma|F_o|)$ of 0.12. A subsequent difference Fourier synthesis revealed the positions

(30) Despite the fact that all the peaks proved to be single, the possibility of twinning was checked by verifying that the hkl values associated with the very weak and very strong reflections at low sin θ/λ refined using the same orientation matrix.
(31) Walker, N.; Stuart, D. Acta Crystallogr. 1983, A39, 158.
(32) Sheldrick, G. M. (1990); SHELXTL PLUS™ Release 4.21/V. Siemens Analytical X-Ray Instruments, Inc., Madison, Wisconsin.

Table I. Summary of Crystal Data and Refinement Results for $N(CH_3)_4^+IOF_6^-$ at –93 and –155 °C

T (°C)	–93	–155
space group	P4/nmm (tetragonal)	
a (Å)	8.8590(10)	8.8151(10)
c (Å)	6.3690(10)	6.3213(12)
V (Å³)	499.85(11)	491.20(10)
molecules/unit cell	2	
molecular weight	331.0	
cryst dimens (mm)	0.4 × 0.5 × 0.2	0.4 × 0.4 × 0.4
calcd density (g cm⁻³)	2.199	2.238
color	very faintly yellow	
cryst decay (%)	no	no
abs coeff (mm⁻¹)	3.259	3.326
wavelength (Å) used for data collection	0.56086	0.71069
sin θ/λ limit (Å⁻¹)	0.8915	0.9045
total no. of reflctns measd	3136	3489
no. of independent reflctns	876	887
no. of reflctns used in structural analysis, $I > 3\sigma(I)$	780	885
no. of variable parameters	28	34
final agreement factors		
R	0.0373	0.0291
R_w	0.0350	0.0255

of two atoms located on special positions, above and below the iodine. It was possible to distinguish a fluorine from an oxygen atom from the difference in bond lengths (i.e., 1.83 and 1.74 Å). The introduction of these positions gave a residual factor R of 0.10. A further difference Fourier synthesis clearly showed the presence of three atoms in the equatorial environment of the iodine. Two of these atoms were positioned on general positions, while the third one was positioned on a special position (..m). Consequently, the model implied a 4-fold disorder in the "pseudo"-equatorial plane consisting of a superposition of four molecules with identical I, axial F, and O positions. Consequently, the site occupancy factors of the equatorial fluorine atoms were set equal to 0.25 and 0.125 (general and special positions, respectively) instead of 1.00 and 0.5. The introduction of these positions and isotropic thermal parameters for the equatorial F atoms (all set equal) resulted in a drop of the residual factor R to 0.057. Another improvement of the structure was achieved by introducing anisotropic thermal parameters for the I, N, C, F_{ax}, and O atoms (the F_{eq} were kept isotropic because of the presence of the 4-fold disorder), and the positions of the hydrogen atoms located from a difference Fourier map ($U(H)$ fixed to 0.08 Å²), as well as a weighting factor ($w = 1/\sigma^2(F) – 0.0003F^2$), dropping the R factor to 0.044 ($R_w = 0.041$).

The structure was solved a second time using data that had been corrected for absorption. The initial model used the atomic coordinates and isotropic thermal parameters defined previously for all the atoms. The solution obtained ($R = 0.043$) indicated a slight improvement over that obtained without absorption corrections ($R = 0.057$). The final refinement was obtained by introducing anisotropic thermal parameters for the I, F_{ax}, O, N, and C atoms and a weighting factor ($w = 1/\sigma^2(F) + 0.0000F^2$) and gave rise to a residual R of 0.0373 ($R_w = 0.0350$). In the final difference Fourier map, the maximum and the minimum electron densities were 1.5 and –1.6 Å³.

All calculations were performed using the SHELXTL PLUS[32] determination package for structure determination molecular graphics.

At Berlin, the crystal was mounted, with the help of a special apparatus,[33] on an Enraf Nonius CAD 4 diffractometer at –155 °C. Oscillating crystal photographs were used to check the reflection quality. There were 25 reflections in the ϑ range 12–25° that were used to obtain the orientation matrix and lattice constants. Space group determination: The lattice constants indicated no deviation from tetragonal symmetry. Reflection intensities obeyed the rules $F(hkl) = F(\bar{h}kl) = F(kh\bar{l})$ with $R_{int} = 0.0204$. Extinction of $hk0 \neq 2n$ left only space group P4/nmm (No. 129), which enforces the 4-fold disorder model. Calculations in orthorhombic space groups Pmmn (No. 59) or $P2_1mn$ (No. 31) generated the same disorder of the equatorial fluorine atoms. Three reflections were used to check for crystal decay and standard reflections orientation. Further details of the measurement routine are given in Tables I and S1 (supplementary material). After applying Lorentz and polarization

(33) Keith, M.; Bärnighausen, H. A. Kristallogr. 1985, 170, 5. Schumann, H.; Genthe, W.; Hahn, F.; Hossein, M. B.; d. Helin, D. V. Organomet. Chem. 1986, 229, 67.

The IOF$_6^-$ Anion

J. Am. Chem. Soc., Vol. 115, No. 7, 1993 2699

Table II. Bond Lengths, Bond Angles, Average Equatorial Plane Angle, and Deviations from the Average O–I–F$_{eq}$ Bond Angle for N(CH$_3$)$_4^+$IOF$_6$ at –93 and –155 °C

	bond lengths (Å)		deviations (deg) from the mean O–I–F$_{eq}$ bond angle	
	–93 °C	–155 °C	–93 °C	–155 °C
I–O	1.772(8)	1.745(4)		
I–F(1)	1.822(6)	1.823(3)		
I–F(2)	1.899(9)	1.894(5)	–0.8(2)	–0.4(1)
I–F(3)	1.852(10)	1.868(7)	5.2(2)	3.7(2)
I–F(4)	1.880(14)	1.868(9)	–8.7(4)	–6.6(3)
N–C	1.483(4)	1.491(3)		

	bond angles (deg)	
	–93 °C	–155 °C
O–I–F(2)	94.3(2)	95.9(1)
O–I–F(3)	88.3(2)	91.8(2)
O–I–F(4)	102.4(4)	102.1(3)
F(1)–I–F(2)	85.7(2)	84.1(1)
F(1)–I–F(3)	91.7(2)	88.2(2)
F(1)–I–F(4)	77.8(4)	77.9(3)
F(3)–I–F(2e)	68.7(4)	69.9(3)
F(4)–I–F(3)	78.6(3)	76.1(2)
F(2c)–I–F(2e)	66.8(5)	67.5(3)
mean O–I–F$_{eq}$	93.5(3)	95.5(2)
mean pucker angle^a	4.14(30)	2.96(20)

^{a} Mean deviation of the equatorial fluorine ligands from the mean O–I–F$_{eq}$ angle.

corrections, the data were used for refinement of the previously published[11] model with the program SHELXS 76.[34] Atomic form factors were taken from the Kynoch tables.[35] The atoms I, O, F(1). N, and C were refined anisotropically and F(2)–F(4) isotropically which resulted in $R = 0.045$. Absorption correction was introduced at this stage. Optical measurements were not possible because of the embedding of the colorless crystal in paraffin oil. The ψ scan method gave no better results. Finally the method DIFABS[31] was used. Maximal and minimal corrections of 1.28 and 0.85 were applied. At this stage, hydrogen atoms were found in difference Fourier maps and refined with fixed isotropic U. This model refined to $R = 0.0291$ and $R_w = 0.0255$ (see Table I). The 4-fold disordered atoms F(2)–F(4) were then treated anisotropically. This resulted in $R = 0.020$ and $R_w = 0.0171$. The F(2), F(3), and F(4) atoms became quite disk-like, with a considerable bond shrinkage effect. Since it is unclear whether or not it is advisable to refine these 4-fold disordered atoms anisotropically because of overlap of these atoms with each other, the calculations with isotropic F(2), F(3), F(4) atoms is regarded as the best solution.

Summaries of the data collection parameters and other crystallographic information for both data sets are given in Table I. The final atomic coordinates, thermal parameters, interatomic distances, bond angles, and deviations from the average O–I–F$_{eq}$ angles are listed in Tables II and S4–S5 (supplementary material). Summaries of the structure determinations and the observed and calculated structure factors are given in Tables S1–S3.

Results and Discussion

Synthesis and Properties of N(CH$_3$)$_4^+$IOF$_6^-$. In a previous study,[36] it was shown that at room temperature, CsF does not react with a large excess of IOF$_5$, while at higher temperatures it tends to undergo deoxygenation. In the same paper it was speculated that the failure to observe fluorine–oxygen exchange in the IF$_7$–CsNO$_3$ system might be due to the lack of formation of an intermediate IOF$_6^-$ salt. The present study clearly demonstrates that under suitable reaction conditions, i.e. using a soluble anhydrous fluoride of a large cation in a compatible solvent, IOF$_6^-$ salts are readily formed according to

(34) Sheldrick, G. M. *Program for Crystal Structure Determination*; Göttingen, 1976.

(35) *International Tables for X-ray Crystallography*; The Kynoch Press: Birmingham, 1968; Vol. III.

(36) Christe, K. O.; Wilson, W. W.; Wilson, R. D. *Inorg. Chem.* **1989**, *28*, 904.
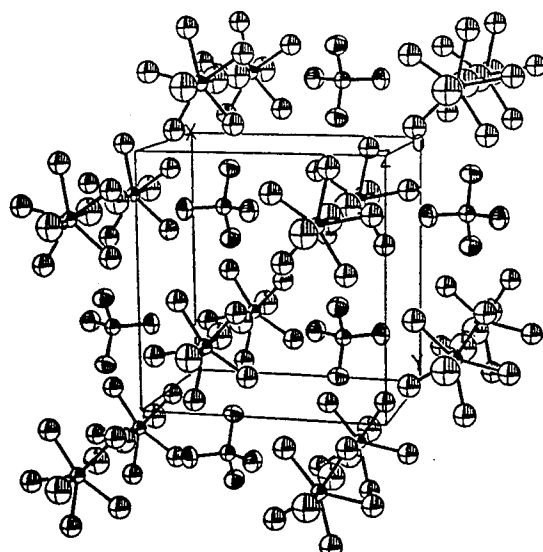
Figure 1. Packing diagram of N(CH$_3$)$_4^+$IOF$_6^-$ viewed along the c axis.
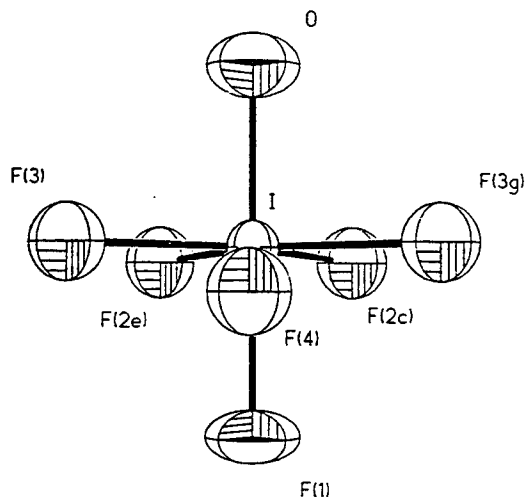
Figure 2. The structure of the IOF$_6^-$ anion showing the puckering pattern of the equatorial fluorine ligands.

$$N(CH_3)_4^+F^- + IOF_5 \xrightarrow{CH_3CN} N(CH_3)_4^+IOF_6^- \qquad (1)$$
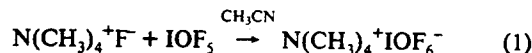
The resulting N(CH$_3$)$_4^+$IOF$_6^-$ is a very pale yellow solid which is thermally stable up to about 137 °C where it starts to decompose to IOF$_4^-$, CF$_4$, and COF$_2$ as the major products. It was characterized by elemental analysis, a crystal structure determination, and vibrational and ^{19}F NMR spectroscopy (see below).

X-ray Crystal Structure of N(CH$_3$)$_4^+$IOF$_6^-$. The crystal structure of N(CH$_3$)$_4^+$IOF$_6^-$ at –93 °C was determined at McMaster University and confirmed at the Freie Universität Berlin for a crystal kept at –155 °C. Although the gross features of both structures are very similar, they exhibit an extremely interesting temperature dependence of the degree of puckering and, therefore, both data sets are given in full detail.

The crystal structure of N(CH$_3$)$_4^+$IOF$_6^-$ consists of well-separated N(CH$_3$)$_4^+$ and IOF$_6^-$ ions. The packing of the ions (see Figure 1) can be described as a cubic close packing of alternating layers of IOF$_6^-$ anions and N(CH$_3$)$_4^+$ cations in which the alternating orientation of the tetrahedral cations results in a cuboctahedral[37] unit cell with $Z = 2$. While the cation is perfectly ordered with the expected bond lengths, the IOF$_6^-$ anion is subject to a positional 4-fold disorder in the equatorial plane. The model results from the superposition of four anions in which the central I atom and the axial O and F(1) atoms occupy identical positions.

(37) Hyde, B. G.; Anderson, S. *Inorganic Crystal Structures*; John Wiley & Sons: New York, 1989; p 7.

One of these anions is shown in Figure 2. There are no significant contacts to iodine other than the directly bonded oxygen and six fluorine ligands, and the anion exhibits a gross pentagonal bipyramidal geometry. The $O-I-F_{ax}$ angle is constrained by symmetry to be 180°, while there are no constraints on the positions of the equatorial fluorines. The equatorial fluorines are bent away from the axial oxygen ligand, as expected for a doubly bonded oxygen being more repulsive than a singly bonded fluorine ligand.[5]

The I–O bond length (1.75–1.77 Å) indicates significant double bond character for the I–O bond.[38-43] Its temperature dependence will be discussed below. The greater I–O bond length in IOF_6^-, when compared with that in IOF_5 (1.715(4) Å),[38] is consistent with the placement of some of the negative charge on oxygen, thereby increasing the polarity and decreasing the bond order of the I–O bond. The axial I–F bond (1.823(3) Å) is, within experimental error (±3σ), significantly shorter than all of the equatorial I–F bonds (average 1.88 Å), and both types of I–F bonds in IOF_6^- are significantly longer than the corresponding bonds in IF_7 (1.786(7) and 1.858(4) Å, respectively).[7] These differences can be attributed again to the formal negative charge on IOF_6^-, which leads to greater $I^{\delta+}-F^{\delta-}$ bond polarities and consequently longer bonds. The greater length of the equatorial bonds in IOF_6^- and IF_7 relative to their axial ones is due to the increased mutual repulsion of the fluorine ligands in the highly congested equatorial plane and their higher ionicity (see below).

Nature and Temperature Dependence of the Equatorial Puckering in IOF_6^-. As mentioned above, the equatorial fluorine atoms in IOF_6^- are bent away from the doubly bonded oxygen atom by about 5°. Furthermore, the plane of the equatorial fluorine atoms is puckered and its I–F bonds are elongated in order to lessen the high degree of ligand–ligand repulsion encountered for these fluorines. Contrary to the rapid dynamic puckering in free, pentagonal-bipyramidal molecules, such as IF_7,[8] the puckering in solid $N(CH_3)_4^+IOF_6^-$ is frozen out by hydrogen···fluorine bridging between the two F(2) atoms of IOF_6^- and hydrogen atoms from two different cations. This bridging results in two close F···C contacts of 3.175(9) and 3.271(9) Å, while the remaining closest F···C contacts occur at 3.317(9), 3.473(9), and 3.416(9) Å and are very close to the accepted sum of the van der Waals radii of CH_3 (2.00 Å)[44] and F (1.35–1.40 Å)[44,45] which is 3.35–3.40 Å.

A pentagonal plane can be puckered in two ways resulting in structures of either C_s or C_2 symmetry, respectively.

C_s   C_2

As mentioned above, the doubly bonded, axial oxygen ligand in IOF_6^- is more repulsive than the singly bonded, axial fluorine ligand. Therefore, the average equatorial plane, which can be defined as a plane perpendicular to the $O-I-F_{ax}$ axis containing all five equatorial fluorine ligands at the averaged $F_{eq}-I-O$ bond angle, drops below the center of the iodine atom. As can be seen from Table II and Figure 2, the puckered plane of IOF_6^- definitely exhibits C_s symmetry.

(38) Bartell, L. S.; Clippard, F. B.; Jacob, J. E. *Inorg. Chem.* **1976**, *15*, 3009.
(39) Smart, L. E. *J. Chem. Soc., Chem. Commun.* **1977**, 519.
(40) Selte, K.; Kjekshus, A. *Acta Chem. Scand.* **1970**, *24*, 1912.
(41) Kálmán, K.; Cruickshank, D. W. J. *Acta Crystallogr.* **1970**, *B26*, 1782.
(42) Feikeman, Y. D. *Acta Crystallogr.* **1961**, *14*, 315.
(43) Feikeman, Y. D. *Acta Crystallogr.* **1966**, *20*, 765.
(44) Pauling, L. *The Nature of the Chemical Bond*, 3rd ed.; Cornell University Press: Ithaca, New York, 1960; p 260.
(45) Bondi, A. *J. Phys. Chem.* **1964**, *68*, 441.
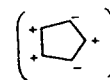
Furthermore, the relative displacements of the equatorial fluorine ligands from the average equatorial plane decrease with decreasing temperature, i.e. *the degree of puckering decreases with decreasing temperature.*

-93 °C   -155 °C
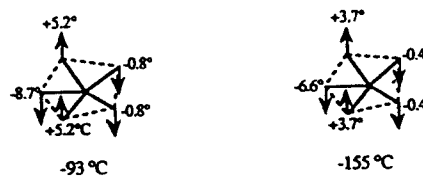
This decrease in the degree of puckering at lower temperatures causes additional important structural changes. Thus, the I–O bond length is significantly shortened and the angle between the oxygen ligand and the average equatorial plane is increased.

-93 °C   -155 °C
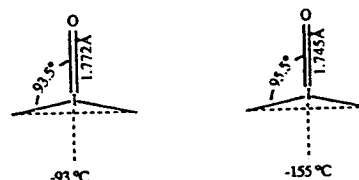
These temperature effects can be explained by a decreasing population of the higher vibrational states of the ring puckering motion which, due to its low frequency of about 141 cm⁻¹, is, even at low-temperatures, still highly populated. The resulting decrease in the thermal motion of the equatorial fluorines diminishes their mutual repulsion and allows the equatorial fluorines to become more coplanar and less repulsive which, in turn, results in a shortening of the I–O bond length. It would therefore be of great interest to determine the crystal structure of $N(CH_3)_4^+IOF_6^-$ at a very low temperature at which the puckering motion is completely frozen out and to compare the resulting structure with those of the present study. Such a study could establish beyond a doubt that in their minimum energy structures these normally puckered, pentagonal bipyramidal molecules indeed possess unpuckered equatorial planes.

¹⁹F NMR Spectrum of the IOF_6^- Anion. The ¹⁹F NMR spectrum (obtained at McMaster University) of $N(CH_3)_4^+IOF_6^-$ was recorded at –40 °C in CH_3CN solution and is in agreement with a pentagonal bipyramidal structure for the IOF_6^- anion. This structure is expected to have an average C_{5v} point group symmetry with the oxygen in the axial position. Accordingly, the ¹⁹F NMR spectrum (Figure 3) displays a broad doublet ($\Delta\nu_{1/2} \approx 170$ Hz) at 166.0 ppm, assigned to the equatorial fluorines, and a broad binomial sextet ($\Delta\nu_{1/2} \approx 360$ Hz) at 111.1 ppm, assigned to the axial fluorine *trans* to oxygen. The weak triplet observed at 114.5 ppm [$^2J(F_{eq}-F_{ax}) = 200$ Hz] is attributed to the F-*trans*-to-O environment of *cis*-$IO_2F_4^-$[46] which probably arose from adventitious hydrolysis of IOF_6^- during synthesis or NMR sample preparation. The observation of separate ¹⁹F resonances for the axial and equatorial ligand environments of IOF_6^- is unusual for a pentagonal bipyramidal species and demonstrates that the IOF_6^- anion does not undergo intramolecular ligand exchange (i.e., pseudorotation) in solution, in contrast with the related TeF_7^- anion[10,11] and IF_7 molecule.[47] This is not surprising because any plausible intermediate in the pseudorotation process for IOF_6^- would require the doubly bonded oxygen ligand to move into an

(46) Christe, K. O.; Wilson, R. D.; Schack, C. J. *Inorg. Chem.* **1981**, *20*, 2104.
(47) (a) Gillespie, R. J.; Quail, J. W. *Can. J. Chem.* **1964**, *42*, 2671. (b) Bartlett, N.; Beaton, S.; Reeves, L. W.; Wells, E. J. *Can. J. Chem.* **1964**, *42*, 2531. (c) Alexakos, L. G.; Cornwell, C. D.; Pierce, St. B. *Proc. Chem. Soc.* **1964**, *86*, 293. (d) Gutowski, H. S.; Hoffmann, C. F. *J. Chem. Phys.* **1951**, *19*, 1259.
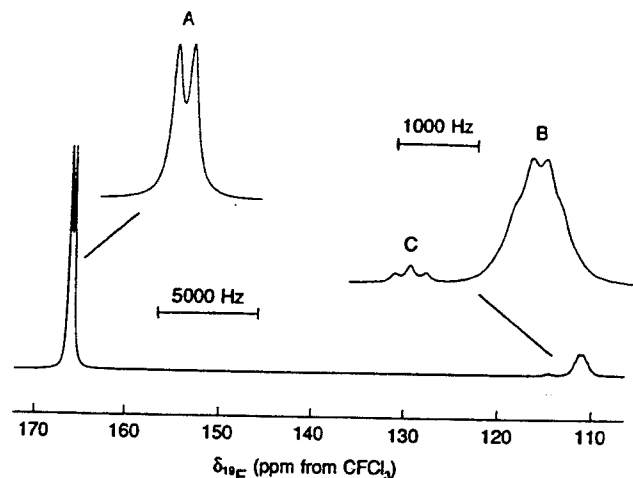
The IOF$_6^-$ Anion

J. Am. Chem. Soc., Vol. 115, No. 7, 1993 2701

Figure 3. The ^{19}F NMR spectrum (470.599 MHz) of a saturated solution of N(CH$_3$)$_4$$^+IOF_6^-$ in CH$_3$CN at –40 °C: (A) F$_{eq}$ environment of IOF$_6^-$; (B) F$_{ax}$ environment of IOF$_6^-$; (C) F-*trans*-to-O environment of *cis*-IO$_2$F$_4^-$ impurity.

equatorial position. The greater space requirement of the oxygen double bond domain, compared with that of a fluorine single bond domain, would render the placement of the oxygen ligand in the more sterically crowded equatorial position energetically unfavorable, thereby creating a high activation barrier for the process. Although the X-ray crystal structure reveals that, in the solid state, the equatorial fluorine ligands of the IOF$_6^-$ anion are unevenly puckered, only a single resonance is observed for these ligands in the ^{19}F NMR spectrum of the solution. Clearly, the puckering, which is frozen out in the solid state, becomes a dynamic process in solution which is fast on the NMR time scale.

It is of interest to compare the ^{19}F chemical shifts of IOF$_6^-$ with those of other related iodine(VII) oxofluoro species. The ^{19}F chemical shifts of the F-*trans*-to-F environments in *trans*-IO$_2$F$_4^-$, *cis*-IO$_2$F$_4^-$,[46] and IOF$_5$[47] occur in a specific region at 65.1, 66.0, and 68 ppm, respectively. Similarly, the ^{19}F chemical shifts of the F-*trans*-to-O environments in *cis*-IO$_2$F$_4^-$ and IOF$_5$ also occur in a distinct region at 112.8[46] and 107 ppm,[48] respectively. In the IOF$_6^-$ anion it can be seen that the F-*trans*-to-O environment (111.1 ppm) also resonates in this region but that the resonance of the five equatorial fluorines (166.0 ppm) is strongly deshielded (i.e., by ca. 100 ppm) from the F-*trans*-to-F environments of IOF$_5$ and *cis*-/*trans*-IO$_2$F$_4^-$. This phenomenon has also been noted for the XeF$_5^-$ anion in which the fluorines in the pentagonal plane resonate 56.8 ppm to high frequency of the fluorine ligands in square-planar XeF$_4$.[49] In the cases of the pentagonal bipyramidal TeF$_7^-$ anion and IF$_7$ molecule, even at low temperature[10,11,47] only average ^{19}F chemical shifts can be obtained owing to their fluxional behavior. Nevertheless, the fact that these average chemical shifts occur at significantly higher frequency than those of the related octahedral TeF$_6$[50] and IF$_6^+$[51] species indicates that the five equatorial fluorines have a higher frequency ^{19}F chemical shift than the two axial fluorine ligands, since the former will contribute the largest weighting to the average chemical shift.

The large chemical shift differences between fluorine ligands in a square plane and those in a pentagonal plane in the aforementioned species are indicative of the dominance of the paramagnetic contribution to the ^{19}F shielding constant. In the theory developed by Pople and Karplus,[52] the paramagnetic contribution to the shielding constant of an atom A bonded to

(48) Remeasured for this work in CH$_3$CN at –40 °C.

(49) Christe, K. O.; Curtis, E. C.; Dixon, D. A.; Mercier, H. P.; Sanders, J. C. P.; Schrobilgen, G. J. *J. Am. Chem. Soc.* **1991**, *113*, 3351.

(50) This work; chemical shift determined as δ = –51.3 ppm for TeF$_6$ in CH$_3$CN at –40 °C.

(51) Brownstein, M.; Selig, H. *Inorg. Chem.* **1972**, *11*, 656.

(52) Karplus, M.; Pople, J. A. *J. Chem. Phys.* **1963**, *38*, 2803.

Figure 4. Vibrational spectra of N(CH$_3$)$_4$$^+IOF_6^-$. Trace A, infrared spectrum of the solid as an AgBr disk; traces B and C, Raman spectra of the solid at 25 and –146 °C; traces D and E, Raman spectra of the CH$_3$CN solution with parallel and perpendicular polarization, respectively.
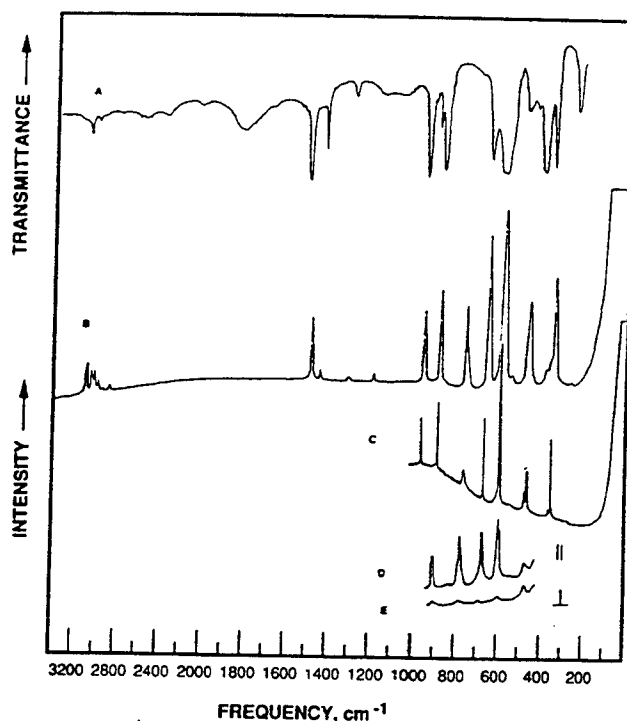
another atom B is given by eq 2

$$\sigma_p^A = \frac{-e^2\hbar^2\langle r^{-3}\rangle_{2p}}{2m^2c^2\Delta E}[Q_{AA} + \sum_{B\neq A} Q_{AB}] \qquad (2)$$

where $\langle r^{-3}\rangle_{2p}$ is the mean inverse cube of the 2p-orbital radial function on atom A, Q_{AA} is the charge density term for atom A, Q_{AB} is the bond order term for the A–B bond, and ΔE is the mean excitation energy.

Compared with the bonds in the corresponding octahedral or pseudooctahedral precursors, MO$_y$F$_x^n$, those in the MO$_y$F$_{x+1}^{n-1}$ species, which contain a pentagonal plane of M–F bonds (where M = Xe, I, Te), exhibit greater ionic character, as indicated by their longer bond lengths and lower vibrational stretching frequencies. This greater ionic character would be expected to bring about a decrease in the $\langle r^{-3}\rangle_{2p}$ and charge density–bond order terms of eq 2. This would result in a decrease in σ_p and a more shielded chemical shift and does not account for the experimentally observed trend. Consequently, it would appear that the origin of the observed deshielding most likely lies in the ΔE term. Unfortunately, the nature of the excited states is unknown at present; however, it is interesting to note that comparison of the HOMO energies in XeF$_4$ and XeF$_5^-$[49] as well as IOF$_5$ and IOF$_6^-$ reveals that the anions have significantly lower values than the neutral molecules and may facilitate excitation to a higher excited state, i.e., ΔE is smaller for XeF$_5^-$ and IOF$_6^-$ than for XeF$_4$ and IOF$_5$.

The two-bond fluorine–fluorine scalar coupling $^2J(^{19}F_{ax}$–$^{19}F_{eq})$ in IOF$_6^-$ has a value of 205 Hz and is almost identical in magnitude to that measured previously for *cis*-IO$_2$F$_4^-$ in CH$_3$CN [$^2J(^{19}F_{ax}$–$^{19}F_{eq})$ = 204 Hz].[46] The couplings in both anions are smaller than the corresponding coupling in the related IOF$_5$ molecule [$^2J(^{19}F_{ax}$–$^{19}F_{eq})$ = 271–280 Hz],[53] which may reflect the anticipated greater ionic character in the bonds of the anionic species.[54] In the ^{19}F NMR spectrum of IOF$_6^-$, both the doublet and sextet

(53) Brownstein, M.; Gillespie, R. J.; Krasznai, J. P. *Can. J. Chem.* **1978**, *56*, 2253.

2702 *J. Am. Chem. Soc., Vol. 115, No. 7, 1993*

Christe et al.

Table III. Vibrational Spectra of N(CH₃)₄⁺IOF₆⁻ and Their Assignment

| | obsd freq, cm⁻¹ (rel intensity) | | | assignments (point group) | |
| | Ra | | CH₃CN sol 25 °C | N(CH₃)₄⁺ (T_d) | IOF₆⁻ (C_{5v}) |
IR 25 °C	solid 25 °C	−150 °C			
3045 mw	3043 (20)	3045 (5)		ν_5(E)	
	2996 (13)			ν_{14}(F₂)	
2970 w	2965 (13)	2970 (4)		ν_1(A₁) + combin bands	
	2927 (6)				
	2819 (5)			ν_{15}(F₂)	
1489 vs				ν_2(A₁), ν_6(E)	
	1464 (46)	1466 (15)		ν_{16}(F₂)	
1418 m	1417 (6)	1416 (3)		ν_{17}(F₂)	
1285 mw	1288 (3)			ν_7(E)	
	1173 (6)	1174 (4)		ν_{18}(F₂)	
949 vs	948 (41)	949 (28)			ν_1(A₁)
873 vs	874 (53)	873 (37)	880 (50) p		
	752 (45)	753 (15)		ν_3(A₁)	
	740 sh	742 sh			ν_2(A₁)
649 s	649 (88)	658 (57)	656 (75) p		ν_5(E₁)
585 vs	578 (100)	584 (100)	581 (100) p		ν_3(A₁)
					ν_9(E₂)
535 w,sh	530 (4)	530 (3)			
490 m		466 (15)		ν_{19}(F₂)	
475 sh					ν_{10}(E₂)
	457 (49)	456 (23)	457 (20) dp		ν_6(E₁)
405 vs				ν_8(E)	
	373 sh	377 (5)			ν_4(A₁)
359 s		354 (4)			ν_7(E₁)
	341 (62)	344 (52)		ν_{12}(F₁)	
		335 (5)			
255 s	260 (2)	260 (2)			ν_8(E₁)

are significantly broadened owing to partially collapsed scalar coupling to the quadrupolar ^{127}I ($I = ^5/_2$) nucleus. The ^{19}F NMR spectra of *cis*-IO₂F₄⁻ [46] and IOF₅ [47a] also show broadening attributed to the same cause. Interestingly, the line width of the sextet of IOF₆⁻ is substantially broader than that of the doublet, indicating that $^1J(^{19}F_{ax}-^{127}I)$ is larger than $^1J(^{19}F_{eq}-^{127}I)$ and therefore less quadrupole collapsed. If it is assumed that the Fermi-contact mechanism provides the dominant coupling contribution, then this observation is consistent with the relatively more covalent (i.e., greater s-character) bond between iodine and the axial fluorine as compared with those between iodine and the equatorial fluorines.[54] The X-ray crystallographic data and vibrational spectra for N(CH₃)₄⁺IOF₆⁻ support this idea in that the I–F_{ax} bond distance is shorter than the average I–F_{eq} bond distance and the I–F_{ax} force constant is larger than the I–F_{eq} one (see below).

Vibrational Spectra. The infrared and Raman spectra of solid N(CH₃)₄⁺IOF₆⁻ and the Raman spectra of its CH₃CN solution were recorded and are shown in Figure 4. The observed frequencies, together with their assignments, are summarized in Table III. A comparison of the observed and calculated (see below) frequencies of IOF₆⁻ with those of the closely related pentagonal IF₇ molecule[8] and XeF₅⁻ anion,[49] together with their approximate mode descriptions, is given in Table IV. After subtraction of the well-known[15,55] bands of the N(CH₃)₄⁺ cation (see Table III), the remaining bands, which are due to IOF₆⁻, can be readily assigned based on the data given in Table IV. Since the vibrational spectra of IOF₆⁻ in solid N(CH₃)₄⁺IOF₆⁻ do not appear to be noticeably affected by the slight equatorial puckering, they were assigned (see Table IV) in point group C_{5v} which is the lowest energy structure of the free anion (see below).

Ab Initio Calculations and Normal Coordinate Analyses. The electronic structure of IOF₆⁻ was calculated at the ab initio level

by using both local density functional (LDF) theory and molecular orbital theory with an effective core potential (ECP) for the core electrons of iodine. Both types of calculations resulted in minimum energy structures of C_{5v} symmetry with the ECP calculations duplicating the experimentally observed geometry (see Table V) and vibrational frequencies (see Table IV) much better than the LDF calculations. In view of the superiority of the ECP calculations, we have also recalculated the structure of the closely related XeF₅⁻ anion, for which previously[49] only LDF values had been available. As can be seen from Tables IV and V, the ECP calculations are in excellent agreement with the observed values, after scaling of the calculated frequencies by empirical factors to maximize their fit with the experimental data, and therefore are invaluable for the correct assignments of the vibrational spectra. For XeF₅⁻, for example, they clearly indicate that the previous assignments[49] for ν_2(A₂″) = 274 cm⁻¹ and ν_4(E₁′) = 290 cm⁻¹ should be reversed. In view of the closeness of these two frequencies, the reversal of their assignments has very little or no impact on the conclusions previously reached[49] for XeF₅⁻.

The eleven fundamental vibrations of a pentagonal bipyramidal AX₅YZ species in point group C_{5v} can be classified as $\Gamma = 4A_1$(IR,Ra) + 4E₁(IR,Ra) + 3E₂(Ra). The internal coordinates, symmetry coordinates, and approximate mode descriptions for IOF₆⁻ are summarized in Figure 5 and Table S6, respectively. The tentative assignments given in our preliminary communication[10] for IOF₆⁻ and IF₇ have been significantly improved resulting in revised assignments for ν_6, ν_7, ν_8, and ν_{10} of IOF₆⁻ and for ν_9 and ν_{10} of IF₇.

By the use of the scaled ECP frequencies, force fields were calculated for IOF₆⁻ (see Table VI) and XeF₅⁻ (see Table VII). The potential energy distribution (PED) for IOF₆⁻ is given in Table VIII. As can be seen from Table VIII, the IF₅ in-plane deformation motions, due to their high frequencies, mix considerably with some of the other symmetry coordinates, and the ν_7(E₁) and ν_8(E₁) modes are antisymmetric and symmetric combinations, respectively, of S₇ and S₈. Consequently, ν_7 and ν_8 are better described as an O–I–F_{ax} rocking motion

(54) Jameson, C. J. In *Multinuclear NMR*; Mason, J., Ed.; Plenum Press: New York, 1987; Chapter 4, pp 97–101.

(55) Christe, K. O.; Wilson, W. W.; Bau, R.; Bunte, S. W. *J. Am. Chem. Soc.* 1992, *114*, 3411 and references cited therein.

The IOF$_6^-$ Anion

J. Am. Chem. Soc., Vol. 115, No. 7, 1993 2703

and an O–I–F$_{ax}$ scissoring motion

respectively, than as separated I=O and I—F$_{ax}$ wagging motions. The only deficiency of the ECP calculation for IOF$_6^-$ was the low-frequency value and resulting force constant for the scaled I–O stretching mode, $\nu_1(A_1)$. Consequently, we prefer to use for this mode the unscaled value of 860 cm^{-1} which is in much better agreement with the observed value of 873 cm^{-1}. The low value calculated for this stretching frequency is surprising as the calculated I–O bond length is shorter than the experimental value. Due to the larger number of symmetry species for XeF$_5^-$, its PED (see Table VII) is highly characteristic and requires no further comment. It should be noted, however, that the symmetry coordinates and internal force constants, previously published[49] for XeF$_5^-$, contained two typographical errors. S_{5b} should read $(2/5)^{1/2}$ [sin 2α ($\Delta r_2 - \Delta r_5$) – sin α ($\Delta r_3 - \Delta r_4$)], and subscripts had been omitted from the last two internal force constants in Table VIII which should read $f_{\gamma\gamma} - f_{\gamma\gamma}'$ and $f_\gamma - f_{\gamma\gamma}$, respectively.

The internal force constants of greatest interest are those involving the stretching of the axial and the equatorial fluorine bonds and the equatorial in-plane deformation constants. These data are summarized for the IF$_7$, IOF$_6^-$, XeF$_5^-$ series in Table IX. As can be seen from this table, the X–F$_{ax}$ bonds are considerably stronger than the X–F$_{eq}$ ones for a given compound, as expected from the bonding scheme proposed below. Furthermore, the stretching force constants decrease significantly on going from IF$_7$ to IOF$_6^-$ and XeF$_5^-$, as expected from an increasing ionicity of the X–F bonds caused by the formal negative charge in the anions and the reduction in the formal oxidation state of the central atom from +VII in IF$_7$ and IOF$_6^-$ to +IV in XeF$_5^-$. The large increase in the value of f_{rr}', the coupling to opposite bonds, from IOF$_6^-$ to XeF$_5^-$, is analogous to those previously observed[46] for going from either *trans*-IO$_2$F$_4^-$ (f_{rr}' = 0.27 mdyn/Å) to IOF$_4^-$ (f_{rr}' = 0.45 mdyn/Å) and IF$_4^-$ (f_{rr}' = 0.47 mdyn/Å) or IOF$_5^-$ (f_{rr}' = 0.18 mdyn/Å) to IF$_5$ (f_{rr}' = 0.38 mdyn/Å) and, hence, appears to be associated with the introduction of a sterically active, free valence electron pair into the ligand sphere around the central atom.

The in-plane deformation constants, f_α, are a measure for the strength of the mutual repulsion of the equatorial ligands and hence for the degree of congestion in this plane which, in turn, is responsible for the puckering. As can be seen from Table IX, the value of f_α decreases markedly on going from IF$_7$ to IOF$_6^-$ and XeF$_5^-$. In IF$_7$, the in-plane deformation constant, f_α, is about five times larger than the out-of-plane deformation constant, f_β, and accounts for the puckering of the equatorial plane in IF$_7$. On the other hand, in XeF$_5^-$ the f_α value has become much smaller and approaches the range of values expected for the out-of-plane deformation constants, f_β. This is in good agreement with the X-ray crystal structure of N(CH$_3$)$_4^+$XeF$_5^-$ which showed[49] that XeF$_5^-$ is planar and not puckered. Hence, it appears that the value of the in-plane deformation force constant, f_α, is a useful parameter for measuring the degree of congestion and the likely occurrence of puckering in the equatorial ligand plane.

It must be pointed out that the problem of calculating the internal deformation constants from the corresponding symmetry force constants is underdetermined (more unknowns than available equations) and, hence, requires additional assumptions. For the calculation of f_α in our compounds, the pure vibrational force field[56] condition of Kuczera, adapted to 5-fold symmetry, f_α +

(56) (a) Kuczera, K.; Czerminski, R. *J. Mol. Struct.* **1983**, *105*, 269. (b) Kuczera, K. *J. Mol. Struct.* **1987**, *160*, 159.

Table IV. Comparison of Observed and Calculated Frequencies of IOF$_6^-$, IF$_7$, and XeF$_5^-$, Together with Their Approximate Mode Descriptions

		IOF$_6^-$ (C$_{5v}$)				IF$_7$ (D$_{5h}$)^c				XeF$_5^-$ (D$_{5h}$)			
		obsd freq, cm^{-1} int (IR,Ra)	approx mode description	calcd freq, cm^{-1} ECP^a	LDF	assign	obsd freq, cm^{-1} int (IR,Ra)	approx mode description	calcd freq, cm^{-1} ECP^c	LDF	assign	approx mode description	obsd freq, cm^{-1} int (IR,Ra)	calcd freq, cm^{-1} ECP^d	LDF^f
assign	approx mode description														
A$_1$ ν_1	ν I=O	873 (vs,53p)	860^b	870	ν_3(A$_2''$)	ν as IF$_2$ax	746 (s,–)	753	710	ν_1(A$_1'$)	ν sym XeF$_5$	502 (–,100)	498	467
ν_2	ν IF$_{ax}$	649 (s,88p)	625	599	ν_1(A$_1'$)	ν sym IF$_2$ax	676 (–,20p)	673	630	ν_2(A$_2''$)	δ umbrella XeF$_5$	290 (m,sh,–)	301	270
ν_3	ν sym IF$_5$	584 (ν_5,100p)	566	537	ν_2(A$_1'$)	ν sym IF$_5$	635 (–,100p)	644	598	ν_3(E$_1'$)	ν as XeF$_5$	450 (vs,–)	449	502
ν_4	δ umbrella IF$_5$	359 (s,4)	371	314	ν_4(A$_2''$)	δ umbrella IF$_5$	365 (s,–)	368	304	ν_4(E$_1'$)	δ as XeF$_5$ in plane	274 (s,–)	273	248
E$_1$ ν_5	ν as IF$_5$	585 (vs,ν_3)	583	568	ν_5(E$_1'$)	ν as IF$_5$	670 (vs,–)	681	647					
ν_6	δ as IF$_5$ in plane	405 (vs,–)	415	365	ν_6(E$_1'$)	δ as IF$_5$ in plane	425 (vs,–)	441	377					
ν_7	δ rock O=I—F$_{ax}$	341 (–,62)	340	292	ν_8(E$_1''$)	δ rock IF$_2$ax	319 (–,6)	320	259					
ν_8	δ sciss O=I—F$_{ax}$	260 (s,2)	273	233	ν_7(E$_1'$)	δ sciss IF$_2$ax	257 (w,–)	265	213	ν_5(E$_2'$)	ν as XeF$_5$	423 (–,16)	420	413
E$_2$ ν_9	δ sciss IF$_5$ in plane	530 (–,4)	530	486	ν_9(E$_2'$)	mixture of δ sciss in plane and ν as IF$_5$	596 (–,2)	605	561	ν_6(E$_2'$)	δ sciss XeF$_5$ in plane	377 (–,23)	373	375
ν_{10}	ν as IF$_5$	457 (–,49)	446	421	ν_{10}(E$_2'$)		510 (–,17)	515	467					
ν_{11}	δ pucker IF$_5$	not obsd	141	111	ν_{11}(E$_2''$)	δ pucker IF$_5$	[68]	59	50i	ν_7(E$_2''$)	δ pucker XeF$_5$	not obsd	105	79

^{a} Frequency values were scaled by an empirical factor of 0.9038. ^{b} Unscaled frequency value; scaled frequency value is 789 cm^{-1}. ^{c} Frequency values were scaled by an empirical factor of 0.932. ^{d} Frequency values were scaled by an empirical factor of 0.8618. ^{e} Data from ref 8. ^{f} Data from ref 49.

2704   *J. Am. Chem. Soc., Vol. 115, No. 7, 1993*

Christe et al.

Table V. Observed and Calculated Geometries of IOF_6^- and the Closely Related IF_7 and XeF_5^-

	IOF_6^-				IF_7				XeF_5^-		
		calcd[a]				calcd[c]				calcd	
	exp[a]	ECP	LDF		exp[b]	ECP	LDF		exp[d]	ECP	LDF
$rI-O$ (Å)	1.75–1.77	1.7255	1.791	$rI-F_{ax}$	1.781	1.7705	1.870	$rXe-F_{eq}$	2.012	1.9924	2.077
$rI-F_{ax}$ (Å)	1.82	1.8087	1.913	$rI-F_{eq}$	1.857	1.8333	1.918				
$rI-F_{eq}$ (Å)	1.88	1.8819	1.969	$F_{ax}-I-F_{eq}$	90	90	90				
$O-I-F_{eq}$ (deg)	94–96	95.76	96.0								

[a] Data from this study. [b] Data from ref 7. [c] Data from ref 8. [d] Data from ref 49.
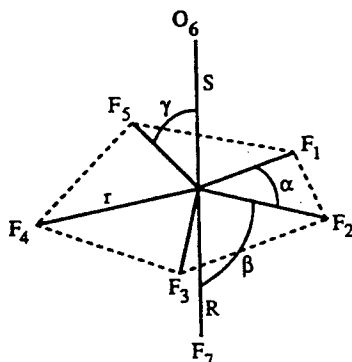
Figure 5. Internal coordinates for IOF_6^-.

Table VI. Symmetry Force Constants[a] of IOF_6^- Calculated from the Scaled ECP Frequencies of Table IV

		F_{11}	F_{22}	F_{33}	F_{44}
A_1	F_{11}	6.077[b]			
		(4.967)[c]			
	F_{22}	0.057	3.899		
	F_{33}	−0.041	0.169	3.656	
	F_{44}	−0.164	0.332	0.078	1.725

		F_{55}	F_{66}	F_{77}	F_{88}
E_1	F_{55}	3.040			
	F_{66}	−1.079	3.246		
	F_{77}	0.230	−0.234	1.087	
	F_{88}	0.176	−0.271	0.085	0.891

		F_{99}	$F_{10,10}$	$F_{11,11}$
E_2	F_{99}	2.844		
	$F_{10,10}$	0.407	2.478	
	$F_{11,11}$	−0.007	−0.064	0.395

[a] Stretching constants in mdyn/Å, deformation constants in mdyn Å/rad², and stretch–bend interaction constants in mdyn/rad. [b] Unscaled value (see text). [c] Scaled value.

$2f_{\alpha\alpha} + 2f_{\alpha\alpha}' \equiv 0$, was used. Since for f_β the case is even more complex, no explicit values were calculated for f_β of IOF_6^- and XeF_5^-; however, we estimate f_β of IOF_6^- to be slightly larger than and that of XeF_5^- to be similar to that of IF_7.

Structure and Bonding in IOF_6^- and Related Molecules and Ions. The pentagonal bipyramidal structure and the co-planarity of the equatorial ligands in the minimum energy configuration of IOF_6^-, which cannot be accounted for by either "repelling points on a sphere" VSEPR arguments[5] or classical, directionally localized molecular orbitals, can be rationalized in terms of a bonding scheme, outlined[49] for XeF_5^- and elaborated on in more detail[8] for IF_7. In this scheme, the structure and bonding of XeF_5^- are explained by a simple model derived from XeF_4. The bonding in the square-planar XeF_4 can be described by two semi-ionic, 3-center 4-electron (3c–4e) bonds[57] for the four Xe–F bonds and two lone valence electron pairs on Xe ($s^2p_z^2$ hybrids). The 3c–4e bonds involve the p_x^2 and p_y^2 orbitals of xenon. Addition

(57) (a) Pimentel, G. C. *J. Chem. Phys.* 1951, *10*, 446. Hach, R. J.; Rundle, R. E. *J. Am. Chem. Soc.* 1951, *73*, 4321. Rundle, R. E. *J. Am. Chem. Soc.* 1963, *85*, 112. (b) Burdett, J. K. In *Molecular Shapes: Theoretical Models of Inorganic Stereochemistry*; Wiley: New York, 1980.

Table VII. Revised Assignments, ECP Force Field,[a] and Potential Energy Distribution[b] for XeF_5^-

assign		approx mode description	freq cm⁻¹ calcd (ECP)	obsd[c]	symmetry force constants	PED
A_1	ν_1	ν sym XeF_5	498	502	$F_{11} = 2.775$	100(1)
A_2''	ν_2	δ umbrella	301	290	$F_{22} = 1.191$	100(2)
E_1'	ν_3	ν asym XeF_5	449	450	$F_{33} = 1.6714$	97(3) + 3(4)
					$F_{34} = -0.193$	
	ν_4	δ asym in plane	273	274	$F_{44} = 1.940$	99(4) + 1(3)
E_2'	ν_5	ν asym XeF_5	420	423	$F_{55} = 1.938$	92(5) + 8(6)
					$F_{56} = 0.1191$	
	ν_6	δ in-plane	373	377	$F_{66} = 1.7505$	91(6) + 9(5)
E_2''	ν_7	δ pucker	105		$F_{77} = 0.2498$	100(7)

[a] Force constants calculated with the ECP frequencies; stretching constants in mdyn/Å, deformation constants in mdyn Å/rad², and stretch–bend interaction constants in mdyn/rad. [b] PED in percent. [c] Data from ref 49.

Table VIII. Potential Energy Distribution for IOF_6^-

		freq, cm⁻¹	PED, %
A_1	ν_1	860	87(1) + 7(2) + 5(4)
	ν_2	625	83(2) + 10(3) + 4(1) + 2(4)
	ν_3	566	88(3) + 12(2)
	ν_4	371	100(4)
E_1	ν_5	583	97(5) + 2(8)
	ν_6	415	44(6) + 26(8) + 25(7) + 5(5)
	ν_7	340	58(8) + 42(7)
	ν_8	273	43(8) + 40(7) + 16(6)
E_2	ν_9	530	73(9) + 27(10)
	ν_{10}	446	72(10) + 28(9)
	ν_{11}	141	100(11)

Table IX. Internal Force Constants[a,b] (mdyn/Å) of IF_7, IOF_6^-, and XeF_5^-

	IF_7	IOF_6^-	XeF_5^-
f_R	5.005	3.897	
f_r	3.947	2.938	2.062
f_{rr}	0.326	0.306	0.198
f_{rr}'	0.0265	0.0536	0.317
f_α	0.847	0.690	0.364
$f_{\alpha\alpha}$	−0.183	−0.147	−0.081
$f_{\alpha\alpha}'$	−0.240	−0.198	−0.102
f_β	0.163		

[a] The deformation constants have been normalized for the following bond distances: IF_7, $rI-F_{eq} = 1.857$ Å; IOF_6^-, $rI-F_{eq} = 1.877$ Å; XeF_5^-, $rXe-F = 2.0124$ Å. [b] f_{rr} and f_{rr}' denote coupling to adjacent and opposite bonds, respectively, and $f_{\alpha\alpha}$ and $f_{\alpha\alpha}'$ coupling to adjacent and opposite bond angles, respectively.

of an F⁻ ion to the equatorial plane in XeF_4 results in pentagonal-planar XeF_5^- and the formation of a semi-ionic, 6-center 10-electron (6c-10e) bond involving the delocalized $p_x^2p_y^2$ hybrid orbitals of Xe and 6 electrons on the 5 F ligands.[49] The two lone valence electron pairs on Xe in XeF_5^- are analogous to those in XeF_4.

Now let us consider the bonding in IF_7 and IOF_6^-. Their planar IF_5 fragments have essentially the same bonding as XeF_5^-, as shown by the atomic population calculations given in Table X. As expected for the replacement of two free valence electron pairs on the central atom by two bonded ligands, each of which

The IOF$_6^-$ Anion
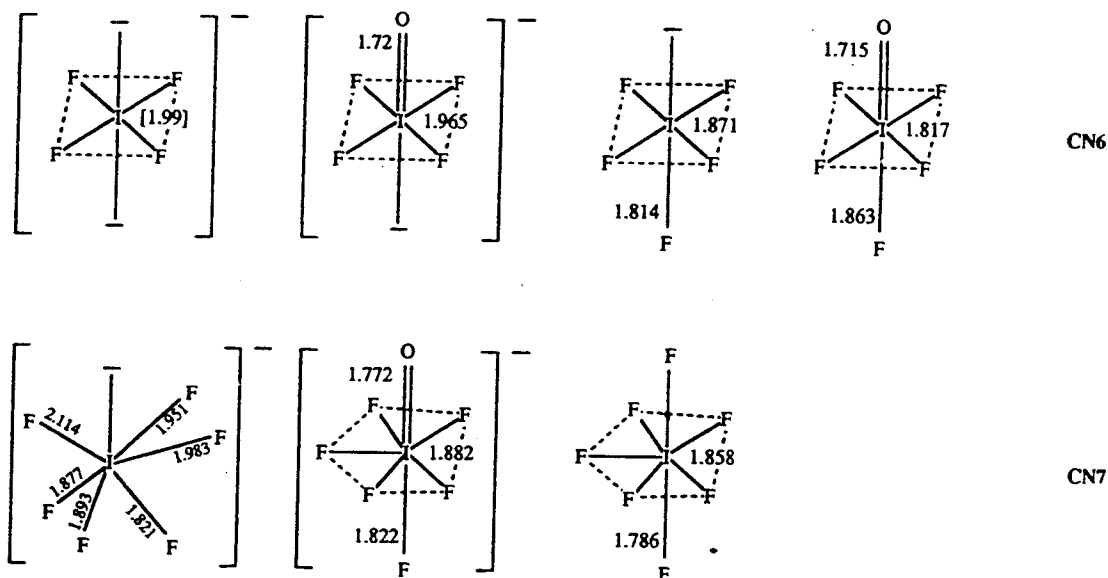
J. Am. Chem. Soc., Vol. 115, No. 7, 1993 2705

Figure 6. A comparison of the structure of IOF$_6^-$ with those of closely related hexa- and heptacoordinated iodine fluorides and oxyfluorides.

Table X. Atomic Populations (e) in the Valence Electron Orbitals and Total Charge Distributions for XeF$_5^-$, IF$_7$, and IOF$_6^-$

	XeF$_5^-$	IF$_7$	IOF$_6^-$
	Central Atom		
s	2.22	1.35	1.43
$p_x = p_y$	0.61	0.64	0.64
p_z	2.02	0.60	0.71
d_{z^2}	0.03	0.11	0.14
$d_{x^2} = d_{y^2}$	0.06	0.12	0.09
d_{xy}	0.14	0.20	0.16
$d_{xz} = d_{yz}$	0.04	0.14	0.15
d total	0.37	0.83	0.78
	Equatorial Fluorines		
s	1.98	1.93	1.94
p bond	1.70	1.57	1.64
p in plane	1.98	1.96	1.97
p_z	1.97	1.94	1.95
d	0	0.03	0.02
	Axial Fluorines and Oxygens		
s		1.92	1.92 (F), 1.86 (O)
p_z		1.54	1.57 (F), 1.16 (O)
$p_x = p_y$		1.94	1.95 (F), 1.83 (O)
d		0.04	0.03 (F), 0.04 (O)
	Total Charges		
central atom	2.15	2.94	2.81
F$_{eq}$	−0.63	−0.43	−0.53
F$_{ax}$		−0.39	−0.44
O$_{ax}$			−0.74

contributes one electron to its bond, the population of the s^2 and p$_z^2$ orbitals of I in IF$_7$ and IOF$_6^-$ has decreased by about two electrons, compared to XeF$_4$ and XeF$_5^-$. The higher oxidation state of the central atoms in IF$_7$ and IOF$_6^-$ (+VII) results in I having a higher positive charge than Xe (+IV) in XeF$_5^-$. This causes the effective electronegativity differences between the central atoms and the ligands in IF$_7$ and IOF$_6^-$ to be smaller than those in XeF$_4$ and XeF$_5^-$ and results in an increased covalency and a shortening of the central atom–fluorine bonds. Furthermore, the axial fluorine ligands in IF$_7$ and IOF$_6^-$ carry less of a negative charge than the equatorial ones which accounts for the axial I–F bonds being more covalent and, hence, shorter than the equatorial ones. The total charge distributions in IF$_7$ and IOF$_6^-$ (see Table X) also demonstrate the effect of replacing an F ligand in IF$_7$ by an O$^-$ ligand. The oxygen substitution results in the release of electron density into the IF$_6$ part of the molecule which increases the negative charges on the six fluorines and weakens the I–F bonds in IOF$_6^-$ relative to those in IF$_7$.

Of course, the above model does not account for the fact that the electrons will try to minimize their mutual repulsions and occupy all of the available orbitals to do so. This results in the participation of some d functions. Although we are not proposing a d hybridization model, the population in the d orbitals does suggest a redistribution into these orbitals beyond that expected if the d orbitals were to act solely as polarization functions.

The above atomic population and total charge distribution analysis qualitatively confirms our simple bonding model for pentagonal-bipyramidal molecules. This model involves the use of delocalized p$_x^2$ and p$_y^2$ hybrid orbitals of the central atom for the formation of a semi-ionic, 6c–10e bond with the five equatorial ligands and of an sp$_z$ hybrid orbital for the formation of two, more covalent, axial bonds. This bonding scheme can account for all the observed structural features and also the observed bond length differences. The planarity of the p$_x^2$ and p$_y^2$ hybrid orbitals of the central atom also explains why these heptacoordinated main group fluorides and oxyfluorides prefer pentagonal-bipyramidal structures and not the monocapped octahedral or trigonal prismatic ones expected from VSEPR arguments.

As far as the puckering of the equatorial plane in pentagonal bipyramidal molecules is concerned, the data given above for IOF$_6^-$ strongly suggest that the congestion in its equatorial plane and hence the driving force toward puckering is intermediate between those of puckered IF$_7$ and planar XeF$_5^-$. Therefore, it might be possible that by a reduction of the thermal motion of the ligands, the mutual repulsion among the equatorial ligands will be sufficiently diminished to allow for the observation of a temperature-dependent transition from a puckered to a planar configuration. Our two crystal structure determinations of N(CH$_3$)$_4^+$IOF$_6^-$ at different temperatures clearly demonstrate such a temperature dependency of the degree of puckering, and the ab initio calculations point to a minimum energy structure with coplanar equatorial ligands.

A comparison of the structure of IOF$_6^-$ with those[7,38,58-61] of other hexa- and heptacoordinated iodine fluorides and oxyfluorides is shown in Figure 6 and suggests the following general effects: (i) If the central iodine atom possesses a free valence electron pair, this pair seeks high s character, i.e. sp^n hybridization. If the number of ligands is larger than four, then as many F ligands

(58) The bond length in IF$_4$ is a value estimated from a normal coordinate analysis: Christe, K. O.; Naumann, D. *Inorg. Chem.* 1973, 12, 59.

(59) Ryan, R. R.; Asprey, L. B. *Acta Crystallogr. Part B* 1972, B28, 979.

(60) Balikci, B.; Brier, P. N. *J. Mol. Spectrosc.* 1981, 89, 254.

(61) Majhoub, A. R.; Seppelt, K. *Angew. Chem., Int. Ed. Engl.* 1991, 30, 323.

Christe et al.

2706 *J. Am. Chem. Soc., Vol. 115, No. 7, 1993*

form semi-ionic, 3-center 4-electron (3c–4e)[57a] or similar multi-center bonds[57b] as are required to allow the free electron pairs to form an sp^n hybrid with any remaining ligands. The resulting semi-ionic, multi-center bonds are considerably longer than the more covalent sp^n hybrid bonds.[62] This effect accounts for the long equatorial I–F bonds in IF_4^-,[58] IOF_4^-,[59] and IF_5,[60] and the short axial I–F bond in IF_5.[60] (ii) If the central atom does not possess any free valence electron pair, the ionicity of the bonds and, as a result, their lengths are influenced by the following secondary effects: (a) An increase in the oxidation state of the central atom generally increases its effective electronegativity and results in increased covalency and, hence, shorter bonds. It must be kept in mind, however, that the addition of two fluorine ligands results in a considerably stronger electron density withdrawal from the central atom than that caused by the addition of one doubly bonded oxygen ligand. Thus, for extremely electronegative central atoms, such as chlorine in ClF_2^+ or ClF_4^-, the addition of an oxygen ligand may even result in the reverse effect, i.e. the release of electron density to the central atom.[62,63] (b) In the case of coordination number (CN) seven, steric crowding and, hence, repulsion effects also become important. The increased congestion in the equatorial planes of IF_7 and IOF_6^-, for example, results in increased mutual repulsion and increased lengths of the equatorial bonds. Thus, the nearest-neighbor $F_{eq}\cdots F_{eq}$ contacts in the IOF_6^- anion at –93 °C are 2.090(16)–2.362(12) Å and are significantly less than twice the nominal van der Waals radius for fluorine, i.e., 2.70–2.80 Å,[44,45] while in hexacoordinated IF_5[38] the nearest neighbor $F_{eq}\cdots F_{eq}$ contacts are 2.571 Å and are still at the limit of the sum of the fluorine van der Waals radii. Similarly, the increased repulsion from the sterically active, free valence electron pair on iodine in hepta-coordinated IF_6^- causes an elongation of the three neighboring I–F bonds.[61] (c) A formal negative charge, as found in an anion, enhances the $F^{\delta-}$–$I^{\delta+}$ bond polarity and hence the ionicity of a bond and, thereby, increases the bond lengths.[62]

The combination of these effects can explain the features of the compounds shown in Figure 6. For IOF_6^-, the relative length of equatorial I–F bonds can be explained by semi-ionic, multi-center bonding, which is enhanced by the formal negative charge and the repulsion effects caused by the steric crowding in the equatorial plane, while the lengthening of the I–O bond is attributed mainly to the formal negative charge and the repulsion effects. There is one piece of data in Figure 6, however, which does not fit the overall picture. This is the axial I–F bond length in IOF_5. The published[38] value of 1.863 Å appears too long and, based on the fact that the axial IF stretching force constant in IOF_5 is larger than the equatorial one[64] and by analogy with the isoelectronic $TeOF_5^-$ anion (Te–F$_{ax}$ = 1.854 Å, Te–F$_{eq}$ = 1.853 Å),[65] the axial bond distance in IOF_5 should be similar to or shorter than the equatorial ones. A cursory examination[66] of the

experimental data[38,64,67–69] available for IOF_5 revealed that these bond distances are not well-determined and are very sensitive to the choice of the O–I–F$_{eq}$ bond angle. Thus, a decreasing angle lengthens the I–O and shortens the I–F$_{ax}$ bond. Furthermore, a lengthening of the I–F$_{eq}$ bond distance results in a shortening of the I–F$_{ax}$ bond distance. Obviously, additional experimental data are required for a more precise structure determination of IOF_5.

Conclusions. The IOF_6^- anion provides unique information on the nature of heptacoordinated molecules. The high degree of fluxionality, which is normally encountered for free heptacoor-dinated molecules, is absent. Dynamic puckering of the equatorial ligand plane is frozen out by crystal forces, and axial–equatorial ligand exchange is precluded by the incorporation of the more repulsive, axial oxygen ligand. It is shown that the statically puckered, equatorial fluorine plane exhibits C_s symmetry in the crystal. Furthermore, it is demonstrated by ab initio calculations and the crystal structure of XeF_5^- that the lowest energy structures of these molecules are pentagonal bipyramids with coplanar equatorial ligands. This coplanarity is explained by a bonding scheme involving delocalized, planar p_x^2–p_y^2 hybrid orbitals of the central atom for the formation of a semi-ionic, 6-center 10-electron system for the five I–F$_{eq}$ bonds which also accounts for their increased lengths. The degree of puckering of the equatorial ligand plane increases with increasing mutual repulsion of the equatorial ligands and, therefore, is temperature dependent as demonstrated for IOF_6^-.

Supplementary Material Available: A structure determination summary (Table S1), final atomic coordinates, equivalent isotropic displacement coefficients, and site occupancy factors (Table S4), anisotropic displacement coefficients (Table S5), and symmetry coordinates (Table S6) (6 pages); calculated and observed structure factor amplitudes (Tables S2 and S3) (16 pages). Ordering information is given on any current masthead page.

(62) Christe, K. O.; Schack, C. J. *Adv. Inorg. Chem. Radiochem.* **1976**, *18*, 331. Christe, K. O. *XXIVth Int. Congr. Pure Appl. Chem.* **1974**, *4*, 115.
(63) Christe, K. O.; Curtis, E. C. *Inorg. Chem.* **1972**, *11*, 2209.

(64) Smith, D. F.; Begun, G. M. *J. Chem. Phys.* **1965**, *43*, 2001. Holloway, J. H.; Selig, H.; Claassen, H. H. *J. Chem. Phys.* **1971**, *54*, 4305.
(65) Miller, P. K.; Abney, K. D.; Rappé, A. K.; Anderson, O. P.; Strauss, S. H. *Inorg. Chem.* **1988**, *27*, 2255.
(66) Kukolich, S. G., private communication of unpublished results.
(67) Brier, P. N. *J. Mol. Spectrosc.* **1987**, *125*, 233.
(68) Brier, P. N.; Winrow, M. J. *J. Mol. Spectrosc.* **1984**, *107*, 21.
(69) Pierce, S. B.; Cornwell, C. D. *J. Chem. Phys.* **1967**, *47*, 1731.

Heptacoordination: Pentagonal Bipyramidal XeF7+ and TeF7- Ions

Karl O. Christe,[*,†] **David A. Dixon,**[‡] **Jeremy C. P. Sanders,**[§] **Gary J. Schrobilgen,**[*,§] **and William W. Wilson**[†]

*Contribution from the Rocketdyne Division of Rockwell International Corporation,
Canoga Park, California 91309, Central Research and Development Department,
E. I. du Pont de Nemours and Company, Inc., Experimental Station,
Wilmington, Delaware 19880-0328, and Department of Chemistry, McMaster University,
Hamilton, Ontario L8S 4M1, Canada*

Received February 18, 1993[®]

Abstract: The TeF7- anion was studied experimentally by vibrational and ^{19}F and [125]Te NMR spectroscopy. Ab initio calculations employing effective core potentials and density functional theory calculations at the self-consistent nonlocal level with the nonlocal exchange potential of Becke and the nonlocal correlation functional of Perdew were used for the analysis of the isoelectronic series TeF7-, IF7, XeF7+. It is shown that XeF7+ is a stable structure, that all three members of this series possess a pentagonal bipyramidal equilibrium geometry, and that from the two closest lying saddle point geometries only the monocapped trigonal prism, but not the monocapped octahedron, is a transition state for the intramolecular axial–equatorial ligand exchange. The results from a normal coordinate analysis reveal the existence of an unusual new effect which counteracts the ligand–ligand repulsion effect and is characterized by axial bond stretching encouraging equatorial bond stretching. While in TeF7- the ligand–ligand repulsion effect dominates, in XeF7+ the new effect becomes preponderant.

Introduction

The problems associated with heptacoordination are manifold and fascinating[1-5] and have recently received significant renewed interest.[3-11] On the basis of the hard sphere model of the valence shell electron pair repulsion (VSEPR) rules of repelling points on a sphere, the energetically preferred structure for a hepta-coordinated species is a monocapped octahedron.[1,2] Two other structures that are only slightly higher in energy are those of a monocapped trigonal prism and a pentagonal bipyramid.[12-15] A study of the relative total repulsive force between seven repelling points of a sphere in terms of the energy law

$$E = \sum_{i \neq j} \frac{1}{r_{ij}{}^n} \qquad (1)$$

where r_{ij} is the distance between two of the points and n is an

† Rocketdyne.
‡ Du Pont.
§ McMaster University.
® Abstract published in *Advance ACS Abstracts*, September 1, 1993.
(1) Gillespie, R. J. *Molecular Geometry*; Van Nostrand Reinhold Company: London, 1972.
(2) Gillespie, R.J.; Hargittai, I. *The VSEPR Model of Molecular Geometry*; Allyn and Bacon, A Division of Simon & Schuster, Inc.: Needham Heights, MA, 1991.
(3) Christe, K. O.; Curtis, E. C.; Dixon, D. A. *J. Am. Chem. Soc.* **1993**, *115*, 1520.
(4) Christe, K. O.; Dixon, D. A.; Mahjoub, A. R.; Mercier, H. P. A.; Sanders, J. C. P.; Seppelt, K.; Schrobilgen, G. J.; Wilson, W. W. *J. Am. Chem. Soc.* **1993**, *115*, 2696.
(5) Gillespie, R. J. *Chem. Soc. Rev.* **1992**, 59.
(6) Christe, K. O.; Christe, E. C.; Dixon, D. A.; Mercier, H. C. P.; Sanders, J. C. P.; Schrobilgen, G. J. *J. Am. Chem. Soc.* **1991**, *113*, 3351.
(7) Christe, K. O.; Sanders, J. C. P.; Schrobilgen, G. J.; Wilson, W. W. *J. Chem. Soc., Chem. Commun.* **1991**, 837.
(8) Mahjoub, A. R.; Seppelt, K. *J. Chem. Soc., Chem. Commun.* **1991**, 840.
(9) Mahjoub, A. R.; Drews, T.; Seppelt, K. *Angew. Chem., Int. Ed. Engl.* **1992**, *31*, 1036.
(10) Christe, K. O.; Dixon, D. A.; Sanders, J. C. P.; Schrobilgen, G. J.; Wilson, W. W. *Inorg. Chem.*, in press.
(11) Mahjoub, A. R.; Seppelt, K. *Angew. Chem., Int. Ed. Engl.* **1991**, *30*, 323.
(12) (a) Hoffmann, R.; Beier, B. F.; Muetterties, E. L.; Rossi, A. R. *Inorg. Chem.* **1977**, *16*, 511. (b) Kepert, D. *Inorganic Stereochemistry*; Springer: Berlin, 1982.

unknown constant, has indicated[13-15] that the minimum energy structure of these heptacoordinated species is a function of n. For $0 < n < 3$, i.e., soft repulsion, the pentagonal bipyramid is the minimum energy structure, while for $3 < n < 6$, the monocapped trigonal prism, and for $n > 6$, i.e., hard repulsion, the monocapped octahedron are the energetically favored structures. Whereas these predictions seem to hold well for heptacoordinated transition-metal compounds,[10] the presently known heptacoordinated main-group compounds, in spite of their expected pronounced hardness, show a strong preference for pentagonal bipyramidal structures.[3,4,6-10] In view of these findings it was of interest to study the isoelectronic series of main-group species XeF7+, IF7, TeF7-, in which the hardness should increase from TeF7- to XeF7+.

For the XeF7+, IF7, TeF7- series, the following information was previously available. For XeF7+, no previous reports could be found in the literature. The IF7 molecule has been known and studied since 1931,[16] but a better understanding of its charac-teristic behavior was achieved only very recently.[3] The TeF7- anion has been known since 1957,[17,18] but again this anion was not well characterized. Whereas some preliminary results on TeF7- were recently published in three short notes,[7-9] a full account and analysis of the data have not been presented before and the vibrational assignments needed revision.

In this paper, we present data on the novel XeF7+ cation and a complete analysis of the TeF7- anion that firmly establishes the vibrational assignments for the isoelectronic XeF7+, IF7, TeF7- series. This analysis resulted in the discovery of a highly unusual reversal of Raman intensities in the A1' symmetry block which contains only two orthogonal and, hence, normally very weakly coupled stretching modes. By means of a normal coordinate analysis, the cause of this intensity reversal was identified and is attributed to a novel effect which counteracts the ligand–ligand repulsion effect. Furthermore, ab initio and density functional

(13) Claxton, T. A.; Benson, G. C. *Can. J. Chem.* **1966**, *44*, 157.
(14) Bradford Thompson, H.; Bartell, L. S. *Inorg. Chem.* **1968**, *7*, 488.
(15) McDowell, H. K.; Chiu, H.-L.; Geldard, J. F. *Inorg. Chem.* **1988**, *27*, 1674.
(16) Ruff, O.; Keim, R. *Z. Anorg. Chem.* **1931**, *201*, 245.
(17) Muetterties, E. L. *J. Am. Chem. Soc.* **1957**, *79*, 1004.
(18) Selig, H.; Sarig, S.; Abramowitz, S. *Inorg. Chem.* **1974**, *13*, 1508.

theory calculations were used to determine the relative energies, minimum energy structures, saddle points, and transition states of the XeF_7^+, IF_7, TeF_7^- series. This work completes our systematic study of these and similar heptacoordinated main-group element compounds.[3,4,6,7,10]

Experimental Section

Apparatus and Materials. Volatile materials were handled in stainless steel–Teflon and Pyrex glass vacuum lines, as described previously.[6] Nonvolatile materials were handled in the dry nitrogen atmosphere of a glovebox (Vacuum Atmospheres Model DLX).

Literature methods were used for the syntheses of $N(CH_3)_4F$[19] and TeF_4[20] and the drying of CH_3CN (Caledon).[21] Tellurium hexafluoride was prepared by fluorination of crude TeF_4 in a Monel reactor using a 50 mol % excess of elemental fluorine under autogeneous pressure at 250 °C for 4 h. Crude TeF_6 was purified by condensation onto a dry sample of NaF in a stainless steel Whitey cylinder at –196 °C and stored at room temperature for several days prior to use.

Synthesis of $N(CH_3)_4TeF_7$. Anhydrous tetramethylammonium fluoride (0.5125 g, 5.5022 mmol) was loaded into a $^1/_2$-in. o.d. Teflon–FEP tube in the drybox. The tube was equipped with a Kel-F valve and attached to a glass vacuum line. Anhydrous CH_3CN (ca. 3 mL) was distilled onto the $N(CH_3)_4F$ at –196 °C. The mixture was warmed briefly to 25 °C in order to dissolve the $N(CH_3)_4F$, frozen to –78 °C, and pressurized with dry N_2 (1.5 atm). The tube was attached to the metal vacuum line and evacuated at –196 °C. Tellurium hexafluoride (5.75 mmol, 4.5 mol % excess) was metered out into the calibrated vacuum line and condensed into the FEP tube at –196 °C. The reaction mixture was warmed to –40 °C and agitated as the CH_3CN and TeF_6 melted. The reaction took place with formation of a white precipitate. In order to ensure that the reaction was complete, the mixture was warmed to 25 °C and allowed to stand at this temperature for 10 min. The excess TeF_6 and CH_3CN solvent were pumped off in a dynamic vacuum, leaving the $N(CH_3)_4$-TeF_7 as a dense white powder (1.7208 g, 93%).

Nuclear Magnetic Resonance Spectroscopy. The ^{19}F and ^{125}Te NMR spectra were recorded unlocked (field drift <0.1 Hz h^{-1}) on a Bruker AM-500 spectrometer equipped with an 11.744-T cryomagnet. The ^{19}F spectra were obtained using a 5-mm combination $^1H/^{19}F$ probe operating at 470.599 MHz. The spectra were recorded in a 32K memory. A spectral width setting of 5000 Hz was employed, yielding a data point resolution of 0.305 Hz/data point and an acquisition time of 3.28 s. No relaxation delays were applied. Prior to Fourier transformation, the free induction decay was zero-filled to 128K of memory, giving a data point resolution of 0.076 Hz/data point. Typically, 16 transients were accumulated. The pulse width corresponding to a bulk magnetization tip angle, θ, of approximately 90° was equal to 1 μs. No line broadening parameters were used in the experimental multiplication of the free induction decays prior to Fourier transformation.

The ^{125}Te NMR spectra were obtained at 157.794 MHz by using a broad-band VSP probe tunable over the range 23–202 MHz. The spectra were recorded in a 32K memory. The spectral width setting was 25 kHz, which yielded a data point resolution of 1.526 Hz/data point and an acquisition time of 0.655 s. Prior to Fourier transformation, the free induction decay was zero-filled to 64K of memory, giving a data point resolution of 0.763 Hz/data point. No relaxation delays were applied. Typically 5000 transients were accumulated. The pulse width corresponding to a bulk magnetization tip angle, θ, of approximately 90° was equal to 10 μs. A line broadening parameter of 1.5 Hz was applied to the exponential multiplication of the free induction decay prior to Fourier transformation.

The spectra were referenced to neat external samples of $CFCl_3$(^{19}F) and $(CH_3)_2Te$(^{125}Te) at ambient temperature. The chemical shift convention used is that a positive sign signifies a chemical shift to high frequency of the reference compound.

NMR samples were prepared in 10- or 5-mm precision glass tubes (Wilmad). Solids were weighed into the tubes in the drybox, and CH_3CN solvent was distilled in vacuo onto the solid at –78 °C. The tubes were flame-sealed in a dynamic vacuum while keeping the contents frozen at –78 °C.

Vibrational Spectra. Infrared spectra of solid $N(CH_3)_4TeF_7$ were recorded on a Perkin-Elmer Model 283 spectrometer. The finely powdered sample was pressed between two AgBr disks in a Wilks minipress inside the drybox. Raman spectra were recorded on a Spex Model 1403 spectrophotometer using the 647.1-nm exciting line of a Kr ion laser and baked-out Pyrex melting point capillaries as sample containers.

Computational Methods. The electronic structure calculations were done by both ab initio molecular orbital and density functional theories. At the ab initio molecular orbital level effective core potentials (ECP) were used for the core electrons on the central atoms. The valence basis sets are of polarized double-ϑ quality. The fluorine basis set is from Dunning and Hay,[22] and the ECP, from Wadt and Hay,[23] including relativistic corrections and augmented by a d function on the central atom.[24] The geometries were optimized by using analytic gradient techniques[25] at the SCF level.[26] Final energies were calculated for the SCF geometries at the MP-2 level. The force fields were calculated analytically.[27,28] The ab initio MO calculations were done with the program GRADSCF,[29] as implemented on a Cray YMP computer system. This computational method generally underestimates these central atom–fluorine bond distances by about 0.01–0.02 Å and, hence, results in vibrational frequency and force constant values which are somewhat too high. Therefore, the calculated values were scaled using empirical factors to give the best fit between calculated and observed frequencies. If the deformation frequencies showed significantly larger deviations than the stretching frequencies, separate scaling factors were used for the two groups.[30] Since the force constants are proportional to the square of the frequencies, the calculated force constants were scaled by the square of the factors used for scaling the corresponding frequencies.

The density functional theory (DFT)[31] calculations were done with the program DGauss,[32] which employs Gaussian orbitals on a Cray YMP computer. Norm-conserving pseudopotentials[33] were generated for I, the Te set for I, Te, and Xe by following the work of Troullier and Martins.[34] The valence basis set for I is [421/31/1] with a fitting basis set of [7/6/1], and the corresponding basis sets for Te and Xe have the form (42/43/1) with a [7/5] fitting basis. The basis set for F is of polarized triple-ζ valence quality and has the form (7111/411/1) with a [7/3/3] fitting basis.[35] The calculations were done with the local

(19) Christe, K. O.; Wilson, W. W.; Wilson, R. D.; Bau, R.; Feng, J. *J. Am. Chem. Soc.* **1990**, *112*, 7619.

(20) Seppelt, K. *Inorg. Synth.* **1980**, *20*, 33.

(21) Christe, K. O.; Wilson, W. W. *J. Fluorine Chem.* **1990**, *47*, 117. Winfield, J. M. *J. Fluorine Chem.* **1984**, *25*, 91.

(22) Dunning, T. H., Jr.; Hay, P. J. In *Methods of Electronic Structure Theory*; Schaefer, H. F., III, Ed.; Plenum Press: New York, 1977; Chapter 1.

(23) Wadt, W. R.; Hay, P. J. *J. Chem. Phy.* **1985**, *82*, 284.

(24) Huzinaga, S.; Andzelm, J.; Klobukowski, M.; Radzio, E.; Sakai, Y. U.; Tatasaki, H. *Gaussian Bassi Sets of Molecular Calculations*; Elsevier: Amsterdam, 1984.

(25) (a) Komornicki, A.; Ishida, K.; Morokuma, K.; Ditchfield, R.; Conrad, M. *Chem. Phys. Lett.* **1977**, *45*, 595. (b) McIver, J. W., Jr.; Komornicki, A. *Chem. Phys. Lett.* **1971**, *10*, 202. (c) Pulay, P. In *Applications of Electronic Structure Theory*; Schaefer, H. F., III, Ed.; Plenum Press: New York, 1977; p 153.

(26) (a) Moller, C.; Plesset, M. S. *Phys. Rev.* **1934**, *46*, 618. (b) Pople, J. A.; Binkley, J. S.; Seeger, R. *Int. J. Quantum Chem., Symp.* **1976**, *10*, 1.

(27) (a) King, H. F.; Komornicki, A. *J. Chem. Phys.* **1986**, *84*, 5465. (b) King, H. F.; Komornicki, A. In *Geometrical Derivatives of Energy Surfaces and Molecular Properties*; Jorgenson, P., Simons, J., Eds.; NATO AESI Series C; D. Reidel: Dordrecht, 1986; Vol. 166, p 207.

(28) Breidung, J.; Thiel, W.; Komornicki, A. *Chem. Phys. Lett.* **1988**, *153*, 76.

(29) GRADSCF is an ab initio program system designed and written by A. Komornicki at Polyatomics Research.

(30) Marsden, C. J. *J. Chem. Phys.* **1987**, *87*, 6626.

(31) (a) Parr, R. G.; Yang, W. *Density Functional Theory of Atoms and Molecules*; Oxford University Press: New York, 1989. (b) Salahub, D. R. In *Ab Initio Methods in Quantum Chemistry* II; Lawley, K. P., Ed.; J. Wiley & Sons: New York, 1987; p 447. (c) Wimmer, E.; Freeman, A. J.; Fu, C.-L.; Cao, P.-L.; Chou, S.-H.; Delley, B. In *Supercomputer Research in Chemistry and Chemical Engineering*; Jensen, K. F., Truhlar, D. G., Eds.; ACS Symposium Series No. 353; American Chemical Society: Washington, DC, 1987; p 49. (d) Jones, R. O.; Gunnarsson, O. *Rev. Mod. Phys.* **1989**, *61*, 689. (e) Zeigler, T. *Chem. Rev.* **1991**, *91*, 651.

(32) Andzelm, J.; Wimmer, E.; Salahub, D. R. In *The Challenge of d and f Electrons: Theory and Computation*; Salahub, D. R., Zerner, M. C., Eds.; ACS Symposium Series No. 394; American Chemical Society: Washington, DC, 1989; p 228. (b) Andzelm, J. In *Density Functional Methods in Chemistry*; Labanowski, J., and Andzelm, J., Eds.; Springer-Verlag: New York, 1991; p 101. Andzelm, J. W.; Wimmer, E. *J. Chem. Phys.* **1992**, *96*, 1280. DGauss is a local density functional program available via the Cray Research Unichem Project, Cray Research, Eagan, MN, 1993.

(33) Chen, H.; Krashowski, M.; Fitzgerald, G. *J. Chem. Phys.*, in press.

(34) Troullier, N.; Martins, J. L. *Phys. Rev. B* **1991**, *43*, 1993.

(35) Godbout, N.; Salahub, D. R.; Andzelm, J.; Wimmer, E. *Can. J. Chem.* **1992**, *70*, 560.

Heptacoordination: TeF7- and XeF7+ Ions

J. Am. Chem. Soc., Vol. 115, No. 21, 1993 9463

potential of Vosko, Wilk, and Nusair[36] and at the self-consistent nonlocal level with the exchange potential of Becke[37] together with the correlation functional of Perdew[38] (NLDFT/BP). Geometries were optimized by using analytical gradients.[32] Second derivatives were calculated by numerical differentiation of the analytic first derivatives. A two-point method with a finite difference of 0.01 au was used.

Results and Discussion

Synthesis. Although the results of our theoretical calculations (see below) suggest that XeF7+ is a stable species, its synthesis has so far not been achieved and is expected to be very difficult. The calculated oxidizer strength of XeF7+ is almost identical to that of KrF+, which is the strongest presently known oxidative fluorinator.[39] Therefore, its synthesis from XeF6 by oxidative fluorination will require an oxidizer that is stronger than KrF+. The synthesis of XeF7+ from XeF8 by F- abstraction will be similarly difficult because XeF8 is unknown and will also be very difficult to synthesize.

The synthesis of N(CH3)4TeF7 is readily accomplished by the reaction of N(CH3)4F with a moderate excess of TeF6 in CH3CN solution.

$$N(CH_3)_4F + TeF_6 \xrightarrow{CH_3CN} N(CH_3)_4TeF_7 \qquad (1)$$

The use of an excess of N(CH3)4F must be avoided since it results in the formation of the TeF8^2- anion.[18] The compound N(CH3)4TeF7 is a stable, white, crystallinic material that can be recrystallized from CH3CN. Two independent single-crystal X-ray diffraction studies,[9,40] have been carried out and yielded identical results. The TeF7- anion in N(CH3)4TeF7 undergoes 4-fold disorder for the five equatorial fluorine ligands. Although these studies established for TeF7- a distorted, pentagonal bipyramidal structure in which the axial bonds are shorter than the equatorial bonds, the remaining structural features were not well determined because of the disorder.

NMR Spectra of TeF7-. The ^{125}Te NMR spectrum of N(CH3)4-TeF7 in CH3CN at 30 °C shows[7,8] a binominal octet [$\delta(^{125}Te)$, 327.4 ppm; $^1J(^{125}Te-^{19}F)$, 2876 Hz]. This demonstrates the equivalence of all seven fluorine ligands on the NMR time scale due to a rapid intramolecular exchange mechanism which cannot be frozen out on cooling the sample down to -48 °C, the freezing point of the CH3CN solution. The ^{125}Te chemical shift of TeF7- is significantly more shielded (i.e., by 217.8 ppm) than that of TeF6 in CH3CN at 30 °C [$\delta(^{125}Te)$, 545.2 ppm; $^1J(^{125}Te-^{19}F)$, 3746 Hz], and this is in accord with the expected trend of increasing shielding with increasing negative charge.[41]

The ^{19}F NMR spectrum of N(CH3)4TeF7 in CH3CN at 30 °C (Figure 1) is also consistent with the TeF7- anion undergoing a rapid intramolecular exchange process and displays a single environment [$\delta(^{19}F)$, 16.1 ppm] flanked by natural abundance (7.14%) ^{125}Te[$^1J(^{19}F-^{125}Te, 2876$ Hz] and (0.908%) ^{123}Te[$^1J(^{19}F-^{123}Te)$, 2385 Hz] satellites. The isoelectronic IF7 molecule displays similar fluxional behavior and a single environment in the ^{19}F NMR spectrum.[42] At an external field strength of 11.744 T, the high-resolution ^{19}F NMR spectrum of the central line of the TeF7- resonance (Figure 2) displays the isotopic shift pattern arising from ^{19}F ligands bonded to the natural abundance spinless tellurium isotopes in the ^{130}TeF7- (33.80%), ^{128}TeF7- (31.69%),
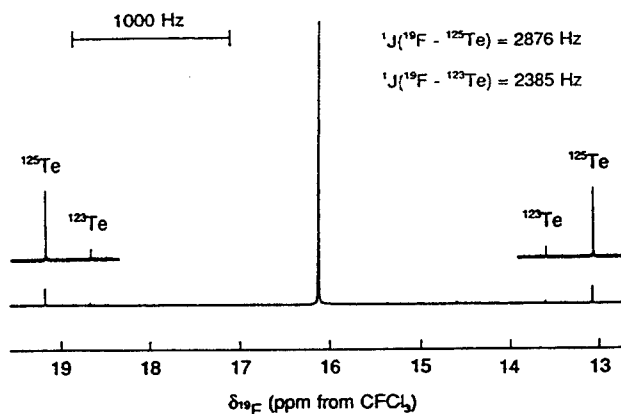
Figure 1. ^{19}F NMR spectrum (470.599 MHz) of N(CH3)4TeF7 in CH3CN solution at 30 °C.
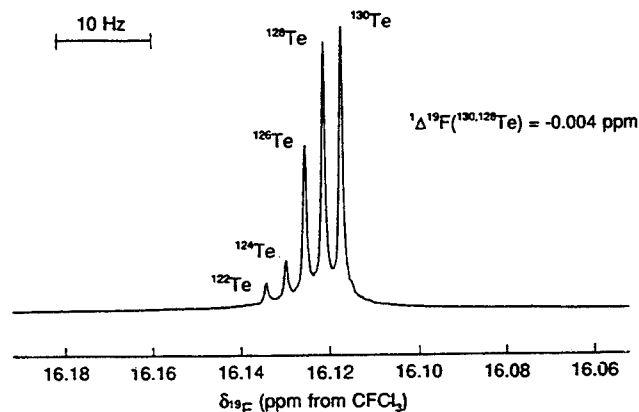
Figure 2. High-resolution ^{19}F NMR spectrum (470.599 MHz) of the central line of TeF7-.

^{126}TeF7- (18.95%), ^{124}TeF7- (4.82%), and ^{122}TeF7- (2.60%) isotopomers. With every increase of two mass units, each isotopomer is shifted successively to low frequency by $^1\Delta^{19}F(Te)$ = -0.0042 ppm. This value is essentially identical, within experimental error, with values obtained for TeF6 and various OTeF5 derivatives.[43] The ^{19}F chemical shift of TeF7- is deshielded by 67.4 ppm with respect to that of TeF6 in CH3CN at 30 °C. The pentagonal planes of fluorine ligands in the XeF5- and IOF6- anions show similar high-frequency chemical shifts which have been suggested to arise from a low-energy HOMO excitation in the paramagnetic contribution to the ^{19}F shielding constant in these anions.[6,10] In TeF7-, the observed ^{19}F chemical shift represents a weighted average of the F_{ax} and F_{eq} chemical shifts (eq 2).

$$\delta(^{19}F)_{av} = {^2/_7}\delta(^{19}F_{ax}) + {^5/_7}\delta(^{19}F_{eq}) \qquad (2)$$

Nevertheless, the fact that this chemical shift occurs at significantly higher frequency than that of TeF6 supports the idea that the five equatorial fluorines in TeF7- have a higher frequency ^{19}F shift than the two axial fluorines, since the former will contribute the larger weighting to the average chemical shift. In fact, it is possible to estimate, to a first approximation, the individual chemical shifts of the F_{ax} and F_{eq} environments of TeF7- in the absence of exchange. The chemical shift of the F_{ax} environment may be estimated from an observation made from the ^{19}F NMR spectrum of IOF6-, in which it is found that the chemical shift of the F-*trans*-to-O environment occurs very close to the F-*trans*-to-O environments in the octahedral IOF5 and *cis*-IO2F4- species.[4] This is not surprising since the nature of the sp$_z$ hybrid bonding in the F_{ax}—I=O moiety changes little as compared with that for the equatorial fluorines on going from IOF5 to IOF6- (i.e., from

(36) Vosko, S. J.; Wilk, L.; Nusair, M. *Can. J. Phys.* **1980**, *58*, 1200.

(37) Becke, A. D. *Phys. Rev. A* **1988**, *38*, 3098. (b) Becke, A. D. In *The Challenge of d and f Electrons: Theory and Computation*; Salahub, D. R.; Zerner, M. C., Eds.; ACS Symposium Series No. 394; American Chemical Society: Washington, DC, 1989; p 166. (c) Becke, A. D. *Inter. J. Quantum Chem., Quantum. Chem. Symp.* **1989**, *23*, 599.

(38) Perdew, J. P. *Phys. Rev. B* **1986**, *33*, 8822.

(39) Christe, K. O.; Dixon, D. A. *J. Am. Chem. Soc.* **1992**, *114*, 2978.

(40) Mercier, H. C. P. Unpublished results.

(41) Jameson, C. J.; Mason, J. In *Multinuclear NMR*; Mason, J., Ed.; Plenum Press: New York, 1987; Chapter 3, pp 66–68.

(42) Gillespie, R. J.; Quail, J. W. *Can. J. Chem.* **1964**, *42*, 2671. Muetterties, E. L.; Packer, K. J. *J. Am. Chem. Soc.* **1964**, *86*, 293.

(43) Sanders, J. C. P.; Schrobilgen, G. J. To be submitted.

Table I. Observed and Calculated Vibrational Spectra of Isoelectronic TeF7⁻, IF7, and XeF7⁺

assignment in point group D_{5h}		approximate mode description	TeF7⁻ obsd freq, cm⁻¹ (intens) Ra	IR	calcd freq, cm⁻¹ (IR intens) SCF[a]	NLDFT[b]	IF7 obsd freq, cm⁻¹ (intens) Ra	IR	calcd freq, cm⁻¹ (IR intens) SCF[a]	NLDFT[c]	XeF7⁺ calcd freq, cm⁻¹ (IR intens) SCF[a]	NLDFT[d]
A_1'	ν_1	ν sym XF₂ ax	640 (10)		644.6	648 (0)	676 (2)		673	670 (0)	681.6	684 (0)
	ν_2	ν sym XF₅ eq inphase	597 (2.6)		595.7	596 (0)	635 (10)		644	621 (0)	625.8	620 (0)
A_2''	ν_3	ν asym XF₂ ax		699 vs	703.0	713 (147)		746 s	753	752 (129)	757.1	776 (88)
	ν_4	δ umbrella XF₅ eq		335 ms	336.7	342 (51)		365 s	368	366 (37)	361.6	360 (23)
E_1'	ν_5	ν asym XF₅ eq		625 vs	618.4	614 (220)		670 vs	681	658 (232)	688.1	677 (158)
	ν_6	δ sciss XF₂ ax		385 s	387.7	377 (306)		425 vs	441	418 (204)	438.6	416 (137)
	ν_7	δ asym XF₅ eq in-plane		not obsd	236.5	238 (0.1)		257 w	265	267 (0.2)	270.1	267 (0)
E_1''	ν_8	δ wag XF₂ ax	295 (0.5) br		291.4	297 (0)	319 (0.6)		320	322 (0)	318.4	320 (0)
E_2'	ν_9	mixture of δ sciss XF₅ in-plane and ν asym XF₅ eq	not obsd		521.1	523 (1.0)	596 (0.2)		605	606 (0)	621.1	617 (0)
	ν_{10}		458 (1.6)		442.5	444 (11)	510 (1.7)		515	508 (0)	541.0	539 (0)
E_2''	ν_{11}	δ pucker XF₅			52.9	59 (0)	[68]		59	82 (0)	81.6	90 (0)

[a] Scaling factors used: TeF7⁻, stretching modes = 0.9293, deformation modes = 0.8810; IF7, all modes = 0.9320; XeF7⁺, all modes = 0.93. [b] Scaling used: stretching modes, +38 cm⁻¹; deformation modes, −38 cm⁻¹; for the scaling, ν_9 was treated as the deformation mode and ν_{10} as the stretching mode in agreement with their PED. [c] Scaling used: stretching modes, +30 cm⁻¹; deformation modes, −10 cm⁻¹; ν_9 and ν_{10} are almost equal mixtures of stretching and bending and both were scaled as stretching modes. [d] Scaling used: stretching modes, +35 cm⁻¹; deformation modes, −15 cm⁻¹; ν_9 and ν_{10} were both scaled as stretching modes.
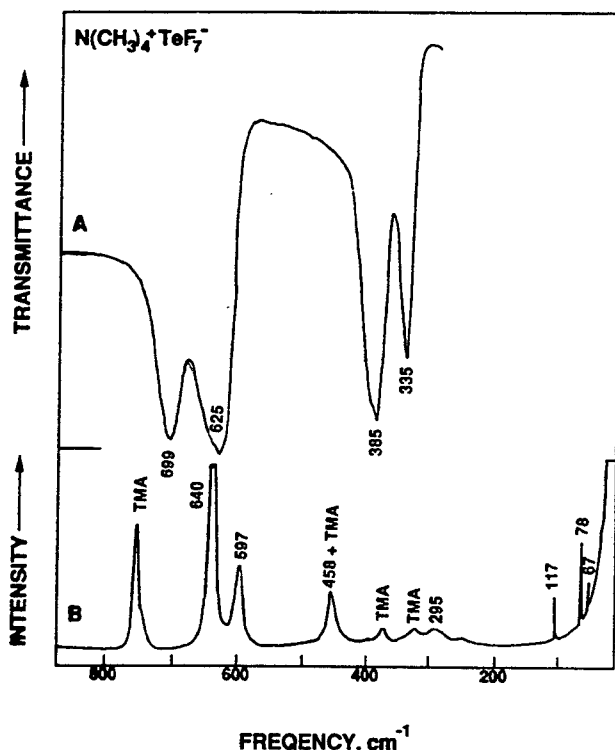
Figure 3. Infrared (trace A) and Raman (trace B) spectra of solid N(CH₃)₄TeF7 recorded at room temperature. The Raman bands marked by TMA are due to the N(CH₃)₄⁺ cation.

two three-center 4-electron bonds to a six-center 10-electron bond system), as has been demonstrated by recent ab initio calculations.[4] If the ideas behind the above ¹⁹F shift observation are extrapolated to other pentagonal bipyramidal fluoro anions, then it can be anticipated that the F_{ax} environment of TeF7⁻ will have an ¹⁹F chemical shift close to that of TeF₆ (i.e., −51.3 ppm). Substitution of this value and the observed average ¹⁹F chemical shift for TeF7⁻ into eq 2 allows the chemical shift of F_{eq} to be estimated as 43 ppm. A similar calculation may be performed for IF7 by using the observed average ¹⁹F chemical shift for IF7 [δ(¹⁹F), 172

ppm][44] and assuming that $\delta(F_{ax})$ will be close to the ¹⁹F chemical shift of IF6⁺ [δ(¹⁹F), 73 ppm].[45] This yields the ¹⁹F chemical shift for the F_{eq} environment of IF7 as 212 ppm.

The magnitude of the one-bond ¹²⁵Te–¹⁹F coupling constant drops from 3746 Hz in TeF₆ to 2876 Hz in TeF7⁻. The latter represents the average value of the $^1J(^{125}Te–^{19}F_{ax})$ and $^1J(^{125}Te–^{19}F_{eq})$ couplings, and its smaller magnitude probably reflects a correspondingly small value for $^1J(^{125}Te–^{19}F_{eq})$ arising from the weaker, more polar Te–F_{eq} bonds in the TeF7⁻ anion.

Vibrational Spectra of TeF7⁻. The infrared and Raman spectra of solid N(CH₃)₄TeF7 are shown in Figure 3. In addition to the bands due to TeF7⁻, that are denoted in Figure 3 by their frequency values, bands due to the N(CH₃)₄⁺ cation have been observed, which are denoted by TMA. Since the vibrational spectra of N(CH₃)₄⁺ are well-known and, for N(CH₃)₄TeF7, are completely analogous to those previously reported and analyzed for the N(CH₃)₄⁺ salts of F⁻,[19] HF₂⁻,[46] XeF₅⁻,[6] IOF₆⁻,[4] TeOF₅⁻,[10] TeOF₆²⁻,[10] or N₃⁻,[47] only the bands due to TeF7⁻ need to be analyzed. This goal was accomplished by a comparison of the observed spectra with those[3] of isoelectronic IF7 and those calculated for the isoelectronic series XeF7⁺, IF7, TeF7⁻ by theoretical methods (see Table I).

Theoretical Calculations for XeF7⁺, IF7, and TeF7⁻. The electronic structure calculations were done by both ab initio molecular orbital and density functional theories. The results are summarized in Tables I and II. There is only a small effect of correlation on the energy differences for IF7 and TeF7⁻, but there is a larger effect for XeF7⁺. The size of the correlation correction to the energy difference seems to follow the congestion in the plane with the most congested structure XeF7⁺ having the largest correlation energy effect. It should be noted that the iodine pseudopotential for the self-consistent nonlocal density functional calculation was very difficult to generate due to the presence of "ghost" states.

Since the geometry and vibrational frequencies of IF7 are well established,[3,48] the quality of our calculations can readily be examined. As can be seen from Table II, the use of a norm-

(44) Recorded for this work as a neat sample at 25 °C.
(45) Brownstein, M.; Selig, H. *Inorg. Chem.* **1972**, *11*, 656.
(46) Wilson, W. W.; Christe, K. O.; Feng, J.; Bau, R. *Can. J. Chem.* **1989**, *67*, 1898.
(47) Christe, K. O.; Wilson, W. W.; Bau, R.; Bunte, S. W. *J. Am. Chem. Soc.* **1992**, *114*, 3411.

Heptacoordination: TeF$_7^-$ and XeF$_7^+$ Ions

J. Am. Chem. Soc., Vol. 115, No. 21, 1993 9465

Table II. Observed and Calculated D_{5h} Geometries of TeF$_7^-$, IF$_7$, and XeF$_7^+$

| | TeF$_7^-$ | | | IF$_7$ | | | XeF$_7^+$ | |
| | | calcd | | | calcd | | | calcd | |
	obsd	SCF	NLDFT[a]	obsd	SCF	NLDFT	SCF	NLDFT
r(X–F$_{ax}$), Å	1.790(17)	1.801	1.769	1.781	1.771	1.781	1.773	1.778
r(X–F$_{eq}$), Å	1.832(20)–1.903(39)	1.872	1.864	1.857	1.833	1.856	1.830	1.850

[a] The bond lengths calculated by the NLDFT method are usually slight longer than those obtained by the SCF method. The shorter values calculated by the NLDFT method for TeF$_7^-$ are attributed to our difficulties of obtaining a good pseudopotential for tellurium.

Table III. Total Energies (au), Zero-Point Energies (kcal/mol) and Imaginary Frequencies (cm^{-1}) for the Pentagonal Bipyramidal (PB), Monocapped Trigonal Prismatic (MTP), and Monocapped Octahedral (MO) Structures of TeF$_7^-$, IF$_7$, and XeF$_7^+$

| | MP-2 | SCF | | | NLDFT/BP | |
structure	total energy[a]	total energy	zero-pt energy[b]	imag freq	total energy	imag freq
TeF$_7^-$ (PB)	−705.555 318	−704.187 658	10.46	none	−707.703 843	none
TeF$_7^-$ (MTP)	−705.550 267	−704.181 746	10.47	89	−707.701 802	93
TeF$_7^-$ (MO)	−705.549 676	−704.181 149	10.41	64e	−707.697 625	77e
IF$_7$ (PB)	−708.412 369	−707.033 247	11.34	none	−710.653 843	none
IF$_7$ (MTP)	−708.408 298	−707.027 062	11.38	93	−710.650 508	94
IF$_7$ (MO)	−708.407 948	−707.026 454	11.32	67e	−710.648 087	75e
XeF$_7^+$ (PB)	−711.696 478	−710.267 925	11.54	none	−714.049 856	none
XeF$_7^+$ (MTP)	−711.690 749	−710.258 962	11.49	108	−714.044 235	99
XeF$_7^+$ (MO)	−711.690 450	−710.258 116	11.42	78e	−714.042 066	79e

[a] Valence electrons only. [b] Scaled by 0.9.

Table IV. Relative Energies (kcal/mol) for the Pentagonal Bipyramidal (PB), Monocapped Trigonal Prismatic (MTP), and Monocapped Octahedral (MO) Structures of TeF$_7^-$, IF$_7$, and XeF$_7^+$.

structure	MP-2	SCF	NLDFT/BP
TeF$_7^-$ (PB)	0	0	0
TeF$_7^-$ (MTP)	3.2	3.7	1.3
TeF$_7^-$ (MO)	3.5	4.1	3.9
IF$_7$ (PB)	0	0	0
IF$_7$ (MTP)	2.6	3.9	2.1
IF$_7$ (MO)	2.8	4.3	3.6
XeF$_7^+$ (PB)	0	0	0
XeF$_7^+$ (MTP)	3.6	5.6	3.5
XeF$_7^+$ (MO)	3.8	6.2	4.9

conserving pseudopotential for the central atom combined with the exchange potential of Becke[37] and the nonlocal correlation functional of Perdew[38] at the self-consistent nonlocal level (NLDFT/BP) exactly duplicates the experimental geometry of IF$_7$, while the ab initio SCF calculations using effective core potentials also result in a geometry which is close to the observed one. The scaled calculated frequencies obtained by both methods are also in excellent agreement with each other and the experimental values (see Table I) and demonstrate the quality of both types of calculations. The agreement between the scaled SCF and NLDFT/BP frequencies is also very good for TeF$_7^-$ and XeF$_7^+$ (see Table I), and for TeF$_7^-$, the calculated frequencies duplicate well the observed ones.

As has been pointed out already in the Introduction, three structures which are very close in energy[15] exist for these heptacoordinated compounds. It was therefore of interest to calculate the total and relative energies of these structures (see Tables III and IV) and to determine their nature on the corresponding potential energy surfaces. Our results show that for all three members of the XeF$_7^+$, IF$_7$, TeF$_7^-$ series the pentagonal bipyramid is the minimum energy structure, followed by the monocapped trigonal prism and the monocapped octahedron. Furthermore, they show that with increasing hardness, i.e., on going from the TeF$_7^-$ anion to the smaller IF$_7$ molecule and XeF$_7^+$ cation, the energy gaps between the pentagonal bipyramid and the monocapped trigonal prism become larger and not smaller, as predicted by the energy law (1) of repelling points on a

sphere.[13–15] This confirms our previously reached conclusion[3,4] that the pentagonal bipyramidal minimum energy structure of these heptacoordinated main group fluorides is not dictated by the hardness of the valence shell electron pair repulsion potential but by the geometry of the valence electron orbitals on the central atom.

Furthermore, our results show that the monocapped octahedron possesses a degenerate imaginary frequency and thus cannot be a transition state. The monocapped trigonal prism has only one imaginary frequency and, thus, is a transition state. Examination of the motion exhibited by the mode with the imaginary frequency shows that it is the motion expected for converting an axial F into an equatorial F. In fact, for XeF$_7^+$, if the convergence is tightened in the geometry optimization, the monocapped trigonal prism can relax to the pentagonal bipyramid. The small energy differences between the three lowest energy structures are in accord with the NMR experiments in which only one type of fluorine was observed, suggesting a low energy barrier toward axial–equatorial ligand exchange.

Normal Coordinate Analysis. The above given results from the theoretical calculations and their close agreement with the experimental vibrational spectra firmly establish their assignments. Inspection of Table I shows the expected frequency trends, i.e., a significant frequency increase with decreasing negative charge on the fluorine ligands which, on going from IF$_7$ to XeF$_7^+$, is partially counteracted by the fact that Xe–F bonds are generally weaker than the corresponding I–F bonds. The assignments for TeF$_7^-$ given in Table I differ for ν_1, ν_2, ν_9, and ν_{10} from those tentatively made[7] in the absence of theoretical calculations.

A particularly interesting and originally most perplexing problem was making the assignments in the A$_1'$ block. This block contains only two modes, the symmetric axial and the symmetric equatorial stretching modes, ν_1 and ν_2, respectively. Since their motions are orthogonal ($G_{12} = 0$) and the central atom is much heavier than the fluorine ligands, the two vibrations were expected to be highly characteristic and analogous for IF$_7$ and TeF$_7^-$. However, the observed Raman bands (i.e., IF$_7$, 676 cm^{-1} (Raman intensity of 2), 635 cm^{-1} (Raman intensity of 10); TeF$_7^-$, 640 cm^{-1} (Raman intensity of 10), 597 cm^{-1} (Raman intensity of 2.6)) show that either their relative frequencies or their intensities are reversed. Since generally the relative intensities are the more reliable guide for making assignments, we had assigned in our preliminary note[7] the more intense Raman bands, at 635 cm^{-1}

(48) Adams, W. J.; Bradford Thompson, H.; Bartell, L. S. *J. Chem. Phys.* **1970**, *53*, 4040.

9466 *J. Am. Chem. Soc., Vol. 115, No. 21, 1993*

Christe et al.

Table V. Scaled SCF Force Fields[a] of the Isoelectric Series TeF_7^-, IF_7, XeF_7^+

assignment		freq, cm^{-1}	symmetry force constants	PED	freq, cm^{-1}	symmetry force constants	PED	freq, cm^{-1}	symmetry force constants	PED
		TeF$_7^-$			**IF$_7$**			**XeF$_7^+$**		
A_1'	ν_1	644.6	$F_{11} = 4.460$ $F_{12} = 0.304$	$72S_1 + 28S_2$	673	$F_{11} = 5.063$ $F_{12} = -0.0058$	$100S_1$	681.6	$F_{11} = 5.134$ $F_{12} = -0.218$	$92S_1 + 8S_2$
	ν_2	595.7	$F_{22} = 4.160$	$72S_2 + 28S_1$	644	$F_{22} = 4.651$	$100S_2$	625.8	$F_{22} = 4.445$	$92S_2 + 8S_1$
A_2''	ν_3	703.0	$F_{33} = 4.361$ $F_{34} = 0.378$	$93S_3 + 7S_4$	753	$F_{33} = 4.947$ $F_{34} = 0.342$	$92S_3 + 8S_4$	757.1	$F_{33} = 4.958$ $F_{34} = 0.206$	$91S_3 + 9S_4$
	ν_4	336.7	$F_{44} = 1.413$	$100S_4$	368	$F_{44} = 1.624$	$100S_4$	361.6	$F_{44} = 1.582$	$100S_4$
E_1'	ν_5	618.4	$F_{55} = 3.429$ $F_{56} = -1.261$ $F_{57} = 0.278$	$98S_5 + 2S_7$	681	$F_{55} = 4.105$ $F_{56} = -1.427$ $F_{57} = 0.231$	$97S_5 + 3S_7$	688.1	$F_{55} = 4.162$ $F_{56} = -1.319$ $F_{57} = 0.126$	$95S_5 + 4S_6 + 1S_7$
	ν_6	387.7	$F_{66} = 3.137$ $F_{67} = -0.300$	$56S_6 + 35S_7 + 9S_5$	441	$F_{66} = 3.879$ $F_{67} = -0.318$	$62S_6 + 33S_7 + 5S_5$	438.6	$F_{66} = 3.799$ $F_{67} = -0.276$	$64S_6 + 33S_7 + 3S_5$
	ν_7	236.5	$F_{77} = 0.828$	$92S_7 + 8S_6$	265	$F_{77} = 0.980$	$93S_7 + 7S_6$	270.1	$F_{77} = 1.021$	$92S_7 + 7S_6 + 1S_5$
E_1''	ν_8	291.4	$F_{88} = 0.708$	$100S_8$	320	$F_{88} = 0.823$	$100S_8$	318.4	$F_{88} = 0.815$	$100S_8$
E_2'	ν_9	521.1	$F_{99} = 2.218$ $F_{9,10} = 0.468$	$77S_{10} + 23S_9$	605	$F_{99} = 3.436$ $F_{9,10} = 0.531$	$57S_{10} + 43S_9$	621.1	$F_{99} = 3.976$ $F_{9,10} = 0.462$	$68S_9 + 32S_{10}$
	ν_{10}	442.5	$F_{10,10} = 3.007$	$76S_9 + 24S_{10}$	515	$F_{10,10} = 3.375$	$61S_9 + 39S_{10}$	541.0	$F_{10,10} = 3.334$	$70S_{10} + 30S_9$
E_2''	ν_{11}	52.9	$F_{11,11} = 0.0548$	$100S_{11}$	59	$F_{11,11} = 0.0647$	$100S_{11}$	81.6	$F_{11,11} = 0.125$	$100S_{11}$

[a] The symmetry coordinates are identical to those used in ref 8 for IF_7; i.e. S_1 = sym ax stretch, S_2 = sym eq stretch, S_9 = asym eq stretch, S_{10} = δ asym XF_5 in-plane. Stretching force constants in mdyn/Å, deformation constants in mdyn Å/rad², and stretch–bend interaction constants in mdyn/rad. The following scaling factors were used for the force constants. TeF_7^-: stretching force constants = $(0.9293)^2 = 0.8636$; deformation constants = $(0.881)^2 = 0.776\ 16$; stretch–bend interaction constants = $(0.9293 \times 0.881) = 0.8187$. IF_7: all constants = $(0.932)^2 = 0.8686$. XeF_7^+: all constants = $(0.93)^2 = (0.8649)$.

Table VI. Detailed Normal Coordinate Analysis of the A_1' Blocks of TeF_7^-, IF_7, and XeF_7^+

	TeF$_7^-$		**IF$_7$**		**XeF$_7^+$**	
	ν_1	ν_2	ν_1	ν_2	ν_1	ν_2
calcd freq, cm^{-1}	644	595.7	673	644	681.6	625.8
obsd rel Ra intens	10	2.6	2	10	---	---
interaction force constant F_{12} (mdyn/Å)	+0.304		-0.006		-0.218	
potential energy distribution (%)	72 axial str. + 28 equat. str.	72 equat. str. + 28 axial str.	100 axial str.	100 equat. str.	92 axial str. + 8 equat. str.	92 equat. str. + 8 axial str.
internal coordinate displacement vectors	$0.849\ S_1 +$ $0.528\ S_2$	$0.849\ S_2 -$ $0.528\ S_1$	$1.0\ S_1$	$1.0\ S_2$	$0.960\ S_1 -$ $0.278\ S_2$	$0.960\ S_2 +$ $0.278\ S_1$
approximate mode description	in-phase combination of S_1 and S_2	out-of-phase combination of S_2 and S_1	pure S_1	pure S_2	out-of-phase combination of S_1 and S_2	in-phase combination of S_2 and S_1
qualitative estimate of rel Ra intens	$2(0.849) +$ $5(0.528) =$ 4.329	$5(0.849) -$ $2(0.528) =$ 3.189	$2(1) = 2$	$5(1) = 5$	$2(0.96) -$ $5(0.278) =$ 0.53	$5(0.96) +$ $2(0.278) =$ 5.356

in IF_7 and 640 cm^{-1} in TeF_7^-, to the symmetric equatorial stretch and the less intense ones, at 676 cm^{-1} in IF_7 and 597 cm^{-1} in TeF_7^-, to the symmetric axial stretch. The results of our ab initio force field calculations and normal coordinate analysis (see Table V), however, clearly show that in IF_7 and TeF_7^- the 676 and 640 cm^{-1} Raman bands, respectively, are the symmetric axial stretches and the 635 and 597 cm^{-1} bands, respectively, are the symmetric equatorial stretches. Consequently, it is the relative Raman intensities of ν_1 and ν_2 and not their frequencies that are reversed.

This intensity reversal can be rationalized by a more detailed inspection of the normal coordinate analysis data for the A_1' blocks of XeF_7^+, IF_7, and TeF_7^- (see Table VI). In IF_7, the F_{12} interaction force constant is essentially zero, ν_1 and ν_2 are pure axial and equatorial stretching, respectively, and the equatorial stretching mode, which involves five fluorine ligands, has a higher Raman intensity than the axial one, which involves only two fluorines. In TeF_7^-, the F_{12} interaction force constant has a substantial, positive value which results in ν_1 and ν_2 becoming 72/28% and 28/72% mixtures of axial and equatorial stretching, respectively. The signs of the internal displacement vectors show

that, in TeF_7^-, ν_1 is an in-phase combination of the symmetry coordinates S_1 and S_2 and ν_2 their out-of-phase combination. The lower frequency and energy of the out-of-phase combination is in accord with our expectations from mutual ligand repulsion arguments that a shortening of the equatorial bonds should result in increased repulsion and, therefore, in a lengthening of the axial bond. This same feature has previously been found and discussed for the A_1' block of the closely related, trigonal bipyramidal PF_5 molecule of D_{3h} symmetry.[30]

For XeF_7^+, the situation is reversed, i.e., F_{12} becomes negative and, as a result, axial stretching encourages equatorial stretching. The exact nature of this effect, which is opposite to the mutual repulsion effect, is not entirely clear at this time but is believed to be electronic in nature. It seems to increase with an increasing positive charge on the species, i.e., in the direction $TeF_7^- \rightarrow IF_7 \rightarrow XeF_7^+$.

The internal relationships between the diagonal and interaction force constants, the potential energy distribution, and in-phase and out-of-phase combinations of the symmetry coordinates for the A_1' blocks of these D_{nh} bipyramidal molecules can be more

Heptacoordination: TeF$_7^-$ and XeF$_7^+$ Ions

J. Am. Chem. Soc., Vol. 115, No. 21, 1993 9467

fully understood by an inspection of the plots of the diagonal force constants F_{11} and F_{22} as functions of their interaction
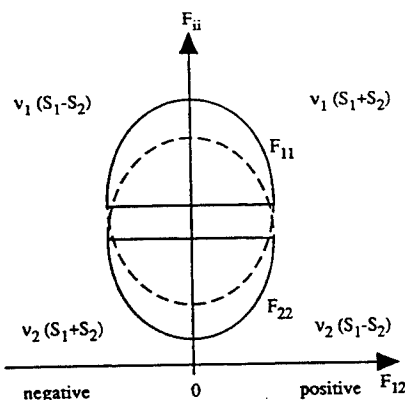
constant F_{12}. The possible solutions of F_{11} and F_{22} have the form of ellipses whose centers for the off-diagonal kinetic energy term G_{12} being zero, as is the case for these D_{nh} molecules,[49] are located on the F_{ii} axis.[50]

From this graph, it is obvious that, for $G_{12} = 0$, F_{12} does not also automatically become zero, as has sometimes been incorrectly assumed in previous force field calculations. If $F_{12} = 0$, then F_{11} and F_{22} are a maximum and a minimum, respectively, and ν_1 and ν_2 are 100% characteristic vibrations, i.e., no mixing of the symmetry coordinates occurs, as is the case for IF$_7$. If F_{12} is nonzero, the numerical values of F_{11} and F_{22} depend only on the size of F_{12} but not on its sign. The sign of F_{12}, however, determines whether ν_1 or ν_2 is the inphase combination of the symmetry coordinates S_1 and S_2 and, therefore, determines their relative Raman intensities. A negtive F_{12} value results in the higher frequency vibration being the out-of-phase combination of S_1 and S_2 and having a decreased Raman intensity. This logic is confirmed by the rough estimates of the relative Raman intensities of ν_1 and ν_2, made in Table VI under the assumption that the polarizabilities of the equatorial and the axial fluorine ligands are identical. These rough estimates are in reasonable agreement with the relative Raman intensities observed for TeF$_7^-$ and IF$_7$

(49) Ohwada, K. *Spectrochim. Acta, Part A* **1981**, 37A, 873.
(50) Sawodny, W. *J. Mol. Spectrosc.* **1969**, 30, 56.

and confirm the observed intensity reversal. Unfortunately, the ultimate question, what makes F_{12} change its sign on going from TeF$_7^-$ to XeF$_7^+$, cannot be answered with confidence at this time.

One final observation for the XeF$_7^-$, IF$_7$, TeF$_7^+$ series concerns the identities of the antisymmetric equatorial stretching mode ν_9 and the equatorial in-plane deformation ν_{10}. As can be seen from the potential energy distributions of Table V, these two vibrations have similar frequencies and are strongly mixed. In TeF$_7^-$, the stretching vibration has the lower frequency, whereas in XeF$_7^+$, it has the higher frequency. The fact that in TeF$_7^-$ the frequency and antisymmetric stretching force constants drop below those of the antisymmetric, in-plane deformation can be explained by the lengthening and weakening of its equatorial Te–F bonds due to the formal negative charge which increases the ionicity of these bonds.

Conclusion

The results of this study show that for all three members of the isoelectronic XeF$_7^+$, IF$_7$, TeF$_7^-$ series the pentagonal bipyramid is the minimum energy structure and the monocapped trigonal prism is a transition state. This finding supports our previous proposal[3,4,10] that the pronounced preference of heptacoordinated main-group element compounds for pentagonal bipyramidal structures is not caused by their relative hardness but is best explained by the geometry of the valence electron orbitals of their central atoms. This geometry is the result of a bonding scheme involving a planar, delocalized p$_{xy}$ hybrid of the central atom for the formation of five equatorial, semi-ionic, six-center 10-electron bonds and an sp$_z$ hybrid for the formation of two mainly covalent axial bonds.[3] In addition, the Raman intensities in the A$_1'$ block of TeF$_7^-$ and IF$_7$ exhibit an unprecedented intensity reversal, which suggests the existence of an electronic effect which counteracts the intuitively obvious ligand–ligand repulsion effect of axial bond shortening encouraging equatorial bond lengthening.

9655

On the Structure of IOF$_5$

Karl O. Christe,[*,†] **Earl C. Curtis,**[†] **and David A. Dixon**[‡]

Contribution from Rocketdyne, A Division of Rockwell International, Canoga Park, California 91309, and Central Research and Development Department, E. I. du Pont de Nemours and Company, Inc., Experimental Station, Wilmington, Delaware 19880-0328

Received March 25, 1993[●]

Abstract: Ab initio and density functional theory calculations were carried out for IOF$_5$ and, together with experimental and ab initio data for isoelectronic TeOF$_5^-$, suggest that the axial and the equatorial I–F bonds of IOF$_5$ are of comparable lengths and that the O–I–F$_{eq}$ bond angle is close to 97.2°. Using these two constraints and the previously published I^{16}OF$_5$ and I^{18}OF$_5$ microwave data, the structure of IOF$_5$ was determined as $rI–O = 1.725$ Å, $rI–F_{ax} \equiv rI–F_{eq} = 1.826$ Å, and $\angle OIF_{eq} = 97.2°$. The finding that the axial I–F bond length is comparable to the equatorial one eliminates the need for invoking for IOF$_5$ either a "secondary relaxation effect" which lengthens the fluorine bond in the trans position to a doubly bonded oxygen ligand or a "trans effect" which shortens this bond.

Introduction

The high symmetry, C_{4v}, of IOF$_5$ renders its structure determination very difficult. Thus, microwave spectroscopy provides only one rotational constant[1–3] because there is no dipole moment change on rotation about the fourfold z-axis and an identical change on rotation about either the x- or y-axes. Furthermore, its nearly identical bond distances result in a severe overlap of peaks in the radial distribution curve from the electron diffraction data.[4] In spite of these enormous difficulties, Bartell, Clippard, and Jacob reported[4] in 1976, on the basis of a combined electron diffraction–microwave study, the following structure for IOF$_5$.
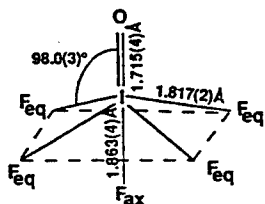
The surprising and unusual feature of this structure is the axial I–F bond being 0.046 Å longer than the equatorial ones. To explain this feature, Bartell and co-workers invoked a novel "secondary relaxation effect" that greatly outweighs the primary repulsion effects. The assumption that a repulsion effect on a bond which is two bonds removed from the repelling ligand should be so much stronger than that exercised on the neighboring bonds is very difficult to rationalize. It was also contrary to the results from a previous force field calculation[5] by Smith and Begun, who concluded that the equatorial and axial I–F bonds in IOF$_5$ were of about equal strength. To counter this force field argument, Bartell and co-workers refitted[4] the observed vibrational frequencies[5,6] with their own force field that provided a force constant for the axial I–F bond which was lower than that of the equatorial bonds. However, in view of the underdetermined nature of these force fields, the observed frequencies can be fitted with a wide

range of force constants and, therefore, provide no compelling evidence either for or against the structural model proposed[4] by Bartell.

In the course of our recent experimental and theoretical structural studies of the IOF$_6^-$[7] and TeOF$_5^-$[8] anions, it became apparent that Bartell's previous structure[4] for IOF$_5$ might need correction. In this paper we analyze the previous data and, in concert with new ab initio and density functional theory calculations, propose a revised structure for IOF$_5$.

Results and Discussion

I. Electron Structure Calculations. A. Computational Methods. The electronic structure calculations were done at the ab initio molecular orbital level using an effective core potential (ECP) for the core electrons on iodine. The valence basis set is of polarized double-ζ quality. The fluorine and oxygen basis sets are from Dunning and Hay[9] and the ECP from Hay and Wadt,[10] including relativistic corrections and augmented by a d function on I with an exponent of 0.266.[11] The geometries were optimized by using analytic gradient techniques[12] at the SCF and MP-2 levels,[13] and the force fields were calculated analytically.[14,15] The SCF/ECP calculations were done with the program GRADSCF,[16] as implemented on a Cray YMP computer system. Because the

† Rocketdyne.
‡ E. I. du Pont de Nemours and Company, Inc.
● Abstract published in *Advance ACS Abstracts*, September 15, 1993.
(1) Pierce, S. B.; Cornwell, C. D. *J. Chem. Phys.* **1967**, *47*, 1731.
(2) Brier, P. N.; Winrow, M. J. *J. Mol. Spectrosc.* **1984**, *107*, 21.
(3) Brier, P. N. *J. Mol. Spectrosc.* **1987**, *125*, 233.
(4) Bartell, L. S.; Clippard, F. B.; Jacob, E. J. *Inorg. Chem.* **1976**, *15*, 3009.
(5) Smith, D. F.; Begun, G. M. *J. Chem. Phys.* **1965**, *43*, 2001.
(6) Holloway, J. H.; Selig, H.; Claassen, H. H. *J. Chem. Phys.* **1971**, *54*, 4305.

(7) Christe, K. O.; Dixon, D. A.; Mahjoub, A. R.; Mercier, H. P. A.; Sanders, J. C. P.; Seppelt, K.; Schrobilgen, G. J.; Wilson, W. W. *J. Am. Chem. Soc.* **1993**, *115*, 2696.
(8) Christe, K. O.; Dixon, D. A.; Sanders, J. C. P.; Schrobilgen, G. J.; Wilson, W. W. *Inorg. Chem.*, in press.
(9) Dunning, T. H., Jr.; Hay, P. J. In *Methods of Electronic Structure Theory*; Schaefer, H. F., III, Ed.; Plenum Press: New York, 1977; Chapter 1.
(10) Hay, P. J.; Wadt, W. R. *J. Chem. Phys.* **1985**, *82*, 299.
(11) Huzinaga, S.; Andzelm, J.; Klobukowski, M.; Radzio, E.; Sakai, Y.; Tatasaki, H. *Gaussian Basis Sets of Molecular Calculations*; Elsevier: Amsterdam, The Netherlands, 1984.
(12) (a) Komornicki, A.; Ishida, K.; Morokuma, K.; Ditchfield, R.; Conrad, M. *Chem. Phys. Lett.* **1977**, *45*, 595. (b) McIver, J. W., Jr.; Komornicki, A. *Chem. Phys. Lett.* **1971**, *10*, 202. (c) Pulay, P. In *Applications of Electronic Structure Theory*; Schaefer, H. F., III, Ed.; Plenum Press: New York, 1977; p 153.
(13) (a) Moller, C.; Plesset, M. S. *Phys. Rev.* **1934**, *46*, 618. (b) Pople, J. A.; Binkley, J. S.; Seeger, R. *Int. J. Quantum Chem. Symp.* **1976**, *10*, 1. Pople, J. A.; Krishnan, R.; Schlegel, H. B.; Binkley, J. S. *Int. J. Quantum Chem. Symp.* **1979**, *13*, 325. Handy, N. C.; Schaefer, H. F., III. *J. Chem. Phys.* **1984**, *81*, 5031.
(14) (a) King, H. F.; Komornicki, A. *J. Chem. Phys.* **1986**, *84*, 5465. (b) King, H. F.; Komornicki, A. In *Geometrical Derivatives of Energy Surfaces and Molecular Properties*; Jorgenson, P., Simons, J., Eds.; NATO ASI Series C, Vol. 106, D; Reidel: Dordrecht, The Netherlands, 1986; p 207.
(15) Breidung, J.; Thiel, W.; Komornicki, A. *Chem. Phys. Lett.* **1988**, *153*, 76.
(16) GRADSCF is an ab initio program system designed and written by A. Komornicki at Polyatomics Research.

Table I. Comparison of the Calculated and Observed Geometries of IOF_5 and Isoelectronic $TeOF_5^-$

| | IOF_5 | | | | $TeOF_5^-$ | |
| | calcd | | | | | |
	SCF/ECP	MP-2	NLDFT/BP	obsd[a]	calcd[b] SCF/ECP	obsd[c]
$rX{-}O$ (Å)	1.706	1.729	1.671	1.725	1.738	1.736(3)
$rX{-}F_{ax}$ (Å)	1.797	1.865	1.815	1.826	1.835	1.854(2)
$rX{-}F_{eq}$ (Å)	1.798	1.866	1.812	1.826	1.838	1.853(2)
$\angle OXF_{eq}$ (deg)	97.24	97.4	96.60	97.2	97.44	95.2(1)

[a] Calculated from the microwave data assuming $\angle OIF_{eq} = 97.2°$ and $rI{-}F_{ax} = rI{-}F_{eq}$. [b] Data from ref 8. [c] Data from ref 28.

calculated vibrational frequencies and force constants are somewhat too high due to the neglect of electron correlation and of anharmonicity, the calculated values require scaling. Since the deformation modes may be more strongly affected by these bond length deviations than the stretching modes, it is often advantageous to use different empirical scaling factors for the stretching and the deformation modes.[17]

In order to investigate whether there are any effects of electron correlation on the molecular parameters, we·reoptimized the geometry of IOF_5 at the MP-2 level using the program system Gaussian 92[18] using the ECP and basis set described above. The geometry was also reoptimized at the density functional theory (DFT)[19] level, as this·level has been shown[20] to yield a good structure for IF_7. The calculations were done with the program DGauss,[21] which employs Gaussian orbitals on a Cray YMP computer. A norm-conserving pseudopotential[22] was used for I following the work of Troullier and Martins.[23] The valence basis set for I is [42/32/1] with a fitting basis set of [7/5]. The basis set for F and O is of polarized triple-ζ valence quality and has the form [7111/411/1] with a [7/3/3] fitting basis.[24] The calculations were done at the self-consistent nonlocal level with the local potential of Vosko, Wilk, and Nusair[25] and with the nonlocal exchange potential of Becke[26] together with the nonlocal correlation functional of Perdew[27] (NLDFT/BP). The geometries were optimized by using analytical gradients.[21]

B. Calculated Geometry of IOF_5. The geometry of IOF_5 was calculated at the uncorrelated SCF/ECP and the correlated MP-2 and NLDFT/BP levels of theory (see Table I). The difference between the axial and the equatorial I–F bond lengths is very small, i.e., about 0.001 Å, for both the uncorrelated and the correlated ab initio calculations and, hence, is not noticeably influenced by correlation. Similarly, the correlated nonlocal

(17) Marsden, C. J. *J. Chem. Phys.* **1987**, *87*, 6626.

(18) Frisch, M. J.; Trucks, G. W.; Head-Gordon, M.; Gill, P. M. W.; Wong, M. W.; Foresman, J. B.; Johnson, B. G.; Schlegel, H. B.; Robb, M. A.; Replogle, E. S.; Gomperts, R.; Andres, J. L.; Raghavachari, K.; Binkley, J. S.; Gonzales, C.; Martin, R. L.; Fox, D. J.; DeFrees, D. J.; Baker, J.; Stewart, J. J. P.; Pople, J. A. *Gaussian 92*; Gaussian Inc.: Pittsburgh, PA, 1992.

(19) Parr, R. G.; Yang, W. *Density Functional Theory of Atoms and Molecules*; Oxford University Press: New York, 1989.

(20) Christe, K. O.; Dixon, D. A.; Sanders, J. C. P.; Schrobilgen, G. J.; Wilson, W. W. *J. Am. Chem. Soc.*, in press.

(21) (a) Andzelm, J.; Wimmer, E.; Salahub, D. R. In *The Challenge of d and f Electrons: Theory and Computation*; Salahub, D. R., Zerner, M. C., Eds.; ACS Symposium Series 394; American Chemical Society: Washington, DC, 1989; p 228. (b) Andzelm, J. In *Density Functional Methods in Chemistry*; Labanowski, J., Andzelm, J., Eds.; Springer-Verlag: New York, 1991; p 101. (c) Andzelm, J. W.; Wimmer, E. *J. Chem. Phys.* **1992**, *96*, 1280. DGauss is a local density functional program available via the Cray Research Unichem Project, Cray Research, Eagan, MN, 1993.

(22) Chen, H.; Kraskowski, M.; Fitzgerald, G. *J. Chem. Phys.*, in press.

(23) Troullier, N.; Martins, J. L. *Phys. Rev. B* **1991**, *43*, 1993.

(24) Godbout, N.; Salahub, D. R.; Andzelm, J.; Wimmer, E. *Can. J. Chem.* **1992**, *70*, 560.

(25) Vosko, S. J.; Wilk, L.; Nusair, M. *Can. J. Phys.* **1980**, *58*, 1200.

(26) (a) Becke, A. D. *Phys. Rev. A* **1988**, *38*, 3098. (b) Becke, A. D. In *The Challenge of d and f Electrons: Theory and Computation*; Salahub, D. R., Zerner, M. C., Eds.; ACS Symposium Series 394; American Chemical Society: Washington, DC, 1989; p 166. (c) Becke, A. D. *Int. J. Quantum Chem. Quantum. Chem. Symp.* **1989**, *23*, 599.

(27) Perdew, J. P. *Phys. Rev. B* **1986**, *33*, 8822.

density functional theory calculation also resulted in axial and equatorial I–F bond lengths which differ by only 0.003 Å. The IOF_{eq} bond angles calculated at these three levels of theory are also very similar. Therefore, the assumptions of $rIF_{ax} = rIF_{eq}$ and $\angle OIF_{eq} \approx 97.2°$ for IOF_5 are well supported by the electronic structure calculations at all three levels of theory and can be used as constraints to calculate the I–O and I–F bond lengths from the published $I^{16}OF_5$ and $I^{18}OF_5$ microwave data[1,2] (see below). Inspection of Table I reveals that, as for IF_7,[20] the NLDFT/BP calculation duplicates best the experimental I–F bond lengths, while the corresponding SCF/ECP and MP-2 values are about 0.03 Å shorter and longer, respectively. The observed I–O bond length is best duplicated by the MP-2 calculation, while the SCF/ECP calculation results in a value which is 0.019 Å too short. This is in accord with our previous findings for the IOF_6^- [7] and the isoelectronic $TeOF_5^-$ [8] anions (see Table I). The shortness of the I–O bond in the NLDFT/BP calculation for IOF_5 is unexpected and suggests that there might be a minor problem with the choice of the basis set.

C. Calculated and Observed Vibrational Frequencies and Infrared Intensities. Another crucial test for the quality of our theoretical calculations for IOF_5 is the agreement between calculated and observed vibrational frequencies and infrared intensities. Since the deviations of the I–O and the I–F bond lengths from the observed ones were most uniform for the SCF/ECP data set, the vibrational frequencies and infrared intensities were calculated by this method and scaled to correct for the usual overestimation of the bond lengths. The results are summarized in Table II and show that the agreement between calculated, and observed values is excellent, particular for the IF_5 part of the molecule. The fact that the I=O stretching mode required its own scaling factor and, contrary to the I–F modes, resulted in a low-frequency value has been found by us for other oxofluorides, such as IOF_6^-,[7] and appears to be systematic for this level of calculation for doubly bonded oxygen ligands.

D. Normal Coordinate Analysis and Force Constants. Since the ab initio SCF/ECP method used here results in a fully determined force field with off-diagonal symmetry force constants that are expected to be very close to those of the general valence force field, the SCF/ECP force field and, in particular, the internal stretching force constants for the axial and the equatorial I–F bonds can be expected to be more reliable than the published,[4,5] underdetermined values. Our scaled force field and its potential energy distributions are summarized in Table III. As can be seen, the two most crucial internal force constants, i.e. the I–F_{ax} and I–F_{eq} stretching force constants, have values of 4.62 and 4.60 mdyn/Å, respectively. This result, together with the calculated and observed[28] $TeOF_5^-$ bond distances of Table I, supports our contention that the axial X–F bonds in these XOF_5 species of C_{4v} symmetry are either equal to or slightly shorter and stronger than the equatorial ones.

II. Comparison with Related Molecules and Ions. The compound that is most closely related to IOF_5 and is best characterized is the isoelectronic $TeOF_5^-$ anion.[8,28] Its geometry is known from a crystal structure determination[28] and agrees well with that calculated at the SCF/ECP level of theory (see Table I), keeping in mind the usual underestimation of the bond lengths at the SCF/ECP level. These data confirm that the equatorial and axial Te–F bonds in $TeOF_5^-$ are, within experimental error, of equal lengths and are closely duplicated by the SCF/ECP calculations. The larger discrepancy between observed and calculated X–O bond length in $TeOF_5^-$ relative to IOF_5 might be attributed to the choices of basis sets and the fact that the calculated distances are for the free gas-phase ion and not an ionic solid which might be influenced by crystal effects. Another known XOF_5^- anion of C_{4v} symmetry is SOF_5^-. Its structure has

(28) Miller, P. K.; Abney, K. D.; Rappé, A. K.; Anderson, O. P.; Strauss, S. H. *Inorg. Chem.* **1988**, *27*, 2255.

Table II. Observed and Calculated Frequencies and Infrared Intensities of IOF_5

point group C_{4v}	assignment	approximate mode description	obsd freq, cm⁻¹, intens		calcd freq^a (IR intens)
			IR gas^b	Ra gas^b	
A_1	ν_1	$\nu I=O$	927.3 s	926.7 s, p	926.7 (57)
	ν_2	$\nu I-F_{ax}$	681.0 s	680.4 vs, p	682.2 (41)
	ν_3	ν sym IF_4 in-phase		640.2 vs, p	638.9 (0.7)
	ν_4	δ umbrella IF_4	362.9 s		367.5 (93)
B_1	ν_5	ν sym IF_4 out-of-phase	not obsd	647 s, dp	644.7 (0)
	ν_6	δ pucker IF_4	not obsd		245.0 (0)
B_2	ν_7	δ sym IF_4 in-plane	not obsd	307 m, dp	303.3 (0)
E	ν_8	ν asym IF_4	710.3 vs	712 w, dp	714.2 (187)
	ν_9	δFIF_4	372.2 s	375 m, dp	378.4 (40)
	ν_{10}	δOIF_4	343 s	341 s, dp	341.6 (49)
	ν_{11}	δ asym IF_4 in-plane	204.8 vw	208 vw, dp	206.9 (0)

^{a} The following scaling factors were used: ν_1, 1.030; remaining stretching modes, 0.943 65; deformation modes, 0.903 64. ^{b} Data from ref 6.

Table III. Ab Initio Force Field^{a-c} of IOF_5

point group C_{4v}	assignment	calcd freq, cm⁻¹	symmetry force constants	PED (%)
A_1	ν_1	926.7	$F_{11} = f_D = 6.999$ $F_{12} = f_{DR} = 0.495$ $F_{13} = f_{Dr} = -0.141$ $F_{14} = 0.139$	86.7 (S₁) + 7.1 (S₂) + 4.5 (S₄) + 1.7 (S₃)
	ν_2	682.2	$F_{22} = f_R = 4.623$	66.5 (S₂) + 26.6 (S₃) + 5.9 (S₁) + 1.0 (S₄) (symmetric combination of S₂ and S₃)
	ν_3	638.9	$F_{23} = f_{Rr} = 0.202$ $F_{24} = -0.494$ $F_{33} = f_r + 2f_{rr} + f_{rr'} = 4.748$	68.6 (S₃) + 31.4 (S₂) (antisymmetric combination of S₂ and S₃)
	ν_4	367.5	$F_{34} = -0.006$ $F_{44} = \frac{1}{2}(f_\beta + 2f_{\beta\beta} + f_{\beta\beta'} + f_\gamma + 2f_{\gamma\gamma} + f_{\gamma\gamma'} - 2f_{\beta\gamma} - 4f_{\beta\gamma'} - 2f_{\beta\gamma''}) = 1.691$	99.4 (S₄)
B_1	ν_5	644.7	$F_{55} = f_r - 2f_{rr} + f_{rr'} = 4.651$ $F_{56} = 0.006$	100 (S₅)
	ν_6	245.0	$F_{66} = \frac{1}{2}(f_\beta - 2f_{\beta\beta} + f_{\beta\beta'} + f_\gamma - 2f_{\gamma\gamma} + f_{\gamma\gamma'} - 2f_{\beta\gamma} + 4f_{\beta\gamma'} - 2f_{\beta\gamma''}) = 1.085$	100 (S₆)
B_2	ν_7	303.3	$F_{77} = f_\alpha - 2f_{\alpha\alpha} + f_{\alpha\alpha'} = 0.845$	100 (S₇)
E	ν_8	714.2	$F_{88} = f_r - f_{rr'} = 4.493$ $F_{89} = f_{r\beta} - f_{r\beta''} = 0.338$ $F_{8,10} = f_{r\gamma} - r_{r\gamma'} = 0.183$ $F_{8,11} = \sqrt{2}(f_{r\alpha} - f_{r\alpha'}) = 0.113$	93.4 (S₈) + 3.3 (S₁₁) + 2.6 (S₁₀)
	ν_9	378.4	$F_{99} = f_\beta - f_{\beta\beta'} = 1.451$ $F_{9,10} = 0.096$ $F_{9,11} = 0.182$	81.3 (S₉) + 16.7 (S₁₁) + 2.0 (S₁₀)
	ν_{10}	341.6	$F_{10,10} = f_\gamma - f_{\gamma\gamma'} = 0.952$ $F_{10,11} = 0.177$	86.0 (S₁₀) + 10.7 (S₁₁) + 3.1 (S₉)
	ν_{11}	206.9	$F_{11,11} = f_\alpha - f_{\alpha\alpha'} = 0.980$	66.6 (S₁₁) + 22.1 (S₁₀) + 11.2 (S₉)

^{a} Stretching constants in mdyn/Å; deformation constants in (mdyn Å)/rad²; stretch–bend interaction constants in mdyn/rad. ^{b} The following scaling factors were used: $F_{11} = (1.030)^2$; all other stretching force constants = $(0.943\ 65)^2$; deformation force constants = $(0.903\ 64)^2$; stretch–bend interaction constants = 0.943 65 × 0.903 64. ^{c} The missing explicit F matrix terms are complex, angle-dependent expressions and, therefore, are not listed. ^{d} The following internal coordinates were used: I–O = D, I–F$_{ax}$ = R, I–F$_{eq}$ = r, $\angle F_{eq}$–I–F$_{eq}$ = α, $\angle F_{eq}$–I–O = γ, $\angle F_{eq}$–I–F$_{ax}$ = β. ^{e} Internal force constants: f_D = 6.999; f_R = 4.623; f_r = 4.596.

been studied[29] by X-ray diffraction; however, the positions of the oxygen and the fluorine atoms could not be distinguished in the structure, and no conclusive structural parameters were given.

A closely related species is the IOF_6^- anion.[7] Although its pentagonal bipyramidal structure with a congested equatorial plane and formal negative charge result in long, highly ionic, equatorial bonds, its mainly covalent I=O and I—F$_{ax}$ bonds should be only slightly longer than those in IOF_5. Indeed, the observed and calculated bond distances[7] (see Table IV) are again in excellent agreement with our findings for IOF_5 but not with the long IF$_{ax}$ bond of 1.863 Å reported[4] previously for IOF_5. It is very difficult to envision that the addition of a negatively charged fluoride ligand to IOF_5 would shorten the I–F$_{ax}$ bond in the resulting anion by 0.04 Å.

III. Proposed Structure of IOF₅ Derived from a Combination of the Theoretical and Microwave Data. Four parameters are required to define the structure of IOF_5 in C_{4v} symmetry, i.e. the I=O, IF$_{eq}$, and IF$_{ax}$ bond lengths and the OIF$_{eq}$ bond angle.

(29) Heilemann, W.; Mews, R.; Pohl, S.; Sack, W. *Chem. Ber.* **1989**, *122*, 427.

Table IV. Comparison of the Calculated (SCF/ECP) and Observed Geometries of the IOF_5 Molecule and the IOF_6^- Anion

	calcd	obsd	calcd	obsd
$rI-O$ (Å)	1.706	1.725	1.726	1.75–1.77
$rI-F_{ax}$ (Å)	1.797	1.826	1.809	1.82
$rI-F_{eq}$ (Å)	1.798	1.826	1.882	1.88

^{a} Data from ref 7.

Since the microwave data published[1] for $I^{16}OF_5$ and $I^{18}OF_5$ provide two independent rotational constants, two assumptions must be made to solve the IOF_5 structure. Since for gas-phase molecules the theoretical calculations generally predict the bond angles quite accurately and for isoelectronic $TeOF_5^-$ also predicted[8] the bond length difference between axial and equatorial Te–F bonds within experimental error (see Table I), the structure of IOF_5 was

calculated using the two rotational constants from the microwave study[1,2] and the following constraints from our theoretical calculations: $\angle OIF_{ax} \equiv 97.2°$ and $rIF_{ax} \equiv rIF_{eq}$. This combined ab initio–microwave calculation resulted in the following geometry for IOF_5: $rI{=}O = 1.725$ Å; $rIF_{ax} \equiv rIF_{eq} = 1.826$ Å; $\angle OIF_{eq} \equiv 97.2°$. These values agree well with our expectations and compare favorably with those observed for closely related compounds[7] and isoelectronic $TeOF_5^-$.[8,28]

IV. Previous Electron Diffraction Study. Without access to the original electron diffraction data, we were not able to examine the compatibility of our revised structural model with the experimental electron diffraction data.[4] However, several general comments concerning the previous electron diffraction study can be made. (i) The eight internuclear distances of IOF_5 overlap badly, forming only three fully resolved peaks in the radial distribution curve. This adds considerable ambiguity to the interpretation of the electron diffraction results. (ii) The electron diffraction pattern is systematically influenced by dynamic scattering because of the rather deep potential well of the heavy iodine.[30] (iii) Six of the eight internuclear distances are almost identical for our revised and Bartell's original model,[4] with the only significant difference being the partitioning of the axial and the equatorial I–F bond distances. It should be pointed out that the mean I–F bond length of all I–F bonds in Bartell's structure (1.826 Å) is identical to that derived from our study for both the equatorial and the axial I–F bonds and that the I–O bond length and the O–I–F$_{eq}$ bond angle of his model also agree within experimental error with those from our study. Therefore, the electron diffraction data would be in good agreement with our revised structure if the unresolved radial distribution curve peaks for the I–F bond distance are fitted for a single I–F bond distance. (iv) The relatively large deviations found[4] in the radial distribution difference curve between 1.5 and 2.0 Å are also indicative of problems with the previously used partitioning of the I–F bond distances. Therefore, it would be interesting to investigate the compatibility of our revised structure with the experimental electron diffraction data.

V. Conclusions. The results of our theoretical calculations for IOF_5, its normal coordinate analysis and force field, and a comparison with known and well-characterized isoelectronic or closely related species all indicate that the equatorial and axial I–F bonds in IOF_5 are of comparable lengths. This finding eliminates the need for the use of a "secondary relaxation effect"[4] to account for its structure. The results of this study, i.e., I–F$_{ax}$ and I–F$_{eq}$ of IOF_5 having about the same bond length, furthermore show that there is also no need for the use of the opposite, so called "*trans* effect"[31] which supposedly causes a significant shortening of the fluorine bond *trans* to the oxygen ligand. The effect which a doubly bonded oxygen has on a fluorine ligand in the *trans* position is governed by the oxidation state and the effective electronegativity of the central atom. For the so called "*trans* effect", the effective electronegativity of the central atom must be lower than that of the oxygen ligand. Then, the oxygen ligand withdraws electron density from the central atom, which increases the covalency and, hence, the strength of the central atom–fluorine bond. If, however, the effective electronegativity of the central atom is higher than that of oxygen, the oxygen ligand releases electron density to the rest of the molecule. This increases the ionicity of the central atom–fluorine bonds and, hence, weakens them. If the effective electronegativities of the central atom and the oxygen ligand are about the same, as appears to be the case for IOF_5, there should be no noticeable effect.

(30) Bartell, L. S. Private communication.
(31) Shustorovich, E. M.; Buslaev, Yu. A. *Inorg. Chem.* **1976**, *15*, 1142.

The TeOF$_6^{2-}$ Anion: The First Example of a Multiply Charged, Pentagonal Bipyramidal, Main-Group Element AX$_5$YZ Species and the Vibrational Spectra of the TeOF$_5^-$ Anion

Karl O. Christe,[*,†] David A. Dixon,[‡] Jeremy C. P. Sanders,[§] Gary J. Schrobilgen,[*,§] and William W. Wilson[†]

Rocketdyne, A Division of Rockwell International, Canoga Park, California 91309, Department of Chemistry, McMaster University, Hamilton, Ontario L8S 4MI, Canada, and Central Research and Development Department, E. I. du Pont de Nemours and Company, Inc., Experimental Station, Wilmington, Delaware 19880-0328

The new TeOF$_6^{2-}$ anion has been isolated in the form of its tetramethylammonium salt from solutions of N(CH$_3$)$_4$F and N(CH$_3$)$_4$TeOF$_5$ in CH$_3$CN. It was characterized by vibrational spectroscopy, a normal coordinate analysis and ab initio calculations. It is shown that its structure is analogous to that of the recently discovered, isoelectronic IOF$_6^-$ anion which makes it only the second known representative of a pentagonal bipyramidal, main-group element AX$_5$YZ species and the first multiply charged example of such a species. The stretching force constant of the TeF$_5$ part of TeOF$_6^{2-}$ is significantly smaller than that in IOF$_6^-$ indicating that the additional negative charge in TeOF$_6^{2-}$ weakens mainly the equatorial Te–F bonds. The vibrational spectra of N(CH$_3$)$_4$TeOF$_5$ are also reported, and the results of ab initio calculations and of a normal coordinate analysis of TeOF$_5^-$ show that six of its fundamental vibrations had previously been assigned incorrectly.

Introduction

Heptacoordinated species are of special interest. According to the hard sphere model of the valence shell electron pair repulsion (VSEPR) rules of repelling points on a sphere, heptacoordinated species should prefer structures derived from a monocapped octahedron.[1,2] Besides the monocapped octahedron, there are two other structures for heptacoordinated species that are only slightly higher in energy. These are the monocapped trigonal prism and the pentagonal bipyramid.[3] Examinations[4,5] of the relative energy E of seven repelling points on a sphere in terms of the energy law

$$E = \sum_{i \neq j} \frac{1}{r_{ij}^n}$$

where r_{ij} is the distance between two of the points and n is a constant, have indicated that for heptacoordinated species the minimum energy structure depends on n. For $0 < n < 3$, i.e., soft repulsion, the pentagonal bipyramid was the minimum energy structure, while for $3 < n < 6$ the monocapped trigonal prism and for $n > 6$, i.e., hard repulsion, the monocapped octahedron were the energetically preferred structures.[5] Although at present no quantitative numbers are available[2] for n, for heptacoordinated transition metal fluorides or oxofluorides the experimental observations qualitatively agree with these predictions. Thus, the most ionic and softest XF$_7$ or XOF$_6$ species, i.e., the triply charged anions ZrF$_7^{3-}$, HfF$_7^{3-}$, TaOF$_6^{3-}$, and NbOF$_6^{3-}$ have pentagonal bipyramidal structures,[2,6,7] the intermediately soft, doubly charged anions NbF$_7^{2-}$ and TaF$_7^{2-}$ have monocapped
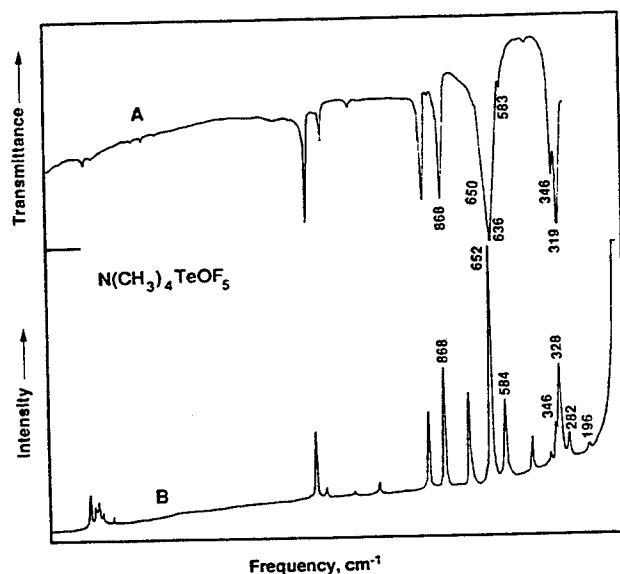
Figure 1. Infrared (A) and Raman (B) spectra of solid N(CH$_3$)$_4$TeOF$_5$.

trigonal prismatic structures,[8,9] and the hardest, singly charged anions MoF$_7^-$, WF$_7^-$, and UF$_7^-$ possess monocapped octahedral structures.[10] On the basis of the presently available structural data, the nature of the central atom or small changes in its d orbital occupation seem to have little influence on the structures of these compounds.

Whereas the aforementioned VSEPR rules and energy law predictions[5] appear to be applicable to transition metal elements, the heptacoordinated main-group elements do not comply. By comparison with identically charged transition metal compounds, the heptacoordinated main-group compounds should be even harder because of the smaller radii of their central atoms and the increased s and p character of their valence electrons. Therefore, the neutral or singly charged heptacoordinated main-group

† Rocketdyne.
‡ DuPont.
§ McMaster University.
(1) Gillespie, R. J. Molecular Geometry; Van Nostrand Reinhold Co.: London, 1972.
(2) Gillespie, R. J.; Hargittai, I. The VSEPR Model of Molecular Geometry; Allyn and Bacon, A Division of Simon & Schuster, Inc.: Needham Heights, MA, 1991.
(3) Kepert, D. Inorganic Stereochemistry; Springer: Berlin, 1982.
(4) Claxton, T. A.; Benson, G. C. Can. J. Chem. 1966, 44, 157.
(5) Bradford Thompson, H.; Bartell, L. S. Inorg. Chem. 1968, 7, 488.
(6) Granzin, J.; Saalfeld, H. Z. Kristallogr. 1988, 183, 71.
(7) (a) Averdunk, F.; Hoppe, R. J. Fluorine Chem. 1989, 42, 413. (b) Stomberg, R. Acta Chem. Scand., Ser. A 1983, A37, 412.
(8) Torardi, C. C.; Brixner, L. H.; Blasse, G. J. Solid State Chem. 1987, 67, 21.
(9) Brown, G. M.; Walker, L. A. Acta Crystallogr. 1966, 20, 220.
(10) Giese, S.; Seppelt, K. J. Fluorine Chem. 1992, 58, 368.

Table I. Vibrational Spectra of $N(CH_3)_4TeOF_5$ and Their Assignments

| | obsd freq, cm⁻¹ (rel intens) | | assignments (point group) | |
| | Raman | | | |
IR 25 °C	25 °C	−150 °C	$N(CH_3)_4^+$ (T_d)	$TeOF_5^-$ (C_{4v})
3110 sh	3043 (13)	3045 (8)		
3042 mw	2995 (7)	3030 (7)		
	2966 (10)	2968 (2)		
2972 w	2928 (w)			
	2820 (3)	2931 (2)	ν_5 (E)	
		2820 (3)	ν_{14} (F_2)	
2759 vw			ν_1 (A_1)	
2660 vvw			+ combination	
2622 vvw			bands	
2588 vw				
2523 vvw				
2485 vw				
2362 vvw				
1492 vs			ν_{15} (F_2)	
	1465 (26)	1477 (10)	ν_2 (A_1), ν_6 (E)	
		1465 (7)		
1419 m	1418 (5)	1421 (2)	ν_{16} (F_2)	
1289 mw	1289 (2)	1288 (1)	ν_{17} (F_2)	
1220 w				(584 + 636)
	1174 (5)	1175 (1)	ν_7 (E)	
951 s	949 (28)	952 (18)	ν_{18} (F_2)	
921 w				
868 s	868 (47)	858 (35)		ν_1 (A_1)
828 vw, sh				
770 w				
	753 (37)	758 (12)	ν_3 (A_1)	
	742 sh	748 (7)		
650 sh	652 (100)	652 (100)		ν_2 (A_1)
636 vs				ν_8 (E)
583 mw	584 (30)	594 (22)		ν_3 (A_1), ν_5 (B_1)
460 w	460 (13)	459 (7)	ν_{19} (F_2)	
	373 (5)	375 (4)	ν_8 (E)	
346 ms	346 (6)	347 (9)		ν_9 (E)
329 sh	328 (40)	329 (40)		ν_{10} (E)
319 s				ν_4 (A_1)
	282 (10)	283 (6)		ν_7 (B_2)
	196 (3)	196 (3)		ν_{11} (E)
		93 (2)	lattice vibrations	
		38 (2)		

element compounds should be very hard and exhibit monocapped octahedral structures. This, however, is not the case, and IF_7,[11,12] TeF_7^-,[13,14] IOF_6^-,[13,15] and XeF_5^- [16] all exhibit pentagonal bipyramidal structures. A rationale for their structures was recently presented in our papers on IF_7[12] and IOF_6^-.[15] It was concluded[12,15] that the pentagonal bipyramidal geometry of their more localized valence electron orbitals, rather than the intramolecular repulsion force, is the main reason for their pentagonal bipyramidal molecular structures.

The bonding in the pentagonal bipyramidal main-group fluorides has been described[12,15] by planar, $p_{x,y}$ hybrid orbitals of the central atom for the formation of a coplanar, semiionic, 6-center–10-electron (6c–10e) bond system for the five equatorial ligands. Depending on the relative bond lengths and radii of the atoms involved, this equatorial plane can become highly congested and, therefore, undergo substantial puckering. Further interest and complexity is added to this problem by the facts that these structures possess 5-fold symmetry, are usually nonrigid, and exhibit fluxionality involving static or dynamic puckering of the equatorial plane and, in some instances,[12] also axial–equatorial ligand exchange.

In view of the strong dependency of the structures of the heptacoordinated transition metal compounds upon the number of their ionic charges, (see above) it was interesting to explore to what extend this also applies to heptacoordinated main-group element compounds. Whereas neutral IF_7 and the singly charged anions TeF_7^-, IOF_6^-, and XeF_5^- are now well understood,[11,16] no data had been available on multiply charged anions. Therefore, we have prepared and characterized the $TeOF_6^{2-}$ anion and, in this paper, report our results.

Experimental Section

Materials. The synthesis of anhydrous $N(CH_3)_4F$ has been previously described.[17] The CH_3CN (Baker, Bio-analyzed, having a water content of 40 ppm) was treated with P_2O_5 and freshly distilled prior to use, thereby reducing its water content to <4 ppm. A literature method[18] was used for the synthesis of anhydrous $N(CH_3)_4TeOF_5$.

Synthesis of $[N(CH_3)_4]_2TeOF_6$. In the drybox, $N(CH_3)_4TeOF_5$ (0.4543 g, 1.45 mmol) and a 2-fold excess of $N(CH_3)_4F$ (0.2726 g, 2.93 mmol) were loaded into separate limbs of a two-limbed Pyrex glass vessel equipped with J. Young glass–PTFE stopcocks. Dry CH_3CN (ca. 5 mL of liquid) was vacuum distilled onto each solid at −196 °C. The two limbs were allowed to warm to −9 °C in order to dissolve the solids. While both solutions were maintained at −9 °C, the $N(CH_3)_4F$ solution was poured into the $N(CH_3)_4TeOF_5$ solution. The reaction mixture was stirred at −9 °C for 15 min, during which time a heavy white precipitate formed. The mixture was cooled to −20 °C and stirred for an additional 45 min. The supernatant solution was decanted from the white precipitate at −20 °C. The residual CH_3CN was pumped off at −9 °C and finally at 25 °C overnight. A fine white powder remained (0.4298 g), which was shown by Raman and infrared spectroscopy to be a mixture of $[N(CH_3)_4]_2$-$TeOF_6$ and $N(CH_3)_4TeOF_5$.

Vibrational Spectroscopy. Raman spectra were recorded on either a Cary Model 83 or a Spex Model 1403 spectrophotometer using the 488-nm exciting line of an Ar ion or the 647.1-nm line of a Kr ion laser, respectively. Baked-out Pyrex melting point capillaries or thin-walled Kel-F tubes were used as sample containers.

Infrared spectra were recorded by using either AgCl, AgBr, or KBr disks on a Perkin-Elmer Model 283 spectrophotometer. The finely powdered samples were sandwiched between two thin disks and pressed together in a Wilks minipress inside the drybox.

Nuclear Magnetic Resonance Spectroscopy. The ^{19}F NMR spectra were recorded unlocked (field drift <0.1 Hz h⁻¹) on a Bruker AM-500 spectrometer equipped with an 11.744-T cryomagnet. The ^{19}F spectra were obtained using a 5-mm combination $^1H/^{19}F$ probe operating at 470.599 MHz. The spectra were recorded in a 32 K memory. A spectral width setting of 50 kHz was employed, yielding a data point resolution of 3.052 Hz/data point and an acquisition time of 0.327 s. No relaxation delays were applied. Typically, 10 000 transients were accumulated. The pulse width corresponding to a bulk magnetization tip angle, θ, of approximately 90° was equal to 1 μs. No line broadening parameters were used in the exponential multiplication of the free induction decays prior to Fourier transformation.

The spectra were referenced to a neat external sample of $CFCl_3$ at ambient temperature. The chemical shift convention used is that a positive (negative) sign signifies a chemical shift to high (low) frequency of the reference compound.

Solids were weighed into 5-mm precision glass tubes (Wilmad) in the drybox, and CH_3CN solvent was distilled *in vacuo* onto the solid at −78 °C. The tubes were flame-sealed in dynamic vacuum while keeping the contents frozen to −78 °C.

Computational Methods. The electronic structure calculations were done at the ab initio molecular orbital level using an effective core potential (ECP) for the core electrons on tellurium. The valence basis set is of polarized double zeta quality. The fluorine and oxygen basis sets are

(11) Adams, W. J.; Bradford Thompson, H.; Bartell, L. S. *J. Chem. Phys.* **1970**, *53*, 4040.
(12) Christe, K. O.; Curtis, E. C.; Dixon, D. A. *J. Am. Chem. Soc.*, in press.
(13) Christe, K. O.; Sanders, J. C. P.; Schrobilgen, G. J.; Wilson, W. W. *J. Chem. Soc., Chem. Commun.* **1991**, 837.
(14) Mahjoub, A. R.; Seppelt, K. *J. Chem. Soc., Chem. Commun.* **1991**, 840.
(15) Christe, K. O.; Dixon, D. A.; Mahjoub, A. R.; Mercier, H. P. A.; Sanders, J. C. P.; Seppelt, K.; Schrobilgen, G. J.; Wilson, W. W. *J. Am. Chem. Soc.*, in press.
(16) Christe, K. O.; Curtis, E. C.; Dixon, D. A.; Mercier, H. P.; Sanders, J. C. P.; Schrobilgen, G. J. *J. Am. Chem. Soc.* **1991**, *113*, 3351.

(17) Christe, K. O.; Wilson, W. W.; Wilson, R. D.; Bau, R.; Feng, J. *J. Am. Chem. Soc.* **1990**, *112*, 7619.
(18) Mercier, H. P. A.; Sanders, J. C. P.; Schrobilgen, G. J. *J. Am. Chem. Soc.*, submitted for publication.

Table II. Observed and Calculated Vibrational Spectra of TeOF$_5^-$

assignment C_{4v}		approx mode description	obsd			calcd		
			freq, cm^{-1} (rel intens)		$^{16}O-^{18}O$ shift[a]	freq,[b] cm^{-1}	IR intens	$^{16}O-^{18}O$ shift
			IR	Raman				
A$_1$	ν_1	ν(TeO)	868 s	868 (47)	40	860	101	39.9
	ν_2	sym combination of ν_{sym}(TeF$_4$) and ν(TeF$_{ax}$)	650 sh	652 (100)	1	658	63	1.5
	ν_3	antisym combination of ν_{sym}(TeF$_4$) and ν(TeF$_{ax}$)	583 mw	584 (30)	0	573	3	0.3
	ν_4	$\delta_{umbrella}$(TeF$_4$)	319 s			339	106	0.8
B$_1$	ν_5	ν_{sym}(TeF$_4$) out-of-phase		584 (30)		582	0	0
	ν_6	δ_{pucker}(TeF$_4$)	not obsd	not obsd		223	0	0
B$_2$	ν_7	δ_{sciss}(TeF$_4$) in-plane		282 (10)	0	280	0	0
E	ν_8	ν_{asym}(TeF$_4$)	636 ms		0	651	221	0
	ν_9	δ(FTeF$_4$)	346 ms	346 (6)	0	348	61	0.2
	ν_{10}	δ(OTeF$_4$)	329 sh	328 (40)	10	329	60	10.2
	ν_{11}	δ_{asym}(TeF$_4$) in-plane		196 (3)		185	0.04	1.9

[a] The oxygen isotopic shift data were taken from ref 32. [b] The calculated frequencies were scaled by the following empirical factors to give the best agreement with the observed values: stretching frequencies, 0.9529; deformation modes, 0.8812.

Table III. Observed and Calculated Geometries of TeOF$_5^-$

	obsd[a]	calcd[b]		obsd[a]	calcd[b]
r(Te–O), Å	1.786(3)	1.738	r(Te–F$_{eq}$), Å	1.853(2)	1.838
r(Te–F$_{ax}$), Å	1.854(2)	1.835	$\angle$(OTeF$_{eq}$), deg	95.2(1)	97.44

[a] Librationally uncorrected values reported in ref 32 for the solid TeOF$_5^-$ salt of protonated 1,8-bis(dimethylamino)naphthalene at –106 °C. [b] Unscaled values calculated for the free TeOF$_5^-$ anion.

Table IV. Ab Initio Force Field[a,b] of TeOF$_5^-$ and Potential Energy Distribution

			sym force consts	PED
A$_1$	ν_1	860	$F_{11} = f_D = 6.164$ $F_{12} = f_{DR} = 0.028$ $F_{13} = f_{Dr} = 0.137$ $F_{14} = 0.198$	92.3 (S_1) + 4.1 (S_2) + 3.3 (S_4)
	ν_2	658	$F_{22} = f_R = 3.929$ $F_{23} = f_{Rr} = 0.448$ $F_{24} = -0.505$	52.8 (S_2) + 44.9 (S_3) + 1.2 (S_4) + 1.1 (S_1)
	ν_3	573	$F_{33} = f_r + 2f_{rr} + f_{rr'} = 4.179$ $F_{34} = -0.027$	50.3 (S_3) + 49.3 (S_2)
	ν_4	339	$F_{44} = 1.514$	98.8 (S_4) + 1.0 (S_2)
B$_1$	ν_5	282	$F_{55} = f_r - 2f_{rr} + f_{rr'} = 3.782$ $F_{56} = 0.027$	100 (S_5)
	ν_6	223	$F_{66} = 0.942$	100 (S_6)
B$_2$	ν_7	280	$F_{77} = f_\alpha - 2f_{\alpha\alpha} + f_{\alpha\alpha'} = 0.755$	100 (S_7)
E	ν_8	651	$F_{88} = f_r - f_{rr'} = 3.789$ $F_{89} = f_{r\beta} - f_{r\beta''} = 0.343$ $F_{8,10} = f_{r\gamma} - f_{r\gamma'} = 0.242$ $F_{8,11} = 2^{1/2}(f_{r\alpha} - f_{r\alpha'}) = 0.141$	94.8 (S_8) + 2.7 (S_{11}) + 2.0 (S_{10})
	ν_9	348	$F_{99} = f_\beta - f_{\beta\beta'} = 1.262$ $F_{9,10} = 0.088$ $F_{9,11} = 0.182$	78.1 (S_9) + 21.6 (S_{11})
	ν_{10}	329	$F_{10,10} = f_\gamma - f_{\gamma\gamma'} = 0.919$ $F_{10,11} = 0.188$	86.0 (S_{10}) + 7.1 (S_9) + 6.9 (S_{11})
	ν_{11}	185	$F_{11,11} = f_\alpha - f_{\alpha\alpha'} = 0.865$	67.1 (S_{11}) + 20.1 (S_{10}) + 12.6 (S_9)

[a] The following symmetry coordinates were used: S_1 = TeO stretch; S_2 = TeF$_{ax}$ stretch; S_3 = TeF$_4$ sym in-phase stretch; S_4 = TeF$_4$ umbrella deform; S_5 = TeF$_4$ sym out-of-phase stretch; S_6 = TeF$_4$ pucker deform; S_7 = TeF$_4$ sym in-plane deform; S_8 = TeF$_4$ asym stretch; S_9 = TeF$_{ax}$ wag; S_{10} = TeO wag; S_{11} = TeF$_4$ asym in-plane deform. For their explicit values, see: Smith, D. F.; Begun, G. M. *J. Chem. Phys.* **1965**, *43*, 2001. [b] The following scaling factors were used: stretching force constants, (0.9529)^2; deformation constants, (0.8812)^2; stretch–bend interactions, 0.9529 × 0.8812. Stretching constants are in mdyn/Å, deformation constants in mdyn Å/rad^2, and stretch–bend interaction constants in mdyn/rad.

from Dunning and Hay,[19] and the ECP is from Hay and Wadt[20] including relativistic corrections and augmented by a d function on Te with an exponent of 0.237.[21] The Te, O, and F basis sets were augmented further by a diffuse p function with exponents of 0.035, 0.059, and 0.074,

Table V. Vibrational Spectra of [N(CH$_3$)$_4$]$_2$TeOF$_6$ and Their Assignment

| obsd freq (25 °C), cm^{-1} (rel intens)		assignment (point group)	
IR	Ra	N(CH$_3$)$_4^+$ (T_d)	TeOF$_6^{2-}$ (C_{5v})
3043 mw	3036 (40)	ν_5 (E)	
2999 w	2996 (5)	ν_{14} (F$_2$)	
	2968 (30)	ν_1 (A$_1$)	
	2945 sh	+ combination	
	2928 (20)	bands	
	2900 sh		
	2825 (9)		
1498 vs		ν_{15} (F$_2$)	
1464 w	1474 (91)	ν_2 (A$_2$), ν_6 (E)	
1421 w	1420 (9)	ν_{16} (F$_2$)	
	1291 (9)	ν_{17} (F$_2$)	
	1185 (9)	ν_7 (E)	
954 vs	952 (72)	ν_{18} (F$_2$)	
921 w	919 (10)		
830 s	830 (71)		ν_1 (A$_1$)
	752 (80)	ν_3 (A$_1$)	
614 m	614 (100)		ν_2 (A$_1$)
	530 (63)		ν_3 (A$_1$)
525 vs			ν_5 (E$_1$)
461 w	459 (25)	ν_{19} (F$_2$)	ν_9 (E$_2$)?
	388 (35)		ν_{10} (E$_2$)
	368 sh	ν_8 (E)	
365 vs			ν_6 (E$_1$)
330 s			ν_4 (A$_1$)
	322 (60)		ν_7 (E$_1$)
	245 (2)		ν_8 (E$_1$)

respectively, to account for the negative ion character. The geometries were optimized by using gradient techniques,[22] and the force fields were calculated analytically.[23,24] The ab initio MO calculations were done with the program GRADSCF,[25] as implemented on a Cray YMP computer system. Because the calculated vibrational frequencies and force constants are somewhat too high due to the neglect of electron correlation and of anharmonicity, the calculated frequencies and force constants require scaling. Since the deformation modes are usually more strongly affected

(21) Huzinaga, S.; Andzelm, J.; Klobukowski, M.; Radzio, E.; Sakai, Y.; Tatasaki, H. *Gaussian Basis Sets of Molecular Calculations*; Elsevier: Amsterdam, 1984.

(22) (a) Komornicki, A.; Ishida, K.; Morokuma, K.; Ditchfield, R.; Conrad, M. *Chem. Phys. Lett.* **1977**, *45*, 595. (b) McIver, J. W., Jr.; Komornicki, A. *Chem. Phys. Lett.* **1971**, *10*, 202. (c) Pulay, P. In *Applications of Electronic Structure Theory*, Schaefer, H. F., III, Ed.; Plenum Press: New York, 1977; p 153.

(23) (a) King, H. F.; Komornicki, A. *J. Chem. Phys.* **1986**, *84*, 5465. (b) King, H. F.; Komornicki, A. In *Geometrical Derivatives of Energy Surfaces and Molecular Properties* Jorgenson, P., Simons, J., Eds.; NATO ASI Series C 166; D. Reidel: Dordrecht, The Netherlands 1986; p 207.

(24) Breiding, J.; Thiel, W.; Komornicki, A. *Chem. Phys. Lett.* **1988**, *153*, 76.

(25) GRADSCF is an ab initio program system designed and written by A. Komornicki at Polyatomics Research.

(26) Marsden, C. J. *J. Chem. Phys.* **1987**, *87*, 6626.

(19) Dunning, T. H., Jr.; Hay, P. J. In *Methods of Electronic Structure Theory*, Schaefer, H. F., III, Ed., Plenum Press: New York, 1977; Chapter 1.

(20) Hay, P. J.; Wadt, W. R. *J. Chem. Phys.* **1985**, *82*, 299.

Table VI. Comparison of Observed and Calculated Frequencies of the Isoelectronic $TeOF_6^{2-}$ and IOF_6^- Anions, Together With Approximate Mode Descriptions

| assignment (C_{5v})		approx mode description	$TeOF_6^{2-}$		IOF_6^-	
			obsd freq, cm^{-1} (intens (IR, Raman))	calcd freq,^{a} cm^{-1}, (IR intens)	obsd freq,^{a} cm^{-1} (intens (IR, Raman))	calcd freq,^{b} cm^{-1}
A_1	ν_1	$\nu(X=O)$	830 (s, 71)	829.7 (122)	873 (vs, 53p)^e	873
	ν_2	$\nu(X-F_{ax})$	614 (m, 100)	629.6 (73)	649 (s, 88p)	639.6
	ν_3	$\nu_{sym}(XF_5)$	530 (..., 80)	527.1 (0.1)	584 (c, 100p)	579.9
	ν_4	$\delta_{umbrella}(XF_5)$	330 (s, ...)	337.9 (104)	359 (s, 4)	363.0
E_1	ν_5	$\nu_{asym}(XF_5)$	525 (vs, ...)	529.9 (202)	585 (vs, d)	597.7
	ν_6	$\delta_{asym}(XF_5)$ in-plane	365 (vs, ...)	368.3 (272)	405 (vs, ...)	406.6
	ν_7	$\delta_{rock}(O=X-F_{ax})$	322 (..., 60)	314.6 (0.1)	341 (..., 62)	333.2
	ν_8	$\delta_{sciss}(O=X-F_{ax})$	245 (..., 2)	244.1 (1.3)	260 (s, 2)	267.4
E_2	ν_9	$\delta_{sciss}(XF_5)$ in plane	459 (w, 25)	456.7 (0)	530 (..., 4)	519.8
	ν_{10}	$\nu_{asym}(XF_5)$	388 (..., 35)	377.4 (0)	457 (..., 49)	457.3
	ν_{11}	$\delta_{pucker}(XF_5)$	not obsd	129.6 (0)	not obsd	138.1

^{a} Frequency values were scaled by the following empirical factors to give the best fit with the observed frequencies: stretching modes, 0.9747; deformation modes, 0.8789. ^{b} The following empirical scaling factors were used: stretching modes, 0.9262 except for $\nu_1 = 1.0146$; deformation modes, 0.8863. The values previously published in ref 15 are slightly different due to the use of a common scaling factor for both the stretching and the deformation modes. ^{c} Very strong IR band at 585 cm^{-1} is due to ν_5 and not ν_3, which should be of vanishingly small IR intensity. ^{d} Very strong Raman band at 584 cm^{-1} is due to ν_3 and not ν_5, which should be of vanishingly small Raman intensity. ^{e} p = polarized.
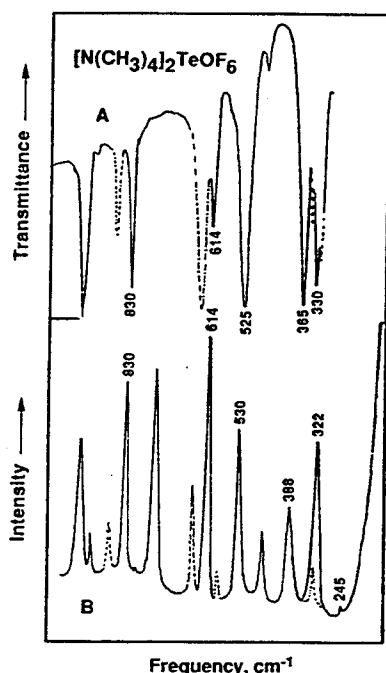
Figure 2. Infrared (A) and Raman (B) spectra of solid $[N(CH_3)_4]_2$-$TeOF_6$. The dashed lines are due to $TeOF_5^-$.

by the bond lengths than the stretching modes, it is advantageous to use two different scaling factors for the stretching and the deformation modes.[26]

Results and Discussion

Synthesis and Properties of $[N(CH_3)_4]_2TeOF_6$. This compound was prepared according to

$$N(CH_3)_4TeOF_5 + N(CH_3)_4F \xrightarrow{CH_3CN} [N(CH_3)_4]_2TeOF_6 \quad (1)$$
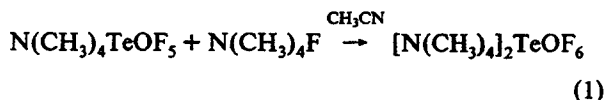
Since both starting materials are soluble in CH_3CN while the desired product is not, the latter can easily be isolated by filtration or decantation. In spite of using a 2-fold excess of $N(CH_3)_4F$, the reaction product always contained some unreacted $TeOF_5^-$ salt as detected by vibrational spectroscopy. Since the dry $[N(CH_3)_4]_2TeOF_6$ salt is thermally stable at room temperature, the observation of some unreacted $N(CH_3)_4TeOF_5$ in the product implies that reaction 1 might be an equilibrium which is only incompletely shifted to the right. Attempts were made to remove the unreacted $N(CH_3)_4TeOF_5$ from the reaction product by repeated extractions with CH_3CN. Although the purity of the

Table VII. Scaled ab Initio Force Field^{a,b} and Potential Energy Distribution of $TeOF_6^{2-}$

			sym force consts	PED
A_1	ν_1	829.7	$F_{11} = 5.727$ $F_{12} = 0.020$ $F_{13} = 0.190$ $F_{14} = -0.213$	$91.3\ (S_1) + 4.6\ (S_2) + 4.0\ (S_4)$
	ν_2	629.6	$F_{22} = 3.811$ $F_{23} = 0.403$ $F_{24} = 0.362$	$78.3\ (S_2) + 18.0\ (S_3) + 2.3\ (S_4) + 1.4\ (S_1)$
	ν_3	527.1	$F_{33} = 3.335$ $F_{34} = 0.086$	$80.0\ (S_3) + 19.5\ (S_2)$
	ν_4	337.9	$F_{44} = 1.525$	$100\ (S_4)$
E_1	ν_5	529.9	$F_{55} = 2.549$ $F_{56} = -0.997$ $F_{57} = 0.269$ $F_{58} = 0.239$	$99.3\ (S_5)$
	ν_6	368.3	$F_{66} = 2.665$ $F_{67} = -0.226$ $F_{68} = -0.275$	$33.0\ (S_6) + 36.1\ (S_8) + 18.1\ (S_7) + 12.8\ (S_5)$
	ν_7	314.6	$F_{77} = 0.937$ $F_{78} = 0.074$	$44.5\ (S_7) + 54.4\ (S_8)^c$
	ν_8	244.1	$F_{88} = 0.825$	$34.2\ (S_8) + 43.8\ (S_7) + 21.3\ (S_6)^d$
E_2	ν_9	456.7	$F_{99} = 2.306$ $F_{9,10} = 0.380$ $F_{9,11} = -0.065$	$87.8\ (S_9) + 12.2\ (S_2)$
	ν_{10}	377.4	$F_{10,10} = 1.742$ $F_{10,11} = -0.058$	$88.6\ (S_{10}) + 11.3\ (S_9)$
	ν_{11}	129.6	$F_{11,11} = 0.356$	$99.9\ (S_{11})$

^{a} The following scaling factors were used: stretching force constants, $(0.9747)^2$; deformation constants, $(0.8789)^2$; stretch–bend interactions, 0.9747×0.8789. Stretching constants were in mdyn/Å, deformation constants in mdynÅ/rad^2, and stretch–bend interaction constants in mdyn/rad. ^{b} The symmetry coordinates used were identical to those previously published in ref 15 for IOF_6^-. ^{c} Antisymmetric combination of S_7 and S_8. ^{d} Symmetric combination of S_7 and S_8.

product was substantially improved in this manner, we did not succeed in the preparation of totally pure $[N(CH_3)_4]_2TeOF_6$.

Since $[N(CH_3)_4]_2TeOF_6$ has very little solubility in CH_3CN, single crystals for a crystal structure determination could not be grown. The ^{19}F NMR spectrum of $[N(CH_3)_4]_2TeOF_6$ in CH_3-CN at -10 °C displays only weak resonances attributable to $TeOF_5^-[\delta(^{19}F_A), -19.1$ ppm; $\delta(^{19}F_B), -36.9$ ppm; $^2J(F_A - F_B)$, 170 Hz] and $F^-[\delta(^{19}F), -70.1$ pm] but none assignable to $TeOF_6^{2-}$. When the temperature to is rasied 25 °C, rapid dissociation of the $TeOF_6^{2-}$ anion into $TeOF_5^-$ and F^- results in solvent attack by F^- and formation of HF_2^-.[27] Similar behavior has been noted previously[13] for $[N(CH_3)_4]_2TeF_8$ in CH_3CN, thereby demon-

(27) Christe, K. O.; Wilson, W. W. *J. Fluorine Chem.* **1990**, *47*, 117.
(28) Christe, K. O.; Wilson, W. W.; Bau, R.; Bunte, S. W. *J. Am. Chem. Soc.* **1992**, *114*, 3411 and references cited therein.

strating the strong propensity of these dinegative anions to dissociate in solution. As a consequence of the insolubility and instability of [N(CH$_3$)$_4$]$_2$TeOF$_6$ in CH$_3$CN, the recording of a ^{125}Te NMR spectrum for the TeOF$_6^{2-}$ anion has also not been possible. Consequently, the characterization of the TeOF$_6^{2-}$ anion was based entirely on its vibrational spectra and their comparison with those of the isoelectronic IOF$_6^-$ anion whose structure has been firmly established by X-ray diffraction and NMR spectroscopy.[9] Since the samples of [N(CH$_3$)$_4$]$_2$TeOF$_6$ used for the spectroscopic study always contained some TeOF$_5^-$, it was necessary to first analyze the vibrational spectra of N(CH$_3$)$_4$-TeOF$_5$.

Vibrational Spectra of N(CH$_3$)$_4$TeOF$_5$. The vibrational spectra of N(CH$_3$)$_4$TeOF$_5$ are shown in Figure 1 and the observed frequencies, together with their assignments, are summarized in Table I. The assignments for the N(CH$_3$)$_4^+$ cation follow those previously given[15,17,28] for other N(CH$_3$)$_4^+$ salts and, therefore, require no further discussion. The bands observed for the TeOF$_5^-$ anion are in general agreement with those previously reported[29-32] for the Cs$^+$, Ag$^+$, [N(n-C$_4$H$_9$)$_4^+$], and 1,8 bis (dimethylamino)-naphthalenium salts. The previous assignments and normal coordinate analyses,[30,32] however, require substantial revision as shown by the results of our ab initio calculations (see Tables II–IV). In the previous studies ν_4, ν_5, ν_6, ν_7, ν_9, and ν_{11} had been incorrectly assigned. Our revised assignments are further supported by ^{16}O–^{18}O isotopic shifts[32] and calculated infrared intensities (see Table II). These results demonstrate again[12,15] the great benefit of reliable ab initio calculations for the correct analysis of vibrational spectra complicated by coincidences and low intensities of some of their bands.

Vibrational Spectra of [N(CH$_3$)$_4$]$_2$TeOF$_6$. The vibrational spectra of [N(CH$_3$)$_4$]$_2$TeOF$_6$ are shown in Figure 2 and the observed frequencies, together with their assignments, are summarized in Table V. Since the TeOF$_6^{2-}$ anion readily loses an F$^-$ ion, it was not possible to obtain spectra which were completely free of TeOF$_5^-$ impurities. The bands due to TeOF$_5^-$ have been indicated in Figure 2 by dashed lines, and those due to TeOF$_6^{2-}$ have been marked by their frequency values. The unmarked bands belong to the N(CH$_3$)$_4^+$ cations.

Since the low solubility of [N(CH$_3$)$_4$]$_2$TeOF$_6$ preempted its characterization by NMR spectroscopy or single-crystal X-ray diffraction, a thorough vibrational analysis was carried out to establish the presence of the novel TeOF$_6^{2-}$ anion. As can be seen from Table VI, the vibrational spectra of TeOF$_6^{2-}$ are in excellent agreement with those of isoelectronic IOF$_6^-$ and our results from ab initio ECP calculations. With the exception of the equatorial TeF$_5$ puckering mode, ν_{11}, which is difficult to detect because of its low intensity and frequency, all fundamental vibrations expected for TeOF$_6^{2-}$ have been observed. The observed frequencies deviate only by an average of 6.6 cm^{-1} from the scaled calculated frequencies, and the observed qualitative infrared intensities are in complete accord with the calculated values. The symmetry force constants and potential energy distribution (see

(29) Sladky, F.; Kropshofer, H.; Leitzke, O.; Peringer, P. *J. Inorg. Nucl. Chem. Suppl.* **1976**, 69.
(30) Mayer, E.; Sladky, F. *Inorg. Chem.* **1975**, *14*, 589.
(31) Thrasher, J. S.; Seppelt, K. *Z. Anorg. Allg. Chem.* **1985**, *529*, 85.
(32) (a) Strauss, S. H.; Abney, K. D.; Anderson, O. P. *Inorg. Chem.* **1986**, *25*, 2806. (b) Miller, P. K.; Abney, K. D.; Rappé, A. K.; Anderson, O. P.; Strauss, S. H. *Inorg. Chem.* **1988**, *27*, 2255.

Table VIII. Internal Stretching Force Constants (mdyn/Å)^a of TeOF$_6^{2-}$ Compared to Those of IOF$_6^-$

	IOF$_6^-$	TeOF$_6^{2-}$	% change
fXO	6.256	5.727	−8.5
fXF$_{ax}$	4.095	3.811	−6.9
fXF$_{eq}$	3.086	2.383	−22.8

^{a} Calculated ab initio ECP values scaled by the square of the scaling factors given in the footnotes of Table VI. The values given for IOF$_6^-$ deviate somewhat from those of ref 15 due to the different scaling procedure (separate scaling of stretching and deformation modes) used to conform with those used for TeOF$_6^{2-}$.

Table IX. Calculated Geometry of TeOF$_6^{2-}$ Compared to the Calculated and Experimental Geometries of Isoelectronic IOF$_6^-$

	TeOF$_6^{2-}$ calcd	IOF$_6^{-a}$ calcd	IOF$_6^{-a}$ exptl
r(X–O), Å	1.7598	1.7255	1.75–1.77
r(X–F$_{ax}$), Å	1.8400	1.8087	1.82
r(X–F$_{eq}$), Å	1.9373	1.8819	1.88
$\angle$(OXF$_{eq}$), deg	95.9922	95.76	94–96

^{a} Values from ref 15.

Table X. Total Charge Distributions for IOF$_6^-$ and TeOF$_6^{2-}$

	IOF$_6^{-a}$	TeOF$_6^{2-}$		IOF$_6^{-a}$	TeOF$_6^{2-}$
central atom	2.71	2.88	F$_{ax}$	−0.44	−0.60
F$_{eq}$	−0.53	−0.66	O$_{ax}$	−0.74	−0.97

^{a} Values from ref 15.

Table VII), the internal stretching force constants (see Table VIII), the calculated geometry (see Table IX), and the total charge distribution (see Table X) are analogous to those[15] of isoelectronic IOF$_6^-$. As expected, the additional negative charge in TeOF$_6^{2-}$ increases the central atom (δ+)–ligand (δ–) bond polarities which can, at least partially, account for the lengthening of the bonds and the decrease in the values of the force constants. Interestingly, the equatorial Te–F stretching force constant decreases and the corresponding bond length increases by a much larger percentage than those of the axial bonds. This is not surprising in view of the bonding scheme previously proposed[15] for IOF$_6^-$. This scheme assumes a semiionic 6-center–10-electron bond system for the equatorial ligands. Therefore, these bonds should be more strongly influenced by the increased ionicity. Since the relationships between either bond lengths or force constants and atomic charges are strongly nonlinear and, at a −1.0 charge on fluorine, complete ionization and bond separation should occur, the changes in the atomic charges of such highly negatively charged fluorine ligands (see Table X) should not be expected to be proportional to those in the force constants or bond lengths.

In summary, the vibrational spectra observed for the adduct between N(CH$_3$)$_4$F and N(CH$_3$)$_4$TeOF$_5$ and their thorough analysis firmly establish the presence of the new TeOF$_6^{2-}$ anion and show that its structure and bonding closely resemble those found[15] for IOF$_6^-$.

11279

Osmium Tetrafluoride Dioxide, *cis*-OsO$_2$F$_4$

Karl O. Christe,[*,†] David A. Dixon,[‡] Hans Georg Mack,[§] Heinz Oberhammer,[§] Alain Pagelot,[∥] Jeremy C. P. Sanders,[⊥] and Gary J. Schrobilgen[⊥]

Contribution from Rocketdyne, A Division of Rockwell International Corporation, Canoga Park, California 91309, Central Research and Development Department, E.I. du Pont de Nemours and Company, Inc., Experimental Station, Wilmington, Delaware 19880, Institut für Physikalische und Theoretische Chemie, Universität Tübingen, 7400 Tübingen, Germany, Department of Chemistry, McMaster University, Hamilton, Ontario L8S 4MI, Canada, and Bruker Spectrospin, G7160 Wissembourg, France

Received June 24, 1993[®]

Abstract: The new osmium(VIII) oxo fluoride obtained from the reaction of KrF$_2$ and OsO$_4$ in anhydrous HF solution and originally identifed as OsOF$_6$ is shown by quantitative material balance, electron diffraction, NMR and vibrational spectroscopy, and density functional theory calculations to be *cis*-OsO$_2$F$_4$. The combined electron diffraction study and DFT calculations result in the following geometry: $r_{Os=O}$ = 1.674(4) Å, r_{Os-F_c} = 1.883(3) Å, r_{Os-F_a} = 1.843(3) Å, $\angle O=Os=O$ = 103.5(25)°, $\angle F_c-Os-F_c$ = 77.3(26)°, $\angle F_a-Os-F_a$ = 172.0(3)°, $\angle O=Os-F_a$ = 92.4(17)°. In addition to the ^{19}F NMR spectrum, the ^{187}Os chemical shift was measured for *cis*-OsO$_2$F$_4$ from its ^{19}F{^{187}Os} inverse correlation spectrum. The results from the density functional theoretical calculations show that for OsO$_2$F$_4$ the *cis*-structure of C_{2v} symmetry is a true minimum and that, in accord with expectations for a d^0 transition metal complex, the *trans*-D_{4h} structure is not a minimum energy structure and distorts to a C_{2v} structure.

Introduction

The synthesis of novel fluorides at the limits of oxidation and coordination is a great challenge. Of particular interest in this respect is osmium because from its oxide chemistry this element is known to possess a rare maximum oxidation state of +VIII. Although the replacement of one doubly bonded oxygen ligand by two singly bonded fluorine ligands does not alter the formal oxidation state of the central atom, such a replacement becomes increasingly more difficult with an increasing number of fluorine ligands. Thus, the effective electron-withdrawing power of two singly bonded fluorine ligands is considerably greater than that of one doubly bonded oxygen ligand,[1] and steric crowding of ligands becomes a problem for coordination numbers in excess of 6.[2] Therefore, it is not surprising that, in the Os(VIII) series, OsF$_8$, OsOF$_6$, OsO$_2$F$_4$, OsO$_3$F$_2$, and OsO$_4$, until recently only OsO$_4$ and OsO$_3$F$_2$ had been known and well characterized.[3-5] Two years ago, Bougon reported[6] the synthesis of a new Os(VIII) oxo fluoride for which he proposed the composition OsOF$_6$. In a subsequent brief note[7] by Christe and Bougon, however, it was shown that this compound is *cis*-OsO$_2$F$_4$ and not OsOF$_6$. In this paper we present the experimental evidence for this new Os-(VIII) oxo fluoride being indeed OsO$_2$F$_4$ and having a *cis*-structure.

† Rocketdyne.
‡ E.I. du pont.
§ Universität Tübingen.
∥ Bruker Spectrospin.
⊥ McMaster University.
® Abstract published in *Advance ACS Abstracts*, October 15, 1993.

(1) Christe, K. O.; Dixon, D. A. *J. Am. Chem. Soc.* **1992**, *114*, 2978.
(2) Christe, K. O.; Curtis, E. C.; Dixon, D. A.; Mercier, H. P. A.; Sanders, J. C. P.; Schrobilgen, G. J.; Wilson, W. W. In *Fluorine and Fluorine-Containing Substituent Groups in Inorganic Chemistry*; Thrasher, J., Strauss, S., Eds.; ACS Symposium Series; American Chemical Society: in press.
(3) Hepworth, M. A.; Robinson, P. L. *J. Inorg. Nucl. Chem.* **1957**, *4*, 24.
(4) Nguyen-Nghi; Bartlett, N. *C. R. Acad. Sci. Paris Sect. C* **1969**, *269*, 756.
(5) Hope, E. G.; Levason, W.; Ogden, J. S. *J. Chem. Soc., Dalton Trans.* **1988**, 61 and 997.
(6) Bougon, R. *J. Fluorine Chem.* **1991**, *53*, 419.
(7) Christe, K. O.; Bougon, R. *J. Chem. Soc., Chem. Commun.* **1992**, 1056.

Experimental Section

Materials and Apparatus. OsO$_4$ (Aldrich, 99.8%) was sublimed prior to use. KrF$_2$ was prepared by UV-photolysis of Kr in liquid F$_2$ at –196 °C using a stainless-steel reactor equipped with a sapphire window.[8] HF (Matheson) was dried by storage over BiF$_5$.[9]

Volatile materials were handled in a stainless-steel vacuum line equipped with Teflon-FEP U-traps, stainless-steel bellows-seal valves, and a Heise Bourdon tube-type pressure gauge.[10] The line and other hardware employed were passivated with ClF$_3$, BrF$_5$, and HF. Nonvolatile materials were handled in the dry nitrogen atmosphere of a glovebox.

Vibrational Spectra. Infrared spectra were recorded in the range 4000–200 cm^{-1} on a Perkin-Elmer Model 283 spectrophotometer. Spectra of solids were obtained by using dry powders pressed between AgCl windows in an Econo press (Barnes Engineering Co.). Spectra of gases were obtained by using a Teflon cell of 5-cm path length equipped with AgCl windows. Raman spectra were recorded on a Spex Model 1403 spectrophotometer using using the 647.1-nm exciting line of a Kr ion laser. Sealed quartz tubes were used as sample containers in the transverse-viewing–transverse-excitation mode. A previously described[11] device was used for recording the low-temperature spectra. For the HF solutions, thin-walled Kel-F tubes were used as sample tubes.

Nuclear Magnetic Resonance Spectroscopy. The ^{19}F NMR spectra were recorded unlocked (field drift <0.1 Hz h^{-1}) on a Bruker AM-500 spectrometer as previously described.[12] No line-broadening parameters were used in the exponential multiplication of the free induction decays prior to Fourier transformation.

The two-dimensional (^{19}F, ^{187}Os) inverse NMR spectra were run on a Bruker AMX-300 spectrometer equipped with a 7.0463-T cryomagnet. The spectra were obtained with a 5-mm triple resonance ^{1}H/^{31}P/X probe with the outer X coil tunable over a broad-band frequency range and the ^{1}H channel retuned to ^{19}F. The experiments were carried out using the phase-sensitive (TPPI) HMQC pulse sequence.[13,14] The ^{19}F dimension was generated with 8 K data points and a spectral width of 20 000 Hz, while the ^{187}Os dimension was generated with 115 data points and a

(8) Christe, K. O.; Wilson, W. W.; Bougon, R. A. *Inorg. Chem.* **1986**, *25*, 2163.
(9) Christe, K. O.; Wilson, W. W.; Schack, C. J. *J. Fluorine Chem.* **1978**, *11*, 71.
(10) Christe, K. O.; Wilson, R. D.; Schack, C. J. *Inorg. Synth.* **1986**, *24*, 3.
(11) Miller, F. A.; Harney, B. M. *Appl. Spectrosc.* **1969**, *23*, 8.
(12) Christe, K. O.; Dixon, D. A.; Mahjoub, A. R.; Mercier, H. P. A.; Sanders, J. C. P.; Seppelt, K.; Schrobilgen, G. J.; Wilson, W. W. *J. Am. Chem. Soc.* **1993**, *115*, 2696.

spectral width of 27 777 Hz. The number of transients collected for each t_1 increment was 256. A recycling time of 2.2 s was used. The $1/2J$ delay was 8 ms. In the ^{187}Os dimension, the free induction decays were zero-filled to 2 K data points prior to Fourier transformation; no zero-filling was applied to free induction decays in the ^{19}F dimension. This gave data point resolutions of 27 Hz/point (^{187}Os) and 4.88 Hz/point (^{19}F). The data were processed using a 90° shifted sine bell in the ^{19}F dimension and a 60° sine bell in the ^{187}Os dimension.

The ^{19}F spectra were referenced to a neat external sample of CFCl$_3$ at ambient temperature. The ^{187}Os chemical shift was calculated from its absolute frequency using the conversion factor 6.850 099 8 MHz for δ(OsO$_4$) = 0.0 ppm (Ξ = 2.282 343 MHz). The chemical shift convention used is that a positive sign signifies a chemical shift to high frequency of the reference compound.

Samples were prepared in prepassivated 25-cm lengths of 4-mm o.d. FEP tubing, heat-sealed at one end and joined to a Kel-F valve. The *cis*-OsO$_2$F$_4$ (0.015 15 g, 0.050 81 mmol) was loaded into the tube in the drybox. The tube was transferred to a Teflon FEP metal vacuum line and anhydrous HF was distilled *in vacuo* into the tube at –78 °C to a depth of 3 cm. The tube was heat-sealed *in vacuo* while the contents were kept frozen at –196 °C. On warming of the sample to room temperature, a pale red saturated solution resulted which contained some solid *cis*-OsO$_2$F$_4$; this solution was decanted into the other end of the tube before the NMR spectrum was run.

Electron Diffraction. The electron diffraction intensities were recorded with a Gasdiffracktograph KD-G2[15] at two camera distances (25 and 50 cm) and with an accelerating voltage of about 60 kV. The electron wavelength was calibrated with ZnO diffraction patterns. The sample was sublimed at a reservoir temperature of 40 °C and the stainless-steel inlet system and nozzle with 0.5-mm diameter were heated to 50 °C. The photographic plates were analyzed by the usual methods.[16]

Synthesis of *cis*-OsO$_2$F$_4$. A $^3/_4$-in. o.d. Teflon-FEP U-trap that was closed by two stainless-steel valves was passivated, and OsO$_4$ (888.7 mg, 3.496 mmol) and dry HF (5.1027 g) were condensed in at –196 °C in a dynamic vacuum. In the same manner, KrF$_2$ (969.1 mg, 7.956 mmol) was added, and the resulting mixture was allowed to warm slowly toward room temperature. On warm up, gas evolution set in and the originally clear, colorless solution and solid OsO$_4$ phase turned orange-brown. To slow down the reaction, the reactor was intermittently cooled with a –78 °C bath when the gas evolution became too rapid. After completion of gas evolution, the solid product in the bottom of the reactor had turned purple. The gas evolution was measured by cooling the reactor first to –196 °C and then to –95 °C and measuring the amounts of noncondensible gas at each temperature by both *P*, *V*, *T* methods and by weight. The gas, noncondensible at –196 °C, was identified as oxygen (3.50 mmol), and that –95 °C as Kr (6.99 mmol). The combined weight loss was 696 mg (weight calculated for 3.496 mmol of O$_2$ and 6.992 mmol of Kr = 697.8 mg). The HF solvent and excess of KrF$_2$ were removed by pumping at –22 °C for 2 h leaving behind 1.047 g of a purple solid (weight calculated for 3.496 mmol of OsO$_2$F$_4$ = 1.043 g).

Computational Methods. The density functional theory (DFT)[17] calculations were done with the program DGauss,[18] which employs Gaussian orbitals on a Cray YMP computer. The initial basis set[19] for O and F is a polarized valence double-ζ set with the form (621/41/1)

(13) Marion, D.; Wuthrich, K. *Biochem. Biophys. Res. Commun.* **1983**, *113*, 967. Bodenhausen, G.; Kogler, H.; Ernst, R. R. *J. Magn. Reson.* **1984**, *58*, 370.

(14) Bax, A.; Subramanian, S. *J. Magn. Reson.* **1986**, *67*, 565.

(15) Oberhammer, H. *Molecular Structure by Diffraction* Methods; The Chemical Society: London, 1976; Vol. 4, p 24.

(16) Oberhammer, H.; Gombler, W.; Willner, H. *J. Mol. Struct.* **1981**, *70*, 273.

(17) (a) Parr, R. G.; Yang, W. *Density Functional Theory of Atoms and Molecules*; Oxford University Press: New York, 1989. (b) Salahub, D. R. In *Ab Initio Methods in Quantum Chemistry-II*; Lawley, K. P., Ed.; J. Wiley & Sons: New York, 1987; p 447. (c) Wimmer, E.; Freeman, A. J.; Fu, C.-L.; Cao, P.-L.; Chou, S.-H.; Delley, B. In *Supercomputer Research in Chemistry and Chemical Engineering*; Jensen, K. F., Truhlar, D. G., Eds.; ACS Symposium Series No. 353; American Chemical Society: Washington, DC, 1987; p 49. (d) Jones, R. O.; Gunnarsson, O. *Rev. Mod. Phys.* **1989**, *61*, 689. (e) Zeigler, T. *Chem. Rev.* **1991**, *91*, 651.

(18) (a) Andzelm, J.; Wimmer, E.; Salahub, D. R. In *The Challenge of d and f Electrons: Theory and Computation*; Salahub, D. R., Zerner, M. C., Eds.; ACS Symposium Series No. 394; American Chemical Society: Washington, DC, 1989; p 228. (b) Andzelm, J. In *Density Functional Methods in Chemistry*; Ed. Labanowski, J., Andzelm, J., Eds.; Springer-Verlag: New York, 1991; p 101. (c) Andzelm, J.; Wimmer, E. *J. Chem. Phys.* **1992**, *96*, 1280. DGauss is a local density functional program available via the Cray Research Unichem Project, Cray Research, Eagan, MN, 1993.

and a [7/3/3] fitting basis set. Norm-conserving pseudopotentials[20] were generated for Os following the work of Troullier and Martins.[21] The valence basis set for Os is (4,2/4/3,1) with a fitting basis set of [7/4/5]. The calculations were initially done at the local density functional (LDFT) level with the local potential of Vosko, Wilk, and Nusair.[22] Subsequently, the calculations were also done at the nonlocal level with the exchange potential of Becke[23] together with the nonlocal correlation functional of Perdew[24] (NLDFT/BP). For this case, a somewhat improved valence basis set of the form (721/51/1) was used for O and F. Geometries were optimized by using analytical gradients.[18] Second derivatives were calculated by numerical differentiation of the analytic first derivatives. A 2 point method with a finite difference of 0.01 au was used.

Results and Discussion

Synthesis and Properties of OsO$_2$F$_4$. The reaction of OsO$_4$ with KrF$_2$ in anhydrous HF solution proceeds quantitatively according to (1), as shown by an excellent material balance. Even

$$OsO_4 + 2KrF_2 \xrightarrow{HF} OsO_2F_4 + 2Kr + O_2 \qquad (1)$$
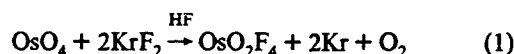
in the presence of a 2-fold excess of KrF$_2$ no further oxygen–fluorine exchange was observed, and the excess of KrF$_2$ was recovered unreacted. These results establish that the product from the OsO$_4$ + KrF$_2$ reaction is OsO$_2$F$_4$ and not OsOF$_6$ as previously reported.[6] The physical and spectroscopic properties of OsO$_2$F$_4$ (see below) are identical to those previously ascribed[6] to OsOF$_6$ and leave no doubt that the two products are identical. The facts that the reaction between KrF$_2$ and OsO$_4$ sets in at temperatures well below the incipient decomposition of KrF$_2$, that the yield of OsO$_2$F$_4$ based on KrF$_2$ is quantitative, and that under these conditions F$_2$ was shown to be unreactive with HF solutions of OsO$_4$ establish that reaction (1) involves a direct attack of KrF$_2$ on OsO$_4$ and does not proceed through an initial KrF$_2$ decomposition to F atoms which then react with OsO$_4$.

The OsO$_2$F$_4$ is a purple solid with a melting point of 90 °C and a vapor pressure of 1 Torr at room temperature. It can be stored at room temperature for extended time periods without significant decomposition. It dissolves in anhydrous HF to give purplish-red solutions. It hydrolyzes rapidly with formation of HF and a black precipitate. The X-ray powder pattern of OsO$_2$F$_4$ was identical to that previously ascribed[6] to OsOF$_6$.

Nuclear Magnetic Resonance Spectra. The ^{19}F NMR spectrum of a saturated solution of OsO$_2$F$_4$ in anhydrous HF shows two triplets of equal intensity characteristic of an A$_2$X$_2$ spin system (Figure 1). This provides definitive proof of the *cis* geometry adopted by OsO$_2$F$_4$, since the *trans*-isomer would have all four fluorine ligands equivalent and the ^{19}F NMR spectrum would only display a singlet arising from the A$_4$ spin system. The triplet multiplicities arise from the two-bond F$_a$–F$_e$ coupling which has a value of 138.3 Hz. At present, it is difficult to make a definitive assignment as to which triplet arises from which fluorine ligand environment, i.e., F-*trans*-to-F (F$_a$) or F-*trans*-to-O (F$_e$). Comparison of the ^{19}F chemical shifts with those in the related octahedral species WOF$_5^-$ [25] and ReOF$_5$,[26] where unambiguous assignment of the two environments can be made from the multiplicities of the resonances, suggests that the low-frequency triplet (δ = 15.8 ppm) should be ascribed to the F-*trans*-to-O

(19) Godbout, N.; Salahub, D. R.; Andzelm, J.; Wimmer, E. *Can. J. Chem.* **1992**, *70*, 560.

(20) Chen, H.; Kraskowski, M.; Fitzgerald, G. *J. Chem. Phys.*, in press.

(21) Troullier, N.; Martins, J. L. *Phys. Rev. B* **1991**, *43*, 1993.

(22) Vosko, S. J.; Wilk, L.; Nusair, M. *Can. J. Phys.* **1980**, *58*, 1200.

(23) (a) Becke, A. D. *Phys. Rev. A* **1988**, *38*, 2098. (b) Becke, A. D. In *The Challenge of d and f Electrons: Theory and Computation*; Salahub, D. R., Zerner, M. C., Eds.; ACS Symposium Series No. 394; American Chemical Society: Washington, DC, 1989; p 166. (c) Becke, A. D. *Int. J. Quantum Chem. Quantum Chem. Symp.* **1989**, *23*, 599.

(24) Perdew, J. P. *Phys. Rev. B* **1986**, *33*, 8822.

(25) McFarlane, W.; Noble, A. M.; Winfield, J. M. *J. Chem. Soc. A* **1971**, 948.

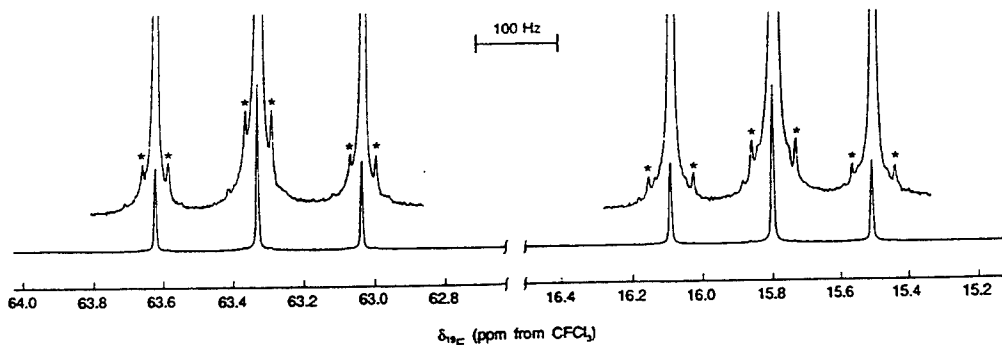(26) Bartlett, N.; Beaton, S.; Reeves, L. W.; Wells, E. J. *Can. J. Chem.* **1964**, *42*, 2531.

Figure 1. ^{19}F NMR spectrum (470.599 MHz) of a saturated solution of *cis*-OsO₂F₄ in anhydrous HF at 30 °C. The vertical expansion (×32) clearly reveals the satellites (denoted by asterisks) arising from spin coupling of the two ^{19}F ligand environments to natural-abundance (1.64%) ^{187}Os.

environment and the high-frequency triplet (δ = 63.3 ppm) to the F-*trans*-to-F environment. In addition, the ^{19}F chemical shifts of the *cis*-WO₂F₄²⁻ anion have also previously been assigned with the F-*trans*-to-F environment to high frequency of the F-*trans*-to-O environment.[27] On the other hand, coupling constant considerations indicate that the assignments for *cis*-OsO₂F₄ should be the reverse of those given above. Since the F_e–Os bonds are, as a consequence of F_e being *trans* to the stronger π-donor oxygen ligand, longer and more polar than the F_a–Os bonds, the $^1J(^{19}F_e$–$^{187}Os)$ coupling would be expected to be smaller than $^1J(^{19}F_a$–$^{187}Os)$ coupling (*vide infra*). On this basis, the F_e environment would be assigned to the high-frequency triplet and the F_a environment to the low-frequency triplet. A similar ambiguity also exists for the assignment of the F_a and F_e environments in the *cis*-ReO₂F₄⁻ [28] and *cis*-TcO₂F₄⁻ [29] anions, and the problem is currently under further investigation.

At high gain, each component of the two triplets displays low-intensity satellites (Figure 1), which arise from ^{19}F coupling to the low-abundance (1.64%) spin-active isotope ^{187}Os ($I = \frac{1}{2}$). The satellites yield two couplings, viz., $^1J(^{19}F_{lf}$–$^{187}Os) = 35.1$ Hz and $^1J(^{19}F_{hf}$–$^{187}Os) = 59.4$ Hz, for the low-frequency and high-frequency resonances, respectively, which represent the first reported couplings between ^{187}Os and ^{19}F. As discussed above, the actual assignment as to which fluorine ligand environment gives rise to which coupling constant is not yet resolved.

Osmium-187 is the least sensitive nuclide (receptivity with respect to ^{13}C = 1.15 × 10⁻³) in the Periodic Table, and its observation by conventional NMR techniques is very difficult.[30] Indeed until very recently, the only known ^{187}os chemical shifts were of the standard, OsO₄,[31] and a few μ-hydrido dinuclear osmium clusters.[32] In 1990, Benn and co-workers[33] obtained ^{187}Os NMR parameters [viz., $\delta(^{187}Os)$, $T_1(^{187}Os)$, $^1J(^{187}Os$–$^{31}P)$, and $^1J(^{187}Os$–$^1H)$] from a range of organo–osmium compounds by use of indirect 2D NMR spectroscopy in which the sensitive ^1H or ^{31}P nuclides were used for observation.

In view of the success of these experiments, it seemed worthwhile to attempt the acquisition of the ^{187}Os NMR spectrum of *cis*-
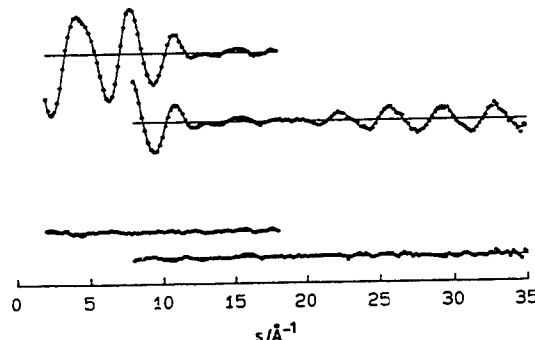
(27) Buslaev, Yu. A.; Petrosynants, S. P. *J. Struct. Chem. (Engl. Transl.)* **1969**, *10*, 983.

(28) (a) Bol'shakov, A. M.; Glushkova, M. A.; Buslaev, Yu. A. *Dokl. Chem. (Engl. Transl.)* **1983**, *273*, 417. (b) Casteel, W. J., Jr.; LeBlond, N.; Mercier, H. P. A.; Schrobilgen, G. J. Unpublished results.

(29) (a) Mercier, H. P. A.; Schrobilgen, G. *J. Inorg. Chem.* **1993**, *32*, 145. (b) Casteel, W. J., Jr.; LeBlond, N.; Lock, P. E.; Schrobilgen, G. J. Unpublished results.

(30) Goodfellow, R. J. In *Multinuclear* NMR; Mason, J., Ed.; Plenum Press: New York, 1987; Chapter 20, pp 521–561.

(31) Schwenk, A. *Prog. NMR Spectrosc.* **1985**, *17*, 69. Schwenk, A. Z. *Phys.* **1968**, *213*, 482. Kaufmann, J.; Schwenk, A. *Phys. Lett.* **1967**, *24A*, 115.

(32) Cabeza, J. A.; Mann, B. E.; Maitlis, P. M.; Brevard, C. *J. Chem. Soc., Dalton Trans.* **1988**, 629. Cabeza, J. A.; Nutton, A.; Mann, B. E.; Brevard, C.; Maitlis, P. M. *Inorg. Chim. Acta* **1986**, *115*, 447. Cabeza, J. A.; Mann, B. E.; Brevard, C.; Maitlis, P. M. *J. Chem. Soc., Chem. Commun.* **1985**, 65.

(33) (a) Benn, R.; Brenneke, H.; Joussen, E.; Lehmkuhl, H.; Ortiz, F. L. *Organometallics* **1990**, *9*, 756. (b) Benn, R.; Joussen, E.; Lehmkuhl, H.; Ortiz, F. L.; Rufinska, A. *J. Am. Chem. Soc.* **1989**, *111*, 8754.

Figure 2. Experimental (dots) and calculated (solid line) molecular intensities and differences for *cis*-OsO₂F₄.

OsO₂F₄ by indirect methods with ^{19}F as the observation nuclide. Hitherto, ^{19}F had only been used in the inverse detection of ^{13}C and ^{183}W.[34] The standard $^{19}F\{^{187}Os\}$ inverse correlation spectrum obtained for a saturated solution of *cis*-OsO₂F₄ in anhydrous HF clearly reveals a correlation with the ^{187}Os dimension and gives the ^{187}Os chemical shift of *cis*-OsO₂F₄ as 1431 ± 10 ppm with respect to OsO₄. This experiment uses multiplet quantum transitions which result in the loss of the passive heteronuclear couplings in the ^{187}Os dimension.[35] So far, attempts to obtain a spectrum by means of a double INEPT inverse experiment,[36] which should have the ^{19}F multiplicity manifest in the ^{187}Os dimension, have been unsuccessful. The ^{187}Os chemical shift of *cis*-OsO₂F₄ is the first to be reported for an Os(VIII) oxo fluoride and is strongly deshielded with respect to OsO₄. The only other precedent for this situation is found in ^{99}Tc NMR spectroscopy, where the chemical shift of the *cis*-TcO₂F₄⁻ anion is deshielded with respect to the corresponding tetraoxo-species TcO₄⁻,[29] although chemical shifts of metal nuclei, such as ^{99}Tc, do not correlate well with the electronegativity of the substituents.[37]

Electron Diffraction Analysis. The observed molecular intensities in the s-ranges 2–18 and 8–35 Å⁻¹ at intervals of Δs = 0.2 Å⁻¹ are shown in Figure 2. The radial distribution function of OsO₂F₄ (Figure 3) was calculated by Fourier transform of the molecular intensities by applying an artificial damping function $\exp(-\gamma s^2)$ with $\gamma = 0.002$ Å². In the least-squares refinements the molecular intensities were modified by a digonal weight matrix, and known scattering amplitudes and phases were used.[38] The electron diffraction analysis of OsO₂F₄ presents two major problems: (1) The equatorial and axial Os–F bond lengths are

(34) Bourdonneau, M.; Brevard, C. *Inorg. Chem.* **1990**, *29*, 3270.

(35) Müller, L. *J. Am. Chem. Soc.* **1979**, *101*, 4481. Bax, A.; Griffey, R. H.; Hawkins, B. L. *J. Am. Chem. Soc.* **1983**, *105*, 7188. Bax, A.; Griffey, R. H.; Hawkins, B. L. *J. Magn. Reson.* **1983**, *55*, 301. Müller, L.; Schiksius, R. A.; Opella, S. J. *J. Magn. Reson.* **1986**, *66*, 379.

(36) Bodenhausen, G.; Ruben, D. J. *Chem. Phys. Lett.* **1980**, *69*, 185. Benn, R.; Brenneke, H.; Frings, A.; Lehmkuhl, H.; Mehler, G.; Rufinska, A.; Wildt, T. *J. Am. Chem. Soc.* **1988**, *110*, 5661.

(37) One of the reviewers has pointed out that the chemical shift of ^{99}Tc in TcO₃CH₃ is substantially downfield from that in TcO₃F.

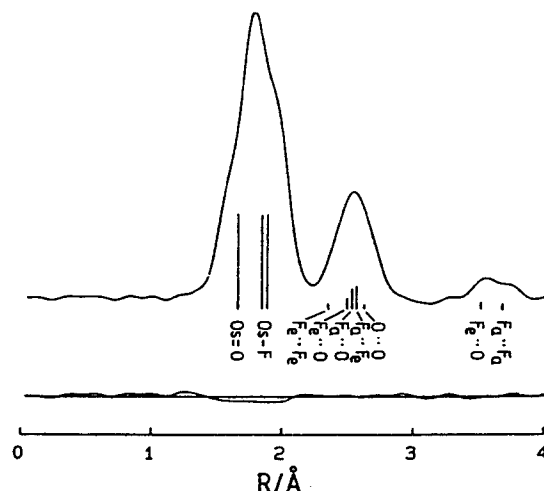11282 *J. Am. Chem. Soc., Vol. 115, No. 24, 1993*

Christe et al.

Figure 3. Experimental radial distribution function and difference curve. The positions of interactomic distances are indicated by vertical lines.

Table I. Results of Electron Diffraction Analyses and Theoretical Calculations

Geometric Parameters

| | electron diffraction[a] | | |
	model I	model II	theoretical
Os=O	1.674(4)	1.674(4)	1.724
(Os–F)$_{mean}$	1.863(3)	1.863(3)	1.901
(Os–F$_e$) – (Os–F$_a$)	0.000[b]	0.040[b]	0.040
Os–F$_e$	1.863(3)[c]	1.883(3)	1.921
Os–F$_a$	1.863(3)[c]	1.843(3)	1.881
O=Os=O	97.4(56)	103.5(25)	102.6
F$_e$–Os–F$_e$	78.5(21)	77.3(26)	78.6
F$_e$–Os=O	92.1(39)[c]	89.6(16)[c]	89.4
F$_e$–Os–F$_a$	85.5(12)	87.0(15)	85.0
O=O–F$_a$	93.8(8)[c]	92.4(17)[c]	94.1
F$_a$–Os–F$_a$	168.6(30)[c]	172.0(35)[c]	169.0

Interatomic Distances and Vibrational Amplitudes for Model II

	r	l		r	l
Os=O	1.674(4)	0.046(4)	F$_e$··F$_e$	2.35(7)	
Os–F	1.863(3)	0.054(3)	O··F$_e$	2.51(4)	
F$_e$··O	3.53(1)	0.080(27)	O··F$_a$	2.54(4)	0.110[b]
F$_a$··F$_a$	3.68(1)		F$_a$··F$_e$	2.57(4)	
			O··O	2.63(5)	

[a] r_a distances in Å and angles in deg. Error limits are 3σ values. [b] Not refined. [c] Dependent geometric parameter.

very similar and cannot be determined separately. A mean value (Os–F)$_{mean}$ = $^1/_2$[(Os–F$_e$) + (Os–F$_a$)] was refined, and the bond length difference (Os–F$_e$) – (Os–F$_a$) was set either to zero (model I) or to the theoretically calculated value of 0.040 Å (model II). (2) In near-octahedral structures all short nonbonded distances, which form the peak near 2.56 Å in our radial distribution function, are closely spaced and their assignment is not unique. As can be seen from Figure 3, two pairs of distances, i.e. the F$_e$··F$_e$ and O··O distances in the equatorial plane and the F$_a$··F$_e$ and F$_a$··O distances between axial and equatorial substituents can be interchanged. The former interchange leads to an F$_e$–Os–F$_e$ angle smaller than or nearly equal to the O=Os=O angle and the latter interchange to F$_e$–Os–F$_a$ angles smaller or larger than the O=Os–F$_a$ angles. The equatorial F$_e$–Os=O angles are nearly unaffected by thes interchanges. While all four possible assign-

(38) Haase, J. Z. *Naturforsch., A* **1970**, *25*, 936. The problems of possibly inadequate scattering amplitudes or phases for atoms of high atomic number and the importance of multiple scattering have recently been studied extensively for the tantalum compound (CH$_3$)$_3$TaF$_2$, which also contains a sixth row element (Elbel, S.; Oberhammer, H. To be published). It was found that these possible inadequacies in scattering theory have a negligible effect on geometric parameters and lead to small changes in vibrational amplitudes only.
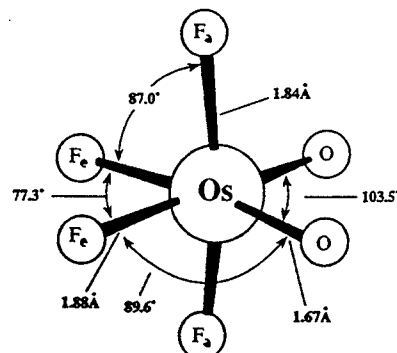

Figure 4. Molecular structure of gaseous *cis*-OsO$_2$F$_4$ from combined electron diffraction and computational data.

ments for the 2.56-Å peak components fit the experimental radial distribution curve and the molecular intensities nearly equally well, only one assignment is in accord with our theoretical calculations (see below) and general VSEPR arguments.[39] On the basis of these, the osmium–oxygen bonding domains are more repulsive than the osmium–fluorine domains and, therefore, the O–Os–O bond angle must be larger than the equatorial F–Os–F angle, and the axial fluorine atoms must be bent away from the oxygen ligands. Using this constraint for the bond angles and the resulting assignments for the individual components of the 2.56-Å peak of the radial distribution curve, the diffraction data were refined for both, model I and model II, and resulted in a slightly lower (by 8%) R-factor for model II (see Table I). Since the vibrational amplitude for the short nonbonded distances causes high correlations in the least-squares analysis, this amplitude was not refined. When five geometric parameters [r(Os–O), r(Os–F)$_{mean}$, ∠OOsO, ∠F$_e$OsF$_e$, ∠F$_e$OsF$_a$] and three vibrational amplitudes were refined simultaneously, only one correlation coefficient had a value larger than |0.5|: F$_e$OsF$_e$/OOsF$_a$ = –0.79. Of the two structural models for OsO$_2$F$_4$, model II (Figure 4) is preferred since it results in the lowest R-factor and because theoretical calculations of the type used in our study are known to reproduce differences between bond lengths of similar types, such as Os–F$_e$ and Os–F$_a$, very well.

A comparison of the structure of *cis*-OsO$_2$F$_4$ with those of OsO$_4$,[40] OsOF$_4$,[41] and OsF$_6$[42] shows the following trends:
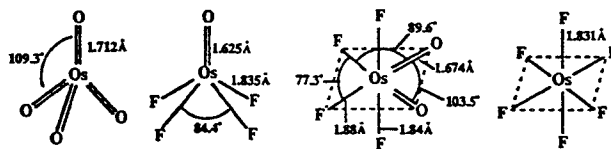
The Os–O bond length increases with an increasing number of oxygen ligands; i.e., oxygen releases electron density to the high oxidation state osmium central atom. This allows the transfer of more negative charge to the remaining ligands, thereby increasing the polarities and lengths of these bonds. The Os–F bond length also increases with increasing oxygen substitution; i.e., it increases from 1.835(7) Å in OsOF$_4$ to an average of 1.863(3) Å in *cis*-OsO$_2$F$_4$. Obviously, secondary effects, such as the formal oxidation state of the central atom and its coordination number, will also contribute to the bonding but cannot be analyzed at the present time in the absence of more precise data and further examples.

(39) (a) Gillespie, R. J. *Molecular Geometry*; Van Nostrand Reinhold: London, 1972. (b) Gillespie, R. J.; Hargittai, I. *The VSEPR Model of Molecular Geometry*; Allyn and Bacon: Boston, 1991.

(40) Seip, H. M.; Stolevik, R. *Acta Chem. Scand.* **1966**, *20*, 385.

(41) Alekseichuk, I. S.; Ugarov, V. V.; Rambidi, N. G.; Legasov, V. A.; Sokolov, V. B. *Proc. Acad. Sci. USSR (Engl. Transl.)* **1981**, *257*, 99.

(42) Weinstock, B.; Claassen, H. H.; Malm, J. G. *J. Chem. Phys.* **1960**, *32*, 181. Claassen, H. H.; Goodman, G. L.; Kimura, M.; Schomaker, V.; Smith, D. W. *J. Chem. Phys.* **1968**, *48*, 4001.

Table II. Vibrational Spectral Data for *cis*-OsO$_2$F$_4$

assgnts and approx mode descriptions in point group C_{2v}		obsd^a freq, cm^{-1} (rel int)		calcd freq, cm^{-1} (IR int)	
		IR (25 °C)	R (−150 °C)	NLDFT/BP^b	LDFT^c
A$_1$ (IR, R)	ν_1 ν_{sym} OsO$_2$	940 s	943 (100)	947 (78)	918 (79)
	ν_2 sym comb of sym ax and sym equat OsF$_2$ stretch		673 (59)	648 (47)	663 (50)
	ν_3 antisym comb of sym ax and sym equat OsF$_2$ stretch	590 vs	580 (17)	578 (24)	595 (33)
	ν_4 δ_{sciss} OsO$_2$		402 (38)	376 (1.3)	374 (5.4)
	ν_5 sym comb of ax and equat OsF$_2$ scissor		350 (31)	321 (6.0)	325 (13)
	ν_6 antisym comb of ax and equat OsF$_2$ scissor		217 (1)	212 (1.5)	212 (2.2)
A$_2$ (-, R)	ν_7 OsO$_2$ torsion		314 (1)	321 (3.9)	322 (14)
	ν_8 OsF$_{2e}$ torsion		95 sh	100 (0)	95 (7.7)
B$_1$ (IR, R)	ν_9 ν_{as} OsF$_{2a}$	680 vs	680 sh	676 (198)	690 (203)
	ν_{10} δ_{rock} OsF$_{2a}$		323 (1)	325 (7.8)	326 (11)
	ν_{11} δ_{rock} OsF$_{2e}$		266 (2)	269 (38)	268 (35)
B$_2$ (IR, R)	ν_{12} ν_{as} OsO$_2$	930 s	933 (31)	950 (111)	929 (110)
	ν_{13} ν_{as} OsF$_{2e}$	570 vs	572 (14)	553 (43)	576 (26)
	ν_{14} sym comb of OOsF$_e$ sciss and OsF$_{2a}$ sciss		344 (31)	311 (20)	317 (25)
	ν_{15} antisym comb of OOsF$_e$ sciss and OsF$_{2a}$ sciss		168 (3)	181 (0.4)	176 (0.5)

^{a} In addition to the bands listed, the following very weak Raman bands were observed: 246 (1) = (168 + 79), 190 (0+), 175 sh, 79 (1) = lattice vibration. ^{b} Unscaled frequencies. ^{c} The stretching frequencies were scaled by an empirical factor of 0.9424 to maximize their agreement with the observed ones.
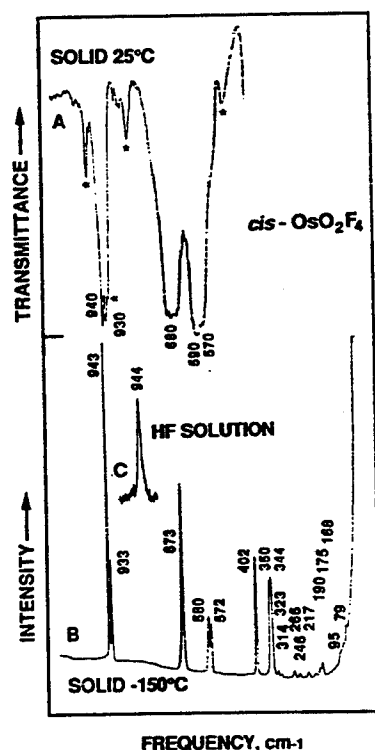

Figure 5. Infrared (A) and Raman (B and C) spectra of *cis*-OsO$_2$F$_4$ in the solid state (A and B) and HF solution (C). The bands marked by an asterisk are due to decomposition products.

Table III. Calculated Structure and Vibrational Frequencies for OsO$_4$

Bond Distances (Å)

	LDFT	NLDFT/BP	expt
r(Os–O)	1.730	1.739	1.71

Vibrational Frequencies (cm^{-1}) and IR Intensities (km/mol)

sym	expt	LDFT	NLDFT/BP
A$_1$	965	1000 (0)	953 (0)
E	333	292 (0)	323 (0)
F$_2$	960	1027 (359)	980 (329)
	329	300 (16)	339 (10)

Table IV. Geometry Parameters^a for OsO$_2$F$_4$

	C_{2v} (cis) (see Figure 4)		C_{2v} (trans) (see Figure 6)		
	LDFT	NLDFT/BP	LDFT	NLDFT/BP	expt
r(Os–O)	1.724	1.735	1.734	1.741	1.674(4)
r(Os–F)	1.881 a	1.902 a	1.882 e2	1.900	1.843(3) a
r(Os–F)	1.921 e	1.944 e	1.927 el	1.965	1.883(3) e
∠O–Os–O	102.6	102.1	137.2	136.9	103.5(25)
∠O–Os–F	89.4 e	89.4 e	106.9 e2	106.9	89.6(16) e
∠O–Os–F	94.1 a	93.8 a	81.0 el	80.9	92.4(17) a
∠F–Os–F	169.0 a,a	167.7 a,a	129.7 el,el	129.2	172.0(35) a,a
∠F–Os–F	78.6 e,e	79.1 e,e	75.2 e2,e2	75.5	77.3(26) e,e
∠F–Os–F	85.0 a,e	85.3 a,e	77.5 el,e2	77.6	87.0(15) a,e

^{a} Bond distances in Å. Bond angles in deg.

Vibrational Spectra. The infrared and Raman spectra of solid OsO$_2$F$_4$ and the Raman spectrum of its HF solution are shown in Figure 5. The observed frequencies, together with their assignments in point-group C_{2v}, are listed in Table II. The assignments were made by comparison with the calculated frequencies and intensities (see Table II and below) and are unambiguous for the seven fundamental vibrations with the highest frequencies, i.e., for the bands above 400 cm^{-1}. In the 300–350-cm^{-1} region, four Raman bands were observed at 350, 344, 323, and 314 cm^{-1}, which must be assigned to ν_5(A$_1$), ν_7(A$_2$), ν_{10}(B$_1$), and ν_{14}(B$_2$). Of these, ν_5(A$_1$) and ν_{14}(B$_2$) involve very similar type of motions and, by comparison with the related SF$_4$[43] and PF$_4^-$[44] species, should be of much higher Raman intensities than the OsO$_2$ rocking and the OsO$_2$ torsion motions. Therefore, ν_5(A$_1$) and ν_{14}(B$_2$) were assigned to the Raman bands at 344 and

350 cm^{-1}, respectively, and ν_7(A$_2$) and ν_{10}(B$_1$) to 314 and 323 cm^{-1}, respectively. In the 200–270-cm^{-1} region, three bands were observed at 217, 246, and 266 cm^{-1}, two of which should belong to the OsF$_{2eq}$ rocking mode, ν_{11}(B$_1$), and the antisymmetric combination of axial and equatorial OsF$_2$ scissoring, ν_6(A$_1$). Since the 246-cm^{-1} band has the lowest Raman intensity and can be assigned to a combination band, i.e., 168 + 79 = 247 cm^{-1}, the 266-cm^{-1} Raman band was assigned to ν_{11}(B$_1$) and the 217-cm^{-1} one to ν_6(A$_1$). The remaining yet unassigned modes, ν_{15}(B$_2$) and ν_8(A$_2$), have calculated frequency values of about 176 and 95 cm^{-1}, respectively, and consequently are assigned to the Raman bands observed at 168 and 95 cm^{-1}, respectively, leaving only two very weak Raman features at 190 (0+) and 175 (sh) cm^{-1} and a probable lattice vibration at 79 cm^{-1} unassigned. Although the assignments below the 344-cm^{-1} Raman line are somewhat

(43) Christe, K. O.; Willner, H.; Sawodny, W. *Spectrochim. Acta, Part A* **1979**, *35A*, 1347 and references cited therein.

(44) Christe, K. O.; Dixon, D. A.; Mercier, H. P.; Sanders, J. C. P.; Schrobilgen, G. J.; Wilson, W. W. Submitted for publication in *J. Am. Chem. Soc.*

Table V. Vibrational Frequencies (cm⁻¹) and IR Intensities (km/mol) for C_{2v} *trans*-OsO_2F_4

sym	LDFT	NLDFT/BP	sym	LDFT	NLDFT/BP
A_1	955 (18)	925 (30)	B_1	968 (132)	950 (97)
	726 (82)	672 (87)		345 (4.9)	336 (2.8)
	589 (18)	527 (20)		256 (3.3)	255 (2.5)
	403 (7.0)	385 (2.5)	B_2	706 (159)	638 (142)
	333 (12)	321 (15)		594 (5.6)	537 (5.2)
	122 (0.4)	117 (0.8)		304 (14)	299 (15)
A_2	419 (0.2)	407 (0)		241 (21)	230 (20)
	96 (3.8)	89 (0)			
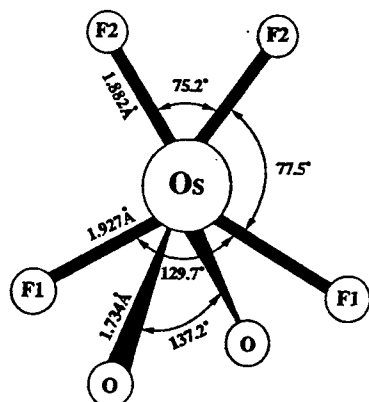
Figure 6. Minimum energy C_{2v} structure of OsO_2F_4 obtained from the *trans*-D_{4h} structure as a starting point in the LDFT calculation. The Os, F1, and F2 atoms are all in one plane.

tentative, the agreement with the calculated frequencies and anticipated intensities is quite good (see Table II). Hence, the observed vibrational spectra strongly support the pseudooctahedral *cis*-structure established by both the electron diffraction and the NMR studies.

Computational Results. The geometries and vibrational spectra of *cis*- and *trans*-OsO_2F_4 were calculated using density functional theory at the local density functional (LDFT) level with the local potential of Vosko et al.[22] and also at the nonlocal level with the exchange potential of Becke[23] together with the nonlocal correlation functional of Perdew[24] (NLDFT/BP). To test the accuracy of these methods, the well-known OsO_4 molecule[40] was first calculated. The results are summarized in Table III. As can be seen, the calculated bond lengths are slightly longer than the observed one, but the calculated frequencies and, in particular those at the NLDFT/BP level, are quite close to the experimental ones even without scaling.

The calculations for *cis*- and *trans*-OsO_2F_4 (see Tables II, IV, and V) show that the *cis*-structure for OsO_2F_4 is a true minimum. The D_{4h} *trans*-structure is not a minimum energy structure and distorts to a C_{2v} structure as shown in the Figure 6. The minimum-energy structure is 17.7 kcal/mol lower in energy as compared to the minimum-energy C_{2v} *trans*-structure at the local DFT level and is 15.5 kcal/mol lower in energy than the *trans*-structure if nonlocal correlations are included. The fact that contrary to $IO_2F_4^-$, which exists as both a *cis*- and *trans*-isomer,[45] OsO_2F_4 forms only a stable *cis*-isomer is in accord with previous conclusions[46-48] that in octahedral dioxo complexes, MO_2X_4, metals with a d^0 configuration prefer a *cis*-structure.

Note Added in Proof. After completion of this work, two publications dealing with OsO_2F_4 appeared. In the first one (*Chem. Ber.* **1993**, *126*, 1331) Bougon, Buu, and Seppelt report a crystal structure. Their results were severely hampered by absorption and disorder problems and, therefore, did not yield a reliable geometry for OsO_2F_4. In the second paper (*Chem. Ber.* **1993**, *126*, 1325) Veldkamp and Frenking report the results from ab initio calculations at the HF and MP2 levels of theory. A comparison of their results with ours shows that our density functional theory calculations reproduce the experimental values much better and, therefore, should be preferred.

(45) Christe, K. O.; Wilson, R. D.; Schack, C. J. *Inorg. Chem.* **1981**, *20*, 2104.

(46) Griffith, W. P.; Wickins, T. D. *J. Chem. Soc. A* **1968**, 400.

(47) Griffith, W. P. *J. Chem. Soc. A* **1969**, 211.

(48) Hope, E. G.; Levason, W.; Ogden, J. S. *J. Chem. Soc., Dalton Trans.* **1988**, 997.

2850

Tetrafluorophosphite, PF_4^-, Anion[†]

Karl O. Christe,[*,1] **David A. Dixon,**[2] **Hélène P. A. Mercier,**[3] **Jeremy C. P. Sanders,**[3]
Gary J. Schrobilgen,[*,3] **and William W. Wilson**[1]

*Contribution from Rocketdyne, A Division of Rockwell International,
Canoga Park, California 91309, Department of Chemistry, McMaster University,
Hamilton, Ontario L8S 4MI, Canada, and Central Research and Development
Department, E. I. du Pont de Nemours and Company, Inc., Experimental Station,
Wilmington, Delaware 19880-0328*

Received July 19, 1993[●]

Abstract: $N(CH_3)_4^+PF_4^-$, the first example of a PF_4^- salt, has been prepared from $N(CH_3)_4F$ and PF_3 using either CH_3CN, CHF_3, or excess PF_3 as a solvent. The salt is a white, crystalline solid which is thermally stable up to 150 °C, where it decomposes to $N(CH_3)_3$, CH_3F, and PF_3. The structure of the PF_4^- anion was studied by variable temperature ^{31}P and ^{19}F NMR spectroscopy, infrared and Raman spectroscopy, SCF, MP2, local and nonlocal density functional calculations, a normal coordinate analysis, and single-crystal X-ray diffraction. The anion possesses a pseudo trigonal bipyramidal structure with two longer axial bonds and an equatorial plane containing two shorter equatorial bonds and a sterically active free valence electron pair. In solution, it undergoes an intramolecular exchange process by the way of a Berry pseudorotation mechanism. The vibrational frequencies observed for PF_4^- in solid $N(CH_3)_4PF_4$ are in excellent agreement with those calculated for free gaseous PF_4^-. The X-ray diffraction study (tetragonal, space group $P\bar{4}2_1m$, $a = 8.465(3)$ Å, $c = 5.674(2)$ Å, $Z = 2$, $R = 0.0723$ for 268 observed [$F \geq \sigma(F)$] reflections suffers from a 3-fold disorder with unequal occupancy factors for the equatorial fluorine atoms of PF_4^- but confirms its pseudo trigonal bipyramidal structure and the axial P–F bond length calculated for the free ion.

Introduction

Although PBr_4^-[4–6] and PCl_4^-[7] salts have been well-known for many years, and the free PF_4^- anion has been observed by mass spectroscopy[8–10] and in ion cyclotron resonance experiments,[11,12] no reports on the isolation of PF_4^- salts could be found in the literature. The only published attempts to prepare such salts were negative. In 1955 Woolf reported that PF_3, when passed over KF *in vacuo* at temperatures up to 240 °C, did not form a salt and that KF and PF_3 at atmospheric pressure and temperatures above 200 °C produced KPF_6 and red phosphorus in an apparent disproportionation reaction.[13] Similarly, Muetterties and co-workers stated[14] in 1960 that KF or CsF absorbs PF_3 at about 150 °C, but that the products were a mixture of PF_6^- salts and red phosphorus and not PF_4^- salts. In 1981, Wermer and Ault reported[15] the isolation of the $Cs^+PF_4^-$ ion pair by codeposition of CsF and PF_3 in an argon matrix; however, their evidence for the presence of such an ion pair is weak since only infrared spectra between about 800 and 550 cm^{-1} were presented, too many bands were observed, and their frequencies do not

correspond well to those found in this study for the PF_4^- anion in $N(CH_3)_4PF_4$.

This lack of evidence for PF_4^- salts in the previous literature was surprising since the F^- affinity of PF_3 (40.2 kcal mol^{-1})[12] is comparable to that of SO_2 (43.8 kcal mol^{-1}),[12] which readily forms stable SO_2F^- salts. Since our recent synthesis[16] of truly anhydrous $N(CH_3)_4F$ had provided us with a source of soluble fluoride ion in combination with a large and relatively inert stabilizing counter cation, we decided to explore whether salts containing the PF_4^- anion could be prepared.

Experimental Section

Apparatus and Materials. Volatile materials were handled in a flamed-out Pyrex glass vacuum line that was equipped with Kontes glass–Teflon valves and a Heise pressure gauge. Nonvolatile materials were handled in the dry nitrogen atmosphere of a glovebox. The infrared and Raman spectrometers and the X-ray diffractometer have previously been described.[17]

Literature methods were used for the syntheses of $N(CH_3)_4F$[16] and the drying of CH_3CN.[18] PF_3 (Ozark Mahoning) and CHF_3 (The Matheson Co.) were purified by fractional condensation prior to their use.

Synthesis of $N(CH_3)_4PF_4$. Three modifications were used for the preparation of this compound, and all three methods gave quantitative yields of the desired $N(CH_3)_4PF_4$ salt.

I. $N(CH_3)_4F$ was loaded in the drybox into a two-piece Pyrex ampule that was closed by a Teflon valve. The vessel was connected to the vacuum line and cooled to –196 °C, and about 4 mL of liquid CH_3CN was added per millimole of $N(CH_3)_4F$. The mixture was briefly warmed to room temperature to dissolve the $N(CH_3)_4F$ and cooled again to –196 °C for the addition of a 50% excess of PF_3. The mixture was allowed to warm to ambient temperature for several hours, and then the volatile products were pumped off, leaving behind white, solid $N(CH_3)_4PF_4$.

† Dedicated to Professor Wolfgang Sawodny on the occasion of his 60th birthday.
● Abstract published in *Advance ACS Abstracts*, February 1, 1994.
(1) E. I. du Pont de Nemours and Company, Inc.
(2) McMaster University.
(3) Rockwell International, Rocketdyne Division.
(4) Dillon, K. B.; Waddington, T. C. *J. Chem. Soc., Chem. Commun.* 1969, 1317.
(5) Sheldrick, W. S.; Schmidpeter, A.; Zwaschka, F.; Dillon, K. B.; Platt, A. W. G.; Waddington, T. C. *J. Chem. Soc., Dalton Trans.* 1981, 413.
(6) Sheldrick, W. S.; Kiefer, J. Z. *Naturforsch., B* 1989, *44B*, 609.
(7) Dillon, K. B.; Platt, A. W. G.; Schmidpeter, A.; Zwaschka, F.; Sheldrick, W. S. Z. *Anorg. Allg. Chem.* 1982, *488*, 7.
(8) Dillard, J. G.; Rhyne, T. C. *J. Am. Chem. Soc.* 1969, *91*, 6521.
(9) Rhyne, T. C.; Dillard, J. G. *Inorg. Chem.* 1971, *10*, 730.
(10) Lane, K. R.; Sallans, L.; Squires, R. R. *J. Am. Chem. Soc.* 1985, *107*, 5369.
(11) Sullivan, S. A.; Beauchamp, J. L. *Inorg. Chem.* 1978, *17*, 1589.
(12) Larson, J. W.; McMahon, T. B. *J. Am. Chem. Soc.* 1983, *105*, 2944.
(13) Woolf, A. A. *J. Chem. Soc.* 1955, 279.
(14) Muetterties, E. L.; Bither, T. A.; Farlow, M. W.; Coffman, D. D. *J. Inorg. Nucl. Chem.* 1960, *16*, 52.
(15) Wermer, P.; Ault, B. S. *Inorg. Chem.* 1981, *20*, 970.

(16) Christe, K. O.; Wilson, W. W.; Wilson, R. D.; Bau, R.; Feng, J. *J. Am. Chem. Soc.* 1990, *112*, 7619.
(17) Christe, K. O.; Curtis, E. C.; Dixon, D. A.; Mercier, H. P.; Sanders, J. C. P.; Schrobilgen, G. J. *J. Am. Chem. Soc.* 1991, *113*, 3351.
(18) Christe, K. O.; Dixon, D. A.; Mahjoub, A. R.; Mercier, H. P. A.; Sanders, J. C. P.; Seppelt, K.; Schrobilgen, G. J.; Wilson, W. W. *J. Am. Chem. Soc.* 1993, *115*, 2696.

II. The N(CH$_3$)$_4$F was dissolved in liquid CHF$_3$ at −78 °C, using about 2 g of CHF$_3$ per millimole of N(CH$_3$)$_4$F, followed by the addition of twice the required amount of PF$_3$ at −196 °C. The mixture was warmed for about 10 h to −78 °C, followed by the pumping off of all material that was volatile at room temperature. The white solid residue consisted of N(CH$_3$)$_4$PF$_4$.

III. The N(CH$_3$)$_4$F was placed into a small volume, stainless steel Hoke cylinder that was closed by a valve. On the vacuum line, a 15-fold excess of PF$_3$ was added to the cylinder at −196 °C, and the cylinder was kept at room temperature for 12 h. The cylinder was cooled again to −196 °C, and all volatile material was removed by pumping during warm-up of the cylinder from −196 °C to room temperature, leaving behind the white solid N(CH$_3$)$_4$PF$_4$.

Pyrolysis of N(CH$_3$)$_4$PF$_4$. A sample of N(CH$_3$)$_4$PF$_4$ (1.68 mmol) in a Pyrex vessel was heated in a dynamic vacuum at 165 °C for 6.5 h. The volatile decomposition products consisted of PF$_3$ (1.51 mmol), CH$_3$F (0.92 mmol), and N(CH$_3$)$_3$ (0.92 mmol), in good agreement with the observed weight loss. The beige-colored residue (85 mg) was identified by infrared and ^{19}F NMR spectroscopy as a mixture of N(CH$_3$)$_4$$^+$ salts of PF$_6^-$, HPF$_5^-$, and POF$_2^-$. Differential scanning calorimetry (DSC) showed three irreversible endotherms for N(CH$_3$)$_4$PF$_4$, a very small one at 158 °C, a medium one at about 238 °C, and a large one at about 246 °C.

Crystal Structure Determination of N(CH$_3$)$_4$PF$_4$. Single crystals of N(CH$_3$)$_4$PF$_4$ were obtained from a CH$_3$CN solution, saturated at 50 °C, by allowing the solution in a Teflon–FEP vessel to cool slowly to room temperature. Large transparent crystals were obtained that were square plates and grew as clusters. The crystal used had the dimensions of 0.3 × 0.3 × 0.05 mm.

The crystal was centered on a Siemens R3m/V diffractometer and diffracted only at low angles because of its dimensions. Accurate cell dimensions were determined at −100 °C from a least-squares refinement of the setting angles (χ, ϕ, and 2θ) obtained from 14 accurately centered reflections (with $5.35° \leq 2\theta \leq 12.77°$). Integrated diffraction intensities were collected using a θ–2θ scan technique with scan rates varying from 1.5 to 14.65°/min (in 2θ) and a scan range of ±0.6° so that the weaker reflections were examined more slowly. The data were collected within $0 \leq h \leq 10$, $0 \leq k \leq 10$, and $0 \leq l \leq 6$ and $3 \leq 2\theta \leq 40°$ using Ag Kα with a graphite monochromator ($\lambda = 0.56086$ Å). The intensities of three standard reflections were monitored every 97 reflections; no decay was observed. A total of 472 reflections were collected, and 270 unique reflections remained after averaging of equivalent reflections. Lorentz and polarization corrections were applied. The $P\bar{4}2_1m$ space group was obtained from the Laue symmetry, the 0k0 extinctions with $k \neq 2n$, and the non-centrosymmetric E$_s$ statistics.

The solution was obtained by direct methods.[19] The structure consisted of well separated, ordered N(CH$_3$)$_4$$^+$ cations and disordered PF$_4^-$ anions. While the positioning of the N(CH$_3$)$_4$$^+$ cation was straightforward (N on $\bar{4}$ and C on 1), the orientation of the PF$_4^-$ anion was problematic since the tetragonal axis of the crystal was incompatible with the expected geometry of the PF$_4^-$ anion. All the atoms of PF$_4^-$ were found on special positions, i.e., P and F(2) on 2.mm and F(1) and F(3) on .mm, requiring disorder of the equatorial fluorines. The assumption of 2-fold disorder (structures a + b given in the Results and Discussion section) along the equatorial P–F(2) axis, i.e., of a positional disorder of one equatorial fluorine atom and the sterically active free valence electron pair on phosphorus, and of site occupancy factors (sof) of 0.25 for both F(2) and F(3), gave R-factors of 0.0876 with 268 reflections and of 0.0544 with 185 reflections.

A second disorder model assuming 3-fold disorder along the axial F(1)–P–F(1) axis with equal occupancy factors of 0.1667 for the three equatorial F positions (structures a + b + c given in the Results and Discussion section) gave R-factors of 0.0867 with 268 reflections and 0.0539 with 185 reflections but did not result in the required equal bond lengths for the three equatorial P–F bonds and the 120° and 180° bond angles for the equatorial and axial PF$_2$ groups, respectively. Instead, the geometry found was similar to that found under the assumption of 2-fold disorder.

A third model was tested with variable proportions of structures (a + b) and c, while maintaining the sum of the sof's of F(2) and F(3) equal to 0.5. Minimum R-values of 0.0723 with 268 reflections and 0.0510 with 185 reflections were obtained with sof's of 0.20 for F(2) and 0.30 for F(3).

(19) Sheldrick, G. M. *SHELXTL PLUS*, Release 4.21/V; Siemens Analytical X-Ray Instruments, Inc.: Madison, WI, 1990.

Table 1. Summary of Crystal Data and Refinement Results for N(CH$_3$)$_4$PF$_4$

space group	$P\bar{4}2_1m$
a	8.465(3) Å
c	5.674(2) Å
V (Å^3)	406.5(2)
molecules/unit cell	2
mol wt (g mol^{-1})	181.1
calcd density (g cm^{-3})	1.480
T (°C)	−100
μ (cm^{-1})	1.8
wavelength (Å) used for data colln	0.560 86
final agreement factors	$R = 0.0723$
	$R_w = 0.0745$

Table 2. Atomic Coordinates (× 10^4) and Equivalent Isotropic Displacement Coefficients (Å^2 × 10^3) in N(CH$_3$)$_4$PF$_4^-$

	x	y	z	U(eq)^a	sof^b
P	5000	0	3962(6)	60(1)	0.25
F(1)	3567(4)	1433(4)	4016(11)	65(2)	0.50
F(2)	5000	0	6645(13)	53(2)	0.20
F(3)	−1087(11)	6087(11)	6759(29)	101(4)	0.30
N	0	0	0	33(2)	0.25
C	1450(6)	104(8)	−1526(8)	42(1)	1.00

^{a} Equivalent isotropic U defined as one-third of the trace of the orthogonalized U_{ij} tensor. ^{b} Site occupancy factor.

Table 3. A Comparison of the Apparent Interactive Distances (Å) and Bond Angles (deg) of PF$_4^-$ from the X-ray Diffraction Study with Those Calculated at the SCF Level for Free Ordered PF$_4^-$ and with the Apparent Geometries of the Free Ion When Subjected to Either 2-Fold or 3-Fold Disorder with Equal Occupancy Factors

	apparent geometry from crystal structure	calcd geometries of the free ion		
		ordered	2-fold disordered	3-fold disordered
P–F(1)$_{ax}$	1.716(1) [1.726]^a	1.741	1.736	1.741
P–F(2)$_{eq}$	1.522(8) [1.559]	1.604	1.604	<1.604
P–F(3)$_{eq}$	1.386(5) [1.410]	1.604	<1.604	
F(2)–P–F(3)	108.0(5)	99.9	99.9	120
F(1)–P–F(1)	178.0(5)	168.3	172.4	180
F(1)–P–F(2)	89.0(2)	86.2	86.2	90
F(1)–P–F(3)	90.3(6)	86.2	90.4	90
F(3)–P–F(3A)	143.9(12)		160.2	120

^{a} The values in square brackets have been corrected for libration.

The possibility of disorder higher than 3, such as the 8-fold disorder found for BF$_4^-$ in N(CH$_3$)$_4$BF$_4$,[20] was also examined but was found to be incompatible with the symmetry requirements of our preferred space group. Furthermore, the Fourier difference map revealed no significant electron density in the equatorial plane after subtraction of the phosphorus and the three original equatorial fluorine positions. In the final difference Fourier map, the maximum and minimum electron densities were 0.92 and −0.58 e Å^{-3}, with the maximum located near the P atom.

A summary of the crystal data and refinement results for the 3-fold disordered model with unequal occupancy factors, the final atomic coordinates, equivalent isotropic thermal parameters and site occupancy factors, and the important apparent bond lengths and angles for the PF$_4^-$ anion are given in Tables 1–3. The apparent bond lengths corrected for librational motion are also given in Table 3 and are used throughout the following discussion. A summary of the structure determination, anisotropic displacement coefficients, H-atom coordinates and their isotropic displacement coefficients, and the observed and calculated structure factors are given in the supplementary material, Tables S1–S4.

Nuclear Magnetic Resonance Spectroscopy. The ^{19}F and ^{31}P NMR spectra were recorded unlocked (field drift < 0.1 Hz h^{-1}) on a Bruker AM-500 spectrometer equipped with an 11.744T cryomagnet. Temperatures were measured with a copper–constantan thermocouple inserted directly into the sample region of the probe and were considered accurate to ±1 °C. The spectra were referenced to neat external samples of CFCl$_3$(^{19}F) and 85% H$_3$PO$_4$(^{31}P) at ambient temperature. The IUPAC chemical shift convention was used.

Samples for ^{31}P NMR spectroscopy were prepared in 9-mm-o.d. FEP NMR tubes as described previously[17] using a 2.4-fold excess of N(CH$_3$)$_4$F

(20) Giuseppetti, G.; Mazzi, F.; Tadini, C. *Z. Kristallogr.* **1992**, *202*, 81.

and CH_3CN as a solvent. The ^{19}F NMR samples were prepared in an analogous fashion using 4-mm-o.d. FEP NMR tubes and a 3.7-fold excess of $N(CH_3)_4F$ and CH_3CN (0.25 mL).

Computational Methods. The density functional theory[21] calculations were done with the programs DGauss,[22] which employs Gaussian orbitals, and DMol,[23] which employs numerical orbitals, on a Cray YMP computer. In DGauss, the local potential of Vosko, Wilk, and Nusair[24] is used. The calculations were done at the self-consistent nonlocal level with the nonlocal exchange potential of Becke[25] together with the nonlocal correlation functional of Perdew.[26] The basis set on P has the form (7321/621/1) and that on F has the form (721/621/1).[27] The fitting basis has the form (9/4/4) for P and (7/3/3) for F.

The DMol calculations were done with a polarized double-ζ numerical basis set,[18] using the local potential of von Barth and Hedin.[28] Geometries were optimized by using analytical gradients.[22] Second derivatives were calculated by numerical differentiation of the analytic first derivatives. A two-point method with a finite difference of 0.01 au was used.

The ab initio molecular orbital calculations were done with the program systems GRADSCF[29] and Gaussian 92[30] on a Cray YMP computer. The geometries were optimized by using analytic gradient methods[31] at the SCF and MP2 levels.[32] Force fields were also evaluated analytically[33] at the SCF and MP2 levels. The basis sets are of polarized double-ζ quality for P[34] and F.[35]

Results and Discussion

Synthesis and Properties of $N(CH_3)_4PF_4$. The synthesis of $N(CH_3)_4PF_4$, the first known example of a PF_4^- salt, was achieved

(21) (a) Parr, R. G.; Yang, W. *Density Functional Theory of Atoms and Molecules*; Oxford University Press: New York, 1989. (b) Salahub, D. R. In *Ab Initio Methods in Quantum Chemistry-II*; Lawley, K. P., Ed.; J. Wiley & Sons: New York, 1987; p 447. (c) Wimmer, E.; Freeman, A. J.; Fu, C.-L.; Cao, P.-L.; Chou, S.-H.; Delley, B. In *Supercomputer Research in Chemistry and Chemical Engineering*; Jensen, K. F., Truhlar, D. G., Eds.; ACS Symposium Series 353; American Chemical Society: Washington, DC, 1987; p 49. (d) Jones, R. O.; Gunnarsson, O. *Rev. Mod. Phys.* **1989**, *61*, 689. (e) Ziegler, T. *Chem. Rev.* **1991**, *91*, 651.

(22) (a) Andzelm, J.; Wimmer, E.; Salahub, D. R. In *The Challenge of d and f Electrons: Theory and Computation*; Salahub, D. R., Zerner, M. C., Eds.; ACS Symposium Series 394; American Chemical Society: Washington, DC, 1989; p 228. (b) Andzelm, J. In *Density Functional Methods in Chemistry*; Labanowski, J., Andzelm, J., Eds.; Springer-Verlag: New York, 1991; p 101. (c) Andzelm, J.; Wimmer, E. *J. Chem. Phys.* **1992**, *96*, 1280. (d) DGauss is a local density functional program available via the Cray Research Unichem Project, Cray Research, Eagan, MN, 1993.

(23) (a) Delley, B. *J. Chem. Phys.* **1990**, *92*, 508. (b) Dmol is available commercially from BIOSYM Technologies, San Diego, CA. The multipolar fitting functions for the model density used to evaluate the effective potential have angular momentum numbers of 3 for F and P.

(24) Vosko, S. H.; Wilk, L.; Nusair, M. *Can. J. Phys.* **1980**, *58*, 1200.

(25) (a) Becke, A. D. *Phys. Rev.* **1988**, *A38*, 3098. (b) Becke, A. D. In *The Challenge of d and f Electrons: Theory and Computation*; Salahub, D. R., Zerner, M. C., Eds.; ACS Symposium Series 394; American Chemical Society: Washington, DC, 1989; p 166. (c) Becke, A. D. *Int. J. Quantum Chem. Symp.* **1989**, *23*, 599.

(26) Perdew, J. P. *Phys. Rev. B* **1986**, *33*, 8822.

(27) Godbout, N.; Salahub, D. R.; Andzelm, J.; Wimmer, E. *Can. J. Chem.* **1992**, *70*, 560.

(28) Von Barth, U.; Hedin, L. *J. Phys. C* **1972**, *5*, 1629.

(29) GRADSCF is an ab initio program system designed and written by A. Komornicki at Polyatomics Research.

(30) *GAUSSIAN 92*; Frisch, M. J.; Trucks, G. W., Head-Gordon, M., Gill, P. M. W., Wong, M. W., Foresman, J. B., Johnson, B. G., Schlegel, H. B., Robb, M. A., Replogle, E. S., Gomperts, R., Andres, J. L., Raghavachari, K., Binkley, J. S., Gonzalez, C., Martin, R. L., Fox, J., DeFrees, D. J., Baker, J., Stewart, J. J. P., Pople, J. A., Eds.; Gaussian Inc.: Pittsburg, PA, 1992.

(31) (a) Komornicki, A.; Ishida, K.; Morokuma, K.; Ditchfield, R.; Conrad, M. *Chem. Phys. Lett.* **1977**, *45*, 595. (b) McIver, J. W., Jr.; Komornicki, A. *Chem. Phys. Lett.* **1971**, *10*, 303. (c) Pulay, P. In *Applications of Electronic Structure Theory*; Schaefer, H. F., III, Ed.; Plenum Press: New York, 1977; p 153.

(32) (a) Moller, C.; Plesset, M. S. *Phys. Rev.* **1934**, *46*, 618. (b) Pople, J. A.; Binkley, J. S.; Seeger, R. *Int. J. Quantum Chem. Symp.* **1976**, *10*, 1. (c) Pople, J. A.; Krishnan, R.; Schlegel, H. B.; Binkley, J. S. *Int. J. Quantum Chem. Symp.* **1979**, *13*, 325. (d) Handy, N. C.; Schaefer, H. F., III. *J. Chem. Phys.* **1984**, *81*, 5031.

(33) (a) King, H. F.; Komornicki, A. *J. Chem. Phys.* **1986**, *84*, 5645. (b) King, H. F.; Komornicki, A. In *Geometrical Derivatives of Energy Surfaces and Molecular Properties*; Jorgenson, P., Simons, J., Eds.; NATO ASI Series C; D. Reidel: Dordrect, 1986; Vol. 166, p 207.

(34) McLean, A. D.; Chandler, G. S. *J. Chem. Phys.* **1980**, *72*, 5639. D exponent = 0.50.
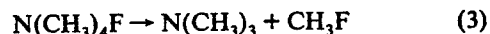
(35) Dunning, T. H., Jr.; Hay, P. J. In *Methods of Electronic Structure Theory*; Schaefer, H. F., III, Ed.; Plenum Press: New York, 1977; Chapter 1.

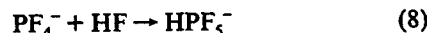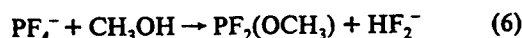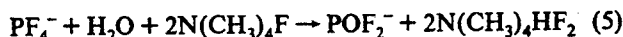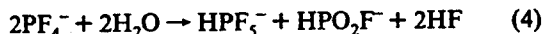according to eq 1. The salt is formed in quantitative yield by

$$N(CH_3)_4F + PF_3 \rightarrow N(CH_3)_4PF_4 \qquad (1)$$

reacting an excess of PF_3 with $N(CH_3)_4F$ in a suitable solvent such as CH_3CN at room temperature, CHF_3 at -78 °C, or liquid PF_3 either at or below room temperature. Due to the relatively low boiling points of CHF_3 and PF_3, the synthesis in CH_3CN solution is preferred and can be carried out in standard glassware. Attempts to prepare $CsPF_4$ from CsF and liquid PF_3 at room temperature were unsuccessful. The only observed reaction product was a small amount of $CsPF_6$.

The $N(CH_3)_4PF_4$ salt is a white crystalline salt which is stable up to about 150 °C, at which temperature it starts to slowly decompose according to eqs 2 and 3, with eq 2 being faster than eq 3.

$$N(CH_3)_4PF_4 \rightarrow N(CH_3)_4F + PF_3 \qquad (2)$$

$$N(CH_3)_4F \rightarrow N(CH_3)_3 + CH_3F \qquad (3)$$

The successful synthesis of the PF_4^- anion and its good thermal stability are in accord with the high F^- affinity of PF_3 (40.2 kcal mol^{-1})[12] and was made possible by the availability of a soluble, anhydrous F^- ion source, i.e., $N(CH_3)_4F$.[16] The use of anhydrous and hydroxyl- and HF-free conditions is important in view of PF_4^- undergoing the following facile reactions 4–8. These reac-

$$2PF_4^- + 2H_2O \rightarrow HPF_5^- + HPO_2F^- + 2HF \qquad (4)$$

$$PF_4^- + H_2O + 2N(CH_3)_4F \rightarrow POF_2^- + 2N(CH_3)_4HF_2 \qquad (5)$$

$$PF_4^- + CH_3OH \rightarrow PF_2(OCH_3) + HF_2^- \qquad (6)$$

$$PF_4^- + 2CH_3OH \rightarrow PF(OCH_3)_2 + HF + HF_2^- \qquad (7)$$

$$PF_4^- + HF \rightarrow HPF_5^- \qquad (8)$$

tions have been studied in detail by multinuclear NMR and vibrational spectroscopy and will be discussed in a separate publication.[36]

^{31}P and ^{19}F NMR Spectroscopy of the PF_4^- Anion. The ^{31}P NMR spectrum of $N(CH_3)_4PF_4$ in CH_3CN at -40 °C reveals a broad singlet ($\Delta\nu_{1/2} = 163$ Hz) at $\delta = 42.3$ ppm. The lack of fine structure indicates that the PF_4^- anion undergoes relatively fast intermolecular exchange under these conditions. However, when a 1.5 M excess of $N(CH_3)_4F$ is added to the sample, the intermolecular exchange is slowed down and the ^{31}P NMR spectrum at -46 °C (Figure 1) reveals a triplet of triplets at $\delta = 40.5$ ppm. This is in agreement with the pseudo trigonal bipyramidal structure expected for PF_4^- according to the VSEPR model.[37,38] The coupling pattern arises from the coupling of the phosphorus to the two inequivalent sets of fluorine ligands: $^1J(^{31}P-^{19}F_{ax}) = 660$ Hz and $^1J(^{31}P-^{19}F_{eq}) = 1405$ Hz. Six of the inner lines of the multiplet are broader than the central and two outer lines. This pattern is indicative of the PF_4^- anion undergoing an intramolecular ligand exchange process in which both equatorial and axial ligands interchange at the same time.[39] In order to confirm this, a series of variable temperature ^{31}P NMR spectra

(36) Christe, K. O.; Dixon, D. A.; Sanders, J. C. P.; Schrobilgen, G. J.; Wilson, W. W. To be published.

(37) Gillespie, R. J. *Molecular Geometry*; Van Nostrand Reinhold Co.: London, 1972.

(38) Gillespie, R. J.; Hargittai, I. *The VSEPR Model of Molecular Geometry*; Allyn and Bacon: Boston, 1991.

(39) Steigel, A. In *NMR–Basic Principles and Progress*; Diel, P., Fluck, E., Kosfeld, R., Eds.; 1978; Vol. 15, p 1 and references therein.
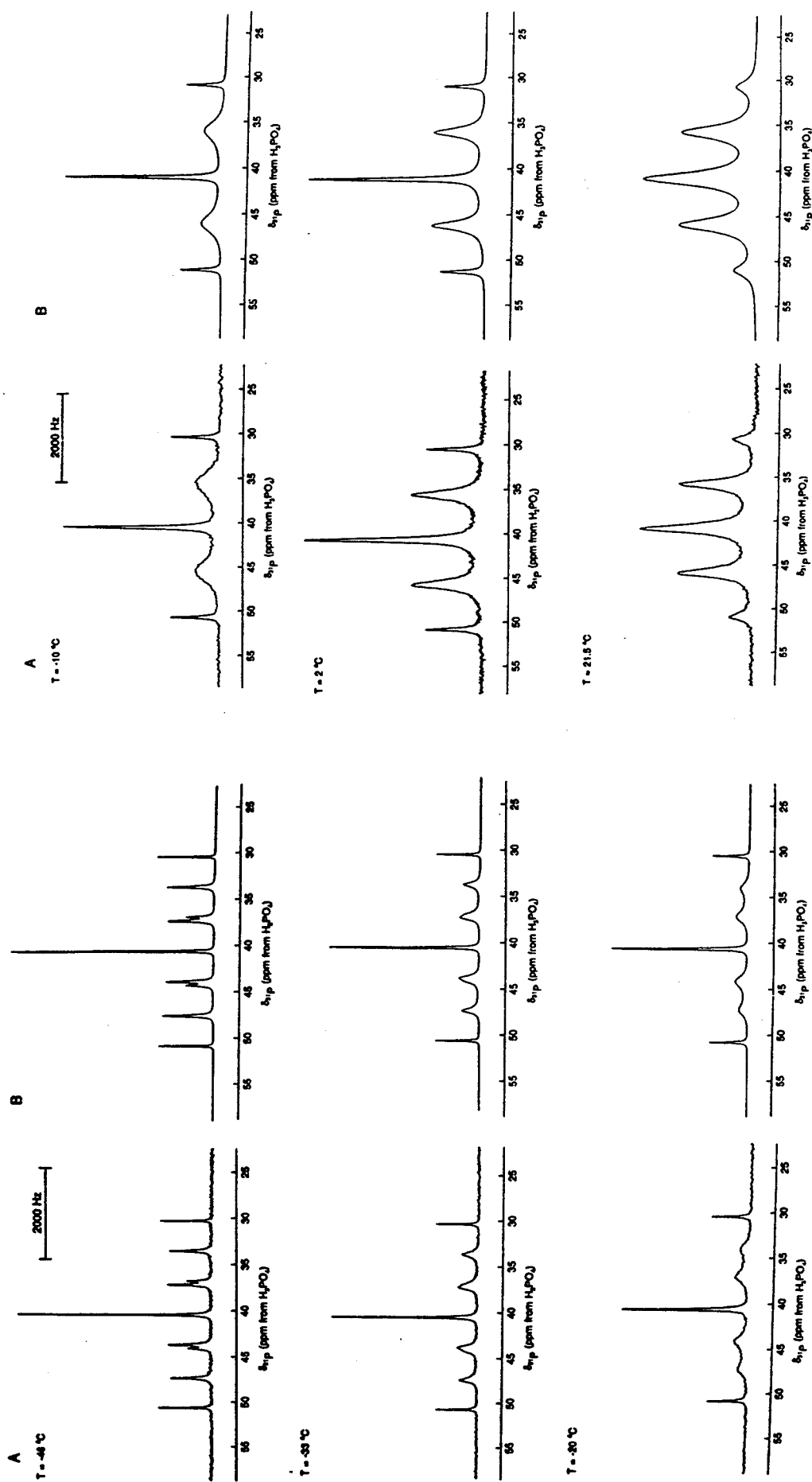
Tetrafluorophosphite, PF₄⁻, Anion

J. Am. Chem. Soc., Vol. 116, No. 7, 1994   2853

Figure 1. Variable temperature ³¹P NMR spectra (202.459 MHz) for N(CH₃)₄PF₄ in CH₃CN containing a 1.5 M excess of N(CH₃)₄F: (A) observed spectra; (B) calculated spectra.
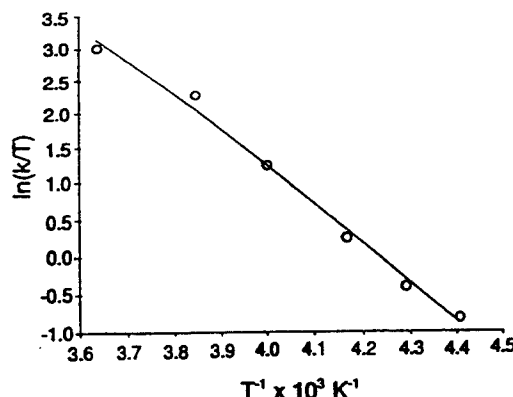
Table 4. Exchange Rate Data Extracted from Variable Temperature ^{31}P NMR Spectra of N(CH$_3$)$_4$PF$_4$ Dissolved in CH$_3$CN Containing a 1.5 M Excess of N(CH$_3$)$_4$F

T, K	k, s^{-1} × 10^2	T, K	k, s^{-1} × 10^2
227	1.00	250	8.50
233	1.60	260	25.0
240	3.10	275	56.0

were obtained over the range –46 to 21 °C (Figure 1). The observed changes in the multiplet pattern on raising the temperature are analogus to those found in the XPF$_4$ series of molecules (where X = N(CH$_3$)$_2$, Cl, or CH$_3$)[40] and are consistent with a mechanism in which both equatorial and axial ligands interchange simultaneously.[39,40] The ^{31}P NMR spectra measured at the highest temperatures reveal significant broadening of the multiplet components as a result of intermolecular fluoride exchange, and in addition, the samples turned orange in color due to attack of the excess F$^-$ on the CH$_3$CN solvent.[41] The mechanism by which the intramolecular ligand exchange process occurs in PF$_4^-$ is most likely the classical Berry pseudorotation mechanism[42] involving a pyramidal C_{4v} transition state with four equivalent fluorine positions.[43]
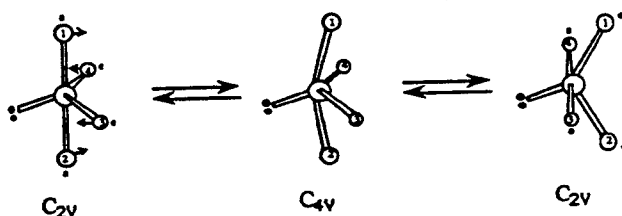
However, it should be noted that NMR spectroscopy alone could not distinguish between this and other mechanisms that result in the same permutation of fluorine nuclei.[39,40] Other mechanisms have been favored for compounds such as ClF$_3$,[44] which possesses two free valence electron pairs on the central atom, or SiH$_4$F$^-$ [45] and PH$_4$F,[46] where in the minimum energy structures, the two axial positions are occupied by one fluorine and one hydrogen ligand. For PF$_4^-$, the rate constants have been determined at different temperatures by visual matching of the experimental spectra with those generated by the DNMR 3 simulation program[47] for exchanging systems (See Table 4). Using previously established equations[48] and an Eyring plot of the rate data (Figure 2), $\Delta H^\ddagger$ and $\Delta S^\ddagger$ were determined to be 43 ± 2 kJ mol and –13 ± 2 J K^{-1} mol^{-1}, respectively. These values compare well with values obtained for the intramolecular exchange process in the isoelectronic SF$_4$ molecule[49–51] and the theoretical value for $\Delta H^\ddagger$ (see Theoretical Calculations section). For SF$_4$, the values obtained for purified neat liquid ($\Delta H^\ddagger$ = 49.2 kJ mol^{-1}, $\Delta S^\ddagger$ = 4.4 J K^{-1} mol^{-1}) and gaseous ($\Delta H^\ddagger$ = 51.9 kJ mol^{-1}, $\Delta S^\ddagger$ = 9.3 J K^{-1} mol^{-1}) samples of SF$_4$ are regarded as the most reliable,

(40) Eisenhut, M.; Mitchell, H. L.; Traficante, D. D.; Kaufman, R. J.; Deutch, J. M.; Whitesides, G. M. *J. Am. Chem. Soc.* **1974**, *96*, 5385.

(41) Christe, K. O.; Wilson, W. W. *J. Fluorine Chem.* **1990**, *46*, 339.

(42) (a) Berry, R. S. *J. Chem. Phys.* **1960**, *32*, 933. (b) Wasada, H.; Hirao, K. *J. Am. Chem. Soc.* **1992**, *114*, 16.

(43) Gordon, M. S.; Windus, T. L.; Burggraf, L. W.; Davis, L. P. *J. Am. Chem. Soc.* **1990**, *112*, 7167.

(44) Minyaev, R. M. *Chem. Phys. Lett.* **1992**, *196*, 203.

(45) Windus, T. M.; Gordon, M. S.; Burggraf, L. W.; Davis, L. P. *J. Am. Chem. Soc.* **1991**, *113*, 4356.

(46) Windus, T. M.; Gordon, M. S. *Theor. Chim. Acta* **1992**, *83*, 21.

(47) (a) Kleier, D. A.; Binsch, G. *Quantum Chemistry Exchange*; Indiana University: Bloomington, 1969; No. 165. (b) Binsch, G. In *Dynamic NMR Spectroscopy*; Jackman, L. M., Cotton, F. A., Eds.; Academic Press: New York, 1975; p 45.

(48) Günther, H. *NMR Spectroscopy–An Introduction*; J. Wiley and Sons: New York, 1973; Chapter 8, p 240.

(49) Seel, F.; Gombler, W. *J. Fluorine Chem.* **1974**, *4*, 327. Gibson, J. A.; Ibbott, D. G.; Janzen, A. F. *Can. J. Chem.* **1973**, *51*, 3203.

(50) Gombler, W. Diploma Thesis, Saarbrücken, FRG, 1974. Gombler, W. Personal communication.

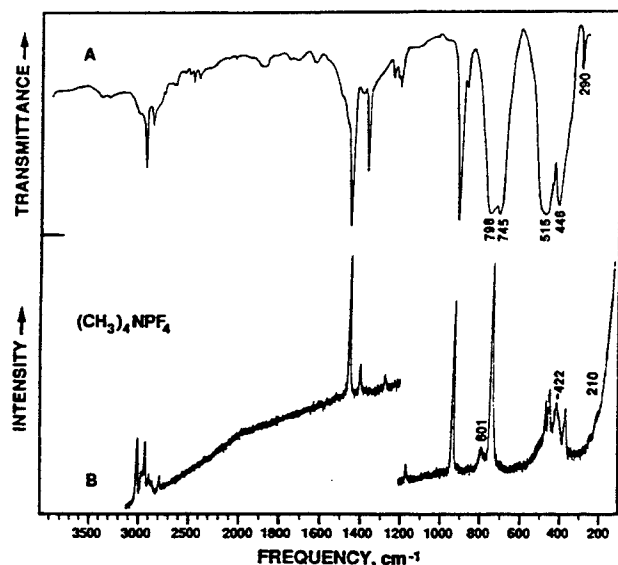(51) Spring, C. A.; True, N. S. *J. Am. Chem. Soc.* **1983**, *105*, 7231.

Figure 2. Eyring plot of the exchange rate data extracted from the variable temperature ^{31}P NMR spectra (202.459 MHz) for N(CH$_3$)$_4$PF$_4$ in CH$_3$CN containing a 1.5 M excess of N(CH$_3$)$_4$F.
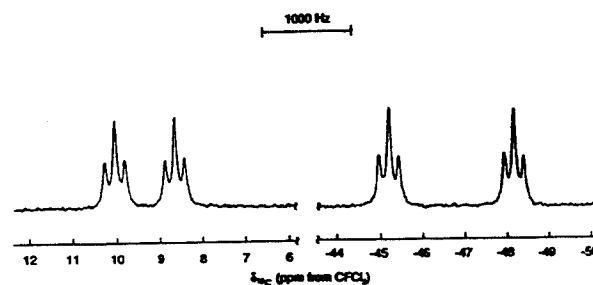
Figure 3. The ^{19}F NMR spectrum (470.599 MHz) at –46 °C of N(CH$_3$)$_4$PF$_4$ in CH$_3$CN containing a 1.5 M excess of N(CH$_3$)$_4$F.

since they represent the highest $\Delta H^\ddagger$ and most positive $\Delta S^\ddagger$ values.[50,51] The somewhat lower values of $\Delta H^\ddagger$ and $\Delta S^\ddagger$ obtained for PF$_4^-$ can probably be ascribed to the effects of some intermolecular fluoride exchange.

The ^{19}F NMR spectrum at –46 °C of N(CH$_3$)$_4$PF$_4$ in CH$_3$CN containing a 3.7 M excess of N(CH$_3$)$_4$F shows, in addition to a signal due to excess F$^-$, resonances attributable to PF$_4^-$, POF$_2^-$, and HPF$_5^-$. The latter two species comprised approximately 10–15% of the total phosphorus in the sample and are thought to have arisen from the adventitious hydrolysis of the PF$_4^-$ anion during synthesis or storage. The reactions giving rise to these products will be described in detail in a separate article.[36] The resonances arising from the PF$_4^-$ anion (Figure 3) comprise two doublets of triplets attributed to the axial (δ = 9.3 ppm) and equatorial (δ = –46.7 ppm) fluorine ligand environments, in accord with the pseudo trigonal bipyramidal structure for PF$_4^-$. The doublet splittings arise from the one-bond couplings $^1J(^{31}P-^{19}F_{ax})$ and $^1J(^{31}P-^{19}F_{eq})$ and are in agreement with those measured from the ^{31}P spectrum. The smaller triplet splittings arise from $^2J(^{19}F_{ax}-^{19}F_{eq})$ = 108 Hz. The chemical shift assignments are based on the magnitudes of the $^1J(^{31}P-^{19}F)$ values for each resonance. The magnitude of $^1J(^{31}P-^{19}F_{eq})$ is expected to be greater than that of $^1J(^{31}P-^{19}F_{ax})$ because of the higher s-character of the equatorial bonds. This agrees with the fact that the P–F$_{eq}$ bond length is shorter than the P–F$_{ax}$ bond length (see below). In the room temperature ^{19}F NMR spectrum of PF$_4^-$ the two doublets of triplets collapse into a single broad (half-width ~ 400 Hz) line due to the above-mentioned axial–equatorial ligand exchange.

Vibrational Spectra. The infrared and Raman spectra of solid N(CH$_3$)$_4$PF$_4$ are shown in Figure 4, and the observed frequencies together with their assignments are summarized in Table 5. The bands due to PF$_4^-$ have been marked in Figure 4 with their frequency values. The remaining bands belong to the N(CH$_3$)$_4^+$ cation, and their assignments have previously been discussed and are well understood.[16,18] As can be seen from Figure 4, the Raman spectrum of N(CH$_3$)$_4$PF$_4$ is dominated by the cation bands, while in the infrared spectrum the PF$_4^-$ bands are more prominent.

Figure 4. Infrared (trace A) and Raman (trace B) spectra of solid N(CH₃)₄PF₄.

Table 5. Vibrational Spectra of N(CH₃)₄PF₄ and Their Assignments

obsd freq, cm⁻¹ (rel int)		assignments (point group)	
IR	Ra	N(CH₃)₄⁺ (T_d)	PF₄⁻ (C₂ᵥ)
3500 vw			
3415 vw	⎫		
3120 sh			
3043 m			
	3042 (30)	ν₅(E)	
2975 w	2996 (10)	ν₁₄(F₂)	
	2962 (23)	ν₁(A₁)	
	2920 (7)	+ combin	
2780 vw	2895 sh	bands	
2755 vw	2813 (7)		
2663 vw			
2622 vw			
2585 w			
2521 vw	⎭		
1940 vw, br			
1815 vw			
1776 vw			
1686 vw			
1550 sh			
1493 s			
		ν₁₅(F₂)	
1444 vw	1476 (73)	ν₂(A₁), ν₆(E)	
1416 m	1419 (14)	ν₁₆(F₂)	
1289 vw	1293 (6)	ν₁₇(F₂)	
1263 vw			
1253 vw			
	1181 (8)	ν₇(E)	
950 s	952 (82)	ν₁₈(F₂)	
918 vw			
798 vs	801 (9)		ν₁(A₁)
	758 (100) ⎱	ν₃(A₁)	
745 vs	745 sh ⎰		ν₈(B₂)
515 vs			ν₆(B₁)
475 vw	476 (28) ⎱	ν₁₉(F₂)	
	459 (35) ⎰		
446 s			ν₃(A₁), ν₇(B₁)
	422 (25)		ν₂(A₁)
	375 (22)	ν₈(E)	
290 mw			ν₉(B₂)
	210 (2)		ν₄(A₁)

The bands due to the PF₄⁻ anion are summarized in Table 6. Their assignments in point group C₂ᵥ were made by comparison with those of isoelectronic SF₄⁵² and with the frequencies

calculated for PF₄⁻ (see below). Their agreement is satisfactory. As expected, the formal negative charge in the PF₄⁻ anion increases the negative charge on the fluorine ligands and, hence, the (δ+)P–F(δ−) bond polarity. This results in a general lowering of the frequencies and stretching force constants relative to the neutral SF₄ molecule.

A comparison of our infrared spectrum for PF₄⁻ in N(CH₃)₄PF₄ with that attributed by Wermer and Ault to a Cs⁺PF₄⁻ ion pair in an argon matrix[15] shows only little similarity. This implies that PF₄⁻ in the two species is either very different or that the species observed in the matrix might not have been PF₄⁻.

Theoretical Calculations and Normal Coordinate Analyses. The electronic structure of PF₄⁻ was calculated using both local (LDF) and nonlocal (NLDF) density functional theories and molecular orbital theory at the self-consistent field (SCF) and MP2 levels. All calculations resulted in a pseudo trigonal bipyramidal structure of C₂ᵥ symmetry as the minimum energy structure (see Table 7). To obtain a better feel for the quality of these calculations, the well-known PF₃ molecule[53–55] was also calculated by the same methods. As can be seen from Table 8, the SCF calculation duplicates best the experimental geometry and vibrational frequencies of PF₃. Therefore, the SCF values are also preferred for PF₄⁻ and are in good agreement with the experimentally observed values (see Table 7). This good agreement clearly demonstrates that the geometries of PF₄⁻ in solid N(CH₃)₄PF₄ and that calculated for the free ion must be very similar, indeed.

The geometry parameters, calculated for PF₄⁻ at different levels of theory (see Table 7), show some interesting trends. Correlation effects are significant and at the MP2 level lengthen r(P–F_eq) by 0.05 Å and the already longer P–F_ax bond by a somewhat smaller value of 0.03 Å. The LDF calculations show bond lengths comparable to those obtained at the MP2 level. Inclusion of self-consistent nonlocal effects increases both the axial and equatorial bond lengths with the larger effect on the axial bond. Comparison of our calculations with those[56] previously carried out by O'Keeffe using a 631G* basis set shows that the results agree within 0.01 Å. The HFS/LDF results[57] of Gutsev are also in reasonable agreement with our LDF results, considering the differences in the basis sets, method, and local potential.

A normal coordinate analysis was carried out for PF₄⁻. The internal and symmetry coordinates and the explicit F matrix used were identical to those previously published[52] for isoelectronic SF₄. The nine fundamental vibrations of PF₄⁻ of C₂ᵥ symmetry can be classified as Γ = 4A₁(IR,Ra) + A₂(Ra) + 2B₁(IR,Ra) + 2B₂(IR,Ra), whereby the B₂ modes were arbitrarily chosen to be symmetric to the symmetry plane defined by the equatorial PF₂ group. Since the scaled SCF frequencies of PF₄⁻ duplicate best the experimentally observed ones, the scaled SCF force field was used and is given in Table 9. The potential energy distribution (PED) is shown in Table 10. The internal stretching force constants of PF₄⁻ are given in Table 11 and are compared to those of isoelectronic SF₄[52] and the phosphorus fluorides PF₃,[55,58,59] PF₆⁻,[60] and PF₅.[61,62]

The results of the normal coordinate analysis demonstrate that, by analogy with isoelectronic SF₄,[52] the symmetric equatorial and axial bending motions, ν₃(A₁) and ν₄(A₁), are highly mixed,

(52) Sawodny, W.; Birk, K.; Fogarasi, G.; Christe, K. O. *Z. Naturforsch., B* **1980**, *35B*, 1137 and references cited therein.

(53) Morino, Y.; Kuchitsu, K.; Moritani, T. *Inorg. Chem.* **1969**, *8*, 867.
(54) Hirota, E.; Morino, Y. *J. Mol. Spectrosc.* **1970**, *33*, 460. Kawashima, Y.; Cox, A. P. *J. Mol. Spectrosc.* **1977**, *65*, 319.
(55) Reichman, S.; Overend, J. *Spectrochim. Acta, Part A* **1970**, *26A*, 379. Reichman, S. *J. Mol. Spectrosc.* **1970**, *35*, 329. Small, C. E.; Smith, J. G. *J. Mol. Spectrosc.* **1978**, *73*, 215.
(56) O'Keeffe, M. *J. Am. Chem. Soc.* **1986**, *108*, 4341.
(57) Gutsev, G. L. *J. Chem. Phys.* **1993**, *98*, 444.
(58) Breidung, J.; Thiel, W. *J. Comput. Chem.* **1992**, *13*, 165.
(59) Breidung, J.; Schneider, W.; Thiel, W. *J. Mol. Spectrosc.* **1990**, *140*, 226.
(60) Sawodny, W. Habilitation Thesis, University of Stuttgart, Germany, 1969.
(61) Marsden, C. J. *J. Chem. Phys.* **1987**, *87*, 6626.
(62) Christen, D.; Kadel, J.; Liedtke, A.; Minkwitz, R.; Oberhammer, H. *J. Phys. Chem.* **1989**, *93*, 6672.

Christe et al.

2856   *J. Am. Chem. Soc., Vol. 116, No. 7, 1994*

Table 6. Comparison of Observed and Calculated Frequencies of PF_4^- with Those of SF_4 and Their Approximate Mode Descriptions

assignment in point group C_{2v}		approximate mode description	PF_4^- obsd freq, cm^{-1}(int) IR	PF_4^- obsd freq, cm^{-1}(int) Ra	calcd freq,[a] (IR int) SCF	SF_4 obsd freq, cm^{-1}(int) IR	SF_4 obsd freq, cm^{-1}(int) Ra
A_1	ν_1	ν sym $XF_{2,eq}$	798 vs	801 ms	795 (218)	892 s	893 (92)
	ν_2	ν sym $XF_{2,ax}$		422 s	416 (0)	558 w	558 (100)
	ν_3	δ sciss $XF_{2,eq,ax}$, sym comb	446 s		464 (28)	532 ms	535 (35)
	ν_4	δ sciss $XF_{2,eq,ax}$, asym comb		210 sh	201 (1.0)	226 w	229 (10)
A_2	ν_5	XF_2 twist			392 (0)		
B_1	ν_6	ν asym $XF_{2,ax}$	515 vs		523 (620)	728 vs	730 (5)
	ν_7	δ wag $XF_{2,eq}$	446 s		446 (56)		474 (7)
B_2	ν_8	ν asym $XF_{2,eq}$	745 vs		746 (209)	867 s	865 sh
	ν_9	δ sciss $XF_{2,ax}$ out of plane	290 mw		293 (7.4)	353 m	356 (0+)

[a] The frequency values were scaled by an empirical factor of 0.9005 to maximize the fit with the observed values.

Table 7. Geometries and Vibrational Frequencies Calculated for PF_4^- by Different Methods

computational method	geometry $r_{PF_{eq}}$ (Å)	$r_{PF_{ax}}$ (Å)	F_{eq}–P–F_{eq} (deg)	$\angle F_{ax}$–P–F_{ax} (deg)	$\angle F_{eq}$–P–F_{ax} (deg)	vibrational freq (cm^{-1}) and relative infrared intensity $\nu_1(A_1)$	$\nu_2(A_1)$	$\nu_3(A_1)$	$\nu_4(A_1)$	$\nu_5(A_2)$	$\nu_6(B_1)$	$\nu_7(B_1)$	$\nu_8(B_2)$	$\nu_9(B_2)$
SCF[a]	1.604	1.741	99.9	168.3	86.2	795 (218)	416 (0)	464 (28)	201 (1.0)	392 (0)	523 (620)	446 (56)	746 (209)	293 (7.4)
MP2[b]	1.651	1.774	98.9	169.7	86.7	808 (174)	461 (2.4)	453 (15)	200 (0.9)	384 (0)	602 (588)	442 (7.2)	750 (188)	285 (6.0)
LDF[b]	1.666	1.768	98.2	169.8	86.7	757	451	408	178	349	607	405	709	261
NLDF/BP[b]	1.673	1.814	99.2	171.0	87.1	735 (168)	405 (3.9)	394 (7.3)	177 (1.3)	344 (0)	537 (547)	390 (27)	673 (252)	252 (5.1)
exptl values		1.73(1)				801 vs	422 (Ra)	446 s	210 (Ra)		515 vs	446 s	745 vs	290 mw

[a] The frequency values were scaled by an empirical factor of 0.9005 to maximize the fit with the observed values. [b] Unscaled frequencies.

Table 8. Experimental and Calculated Geometries and Vibrational Frequencies of PF_3

computational method	geometry r_{PF} (Å)	$\angle FPF$ (deg)	vibrational freq (cm^{-1}) and relative infrared intensity $\nu_1(A_1)$	$\nu_2(A_1)$	$\nu_3(E)$	$\nu_4(E)$
SCF[a]	1.562	97.2	896 (182)	486 (43)	859 (468)	347 (15)
MP2[b]	1.602	97.4	884 (143)	465 (30)	853 (418)	330 (12)
LDF[b]	1.616	96.9	834	420	823	300
NLDF/BP[b]	1.622	97.6	813 (134)	431 (21)	780 (420)	206 (8)
exptl values	1.561(1)	97.7(2)	892 s	488 m	860 vs	347 w

[a] Frequency values scaled by an empirical factor of 0.9283 to maximize the fit between calculated and experimental values. [b] Unscaled frequencies.

Table 9. Symmetry Force Constants[a] of PF_4^- Calculated from the Scaled SCF Frequencies of Table 8
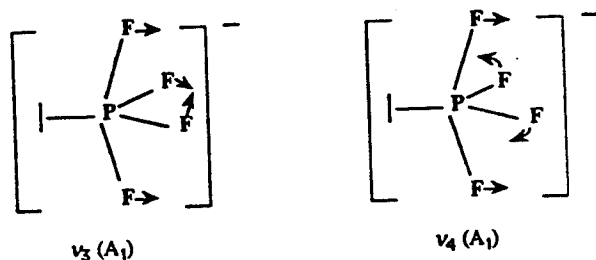
	F_{11}	F_{22}	F_{33}	F_{44}			F_{66}	F_{77}
F_{11}	4.204				F_{66}		1.484	1.679
F_{22}	0.721	2.159			F_{77}		0.577	
F_{33}	0.303	−0.055	1.152				F_{88}	F_{99}
F_{44}	0.163	0.034	0.489	1.078	F_{88}		3.676	1.524
F_{55}	1.482				F_{99}		−0.328	

[a] Stretching constants in mdyn/Å, deformation constants in mdyn Å/rad^2, and stretch–bend interaction constants in mdyn/rad.

Table 10. Potential Energy Distribution for PF_4^-

		freq, cm^{-1}	PED, %
A_1	ν_1	795	60.2(1) + 20.5(3) + 15.7(4) + 3.6(2)
	ν_2	416	91.7(2) + 7.8(2) + 0.5(4)
	ν_3	464	50.2(3) + 45.5(4) + 4.0(1) + 0.3(2)
	ν_4	201	52.7(4) + 46.9(3) + 0.3(2) + 0.1(1)
A_2	ν_5	392	100(5)
B_1	ν_6	523	57.8(6) + 42.2(7)
	ν_7	446	57.2(7) + 42.8(6)
B_2	ν_8	746	89.9(8) + 10.1(9)
	ν_9	293	99.7(9) + 0.3(8)

Table 11. Stretching Force Constants (mdyn/Å) of PF_4^- Compared to Those of SF_4, PF_3, PF_6^-, and PF_5

	SF_4[a]	PF_4^-	PF_3[b]	PF_6^-[c]	PF_5[d]
$f_{r,eq}$	5.405	3.940	5.470	4.02	6.47
f_{rr}	0.240	0.264	0.449		
$f_{R,ax}$	3.150	1.822			5.45
f_{RR}	0.329	0.338			

[a] Values from ref 52. [b] Values from refs 55, 58. [c] Values from ref 60. [d] Values from ref 62.

with ν_3 being a symmetric combination and ν_4 being an antisymmetric combination of the corresponding symmetry coordinates.

ν_3 (A_1) ν_4 (A_1)

The $\nu_4(A_1)$ mode has the lowest frequency of all the PF_4^- modes and represents the motion involved in the Berry pseudorotation mechanism (see above). Its frequency is comparable with but slightly lower than that in SF_4 and supports the conclusion from our NMR study (see above) that the activation energies for the intramolecular exchange in these two species have similar values. The fact that ν_6 and ν_7 in the B_1 block are also almost equal mixtures of the corresponding symmetry coordinates differs from SF_4 and is due to the more similar frequency values of ν_6 and ν_7 in PF_4^-.

To verify the Berry pseudorotation mechanism, we have also calculated the C_{4v} structure of PF_4^- at the SCF level and obtained an MP2 energy for this geometry. The C_{4v} structure is a transition state with an imaginary frequency of $174i$ cm^{-1}. The P–F bond distance is 1.675 Å, and the F–P–F bond angle is 82.1°. The C_{4v}
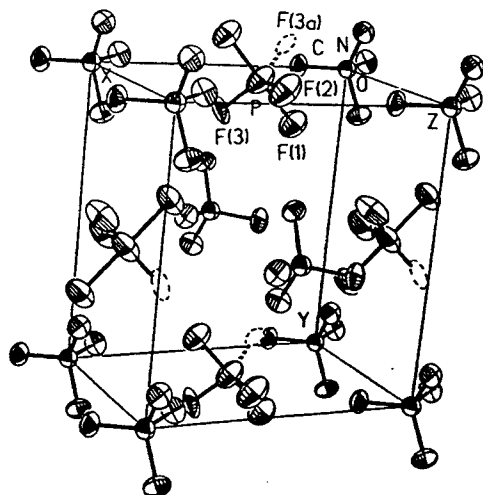
Tetrafluorophosphite, PF$_4^-$, Anion

J. Am. Chem. Soc., Vol. 116, No. 7, 1994 2857

Figure 5. ORTEP drawing of the unit cell of N(CH$_3$)$_4$PF$_4$ showing the packing of the PF$_4^-$ anions and N(CH$_3$)$_4^+$ cations with thermal ellipsoids drawn at the 50% probability.

structure is 48.7 kJ mol^{-1} above the C_{2v} structure at the SCF level and 43.7 kJ mol^{-1} higher at the MP2 level. These values are in excellent agreement with the experimental value of 43.5 kJ mol^{-1} for $\Delta H^{\ddagger}$.

The large differences between the equatorial and the axial stretching force constants, f_r and f_R, respectively, in PF$_4^-$ and SF$_4$ are in agreement with the observed large differences in bond lengths and can be rationalized in terms of semi-ionic, three-center four-electron bonding for the axial fluorine ligands. The high polarity of the bonds in PF$_4^-$ also explains why the equatorial stretching force constant in PF$_4^-$ (3.94 mdyn/Å) is significantly smaller than that found for PF$_3$ (5.47 mdyn/Å).[55,58] The same effect of bond weakening by the formal negative charge is found for the PF$_5$–PF$_6^-$ couple (see Table 11). The higher force constants in the (+V) phosphorus compounds, when compared to those in the corresponding (+III) compounds, is due to the increased effective electronegativity of the central atom and the resulting decrease in polarity of the P–F bonds. The stretch–stretch interaction constants, f_{rr} and f_{RR}, in PF$_4^-$ and SF$_4$ also have very similar values (see Table 11) and provide further evidence for the pronounced similarity of these two isoelectronic species.

X-ray Crystal Structure of N(CH$_3$)$_4$PF$_4$. The crystal structure consists of well-separated N(CH$_3$)$_4^+$ and PF$_4^-$ ions and can be derived from a primitive cubic CsCl-type structure in which the cube formed by the cations is regular, while the cube formed by the anions is somewhat distorted (see Figure 5). The volume of the unit cell is 27 Å^3 smaller than that determined for N(CH$_3$)$_4$PF$_6$ at the same temperature.[63] It is generally accepted that the effective volume of a lone pair is only slightly smaller than that of a fluorine atom (i.e., 20 Å^3).[64] Consequently, the expected volume difference between N(CH$_3$)$_4$PF$_6$ and N(CH$_3$)$_4$PF$_4$ should be slightly larger than 20 Å^3, as was observed.

The N(CH$_3$)$_4^+$ cation is tetrahedral with the expected C–N bond lengths (1.505(6) Å) and C–N–C angles (109.5(2)°). The gross geometry of the PF$_4^-$ anion can be described as a pseudo trigonal bipyramid in which (i) the lone valence electron pair of phosphorus and two fluorines occupy the equatorial positions and (ii) the axial P–F bonds are longer than the equatorial P–F bonds (Figure 5).

The disorder of the PF$_4^-$ anion in its equatorial plane involves two fluorine ligands and one sterically active free valence electron pair, which can be considered much shorter and more repulsive than a P–F bond. Therefore, the apparent equatorial bond lengths,

resulting from the averaging of P–F bonds with the free pair, are too short for normal P–F bonds, and the apparent bond angles also deviate significantly from the theoretical predictions for ordered PF$_4^-$ (see Theoretical Calculations section). As can be seen from Table 3, the observed apparent geometry of ordered PF$_4^-$ is intermediate between those derived from subjecting the free ordered ion to either 2-fold or 3-fold disorder with equal occupancy factors. Therefore, the crystal structure of N(CH$_3$)$_4$-PF$_4$ is best interpreted in terms of a mixture of 2-fold and 3-fold disorder, which amounts to a 3-fold disorder with unequal occupancy factors. A minimum R-value was obtained for the set of occupancy factors listed in Table 2. The superposition of the different equatorial positions results in close, but distinct, positions for the F(3) atom, as reflected in the large value for the thermal parameters, U_{33} = 0.159 Å^2 (supplementary Table 2) and the correspondingly large correction for libration for the P–F(3) bond length (Table 3). The positional disorder of the F(3) atoms is
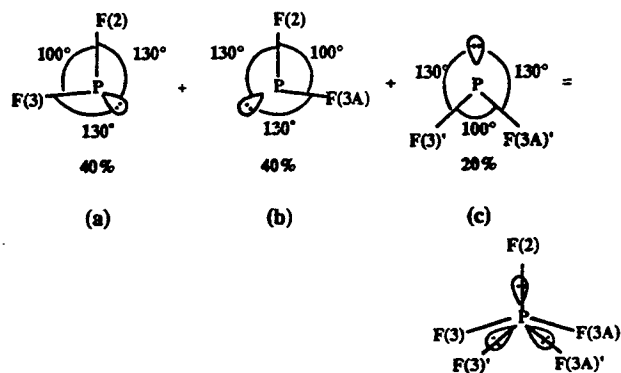
also responsible for the apparent equatorial F–P–F bond angle to be larger than 100°.

In view of the disorder of PF$_4^-$ in N(CH$_3$)$_4$PF$_4$, only the axial P–F bond length is well determined by the X-ray data. The remaining geometrical parameters of PF$_4^-$ are strongly influenced by the disorder, but are consistent with the theoretically calculated structure assuming 3-fold disorder with unequal occupancy factors. In view of this consistency and the agreement between the calculated and observed axial bond length and vibrational frequencies (see above), the structure of PF$_4^-$ is best described by the following geometry.
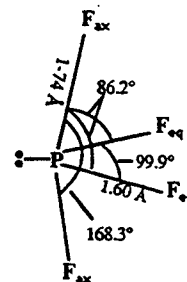
It is interesting to compare this geometry with those established for other similar molecules and ions. As can be seen from Table 12, the geometry of PF$_4^-$ is very similar to that[65] of isoelectronic SF$_4$, with the bonds in PF$_4^-$ being slightly longer, as has been discussed before. The increased length of the axial bonds over that of the equatorial bonds is consistent with the hypervalent nature of these pseudo trigonal bipyramidal compounds and with strong contributions from semi-ionic, three-center four-electron bonding[66] to the axial bonds. Furthermore, the fact that the axial fluorine ligands are bent away from the sterically active
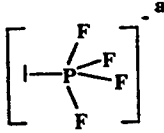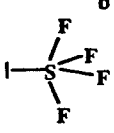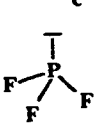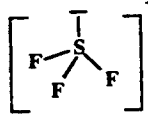
(63) Wang, Y.; Calvert, L. D.; Brownstein, S. K. *Acta Crystallogr.* **1980**, *B36*, 1523.

(64) (a) Zachariasen, W. H. *J. Am. Chem. Soc.* **1948**, *70*, 2147. (b) Edwards, A. J.; Silkos, R. J. C. *J. Chem. Soc. A* **1971**, 942.

(65) Tolles, W. M.; Gwinn, W. D. *J. Chem. Phys.* **1962**, *36*, 1119.

(66) Pimentel, G. C. *J. Chem. Phys.* **1951**, *19*, 446. Hach, R. J.; Rundle, R. E. *J. Am. Chem. Soc.* **1951**, *73*, 4321. Rundle, R. E. *J. Am. Chem. Soc.* **1963**, *85*, 112.

Table 12.   A Comparison of the Geometry of PF_4^- with Those of Closely Related Molecules and Ions

	a	b	c	d
$X-F_{ax}$	1.74	1.646(3)		
$X-F_{eq}$	1.60	1.545(3)	1.570(1)	1.515(2)
$F_{ax}-X-F_{ax}$	168.3	173.1(5)		
$F_{eq}-X-F_{eq}$	99.9	101.6(5)	97.8(2)	96.2(1)

[a] Values from our SCF calculation. [b] Data from ref 65. [c] Data from ref 53. [d] Data from ref 63.

free valence electron pair in the equatorial plane is in accord with the increased repulsion from a free valence electron pair and the VSEPR rules.[37,38] The equatorial bonds in PF_4^- are also somewhat longer than those[53] in PF_3, which again can be attributed to the formal negative charge on PF_4^-. Finally, the isoelectronic pairs, $PF_4^- - SF_4$ and $PF_3-SF_3^+$,[67] exhibit about the same amount of bond shortening (~ 0.06 Å) on going from the phosphorus to the sulfur species.

The cation–anion interactions in $N(CH_3)_4PF_4$ were also examined and show four short P- - -C contacts (supplementary Figure S1) of 3.95 Å (sum of the CH_3 and P van der Waals contacts, 3.85 Å[68,69]) and sixteen short F- - -C contacts (four per fluorine atom) ranging from 3.29 to 3.53 Å (sum of the CH_3 and F van der Waals contacts, 3.35–3.40 Å[68,69]). The nearest neighbor P- - -F contacts of 4.42 Å (sum of the P and F van der Waals contacts, 3.20–3.25 Å[69]) preclude Hal- - -P- - -Hal bridge interactions, which have been observed for $N(n-C_3H_7)_4^+PBr_4^-$[5] but not for $N(C_2H_5)_4^+PCl_4^-$.[7]

The successful synthesis and characterization of the PF_4^- anion completes the PF_4^-, PCl_4^-, PBr_4^- triad. The structures of the PCl_4^- and PBr_4^- anions are unusual because their axial Hal–P–Hal groups are easily distorted. For example, in $N(nPr)_4PBr_4$, the PBr_4^- anion has an almost ideal pseudo trigonal bipyramidal C_{2v} structure,[5] while in $N(C_2H_5)_4PBr_4$, its structure is better described as one of a PBr_3 molecule with a loosely attached fourth Br^- ion.[6]

Obviously, the energy difference between the symmetric and the asymmetric PBr_4^- structures must be very small, and their geometries are influenced by effects such as the size of the counter cation and crystal packing. In $N(C_2H_5)_4PCl_4$, the asymmetry of the axial PCl_2 group is even more pronounced (2.118(4) and 2.850(4) Å[7]) and, by extrapolation, one might predict that, on going from PBr_4^- and PCl_4^- to PF_4^- and from $N(C_2H_5)_4^+$ to the even smaller $N(CH_3)_4^+$ counter cation, the asymmetry of the

axial phosphorus–halogen bonds should further increase. This, however, is not the case; the axial P–F bonds in $N(CH_3)_4PF_4$ are perfectly symmetric, and the PF_4^- anion closely resembles the isoelectronic SF_4 molecule, with both undergoing facile equatorial–axial ligand exchanges with comparable activation enthalpies. It appears that the chemical and physical properties of PF_4^- and PCl_4^- closely follow those of isoelectronic SF_4 and SCl_4. Sulfur tetrafluoride is a covalent, stable molecule, while SCl_4 decomposes at -31 °C and, as a solid, probably has the ionic structure $SCl_3^+Cl^-$.[70-72] The fact that in the chlorides the energy difference between the covalent, pseudo trigonal bipyramidal C_{2v} structure and the more ionic X- - -MX_3 C_{3v} structure is quite small while in the fluorides it is large has recently been also demonstrated by Gutsev through local density functional method calculations for PF_4^- and SCl_4.[57,73]

Supplementary Material Available: A structure determination summary (Table S1), tables of anisotropic thermal paramters and hydrogen atomic coordinates (Tables S2 and S3), a drawing showing the shortest P- - -C contacts (Figure S1) (5 pages); tabulation of calculated and observed structure factor amplitudes (Table S4) (1 page). This material is contained in many libraries on microfiche, immediately follows this article in the microfilm version of the journal, and can be ordered from the ACS; see any current masthead page for ordering information.

(67) Mallouk, T. E.; Rosenthal, G. L.; Müller, G.; Brusasco, R.; Bartlett, N. *Inorg. Chem.* **1984**, *23*, 3167.
(68) Pauling, L. *The Nature of the Chemical Bond*, 3rd ed.; Cornell University Press: Ithaca, NY, 1960; p 261.
(69) Bondi, A. *J. Phys. Chem.* **1964**, *68*, 441.

(70) Steudel, R.; Jensen, D.; Plinke, B. *Z. Naturforsch., B* **1987**, *42*, 163.
(71) Kniep, R.; Korte, L.; Mootz, D. *Z. Naturforsch., B* **1984**, *39*, 305.
(72) Greenwood, N. N.; Earnshaw, A. *Chemistry of the Elements*; Pergamon Press: Oxford, 1989; p 816.
(73) Gutsev, G. L. *J. Phys. Chem.* **1992**, *96*, 10242.

ACS SYMPOSIUM SERIES **555**

Inorganic Fluorine Chemistry

Toward the 21st Century

Joseph S. Thrasher, EDITOR
University of Alabama

Steven H. Strauss, EDITOR
Colorado State University

Developed from a symposium sponsored
by the Division of Fluorine Chemistry
at the 203rd National Meeting
of the American Chemical Society,
San Francisco, California,
April 5–10, 1992

American Chemical Society, Washington, DC 1994

Chapter 5

Heptacoordinated Main-Group Fluorides and Oxofluorides

K. O. Christe[1], E. C. Curtis[1], D. A. Dixon[2], H. P. A. Mercier[3],
J. C. P. Sanders[3], G. J. Schrobilgen[3], and W. W. Wilson[1]

[1]Rocketdyne, Division of Rockwell International Corporation,
Canoga Park, CA 91309
[2]Central Research and Development, DuPont, Experimental Station,
Wilmington, DE 19880–0328
[3]Department of Chemistry, McMaster University, Hamilton,
Ontario L8S 4M1, Canada

The major problems associated with heptacoordination in main-group fluorides and oxofluorides have been resolved. A detailed discussion of the structures of ClF_6^-, BrF_6^-, IF_6^-, XeF_5^-, IF_7, TeF_7^-, IOF_6^- and $TeOF_6^{2-}$ is given. It is shown (i) that the steric activity of a free valence electron pair (E) in XF_6E species depends on the size of X; (ii) that in the XeF_5^- anion, which is the first known example of a pentagonal planar XF_5E_2 species, the two free valence electron pairs are sterically active and occupy the two axial positions; (iii) that the XF_7 and XOF_6 species possess pentagonal bipyramidal structures with five equatorial fluorine ligands which, in free molecules, are highly fluxional and dynamically distorted; (iv) that the dynamic distortion in XF_7 is the result of a rapid puckering motion of the five equatorial fluorines and of a much slower intramolecular, axial-equatorial ligand exchange; (v) that, in the XOF_6 species, this axial-equatorial ligand exchange is precluded by the more repulsive oxygen ligand which resides exclusively in one of the less congested axial positions; (vi) that, in solid $N(CH_3)_4^+IOF_6^-$, the dynamic puckering of the equatorial ligands is frozen out by hydrogen-fluorine bridges; (vii) that the pentagonal bipyramidal structures of these fluorides and oxofluorides cannot be explained by the VSEPR rules of repelling points on a sphere but are governed by the spatial distribution of the valence orbitals of the central atom; and (viii) that the bonding in these heptacoordinated species is best explained by a model involving delocalized $p_{x,y}$ hybrid orbitals of the central atom for the formation of a coplanar, semi-ionic, 6-center 10-electron bond system for the five equatorial bonds and of an sp_z hybrid orbital for the formation of two, more covalent, colinear, axial bonds; this bonding scheme can account for all the observed structural features and also the observed differences in bond lengths.

Inorganic main-group fluorides or oxofluorides offer a unique opportunity to study unusually high coordination numbers and problems associated with them, such as the steric activity of free valence electron pairs, steric crowding of the ligands, and fluxionality. Of particular interest are heptacoordinated species which could exist either

as a monocapped octahedron, a monocapped trigonal prism, or a pentagonal bipyramid. According to the VSEPR model of "repelling points on a sphere", the preferred structures should be the monocapped octahedron or trigonal prism ($1,2$). However, for main-group elements, the pentagonal bipyramid is favored (3), as found for IF_7 (4) and TeF_7^- (5-7). These pentagonal bipyramidal structures possess five-fold symmetry. Their highly congested equatorial planes result in increased equatorial bond lengths and usually some kind of puckering. The puckering of the five equatorial ligands represents a special problem. The odd number of ligands does not allow for a highly symmetric arrangement in which all five equatorial ligands can be placed into equivalent positions, i.e., with identical displacements alternately above and below the equatorial plane. This poses several interesting questions, such as: (i) are the five equatorial ligands equivalent and, if so, how is this equivalency achieved; (ii) are these molecules rigid or fluxional and, if they are fluxional, on what time scale; and (iii) what causes these heptacoordinated molecules to adopt, contrary to the VSEPR rules ($1,2$), pentagonal bipyramidal structures with either planar or only slightly puckered equatorial fluorines? In this paper we will give a brief review of the work recently done in our laboratories in this field which, to a large extent, was made possible by the development of a convenient preparative scale synthesis of truly anhydrous $N(CH_3)_4^+F^-$ (8) and the realization that this salt is an excellent reagent for the preparation of novel, high-oxidation state complex fluoro- or oxofluoro-anions ($9,10$). Furthermore, the high solubilities of these $N(CH_3)_4^+$ salts in solvents such as CH_3CN or CHF_3 permit the gathering of valuable structural information through NMR and vibrational studies and the growth of single crystals suitable for X-ray structure determinations.

XF_6E Species

Typical representatives of this structural type are the hexafluorohalate (V) anions, ClF_6^-, BrF_6^- and IF_6^-. Vibrational spectroscopy on the BrF_6^- ($11,12$) and IF_6^- ($12,13$) anions strongly indicated that BrF_6^- is octahedral while IF_6^- is strongly distorted. This was subsequently confirmed by X-ray crystal structure determinations ($14,15$). For ClF_6^-, only vibrational data are known (10) which show that this anion is also octahedral. These results demonstrate that in the $HalF_6^-$ anions the steric activity of the free valence electron pair on the central atoms is governed by the size of the central atom. For the relatively large iodine atom, the maximum coordination number (CN) towards fluorine exceeds six, thus providing sufficient space for a sterically active free electron pair, whereas for the smaller bromine and chlorine atoms, the maximum CN is only six and, hence, the free valence electron pair occupies a centrosymmetric s orbital and is sterically inactive (12).

XF_5E_2 Species

Only one representative of this type is known, namely the XeF_5^- anion. The structure of this anion was established by ^{19}F and ^{129}Xe NMR and infrared and Raman spectroscopy and an X-ray crystal structure determination (16). The structure of this unique anion is shown in Figures 1 and 2 and demonstrates that the two free valence electron pairs are sterically active and, as expected from their increased repulsive character, occupy the two less congested axial positions of a pentagonal bipyramid.

The chemical equivalence of the five equatorial fluorine ligands in XeF_5^- was confirmed by its ^{129}Xe NMR spectrum which displays a well-resolved binominal sextet (see Figure 3). Due to its relatively long Xe-F bonds, the XeF_5^- anion experiences only mild congestion in the equatorial plane (as shown below, the in-plane deformation force
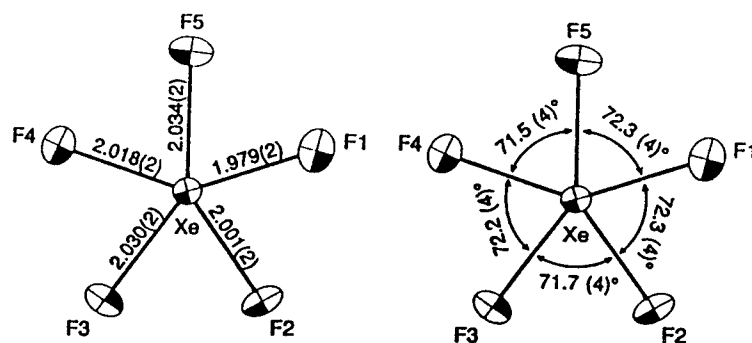
Figure 1. Atom numbering scheme, bond lengths (Å) and angles (deg) for XeF$_5^-$ at -86 °C in [N(CH$_3$)$_4$]$^+$[XeF$_5$]$^-$. Projection of the XeF$_5^-$ anion on (111). Esd's are given in parentheses; thermal ellipsoids are shown at the 50% probability level.
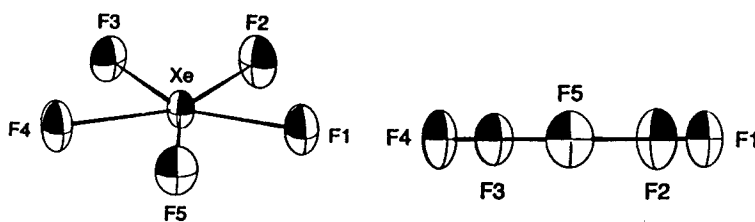

Figure 2. Projections of the XeF$_5^-$ anion on (130) (left) and (010) (right). Thermal ellipsoids are shown at the 50% probability level.
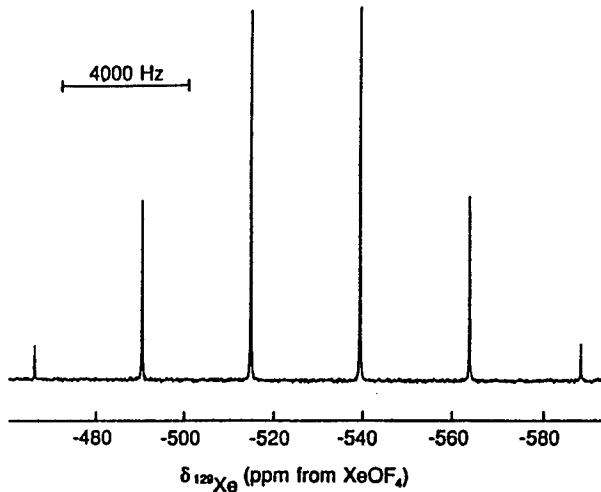

Figure 3. ^{129}Xe NMR spectrum (139.05 MHz) at 24 °C of a saturated solution of N(CH$_3$)$_4^+$XeF$_5^-$ in CH$_3$CN containing a 1 M excess of N-(CH$_3$)$_4^+$F$^-$.

constant, f_α, is only 0.364 mdyn/Å) and therefore is, within experimental error, unpuckered.

XF$_7$ Species, IF$_7$

The two representatives, known for this type, are the IF$_7$ molecule and the TeF$_7^-$ anion. Although IF$_7$ had been known for 61 years (*17*) and numerous papers dealing with its properties had been published, this molecule was only poorly understood and presented many mysteries. Since IF$_7$ is the prototype of a pentagonal bipyramidal, heptacoordinated species, it was imperative to better understand this molecule. The following paragraph summarizes the salient features and conclusions from the previous studies: (i) Crystal structure determinations of solid IF$_7$ were inconclusive due to disorder problems (*18-23*). (ii) In the liquid and gas phases, all seven fluorine ligands were shown to be magnetically equivalent on the time scale of NMR spectroscopy due to an intramolecular exchange of equatorial and axial fluorines (*24-28*). (iii) Gaseous IF$_7$ at room temperature does not possess a permanent dipole moment, as shown by the absence of microwave transitions (*29*) and of deflections in inhomogenous electric fields (*30*). (iv) Gas phase electron diffraction data (*4,31,32*) show that IF$_7$ closely approaches D$_{5h}$ symmetry with a misfit in the 2.1-2.7Å region which is not much larger than common amplitudes of vibration. The breadth and skewing of the 2.5Å nonbonded F$_{ax}$...F$_{eq}$ radial distribution peak were explained by an asymmetric molecule involving fluxionality and a dynamic pseudorotational ring-puckering which resulted in average displacements of 7.5° for the equatorial fluorines and of 4.5° for the axial fluorines (*4*). (v) At least nine studies of the vibrational spectra of IF$_7$ have previously been reported (*33-42*), and although all nine studies analyzed the observed spectra in point group D$_{5h}$, all sets of assignments were different and none was able either to duplicate the experimental mean square amplitudes of vibration (*4*) or to assign the observed infrared combination bands without violations of the D$_{5h}$ selection rules. (vi) Results from a pseudopotential SCF-MO study (*43*) yielded a minimum energy structure with D$_{5h}$ symmetry and an alternative assignment for the vibrational spectra, however, the agreement between calculated and observed frequencies was poor, and a complete vibrational spectrum was not calculated at that time due to the lack of analytic second derivative methods for pseudopotentials.

Ab Initio Calculations for IF$_7$. Because our results on the vibrational spectra and structures of the pentagonal planar XeF$_5^-$ (*16*) and pentagonal bipyramidal IOF$_6^-$ anions substantially differed from those (*4,33-43*) previously reported for pentagonal bipyramidal IF$_7$, ab initio calculations were carried out for IF$_7$ at the following levels of theory: (i) local density functional (LDF) theory with numerical functions; (ii) all electron MO calculations; and (iii) MO calculations with an effective core potential (ECP) on iodine. All three calculations resulted in a pentagonal bipyramid of D$_{5h}$ symmetry as the lowest energy structure. The calculated geometries and vibrational frequencies are summarized in Table I and compared with the revised (see below) experimental values. Reducing the symmetry to C$_2$ or C$_1$ resulted at the LDF level in structures with only one component of the E$_2''$ mode being imaginary and having smaller values, but led to structures that were higher in energy by <0.05 kcal/mol. The remaining frequencies, excluding the E$_2''$ mode, were within 10 cm^{-1} of those for the LDF D$_{5h}$ structure. As can be seen from Table I, the resulting changes in the frequencies and geometries for the C$_2$ and C$_1$ structures from the D$_{5h}$ structure are rather small and demonstrate the great similarities between the ideal D$_{5h}$ structure and the other structures which are somewhat deformed by equatorial puckering and slight axial bending. This is in accord with the previous conclusion that the potential energy well for IF$_7$ at D$_{5h}$ is very flat and shallow and has a nearly quartic contour for buckling along either a C$_2$ or a C$_s$ symmetry coordinate (*3*). Table I shows that the effective core

Table I. Observed and Calculated Vibrational Frequencies and Geometries for IF$_7$

assignments and approximate mode descriptions in point group D$_{5h}$		obsd frequencies, cm⁻¹		calculated frequencies, cm⁻¹				
		IR	Ra	ECP[a] D$_{5h}$	SCF D$_{5h}$	LDF D$_{5h}$	LDF C$_2$	LDF C$_1$
A$_1'$	ν_1 ν sym XF$_2$ ax	—	676(2)p	673	743	630	629	625
	ν_2 ν sym XF$_5$ eq	—	635(10)p	644	704	598	596	596
A$_2''$	ν_3 ν as XF$_2$ ax	746s	—	753	834	710	708	703
	ν_4 δ umbrella XF$_5$ eq	365s	—	368	366	304	310	305
B$_1'$	ν_5 ν as XF$_5$ eq	670vs		681	761	647	644	646
	ν_6 δ as XF$_5$ in plane	425vs		441	454	377	375	376
	ν_7 δ sciss XF$_2$ ax	257w		265	261	213	211	212
E$_1''$	ν_8 δ rock XF$_2$ ax	—	319(0.6)[b]	320	321	259	268	282
E$_2'$	ν_9 mixture of δ sciss XF$_5$ in plane	—	596(0.2)	605	651	561	559	560
	ν_{10} and ν as XF$_5$ eq	—	510(1.7)	515	555	467	464	458
E$_2''$	ν_{11} δ pucker XF$_5$ eq		[68][c]	59	39	50i	41,33i	42,23i
Total Energy								

Geometry	observed[4]		calculated				
	C$_2$-C$_3$	D$_{3h}$					
r(I - F$_{ax}$) (Å)	1.786(7)	1.781	1.7705	1.807	1.870	—	1.874
r(I - F$_{eq}$) (Å)	1.858(4)	1.857	1.8333	1.862	1.918	—	1.917
average equat. puckering angle (deg)	7.5	0	0[d]	0[d]	0[d]	—	4.0[e]
deviation of ax. bonds from 180°	4.5	0	0	0	0	—	1.7[e]

[a] The ECP frequencies were scaled by a factor of 0.932. [b] This frequency value was derived from the two Raman bands at 310(0.6) and 352(0.6) by correction for Fermi resonance (see text). [c] Estimated from the ($\nu_7 + \nu_{11}$) combination band (see text). [d] Although D$_{5h}$ symmetry requires the equatorial plane in the average to be planar, the low frequency of ν_{11} combined with the large F$_{ax}$...F$_{eq}$ amplitude of vibration makes the effective equatorial puckering comparable to that found for the lower symmetries (see text). [e] The actual displacements of the five equatorial fluorines from the ideal plane in a clockwise sense were (deg): +0.35, -3.15, +6.65, -6.65, +3.25 with the axial fluorines being bent toward the equatorial fluorine with the smallest (0.35) equatorial displacement.

potential data set, after scaling by a factor of 0.932 to account for electron correlation and anharmonicity effects, duplicates best the experimental frequencies (*37,40*) with an average frequency deviation of only 7 cm^{-1}. This small deviation is excellent considering that the original calculated values are harmonic, gas-phase frequencies, while the observed values are anharmonic frequencies measured in some cases even in liquid or solid phases.

Raman Spectrum of Solid IF$_7$.   A comparison between the calculated (see Table I) and previously reported (*33-42*) vibrational frequencies, irrespective of their detailed assignments, revealed the following general problems: (i) a Raman active mode having a predicted frequency of about 605 cm^{-1} was missing; (ii) there was one excess fundamental vibration in the 300-400 cm^{-1} region; and (iii) the puckering mode of the equatorial plane which should be inactive in both the Raman and infrared spectra, should have a very low frequency of about 60 cm^{-1} and be observable only indirectly in the form of combination bands.

For these reasons, the Raman spectrum of solid IF$_7$ was reinvestigated at different temperatures.   As can be seen from Figure 4, at -142°C a distinct Raman band is observed at 596 cm^{-1} exhibiting about the right intensity for the missing equatorial IF$_5$ antisymmetric stretching or in-plane scissoring modes. At higher temperature, this band becomes hidden in the foot of the intense 635 cm^{-1} band due to the increased line widths. In the 300-360 cm^{-1} region, two fundamental vibrations had previously been identified (*37*) at 310 and 352 cm^{-1}. Figure 4 shows that on cooling from -13° to -142°C, the frequency separation of these two bands decreases from 42 to 29 cm^{-1} while at the same time the relative intensity of the higher frequency band decreases markedly.   This behaviour is characteristic for a Fermi resonance between a fundamental vibration and a combination band where the population of the combination band decreases with decreasing temperature. Therefore, the 352 cm^{-1} Raman band does not represent a fundamental vibration. It is due (see below) to a combination band which involves the inactive equatorial ring puckering mode and confirms the predicted low frequency value of the latter.

Vibrational Assignments. In view of the above findings, the vibrational assignments for IF$_7$ (see Table I) can now be easily made by comparison with the calculated ECP frequencies. All bands strictly follow the selection rules for D$_{5h}$ symmetry, 2A$_1$'(R) + 2A$_2$"(IR) + 3E$_1$'(IR) + 1E$_1$"(R) + 2E$_2$'(R) + 1E$_2$"(ia), and exhibit the expected relative intensities, infrared gas-phase band contours and Raman polarization. The agreement between calculated and observed frequencies (average $\Delta v = 7$ cm^{-1}) is excellent and supports the present assignments.

The difficulty of assigning the vibrational spectra of IF$_7$ without the help of reliable ab initio calculations is best reflected by the failures of the previous vibrational analyses (*33-42*) in which no more than four out of the eleven fundamental vibrations had been correctly assigned, a disappointing result if one considers the large number of studies and the expertise of the previous investigators. The only significant improvement over these poor results had previously been achieved by Bartell and coworkers who, with the aid of pseudopotential SCF-MO calculations, correctly located seven of the eleven fundamental vibrations and predicted the right frequency range for two additional ones (*43*). Most of these difficulties can be attributed to the fact that the previous investigators did not realize that the equatorial in-plane bending modes of IF$_7$ have such unusually high frequencies.

In several of the previous studies, the inability to assign the observed infrared combination bands of IF$_7$ without violations of the D$_{5h}$ selection rules had been explained by a strong coupling between the E$_2$" and E$_1$' modes which should make the E$_2$" overtones and the pseudoradial, pseudoangular combination bands slightly infrared

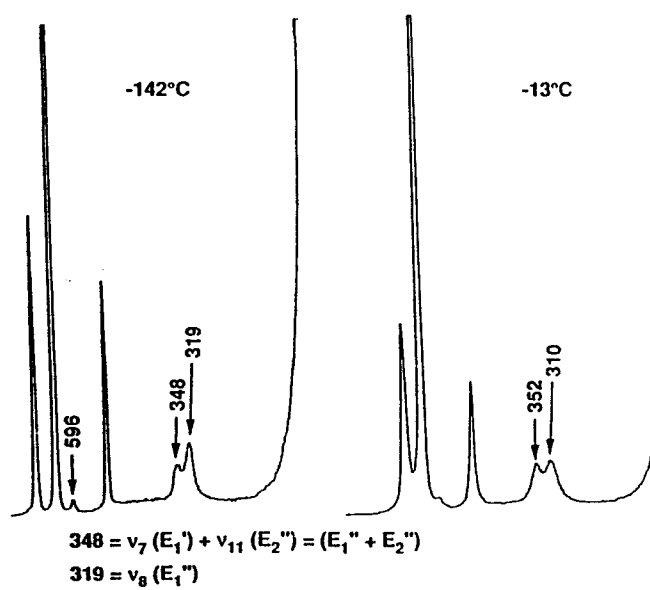$348 = \nu_7 (E_1') + \nu_{11} (E_2'') = (E_1'' + E_2'')$
$319 = \nu_8 (E_1'')$

Figure 4. Raman spectra of solid IF$_7$ recorded at -142 and -13 °C.

active, with intensity borrowed from the induced E_1' displacements (*4,40,44*). The revised assignments for IF_7 given in Table I permit the assignment of all the observed infrared overtones and combination bands without any violations of the D_{5h} selection rules, thus eliminating one of the arguments previously advanced (*40,43*) against IF_7 having an average symmetry of D_{5h}.

The aforementioned, Raman active combination band at 352 cm^{-1} which is in Fermi resonance with v_8 (E_1'') requires some special comment. First of all, Fermi resonance requires this band to have the same E_1'' symmetry as v_8; secondly, the band cannot be assigned using any of the remaining fundamental vibrations of IF_7; and thirdly, there are only two fundamental vibrations, v_7 (E_1') and v_{11} (E_2''), that have frequencies lower than that of v_8. Therefore, the 352 cm^{-1} band can only be due to a combination of v_7 (E_1') with the inactive equatorial ring puckering mode, v_{11} (E_2''), which results in the required E_1'' symmetry for the ensuing combination band. After a correction for the Fermi resonance induced frequency shift (*45*), a frequency of about 68 cm^{-1} is obtained for the ring puckering mode, v_{11}, which is in good agreement with the value of 59 cm^{-1} predicted by our ECP calculations. Furthermore, this [v_7 (E_1') + v_{11} (E_2'')] combination band represents the mode proposed (*4,43*) by Bartell for the pseudorotation in IF_7.

Force Constants and Mean Square Amplitudes of Vibration. Another problem in the previous IF_7 studies (*33-43*) was the discrepancy between the mean square amplitudes of vibration from the electron diffraction study (*4*) and those derived from normal coordinate analyses of the vibrational spectra. Since all the previous normal coordinate analyses for IF_7 had been carried out with partially incorrect assignments, such an analysis was repeated using our ab initio (ECP) force field. Inspection of the internal force constants of IF_7 (see Table II) reveals several interesting features: (i) the stretching force constant of the axial bonds, f_D, is considerably larger than that of the equatorial bonds, as expected from the observed bond lengths (*4*) and general valence shell electron pair repulsion (VSEPR) arguments (*1,2*) which attribute the longer equatorial bonds to the congestion and increased mutual repulsion of the ligands in the equatorial plane. The absolute value of f_D, 5.01 mdyn/Å, is lower than that of 5.42 mdyn/Å previously found for the IF_6^+ cation (*46*), as expected for going from a fluorocation to its parent molecule, and (ii) the values of the equatorial angle deformation constants, f_α and f_β, exhibit a huge difference. As expected, the in-plane deformation, f_α, is very large (0.84 mdyn/Å) due to the severe crowding in the equatorial plane, while the out-of-plane deformation, f_β, is very small (0.16 mdyn/Å) because of the ease of equatorial ring puckering. These force constants lend strong support to our model of the bonding and fluxionality in IF_7 (see below).

The previous electron diffraction study (*4*) had resulted in two different sets of mean square amplitudes of vibration which, depending on the choice of the structural model, strongly differed in their value for the nonbonded $\ell(F_{ax}...F_{eq})$ amplitude. For a static D_{5h} model, this amplitude had a value of 0.169Å, whereas for the statically or dynamically distorted C_2, (50% C_2 + 50% C_s), or C_s models values ranging from 0.104 to 0.107Å were obtained. Since the analysis of the vibrational spectra provides an independent experimental set of mean square amplitudes for IF_7, this set can be used to distinguish between the two structural models which were proposed (*4*) on the basis of the electron diffraction data. As can be seen from Table III, the mean square amplitudes from the vibrational spectra are in good agreement with the D_{5h} but not the other models. It must be kept in mind, however, that the unusually large vibrational amplitude of 0.16Å for $\ell(F_{ax}...F_{eq})$ in the D_{5h} model corresponds to a 6.9° displacement of a fluorine ligand from the equatorial plane and is very close to the

average equatorial puckering angle of 7.5° deduced from the electron diffraction data for the distorted models (4). The good agreement between the mean square amplitudes of vibration, derived from our force field, and those deduced for the D_{5h} model from the electron diffraction data (4), is very gratifying and attests to the correctness of our revised assignments.

Table II. Internal Force Constants[a] (mdyn/Å)[b] of IF_7

$f_D = 5.005$	$f_\beta = 0.163$
$f_{DD} = 0.058$	$f_{\beta\beta} = 0.078$
$f_{Dd} = -0.0018$	$f_{\beta\beta}' = -0.042$
$f_d = 3.947$	$f_{\beta\beta}'' = -0.038$
$f_{dd} = 0.326$	$f_{\beta\beta}''' = -0.044$
$f_{dd}' = 0.0265$	$f_{\beta\beta}'''' = -0.058$
$f_\alpha = 0.841$	$f_{d\beta} = 0.090$
$f_{\alpha\alpha} = -0.187$	$f_{d\beta}' \equiv f_{d\beta}'' \equiv 0$
$f_{\alpha\alpha}' = -0.243$	$f_{\alpha\beta} \equiv f_{\alpha\beta}' \equiv -f_{\alpha\beta}'' = -0.021$
$f_{d\alpha} \equiv f_{d\alpha}' \equiv -f_{d\alpha}'' = -0.238$	$f_{D\beta} \equiv -f_{D\beta}' = 0.042$

[a]$D = IF_{ax}$, $d = IF_{eq}$, $\alpha = \sphericalangle F_{eq}IF_{eq}$, $\beta = \sphericalangle F_{ax}IF_{eq}$, dd = coupling to adjacent d, dd' = coupling to opposite d, $\alpha\alpha$ = adjacent α, $\alpha\alpha'$ = opposite α, $d\alpha$ = α opposite to d, $d\alpha'$ = remote α, $d\alpha''$ = adjoining α, $\beta\beta$ = common D and adjoining d, $\beta\beta'$ = noncommon D and common d, $\beta\beta''$ = common D and remote d, $\beta\beta'''$ = noncommon D and adjoining d, $\beta\beta''''$ = noncommon D and remote d, $d\beta$ = common d, $d\beta'$ = adjoining d, $d\beta''$ = remote d, $\alpha\beta$ = opposite d, $\alpha\beta'$ = adjoining d, $\alpha\beta''$ = common d, $D\beta$ = common D, $D\beta'$ = opposite D. [b]The internal force constants have been normalized for distance assuming $D = 1.781$Å and $d = 1.857$Å.

Table III. Comparison of the Mean Square Amplitudes (Å) of Vibration of IF_7 Obtained from the Vibrational Spectra with Those Derived from the Electron Diffraction Study under the Assumption of Different Structural Models

		Electron Diffraction[5]	
	Vibrational Spectra (D_{5h})	D_{5h}	50% C_2 - 50% C_s
ℓ (I...F_{ax})	0.039	0.042[a]	0.043±0.003
ℓ (I...F_{eq})	0.043	0.044	0.045±0.003
ℓ (F_{eq}...F_{eq}) short	0.061	0.061	0.061±0.005
ℓ (F_{eq}...F_{eq}) long	0.060 ⎫	0.093[b]	0.091[b]±0.006
ℓ (F_{ax}...F_{ax})	0.053 ⎭		
ℓ (F_{eq}...F_{ax})	0.163	0.169	0.106±0.008

[a]Obtained from constraint ℓ (I...F_{ax}) = ℓ (I...F_{eq}) -0.002Å. [b]Overlapping peak which could not be resolved into its two components.

Axial-Equatorial Ligand Exchange. In addition to the above described very fast, dynamic puckering of the pentagonal equatorial fluorine plane which requires very little energy ($\nu_{11} = 59$ cm^{-1} = 0.17 kcal mol^{-1}) and hence is thermally populated at higher vibrational levels even at low temperatures, a second type of fluxionality is possible for IF$_7$. This second type of fluxionality involves an intramolecular exchange of axial and equatorial fluorines. This was shown by the magnetic equivalence of all seven fluorine ligands of IF$_7$ (*24-28*) or the isoelectronic TeF$_7^-$ anion (*6,7*) on the NMR time scale. This exchange process, with an estimated (*27*) lifetime of a given configuration of ~2.5 x 10^{-3} sec, is considerably slower than that for ring puckering and involves higher vibrational levels of ν_7 (E$_1$'). This motion can best be described as an antisymmetric combination of the axial and equatorial bending symmetry coordinates, S$_6$ and S$_7$, which is accompanied by an out-of-plane twisting motion of the three remote equatorial fluorine ligands.

$$\nu_7 (E_1') = 265 \text{ cm}^{-1}$$
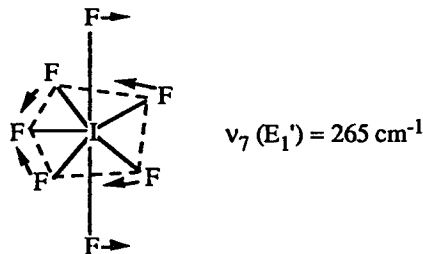
This axial-equatorial exchange mechanism is analogous to that previously proposed by Berry (*47*) for trigonal bipyramidal molecules, such as PF$_5$ or SF$_4$, and involves a substantial energy barrier of several vibrational levels of ν_7.

Structure and Bonding of IF$_7$. Whereas the results of the ab initio calculations, the microwave study and the normal coordinate analysis are best interpreted in terms of a structural model of average D$_{5h}$ symmetry that undergoes a rapid dynamic puckering of the equatorial plane with very large vibrational amplitudes, the previous electron diffraction data (*4*) favored a pseudorotational C$_2$–C$_s$ model with an equilibrium structure that is distorted from D$_{5h}$ symmetry. The question then arises whether one of these seemingly different models is incorrect or if the differences are only due to the semantics of how to best describe a highly fluxional and dynamically distorted molecule.

First of all, one must understand what type of information can be gained from the different methods of investigation. Electron diffraction results generally describe the average structure of vibrating molecules and not the minimum energy geometries (*48*). If a highly fluxional molecule, such as IF$_7$, undergoes a large dynamic distortion at low energy, then electron diffraction will only see a distorted molecule. A classic example for such a case is the linear CO$_2$ molecule which, according to its electron diffraction data, would be bent because in the vibrating molecule the average nonbonded O...O distance becomes shorter than twice the bonded C–O distance (*48*). Returning to the electron diffraction data for IF$_7$, the conclusions (*4,43*) reached by Bartell and coworkers are compelling by their logic and thoroughness. The plane of the five equatorial fluorines of IF$_7$ is highly congested. This congestion can be relieved by a large-amplitude, dynamic puckering. For a five-fold symmetry, the five ligands cannot be displaced from the equatorial plane in a manner which renders them at any given time equivalent and equidistant from the ideal equatorial plane as shown by the previously published (*4*) geometries of the C$_2$ or C$_s$ models of IF$_7$. As a consequence of these

uneven equatorial ligand displacements, the axial ligands experience an uneven repulsion from the equatorial plane and will bend away from those ligands which exhibit the largest displacements from the equatorial plane (1). Since the experimental evidence overwhelmingly suggests that all the equatorial ligands are equivalent, a rapid dynamic pseudorotation of the puckering motion must be invoked which is phase-coupled to a precession of the slightly bent axial FIF group (i.e., Bartell's pseudorotational model) (4). Due to the short time scale of the electron diffraction technique, it detects at all times a distorted IF_7 molecule that exhibits a strong and uneven equatorial puckering and as a consequence also an axial bend which results in an equilibrium symmetry lower than D_{5h}.

On the other hand, ab initio calculations and vibrational spectroscopy generally describe the symmetry of the minimum energy geometry which for IF_7 would be D_{5h} if the distortions are only dynamic in nature and not static. Although the knowledge of the exact potential energy curve of IF_7 would be desirable to distinguish between a distorted and an undistorted ground state configuration, the absence of a permanent dipole moment (30) and microwave transitions (29) and the results from this study strongly favor an undistorted D_{5h} ground state which undergoes facile dynamic distortion, most likely by Bartell's pseudorotation mechanism (4). This signifies that both the D_{5h} and the dynamically distorted model descriptions for IF_7 are, in principal, correct because they describe different time domains. The undistorted D_{5h} model describes the nonvibrating ground state whereas the distorted, dynamically puckered, pseudorotational model depicts the vibrating molecule.

Corroborating evidence that heptacoordinated molecules, with either fluorine, oxygen or free valence electron pairs as ligands, possess in their ground states pentagonal bipyramidal structures with an unpuckered equatorial plane, comes from ongoing ab initio calculations and two X-ray crystal structure determinations. It has experimentally been shown that in XeF_5^-, in which the longer Xe-F bond distances of 1.979(2)-2.034(2)Å lessen the equatorial ligand-ligand repulsions ($f_\alpha = 0.364$ mdyn/Å), the equatorial fluorines are essentially coplanar (16). It has also been shown (see below) that in IOF_6^- ($f_\alpha = 0.690$ mdyn/Å), which has considerably shorter (1.88Å) equatorial bonds than XeF_5^-, the equatorial fluorines are puckered, but that with decreasing temperature the degree of puckering strongly decreases (49).

The fact that heptacoordinated species in their ground states exhibit pentagonal bipyramidal structures with an unpuckered equatorial plane, cannot be rationalized by VSEPR theory (1,2) in terms of a "repelling points on a sphere" (POS) model which should result in either a monocapped octahedron or a monocapped trigonal prism. Furthermore, it cannot be explained by conventional bonding schemes involving localized electron orbitals of the central atom to enforce the coplanarity of a central atom and five equatorial ligands. The best explanation to account for this planarity is the bonding scheme first proposed (16) for XeF_5^- based on an ab initio calculation of the molecular orbital population. In this scheme, the structure and bonding of XeF_5^- are explained by a simple model derived from XeF_4. The bonding in the square planar XeF_4 can be described by two semi-ionic, 3-center 4-electron (3c-4e) bonds (50-52) for the four Xe-F bonds and two lone valence electron pairs on Xe ($s^2p_z^2$ hybrids). The 3c-4e bonds involve the p_x^2 and p_y^2 orbitals of xenon. Addition of an F^- ion to the equatorial plane in XeF_4 results in pentagonal planar XeF_5^- and the formation of a semi-ionic, 6-center 10-electron (6c-10e) bond involving the delocalized $p_x^2 p_y^2$ hybrid orbitals of Xe and 6 electrons on the 5 F ligands (16). The two lone valence electron pairs on Xe in XeF_5^- are analogous to those in XeF_4.

The planar IF_5 fragment of IF_7 has essentially the same bonding as XeF_5^-, as shown by the atomic population calculations given in Table IV. As expected for the

Table IV. Atomic Populations (e) in the Valence Electron Orbitals and Total Charge Distributions for XeF₅⁻, IF₇ and IOF₆⁻[a]

Central Atom

	XeF_5^-	IF_7	IOF_6^-	
s	2.22	1.35	1.43	
$p_x = p_y$	0.61	0.64	0.64	
p_z	2.02	0.60	0.71	
$d_z{}^2$	0.03	0.11	0.14	
$d_x{}^2 = d_y{}^2$	0.06	0.12	0.09	
d_{xy}	0.14	0.20	0.16	
$d_{xz} = d_{yz}$	0.04	0.14	0.15	
d total	0.37	0.83	0.78	

Equatorial Fluorines

s	1.98	1.93	1.94	
p bond	1.70	1.57	1.64	
p in plane	1.98	1.96	1.97	
p_z	1.97	1.94	1.95	
d	0	0.03	0.02	

Axial Fluorines and Oxygens

			F	O
s	—	1.92	1.92	1.86
p_z	—	1.54	1.57	1.16
$p_x = p_y$	—	1.94	1.95	1.83
d	—	0.04	0.03	0.04

Total Charges

Central Atom	2.15	2.94	2.81	
F_{eq}	-0.63	-0.43	-0.53	
F_{ax}	—	-0.39	-0.44	
O_{ax}	—	—	-0.74	

[a]The Z axis is the five-fold axis.

replacement of two free valence electron pairs on the central atom by two bonded ligands, each of which contributes one electron to its bond, the population of the s^2 and $p_z{}^2$ orbitals of I in IF₇ has decreased by about two electrons, compared to XeF₄ and XeF₅⁻. The higher oxidation state of the central atom in IF₇ (+VII) results in I having a higher positive charge than Xe (+IV) in XeF₅⁻. This causes the effective electronegativity difference between the central atom and the ligands in IF₇ to be smaller than those in XeF₄ and XeF₅⁻ and results in an increased covalency and a shortening of

the central atom-fluorine bonds. Furthermore, the axial fluorine ligands in IF_7 carry less of a negative charge than the equatorial ones and their bonds have higher s-character which accounts for the axial I-F bonds to be shorter than the equatorial ones.

Of course, the above model does not account for the fact that the electrons will try to minimize their mutual repulsions and occupy all of the available orbitals to do so. This results in the participation of some d functions. Although we are not proposing a d hybridization model, the population in the d orbitals does suggest a redistribution into these orbitals beyond that expected if the d orbitals were acting solely as polarization functions.

The above atomic population and total charge distribution analysis qualitatively confirms our simple bonding model for pentagonal bipyramidal molecules. This model involves the use of delocalized p_x^2 and p_y^2 hybrid orbitals of the central atom for the formation of a semi-ionic, 6c-10e bond with the five equatorial ligands and of an sp_z hybrid orbital for the formation of two, more covalent, axial bonds. This bonding scheme can account for all the observed structural features and also the observed bond length differences. The planarity of the p_x^2 and p_y^2 hybrid orbitals of the central atom also provides the explanation why the heptacoordinated main-group fluorides prefer pentagonal-bipyramidal structures and not the monocapped octahedral or trigonal prismatic ones expected from VSEPR arguments (1,2).

The possible puckering of the equatorial plane in pentagonal bipyramidal molecules is due to the high degree of congestion in this plane. In XeF_5^- ($r_{XeF} \approx 2.00$ Å) (16), the congestion is relatively low and, therefore, the anion is still planar, whereas the considerably shorter equatorial I-F bonds (r = 1.857 Å) (4) in IF_7 result in increased repulsion and significant dynamic puckering.

XF_7 Species, TeF_7^-

The structure of the TeF_7^- anion which is isoelectronic with IF_7 was shown by ^{19}F NMR and vibrational spectroscopy to be analogous to that of IF_7 (6,7). The [125]Te NMR spectrum (see Figure 5) of TeF_7^- in CH_3CN solution demonstrated that on the NMR time scale all seven fluorine ligands are chemically equivalent and, therefore, the free TeF_7^- anion is fluxional. The pentagonal bipyramidal structure of TeF_7^- has also been recently confirmed by the results from an X-ray crystal structure determination (53) and, hence, does not require any further discussion.

XOF_6 Species

Two isoelectronic anions, IOF_6^- and $TeOF_6^{2-}$, have been prepared (6,7) and are the only known main-group representatives of this structural type. Of the two, the IOF_6^- has been fully characterized by ab initio calculations, NMR and vibrational spectroscopy and an X-ray crystal structure determination, while for $TeOF_6^{2-}$ only the vibrational spectra are known.

Synthesis and Properties of $N(CH_3)_4^+IOF_6^-$. This salt was prepared according to

$$N(CH_3)_4^+F^- + IOF_5 \xrightarrow{ CH_3CN } N(CH_3)_4^+IOF_6^-$$
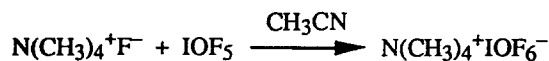
and is a very pale yellow solid which is thermally stable up to about 137°C where it starts to decompose to IOF_4^-, CF_4 and COF_2 as the major products. Its crystal

structure consists of well separated $N(CH_3)_4^+$ and IOF_6^- ions. The packing of the ions (see Figure 6) can be described as a cubic close packing of alternating layers of IOF_6^- anions and $N(CH_3)_4^+$ cations in which the alternating orientation of the tetrahedral cations results in a cuboctahedral (54) unit cell with $Z = 2$. While the cation is perfectly ordered with the expected bond lengths, the IOF_6^- anion is subject to a positional four-fold disorder in the equatorial plane. The model results from the superposition of four anions in which the central I atom and the axial O and F(1) atoms occupy identical positions. One of these anions is shown in Figure 7. There are no significant contacts to iodine other than the directly bonded oxygen and six fluorine ligands, and the anion exhibits a gross pentagonal bipyramidal geometry. The $O\text{-}I\text{-}F_{ax}$ angle is constrained by symmetry to be 180°, while there are no constraints on the positions of the equatorial fluorines. The equatorial fluorines are bent away from the axial oxygen ligand, as expected for a doubly bonded oxygen being more repulsive than a singly bonded fluorine ligand (2).

The I-O bond length (1.75-1.77Å) indicates significant double bond character for the I-O bond (55-60). Its temperature dependence will be discussed below. The greater I-O bond length in IOF_6^-, when compared with that in IOF_5 [1.715(4)Å] (55), is consistent with the placement of some of the negative charge on oxygen, thereby increasing the polarity and decreasing the bond order of the I-O bond. The axial I-F bond [1.823(3)Å] is, within experimental error ($\pm3\sigma$), significantly shorter than all of the equatorial I-F bonds (average 1.88Å), and both types of I-F bonds in IOF_6^- are significantly longer than the corresponding bonds in IF_7 [1.786(7)Å and 1.858(4)Å, respectively] (4). These differences can be attributed again to the formal negative charge on IOF_6^-, which leads to greater $\overset{\delta+}{I}\,\overset{\delta-}{-F}$ bond polarities and consequently longer bonds. The greater length of the equatorial bonds in IOF_6^- and IF_7 relative to their axial ones is due to the increased mutual repulsion of the fluorine ligands in the highly congested equatorial plane and their higher ionicity.

Nature of the Equatorial Puckering in IOF_6^-. As mentioned above, the equatorial fluorine atoms in IOF_6^- are bent away from the doubly bonded oxygen atom by about 5°. Furthermore, the plane of the equatorial fluorine atoms is puckered and its I-F bonds are elongated in order to lessen the high degree of ligand-ligand repulsion encountered for these fluorines. Contrary to the rapid dynamic puckering in free, pentagonal bipyramidal molecules, such as IF_7 (see above), the puckering in solid $N(CH_3)_4^+IOF_6^-$ is frozen out by hydrogen$\cdots$fluorine bridging between the two F(2) atoms of IOF_6^- and hydrogen atoms from two different cations. This bridging results in two close $F\cdots C$ contacts of 3.175(9)Å and 3.271(9)Å, while the remaining closest $F\cdots C$ contacts occur at 3.317(9), 3.473(9) and 3.416(9)Å and are very close to the accepted sum of the van der Waals radii of CH_3 (2.00Å) (61) and F(1.35-1.40Å) (61,62) which is 3.35-3.40Å.

A pentagonal plane can be puckered in two ways resulting in structures of either C_s or C_2 symmetry, respectively.
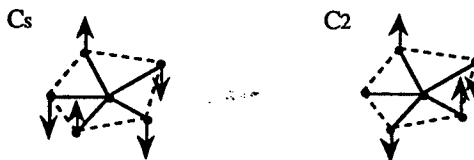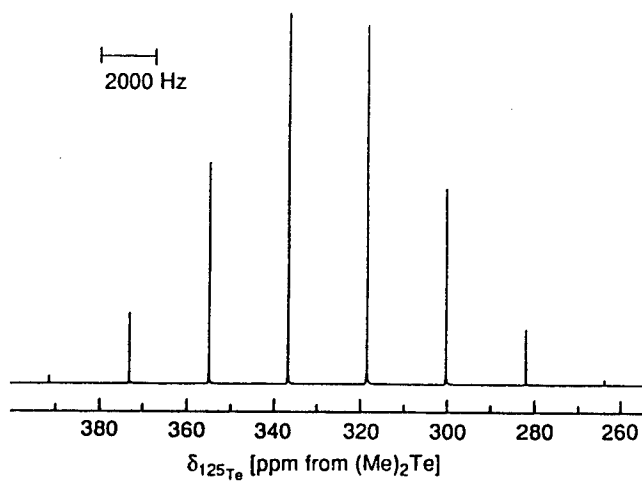
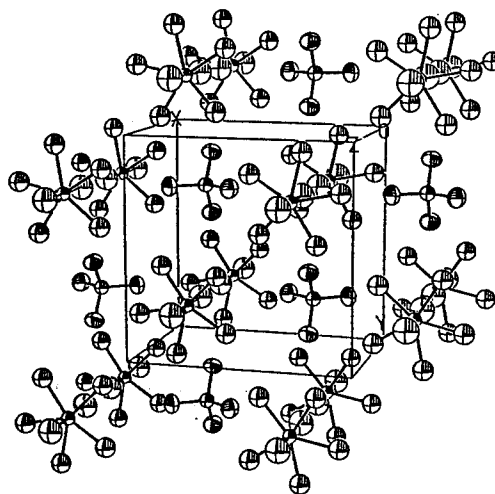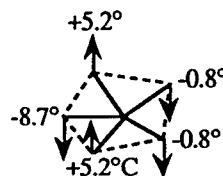Figure 5. The ^{125}Te NMR spectrum of $N(Me)_4^+TeF_7^-$ recorded at 157.792 MHz in MeCN solvent at 30 °C.

Figure 6. Packing diagram of $N(CH_3)_4^+IOF_6^-$ viewed along the c-axis.

As mentioned above, the doubly bonded, axial oxygen ligand in IOF_6^- is more repulsive than the singly bonded, axial fluorine ligand. Therefore, the average equatorial plane, which can be defined as a plane perpendicular to the $O-I-F_{ax}$ axis containing all five equatorial fluorine ligands at the averaged $F_{eq}-I-O$ bond angle, drops below the center of the iodine atom. As can be seen from Figure 7, the puckered plane of IOF_6^- definitely exhibits C_s symmetry with the following out of plane displacements.

^{19}F NMR Spectrum of the IOF_6^- Anion. The ^{19}F NMR spectrum of $N(CH_3)_4^+IOF_6^-$ was recorded at -40 °C in CH_3CN solution and is in agreement with a pentagonal bipyramidal structure for the IOF_6^- anion. This structure is expected to have an average C_{5v} point group symmetry with the oxygen in the axial position. Accordingly, the ^{19}F NMR spectrum (Figure 8) displays a broad doublet ($\Delta v_{1/2} \approx 170$ Hz) at 166.0 ppm, assigned to the equatorial fluorines, and a broad binomial sextet ($\Delta v_{1/2} \approx 360$ Hz) at 111.1 ppm, assigned to the axial fluorine trans to oxygen. The observation of separate ^{19}F resonances for the axial and equatorial ligand environments of IOF_6^- is unusual for a pentagonal bipyramidal species and demonstrates that the IOF_6^- anion does not undergo intramolecular ligand exchange (i.e., pseudorotation) in solution, in contrast with the related TeF_7^- anion (6,7) and IF_7 molecule (see above). This is not surprising because any plausible intermediate in the pseudorotation process for IOF_6^- would require the doubly bonded oxygen ligand to move into an equatorial position. The greater space requirement of the oxygen double bond domain, compared with that of a fluorine single bond domain, would render the placement of the oxygen ligand in the more sterically crowded equatorial position energetically unfavorable, thereby creating a high activation barrier for the process. Although the X-ray crystal structure reveals that, in the solid state, the equatorial fluorine ligands of the IOF_6^- anion are unevenly puckered, only a single resonance is observed for these ligands in the ^{19}F NMR spectrum of the solution. Clearly, the puckering, which is frozen out in the solid state, becomes a dynamic process in solution which is fast on the NMR time scale.

Vibrational Spectra. The infrared and Raman spectra of solid $N(CH_3)_4^+IOF_6^-$ and the Raman spectra of its CH_3CN solution were recorded and are shown in Figure 9. A comparison of the observed and calculated (see below) frequencies of IOF_6^- with those of the closely related pentagonal IF_7 molecule (see above) and XeF_5^- anion (16), together with their approximate mode descriptions, are given in Table V. After subtraction of the well known (8,61) bands of the $N(CH_3)_4^+$ cation, the remaining bands, which are due to IOF_6^-, can be readily assigned based on the data given in Table V. Since the vibrational spectra of IOF_6^- in solid $N(CH_3)_4^+IOF_6^-$ do not appear to be noticeably affected by the slight equatorial puckering, they were assigned (see Table V) in point group C_{5v} which is the lowest energy structure of the free anion (see below).
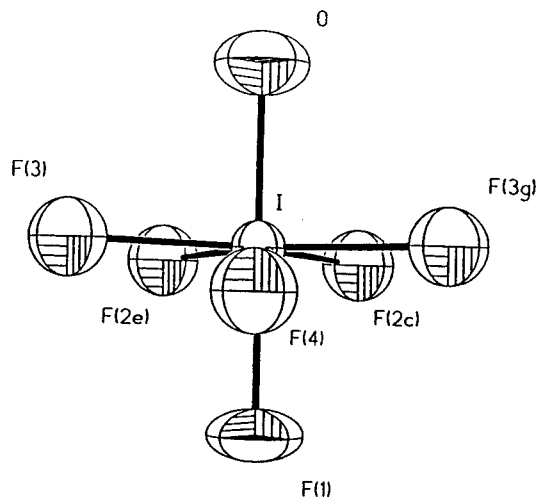
Figure 7. The structure of the IOF_6^- anion showing the puckering pattern of the equatorial fluorine ligands.
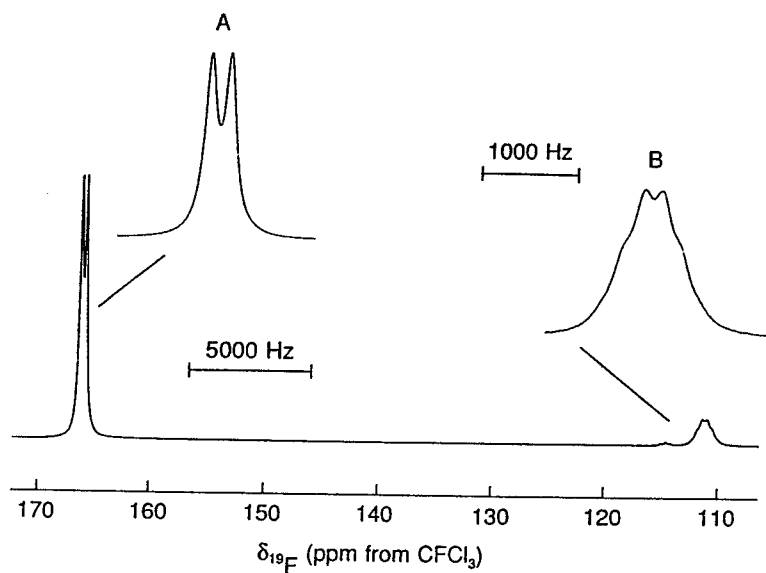

Figure 8. The ^{19}F NMR spectrum (470.599 MHz) of a saturated solution of $N(CH_3)_4^+IOF_6^-$ in CH_3CN at -40 °C. (A) F_{eq} environment of ; (B) F_{ax} environment of IOF_6^-.
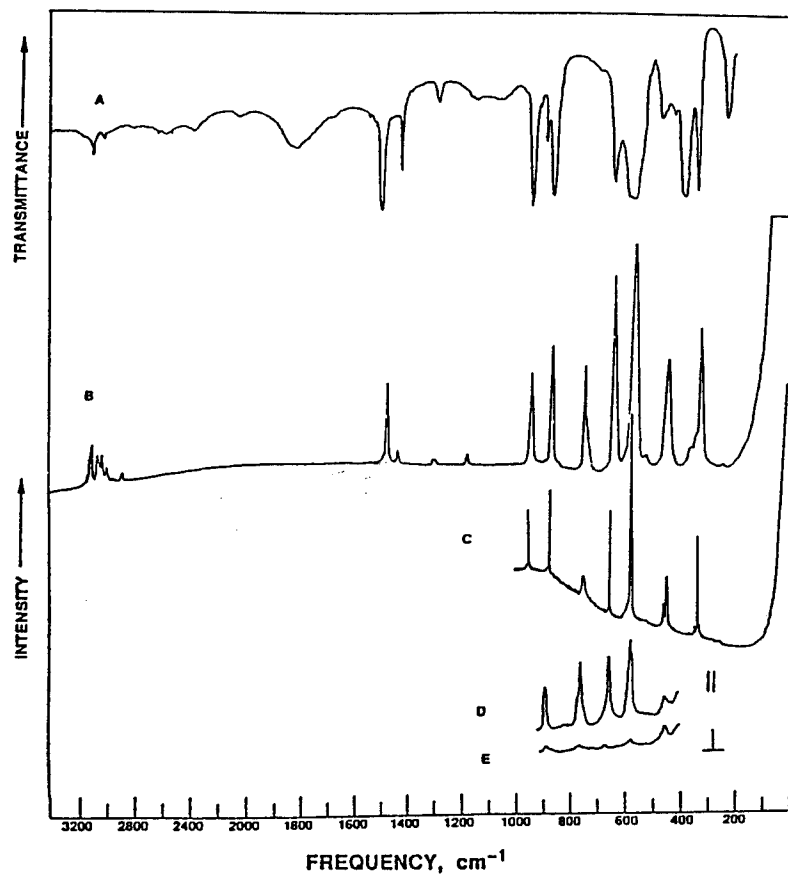
Figure 9. Vibrational spectra of $N(CH_3)_4^+IOF_6^-$. Trace A, infrared spectrum of the solid as an AgBr disk; traces B and C, Raman spectra of the solid at 25 and -146 °C; traces D and E, Raman spectra of the CH_3CN solution with parallel and perpendicular polarization, respectively.

Table V. Comparison of Observed and Calculated Frequencies of IOF_6^-, IF_7 and XeF_5^-, Together with Their Approximate Mode Descriptions

IOF_6^- (C_{5v})					IF_7 (D_{5h})[a]					XeF_5^- (D_{5h})				
assign-ment	approximate mode description	obsd freq, cm⁻¹ int (IR,Ra)	calcd freq, cm⁻¹ ECP[a]	LDF	assign-ment	approximate mode description	obsd freq, cm⁻¹, int (IR,Ra)	calcd freq, cm⁻¹ ECP[c]	LDF	assign-ment	approximate mode description	obsd freq, cm⁻¹, int (IR,Ra)[f]	calcd freq, cm⁻¹ ECP[d]	LDF
A_1 ν_1	ν I=O	873 (vs,53p)	860[b]	870	$\nu_3(A_2'')$	ν as IF_{2ax}	746 (s,–)	753	710	–				
ν_2	νIF_{ax}	649 (s,88p)	625	599	$\nu_1(A_1')$	ν sym IF_{2ax}	676 (–,20p)	673	630	–				
ν_3	ν sym IF_5	584 (vs,100p)	566	537	$\nu_2(A_1')$	ν sym IF_5	635 (–,100p)	644	598	$\nu_1(A_1')$	ν sym XeF_5	502 (–,100)	498	467
ν_4	δ umbrella IF_5	359 (s,4)	371	314	$\nu_4(A_2'')$	δ umbrella IF_5	365 (s,–)	368	304	$\nu_2(A_2'')$	δ umbrella XeF_5	290 (m,sh,–)	301	270
E_1 ν_5	ν as IF_5	585 (vs,vs)	583	568	$\nu_5(E_1')$	ν as IF_5	670 (vs,–)	681	647	$\nu_3(E_1')$	ν as XeF_5	450 (vs,–)	449	502
ν_6	δ as IF_5 in plane	405 (vs,–)	415	365	$\nu_6(E_1')$	δ as IF_5 in plane	425 (vs,–)	441	377	$\nu_4(E_1')$	δ as XeF_5 in plane	274 (s,–)	273	248
ν_7	δ rock O=I-F_{ax}	341 (–,62)	340	292	$\nu_8(E_1'')$	δ rock IF_{2ax}	319 (–,6)	320	259					
ν_8	δ sciss O=I-F_{ax}	260 (s,2)	273	233	$\nu_7(E_1')$	δ sciss IF_{2ax}	257 (w,–)	265	213					
E_2 ν_9	δ sciss IF_5 in plane	530 (–,4)	530	486	$\nu_9(E_2')$	mixture of δ sciss in-plane and ν as IF_5	596 (–,2)	605	561	$\nu_5(E_2')$	ν as XeF_5	423 (–,16)	420	413
ν_{10}	ν as IF_5	457 (–,49)	446	421	$\nu_{10}(E_2')$		510 (–,17)	515	467	$\nu_6(E_2')$	δ sciss XeF_5 in-plane	377 (–,23)	373	375
ν_{11}	δ pucker IF_5	n. obsd	141	111	$\nu_{11}(E_2'')$	δ pucker IF_5	[68]	59	50i	$\nu_7(E_2'')$	δ pucker XeF_5	n. obsd	105	79

[a]Frequency values were scaled by an empirical factor of 0.9038. [b]Unscaled frequency value; scaled frequency value is 789 cm⁻¹. [c]Frequency values were scaled by an empirical factor of 0.932.
[d]Frequency values were scaled by an empirical factor of 0.8618. [e]Data from ref. 8. [f]Data from ref. 49.

Ab Initio Calculations and Normal Coordinate Analyses. The electronic structure of IOF_6^- was calculated at the ab initio level by using both local density functional (LDF) theory and molecular orbital theory with an effective core potential (ECP) for the core electrons of iodine. Both types of calculations resulted in minimum energy structures of C_{5v} symmetry with the ECP calculations duplicating the experimentally observed geometry (see Table VI) and vibrational frequencies (see Table V) much better than the LDF calculations. In view of the superiority of the ECP calculations, we have also recalculated the structure of the closely related XeF_5^- anion, for which previously (16) only LDF values had been available. As can be seen from Tables V and VI, the ECP calculations are in excellent agreement with the observed values, after scaling of the calculated frequencies by empirical factors to maximize their fit with the experimental data, and therefore, are invaluable for the correct assignments of the vibrational spectra. For XeF_5^-, for example, they clearly indicate that the previous assignments (16) for $\nu_2(A_2") = 274$ cm^{-1} and $\nu_4(E_1') = 290$ cm^{-1} should be reversed. In view of the closeness of these two frequencies, the reversal of their assignments has very little or no impact on the conclusions previously reached (16) for XeF_5^-.

A normal coordinate analysis was carried out for IOF_6^-, and the most important internal force constants are compiled in Table VII and compared to those of IF_7 and XeF_5^-. As can be seen, the $X-F_{ax}$ bonds are considerably stronger than the $X-F_{eq}$ ones for a given compound, as expected from the bonding scheme proposed below. Furthermore, the stretching force constants decrease significantly on going from IF_7 to IOF_6^- and XeF_5^-, as expected from an increasing ionicity of the X-F bonds caused by the formal negative charge in the anions and the reduction in the formal oxidation state of the central atom from +VII in IF_7 and IOF_6^- to +IV in XeF_5^-. The large increase in the value of $f_{rr'}$, the coupling to opposite bonds, from IOF_6^- to XeF_5^- is analogous to those previously observed (62) for going from either *trans*-$IO_2F_4^-$ ($f_{rr'} = 0.27$ mdyn/Å) to IOF_4^- ($f_{rr'} = 0.45$ mdyn/Å) and IF_4^- ($f_{rr'} = 0.47$ mdyn/Å) or IOF_5 ($f_{rr'} = 0.18$ mdyn/Å) to IF_5 ($f_{rr'} = 0.38$ mdyn/Å) and, hence, appears to be associated with the introduction of a sterically active, free valence electron pair into the ligand sphere around the central atom.

The in-plane deformation constants, f_α, are a measure for the strength of the mutual repulsion of the equatorial ligands and hence, for the degree of congestion in this plane which, in turn, is responsible for the puckering. As can be seen from Table VII, the value of f_α decreases markedly on going from IF_7 to IOF_6^- and XeF_5^-. In IF_7, the in-plane deformation constant, f_α, is about five times larger than the out-of-plane deformation constant, f_β, and accounts for the puckering of the equatorial plane in IF_7. On the other hand, in XeF_5^- the f_α value has become much smaller and approaches the range of values expected for the out-of-plane deformation constants, f_β. This is in good agreement with the x-ray crystal structure of $N(CH_3)_4^+XeF_5^-$ which showed (16) that XeF_5^- is planar and not puckered. Hence, it appears that the value of the in-plane deformation force constant, f_α, is a useful parameter for measuring the degree of congestion and the likely occurrence of puckering in the equatorial ligand plane.

Structure and Bonding in IOF_6^-. The structure and bonding of IOF_6^- can be rationalized by the same 6-center 10-electron bonding scheme outlined above for IF_7 (see Table IV). The only significant differences between IOF_6^- and IF_7 are that in IOF_6^- the congestion in the equatorial plane is lessened due to more ionic and, hence,

Table VI. Observed and Calculated Geometries of IOF_6^- and the Closely Related IF_7 and XeF_5^-

IOF_6^-	exp[a]	calcd[a] ECP	calcd[a] LDF	IF_7	exp[b]	calcd[a] ECP	calcd[a] LDF	XeF_5^-	exp[c]	calcd ECP	calcd LDF
r I–O(Å)	1.75-1.77	1.7255	1.791	r I–F_{ax}	1.781	1.7705	1.870	r Xe–F_{eq}	2.012	1.9924	2.077
r I–F_{ax}(Å)	1.82	1.8087	1.913	r I–F_{eq}	1.857	1.8333	1.918				
r I–F_{eq}(Å)	1.88	1.8819	1.969	∢F_{ax}–I–F_{eq}	90	90	90				
∢O–I–F_{ax}(deg)	94-96	95.76	96.0								

[a]Data from this study. [b]Data from ref. 4. [c]Data from ref. 49.

Table VII.   Internal Force Constants[a,b] (mdyn/Å) of
IF_7, IOF_6^- and XeF_5^-

	IF_7	IOF_6^-	XeF_5^-
f_R	5.005	3.897	—
f_r	3.947	2.938	2.062
f_{rr}	0.326	0.306	0.198
f_{rr}'	0.0265	0.0536	0.317
f_α	0.847	0.690	0.364
$f_{\alpha\alpha}$	-0.183	-0.147	-0.081
$f_{\alpha\alpha}'$	-0.240	-0.198	-0.102
f_β	0.163		

(a) The deformation constants have been normalized for the following bond distances: IF_7, r $I-F_{eq}$ = 1.857Å; IOF_6^-, r $I-F_{eq}$ = 1.877Å; XeF_5^-, r Xe–F = 2.0124Å. (b) f_{rr} and f_{rr}' denote coupling to adjacent and opposite bonds, respectively, and $f_{\alpha\alpha}$ and $f_{\alpha\alpha}'$ coupling to adjacent and opposite bond angles, respectively.

longer bonds and that in IOF_6^- the intramolecular, equatorial-axial ligand exchange is precluded.

The $TeOF_6^{2-}$ Anion.   The $[N(CH_3)_4^+]_2TeOF_6^{2-}$ salt was prepared from $N(CH_3)_4^+TeOF_5^-$ and excess $N(CH_3)_4^+F^-$ in CH_3CN solution. It could not be isolated in pure form and always contained some unreacted $N(CH_3)_4^+TeOF_5^-$ starting material as a byproduct. Due to its insolubility in CH_3CN, its characterization was limited to vibrational spectroscopy of the solid. These vibrational spectra were completely analogous to those of IOF_6^-, thereby confirming the close structural relationship of the two anions.

Conclusions

The present study shows that the preferred structures of heptacoordinated main-group fluorides and oxofluorides are pentagonal bipyramids. The structure, bonding, and fluxionality of these molecules is now well understood. The pentagonal bipyramidal arrangement cannot be explained by VSEPR-type arguments of repelling points on a sphere but is due to the spatial distribution of the valence orbitals on the central atom. The extensive ligand congestion in the equatorial plane, combined with the special requirements for five-fold symmetry, result in facile, dynamic puckering of the equatorial plane and high degrees of fluxionality. The novel XeF_5^-, IOF_6^-, and $TeOF_6^{2-}$ anions have been prepared and characterized and are the first known examples of pentagonal bipyramidal XF_5E_2 and XOF_6 species.

Acknowledgments

Literature Cited

(1) Gillespie, R.J. *Molecular Geometry*; Van Nostrand Reinhold Co.: London, 1972.

(2) Gillespie, R.J.; Hargittai, I. *The VSEPR Model of Molecular Geometry*; Allyn and Bacon, A Division of Simon & Schuster, Inc: Needham Heights, MA, 1991; p 58.

(3) Bradford-Thompson, H.; Bartell, L.S. *Inorg. Chem.* **1968**, *7*, 488.

(4) Adams, W.J.; Bradford-Thompson, H.; Bartell, L.S. *J. Chem. Phys.* **1970**, *53*, 4040.

(5) Selig, H.; Sarig, S.; Abramowitz, S. *Inorg. Chem.* **1974**, *13*, 1508.

(6) Christe, K.O.; Sanders, J.C.P.; Schrobilgen, G.J.; Wilson, W.W. *J. Chem. Soc., Chem. Commun.* **1991**, 837.

(7) Majhoub, A.R.; Seppelt, K. *J. Chem. Soc., Chem. Commun.* **1991**, 840.

(8) Christe, K.O.; Wilson, W.W.; Wilson R.D.; Bau, R.; Feng, J. *J. Am. Chem. Soc.* **1990**, *112*, 7619.

(9) Wilson, W.W.; Christe, K.O. *Inorg. Chem.* **1989**, *28*, 4172.

(10) Christe, K.O.; Wilson, W.W.; Chirakal, R.V.; Sanders, J.C.P.; Schrobilgen, G.J. *Inorg. Chem.* **1990**, *29*, 3506.

(11) Bougon, R.; Charpin, P.; Soriano, J. *C.R. Hebd. Seances Acad. Sci., Ser. C* **1971**, *272*, 565.

(12) Christe, K.O.; Wilson, W.W. *Inorg. Chem.* **1989**, *28*, 3275.

(13) Christe, K.O. *Inorg. Chem.* **1972**, *11*, 1215.

(14) Mahjoub, A.R.; Hoser, A.; Fuchs, J.; Seppelt, K. *Angew. Chem., Int. Ed. Engl.* **1989**, *28*, 1526.

(15) Mahjoub, A.R.; Seppelt, K. *Angew. Chem. Int. Ed. Engl.* **1991**, *30*, 323.

(16) Christe, K.O.; Curtis, E.C.; Dixon, D.A.; Mercier, H.P.; Sanders, J.C.P.; Schrobilgen, G.J. *J. Am. Chem. Soc.* **1991**, *113*, 3351.

(17) Ruff, O.; Keim, R. *Z. Anorg. Chem.* **1931**, *201*, 245.

(18) Burbank, R.D.; Bensey, Jr., F.N. *J. Chem. Phys.* **1957**, *27*, 981.

(19) Donohue, J. *J. Chem Phys.* **1959**, *30*, 1618.

(20) Burbank, R.D. *J. Chem Phys.* **1959**, *30*, 1619.

(21) Lohr, Jr., L.L.; Lipscomb, W.N. *J. Chem. Phys.* **1962**, *36*, 2225.

(22) Burbank, R.D. *Acta Crystallogr.* **1962**, *15*, 1207.

(23) Donohue, J. *Acta Crystallogr.* **1965**, *18*, 1018.

(24) Gutowski, H.S.; Hoffmann, C.J. *J. Chem. Phys.* **1951**, *19*, 1259.

(25) Muetterties, E.L.; Packer, K.J. *J. Am. Chem. Soc.* **1964**, *86*, 293.

(26) Alexakos, L.G.; Cornwell, C.D.; Pierce, St. B. *Proc. Chem. Soc. (London)* **1963**, 341.

(27) Bartlett, N.; Beaton, S.; Reeves, L.W.; Wells, E.J. *Can. J. Chem.* **1964**, *42*, 2531.

(28) Gillespie, R.J.; Quail, J.W. *Can. J. Chem.* **1964**, *42*, 2671.

(29) Kukolich, S.G. private communication, 1991.

(30) Kaiser, E.W.; Muenter, J.S.; Klemperer, W.; Falconer, W.E. *J. Chem. Phys.* **1970**, *53*, 53.

(31) Bradford-Thompson, H.; Bartell, L.S. *Trans. Am. Cryst. Soc.* **1966**, *2*, 190.

(32) La Villa, R.E.; Bauer, S.H. *J. Chem. Phys.* **1960**, *33*, 182.

(33) Lord, R.C.; Lynch, M.A.; Schumb, W.C.; Slowinski, E.J. *J. Am. Chem.* **1950**, *72*, 522.

(34) Nagarajan, G. *Curr. Sci. (India)* **1961**, *30*, 413; *Bull. Soc. Chim. Belges* **1962**, *71*, 82.

(35) Khanna, R.K. *J. Mol. Spectrosc.* **1962**, *8*, 134.

(36) Arighi, L.S. Ph.D. Thesis, University of Wisconsin, **1965**.

(37) Claassen, H.H.; Gasner, E.L.; Selig, H. *J. Chem. Phys.* **1968**, *49*, 1803.

(38) Ramaswamy, K.; Muthusubramanian, J. *Mol. Struct.* **1970**, *6*, 205.

(39) Wendling, E.; Mahmoudi, S. *Bull. Soc. Chim.* **1972**, 33.
(40) Eysel, H.H.; Seppelt, K. *J. Chem. Phys.* **1972**, *56*, 5081.
(41) Mohan, S. *Acta Cient Indica* **1978**, *1*, 31.
(42) Bernstein, L.S. Ph.D. Thesis, University of California, Berkeley, **1974**.
(43) Bartell, L.S.; Rothman, M.J.; Gavezzotti, A. *J. Chem. Phys.* **1982**, *76*, 4136.
(44) Jacob, E.J.; Bartell, L.S. *J. Chem. Phys.* **1970**, *53*, 2235.
(45) Weidlein, J.; Müller, U.; Dehnicke, K. In *Schwingungsspektroskopie*; Georg Thieme Verlag: Stuttgart, 1982; p 37.
(46) Christe, K.O.; Wilson, R.D. *Inorg. Chem.* **1975**, *14*, 694.
(47) Berry, R.S. *J. Chem. Phys.* **1960**, *32*, 933.
(48) Bartell, L.S. In *Physical Methods of Chemistry*; Weissberger, A.; Rossiter, B.A., Ed. Wiley Interscience: New York, 1972, Vol. I., Part IIID; p 125.
(49) Christe, K.O.; Dixon, D.A.; Mahjoub, A.R.; Mercier, H.P.A.; Sanders, J.C.P.; Seppelt, K.; Schrobilgen, G.J.; Wilson, W.W. to be published.
(50) Pimentel, G.C. *J. Chem. Phys.* **1951**, *10*, 446.
(51) Hach, R.J.; Rundle, R.E. *J. Am. Chem. Soc.* **1951**, *73*, 4321.
(52) Rundle, R.E. *J. Am. Chem. Soc.* **1963**, *85*, 112.
(53) Mahjoub, A.R.; Drews, T.; Seppelt, K. *Angew. Chem., Int. Ed. Engl.* **1992**, *31*, 1036.
(54) Hyde, B.G.; Anderson, S. *Inorganic Crystal Structures*; John Wiley & Sons: New York, 1989; p 7.
(55) Bartell, L.S.; Clippard, F.B. Jacob, J.E. *Inorg. Chem.* **1976**, *15*, 3009.
(56) Smart, L.E. *J. Chem. Soc., Chem. Commun.* **1977**, 519.
(57) Selte, K.; Kjekshus, A. *Acta Chem. Scand.* **1970**, *24*, 1912.
(58) Kálmán, K.; Cruickshank, D.W.J. *Acta Crystallogr.* **1970** *B26*, 1782.
(59) Feikeman, Y.D. *Acta Crystallogr.* **1961**, *14*, 315.
(60) Feikeman, Y.D. *Acta Crystallogr.* **1966**, *20*, 765.
(61) Christe, K.O.; Wilson, W.W.; Bau, R.; Bunte, S.W. *J. Am. Chem. Soc.* **1992**, *114*, 3411, and references cited therein.
(62) Christe, K.O.; Wilson, R.D.; Schack, C.J. *Inorg. Chem.* **1981**, *20*, 2104.

Appendix V

Reprinted from the Journal of the American Chemical Society, 1994, *116*.   5671
Copyright © 1994 by the American Chemical Society and reprinted by permission of the copyright owner.

Electrophilic Fluorination of Methane with "F+" Equivalent N2F+ and NF4+ Salts[1]

George A. Olah,[*,†] **Nikolai Hartz,**[†] **Golam Rasul,**[†] **Qi Wang,**[†] **G. K. Surya Prakash,**[†]
Joseph Casanova,[†] **and Karl O. Christe**[‡]

*Contribution from the Loker Hydrocarbon Research Institute and Department of Chemistry,
University of Southern California, University Park, Los Angeles, California 90089-1661, and
Rocketdyne, A Division of Rockwell International, Canoga Park, California 91304*

Received March 2, 1994[*]

Abstract: The electrophilic fluorination of methane with "F+" equivalent N_2F^+ and NF_4^+ salts was studied by experiment and theory. Reaction of excess methane with $NF_4^+SbF_6^-$ in pyridinium polyhydrogen fluoride solution gave exclusively methyl fluoride. The reaction of $N_2F^+AsF_6^-$ and $NF_4^+AsF_6^-$ with methane (with 1:2 to 4:1 mole ratio, respectively) in HF solution gave methyl fluoride in 63–92% relative yield with 26–6% methylene fluoride and 2–11% fluoroform with no carbon tetrafluoride formed. In a theoretical study of the $CH_4 + F^+$ model reaction stationary points on the potential energy surface were calculated at the QCISD/6-31G*//QCISD/6-31G* + ZPE level. The mechanistic consequences of these reactions are discussed.

Introduction

The concept of electrophilic fluorination of organic compounds was pioneered by Barton and Hesse in their work with CF_3OF.[2] Adcock and Lagow developed the use of highly diluted fluorine in the polyfluorination of hydrocarbons in a radical reaction.[3] The electrophilic fluorination of aromatics, such as benzene and toluene, was studied with highly diluted F_2 by Cacace and Wolf.[4] Selective electrophilic fluorination of saturated hydrocarbons with F_2 leading to monofluorinated product was demonstrated by Rozen[5] using the $CHCl_3/CFCl_3$ solvent system. They proposed a mechanism involving electrophilic insertion of fluorine into the C–H bond of the alkane in a typical electrophilic fashion with $CHCl_3$ acting as the acceptor of the fluoride ion.

$$R_3CH + F_2 \xrightarrow{CHCl_3, CFCl_3} \left[R_3C \cdots \overset{H}{\underset{F}{\cdots}} \quad F \cdots HCCl_3 \right] \longrightarrow R_3CF + HF$$
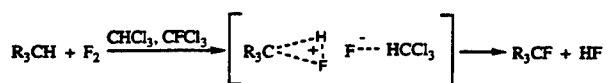
The electrophilic fluorination of methane, the parent alkane, was, however, so far not investigated. Herein we report direct electrophilic fluorination of methane using $N_2F^+AsF_6^-$ and $NF_4^+AsF_6^-$ (SbF_6^-) salts, as well as related theoretical studies and discuss the results and their mechanistic consequences.

Results and Discussion

In order to study the electrophilic fluorination of methane and to avoid any possible free radical reactions we have chosen the ionic salts $N_2F^+AsF_6^-$ and $NF_4^+AsF_6^-$ (SbF_6^-) as fluorinating

Table 1. Fluorination of Alkanes

Mole Ratio of Reagents			% Conversion[*]	% Product				
CH₄	+	N₂F⁺AsF₆⁻ $\xrightarrow[\text{4 hrs., r.t.}]{\text{HF}}$		CH₃F	+	CH₂F₂	+	CHF₃
1	:	2	87	67	:	24	:	9
1	:	1	81	73	:	22	:	5
2	:	1	64	84	:	12	:	4
4	:	1	68	89	:	8	:	3
CH₄	+	NF₄⁺AsF₆⁻ $\xrightarrow[\text{4 hrs., r.t.}]{\text{HF}}$		CH₃F	+	CH₂F₂	+	CHF₃
1	:	2	60	63	:	26	:	11
1	:	1	70	76	:	18	:	6
2	:	1	24	85	:	15	:	0.5
4	:	1	25	92	:	6	:	2
CH₄	+	NF₄⁺SbF₆⁻ $\xrightarrow[\text{24 hrs., r.t.,30 mL}]{\text{Pyridine-HF}}$		CH₃F	+	CH₂F₂	+	CHF₃
16	:	1	100	:	0	:	0	

based on methane consumption.

agents. Olah, Christe, et al. investigated[6] previously the fluorination of aromatics with N_2F^+. It is unlikely that even in this system "F+" can be involved as the *de facto* electrophilic species. An electrophilic mechanism was envisioned with concomitant elimination of nitrogen. N_2F^+ was found to be highly oxidizing in nature resulting also in significant decomposition products. Shack and Christe[7] have studied the reaction of $NF_4^+SbF_6^-$ with toluene and other aromatics. The nature of the ring fluorination products and the lack of side chain substitution seem to imply direct electrophilic fluorination. We have now investigated the fluorination of methane with N_2F^+ and NF_4^+ salts in HF and pyridinium poly(hydrogen fluoride) (PPHF) solvents.

Whereas free "F+" is unknown in the condensed state, electrophilic fluorination of hydrocarbons is of substantial interest. Barton's pioneering work[2] on low-temperature fluorination with CF_3OF opened up intensive investigations in the field. Others

† University of Southern California.
‡ Rocketdyne.
● Abstract published in *Advance ACS Abstracts*, June 1, 1994.
(1) Electrophilic Reactions at Single Bonds. 27. For part 26 see: Olah, G. A.; Ramaiah, P. *J. Org. Chem.* **1993**, *58*, 4639.
(2) (a) Barton, D. H. R.; Godhino, L. S.; Hesse, R. H.; Pechet, M. M. *J. Chem. Soc., Chem. Commun.* **1968**, 804. (b) Barton, D. H. R.; Danks, L. J.; Ganguly, A. K.; Hesse, R. H.; Tarzia, G.; Pechet, M. M. *J. Chem. Soc., Chem. Commun.* **1969**, 227. (c) Hesse, R. H. *Isr. J. Chem.* **1978**, *17*, 60.
(3) Adcock, J. L.; Lagow, R. J. *J. Am. Chem. Soc.* **1974**, *96*, 7588.
(4) Cacace, F.; Wolf, A. P. *J. Am. Chem. Soc.* **1978**, *100*, 3639.
(5) Rozen, S.; Gal, C. *J. Org Chem.* **1987**, *52*, 2769, **1988**, *53*, 2803. Rozen, S. In *Synthetic Fluorine Chemistry*; Olah, G. A., Chamber, R. D., Prakash, G. K. S., Eds.; Wiley: New York, 1992, p 143.

(6) Olah, G. A.; Laali, K.; Farnia, M.; Shih, J.; Sing, B. P.; Shack, J. C.; Christie, K. O. *J. Org. Chem.* **1985**, *50*, 1338.
(7) Shack, J. C.; Christie, K. O. *J. Fluorine Chem.* **1981**, *18*, 363.

0002-7863/94/1516-5671$04.50/0   © 1994 American Chemical Society

Table 2. Calculated Energies (-au), ZPE (kcal/mol), and Relative Energies (kcal/mol) of CH$_4$F$^+$

	MP2(FU)6-31G*// MP2(FU)/6-31G*	ZPE[a]	MP4(SDTQ)/6-31G*// MP2(FU)/6-31G*	rel[b]	QCISD/6-31G*// QCISD/6-31G*	rel[c]
1 (C_s)	139.578 26	31.4	139.598 46	0.0	139.594 00	0.0
2 (C_s)	139.522 15	25.5	139.546 54	26.7	139.540 46	27.7
3 (C_s)	139.577 51	31.1[d]	139.584 44	8.5	139.593 32	0.1
4 (C_{4v})	139.503 44	26.9[e]	139.522 96	42.9	139.516 25	44.3
5 (C_{3v})	139.423 88	26.9[e]	139.444 04	92.4	139.436 87	94.1
CH$_3$F (C_{3v})	139.342 66	25.5	139.360 68		139.355 18	
CH$_4$ (T_d)	40.195 07	29.1	40.354 79		40.353 37	
F$^+$	98.730 38		98.750 66		98.769 92	

[a] At MP2(FU)/6-31G*//MP2(FU)/6-31G*. [b] At MP4(SDTQ)/6-31G*//MP2(FU)/6-31G*+ZPE. [c] At QCISD/6-31G*//QCISD/6-31G*+ZPE.
[d] NIMAG=1. [e] NIMAG=2.

used CH$_3$COOF, whereas Rozen[5] pioneered HOF and other reagents.

The electrophilic fluorination of methane with N$_2$F$^+$AsF$_6^-$ and NF$_4^+$AsF$_6^-$ in HF gave high yields of methyl fluoride. With a 2:1 CH$_4$ to N$_2$F$^+$ (or NF$_4^+$) mole ratio, CH$_3$F is formed in 67 and 63% relative yield, repectively, with 24–26% CH$_2$F$_2$ and 9–11% CHF$_3$ (no CF$_4$ was observed). When using a 1:1 CH$_4$ to N$_2$F$^+$ (or NF$_4^+$) ratio, CH$_3$F relative yield was around 73–76%, and with a 4:1 mol value 89–92% of CH$_3$F was obtained with only 6–8% CH$_2$F$_2$ and 2–3% CHF$_3$. When a large excess (16:1) of methane was used with NF$_4^+$SbF$_6^-$ in pyridinium polyhydrogen fluoride only methyl fluoride was observed. To account for the data, an electrophilic insertion of N$_2$F$^+$ and NF$_4^+$, respectively, into the C–H bond of methane can be envisioned giving methyl fluoride. One of the referees suggested that as the reaction solutions also contain strong superacids, protonation of methane can also occur to give CH$_5^+$ which may affect the reaction. However, formation of CH$_5^+$ we believe has no consequence on the experimentally observed direct fluorination reaction. Even if a limited CH$_4$ + H$^+$ $\rightleftharpoons$ CH$_5^+$ equilibrium exists due to some superacid present in the system, there must be at any given time a large excess of methane present to react with the strong electrophilic fluorinating reagents.

Since electrophilic fluorination of methane with insertion of FN$_2^+$ and NF$_4^+$ is difficult to study by theory we have investigated simplified model, singlet F$^+$ cation insertion into methane and explored the CH$_4$F$^+$ potential energy surface. The related protonation of methyl fluoride was previously investigated experimentally by McMahon and Kebarle in the gas phase.[8] On the basis of the variation of the proton affinities of methyl halides as a function of their valence ionization potential, the authors concluded that 3c–2e bonding occurs upon protonation of a C–H bond in CH$_3$F. This was based on the fact that the proton affinity of CH$_3$F does not correlate with its valence ionization potential. This behavior suggested that the CH$_4$F$^+$ ions may be structurally different from other CH$_3$XH$^+$ ions (hydrido halonium ions) and may possess the 3c–2e bond.[8]

Optimizations on CH$_4$F$^+$ isomers were carried out at the MP2-(FU)/6-31G* and QCISD/6-31G* levels. At QCISD/6-31G*//QCISD/6-31G*+ZPE structure 1 is 27.7 kcal/mol more stable than structue 2 (Table 2). Structure 1 can be considered as a complex between the CH$_3^+$ ion and the HF molecule predominantly having hydridofluoronium ion character. Structure 2 is a loosely held complex between CH$_2$F$^+$ and H$_2$ (Figure 1). The structure 1 was also calculated previously at the Hartree–Fock level, and results similar to those reported here were observed.[9] Structure 3 is the transition structure of rotation of 1 around the C–F bond and is only 0.1 kcal/mol less stable than structure 1, indicating the facile rotation around the C–F bond. The C_{4v} symmetrical structure 4 and the C_{3v} symmetrical structure 5 are
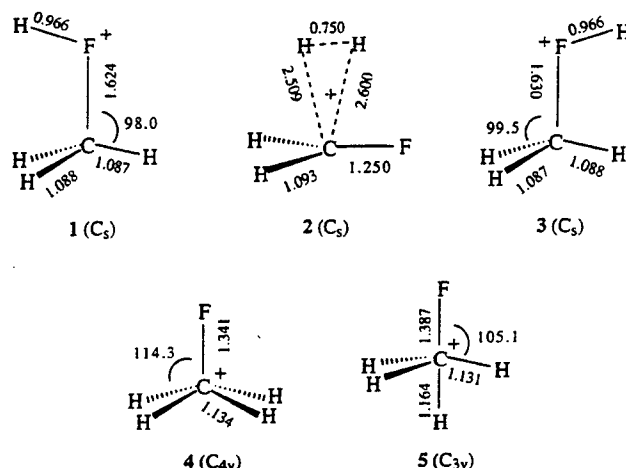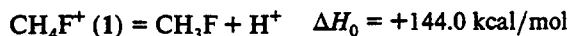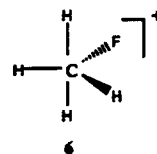
(8) McMahon, T. B.; Kebarle, P. *Can. J. Chem.* **1985**, *63*, 3160.
(9) Alcami, M.; Mo, O.; Yanez, M.; Abboud, J. L.; Elguero, J. *J. Chem. Phys. Lett.* **1990**, *172*, 471. Hess, B., Jr.; Zahradnik, R. *J. Am. Chem. Soc.* **1990**, *112*, 5731. Ikuta, S. *J. Mol. Struct. (Theochem)* **1987**, *149*, 297. Smith, S. F.; Chandrasekhar, J.; Jorjensen, W. L. *J. Phys. Chem.* **1982**, *86*, 3308. Jorjensen, W. L.; Cournoyer, M. E. *J. Am. Chem. Soc.* **1978**, *110*, 5278.

Figure 1. QCISD/6-31G* optimized structures of CH$_4$F$^+$. Bond lengths are in angstroms and angles are in degrees.

not minima as each of them contains two imaginary frequencies in their calculated vibrational spectrum. The dissociation of 1 into CH$_3$F and H$^+$ is endothermic by 144.0 kcal/mol (at QCISD/6-31G*//QCISD/6-31G*+ZPE). However, formation of 1 from CH$_4$ and F$^+$ is exothermic by as much as 293.1 kcal/mol at the same level. Thus the overall reaction to form CH$_3$F and H$^+$ from "F$^+$" and CH$_4$ is exothermic by 149.1 kcal/mol.

$$CH_4F^+ \ (1) = CH_3F + H^+ \quad \Delta H_0 = +144.0 \ \text{kcal/mol}$$

$$CH_4 + F^+ = CH_4F^+ \ (1) \quad \Delta H_0 = -293.1 \ \text{kcal/mol}$$

The electrophilic fluorination of methane with N$_2$F$^+$ and NF$_4^+$ in HF solution gives methyl fluoride in 89–92% relative yield with high selectivity. Theoretical studies of the reaction of methane with "F$^+$" are in accord with insertion of "F$^+$" into the C–H bond leading to the intermediate CF$_3$FH$^+$, 1. However, attempts to locate the transition state of the reaction CH$_4$ + "F$^+$" leading to formation of 3c–2e structure 6 (involving initial "F$^+$" insertions directly into the C–H bond) failed. This is due to the extremely high reactivity of electrophilic "F$^+$" reacting with methane practically without any activation energy barrier. Structure 1 was found to be the global minimum on the CH$_4$F$^+$ potential energy surface.

6

We have also carried out a similar experimental study of the fluorination of ethane with NF$_4^+$AsF$_6^-$ in HF solution. Whereas the results are more complex, CH$_3$F and C$_2$H$_5$F were formed in a 1.8:1 ratio. Thus NF$_4^+$ attack takes place in this case in not only the C–H bond of ethane but also the C–C bond. A more

detailed study of the electrophilic fluorination of ethane and higher alkanes will be reported elsewhere.

Experimental Section

Fluorinating agents ($N_2F^+AsF_6^-$, $NF_4^+AsF_6^-$, and $NF_4^+SbF_6^-$) and pyridinium poly(hydrogen fluoride), PPHF, were prepared according to published procedures.[10] All gaseous chemicals used were purchased either from Matheson Gas Products or PCR Inc. NMR spectra were obtained on a Varian Associate Model VXR-200. GC analyses were carried out on a Varian 3400 gas chromatograph on a DB-1 column. MS analyses were performed on a Hewlett Packard 5971 mass spectrometer (EI). Identity and relative response factors of products were confirmed by comparison with authentic CH_3F, CH_2F_2, and CHF_3 samples. The error margin in the data reported in Table 1 is ±2%. All the fluorinating agents as well as HF and PPHF are exceedingly corrosive and toxic. Therefore, the experiments should be performed in a well-ventilated hood with great caution and precautions are needed for such work.

Typical Fluorination Procedure. (a) Fluorination of Methane with $NF_4^+SbF_6^-$. Methane (500 psi, 150 mmol) was charged to a stirred solution of 3.05 g of $NF_4^+SbF_6^-$ (9.3 mmol) dissolved in 30 mL of pyridinium poly(hydrogen fluoride) (30:70) in a 100-mL monel autoclave.

After the reaction mixture was kept at room temperature for 24 h, the gaseous product was passed through a KF trap and collected at −95 °C. GC and MS analysis showed only CH_3F. The identity of CH_3F was further confirmed by its ^1H and ^{19}F NMR spectrum by dissolving the gas in $CDCl_3$.

(b) Fluorination of Methane with $N_2F^+AsF_6^-$ and $NF_4^+AsF_6^-$. The appropiate stoichiometric amounts of fluorinating agents ($N_2F^+AsF_6^-$ and $NF_4^+AsF_6^-$) were placed in 10-mL stainless steel Hoke cylinders under dry nitrogen. Anhydrous HF and methane gas were introduced at −196 °C using a stainless steel Teflon vacuum system (for the ratios, see Table 1). After the samples were kept at room temperature for 4 h, the gaseous products were passed through a KF trap, collected at −196 °C (using liquid nitrogen), and analyzed by GC and MS .

Calculations. All calculations were carried out with the Spartan[11] and Gaussian[12] packages of programs.

(10) (a) Christe, K. O.; Guertin, J. P.; Pavlath, A. E. *Inorg. Nucl. Chem. Lett.* **1966**, *2*, 83. (b) Christe, K. O.; Schack, C. J.; Wilson, R. D. *Inorg. Chem.* **1976**, *15*, 1275. (c) Mason, J.; Christe, K. O. *Inorg. Chem.* **1983**, *22*, 1849. (d) Olah, G. A.; Welch, J. T.; Vankar, Y. D.; Nojima, M.; Kerekes, I.; Olah, J. A. *J. Org. Chem.* **1979**, *44*, 3872.

(11) Spartan, Version 2.0.0; Wavefunction Inc.: Irvine, CA, 1991.
(12) Gaussian 92, Revision B, Frisch, M. J.; Trucks, G. W.; Head-Gordon, M.; Gill, P. M. W.; Wong, M. W.; Foresman, J. B.; Johnson, B. G.; Schlegel, H. B.; Robb, M. A.; Replogle, E. S.; Gomperts, R.; Andres, J. L.; Raghavachari, K.; Binkley, J. S.; Gonzalez, C.; Martin, R. L.; Fox, D. J.; Defrees, D. J.; Baker, J.; Steward, J. J. P.; Pople, J. A.; GAUSSIAN, Inc.: Pittsburgh, PA, 1992.

Vibrational Spectra and Mutual Ligand Interactions in the Hydrogen-Substituted Main Group Hexafluorides HPF$_5^-$ and HSF$_5$[†]

Karl O. Christe,[*,1] David A. Dixon,[2] and William W. Wilson[1]

Contribution from Rocketdyne, A Division of Rockwell International Corporation, Canoga Park, California 91309, and the DuPont Corporation, Central Research and Development, Experimental Station, Wilmington, Delaware 19880-0328

Abstract: The new HPF$_5^-$ salt, N(CH$_3$)$_4$HPF$_5$, was prepared and the infrared and Raman spectra of N(CH$_3$)$_4$HPF$_5$ and CsHPF$_5$ were recorded. The spectra were assigned with the help of ab initio molecular orbital and local density functional calculations, and a normal coordinate analysis was carried out. For comparison, the unknown isoelectronic molecule HSF$_5$ was also calculated by the same methods. The internal stretching force constants of HPF$_5^-$ are compared to those of closely related phosphorus and sulfur fluorides and hydrides and confirm the existence of a *cis*-effect in these hydrogen-substituted main group hexafluorides. The observed substitution effects are explained in terms of a hypervalent bonding scheme and result in a preferential weakening of the four equatorial *cis*-bonds.

Introduction

During recent studies of the novel PF$_4^-$ anion[3] and its reaction chemistry,[4] the HPF$_5^-$ anion was observed as one of the reaction products. Although this anion is known and has been characterized by ^{1}H, ^{19}F, and ^{31}P NMR spectroscopy,[5-10] the reports on its vibrational spectra were limited to an incomplete listing of some of the infrared bands without assignments.[8] Since the HPF$_5^-$ anion is the only known main group element species containing five fluorine ligands and one hydrogen ligand, it offered a unique opportunity to examine experimentally the mutual ligand interaction effects exercised by the hydrogen ligand on fluorines in *cis*- and *trans*-positions.

Mutual ligand interaction effects in monosubstituted main group element hexafluorides have been the subject of several previous studies.[11-13] For example, Armstrong and co-workers published in 1975 the results from CNDO/MO calculations on monosubstituted tellurium hexafluorides, TeF$_5$X. They concluded that generally the four fluorine ligands in *cis*-positions to X become more labile than the one in the *trans*-position, except for HTeF$_5$ where the hydrogen substitution produced a weaker *trans* Te–F bond and, surprisingly, exhibited the weakest ligand interaction within the H, OH, NH$_2$, Cl, CH$_3$, Br, SH, PH$_2$, and SiH$_3$ series of ligands.[11] In 1976, Shustorovich and Buslaev proposed the terms *trans*- or *cis*-effect, depending on which bond is more strongly affected by the substitution.[12] On the basis of qualitative MO arguments, they predicted for MF$_5$X compounds, where the

main group central atom M is in its highest oxidation state and X is a strong σ donor such as H or CH$_3$, a *cis*-effect consisting of a weakening of the *cis* M–F bonds and a strengthening of the *trans* M–F bond. They also used the difference Δ between equatorial and axial M–F bond lengths for distinguishing a *cis*-effect from a *trans*-effect. If Δ is positive, the *cis*-effect dominates, while for a negative Δ the *trans*-effect prevails. In 1987, Oberhammer and co-workers determined the structure of SF$_5$Br by a combined electron diffraction–microwave study and established the presence of a small *cis*-effect. They also carried out ab initio calculations with various basis sets (3-21G, 3-21G*, and 6-31G*) for SF$_6$ and HSF$_5$ to confirm the *cis*-effect of a donating substituent in these monosubstituted sulfur hexafluorides but for HSF$_5$ reported only the calculated bond lengths and angles.[13]

Experimental Section

Apparatus and Materials. Volatile materials were handled in a passivated (with ClF$_3$) stainless steel–Teflon FEP vacuum line.[14] Nonvolatile materials were handled in the dry nitrogen atmosphere of a glovebox. The infrared, Raman, and NMR spectrometers have previously been described.[3] Literature methods were used for the synthesis of N(CH$_3$)$_4$F[15] and the drying of HF,[16] CH$_3$CN,[17] and CsF.[18] The PF$_3$ (Ozark Mahoning) was purified by fractional condensation prior to its use.

Syntheses of N(CH$_3$)$_4$HPF$_5$ and CsHPF$_5$. Typically, 2 mmol of MF (M = N(CH$_3$)$_4$ or Cs) was loaded in the drybox into a prepassivated 0.75 in. o.d. Teflon FEP ampule that was closed by a stainless steel valve. On the vacuum line, about 4 mL of liquid HF was added and the mixture was agitated at room temperature for 1 h. The excess of unreacted HF was pumped off at room temperature leaving behind MHF$_2$·nHF (*n* = 1–2). Dry CH$_3$CN (about 3 mL of liquid) and PF$_3$ (about 6 mmol) were added to the ampule at –196 °C, and the mixture was agitated at room temperature for 1 h which resulted in the precipitation of a white solid. All volatile material was pumped off at room temperature leaving behind MHPF$_5$ in quantitative yield (found weights were within 1 mg of those

† Dedicated to Prof. Wolfgang Sawodny on the occasion of his 60th birthday.
● Abstract published in *Advance ACS Abstracts,* June 15, 1994.
(1) Rocketdyne.
(2) DuPont, Contribution No. 6825.
(3) Christe, K. O.; Dixon, D. A.; Mercier, H. P. A.; Sanders, J. C. P.; Schrobilgen, G. J.; Wilson, W. W. *J. Am. Chem. Soc.,* in press.
(4) Christe, K. O.; Dixon, D. A.; Sanders, J. C. P.; Schrobilgen, G. J.; Wilson, W. W., to be submitted for publication.
(5) Nixon, J. F.; Swain, J. R. *Inorg. Nucl. Chem. Lett.* 1969, *5,* 295.
(6) Nixon, J. F.; Swain, J. R. *J. Chem. Soc. A* 1970, 2075.
(7) McFarlane, W.; Nixon, J. F.; Swain, J. R. *Mol. Phys.* 1970, *19,* 141.
(8) Cowley, A. H.; Wisian, P. J.; Sanchez, M. *Inorg. Chem.* 1977, *16,* 1451.
(9) Minkwitz, R.; Liedtke, A. *Z. Naturforsch. B* 1989, *44B,* 679.
(10) Lindemann, D.; Riesel, L. *Z. Anorg. Allg. Chem.* 1992, *615,* 66. Riesel, L.; Kant, M. *Z. Chem.* 1984, *24,* 382.
(11) Armstrong, D. R.; Fraser, G. W.; Meikle, G. D. *Inorg. Chem. Acta* 1975, *15,* 39.
(12) Shustorovich, E. M.; Buslaev, Yu. A. *Inorg. Chem.* 1976, *15,* 1142.
(13) Christen, D.; Mack, H. G.; Oberhammer, H. *J. Chem. Phys.* 1987, *87,* 2001.

(14) Christe, K. O.; Wilson, R. D.; Schack, C. J. *Inorg. Synth.* 1986, *24,* 3.
(15) Christe, K. O.; Wilson, W. W.; Wilson, R. D.; Bau, R.; Feng, J. *J. Am. Chem. Soc.* 1990, *112,* 7619.
(16) Christe, K. O.; Wilson, R. D.; Schack, C. J. *J. Fluorine Chem.* 1978, *11,* 71.
(17) Christe, K. O.; Dixon, D. A.; Mahjoub, A. R.; Mercier, H. P. A.; Sanders, J. C. P.; Seppelt, K.; Schrobilgen, G. J.; Wilson, W. W. *J. Am. Chem. Soc.* 1993, *115,* 2696.
(18) Christe, K. O.; Wilson, W. W.; Bau, R.; Bunte, S. W. *J. Am. Chem. Soc.* 1992, *114,* 3411.

Table 1. Vibrational Spectra of $CsHPF_5$ and $N(CH_3)_4HPF_5$ and Their Assignments

CsHPF5 IR	CsHPF5 Raman	N(CH3)4HPF5 IR	N(CH3)4HPF5 Raman	assignment HPF5⁻ (C_{4v})	assignment N(CH3)4⁺ (T_d)
		3130 w			
		3047 m	3046 (25)		
			3004 (9)		$\nu_5(E)$
			2988 sh		
		2975 w	2968 (15)		$\nu_{14}(F_2)$
			2927 (6)		$\nu_1(A_1)$
			2888 (2)		+combination
			2821 (5)		bands
2508 sh					
2478 m		2487 ms	2486 (4)	$2\nu_8(A_1)$	
2378 s		2375 s	2373 (8)		
2360 sh		2355 m	2355 (4)	$\nu_1(A_1)$	
			1530 (1)		
		1494 vs			$\nu_{15}(F_2)$
			1470 (85)		$\nu_2(A_1), \nu_6(E)$
		1442 w			
		1419 ms	1418 (7)		$\nu_{16}(F_2)$
		1303 w			
		1287 w	1287 (3)		$\nu_{17}(F_2)$
1235 vs		1238 vs	1238 (11)	$\nu_8(E)$	
			1175 (8)		$\nu_7(E)$
		949 vs	948 (100)		$\nu_{18}(F_2)$
945 vw				$(\nu_3 + \nu_{11})(E)$	
		918 vw	918 (2)		$2\nu_{19}(F_2)$
740–840 vs, br		750–820 vs, br	800 (3)	$\nu_9(E)$	
762 vs	769 (65)		768 (15)	$\nu_2(A_1)$	
			754 (47)		
			740 sh		$\nu_3(A_1)$
672 vw		672 vw		$2\nu_{11}(A_1)$	
602 s	607 (100)	602 s	608 (20)	$\nu_3(A_1)$	
		579 vw			
558 ms		558 ms	558 (3)	$\nu_4(A_1)$	
	542 (30)	537 vw	542 (6)	$\nu_5(B_1)$	
512 s	514 (25)	512 s	514 (7)	$\nu_{10}(E)$	
			458 (15)		$\nu_{19}(F_2)$
	440 (25)		440 (7)	$\nu_7(B_2)$	
			373 (18)		$\nu_8(E)$
333 mw		333 mw	337 (1)	$\nu_{11}(E)$	

calculated for $MHPF_5$). The products were identified by vibrational and NMR spectroscopy as $MHPF_5$ salts.[4–10]

Computational Methods. The geometries, vibrational frequencies, and force fields of HPF_5^- and HSF_5 were calculated, as previously described,[19] in the local density functional (LDF) approximation by using the program system DMol with a polarized double numerical basis set. Ab initio molecular orbital calculations were also performed with the program GRADSCF[20] with a polarized double-ζ basis set and with a polarized double-ζ basis set augmented with a set of diffuse p functions on the heavy atoms and a diffuse s function on hydrogen with ζ(s) = 0.041.[21]

(19) (a) Christe, K. O.; Wilson, R. D.; Wilson, W. W.; Bau, R.; Sukumar, S.; Dixon, D. A. *J. Am. Chem. Soc.* **1991**, *113*, 3795. (b) Dixon, D. A.; Andzelm, J.; Fitzgerald, G.; Wimmer, E.; Jasien, P. In *Density Functional Methods in Chemistry*; Labanowski, J., Andzelm, J., Eds.; Springer Verlag: New York, 1991; p 33. (c) Dixon, D. A.; Christe, K. O. *J. Phys. Chem.* **1992**, *96*, 1018. (d) Delley, B. *J. Chem. Phys.* **1990**, *92*, 508. Dmol is available commercially from BIOSYM Technologies, San Diego, CA. A FINE grid was used.
(20) (a) GRADSCF is an ab initio program system designed and written by A. Komornicki at Polyatomics Research. (b) Komornicki, A.; Ishida, K.; Morokuma, K.; Ditchfield, R.; Conrad, M. *Chem. Phys. Lett.* **1977**, *45*, 595. (c) McIver, J. W., Jr.; Komornicki, A. *Chem. Phys. Lett.* **1971**, *10*, 202. (d) Pulay, P. In *Applications of Electronic Structure Theory*; Schaefer, H. F., III, Ed.; Plenum Press: New York, 1977; p 153. (e) King, H. F.; Komornicki, A. *J. Chem. Phys.* **1986**, *84*, 5465. (f) King, H. F.; Komornicki, A. In *Geometrical Derivatives of Energy Surfaces and Molecular Properties*; Jorgenson, P., Simons, J., Eds.; D. Reidel: Dordrecht, 1986; NATO ASI Series C, Vol. 166, p 207.
(21) (a) For F, H, and O basis sets and for diffuse functions see: Dunning, T. H., Jr.; Hay, P. J. In *Methods of Electronic Structure Theory*; Schaefer, H. F., III, Ed.; Plenum Press: New York, 1977; Chapter 1. (b) For P and S basis sets see: (b) McLean, A. D.; Chandler, G. S. *J. Chem. Phys.* **1980**, *72*, 5639.

Results and Discussion

Syntheses of the HPF_5^- Salts. Attempts to prepare the HPF_5^- salts from the corresponding fluorides and excess PF_3 in anhydrous HF solution were unsuccessful and resulted in the exclusive formation of the corresponding bifluorides. This is attributed to HF being a stronger Lewis acid than HPF_4 and, therefore, displacing HPF_4 from its HPF_5^- salts. Consequently, the syntheses of the HPF_5^- salts were advantageously carried out in two separate steps. The first one involved the conversion of the fluorides to the bifluorides in anhydrous HF solution,

$$MF + HF \xrightarrow{HF} MHF_2$$

followed by removal of the unreacted HF and the reaction of the resulting bifluoride with PF_3 in CH_3CN solution.

$$MHF_2 + PF_3 \xrightarrow{CH_3CN} MHPF_5$$
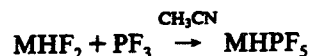
This approach offers the additional advantage that for M being cesium, the $CsHF_2$ is quite soluble in CH_3CN while CsF is not. The purity of the $MHPF_5$ salts prepared in this manner is excellent and the yields are quantitative. The use of an excess of PF_3 in this reaction is important to ensure that all MHF_2 is converted to $MHPF_5$ and any excess HF is converted to HPF_4.

Vibrational Spectra of $N(CH_3)_4HPF_5$ and $CsHPF_5$. The infrared and Raman spectra of these two HPF_5^- salts were recorded. The observed frequencies and their assignments are
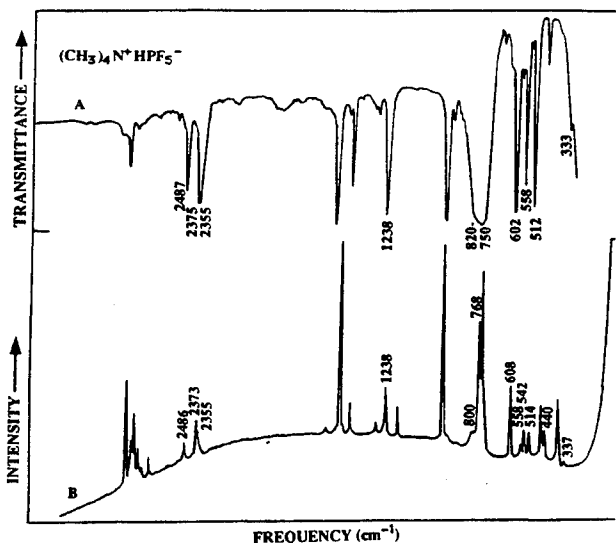
Figure 1. Infrared (A) and Raman (B) spectra of solid N(CH$_3$)$_4$HPF$_5$ recorded at room temperature. The bands due to the anion are marked by their frequency values.

summarized in Table 1. The spectra of N(CH$_3$)$_4$HPF$_5$ were of better quality than those of CsHPF$_5$ and are shown in Figure 1. The bands due to HPF$_5^-$ are marked by their frequency values; the remaining bands belong to the N(CH$_3$)$_4^+$ cation.

The assignments for the N(CH$_3$)$_4^+$ cation are well understood[3,15,17] and were made accordingly. The assignments for HPF$_5^-$ were made in point group C_{4v}, based on frequency and intensity arguments, and above all a comparison with the results from the local density functional and ab initio calculations (see below). The agreement between the observed and calculated frequencies is very good and firmly establishes the assignments given in Tables 1 and 2.

Ab Initio Electronic Structure Theory Calculations. Ab initio molecular orbital (MO) theory and LDF theory were used to calculate the vibrational frequencies (Table 2), geometries (Table 3), force fields (Table 4), and potential energy distributions (Table 5) for the HPF$_5^-$ anion and the isoelectronic HSF$_5$ molecule. The LDFT vibrational frequencies calculated for HPF$_5^-$ are in excellent agreement with the experimentally observed ones after scaling of the deformation modes by an empirical factor of 1.1012 to maximize the fit. The scaling of the deformation frequencies is necessary because the bond lengths, calculated at the LDFT

level, tend to be long by about 0.02–0.05 Å for these types of compounds[3] and the deformation frequencies are more strongly influenced by the bond length changes than the stretching modes. The MO results also show very good agreement with the experimental frequencies if empirical scaling factors are used. In general, the MO methods tend to underestimate bond lengths so that the frequencies are overestimated. It is also worth noting that the calculated values are harmonic and anharmonicity lowers the observed frequencies. The MO bond lengths are about 0.04 Å shorter than the corresponding LDFT values for HPF$_5^-$, whereas for HSF$_5$, the differences increase to about 0.05 Å. The calculated angles agree with each other. There is only a small effect of adding diffuse functions to the basis set at the MO level on the frequencies and there is no effect within 0.001 Å on the geometries. Furthermore, the S–F bond lengths calculated by us for HSF$_5$ at the HF/DZP+ level of theory are in good agreement with those previously obtained[13] at the 3-21G* and 6-31G* levels. The quality of our LDFT and HF/DZP+ methods was also examined by calculating the geometries of the closely related PF$_6^-$ and SF$_6$ species for which experimental values are known.[22,23] The results from the calculations are given in Table 3 and the following predictions can be made for the actual geometries of HPF$_5^-$ and HSF$_5$: HPF$_5^-$, r(P–F$_{ax}$) = 1.628 Å, r(P–F$_{eq}$) = 1.649 Å, r(P–H) = 1.404 Å, $\angle$(F$_{ax}$–P–F$_{eq}$) = 89.3°; HSF$_5$, r(S–F$_{ax}$) = 1.574 Å, r(S–F$_{eq}$) = 1.586 Å, r(S–H) = 1.324 Å, $\angle$(F$_{ax}$–S–F$_{eq}$) = 89.5°.

Structure and Bonding in HPF$_5^-$ and HSF$_5$. The species HPF$_5^-$ and HSF$_5$ can be derived from octahedral PF$_6^-$ and SF$_6$, respectively, by substitution of one fluorine ligand by one hydrogen ligand. Since no experimental data were available on how hydrogen substitution in a perfluorinated XF$_6$ species influences the rest of the molecule,[12,24] it was interesting to analyze this situation more closely.

First, consider the repulsion effects of the hydrogen ligand. According to the second basic tenet of the valence shell electron pair domain (VSEPD) model,[25] the size of a single bond domain in the valence shell of a central atom decreases with increasing electronegativity of the ligand. Since hydrogen has a much lower electronegativity than fluorine, the electron pair domain of a P–H bond should be larger than that of a P–F bond and, therefore, a P–H bond domain should be more repulsive than that of a P–F bond. As has already previously been pointed out, this tenet is not generally valid, as was shown by the bond angles of PH$_3$ and PF$_3$ and 30 additional examples.[26] Contrary to the VSEPD expectations, the bond angle in PF$_3$ (97.8°) is significantly larger than that in PH$_3$ (93.8°), suggesting that the size of the ligands is also important.[26] On the basis of general considerations, one

Table 2. Comparison of Observed and Calculated Frequencies of HPF$_5^-$ and Calculated Frequencies of HSF$_5$ and Their Approximate Mode Descriptions

IR and Raman activity	assignmt in Pt group C_{4v}	approx mode description	HPF$_5^-$					HSF$_5$[d]		
			obsd freq, cm^{-1} (int)		calcd freq, cm^{-1} (IR int)			calcd freq, cm^{-1} (IR int)[e]		
			IR	Raman	LDFT/DNP[a]	HF/DZP[b]	HF/DZP+[c]	LDFT/DNP	HF/DZP	HF/DZP+
IR, RA	A$_1$ ν_1	ν XH	2375 s	2373 (8)	2368	2367 (244)	2394 (246)	2661	2756 (17)	2727 (14)
	ν_2	ν XF$_{ax}$	762 vs	768 (15)	773	793 (268)	794 (277)	821	875 (261)(	867 (263)
	ν_3	ν sym XF$_4$ in phase	602 s	608 (20)	591	599 (45)	598 (52)	652	688 (32)	681 (34)
	ν_4	δ umbrella XF$_4$	558 ms	558 (3)	571	556 (25)	556 (22)	619	619 (42)	618 (41)
–, RA	B$_1$ ν_5	ν sym XF$_4$ out of phase		542 (6)	538	528 (0)	526 (0)	603	629 (0)	622 (0)
	ν_6	δ pucker, XF$_4$		not obsd	281	287 (0)	288 (0)	314	328 (0)	327 (0)
–, RA	B$_2$ ν_7	δ sciss XF$_4$		440 (7)	436	432 (0)	432 (0)	487	492 (0)	489 (0)
IR, RA	E ν_8	δ wag XH	1238 vs	1238 (11)	1236	1293 (144)	1288 (128)	1328	1420 (25)	1411 (27)
	ν_9	ν asym XF$_4$	750–820 vs	800 (3)	801	803 (1070)	798 (1158)	890	923 (1080)	912 (1124)
	ν_{10}	δ wag XF$_{ax}$	512 s	514 (7)	510	505 (27)	505 (28)	556	565 (40)	562 (39)
	ν_{11}	δ asym XF$_4$ in plane	333 mw	337 (1)	331	333 (1.7)	334 (1.5)	371	385 (4.8)	383 (4.6)

[a] The deformation frequencies were multiplied by a factor of 1.1012 to maximize their fit with their observed frequencies. [b] The stretching and deformation frequencies were multiplied by factors of 0.90624 and 0.92748, respectively. [c] The stretching and deformation frequencies were multiplied by factors of 0.89874 and 0.92345, respectively. [d] In the absence of experimental data, the same scaling factors as for HPF$_5^-$ were used. [e] In km mol^{-1}.

Table 3. Calculated Geometries of HPF$_5^-$ and HSF$_5$ Compared to Those Calculated and Observed for PF$_6^-$ and SF$_6$

	HPF$_5^-$		HSF$_5$				
	LDFT/DNP	HF/DZP+	LDFT/DNP	HF/DZP+	3-21G* [a]	6-31G* [a]	MP2/6-31G* [a]
r(X–F$_{ax}$)	1.642	1.607	1.602	1.553	1.556	1.560	1.602
r(X–F$_{eq}$)	1.662	1.628	1.613	1.567	1.565	1.573	1.611
r(X–H)	1.418	1.382	1.351	1.305			
$\angle$(F$_{ax}$–X–F$_{eq}$)	89.3	89.3	89.6	89.5	89.3	89.4	89.4

	PF$_6^-$			SF$_6$				
	obsd[b]	LDFT/DNP	HF/DZP+	obsd[c]	LDFT/DNP	HF/DZP+	3-21G* [a]	6-31G* [a]
r(X–F)	1.625	1.639	1.603	1.563	1.593	1.548	1.550	1.554

[a] Values from ref 13. [b] Values from ref 23. [c] Values from ref 22.

Table 4. Scaled[a] LDFT/DNP and HF/DZP+ Force Fields[b] of HPF$_5^-$ and HSF$_5$

HPF$_5^-$

	A$_1$					B$_1$			E			
	F_{11}	F_{22}	F_{33}	F_{44}		F_{55}	F_{66}		F_{88}	F_{99}	$F_{10,10}$	$F_{11,11}$
F_{11}	3.228 (3.247)				F_{55}	3.234 (3.034)		F_{88}	0.873 (0.892)			
F_{22}	−0.003 (−0.001)	4.018 (4.109)			F_{66}	−0.131 (−0.096)	1.116 (1.228)	F_{99}	0.444 (0.469)	3.597 (3.605)		
						B$_2$						
F_{33}	0.184 (0.330)	0.580 (0.803)	4.218 (4.341)		F_{77}	1.467 (1.373)		$F_{10,10}$	0.050 (0.060)	0.515 (0.554)	1.724 (1.627)	
F_{44}	−0.119 (−0.137)	0.744 (0.778)	−0.095 (−0.029)	2.154 (1.988)				$F_{11,11}$	0.108 (0.113)	0.393 (0.431)	0.217 (0.192)	1.649 (1.577)

HSF$_5$

	A$_1$					B$_1$			E			
	F_{11}	F_{22}	F_{33}	F_{44}		F_{55}	F_{66}		F_{88}	F_{99}	$F_{10,10}$	$F_{11,11}$
F_{11}	4.062 (4.267)				F_{55}	4.062 (4.316)		F_{88}	0.917 (0.968)			
F_{22}	−0.103 (−0.043)	4.626 (5.188)			F_{66}	−0.183 (−0.151)	1.450 (1.480)	F_{99}	0.488 (0.537)	4.467 (4.800)		
						B$_2$						
F_{33}	0.002 (0.017)	0.408 (0.687)	4.952 (5.520)		F_{77}	1.728 (1.650)		$F_{10,10}$	0.042 (0.066)	0.537 (0.624)	1.952 (1.918)	
F_{44}	0.039 (0)	0.810 (0.890)	−0.195 (−0.095)	2.431 (2.270)				$F_{11,11}$	0.090 (0.097)	0.448 (0.505)	0.223 (0.194)	1.928 (1.887)

[a] For the LDFT/DNP force fields, the deformation constants were scaled by a factor of $(1.1012)^2$ and the stretch–bend interaction constants by 1.1012. For the HF/DZP+ force fields, the following scaling factors were used: stretching constants, $(0.89874)^2$; deformation constants, $(0.92345)^2$; and stretch–bend interaction constants (0.89874×0.92345). [b] The HF/DZP+ force fields are listed in parentheses.

Table 5. Potential Energy Distributions for HPF$_5^-$ and HSF$_5$ for the LDFT/DNP Force Field

		HPF$_5^-$		HSF$_5$	
		freq, cm^{-1}	PED, %	freq, cm^{-1}	PED, %
A$_1$	ν_1	2368	99.6S_1	2661	99.5S_1 + 0.3S_4 + 0.1S_2
	ν_2	773	53.3S_2 + 42.0S_4 + 4.7S_3	821	51.7S_2 + 45.2S_4 + 2.9S_3 + 0.2S_1
	ν_3	591	73.0S_3 + 14.1S_4 + 12.6S_2 + 0.35S_1	652	84.1S_3 + 11.2S_2 + 4.7S_4
	ν_4	571	92.3S_4 + 7.4S_2 + 0.2S_3	619	92.9S_4 + 6.7S_2 + 0.3S_3 + 0.1S_1
B$_1$	ν_5	538	99.9S_5 + 0.1S_6	603	99.8S_5 + 0.2S_6
	ν_6	281	99.8S_6 + 0.2S_5	315	99.7S_6 + 0.3S_5
B$_2$	ν_7	436	100S_7	487	100S_7
E	ν_8	1236	99.9S_8	1328	99.9S_8
	ν_9	801	59.6S_9 + 17.4S_{11} + 13.9S_8 + 9.1S_{10}	890	55.5S_9 + 18.7S_8 + 16.9S_{11} + 8.9S_{10}
	ν_{10}	510	61.5S_{10} + 29.8S_{11} + 6.9S_8 + 1.8S_9	556	60.8S_{10} + 31.7S_{11} + 5.8S_8 + 1.7S_9
	ν_{11}	331	59.0S_{11} + 38.0S_{10} + 2.7S_8 + 0.3S_9	372	57.7S_{11} + 40.2S_{10} + 1.9S_8 + 0.2S_9

should expect at least three factors to influence the bond angles in HPF$_5^-$. These are the sizes of the ligands, the phosphorus–ligand bond distances, and the electronegativities of the ligands which influence the size of the electron pair domains. Since these factors can partially compensate each other,[27] it is difficult to predict the net effect. The slight compression of the F$_{ax}$–P–F$_{eq}$ bond angle in HPF$_5^-$ (see Table 3) indicates that the effective repulsions from the hydrogen ligand or its bonding electron pair domain are somewhat larger than those from the fluorine ligands but the overall effect is quite small.

IR and Raman Spectra of N(CH₃)₄HPF₅ and CsHPF₅

J. Am. Chem. Soc., Vol. 116, No. 16, 1994 7127

Table 6. Internal Stretching Force Constants of HPF₅⁻ and HSF₅ Compared to Those of Closely Related Pseudooctahedral Species and Some Hydrides

compd	stretching force constant, mdyn/Å		
	M–F$_{eq}$	M–F$_{ax}$	M–H
PF₆⁻ [a]	4.39	4.39	
HPF₅⁻ [b]	3.66	4.02	3.23
H₂PF₄⁻ [c]	3.07		3.19
PH₄⁺ [d]			3.19
PH₃ [d]			3.10
SF₆ [e]	5.26	5.26	
SF₅Cl [f]	4.51	4.83	
HSF₅ [g]	4.49	4.63	4.06
SF₅Br [h]	4.29	4.50	
SOF₅⁻ [i]	3.60	3.75	
SF₅⁻ [k]	2.06	4.12	
H₂S [d]			3.95
H₃S⁺ [j]			3.65

[a] Reference 29. [b] This work; frr = 0.246, frr' = 0.0645. [c] Reference 30. [d] Reference 31. [e] Reference 32. [f] Reference 33. [g] This work; frr = 0.2225, frr' = 0.020. [h] Reference 34. [i] Reference 35. [k] Reference 36. [j] Reference 37.

The second point of interest concerns the influence of hydrogen substitution on the X–F bond strengths and whether there is a significant *cis-* or *trans-*effect.[12,13] Since hydrogen substitution releases additional electron density into the rest of these molecules, the (δ–)F–X(δ+) bond polarities and, hence, the lengths of their X–F bonds should increase. The calculated bond distances clearly show this. In HPF₅⁻, the P–F$_{ax}$ distance is essentially the same as that in PF₆⁻ whereas the P–F$_{eq}$ bond distances are 0.02 Å longer (see Table 3). Another measure of the bond strengths are the internal stretching force constants (see Table 6). The HPF₅⁻ force constants were derived from the scaled LDFT vibrational frequencies which are almost identical to the experimentally observed ones (see Table 2) and, hence, should be very close to the true force field.[28] As can be seen from Table 6, the averaged P–F stretching force constant decreases, as expected, from PF₆⁻ (4.39 mdyn/Å)[29] to HPF₅⁻ (3.73 mdyn/Å). Substitution of a second fluorine ligand by hydrogen, i.e., going from HPF₅⁻ to *trans*-H₂PF₄⁻, causes a comparable further weakening of the P–F bonds (*trans*-H₂PF₄⁻ = 3.07 mdyn/Å).[30] Calculations carried out by us for H₂PF₄⁻ at the SCF and MP-2 levels of theory with the DZP basis set confirmed this trend and showed that *trans*-H₂PF₄⁻ is favored over the *cis*-isomer by 5.3 and 6.4 kcal/mol, respectively. This agrees with the previous experimental studies[8,30] on H₂PF₄⁻ in which only the *trans*-isomer was observed.

(22) McDowell, R. S.; Aldridge, J. P.; Holland, R. F. *J. Chem. Phys.* **1976**, *80*, 1203.

(23) Gutsev, G. L. *J. Chem. Phys.* **1993**, *98*, 444.

(24) Gillespie, R. J.; Hargittai, I. *The VSEPR Model of Molecular Geometry*; Allyn and Bacon: Boston, 1991.

(25) Gillespie, R. J. *Can. J. Chem.* **1992**, *70*, 742.

(26) Myers, T. *Monatsh. Chem.* **1992**, *123*, 363.

(27) The partial compensation of the ligand size and bond length effects on the bond angles is demonstrated by the following two examples: (a) NF₃ ∠ 102.2° and r = 1.37 Å, NH₃ ∠ 106.6 and r = 1.01 Å, PF₃ ∠ 97.8° and r = 1.56 Å, PH₃ ∠ 93.8° and r = 1.42 Å; (b) OF₂ ∠ 103.3° and r = 1.41 Å, OH₂ ∠ 104.8° and r = 0.965 Å, SF₂ ∠ 98.3° and r = 1.59 Å, SH₂ ∠ 92.2° and r = 1.34 Å. For the same ligands, but decreasing sizes of the central atoms and hence decreasing bond lengths, the ligand–ligand repulsions and thereby the bond angles increase, i.e., from PF₃ to NF₃, PH₃ to NH₃, SF₂ to OF₂, and SH₂ to OH₂. For the same central atom but different ligands, the size of the ligands and the bond length changes are much smaller than for the second period ones and, therefore, the ligand size effect dominates and the bond angles increase on going from SH₂ to SF₂ and PH₃ to PF₃. For the second period central atoms the relative bond length shortening dominates and, hence, the bond angles increase on going from OF₂ to OH₂ and from NF₃ to NH₃.

(28) The scaled LDF frequencies closely duplicate the experimentally observed ones and LDF force fields generally predict the actual off-diagonal symmetry force constants very well. Therefore, the scaled stretching force constants for HPF₅⁻ and HSF₅ used for the discussion in this paper should be very good measures for the relative strengths of the axial and equatorial bonds in these species.

(29) Christe, K. O.; Wilson, R. D. *Inorg. Chem.* **1975**, *14*, 694.

(30) Christe, K. O.; Schack, C. J.; Curtis, E. C. *Inorg. Chem.* **1976**, *15*, 843.

Table 6 also shows that in HPF₅⁻ the *cis*-fluorines are more strongly affected by hydrogen substitution than the *trans*-fluorine. These results confirm the *cis*-effect previously predicted[12] by Shustorovich and Buslaev; however, there is no evidence for a simultaneous shortening of the M–F$_{trans}$ bond. The M–F$_{trans}$ bond is also weakened, although to a lesser extent than the M–F$_{cis}$ bonds. Shustorovich and Buslaev also analyzed correctly[12] that when in MXF₅ the ligand X is multiply bonded such as a terminal oxygen and the *cis*-M–F bonds may be slightly longer than the *trans*-M–F bonds, as shown for SOF₅⁻ (see Table 6)[35] and recently also for IOF₅.[38]

The following model can account for the main features and ligand interactions in these hypervalent, substituted, pseudooctahedral main group fluorides. Ideally, only s and p orbitals are being used for the central atom requiring the assumption of semi-ionic, 3 center–4 electron (3c–4e) bonds[39] to compensate for the resulting electron deficiency. Since 3c–4e bonds involve one p-orbital of the central atom for binding two fluorine ligands, 3c–4e bonding is possible only for approximately linear FMF groups possessing highly electronegative ligands because each ligand must carry half a negative formal charge. In MXF₅ or *trans*-MX₂F₄ where X is either a sterically active free valence electron pair or a highly electropositive ligand, the ligand X is ill-suited for the formation of a semi-ionic 3c–4e bond and, therefore, seeks high s-character, i.e., increased covalency. As a consequence, the four equatorial M–F$_{cis}$ bonds are favored to form two semi-ionic, 3c–4e bond pairs. Since the axial F ligand which is *trans* to X either cannot, if X is a free valence electron pair, form or is less favored, if X is less electronegative than fluorine, to form a linear semi-ionic, 3c–4e bond pair, it seeks to form a regular covalent M–F bond. This scheme accounts for the very large difference[36] between axial and equatorial bond strengths in SF₅⁻, where X is a sterically active free valence electron pair, and the much smaller, but significant, differences in MXF₅ species, where X is either H, Br,[34] or Cl.[33] If X is a doubly bonded ligand, such as a terminal oxygen,[35] the M–O π bond competes with the equatorial semi-ionic bonds for p$_x$ and p$_y$ orbital electron density and, thus, weakens the *cis*-M–F$_{eq}$ bonds. However, this effect appears to be relatively weak.

The M–H stretching force constants are surprisingly insensitive to changes in the ligands, the oxidation state of the central atom, and formal positive or negative charges. Thus, the P–H stretching force constant of PH₄⁺ (3.19 mdyn/Å)[31] is almost identical to that found for HPF₅⁻ (3.23 mdyn/Å), and the same holds for the analogous sulfur compounds (see Table 6).

We would like to briefly comment on HSF₅. Although this molecule is still unknown, the LDF calculations indicate that the molecule is vibrationally stable. We anticipate that the molecule, if prepared, will undergo relatively easy HF elimination to give SF₄ + HF.

Finally, it is interesting to compare the results from this study with the reverse substitution effect, i.e., the influence of one or two fluorine atoms on hydrogen ligands in pseudooctahedral main group compounds. In a previous theoretical study[40] on H₅SbF⁻,

(31) Siebert, H. *Anwendungen der Schwingungsspektroskopie in der Anorganischen Chemie*; Springer-Verlag: Berlin, 1966.

(32) Ruoff, A. *J. Mol. Struct.* **1969**, *4*, 332.

(33) Sawodny, W. Habilitation, University of Stuttgart, Germany, 1969.

(34) Christe, K. O.; Curtis, E. C.; Schack, C. J.; Roland, A. *Spectrochim. Acta, Part A* **1977**, *33A*, 69.

(35) Christe, K. O.; Schack, C. J.; Pilipovich, D.; Curtis, E. C.; Sawodny, W. *Inorg. Chem.* **1973**, *12*, 620.

(36) Christe, K. O.; Curtis, E. C.; Schack, C. J.; Pilipovich, D. *Inorg. Chem.* **1972**, *11*, 1679.

(37) Christe, K. O. *Inorg. Chem.* **1975**, *14*, 2230.

(38) Christe, K. O.; Curtis, E. C.; Dixon, D. A. *J. Am. Chem. Soc.* **1993**, *115*, 9655.

(39) (a) Pimentel, G. C. *J. Chem. Phys.* **1951**, *19*, 446. (b) Hach, R. J.; Rundle, R. E. *J. Am. Chem. Soc.* **1951**, *73*, 4321. (c) Rundle, R. E. *J. Am. Chem. Soc.* **1963**, *85*, 112.

(40) Yamamoto, Y.; Fujikawa, H.; Fujishima, H.; Akiba, K. *J. Am. Chem. Soc.* **1989**, *111*, 2276.

H_5SbOH^-, and $H_4SbF_2^-$ it was shown that the electron-withdrawing effect of fluorine dominates and mainly affects the hydrogen in the *trans*-position by increasing the $(\delta+)H–Sb(\delta-)$ bond polarity and thereby its bond length. Hence, the effect of hydrogen substitution strongly differs from that of fluorine substitution. Whereas fluorine substitution results in a simple, electron-withdrawing and bond-weakening *trans*-effect, hydrogen substitution results in a preferential weakening of the *cis*-ligands

due to increased contributions from semi-ionic 3c–4e bonding to the *cis*-bonds.

Karl O. Christe,* David A. Dixon,
Jeremy C.P. Sanders, Gary J. Schrobilgen,*
and William W. Wilson

On the Hydrolysis and Methanolysis of PF_4^- and Nuclear Magnetic Resonance and Vibrational Spectra of the POF_2^- and HPO_2F^- Anions

The hydrolysis and methanolysis of $N(CH_3)_4PF_4$ were studied by multinuclear NMR and vibrational spectroscopy. With an equimolar amount of water in CH_3CN solution, PF_4^- forms HPO_2F^- and HPF_5^- in a 1:1 mole ratio. With an excess of water, HPO_2F^- is the sole product which was also obtained by the hydrolysis of HPF_5^-. In the presence of a large excess of F−, the hydrolysis of PF_4^- with an equimolar amount of water produces POF_2^-. The resulting $N(CH_3)_4POF_2$ is the first known example of a stable POF_2^- salt. The geometries and vibrational spectra of POF_2^- and HPO_2F^- were calculated by ab initio methods, and normal coordinate analyses were carried out for POF_2^-, HPO_2F^- and the isoelectronic SOF_2, HSO_2F and $ClOF_2^+$ species. The F− affinities of FPO, HPO_2 and related species and the reaction enthalpies of the hydrolysis reactions of the PF_4^- and HPF_5^- anions were also calculated by ab initio methods and are in accord with the experimental data. The methanolysis of PF_4^- produces $PF_2(OCH_3)$ and $PF(OCH_3)_2$ as the main products.

$+CH_3OH$ → $PF_2(OCH_3) + HF_2^-$

$+CH_3OH$ → $PF(OCH_3)_2 + HF$

On the Hydrolysis and Methanolysis of PF_4^- and Nuclear Magnetic Resonance and Vibrationl Spectra of the POF_2^- and HPO_2F^- Anions†

Karl O. Christe,[1] *David A. Dixon,*[2] *Jeremy C.P. Sanders,*[3] *Gary J. Schrobilgen,*[3] *and William W. Wilson*[1].

Contribution from Rocketdyne, A Division of Rockwell International Corporation, Canoga Park, California 91309, the Department of Chemistry, McMaster University, Hamilton, Ontario L8S 4M1, Canada, and The DuPont Company, Central Research and Development, Experimental Station, Wilmington, Delaware 19880-0328.

ABSTRACT

The hydrolysis and methanolysis of $N(CH_3)_4PF_4$ were studied by multinuclear NMR and vibrational spectroscopy. With an equimolar amount of water in CH_3CN solution, PF_4^- forms HPO_2F^- and HPF_5^- in a 1:1 mole ratio. With an excess of water, HPO_2F^- is the sole product which was also obtained by the hydrolysis of HPF_5^-. In the presence of a large excess of F^-, the hydrolysis of PF_4^- with an equimolar amount of water produces POF_2^-. The resulting $N(CH_3)_4POF_2$ is the first known example of a stable POF_2^- salt. The geometries and vibrational spectra of POF_2^- and HPO_2F^- were calculated by ab initio methods, and normal coordinate analyses were carried out for POF_2^-, HPO_2F^- and the isoelectronic SOF_2, HSO_2F and $ClOF_2^+$ species. The F^- affinities of FPO, HPO_2 and related species and the reaction enthalpies of the hydrolysis reactions of the PF_4^- and HPF_5^- anions were also calculated by ab initio methods and are in accord with the experimental data. The methanolysis of PF_4^- produces $PF_2(OCH_3)$ and $PF(OCH_3)_2$ as the main products.

INTRODUCTION

$N(CH_3)_4^+PF_4^-$, the first example of a PF_4^- salt, was recently prepared and characterized in our laboratories.[4] In the course of this work, we observed that this salt undergoes very interesting hydrolysis reactions. Depending on the reaction conditions, this reaction produces either POF_2^- which previously had been observed as a free ion[5a] only at low temperature by NMR spectroscopy[5b] and in an ion cyclotron resonance spectrometer,[6] or HPO_2F^- and HPF_5^- which had previously been characterized only incompletely.[7-15] In this paper, the hydrolysis and methanolysis reactions of PF_4^- and spectroscopic data for POF_2^- and HPO_2F^- are reported. Our results on HPF_5^- have been included in a separate paper[16] discussing mutual ligand interaction effects in monosubstituted main group hexafluorides.

EXPERIMENTAL SECTION

Apparatus and Materials. The syntheses of $N(CH_3)_4PF_4$[4] and $N(CH_3)_4HPF_5$[16] have previously been described. Volatile materials were handled in a Pyrex glass vacuum line that was equipped with Kontes glass-Teflon valves and a Heise pressure gage. Nonvolatile materials were handled in the dry nitrogen atmosphere of a glove box. The infrared and Raman spectrometers have previously been described.[17]

Hydrolysis of $N(CH_3)_4PF_4$. In a typical experiment, $N(CH_3)_4PF_4$ (1.104 mmol) was placed in the dry box into a baked out 3/4 inch o.d. Teflon-FEP ampule that contained a Teflon coated magnetic stirring bar and was closed by a stainless steel valve. A sample of "wet" CH_3CN was made up by the addition of a known amount of H_2O to a known amount of dry CH_3CN, and the water content of the resulting solution was verified by a Karl Fischer titration. An amount of wet CH_3CN (3.155 mL) with a total water content of 1.104 mmol was pipetted inside the dry box into the ampule containing the $N(CH_3)_4PF_4$, and the resulting mixture was stirred for 1 hour at room temperature. Then, all volatile material was pumped off for 12 hours at 25°C leaving behind 198.4 mg of a white solid that was identified

by NMR and vibrational spectroscopy as an equimolar mixture of $N(CH_3)_4HPF_5$ and $N(CH_3)_4HPO_2F$ (weight calculated for 0.552 mmol of $N(CH_3)_4HPF_5$ plus 0.552 mmol of $N(CH_3)_4HPO_2F = 197.8$ mg).

Preparation of $N(CH_3)_4HPO_2F$. When the hydrolysis reaction of $N(CH_3)_4PF_4$ was repeated with a five-fold excess of H_2O and a reaction time of 5 days, followed by removal of all volatile material in a dynamic vacuum at 85°C for 2 days, the sole product was $N(CH_3)_4HPO_2F$.

Hydrolysis of $N(CH_3)_4HPF_5$. A hydrolysis reaction of $N(CH_3)_4HPF_5$ with 2 moles of H_2O was carried out at room temperature, as described above for $N(CH_3)_4PF_4$. After agitation for 16 hours, the originally present white solid had completely dissolved. Removal of all volatile material at 60°C for 15 hours in a dynamic vacuum resulted in a white product consisting of $N(CH_3)_4HPO_2F$ and some unreacted $N(CH_3)_4HPF_5$.

Hydrolysis of $N(CH_3)_4PF_4$ in the Presence of $N(CH_3)_4F$. A 3/4 inch o.d. Teflon-FEP ampule that was closed by a stainless steel valve was loaded in the dry box with $N(CH_3)_4F$ (16.31 mmol). Wet CH_3CN (12.5 g), containing 4.05 mmol of H_2O, was added to the ampule and PF_3 (4.05 mmol) was added at -196°C on the vacuum line. The mixture was warmed to -30°C for 1 hour with agitation, and a voluminous white precipitate formed. After warming for 1 hour to room temperature, all material volatile at room temperature was pumped off for 8 hours leaving behind a white solid residue (1949.4 mg, weight calculated for 4.05 mmol $N(CH_3)_4POF_2$ + 8.10 mmol $N(CH_3)_4HF_2$ + 4.6 mmol $N(CH_3)_4F = 1946.0$ mg) which, based on its infrared spectrum, was a mixture of $N(CH_3)_4POF_2$, $N(CH_3)_4HF_2$, and $N(CH_3)_4F$.

Nuclear Magnetic Resonance Measurements. Samples for ^{31}P and ^{19}F NMR spectroscopy were prepared in 9 mm and 5 mm o.d. Teflon-FEP NMR tubes, respectively, and recorded as previously described[4] on a Bruker AM-500 spectrometer. The spectra were

3

referenced to neat external samples of $CFCl_3$ (^{19}F), 85% H_3PO_4 (^{31}P) and H_2O (^{17}O) at ambient temperature. The chemical shift convention used is that a positive sign signifies a chemical shift to high frequency of the reference compound.

(a) Reaction of $N(CH_3)_4PF_4$ with H_2O in CH_3CN. Typically, $^{17,18}O$-enriched H_2O (8.66 μL, 0.454 mmol) was injected into a 9 mm FEP tube from a microsyringe in a nitrogen-filled glove bag. The tube was closed with a Kel-F valve and attached to a glass vacuum line. Anhydrous CH_3CN (1.8 mL) was distilled *in vacuo* into the tube at -196°C. The tube was pressurized with dry N_2 at -78°C and then allowed to warm to room temperature and mixed well. The tube was taken into the dry box and cooled to -196°C in a cold well. The $N(CH_3)_4PF_4$ (0.0822 g, *ca.* 0.45 mmol), containing 10-15% $N(CH_3)_4POF_2$ and $N(CH_3)_4HPF_5$ as impurities, was added on top of the frozen $^{17,18}O$-enriched H_2O/CH_3CN mixture contained in the FEP tube. The sample tube was kept at -196°C while removing it from the dry box, heat sealing it under a dynamic vacuum, and storing it until the NMR spectra could be obtained.

(b) Reaction of $N(CH_3)_4PF_4$ with H_2O in the Presence of $N(CH_3)_4F$ in CH_3CN. These samples were prepared in a similar way to (a) using the following typical quantities: $^{17,18}O$-enriched H_2O (8.5 μL, 0.45 mmol); $N(CH_3)PF_4$ (containing 10 - 15% $N(CH_3)_4POF_2$ and $N(CH_3)_4HPF_5$ as impurities, 0.08081 g, *ca* 0.46 mmol); $N(CH_3)_4F$ (0.10923 g, 1.1727 mmol). The $N(CH_3)_4F$ was added with the $N(CH_3)_4PF_4$ on top of the frozen $^{17,18}O$-enriched H_2O/CH_3CN mixture. The sample tube was kept at -196°C until the NMR spectra could be obtained.

The ^{19}F NMR samples were prepared in an analogous fashion to the ^{31}P samples by using 4 mm o.d. FEP NMR tubes and the following typical quantities: (a) $N(CH_3)_4PF_4$ (0.0100 g, 0.0552 mmol); $^{17,18}O$-enriched H_2O (1.1 μL, 0.055 mmol) and CH_3CN (0.25 mL); (b) $N(CH_3)_4PF_4$ (0.0096 g, 0.053 mmol); $N(CH_3)_4F$ (0.0194 g, 0.208 mmol);

4

^{17,18}O-enriched H_2O (1.1 μL, 0.055 mmol) and CH_3CN (0.25 mL). Samples were not warmed above -78°C until just prior to recording the spectra.

The sealed FEP sample tubes were inserted into 10 mm or 5 mm thin-walled precision NMR tubes (Wilmad) before being placed in the probe.

Computational Methods. The electronic structure calculations were done at three different levels on a Cray YMP computer. The local density functional calculations were done with the program DMol as previously described[18] with a polarized double numerical basis set (LDFT/DNP). Gradient corrected or non-local density functional calculations were done with the program DGauss[19] which employs Gaussian basis sets. The basis sets for the atoms are triple zeta in the valence space augmented with a set of polarization functions (TZVP).[20] These calculations were done at the self-consistent gradient-corrected (non-local) level (NLDFT) with the non-local exchange potential of Becke[21] together with the non-local correlation functional of Perdew[22] (BP). The ab initio molecular orbital (MO) theory calculations were done at the Hartree-Fock level with the program GRADSCF[23] with a polarized double zeta basis set augmented by polarization and diffuse (p on heavy atoms and s on H(zeta(s) = 0.041)) functions.[24] Geometries at all levels were optimized by using analytical gradients.[19,25] The second derivatives for the DFT calculations were calculated by numerical differentiation of the analytic first derivatives. A 2 point method with a finite difference of 0.01 a.u. was used. Analytical second derivatives were used for the MO calculations.[25]

RESULTS AND DISCUSSION

The hydrolysis of PF_4^- in CH_3CN solution was studied by multinuclear NMR and vibrational spectroscopy. As shown in the following paragraphs, the nature of the formed products strongly depends on the stoichiometry of the reagents and the reaction conditions.

Hydrolysis of PF$_4^-$ with Equimolar Amounts of Water. The hydrolysis of PF$_4^-$ with an equimolar amount of water in CH$_3$CN solution at ambient temperature proceeds rapidly and almost quantitatively according to Equation (1).

$$2PF_4^- + 2H_2O \xrightarrow[20°C]{CH_3CN} HPO_2F^- + HPF_5^- + 2HF \qquad (1)$$
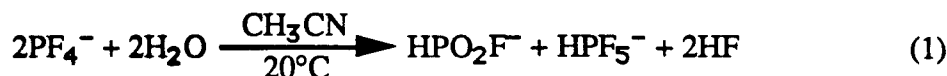
This result was confirmed by multinuclear NMR spectroscopy.

The ^{31}P NMR spectrum of a sample containing equimolar quantities of N(CH$_3$)$_4$PF$_4$ and H$_2$O (oxygen isotopic composition: ^{16}O, 35.4%; ^{17}O, 21.9%, ^{18}O, 42.7%) in CH$_3$CN at -45°C is shown in Figure 1a and reveals five resonances. Three of these resonances, A,C, and D, are assigned to the POF$_2^-$,[5] HPO$_2$F$^-$,[7-9] and HPF$_5^-$,[10-15] anions, respectively, and their NMR data are collected in Table 1. The weak quartet at high frequency, B, is assigned to PF$_3$ [δ = 103.5 ppm; $^1J(^{31}P-^{19}F)$ = 1401 Hz] by comparison with the literature data[26]. A very weak multiplet, E, was also observed overlapping with the HPF$_5^-$ resonance. Since the resonance occurs in the hexacoordinate P(V) region of the spectrum, it is tentatively assigned to the [HPF$_4$(OH)]$^-$ anion which is a proposed intermediate in the hydrolysis reaction (see below). Although the HPO$_2$F$^-$ and POF$_2^-$ anions had been reported previously,[7-15] prior to the present study these anions had not been fully characterized in solution by multi-NMR spectroscopy. The formation of ^{17,18}O-enriched HPO$_2$F$^-$ and POF$_2^-$ in our studies has allowed unequivocal identification of these two anions by the observation of the ^{17}O NMR spectra as well as the ^{16,18}O induced secondary isotopic shifts in the ^{31}P NMR spectra (see below). The small amount of POF$_2^-$ observed in the spectrum was present as an impurity in the N(CH$_3$)$_4$PF$_4$ starting material used to prepare the NMR sample and was not generated by the hydrolysis as shown by the ^{17}O NMR spectrum at -36°C. This spectrum displayed only a broad doublet ($\Delta\nu$ 1/2 = 76 Hz) due to HPO$_2$F$^-$ and no resonance ascribable to POF$_2^-$.

When the ^{31}P NMR spectrum was recorded at 30°C, the hydrolysis had gone to completion and all the PF_3 had disappeared (Figure 1b). The ^{31}P, ^{19}F and ^{17}O NMR data for the observed species are also given in Table 1. The resonance due to POF_2^- had become somewhat more intense and now displayed ^{17}O satellites, thereby indicating a small amount of side reaction in which POF_2^- was produced. Each component of the doublet of doublets (resonance C and Figure 1c) arising from HPO_2F^- was now resolved into three lines which correspond to the $^{16,18}O$ induced secondary isotopic shifts for the three isotopomers $HP^{16}O_2F^-$, $HP^{16}O^{18}OF^-$ and $HP^{18}O_2F^-$. The isotopic shift $^1\Delta^{31}P(^{18,16}O)$ was measured as -0.0358 ± 0.0008 ppm. The observation of these three isotopomers proves that the anion has two oxygen atoms bonded to phosphorus. In addition, each component displayed well resolved, equal-intensity sextet satellites resulting from coupling of ^{31}P to ^{17}O ($I = 5/2$). The ^{17}O satellites are well-resolved at 30°C owing to the slower rate of quadrupolar relaxation of the ^{17}O nucleus at higher temperatures. The spectrum also reveals that the weak multiplet, E, which was partially obscured by the intense HPF_5^- multiplet at -36°C has disappeared on warming, thereby indicating that it might have arisen from the proposed $[HPF_4(OH)]^-$ intermediate (see below). The ^{17}O NMR spectrum (Figure 2) of the same sample at 30°C shows two resonances: an intense doublet, B, assigned to HPO_2F^- and a weaker doublet, A, assigned to POF_2^-. Each component of the doublet resonance of HPO_2F^- is further split into an overlapping doublet of doublets (Figure 2) by the two-bond couplings to ^1H and ^{19}F $[^2J(^{17}O\text{-}^1H) \approx 12 \text{ Hz}; \ ^2J(^{17}O\text{-}^{19}F) \approx 12 \text{ Hz}]$.

The ^{19}F NMR spectrum at 30°C of a sample containing equimolar quantities of $N(CH_3)_4PF_4$ and $^{17,18}O$-enriched H_2O in CH_3CN (Figure 3) reveals a doublet of doublets, A, arising from HPO_2F^-, as well as the resonances B and C attributable to the axial and equatorial fluorine ligand environments, respectively, of HPF_5^-. Under high resolution, each component of the HPO_2F^- resonance is found to comprise three lines corresponding to the three isotopomers $HP^{16}O_2F^-$, $HP^{16}O^{18}OF^-$ and $HP^{18}O_2F^-$. The two-bond isotopic

7

shift, $^2\Delta^{19}F(^{18,16}O)$, was measured as -0.0125 ± 0.0004 ppm and, to the best of our knowledge, is the first experimentally determined $^2\Delta^{19}F(^{18,16}O)$ value. In addition, a broad unresolved hump is visible at the base of each component of the HPO_2F^- multiplet which results from the two-bond coupling of ^{19}F to ^{17}O in the $HP^{16}O^{17}OF^-$ and $HP^{18}O^{17}OF^-$ isotopomers. Attempts to observe the ^{19}F resonance of the intermediate species $HPF_4(OH)^-$ were unsuccessful owing to the difficulty in mixing the reagents and moderating the vigor of the hydrolysis reaction at $-45°C$ in a 4-mm FEP NMR tube.

<u>Hydrolysis of PF_4^- with an Excess of Water</u>. If a large excess of water is used in the hydrolysis of PF_4^- in CH_3CN solution, the originally formed HPF_5^- also undergoes slow hydrolysis and HPO_2F^- becomes the sole product, as shown in Equation (2).

$$PF_4^- + 2\,H_2O \xrightarrow[\text{20°C}]{CH_3CN} HPO_2F^- + 3HF \qquad (2)$$
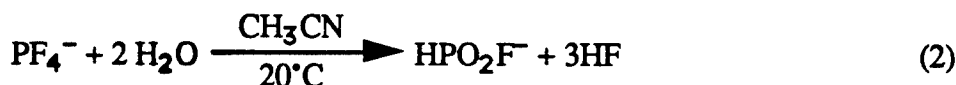
The slow hydrolysis of HPF_5^- to HPO_2F^- was verified by hydrolysing a sample of HPF_5^- with excess water, as shown in Equation (3). After 16 hours at room

$$HPF_5^- + 2\,H_2O \xrightarrow[\text{20°C}]{CH_3CN} HPO_2F^- + 4HF \qquad (3)$$
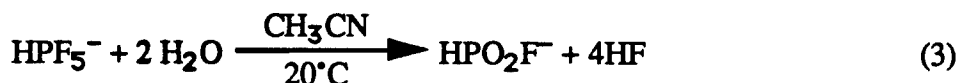
temperature most of the HPF_5^- had been converted to HPO_2F^-.

<u>Hydrolysis of $N(CH_3)_4PF_4$ in the Presence of $N(CH_3)_4F$ in CH_3CN</u>. If the hydrolysis of PF_4^- with an equimolar amount of water is carried out in the presence of an excellent HF scavenger, such as the fluoride anion, the products are different, and POF_2^- is formed in high yield, as shown in Equation (4).

$$PF_4^- + H_2O + 2F^- \xrightarrow[\text{20°C}]{CH_3CN} POF_2^- + 2HF_2^- \qquad (4)$$

8

Reaction (4) is of particular interest since it provided, for the first time, a stable salt of the POF_2^- anion which previously had been observed only by either ion cyclotron resonance spectroscopy[6] or NMR spectroscopy at temperatures below -50°C during the deprotonation of $HPOF_2$ using $[Ir(CO)H(PPh_3)_3]$.[5]

The ^{31}P NMR spectrum of a sample of $N(CH_3)_4PF_4$ at -45°C in CH_3CN, containing a 2.6 molar excess of $N(CH_3)_4F$ and an equimolar quantity of $^{17,18}O$-enriched H_2O, is shown in Figure 4. It reveals three resonances, A,B, and C, attributable to POF_2^-,[5] PF_4^-,[4] and HPF_5^-,[10-15] respectively. The HPF_5^- was present as an impurity in the $N(CH_3)_4PF_4$ starting material and did not arise from the hydrolysis. The triplet A due to POF_2^- was significantly more intense than that in the sample of $N(CH_3)_4PF_4$ in CH_3CN alone; furthermore the resonance exhibited a small "doublet" splitting due to the $^{16,18}O$ secondary isotopic shift, thereby providing conclusive proof that most of the POF_2^- had arisen from the hydrolysis of $N(CH_3)_4PF_4$ with the $^{17,18}O$-enriched H_2O. On warming the sample to -10°C, the amount of POF_2^- increased further and, after warming to room temperature, complete hydrolysis of PF_4^- to POF_2^- had taken place with the $N(CH_3)_4F$ complexing the HF.

The ^{31}P NMR spectrum of the sample at 30°C (Figure 5) shows two triplets [$^1J(^{31}P-^{19}F) = 1183$ Hz] ascribed to the two isotopomers $P^{16}OF_2^-$ and $P^{18}OF_2^-$[$^1\Delta^{31}P(^{18,16}O) = -0.0689 \pm 0.0010$ ppm]. The observation of these two isotopomers demonstrates that the phosphorus is only bonded to one oxygen atom and identifies the POF_2^- anion. In addition, each component of the triplet is flanked by equal-intensity sextet satellites arising from coupling to ^{17}O. These satellites are highly resolved and demonstrate that there is a fortuitously small electric field gradient at the ^{17}O nucleus and consequently the quadrupolar relaxation of the ^{17}O nucleus is very slow. Correspondingly, the ^{17}O NMR spectrum (Figure 6) displays a very sharp doublet, A, ($\Delta v_{1/2} = 5$ Hz) due to the $P^{17}OF_2^-$ anion. A weak resonance, B, attributable to the HPO_2F^- anion was also observed. The ^{19}F NMR

spectrum at 30°C reveals two sharp doublets arising from POF_2^- (Table 1) and HF_2^- ($\delta = $ -144.5 ppm; $^1J(^{19}F-^1H) = 122$ Hz)[27], as well as some weak signals attributable to HPF_5^-.[10-15]

It should be pointed out that some of the NMR parameters of HPO_2F^- and POF_2^- exhibit a pronounced temperature and fluoride ion concentration dependence which accounts for the variances (see Table 1 and Figures 2 and 6) observed in some of the spectra.

Proposed Reaction Mechanism. The formation of the observed products can be rationalized by the following mechanism. (i) Pentacoordinated phosphorus compounds are thermodynamically less favorable than tetra- or hexa-coordinated compounds. Consequently, they exhibit a pronounced tendency to either dismutate to tetra- and hexa-coordinated compounds or add an extra molecule, such as HF or H_2O, to achieve hexacoordination. A typical example for the latter type of reaction is the addition of HF to pentacoordinated PF_4^-, counting the sterically active free valence electron pair on phosphorus in PF_4^- as a ligand, to give hexacoordinated HPF_5^-. [15,16] Similarly, it is very probable, and there is evidence for it in our ^{31}P NMR spectra (see above), that PF_4^- adds one molecule of water to form an intermediate $[HPF_4(OH)]^-$ anion which, in the absence of more information, is written here as the cis-isomer.
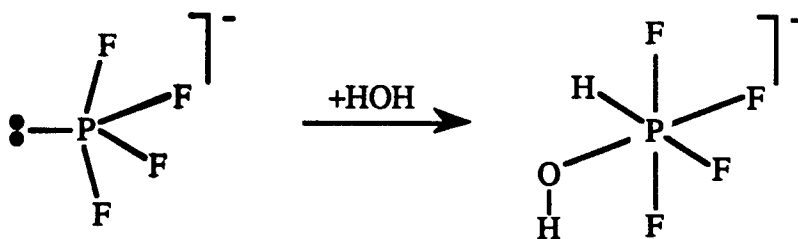
(ii) The resulting unstable $[HPF_4(OH)]^-$ anion could undergo a facile intramolecular HF elimination to give a trigonal bipyramidal $HPOF_3^-$ anion which, by analogy to the closely related POF_4^- anion, [28,29] then could undergo dismutation to a tetrahedral dioxo and an octahedral oxygen-free anion.

10
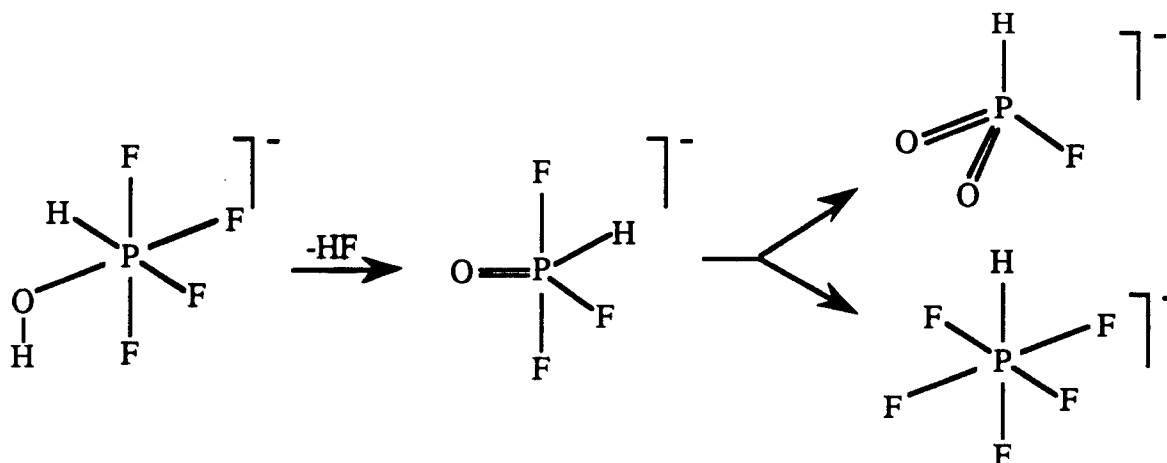
The slower hydrolysis of HPF_5^- with excess water probably involves the same mechanism with the required PF_4^- starting material being generated from HPF_5^- by HF loss. The facts that the

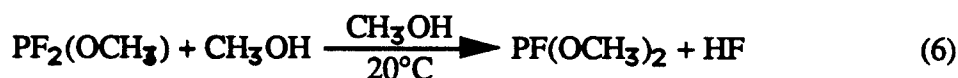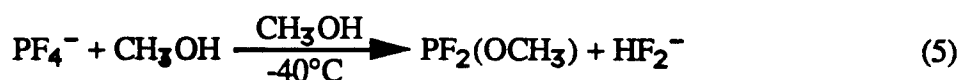$$PF_4^- + HF \rightleftharpoons HPF_5^-$$

equilibrium lies far to the right and half a mole of HPF_5^- is being regenerated during the hydrolysis, thus requiring many hydrolysis cycles in order to achieve a high conversion of HPF_5^- to HPO_2F^-, could explain the slowness of the HPF_5^- hydrolysis.

The exclusive formation of POF_2^- as the hydrolysis product of PF_4^- in the presence of an HF scavenger can also be explained by the same mechanism, i.e., the formation of $HPOF_3^-$ as an intermediate. However, instead of dismutating to HPO_2F^- and HPF_5^-, this anion could undergo a faster F^- promoted HF elimination to POF_2^-.

11
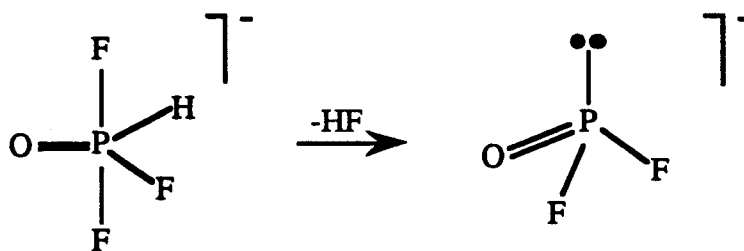
It should be emphasized that in all of the above dismutation reactions, the phosphorus central atom maintains the same formal oxidation state; i.e., in the case of PF_4^- as the starting material, all intermediates and products are phosphorus (+III) compounds and, therefore, derivatives of fluorophosphorous acids.

Methanolysis of PF_4^-. The methanolysis of PF_4^- in CH_3OH solution was also studied by NMR spectroscopy. At -40°C, the main reaction product was $PF_2(OCH_3)$[26,30,31] [^{31}P: triplet [$^1J(^{31}P$-$^{19}F) = 1286$ Hz] of quartets [$^3J(^{31}P$-$^1H) = 8.2$ Hz] at $\delta = 113.2$], while after a brief warming to room temperature, $PF(OCH_3)_2$[30] [^{31}P: doublet [$^1J(^{31}P$-$^{19}F) = 1202$ Hz] of septets [$^3J(^{31}P$-$^1H) = 10$ Hz] at $\delta = 132.9$] became also a major product.

$$PF_4^- + CH_3OH \xrightarrow[-40°C]{CH_3OH} PF_2(OCH_3) + HF_2^- \qquad (5)$$

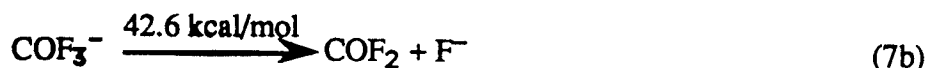$$PF_2(OCH_3) + CH_3OH \xrightarrow[20°C]{CH_3OH} PF(OCH_3)_2 + HF \qquad (6)$$

In addition to these two phosphorous acid methylesters, a small amount of a phosphorus (+V) by-product was observed which is attributed to $OPF(OCH_3)_2$ [^{31}P: doublet [$^1J(^{31}P$-$^{19}F) = 712$ Hz] of septets [$^3J(^{31}P$-$^1H) = 12$ Hz] at $\delta = 13.6$] which could arise from methanolysis of PF_3O.

Ab Initio Calculations and Vibrational Spectra. Since the HPO_2F^- and POF_2^- anions had previously been only partially characterized, it was of interest to analyze their vibrational spectra (Figures 7 and 8 and Tables 4 and 5) and force fields with the help of ab initio calculations (Tables 2-10). For comparison, the geometries and vibrational spectra of the isoelectronic sulfur compounds, HSO_2F and SOF_2 were also calculated. Since the known SOF_2 molecule has been well characterized,[32-34] its experimental data can be used to test the quality of our calculations which were done at the local density functional (LDFT), non-local
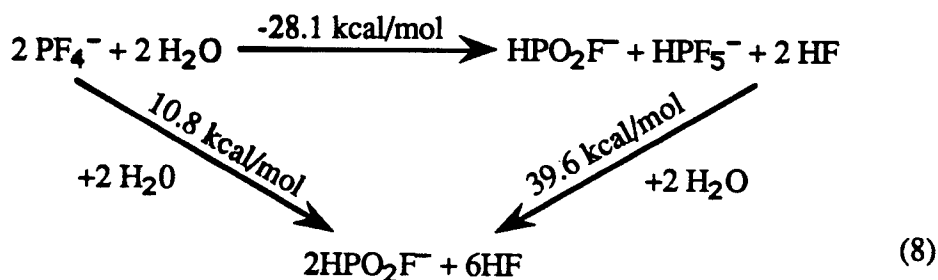
12

density functional (NLDFT/TZVP), and Hartree Fock (HF/DZP+) levels of theory. As can be seen from Table 3, the HF/DZP+ calculation predicts best the experimental geometry of SOF_2[32] and the resulting bond lengths are slightly shorter than the experimentally observed ones. As expected, the density functional theory calculations can predict well the bond angles, but the resulting bond lengths are about 0.05Å longer than the experimentally observed ones. Another test for the quality of our calculations is a comparison of the calculated and observed vibrational frequencies. As can be seen from Tables 4 and 5, the LDFT frequencies, after appropriate scaling to compensate for the overestimation of the bond lengths, yield the best prediction of the experimentally observed values and establish their assignments. The calculated force fields and potential energy distributions are given in Tables 6-9. The valence force constants are summarized in Table 10 and show that within the XOF_2 series, SOF_2 exhibits the strongest bonds and that the bonds in HXO_2F are stronger than those in the corresponding XOF_2 species which is in line with the calculated bond lengths.

The successful synthesis of a stable POF_2^- salt is in accord with the well known stabilities of the isoelectronic species SOF_2, PF_3, SO_2F^-, and SF_3^+ all of which possess 26 valence electrons and with a previous value of 56±4 kcal/mol for the F^- affinity of POF, determined by ion cyclotron resonance spectroscopy.[6] The relative F^- affinities of the various phosphorus species involved in the present study (7a) were obtained by subtracting the experimentally known[6] value of 42.6 kcal/mol for (7b) from the reaction enthalpies, ΔH, of 7(c) which were calculated from the total energies of their components using the DZP+ basis set. The results are summarized in Table 11 and agree well with the available experimental data.[6]. Table 11 shows that all these molecules possess sufficiently high F^-

13

$$A + F^- \longrightarrow AF^- \tag{7a}$$

$$COF_3^- \xrightarrow{\text{42.6 kcal/mol}} COF_2 + F^- \tag{7b}$$

$$A + COF_3^- \xrightarrow{\Delta H} AF^- + COF_2 \tag{7c}$$

all these molecules possess sufficiently high F^- affinities for the formation of stable salts and that FPO and HPO_2 are stronger Lewis acid than either PF_3, HF, POF_3, or SO_2 (F^- affinity of SO_2 = 44 kcal/mol)[6].

The reaction enthalpies of the hydrolysis reactions of HPF_5^- and of PF_4^- with either equimolar amounts or excess of H_2O were also estimated from the heats of formation of the gaseous species calculated with the DZP+ basis set. As can be seen from the Born Haber cycle (8), the calculated values for the two paths are practically identical, thus demonstrating

$$2\,PF_4^- + 2\,H_2O \xrightarrow{\text{-28.1 kcal/mol}} HPO_2F^- + HPF_5^- + 2\,HF$$

$+2\,H_2O$ ↘ 10.8 kcal/mol   39.6 kcal/mol ↙ $+2\,H_2O$

$$2HPO_2F^- + 6HF \tag{8}$$

the consistency of these calculations. The endothermicity of the hydrolysis of HPF_5^- is also in accord with the experimentally observed slowness of this reaction.

14

REFERENCES

†Dedicated to Prof. Reinhard Schmutzler on the occasion of his 60th birthday.

1. Rockwell International

2. DuPont, contribution No. 6869

3. McMaster University

4. Christe, K.O.; Dixon, D.A.; Mercier, H.P.A.; Sanders, J.C.P.; Schrobilgen, G.J.; Wilson, W.W. *J. Am. Chem. Soc.* 1994, **116**, 2850.

5a. Although the free POF_2^- anion was unknown, the existence of the $-P(O)F_2$ ligand in transition metal complexes had been well known from the publications of R. Schmutzler and coworkers (Grosse, J.; Schmutzler, R. *Z. Naturforsch.* 1973, **28b**, 515; *J. Chem. Soc. Dalton*, 1976, 405 and 412; *Acta Cryst.* 1974, **B30**, 1623; Neumann, S.; Schomburg, D.; Schmutzler, R. *J. Chem. Soc. Chem. Comm.* 1979, 848; Hietkamp, S.; Schmutzler, R. *Z. Naturforsch.* 1980, **35b**, 548; Krüger, W.; Sell, M.; Schmutzler, R. *Z. Naturforsch.* 1983, **38b**, 1074; Plinta, H.J.; Gereke, R.; Fischer, A.; Jones, P.G.; Schmutzler, R. *Z. Naturforsch.* 1993, **48b**, 737).

5b. Ebsworth, E.A.V.; Page, P.G.; Rankin, W.H. *J. Chem. Soc. Dalton Trans.* 1984, 2569.

6. Larson, J.W.; McMahon, T.B. *Inorg. Chem.* 1987, **26**, 4018; *J. Am. Chem. Soc.* 1983, **105**, 2944.

7. Schülke, U.; Kayser, R. *Z. Anorg. Allg. Chem.* 1991, **600**, 221.

8. Blaser, B.; Worms, K.H. *Z. Anorg. Allg. Chem.* 1968, **360**, 117.

9. Falius, H. *Angew. Chem. Internat. Edit. Engl.* 1970, **9**, 733; and Ahrens, H.; Falius, H. *Chem. Ber.* 1972, **105**, 3317.

10. Nixon, J.F.; Swain, J.R. *Inorg. Nucl. Chem. Letters*, 1969, **5**, 295.

11. Nixon, J.F.; Swain, J.R. *J. Chem. Soc. A* 1970, 2075.

12. McFarlane, W.; Nixon, J.F.; Swain, J.R. *Mol. Phys.* 1970, **19**, 141.

13. Cowley, A.H.; Wisian, P.J.; Sanchez, M. *Inorg. Chem.* 1977, **16**, 1451.

14. Minkwitz, R.; Liedtke, A. *Z. Naturforsch. B* 1989, **44B**, 679.

15. Lindemann, D.; Riesel, L. *Z. Anorg. Allg. Chem.* 1992, **615**, 66; and Riesel L.; Kant, M. *Z. Chem.* 1984, **24**, 382.

16. Christe, K.O.; Dixon, D.A.; Wilson, W.W. *J. Am. Chem. Soc.* in press.

17. Christe, K.O.; Curtis, E.C.; Dixon, D.A.; Mercier, H.P.; Sanders, J.C.P.; Seppelt, K.; Schrobilgen, G.J.; Wilson, W.W. *J. Am. Chem. Soc.* 1991, **113**, 3351.

18. (a) Christe, K.O.; Wilson, R.D.; Wilson, W.W.; Bau, R.; Sukumar, S.; Dixon, D.A. *J. Am. Chem. Soc.* 1991, **113**, 3795. (b) Dixon, D.A.; Andzelm. J.; Fitzgerald, G.; Wimmer, E.; Jasien, P. In Density Functional Methods in Chemistry; Labanowski, J.; Andzelm. J., Eds.; Springer Verlag: New York, 1991; p. 33. (c) Dixon, D.A.; Christe, K.O. *J. Phys. Chem.* 1992, **96**, 1018. (d) Delley, B. *J. Chem. Phys.* 1990, **92**, 508. DMol is available commercially from BIOSYM Technologies, San Diego, CA. A FINE grid was used.

19. (a) Andzelm, J.; Wimmer, E.; Salahub, D.R. in "The Challenge of d and f Electrons: Theory and Computation"; Eds Salahub, D.R.; Zerner, M.C. ACS Symposium Series, No. 394, American Chemical Society, Washington, D.C. 1989, p.228. (b) Andzelm, J. in "Density Functional Methods in Chemistry", Labanowski, J., Andzelm, J., Eds.; Springer Verlag: New York, 1991, p.101. (c) Andzelm, J.W.; Wimmer, E. *J. Chem. Phys.* 1992, **96**, 1280. DGauss is a local density functional program available via the Cray Unichem Project.

20. Godbout, N.; Salahub, D.R.; Andzelm, J.; Wimmer, E. *Can. J. Chem.* 1992, **70**, 560.

21. (a) Becke, A.D., *Phys. Rev. A* 1988, **38**, 3098. (b) Becke, A.D. in "The Challenge of d and f Electrons: Theory and Computation", Salahub, D.R.; Zerner, M.C., Eds.; ACS Symposium Series No. 394, American Chemical Society, Washington, D.C.

1989, P.166. (c) Becke, A.D. *Inter. J. Quantum Chem. Quantum. Chem. Symp.* 1989, **23**, 599.

22. Perdew, J.P. *Phys. Rev. B* 1986, **33**, 8822.

23. (a) GRADSCF is an ab initio program system designed and written by A. Komornicki at Polyatomics Research. (b) Komornicki, A.; Ishida, K.; Morokuma, K.; Ditchfield, R.; Conrad, M. *Chem. Phys. Lett.* 1977, **45**, 595. (c) McIver, J.W., Jr.; Komornicki, A. *Chem. Phys. Lett.* 1971, **10**, 202. (d) Pulay, P. in "Applications of Electronic Structure Theory," Schaefer, H.F. III, Ed.; Plenum Press: New York, 1977, p.153; (e) King, H.F.; Komornicki, A. *J. Chem. Phys.* 1986, **84**, 5465. (f) King, H.F.; Komornicki, A. in "Geometrical Derivatives of Energy Surfaces and Molecular Properties", Jorgenson, P.; Simons, J., Eds. NATO ASI Series C. Vol. 166, D. Reidel: Dordrecht 1986, p.207.

24. (a) Dunning, T.H., Jr.; Hay, P.J. in "Methods of Electronic Structure Theory," Schaefer, H.F., III, Ed., Plenum Press: New York, 1977, Ch. 1 for F, H and O basis sets and for diffuse functions; (b) McLean, A.D.; Chandler, G.S. *J. Chem. Phys.* 1980, **72**, 5639 for P, S, and Cl basis sets.

25. Ref (b)-(f) of Ref 23.

26. Gutowsky, H.S.; McCall, D.W.; Slichter, C.P. *J. Chem. Phys.* 1953, **21**, 279; Gutowsky, H.S.; McCall, D.W.; Slichter, C.P. *J. Chem. Phys.* 1954, **22**, 162; Martin, D.R.; Pizolato, P.J. *J. Am. Chem. Soc.* 1950, **72**, 4584.

27. Christe, K.O.; Wilson, W.W. *J. Fluorine Chem.* 1990, **46**, 339.

28. Christe, K.O.; Dixon, D.A.; Wilson, W.W.; Schrobilgen, G.J. to be published.

29. Lustig, M.; Ruff, J.K. *Inorg. Chem.* 1967, **6**, 2115.

30. Cameron, J.H.; McLennan, A.J.; Rycroft, D.S.; Winfield, J.M. *J. Fluorine Chem.* 1981, **19**, 135, and references cited therein; Reddy, G.A.; Schmutzler, R. *Z. Naturforsch.* 1970, **25b**, 1199.

31. Kwiatkowski, J.S.; Leszczynski, J. *J. Mol Struct.* 1992, **258**, 287, and references cited therein.

32. Lucas, N.J.D.; Smith, J.G. *J. Mol. Spectrosc.* 1972, **43**, 327.

33. Boyd, R.J.; Szabo, J.P. *Can. J. Chem.* 1982, **60**, 730.

34. (a) Shimanouchi, T. *J. Phys. Chem. Ref. Data* 1977, **6**, 993. (b) Pace, E.L.; Samuelson, H.V. *J. Chem. Phys.* 1966, **44**, 3682.

35. O'Hara, T.J.; Noftle, R.E. *J. Fluorine Chem.* 1982, **20**, 149.

36. Christe, K.O.; Curtis, E.C.; Schack, C.J. *Inorg. Chem.* 1972, **11**, 2212.

Figure 1. ^{31}P NMR spectrum (202.459 MHz) of a sample containing equimolar quantities of $N(CH_3)_4PF_4$ and H_2O (oxygen isotopic composition: ^{16}O,35.4%; ^{17}O, 21.9%; ^{18}O, 42.7%) in CH_3CN. (a) At -45°C: (A) POF_2^-; (B) PF_3; (C) HPO_2F^-; (D) HPF_5^-; (E) $[HPF_4(OH)]^-$? (b) same region at 30°C; (c) at 30°C: expansion of HPO_2F^- multiplet revealing $^{16,18}O$ isotope shifts arising from the $HP^{16}O_2F^-$, $HP^{16}O^{18}OF^-$ and $HP^{18}O_2F^-$ isotopomers. The equal-intensity sextet satellites at the bases of the four main components of the multiplet arise from coupling to ^{17}O in the $HP^{16}O^{17}OF^-$ and $HP^{17}O^{18}OF^-$ isotopomers.

Figure 2. ^{17}O NMR spectrum (67.801 MHz) of the same sample as in Figure 1 at 30°C. (A) POF_2^-; (B) HPO_2F^-. Insert shows a resolution enhanced expansion of the HPO_2F^- multiplet and displays the fine structure arising from the $^2J(^{17}O\text{-}^1H)$ and $^2J(^{17}O\text{-}^{19}F)$ couplings which have similar magnitudes ($\approx$12 Hz).

Figure 3. ^{19}F NMR spectrum (470.599 MHz) of the same sample as in Figure 1 at 30°C. (A) HPO_2F^-; (B) F_{eq} HPF_5^- (C) F_{ax} HPF_5^-. Expansion displays two-bond $^{16,18}O$ isotope shifts arising from the $HP^{16}O_2F^-$, $HP^{16}O^{18}OF^-$ and $HP^{18}O_2F^-$ isotopomers.

Figure 4. ^{31}P NMR spectrum (202.459 MHz) of a sample containing equimolar quantities of $N(CH_3)_4PF_4$ and H_2O (oxygen isotopic composition: ^{16}O, 35.4%; ^{17}O, 21.9%; ^{18}O, 42.7%) and a 2.6 molar excess $N(CH_3)_4F$ in CH_3CN at -45°C. (A) POF_2^-; (B) PF_4^-; (C) HPF_5^-.

Figure 5. ^{31}P NMR spectrum (202.459 MHz) of the same sample as in Figure 4 at 30°C. Expansion of POF_2^- multiplet revealing $^{16,18}O$ isotope shifts arising from the $P^{16}OF_2^-$ and $P^{18}OF_2^-$ isotopomers. The equal-intensity sextet satellites at the

bases of the three main components of the multiplet arise from coupling to ^{17}O in the $P^{17}OF_2^-$.

Figure 6. ^{17}O NMR spectrum (67.801 MHz) of the same sample as in Figure 4 at 30°C. A (POF_2^-); B(HPO_2F^-).

Figure 7. Infrared spectrum of solid $N(CH_3)_4HPO_2F$ recorded as an AgBr disk at room temperature. The bands marked by an asterisk are due to $N(CH_3)_4^+$ and their assignments have previously been discussed in Ref. 17.

Figure 8. Infrared spectrum of solid $N(CH_3)_4POF_2$ recorded as an AgBr disk at room temperature. The bands marked by an asterisk are due to $N(CH_3)_4^+$.

a

D + E

C

B

A

10,000 Hz

$\delta_{31}P$ (ppm from H_3PO_4)

100   50   0   -50   -100   -150

b

10,000 Hz

POF_2^-

HPO_2F^-

HPF_5^-

$\delta_{^{31}P}$ (ppm from H_3PO_4)

120   80   40   0   -40   -80   -120   -160

C

$HP^{16}O^{18}OF^-$

$HP^{18}O_2F^-$

$HP^{16}O_2F^-$

1000 Hz

δ_{31P} (ppm from H_3PO_4)

-8   -6   -4   -2   0   2   4   6

$\delta_{17}O$ (ppm from H_2O)

$^{16}O^{18}O$

$^{18}O_2$

$^{16}O_2$

2000 Hz

B

A

C

$\delta_{^{19}F}$ (ppm from CFCl$_3$)

-52   -54   -56   -58   -60   -62   -64   -66   -68

10,000 Hz

B

A

C

$\delta_{31}P$ (ppm from H_3PO_4)

150   100   50   0   -50   -100   -150

1000 Hz

$P^{16}OF_2^-$

$P^{18}OF_2^-$

135   130   125   120

δ_{31P} (ppm from H_3PO_4)

1000 Hz

A

B
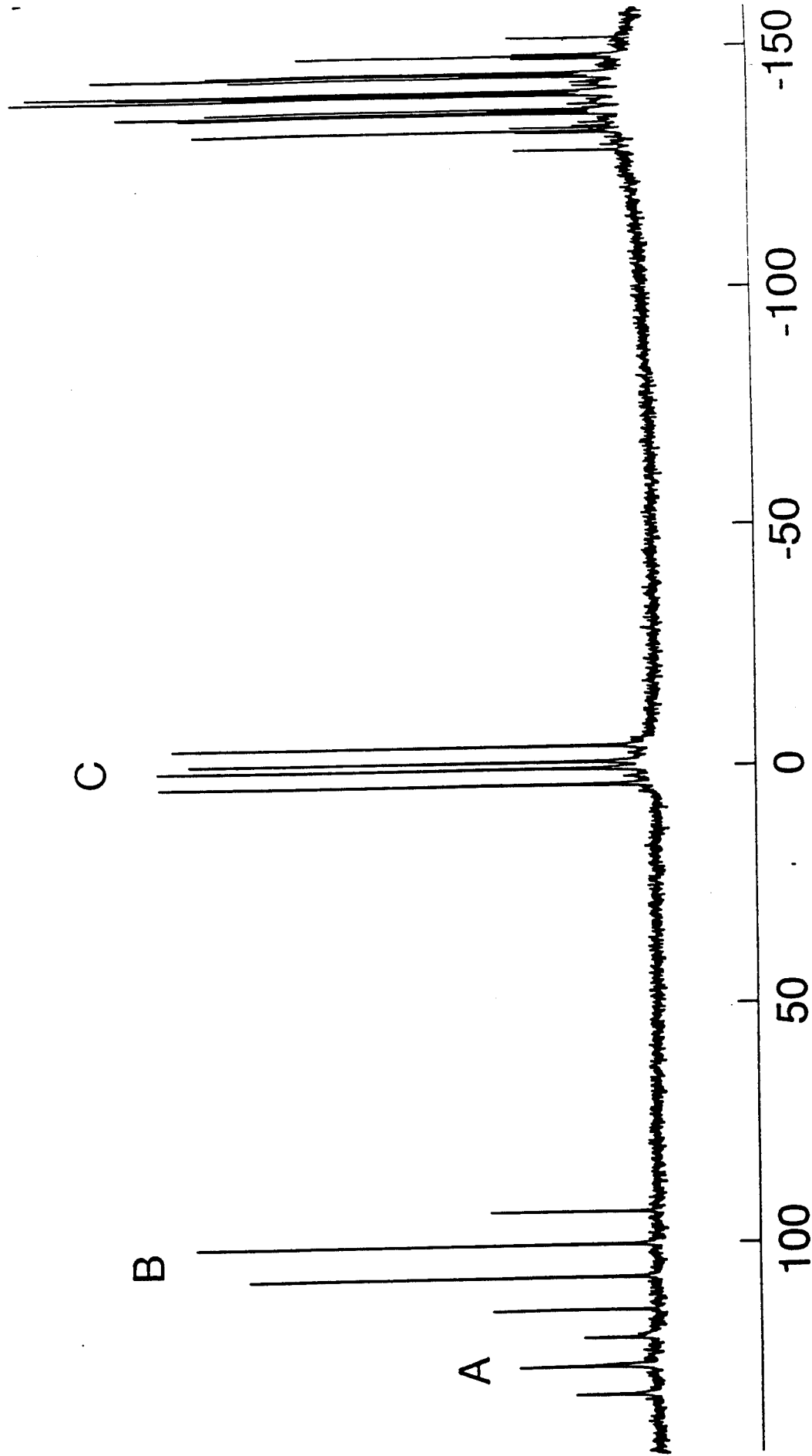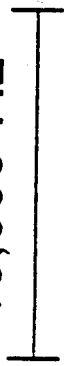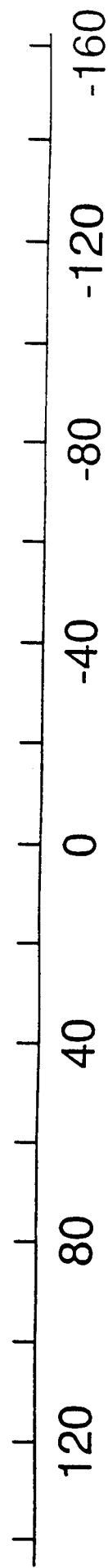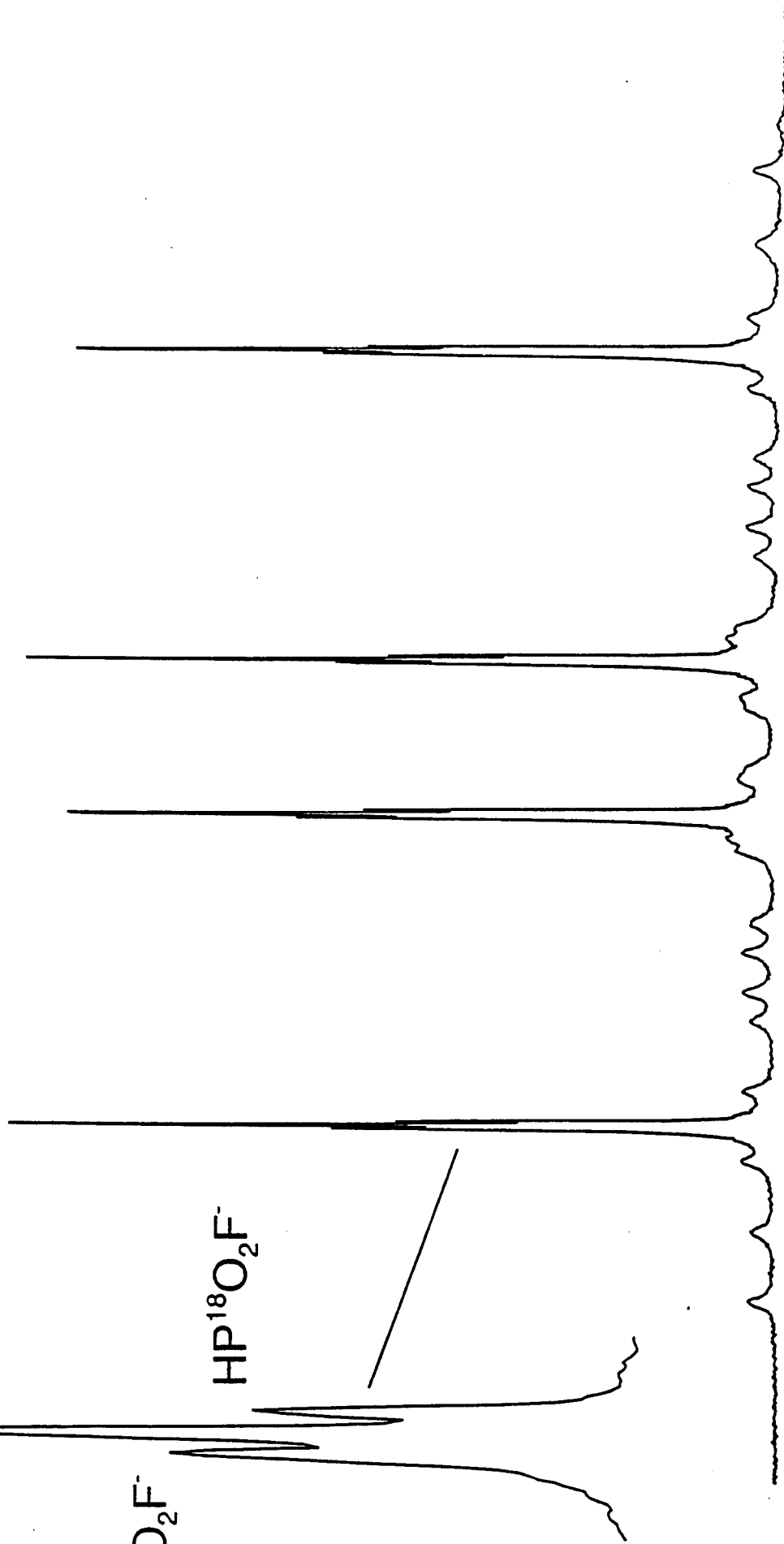
$\delta_{17}O$ (ppm from H_2O)
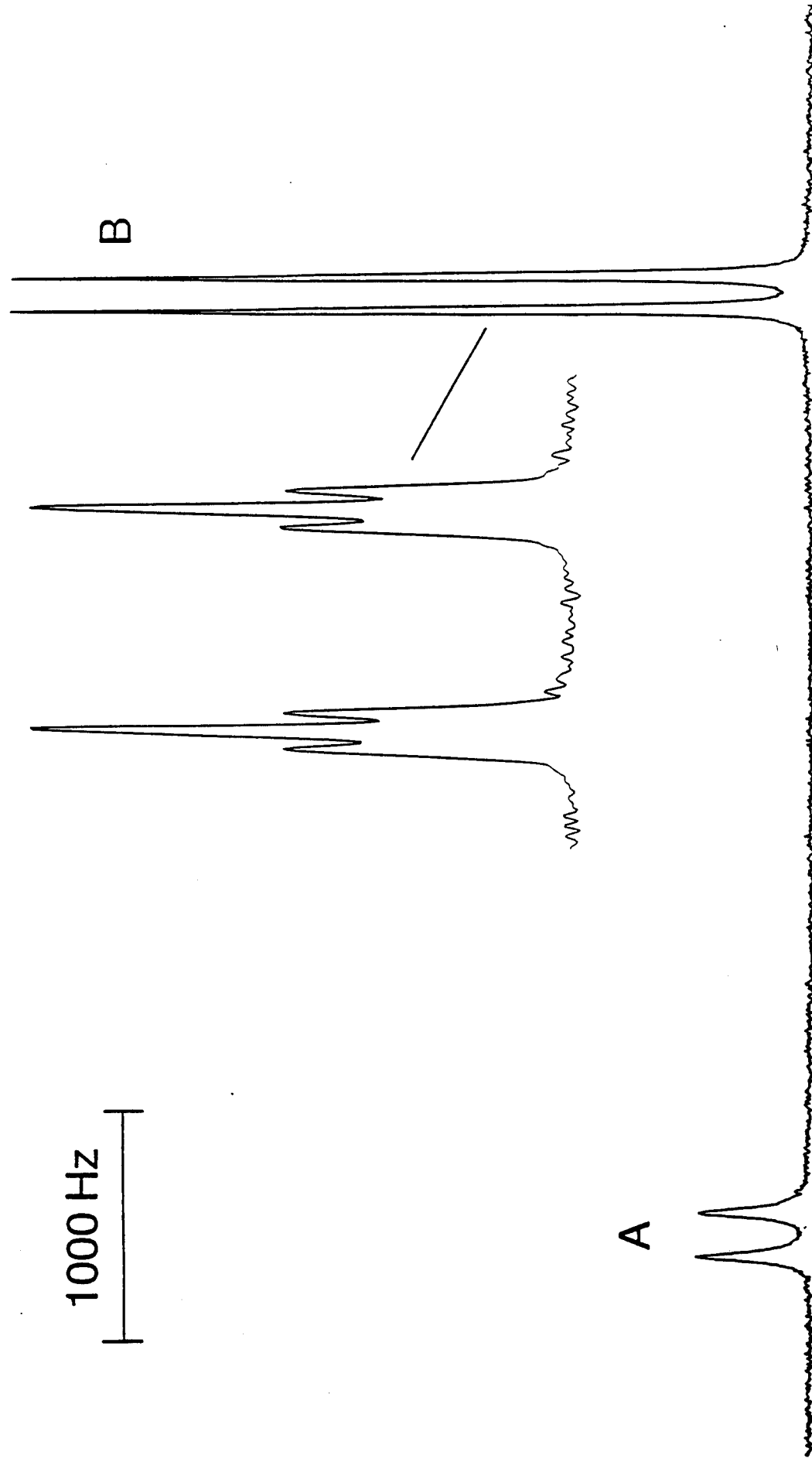
220 210 200 190 180 170 160 150 140 130

$[(CH_3)_4N]^+ HPO_2F^-$

Peaks labeled (reading from spectrum): 392, 427, 539, 755, 866, 998, 1029, 1110, 1279, 2374

TRANSMITTANCE

FREQUENCY (cm^{-1})

$[(CH_3)_4 N]^+ POF_2^-$
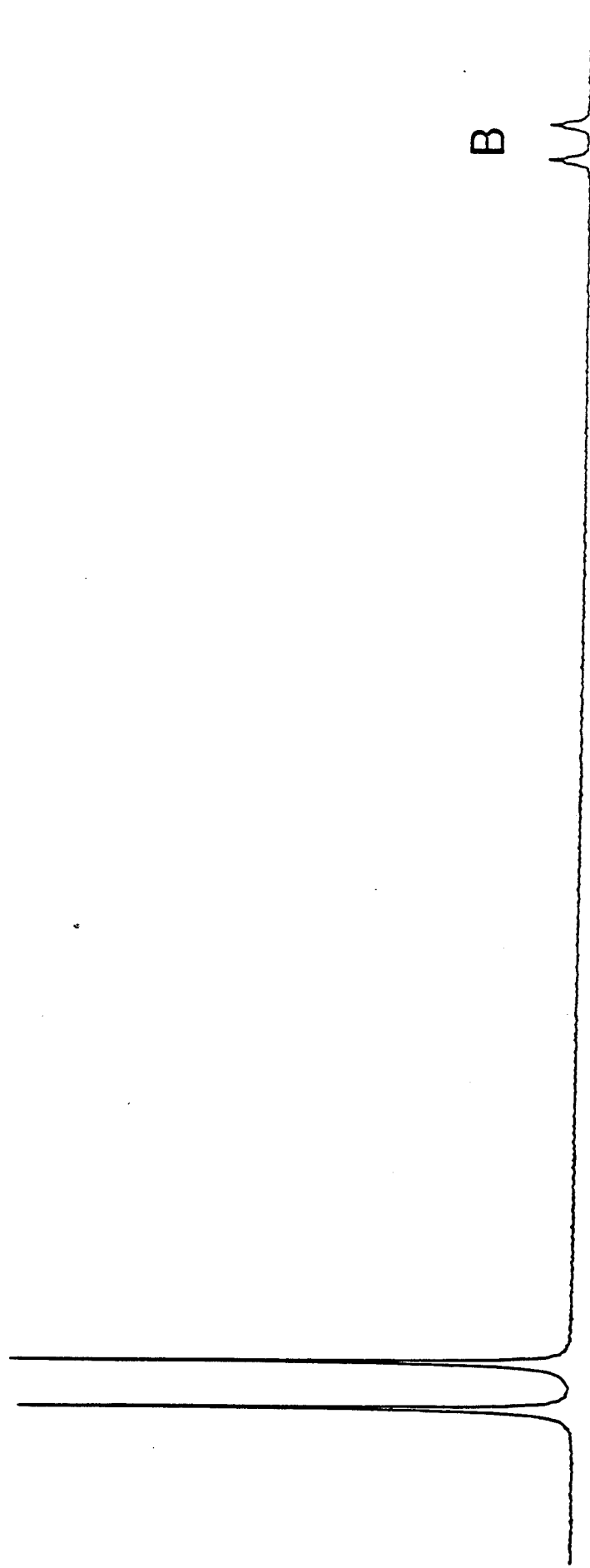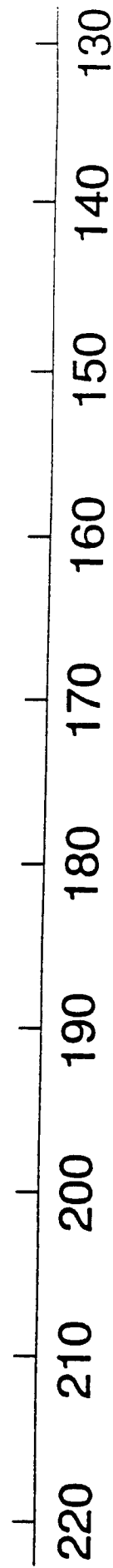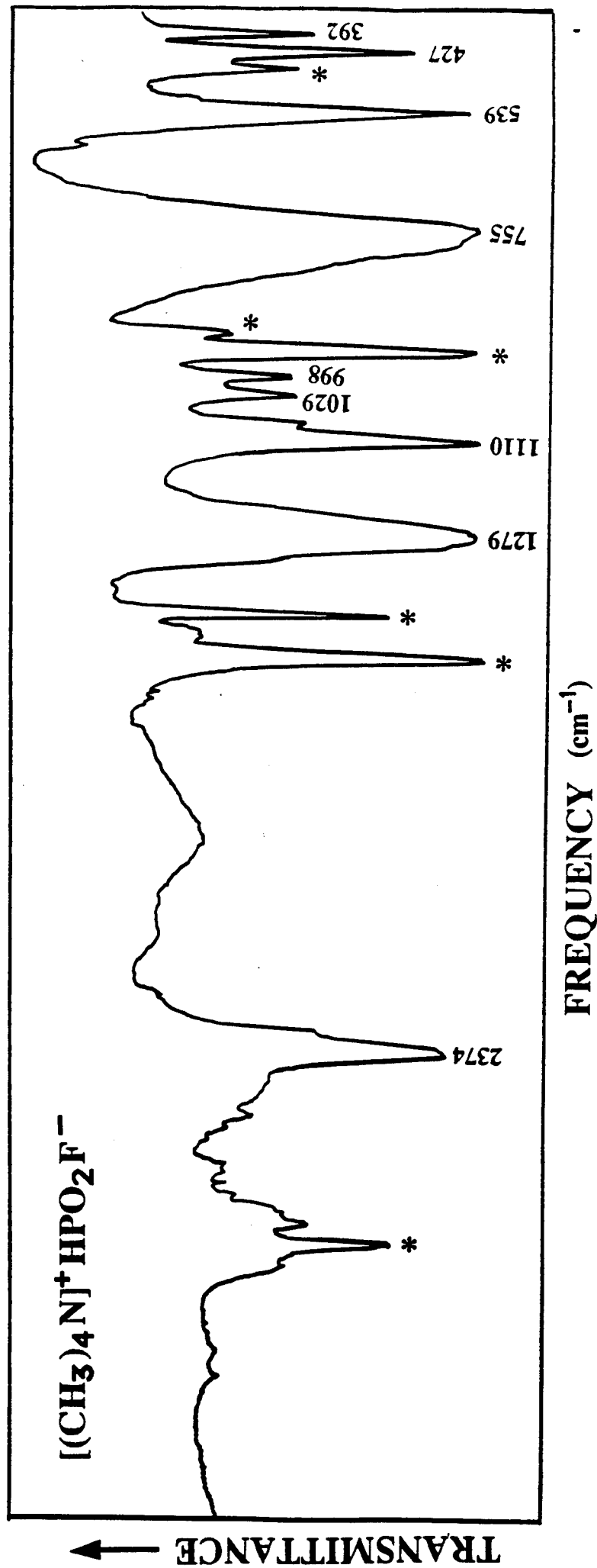
TRANSMITTANCE →

FREQUENCY (cm^{-1})

1148

*

*

691

610

482

*

351

332
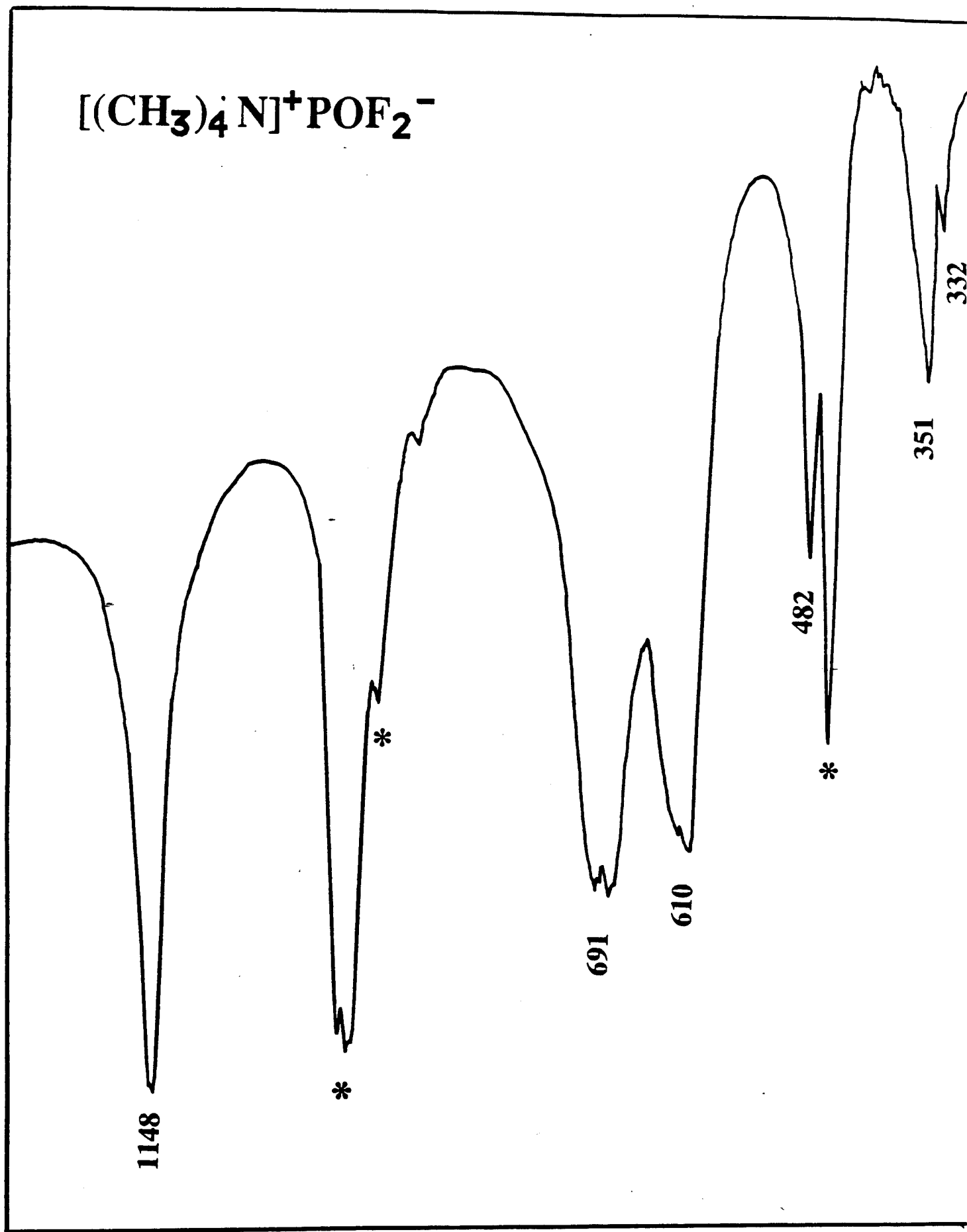
Table 1. NMR Parameters for the $HPF_5{}^-$, HPO_2F^- and $POF_2{}^-$ Anions Produced in the Hydrolysis of $N(CH_3)_4PF_4$

ANION	TEMP °C	$\delta(^{31}P)$, ppm	$\delta(^{19}F)$, ppm	$\delta(^{17}O)$, ppm	$^1J(^{31}P\text{-}^{19}F)$, Hz	$^1J(^{31}P\text{-}^{17}O)$, Hz	$^1J(^{31}P\text{-}^1H)$, Hz	$^2J(^1H\text{-}^{19}F)$, Hz
$HPF_5{}^-$ [a]	30	-140.2	-66.6 (F_a)		731 (F_a)		939	
			-55.8 (F_e)		817 (F_e)			127(F_e)
HPO_2F^-	30[b]	-0.7	-53.6	131.8[c]	947	145	636	127
	-36[b]			117		131		
	-45[b]	-0.5			967		684	
	30[d]			136.4		148		
$POF_2{}^-$	30[b]	127.2	-7.5	191.4	1200	187		
	30[d]	129.1		211.9	1183	189		
	-45[d]	129.4		211.8	1184			

a) F_a and F_e refer to the axial and equatorial fluorine ligand environments, respectively; $^2J(F_a\text{-}F_e) = 42$ Hz. The NMR parameters of $HPF_5{}^-$ exhibited only a very small temperature and F^- ion dependence between 30°C and -45°C.

b) No $N(CH_3)_4F$ added.

c) $^2J(^{17}O\text{-}^{19}F) \approx {}^2J(^{17}O\text{-}^1H) \approx 11.8$Hz.

d) Recorded in the presence of a 2.6 molar excess of $N(CH_3)_4F$.

Table 2. Calculated Geometries of HPO_2F^- and HSO_2F

	HPO_2F^-			HSO_2F		
	LDFT	NLDFT/TZVP	HF/DZP+	LDFT	NLDFT/TZVP	HF/DZP+
rXO (Å)	1.506	1.514	1.474	1.444	1.456	1.407
rXF (Å)	1.661	1.679	1.609	1.612	1.643	1.549
rXH (Å)	1.437	1.444	1.401	1.371	1.379	1.326
∡ OXO or FXF (deg)	125.6	125.2	123.9	125.2	124.5	123.4
∡ OXH (deg)	106.8	106.7	107.1	107.1	107.0	107.7
∡ OXH (deg)	109.2	109.5	109.5	109.2	109.8	109.9
∡ FXH (deg)	94.5	94.9	96.0	94.6	94.4	95.8

Table 3. Calculated and Experimental Geometries for the Isoelectronic Series POF$_2^-$, SOF$_2$, and ClOF$_2^+$

	POF$_2^-$			SOF$_2$				ClOF$_2^+$		
	LDFT	NLDFT/TZVP	HF/DZP+	LDFT	NLDFT/TZVP	HF/DZP+	EXP[a]	LDFT	NLDFT/TZVP	HF/DZP+
rXO (Å)	1.522	1.522	1.481	1.456	1.457	1.409	1.413	1.431	1.440	1.374
rXF (Å)	1.717	1.733	1.653	1.647	1.657	1.570	1.585	1.625	1.652	1.535
∠FXF (deg)	90.8	91.2	91.4	92.7	92.9	92.5	92.83	94.9	95.6	93.4
∠OXF (deg)	105.3	105.6	105.0	106.8	107.0	106.4	106.82	109.6	109.2	108.8

a) Data from Ref. 31.

Table 4. Vibrational Frequencies of HPO_2F^- and HSO_2F

Assignment in Point Group C_s	Approximate Mode Description	HPO_2F^- Observed[a] cm^{-1} (int) IR	RA	HPO_2F^- Calcd (IR int) LDFT[b]	NLDFT/TZVP[d]	HF/DZP+[e]	HSO_2F Calcd (IR int)[f] LDFT	NLDFT/TZVP	HF/DZP+
A' ν_1	νXH	2374s	2370(2.4)	2352	2376(248)	2321(312)	2634	2615(24)	2646(19)
ν_2	ν sym XO_2	1110s	1110(10)	1114	1128(147)	1098(236)	1220	1220(113)	1213(193)
ν_3	δ sciss HXF	998w	1000(0.3)	1006	1013(23)	1076(50)	1095	1074(2.2)	1125(5.9)
ν_4	νXF	755vs	754[c]	728	710(213)	732(269)	803	753(206)	833(262)
ν_5	δ rock XO_2	539ms	540(1)	550	533(59)	540(119)	603	565(54)	591(102)
ν_6	δ sciss XO_2	427m	427(0+)	425	419(14)	421(33)	466	449(10)	466(32)
A" ν_7	ν asym XO_2	1279vs	1281(0.5)	1342	1341(358)	1280(544)	1485	1466(260)	1428(425)
ν_8	δ wag XH	1029w	1029(0.5)	1023	1049(20)	1061(45)	1121	1126(2.0)	1159(8.4)
ν_9	δ wag XF	392mw		384	392(7.4)	384(14)	417	412(13)	464(23)

a) Frequencies are for the solid $N(CH_3)_4^+$ salt from this study. The following infrared band have previously been reported in Ref. 9; Li(HPO₂F): 2462vs, 1247vs, 1137vs, 1053s, 1010vs, 857vs, 565s, 479s, 372s; Li(DPO₂F): 1747s, 1241vs, 1140vs, 855vs, 776s, 742s, 560s, 478s, 381s.

b) Empirical scaling factors used to maximize the fit between observed and calculated frequencies: stretching modes: 1.039; deformation modes 1.121.

c) Coincides with intense $\nu_3(A_1)$ band of $N(CH_3)_4^+$.

d) Empirical scaling factors of 1.0699 and 1.0890 were used for the stretching and deformation modes, respectively.

e) An empirical scaling factor of 0.9133 was used.

f) The same scaling factors were used as for HPO_2F^-.

Table 5. Vibrational Spectra of Isoelectronic POF_2^-, SOF_2, and $ClOF_2^+$

Assignment in Point Group C_s	Approximate Mode Description	POF_2^- obsd[a] IR	RA	calcd (IR int) LDFT[b]	NLDFT/ TZVP[c]	HF/ DZP+[d]	SOF_2 obsd[e] IR	RA	calcd (IR int) LDFT[f]	NLDFT/ TZVP[g]	HF/ DZP+[h]	$ClOF_2^+$ obsd[l] IR	RA	calcd LDFT[k]	NLDFT/ TZVP[l]	HF/ DZP+[m]
A' ν_1	νXO	1148vs	1146	1158	1235(184)	1165(317)	1340.8s 1330.9s	1339.3vs 1329.9vs	1333	1388(147)	1309(263)	1331ms	1333(2)	1265	1307(67)	1253(182)
ν_2	ν sym XF_2	691vs		678	675(220)	686(330)	808.2vs	808.3vs	801	802(177)	815(259)	750br,s	757br(3)	747	748(84)	794(119)
ν_3	δ sym F_2XO	482m		476	486(17)	480(32)	530.4m	529.6s	535	549(23)	534(46)	509ms	511(2)	532	541(22)	509(42)
ν_4	δ sciss XF_2	332w		330	316(0.9)	329(2.4)	377.8w	379.5w	372	354(3.5)	379(8.9)	378sh	378sh(1)	374	348(5.4)	369(6.9)
A" ν_5	ν asym XF_2	610s		616	583(202)	613(269)	747.0vs	746.8w	756	726(212)	757(277)	695vs	696(1)	745	716(133)	776(162)
ν_6	δ asym OXF_2	351mw		358	367(0.3)	351(5.6)	392.5w	398.6w	398	408(2.4)	390(9.0)	407sh	406(2)	394	419(2.8)	382(16)

a) Frequencies are for the solid $N(CH_3)_4^+$ salt from the present study.
b) Using empirical scaling factors of 1.0162 and 1.1650 for the stretching and deformation modes, respectively, to maximize the fit between observed and calculated frequencies.
c) Using empirical scaling factors of 1.0951 and 1.1615 for the stretching and deformation modes, respectively.
d) Using an empirical scaling factor of 0.91115 for all modes.
e) Data from Ref. 33-35.
f) Using empirical scaling factors of 1.0438 and 1.1840 for the stretching and deformation modes, respectively.
g) Using empirical scaling factors of 1.0996 and 1.1698 for the stretching and deformation modes, respectively.
h) Using an empirical scaling factor of 0.9006.
i) Data from Ref. 36.
k) Using empirical scaling factors of 0.9919 and 1.2080 for the stretching and deformation modes, respectively.
l) Using empirical scaling factors of 1.0577 and 1.2555 for the stretching and deformation modes, respectively.
m) Using an empirical scaling factor of 0.8694.

Table 6. Scaled LDFT Force Fields[a] for HPO_2F^- and HSO_2F

HPO_2F^-

A'

	F_{11}	F_{22}	F_{33}	F_{44}	F_{55}	F_{66}
F_{11}	3.201					
F_{22}	0.093	9.457				
F_{33}	0.086	-0.068	1.489			
F_{44}	0.101	0.186	0.154	3.787		
F_{55}	0.124	0.071	1.387	-0.409	4.340	
F_{66}	-0.007	0.132	0.570	-0.377	2.015	2.469

A"

	F_{77}	F_{88}	F_{99}
F_{77}	9.405		
F_{88}	0.259	0.672	
F_{99}	0.222	0.129	1.134

HSO_2F

A'

	F_{11}	F_{22}	F_{33}	F_{44}	F_{55}	F_{66}
F_{11}	3.977					
F_{22}	-0.092	11.227				
F_{33}	-0.029	-0.039	1.668			
F_{44}	-0.019	-0.056	0.206	4.649		
F_{55}	-0.079	0.187	1.624	-0.370	4.909	
F_{66}	-0.031	0.156	0.667	-0.390	2.225	2.697

A"

	F_{77}	F_{88}	F_{99}
F_{77}	11.713		
F_{88}	0.259	0.738	
F_{99}	0.237	0.132	1.249

a) Stretching constants in mdyn/Å, deformation constants in mdyn Å/rad², and stretch-bend interaction constants in mdyn/rad. The following scaling factors were used: Stretching force constants, $(1.039)^2$; deformation constants, $(1.121)^2$; stretch-bend interaction constants, 1.039 x 1.121.

Table 7. Scaled[a] LDFT Force Fields for POF_2^-, SOF_2, and $ClOF_2^+$

POF_2^-

	F_{11}	F_{22}	F_{33}	F_{44}			F_{55}	F_{66}
A' F_{11}	8.338				A" F_{55}	F_{55}	2.464	
F_{22}	0.344	2.886			F_{66}		0.018	1.210
F_{33}	0.118	-0.070	1.874					
F_{44}	0.024	0.045	0.478	1.631				

SOF_2

	F_{11}	F_{22}	F_{33}	F_{44}			F_{55}	F_{66}
A' F_{11}	11.120				A" F_{55}	F_{55}	3.823	
F_{22}	0.203	4.293			F_{66}		0.079	1.365
F_{33}	0.156	-0.090	2.196					
F_{44}	-0.039	0.071	0.601	1.823				

$ClOF_2^+$

	F_{11}	F_{22}	F_{33}	F_{44}			F_{55}	F_{66}
A' F_{11}	10.018				A" F_{55}	F_{55}	3.850	
F_{22}	-0.310	4.096			F_{66}		0.180	1.176
F_{33}	0.019	-0.045	2.212					
F_{44}	-0.121	0.138	0.563	1.717				

a) Using the squares and the product of the scaling factors, given in Table 5, for the stretching, deformation, and stretch-bend interaction constants, respectively.

Table 8. Potential Energy Distributions for HPO_2F^- and HSO_2F

		HPO_2F^-		HSO_2F
		freq, cm^{-1}	PED, %	freq, cm^{-1}	PED, %
A'	ν_1	2352	99.8(1)	2634	99.6(1)
	ν_2	1114	67.2(2) + 17.4(3) + 10.8(6) + 4.5(4)	1220	65.4(2) + 16.7(3) + 11.6(6) + 5.8(4)
	ν_3	1006	81.1(3) + 18.6(5)	1095	80.4(3) + 19.3(5)
	ν_4	728	90.4(4) + 5.0(5) + 4.0(6) + 0.4(2)	803	89.1(4) + 6.7(5) + 3.0(6) + 1.0(2)
	ν_5	550	49.2(5) + 40.9(6) + 8.4(3) + 1.1(4)	603	46.6(5) + 40.5(6) + 10.6(3) + 1.8(4)
	ν_6	425	76.8(6) + 16.3(3) + 5.2(5) + 1.7(4)	466	78.3(6) + 14.7(3) + 5.5(5) + 1.5(4)
A"	ν_7	1342	69.3(7) + 20.0(8) + 10.7(9)	1485	69.2(7) + 19.8(8) + 11.0(9)
	ν_8	1023	99.8(8)	1121	99.9(8)
	ν_9	384	93.2(9) + 6.8(8)	417	94.0(9) + 6.0(8)

Table 9. Potential Energy Distributions for POF_2^-, SOF_2, and $ClOF_2^+$

		POF_2^-		SOF_2		$ClOF_2^+$
		freq, cm^{-1}	PED, (%)	freq, cm^{-1}		freq, cm^{-1}
A'	ν_1	1158	89.8(1)+7.9(3)+1.3(2)+1(4)	1333	88.5(1)+7.3(3)+2.6(2)+1.6(4)	1265	86.2(1)+6.0(3)+5.4(2)+2.4(4)
	ν_2	678	73.7(2)+13.5(4)+12.7(3)	801	76.0(2)+12.7(4)+11.2(3)	747	80.7(2)+9.8(4)+8.4(3)+1.1(1)
	ν_3	476	84.1(3)+9.7(2)+5.9(4)	535	86.8(3)+7.4(4)+5.7(2)	532	91.8(3)+5.2(4)+2.8(2)
	ν_4	330	78.6(4)+20.9(3)+0.5(2)	372	78.7(4)+21.0(3)+0.2(2)	374	83.7(4)+16.1(3)
A"	ν_5	616	84.5(5)+15.5(6)	756	84.8(5)+15.2(6)	745	86.7(5)+13.3(6)
	ν_6	358	97.7(6)+2.3(5)	398	99.0(6)+1.0(5)	394	99.8(6)

Note: The SOF$_2$ and ClOF$_2^+$ sections each also have a PED, (%) column header (labeled as part of their spanning headers) containing the values shown in the rightmost cells above.

Table 10. Valence Force Constants (mdyn/Å) of POF_2^-, SOF_2, $ClOF_2^+$, HPO_2F^-, and HSO_2F

	POF_2^-	SOF_2	$ClOF_2^+$	HPO_2F^-	HSO_2F
f_{XO}	8.34	11.12	10.02	9.43	11.47
f_{XF}	2.68	4.06	3.97	3.79	4.65
f_{XH}	--	--	--	3.20	3.98

Table 11. Calculated and Experimental F⁻ Affinities of Various Phosphorus Fluorides and HF

Molecule	F⁻ Affinity (kcal/mol)	
	Calcd	Exp[a]
PF_3	41.0	40
HF	41.1	39
POF_3	52.3	48
FPO	59.0	56
HPF_4	73.5	
HPO_2	79.9	
PF_5	87.3	85

a) Data from Ref. 6.

ON THE INSTABILITY OF SALTS CONTAINING THE TRIFLUORIDE ANION

Karl O. Christe

Rocketdyne Division of Rockwell International Corporation, Canoga Park, CA 91309 (USA)

ABSTRACT

Elemental fluorine does not form a stable $N(CH_3)_4{}^+F_3{}^-$ salt with solutions of $N(CH_3)_4F$ in either CH_3CN at -31°C or CHF_3 at -142°C.

The trifluoride anion, $F_3{}^-$, has been the subject of numerous theoretical calculations [1-4] ranging from SCF (Self Consistent Field) to CCSDT (Coupled Cluster Single Double Triple). The most sophisticated methods [3] duplicated well the vibrational frequencies which were observed [5] by Ault and Andrews for the $Cs^+F_3{}^-$ and $Rb^+F_3{}^-$ ion pairs in argon matrices at 15K. The best estimates for the stability of $F_3{}^-$ indicate that $F_3{}^-$ is thermodynamically more stable than $(F_2 + F^-)$ by about 110 kJ mol^{-1} [3]. This value is comparable to those found for $Br_3{}^-$ (D_0=105kJ mol^{-1}) and $I_3{}^-$ (D_0=109kJ mol^{-1}) and larger than that of $Cl_3{}^-$ (D_0=75kJ mol^{-1}). Since the $Cl_3{}^-$, $Br_3{}^-$ and $I_3{}^-$ anions are all well known, both in solution and in the solid state, and anhydrous $N(CH_3)_4F$ provides a source of soluble fluoride anions in the presence of a large and oxidizer resistant cation [6], it was interesting to examine whether $N(CH_3)_4{}^+F_3{}^-$ can be prepared on a macroscopic scale using experimental techniques which recently provided novel anions such as $XeF_5{}^-$ [7], $IOF_6{}^-$ [8], $TeOF_6{}^{2-}$ [9], $PF_4{}^-$ [10] or $ClF_6{}^-$ [11].

The possibility of preparing $N(CH_3)_4{}^+F_3{}^-$ was examined by pressurizing solutions of $N(CH_3)_4{}^+F^-$ with up to five hundred torr of F_2 in either CH_3CN at -31°C or CHF_3 at -142°C (Caution! These experiments are potentially hazardous and appropriate safety precautions must be used at all times). The resulting mixtures were gently agitated for about

two hours, followed by removal of all material, volatile at these low temperatures, in a dynamic vacuum. The solid residues were then allowed to warm in the closed Teflon-FEP reaction vessels to room temperature. No fluorine evolution was observed during these warm-up steps. The nonvolatile residues were characterized by the observed material balances and vibrational spectra. In the case of the CHF_3 solution, the low-temperature product was the known [6] $N(CH_3)_4^+F^- \cdot nCHF_3$ adduct which decomposed at higher temperature to $N(CH_3)_4F$ and CHF_3. In the case of the CH_3CN solution, the solid product was $N(CH_3)_4^+HF_2^-$ formed by slow attack of the solvent by both F_2 and F^- [12]. The absence of an oxidizing species in the solid products was also demonstrated by their inability to liberate iodine from aqueous KI solutions.

These results demonstrate that, in spite of the large and strongly stabilizing $N(CH_3)_4^+$ counter ion, F_2 does not form a stable F_3^- salt with $N(CH_3)_4^+F^-$ in either CH_3CN or CHF_3 solutions at low temperatures. The failure of F_3^- formation under the above conditions, in spite of the bond energy of F_2 and the dissociation energy of F_3^- being comparable to those of I_2 and I_3^-, respectively, is surprising and might be attributed to the high solvation energies of F^- in highly polar solvents, such as CHF_3 or CH_3CN. Reactions between $N(CH_3)_4F$ and F_2 in the absence of a solvent were not studied due to the experimental difficulties expected for controlling the reaction.

ACKNOWLEDGEMENT

REFERENCES

1. P.A. Cahill, C.E. Dykstra, and J.C. Martin, *J. Am. Chem. Soc.*, **107** (1985) 6359.

2. J.J. Novoa, F. Mota, and S. Alvarez, *J. Phys. Chem.*, **92** (1988) 6561.

3. G.L. Heard, C.J. Marsden, and G.E. Scuseria, *J. Phys. Chem.*, **96** (1992) 4359.

4. C. Sosa, C. Lee, G. Fitzgerald, and R.A. Eades, *Chem. Phys. Letters*, **211** (1993) 265.

5. B.S. Ault and L. Andrews, *Inorg. Chem.*, **16** (1977) 2024, and *J. Am. Chem. Soc.*, **98** (1976) 1591.

6. K.O. Christe, W.W. Wilson, R.D. Wilson, R. Bau, and J. Feng, *J. Am. Chem. Soc.*, **112** (1990) 7619.

7. K.O. Christe, E.C. Curtis, D.A. Dixon, H.P. Mercier, J.C.P. Sanders, and G.J. Schrobilgen, *J. Am. Chem. Soc.*, **113** (1991) 3351.

8. K.O. Christe, D.A. Dixon, A.R. Mahjoub, H.P.A. Mercier, J.C.P. Sanders, K. Seppelt, G.J. Schrobilgen, and W.W. Wilson, *J. Am. Chem. Soc.*, **115** (1993) 2696.

9. K.O. Christe, D.A. Dixon, J.C.P. Sanders, G.J. Schrobilgen, and W.W. Wilson, *Inorg. Chem.*, **32** (1993) 4089.

10. K.O. Christe, D.A. Dixon, H.P.A. Mercier, J.C.P. Sanders, G.J. Schrobilgen, and W.W. Wilson, *J. Am .Chem. Soc.*, in press.

11. K.O. Christe, W.W. Wilson, R.V. Chirakal, J.C.P. Sanders, and G.J. Schrobilgen, *Inorg. Chem.*, **29** (1990) 3506.

12. W.W. Wilson, K.O. Christe, J. Feng, and R. Bau, *Can. J. Chem.*, **67** (1989) 1898.

Theoretical Prediction of the Structures and Stabilities of Azidamines

H. Harvey Michels,[*1] John A. Montgomery, Jr.,[1] Karl O. Christe[*2], and David A. Dixon[*3]

Contribution from the United Technologies Research Center, East Hartford, CT 06108, Rocketdyne, A Division of Rockwell International Corporation, Canoga Park, CA 91309, and The DuPont Company, Central Research and Development, Experimental Station, Wilmington, DE 19880-0328

Abstract

Ab initio molecular orbital and density functional theory calculations show that azidamines, a new family of polynitrogen compounds, are minima on their respective potential energy surfaces. The geometries, vibrational frequencies, and heats of formation are predicted for $N(N_3)_3$, $HN(N_3)_2$, the $N(N_3)_2^-$ anion, and the $N(N_3)_4^+$ cation. All of these compounds are highly energetic materials with large positive heats of formation. The results suggest that these polynitrogen compounds could be synthetically accessible, and potential methods for their syntheses are proposed.

Introduction

The recent discovery of new allotropic forms of carbon and the rich and fascinating chemistry that it has produced, has also stimulated a renewed search for new allotropic forms of nitrogen.[4-17] Although nitrogen and the CH group are pseudoelements[18] and numerous stable (CH_n) compounds, such as benzene, or polyacetylene are well known, the analogous polynitrogen compounds, N_n, where n exceeds 3, have so far not been prepared. The main reasons for this difference are the relative energies of their triple, double and single bonds. For nitrogen, the average thermochemical bond energy of the triple bond (946 kJ mol^{-1}) is 368 kJ mol^{-1} larger than the sum of a double (418 kJ mol^{-1}) and a single (160 kJ mol^{-1}) bond.[19] Thus, dinitrogen, N_2, is by far the most stable polynitrogen compound. For carbon the situation is reversed. The

1

bond energy of a triple bond (813 kJ mol^{-1}) is 141 kJ mol^{-1} smaller than the sum of a double (598 kJ mol^{-1}) and a single (356 kJ mol^{-1}) bond.[19] Thus, acetylene, $(CH)_2$, is thermodynamically unstable with respect to its higher homologues.

In view of the above energetic considerations, it is not surprising that the polynitrogen compounds with n >2 are highly energetic and thus, are of interest for halogen-free high energy density materials (HEDM). The obvious challenge to their use is their thermodynamic instability which renders their syntheses and handling very difficult. Most publications dealing with polynitrogen compounds have been limited to theoretical predictions of their behavior, and experimental studies, such as the one by Vogler,[20] are rare. Previously calculated, but presently still unknown polynitrogen (n >3) compounds include N_4,[5] N_4^+,[13-17] N_5^-,[9] N_6,[5-7,9] N_8,[5,6,12] N_{12},[10] and N_{20}.[8,10,11] Most of these compounds are cyclic or polycyclic and, hence, would require synthetically very difficult ring closing methods. In order to avoid this difficulty, we are searching for stable polynitrogen structures which would be more amenable to an actual synthesis. As an aid to the synthetic chemist, we have calculated energies, stabilities, and vibrational spectra of a set of polynitrogen compounds, the azidamines.

Computational Methods

Ab initio molecular orbital (MO) calculations were carried out by using the Gaussian 92 programs.[21] RHF/6-31G* and MP2/6-31G* geometry optimizations were performed for all species; additonal calculations with the 6-31G* set augmented with diffuse functions (RHF/6-31+G*) were performed for the anion. The density functional theory[22] calculations were done with the program DGauss[23], which employs Gaussian basis sets on a Cray YMP computer. The basis sets for N and H are triple zeta in the valence space augmented with a set of polarization functions (TZVP) with the form (7111/411/1) for N and (311/1) for H.[24] The auxiliary fitting basis set for the electron density and the exchange-correlation potential has the form [8/4/4] for N and [4/1] for H. The calculations were done at the self-consistent gradient-corrected (non-local) level (NLDFT) with the non-local exchange potential of Becke[25] together with the non-local correlation functional of Perdew[26] (BP). The local potential of Vosko, Wilk and Nusair[27] was used. Geometries were optimized by using

2

analytical gradients.[23] Second derivatives were calculated by numerical differentiation of the analytic first derivatives. A 2-point method with a finite difference of 0.01 a.u. was used.

$N(N_3)_2^-$

The MO electronic structure calculations for $N(N_3)_2^-$ were carried out in both C_2 and C_s symmetries. The dinitramide[28] analogue structure, **A**, of C_s

$$\left[N \left(-N \overset{N}{\underset{N}{\diagup}} \right)_2 \right]^-$$
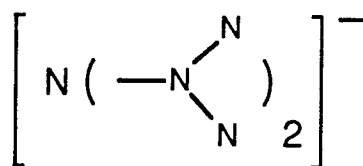
A

symmetry was not vibrationally stable, exhibiting two imaginary vibrational frequencies at the RHF/6-31G* level of theory. This is in accord with our inability to find a satisfactory electronic structure which possesses 8 valence electrons on each nitrogen atom. In contrast, the open chain, diazidamide structure, $(N_3\text{-}N\text{-}N_3)^-$, was a minimum at the RHF/6-31G* level and exhibited all real frequencies. Additional calculations including diffuse functions (RHF/6-31+G*) and electron correlation (MP2/6-31G*), also yielded true minima on the potential energy surface (PES). The results are given in Tables 1 and 2, and the stable C_2 conformation is shown in Figure 1. At the MP2/6-31+G* correlated level of theory, the central N1-N2 bond distance (1.44 Å) is only slightly longer than that of 1.38 Å previously reported for the dinitramide anion, $N(NO_2)_2^-$.[28] Other known compounds of nitrogen exhibit even larger N-N bond lengths: N_2O_3 (1.86 Å),[29] N_2O_4 (1.78 Å)[30] and N_2H_4 (1.45 Å).[29] The N2-N3 and N3-N4 bond lengths are typical of those found in other covalent azides such as hydrogen azide and the halogen azides.[29,31-35] The longest and weakest bonds in $N(N_3)_2^-$ are the central N1-N2 bonds whose lengths are comparable to those in N_2H_4[29] and $N(NO_2)_2^-$.[28] Typically, N-N single bond strengths are 150-180 kJ/mol. As shown below, our calculations give a much smaller value for the activation barrier for N_2 elimination, suggesting that N_2 elimination, rather than cleavage of the N-N single bond, is the lowest energy decomposition path. The

central bond angle, $\Theta(2'12)$, of 101° is consistent with a simple valence bond model with sp^3 hybridization on the central nitrogen atom involving two ligands and two more repulsive, sterically active, free valence electron pairs. These free electron pairs are more repulsive than the two N1-N2 bonds which is consistent with the N2'-N1-N2 bond angle being somewhat smaller than the ideal tetrahedral angle of 109.5°.

Because of the bonding patterns in these molecules there is the possibility that even at the MP2 level, we are not providing an adequate description of the wavefunction. In order to test whether this level is providing an adequate treatment, we used density functional theory which we have shown is a good method to use in the prediction of geometries and energies for structures that are often difficult to treat with traditional ab initio MO methods.[36] These results are also shown in Table 1 for the geometry parameters and in Table 2 for the frequencies. The predicted geometry is quite sensitive to the level of theory, as the RHF/6-31G* and NDLFT/TZVP calculations give a C_{2v} structure, whereas the RHF/6-31+G* and MP2/6-31G* calculations give a C_2 structure. Other than these differences, the agreement in the predicted geometry parameters between the MP2/6-31+G* and NLDFT/TZVP levels is quite good showing that the MO calculations are predicting reasonable structures. The frequencies at the best MO and DFT levels are in qualitative agreement. Usually, the MO frequencies are higher than the experimental values whereas the DFT values are comparable or a little low. Thus it is surprising that the DFT frequencies for the weaker N-N stretches are higher than the MP2 values. This is consistent with the differences in geometry and suggests that the MP2 values for the lower frequency N-N stretches are probably too low. The lowest stretching frequency is at 937 cm^{-1} so there are no very low frequency modes (<250 cm^{-1}) which could lead to decomposition.

Mulliken and CHELPG[37] charge distribution analyses were carried out (Table 3) at the MO level and indicate that much of the excess negative charge resides on the central nitrogen atom. The DFT Mulliken charges show a similar pattern but the charge differences are smaller. Based on the calculated geometry and charge distributions, the structure and bonding in $N(N_3)_2^-$ can be described as a sum of the following two resonance structures. Of course, the

4

charges derived from the resonance structures are larger than the calculated values because charge separation will be minimized in the actual ion.
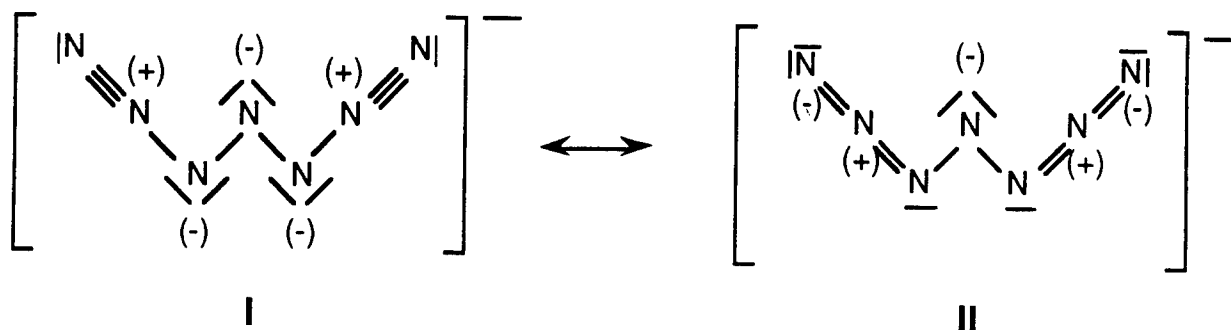
The total valence electron density calculated at the DFT level for $N(N_3)_2^-$ in the molecular plane is shown in Figure 2. Consistent with the resonance structures shown above, there is clearly additional electron density at N1 and N2 with (very) approximate angles of 120° with respect to the N-N bonds. The additional density at N4 is parallel to the N-N bond. These results are consistent with the presence of at least one lone pair on N1, N2 and N4.

$HN(N_3)_2$

Adding a proton to $N(N_3)_2^-$ yields diazidamine, $HN(N_3)_2$. Geometry optimizations were carried out at the RHF/6-31G*, MP2/6-31G* and NLDFT/TZVP levels of theory (Table 4). The calculated second derivatives (see Table 5) reveal a C_s structure (Figure 3a) that is a minimum on the potential energy surface. The lowest frequency stretch at 802 cm^{-1} is 135 cm^{-1} below the lowest energy stretch in $N(N_3)_2^-$. The geometric parameters calculated for $HN(N_3)_2$ are, as expected, very similar to those obtained for the $N(N_3)_2^-$ anion. Addition of the proton leads to enhancment of the contribution of resonance structure I. The charges at the DFT level are shown in Table 3. Protonation of the anion actually leads to an increase in the negative charge at N2 consistent with the increased contribution of resonance structure I. As would be expected, the charge on N3 increases on protonation whereas the charges on N1 and N4 decrease.

We also calculated a C_1 structure obtained by twisting about the N1-N2 bond as shown in Figure 3b. This structure is 9.2 kJ/mol higher in energy

5

and except for the torsion τ (H-N1-N2-N3), the geometry parameters are essentially unchanged from those of the C_s structure.

$N(N_3)_3$

The structure of the triazidamine molecule was investigated in a similar manner. Geometry optimization was first carried out at the RHF/6-31G* level of theory. Harmonic frequency calculations confirmed a vibrationally stable structure of C_3 symmetry with the lowest energy stretch at 771 cm^{-1}. Based on this structure, the geometry was optimized at the MP2/6-31G* level and again a minimum with C_3 symmetry was found as shown in Figure 4. Inclusion of diffuse functions at the RHF level resulted in only minor changes in calculated bond lengths and angles. The results are summarized in Tables 6 and 7. The DFT calculations yield a similar structure except that it has only C_s symmetry. The only real asymmetry in the parameters is found for R_{12} and $R_{12'}$.

Our calculations show that $N(N_3)_3$ is pyramidal as found for the related compounds NH_3, NF_3, $N(CH_3)_3$[29] and $N(NO_2)_3$[38] molecules. The N1-N2 central bond distance (1.46-1.48 Å) is similar to those in $N(N_3)_2^-$, $HN(N_3)_2$ and hydrazine[29] and considerably shorter than that of 1.54 Å calculated[38] for $N(NO_2)_3$. As expected for the approximately linear, nonbulky azide groups, ligand-ligand repulsion effects and ligand crowding appear to be minimal. The charges in $N(N_3)_3$ (Table 3) are essentially the same as those in $HN(N_3)_2$ except that the charge at N1 is less negative than the charge on N1 in $N(N_3)_2H$.
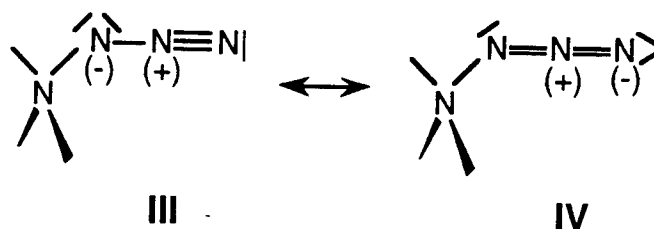
$N(N_3)_4^+$

The last member of this series of azidamine compounds is the tetraazidammonium cation. Geometry and vibrational frequency calculations at the RHF/6-31G* level of theory show a minimum energy structure of D_{2d} symmetry which was again optimized at the MP2/6-31G* level (see Tables 8 and 9 and Figure 5). As can be seen, the central N1-N2 bond length (1.465 Å) is again very similar to those calculated for $N(N_3)_3$ (1.463 Å) and $HN(N_3)_2$ (1.467 Å) at the MP2 level indicating little effect of adding a fourth azido ligand to the central nitrogen atom. The slight distortion of the $N1(N2)_4$ tetrahedron to D_{2d} symmetry can be attributed to unequal repulsion effects caused by the two

6

sterically active free valence electron pairs on each N2 atom. Due to the strongly bent N1-N2-N3 angle of 106°, the four azido groups are arranged in an up-down-up-down manner which minimizes their mutual repulsion (see Figure 4). The DFT geometry is in reasonable agreement with the MP2 geometry. The distance R_{12} is predicted to be longer at the DFT level and R_{23} and R_{34} are thus shorter than the MP2 values. Addition of the fourth N_3 group to form $N(N_3)_4^+$ leads to both N1 and N4 becoming more positive (Table 3) but the charges on N2 and N3 do not show significant variations.
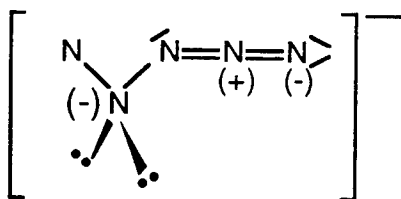
The stretching frequencies for $N(N_3)_4^+$ differ from the other azidamines. The band at 350 cm^{-1} is the asymmetric sum of the symmetric stretches of the N_3 groups from the central N. The band at 453 cm^{-1} is the symmetric sum of these symmetric N-(N_3) stretches coupled with a bend. Thus, there are much lower frequency modes in $N(N_3)_4^+$ that could lead to decomposition than predicted for the other azidamines.

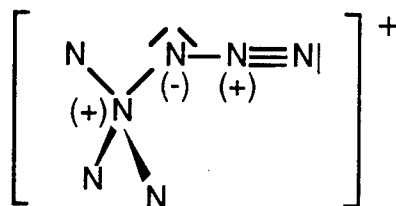**Bond Lengths in the Azido Groups**

Although the N-N bond lengths in the azido groups do not change dramatically on going from the $N(N_3)_2^-$ anion to the $N(N_3)_4^+$ cation and are all within the range expected for predominantly covalent azides, the relative contributions from the two resonance strucures **III** and **IV** are influenced by the sign of the charge on the central nitrogen atom N1. In the $N(N_3)_2^-$ anion, the N1 central atom possesses two free valence electron pairs and, hence, carries a

III   IV

formal negative charge. This formal negative charge on N1 and the undesirability of neighboring charges having the same sign increase the relative contribution from resonance structure IV in the anion. On the other

7

$$\left[\begin{array}{c} \underset{\underset{\cdot\cdot}{N}}{N} \diagdown \underset{(-)N}{\overset{\diagup}{}} \diagup \overset{\frown}{N} = N = N \overset{\diagdown}{\underset{(-)}{}} \\ \end{array} \right]^{-}$$

hand, in the $N(N_3)_4^+$ cation, the N1 atom no longer possesses any free valence electron pair and, hence, carries a formal positive charge. In the cation, therefore, the contribution from resonance structure III should be enhanced. In

$$\left[\begin{array}{c} \underset{N}{N} \diagdown \underset{(+)N}{\overset{\diagup}{}} \diagup \overset{\frown}{\underset{(-)}{N}} - N \underset{(+)}{\equiv} N| \\ N \diagdown N \end{array} \right]^{+}$$

the neutral amines, i.e., $N(N_3)_3$ and $HN(N_3)_2$, the N1 atom does not carry any excess formal charge and, hence, does not influence the relative contributions from the two resonance structures III and IV. This influence of the excess formal charge residing on N1 on the N-N bond lengths of the azido groups is clearly reflected by the results of our calculations. In $N(N_3)_2^-$, the N2-N3 bond has more double bond character (1.247 Å) relative to that in $N(N_3)_4^+$ (1.271 Å), whereas the terminal N3-N4 bond has less triple bond character (1.174 Å) relative to that in $N(N_3)_4^+$ (1.155 Å). The partial equalization of the bond lengths in an azido group strengthens the weak N-N single bond and, hence, increases the activation energy barrier against N_2 elimination, shown schematically in (1) and discussed below.

$$X\text{-}N\text{-}N\text{-}N \; \rightarrow \; X\text{-}N \; + \; N\text{-}N \tag{1}$$

Thus the $N(N_3)_2^-$ anion is expected to possess a somewhat higher energy barrier to N_2 elimination than the $N(N_3)_4^+$ cation.

Thermochemistry

The gas phase heats of formation of the molecules (Table 12) discussed above can be calculated from the enthalpy changes of the reactions shown in Table 11 by using the calculated total energies given in Table 10 and the known heats of formation[39-41] given in Table 12. There is reasonable agreement for the calculated DFT and MO heats of formation for $HN(N_3)_2$ with the NLDFT value being more positive by 27 kJ/mol. The deviation between the two methods increases to 48 kJ/mol for $N(N_3)_3$. For $N(N_3)_4^+$ both DFT values are considerably more positive than the MO value.

Two different methods were used to calculate the heat of formation of the anion $N(N_3)_2^-$. The simplest method is to calculate the proton affinity of the anion as shown in Reaction (10). In order to check the accuracy of the method, we calculated the proton affinity of NH_2^- as shown in Reaction (13). The NLDFT calculated, absolute value for the proton affinity is 31 kJ/mol too high. The NLDFT value for $\Delta H_f(N(N_3)_2^-)$ from Reaction (10) is 37.6 kJ/mol higher than that from Reaction (4). If the error from Reaction (13) is used to correct the value from Reaction (10) giving $\Delta H_f(N(N_3)_2^-)$ = 703.3 kJ/mol, the agreement is significantly improved. At the MO level, additional calculations were carried out. Because of the presence of anions, diffuse functions were added to the 6-31G* basis set to give the 6-31+G* basis set. The MP2 values of $\Delta H_f(N(N_3)_2^-)$ with the 6-31G* basis set, calculated from Reaction (4) and Reaction (14), differ by 131 kJ/mol whereas with the 6-31+G* basis set this difference is only 8 kJ/mol. Taking an average of the 6-31+G* basis set results gives $\Delta H_f(N(N_3)_2^-)$ = 736 kJ/mol. The value of $\Delta H_f(N(N_3)_2^-)$ from Reaction (14) from the NLDFT calculations is 734 kJ/mol which is in good agreement with the uncorrected value from Reaction (10) but not in as good agreement with the value from Reaction (4). If we take the corrected value from Reaction (10) and average it with the NLDFT values from Reactions (4) and (14), we obtain $\Delta H_f(N(N_3)_2^-)$ = 711 kJ/mol. The difference between the MO and DFT values is 25 kJ/mol, similar to some of the differences found above but in the opposite direction.

The two proton affinities that have been calculated, those for $N(N_3)_2^-$ and $HN(N_3)_2$ can be compared to the simple amines, NH_2^- and NH_3. The substitutiion of two hydrogens by two N_3 groups lowers the proton affinity by

9

almost 85 kJ/mol. For example, PA(NF$_3$) equals 573.2 kJ/mol. Thus the azide group is lowering the proton affinity in the same direction as the very electronegative fluorine. As a check, we calculated PA(NH$_3$) = 856.0 kJ/mol in excellent agreement with the experimental value of 853.5 kJ/mol.[40] Substitution of H by N$_3$ makes for a much stronger acid in the gas phase as shown by the large decrease in the proton affinity of the N(N$_3$)$_2^-$ anion by 300.4 kJ/mol as compared to that of NH$_2^-$. The corrected acidity of HN(N$_3$)$_2$ is 1394.9 kJ/mol which can be compared to the value for HNF$_2$ of 1502.1 kJ/mol showing that HN(N$_3$)$_2$ is a stronger acid than HNF$_2$.

These results show that the azidiamines are highly energetic materials and good HEDM candidates. As noted previously, their high energy content arises from the large energy difference between the NN triple bond and the sum of the single and double NN bonds.

Decomposition of covalent azides usually proceeds via N$_2$ elimination and has been well studied for a number of XN$_3$ species where X = H or halogen.[42-47] For example, the N-F bond strength in FN$_3$ is ~230 kJ/mol whereas decomposition to FN($^3\Sigma^-$) and N$_2$ is exothermic by ~125 kJ/mol.[47] Thus the formation of the first excited singlet state as shown in reaction (15) is endothermic by ~20 kJ/mol.[48] There is an experimentally determined activation energy of about

$$FN_3 \rightarrow FN(a^1\Delta) + N_2 \tag{15}$$

61 kJ/mol for Reaction (15). Calculations[43,49] at the HF/6-31G* level give a classical energy barrier of 45.6 kJ/mol which is reduced to 40.4 kJ/mol when zero point effects are included; these results are in qualitative agreement with the experimental value. The decomposition of the azidamines is formally analogous to Reaction (15) as long as it proceeds on the potential energy surface leading to a singlet nitrene (Reaction (16)).

$$RN(N_3)_2 \rightarrow R(N_3)N\text{-}\dot{N}: + N_2 \tag{16}$$

Furthermore, the resulting azido nitrenes may be very unstable leading to a rapid loss of a second N$_2$ molecule as shown in Reaction (17)

10

$$R\text{-}N\text{-}N: \rightarrow R\text{-}N\text{-}N: + N_2 \qquad\qquad (17)$$
$$\;\;\; | \qquad\qquad\quad |$$
$$\;\;\; N_3 \qquad\qquad\;\; N:$$

where the resulting compound should be very unstable and lose yet another N_2. For example, generation of an $N(N_3)_2^-$ structure by removal of a proton from the higher energy structure for $HN(N_3)_2$ led to a structure for the anion that is 54 kJ/mol higher in energy than the optimized anion structure. Optimization of this higher energy form led to dissociation into $2N_2 + N_3^-$ showing that the anion may not be stable to changes in conformation. In order to further study the N_2 elimination process, the transition states (see Figures 7 and 8) for loss of N_2 from $HN(N_3)_2$ and $N(N_3)_3$ were calculated at the HF/6-31G* level following the results noted above for FN_3. For $HN(N_3)_2$, the calculated classical energy barrier for N_2 elimination (Reaction (16)) is 41.3 kJ/mol whereas for $N(N_3)_3$, the classical barrier is 45.8 kJ/mol.[50] Correction of these energy barriers for zero point effects lowers the barriers to 34.1 kJ/mol for $HN(N_3)_2$ and to 38.7 kJ/mol for $N(N_3)_3$. (The geometry parameters and frequencies are given as Supplementary Material.) This result suggests that the predicted shock sensitivity of the azidamines is no better than that of FN_3.[46]

Potential Methods for the Synthesis of Azidamines

Since the polynitrogen compounds of our study are azidamines and, therefore, do not require synthetically difficult ring closing methods, they are more amenable to chemical synthesis than cyclic or polycyclic compounds, such as hexaazabenzene or octaazacubane. Potential methods for the synthesis of azidamines include either the replacement of halogen ligands in nitrogen halides by azido groups using commercially available reagents such as trimethylsilylazide, $(CH_3)_3SiN_3$,

$$NX_3 + 3(CH_3)_3SiN_3 \rightarrow N(N_3)_3 + 3(CH_3)_3SiX \qquad\qquad (18)$$
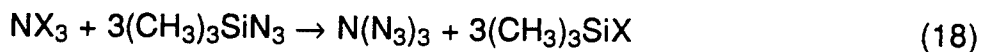
or the reverse approach, i.e., the reactions of trimethysilylamines with halogen azides:

11

$$NSi(CH_3)_{33} + 3XN_3 \rightarrow N(N_3)_3 + 3(CH_3)_3SiX \qquad (19)$$
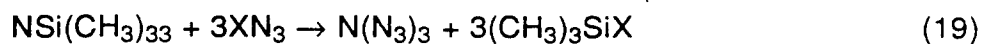
The use of appropriate solvents will be important to better control the reaction conditions and decrease the risk of explosions.

Acknowledgements

Supplementary Material

Cartesian coordinates, geometry parameters and vibrational frequencies for the transition states for reaction (16) for $HN(N_2)_3$ and $N(N_3)_3$ at the HF/6-31G* level.

References

1. United Technologies Research Center, East Hartford, CT 06108.

2. Rocketdyne, A Division of Rockwell International Corporation, Canoga Park, CA 91309. New address: Phillips Laboratory, Edwards Air Force Base, CA 93524-7001.

3. The DuPont Company, Central Research and Development, Experimental Station, Wilmington, DE 19880-0328. Contribution No. 6824

4. Janoschek, R. *Angew, Chem. Int. Ed. Engl.* **1993**, *32*, 230.

5. (a) Ferris, K. F.; Bartlett, R. J. *J. Am. Chem. Soc.* **1992**, *114*, 8302. (b) Lauderdale, W. J.; Stanton, J. F.; Bartlett, R. J. *J. Phys. Chem.* **1992**, *96*, 1173.

6. (a) Engelke, R. *J. Phys. Chem.* **1992**, *96*, 10789. (b) Engelke, R. *J. Phys. Chem.* **1989**, *93*, 5722. (c) Engelke, R.; Stine, J. R. *J. Phys. Chem.* **1990**, *94*, 5689. (d) Engelke, R. *J. Org. Chem.* **1992**, *57*, 4841.

7. Glukhovtsev, M. N.; von Ragué Schleyer, P. *Chem. Phys. Lett.* **1992**, *198*, 547.

8. Bliznyuk, A. A.; Shen, M.; Schaefer III, H. F. *Chem. Phys. Lett.* **1992**, *198*, 249.

9. (a) Nguyen, M. T. *J. Phys. Chem.* **1990**, *94*, 6923. (b) Nguyen, M. T.; Sana, M.; Leroy, G.; Elguero, J. *Can. J. Chem.* **1983**, *61*, 1435. (c) Nguyen, M. T.; McGinn, M. A.; Hegarty, A. F.; Elguero, J. *Polyhedron, Part A,* **1985**, 1721.

10. (a) Alkorta, I.; Elguero, J.; Rozas, I.; Balaban, A. T. *J. Mol. Struct.* **1991**, *228*, 47.

11. Chen, C.; Lu, L.-H.; Yang, Y.-W. *J. Mol. Struct.* **1992**, *253*, 1.

12. Cano, Gorini, J. A.; Farras, J.; Feliz, M.; Olivella, S.; Sole, A.; Villarasa, J. *J. Chem. Soc., Chem. Commun.* **1986**, 959.

13. Hiraoka, K.; Nakajima, G. *J. Chem. Phys.* **1998**, *88*, 7709.

14. Norwood, K.; Luo, G.; Ng, C. Y. *J. Chem. Phys.* **1989**, *91*, 849.

15. Knight, L. B.; Johannessen, K. D.; Cobranchi, C. B.; Earl, E. A.; Feller, D.; Davidson, E. R. *J. Chem. Phys.* **1987**, *87*, 885.

16. Smith, G. P.; Lee, L. C. *J. Chem. Phys.* **1978**, *69*, 5393.

17. Thompson, W. E.; Jacox, M. E. *J. Chem. Phys.* **1990**, *93*, 3856.

18. (a) Haas, A. *Chemiker Zeitung,* **1982**, *106*, 239. (b) Haas, A. *Adv. Inorg. Chem. Radiochem.* **1984**, *28*, 167.

19. Cotton, F. A.; Wilkinson, G. in "Advanced Inorganic Chemistry", Third Edit., Interscience Publishers, John Wiley & Sons, New York, 1972, pg. 113.

20. Vogler, A.; Wright, R. E.; Kunkley, H. *Angew. Chem., Int. Ed. Engl.* **1980**, *19*, 717.

21. Gaussian 92. Frisch, M. J.; Trucks, G. W.; Head-Gordon, M.; Gill, P. M. W.; Wong, M. W.; Foresman, J. B.; Johnson, B. G.; Schlegel, H. B.; Robb, M. A.; Replogle, E. S.; Gomperts, R.; Andrews, J. L.; Raghavachari, K.; Binkley, J. S.; Gonzales, C.; Martin, R. L.; Fox, J.; DeFrees, D. J.; Baker, J.; Stewart, J. J. P.; Pople, J. A.; Gaussian Inc., Pittsburg, PA 1992.

22. (a) Parr, R. G.; Yang, W. "Density Functional Theory of Atoms and Molecules", Oxford University Press, New York, 1989; (b) Salahub, D. R. in "Ab Initio Methods in Quantum Chemistry-II", ed. Lawley, K. P., J. Wiley

& Sons, New York, 1987, p. 447; (c) Wimmer, E.; Freeman, A. J.; Fu, C.-L.; Cao, P.-L.; Chou, S.-H.; Delley, B. in "Supercomputer Research in Chemistry and Chemical Engineering" Jensen, K. F.: Truhlar, D. G., Eds.; ACS Symposium Series, American Chemical Society, Washington, D.C. p.49, 1987; (d) Jones, R. O.; Gunnarsson, O. *Rev. Mod. Phys.* **1989**, *61*, 689; (e) Zeigler, T. *Chem. Rev.* **1991**, *91*, 651.

23.   (a) Andzelm, J.; Wimmer, E.; Salahub, D. R. in "The Challenge of d and f Electrons: Theory and Computation"; Eds Salahub, D. R.; Zerner, M. C. ACS Symposium Series, No. 394, American Chemical Society, Washington, D.C. 1989, p.228.   (b) Andzelm, J. in "Density Functional Methods in Chemistry", Ed. J. Labanowski and J. Andzelm, Springer-Verlag:New York,1991, p.101.   (c) Andzelm, J. W.; Wimmer, E. *J. Chem. Phys.* **1992**, *96*, 1280.   DGauss is a local density functional program available via the Cray Unichem Project.

24.   Godbout, N., Salahub, D. R., Andzelm, J., and Wimmer, E. *Can. J. Chem.* **1992**, *70*, 560.

25.   (a) Becke, A. D., *Phys. Rev. A* **1988**, *38*, 3098.   (b) Becke, A.D. in "The Challenge of d and f Electrons: Theory and Computation" Eds. Salahub, D. R.; Zerner, M. C. ACS Symposium Series No. 394, American Chemical Society, Washington, D.C. 1989, p. 166.   (c) Becke, A. D. *Inter. J. Quantum Chem. Quantum. Chem. Symp.* **1989**, *23*, 599.

26.   Perdew, J. P. *Phys. Rev. B* **1986**, *33*, 8822

27.   Vosko, S. J., Wilk, L. and Nusair, M., *Can. J. Phys.* **1980**, *58*, 1200.

28.   Michels, H. H.; Montgomery, Jr., J. A. *J. Phys. Chem.* **1993**, *97*, 6602.

29.   Harmony, M. D.; Laurie, V. W.; Kuczkowski, R. L.; Schwendeman, R. H.; Ramsay, D. A.; Lovas, F. JH.; Lafferty, W. J.; Maki, A. G. *J. Phys. Chem. Ref. Data* **1979**, *8*, 619.

30. McClelland, B. W. Gundersen, G.; Hedberg, K. *J. Chem. Phys.* **1972**, *56*, 4541.

31. Winnewisser, B. P. *J. Mol. Spectrosc.* **1980**, *82*, 220.

32. Christen, D.; Mack, H. G.; Schatte, G.; Willner, H. *J. Am. Chem. Soc.* **1988**, *110*, 707.

33. Cook, R. L.; Gerry, M. C. L. *J. Chem. Phys.* **1970**, *53*, 2525.

34. Buzek, P.; Klapötke, T. M.; von Ragué Schleyer, P.; Tornieporth-Oetting, I. C.; White, P. S. *Angew. Chem. Int. Ed. Engl.* **1993**, *32*, 275.

35. Hargittai, M.; Tornieporth-Oetting, I. C.; Klapötke, T. M.; Kolonits, M.; Hargittai, I. *Angew. Chem. Int. Ed. Engl.* **1993**, *32*, 759.

36. (a) Dixon, D. A.; Andzelm, J.; Fitzgerald, G.; Wimmer, E. *J. Phys. Chem.* **1991**, *95*, 9197. (b) Christe, K. O.; Curtis, E. C.; Mercier, H. P.; Sanders, J. C. P.; Schrobilgen, G. J.; Dixon, D. A. *J. Am. Chem. Soc.* **1991**, *113*, 3351. (c) Christe, K. O.; Wilson, R. D.; Wilson, W. W.; Bau, R.; Sukumar, S.; Dixon, D. A. *J. Am Chem. Soc.* **1991**, *113*, 3795. (d) Dixon, D. A.; Christe, K. O.; J. Phys. Chem. **1992**, *96*, 1018. (e) Arduengo, A. J., III; Lattman, M.; Dixon, D. A.; Calabrese, J. C. *Heteroatom* **1991**, *2*, 395. (f) Dixon, D. A.; Arduengo, A. J., III; Intl. *J. Quantum Chem. Symp.* **1991**, *25*, 269. (g) Sosa, C.; Andzelm, J.; Wimmer, E.; Dobbs, K. D.; Dixon, D. A. *J. Phys. Chem.* **1992**, *96*, 6630. (h) Dixon, D. A.; Gole, J. L. *Chem. Phys. Lett.* **1992**, *188*, 560. (i) Dixon, D. A.; Matsuzawa, N.; Walker, S. C. *J. Phys. Chem.* **1993**, *96*, 10740.

37. Breneman, C. M.; Wiberg, K. B. *J. Comp. Chem.* **1990**, *11*, 361.

38. Montgomery, Jr., J. A. ; Michels, H. H. *J. Chem. Phys.* **1993**, *97*, 6774.

39. Wagman, D. D.; Evans, W. H.; Parker, V. B.; Schumm, R. H.; Halow, I.; Bailey, S. M.; Churney, K. L.; Nuttal, R. L. *J. Phys. Chem. Ref. Data* **1982**, *11*, Suppl. 2.

40. Lias, S. G.; Bartmess, J. E.; Liebman, J. F.; Holmes, J. L.; Levin,. R. D.; Mallard, W. G. *J. Phys. Chem. Ref. Data*, **1988**, *17*, Suppl 1.

41. Chase, M. W., Jr.; Davies, C. A.;. Downey, J. R.; Jr.; Frurip, D. J.; McDonald, R. A.; Syverud, A. N. *J. Phys. Chem. Ref. Data*, **1985**, *14*, Suppl 1.

42. Benard, D. J.; Winker, B. K.; Seder, T. A.; Cohn, R. H. *J. Phys. Chem.* **1989**, *93*, 4790.

43. Benard, D. J.; Chowdhury, M. A.; Winker, B. K.; Seder, T. A.; Michels, H. H. *J. Phys. Chem.* **1990**, *94*, 7507.

44. Bock, H.; Dammel, R.; DesMarteau, D. D. *Z. Naturforsch., Teil B* **1987**, *42B*, 308.

45. Gericke, K. H.; Lock, M.; Comes, F. J. *Chem. Phys. Lett.* **1991**, *186*, 427.

46. Gholivand, K., Schatte, G.; Willner, H. *Inorg. Chem.* **1987**, *26*, 2137.

47. Otto, M.; Lotz, S. D.; Frenking, G. *Inorg. Chem.* **1992**, *31*, 3647.

48. Huber, K. P.; Herzberg, G. "Constants of Diatomic Molecules," Van Nostrand Reinhold:New York (1979).

49. Michels, H.H,; Montgomery, J.A., Jr. unpublished results.

50. $E(TS(rxn\ 16)) = -381.455869$ a.u. for $HN(N_3)_2$ and $= -544.094226$ a.u. for $N(N_3)_3$ at the HF/6-31G* level.

Table 1. Calculated Geometries (Angstroms and Degrees) of the Diazidamide Anion [$N(N_3)_2^-$].

Level of Theory	RHF/6-31G*(C$_{2v}$)	RHF/6-31G*(C$_1$)	MP2/6-31G*(C$_2$)	MP2/6-31G*(C$_1$)	NLDFT/TZVP(C$_{2v}$)
Geometry					
R_{12}	1.418	1.409	1.451	1.442	1.430
R_{23}	1.197	1.198	1.244	1.247	1.230
R_{34}	1.133	1.131	1.174	1.174	1.183
$\theta_{2'12}$	101.8	102.7	100.6	101.2	102.6
θ_{123}	113.2	112.8	115.8	113.6	116.2
θ_{234}	176.6	177.1	170.2	171.5	174.9
$\tau_{2'123}$	180	-173.7	-150.9	-156.4	180
τ_{1234}	180	-154.7	-144.4	-137.6	180

Table 2. Calculated Harmonic Frequencies in cm⁻¹ and Infrared Intensities [ ] in km/mol of $N(N_3)_2^-$

	Mode	RHF/6-31G* (C₂)	MP2/6-31G* (C₂)	MP2/6-31+G* (C₂)	Mode	RHF/6-31+G* (C₂ᵥ)	NLDFT/TZVP (C₂ᵥ)
A	ν_1	2388 [256]	2291 [14]	2263 [47]	A₁	2359 [190]	2069 [93]
	ν_2	1476 [14]	1188 [9]	1184 [21]		1473 [7]	1252 [10]
	ν_3	1001 [16]	914 [4]	911 [1]		991 [20]	948 [3]
	ν_4	629 [2]	610 [7]	593 [1]		622 [4]	552 [3]
	ν_5	510 [0]	425 [0]	408 [0]		459 [4]	410 [1]
	ν_6	465 [5]	396 [0]	379 [0]		140 [1]	137 [3]
	ν_7	145 [5]	150 [1]	145 [0]	A₂	523 [0]	251 [0]
	ν_8	107 [0]	63 [0]	85 [0]		72 [0]	107 [0]
B	ν_9	2304 [2970]	2280 [1197]	2255 [1422]	B₁	2318 [2634]	2059 [1333]
	ν_{10}	1428 [9]	1162 [2]	1159 [2]		1421 [7]	1218[154]
	ν_{11}	1024 [173]	869 [47]	899 [78]		982 [114]	937 [59]
	ν_{12}	796 [159]	743 [60]	737 [4]		799 [118]	693 [144]
	ν_{13}	492 [30]	385 [12]	326 [13]	B₂	278 [24]	258 [23]
	ν_{14}	282 [23]	218 [25]	227 [23]		525 [33]	212 [5]
	ν_{15}	74 [8]	35 [3]	44 [6]		56 [5]	90 [3]

Table 3. Calculated Atomic Charges

Method	N1	N2	N3	N4
		$N(N_3)_2^-$		
Mulliken/HF	-0.43	-0.27	0.38	-0.40
CHELPG/HF	-0.42	-0.38	0.66	-0.57
Mulliken/DFT	-0.33	-0.12	0.11	-0.32
		$N(N_3)_2H$		
Mulliken/DFT	-0.19(0.07)[a]	-0.18	0.25	-0.10
		$N(N_3)_3$		
Mulliken/DFT	-0.02	-0.15	0.24	-0.09
		$N(N_3)_4^+$		
Mulliken/DFT	0.09	-0.11	0.28	0.06

[a] Charge in parentheses is the sum of the N1 and H charges.

Table 4. Calculated Geometries (Angstroms and Degrees) of Diazidamine [HN(N$_3$)$_2$].

Parameter	RHF/6-31G* C$_s$	RHF/6-31G* C$_1$	MP2/6-31G* C$_s$	MP2/6-31G* C$_1$	NLDFT/TZVP C$_s$	NLDFT/TZVP C$_1$
R$_{12}$	1.425	1.418	1.466	1.455	1.471	1.468
R$_{12'}$		1.423		1.463		1.473
R$_H$	0.999	1.001	1.021	1.025	1.026	1.029
R$_{23}$	1.251	1.261	1.268	1.273	1.256	1.263
R$_{23'}$		1.255		1.268		1.257
R$_{34}$	1.097	1.096	1.156	1.158	1.149	1.150
R$_{34'}$		1.095		1.155		1.148
θ$_{2'12}$	109.6	112.2	108.0	110.1	108.7	111.1
θ$_{215}$	104.2	109.7	101.2	107.4	101.2	107.3
θ$_{2'15}$		105.3		101.7		101.3
θ$_{123}$	108.1	111.2	108.4	112.0	110.9	112.4
θ$_{12'3'}$		107.9		108.2		110.7
θ$_{234}$	173.8	174.0	171.3	171.6	170.3	173.4
		174.1		171.3		171.2
τ$_{H123}$	-136.2	61.7	-153.0	57.4	145.2	47.1
		139.6		154.7		160.9
τ$_{1234}$	-178.2	176.9	-173.0	171.0	179.3	175.6
				172.5		167.4

Table 5. Calculated Harmonic Frequencies in cm^{-1} and Infrared Intensities [ ] in km/mol of HN(N$_3$)$_2$

	Mode	RHF/6-31G* (C$_s$)	MP2/6-31G* (C$_s$)	NLDFT/TZVP (C$_s$)	RHF/6-31G* (C$_1$)	MP2/6-31G* (C$_1$)	NLDFT/TZVP (C$_n$)
A'	ν_1	3807 [26]	3537 [35]	3425 [43]	3762 [8.8]	3472 [11]	3372 [9.2]
	ν_2	2485 [575]	2382 [212]	2134 [328]	2497 [344]	2365 [216]	2126 [258]
	ν_3	1344 [128]	1303 [83]	1260 [70]	2467 [807]	2337 [348]	2096 [530]
	ν_4	1119 [73]	1059 [46]	1030 [56]	1626 [9.4]	1472 [16]	1426 [17]
	ν_5	1055 [62]	891 [2]	847 [4.2]	1287 [132]	1262 [83]	1222 [91]
	ν_6	706 [26]	670 [10]	612 [1.0]	1167 [249]	1130 [124]	1099 [157]
	ν_7	663 [24]	545 [10]	548 [5.4]	1070 [116]	1080 [22]	1043 [12]
	ν_8	495 [11]	444 [5]	399 [5.5]	1054 [75]	881 [20]	825 [4.9]
	ν_9	328 [2]	283 [5]	259 [2.8]	1004 [56]	859 [20]	802 [61]
	ν_{10}	65 [1]	57 [1]	61 [0.8]	821 [17]	736 [20]	691 [21]
A"	ν_{11}	2447 [589]	2367 [286]	2108 [4.4]	738 [39]	665 [43]	624 [75]
	ν_{12}	1659 [13]	1509 [27]	1440 [30]	662 [29]	550 [13]	558 [5.6]
	ν_{13}	1179 [10]	1141 [68]	1133 [114]	653 [15]	537 [7.6]	544 [13]
	ν_{14}	1071 [5]	846 [57]	805 [58]	485 [4.8]	434 [3.0]	410 [5.4]
	ν_{15}	777 [6]	674 [38]	637 [69]	323 [8.0]	267 [8.5]	273 [1.3]
	ν_{16}	648 [5]	533 [3]	543 [0.1]	224 [1.6]	178 [2.2]	169 [1.5]
	ν_{17}	261 [1]	204 [1]	190 [0]	109 [5.1]	96 [3.4]	122 [2.1]
	ν_{18}	50 [2]	44 [1]	66 [0.1]	58 [0.6]	46 [0]	48 [0.2]

Table 6. Calculated Geometries (Angstroms and Degrees) of Diazidamine $[(N_3)_3]$.

Geometry Parameter	RHF/6-31G*	RHF/6-31+G*	MP2/6-31G*	NLDFT/TZVP
R_{12}	1.422	1.421	1.463	1.451
$R_{12'}$ (x2)				1.486
R_{23}	1.251	1.252	1.271	1.259
$R_{2'3'}$ (x2)				1.257
R_{34}	1.097	1.096	1.155	1.147
$R_{3'4'}$ (x2)				1.149
$\theta_{2'12'}$	106.6	106.7	103.9	106.3
$\theta_{212'}$ (x2)				103.0
θ_{123}	107.4	107.5	106.5	108.6
$\theta_{12'3'}$ (x2)				108.3
θ_{234}	174.0	173.9	171.6	170.1
$\theta_{2'3'4'}$ (x2)				170.8
$\tau_{2'123}$	147.6	150.5	147.3	124.8(x2)
$\tau_{212'3'}$ (x2)				149.8
τ_{1234}	174.6	174.2	177.3	179.1
$\tau_{12'3'4'}$ (x2)				171.8

Table 7. Calculated Harmonic Frequencies in cm^{-1} and Infrared Intensities [] in km/mol of N(N$_3$)$_3$

Mode	RHF/6-31G* (C$_3$)	RHF/6-31+G* (C$_3$)	MP2/6-31G* (C$_3$)	NLDFT/TZVP(C$_s$)
A				
ν_1	2490 [403]	2485 [445]	2387 [103]	A' 2142 [257]
ν_2	1276 [107]	1272 [126]	1221 [15]	2101 [333]
ν_3	1109 [4]	1098 [5]	931 [0]	1223 [39]
ν_4	649 [1]	635 [0]	549 [0]	1170 [177]
ν_5	593 [0]	592 [0]	524 [0]	944 [41]
ν_6	536 [15]	539 [15]	486 [3]	836 [12]
ν_7	155 [0]	164 [0]	129 [0]	543 [35]
ν_8	52 [0]	59 [1]	35 [0]	504 [3.4]
				481 [1.2]
				387 [7.5]
				235 [0.4]
				126 [0.0]
				52 [0.1]
E				
ν_9	2457 [1478]	2454 [1542]	2380 [750]	A" 2128 [564]
ν_{10}	1217 [628]	1220 [642]	1171 [188]	1164 [93]
ν_{11}	1130 [46]	1129 [78]	897 [166]	771 [65]
ν_{12}	796 [26]	793 [24]	713 [48]	702 [38]
ν_{13}	644 [32]	626 [26]	526 [4]	621 [76]
ν_{14}	468 [24]	466 [22]	413 [12]	551 [1.5]
ν_{15}	252 [4]	251 [4]	212 [2]	532 [3.6]
ν_{16}	36 [2]	39 [2]	19 [0]	380 [1.2]
				221 [0.7]
				58 [0.0]
				36 [0.1]

Table 8. Calculated Geometries (Angstroms and Degrees) of the Tetraazidammonium Cation, $N(N_3)_4^+$.

Geometry	RHF/6-31G*	MP2/6-31G*	NLDFT/TZVP
R_{12}	1.436	1.465	1.486
R_{23}	1.293	1.292	1.280
R_{34}	1.085	1.149	1.140
$\theta_{2'12}$	100.1	99.2	97.7
θ_{123}	106.8	106.1	109.4
θ_{234}	171.8	169.9	167.8

Table 9. Calculated Harmonic Frequencies in cm^{-1} and Infrared Intensities [] in km/mol of $N(N_3)_4^+$

	Mode	RHF/6-31G*	MP2/6-31G*	NLDFT/TZVP
A_1	υ_1	2599 [0]	2327 [0]	2145 [0]
	υ_2	1112 [0]	1185 [0]	1139 [0]
	υ_3	943 [0]	839 [0]	785 [0]
	υ_4	547 [0]	496 [0]	453 [0]
	υ_5	348 [0]	322 [0]	326 [0]
	υ_6	113 [0]	100 [0]	69 [0]
A_2	υ_7	582 [0]	478 [0]	509 [0]
	υ_8	118 [0]	69 [0]	29 [0]
B_1	υ_9	614 [0]	499 [0]	524 [0]
	υ_{10}	423 [0]	357 [0]	321 [0]
	υ_{11}	82 [0]	59 [0]	81 [0]
B_2	υ_{12}	2589 [52]	2312 [17.4]	2136 [54]
	υ_{13}	1231 [1]	1167 [5.0]	1168 [1.1]
	υ_{14}	1074 [26]	944 [2.0]	843 [14]
	υ_{15}	592 [1]	517 [0.1]	478 [2.0]
	υ_{16}	443 [6]	409 [2.8]	350 [4.5]
	υ_{17}	163 [0]	142 [0]	138 [0.4]
E	υ_{18}	2589 [584]	2318 [697]	2131 [461]
	υ_{19}	1161 [462]	1124 [581]	1084 [517]
	υ_{20}	965 [192]	912 [200]	808 [280]
	υ_{21}	842 [98]	755 [0.1]	668 [17]
	υ_{22}	615 [78]	510 [32.1]	540 [16]
	υ_{23}	473 [22]	418 [10.7]	376 [1.2]
	υ_{24}	226 [6]	196 [4.4]	190 [3.5]
	υ_{25}	87 [4]	66 [1.6]	92 [1.0]

Table 10. Total Energies and Zero Point Energies in a.u.

Molecule	RHF/6-31G*	MP2/6-31G*	MP2/6-31+G*	NLFDT/TZVP	ZPE(MO)	ZPE(DFT)
$[N(N_3)_2]^-$	-380.866256	-380.049745	-382.097251	-383.279397	0.026488	0.025501
$HN(N_3)_2$	-381.471597	-382.633146	-382.657992	-383.834412	0.041008	0.039862
$N(N_3)_3$	-544.111653	-545.773964		-547.457127	0.042438	0.040803
$[N(N_3)_4]^+$	-707.070221	-709.216858		-711.372735	0.055930	0.053014
HN_3	-163.838696	-164.341069	-164.351371	-164.866574	0.020720	0.020779
H_2	-1.126828	-1.144141		-1.177316	0.009450	0.009872
$[NH_2]^-$	-55.476076	-55.646944	-55.708453	-55.914567	0.017038	0.018145
NH_3	-56.184356	-56.354212	-56.363197	-56.585095	0.033040	0.033479
$[NH_4]^+$	-56.530771	-56.700294		-56.923952	0.047572	0.048538
$[N(N_3)_2H_2]^+$				-384.138845		0.052747
$H_2N(N_3)$				-220.206859		0.037762

Table 11. Reactions Used to Calculate Heats of Formation

	Reaction	ΔH(rxn) kJ/mol NLDFT
2	$NH_3 + 2HN_3 \rightarrow HN(N_3)_2 + 2H_2$	296.2
3	$NH_3 + 3HN_3 \rightarrow N(N_3)_3 + 3H_2$	443.5
4	$[NH_2]^- + 2HN_3 \rightarrow [N(N_3)_2]^- + 2H_2$	-4.5
5	$[NH_4]^+ + 4HN_3 \rightarrow [N(N_3)_4]^+ + 4H_2$	746.0
6	$HN_3 + NH_3 \rightarrow H_2 + H_2N(N_3)$	158.5
7	$H_2NN_3 + HN_3 \rightarrow H_2 + HN(N_3)_2$	137.6
8	$HN(N_3)_2 + HN_3 \rightarrow H_2 + N(N_3)_3$	147.3
9	$NH_3 + H^+ \rightarrow [NH_4]^+$	-856.2
10	$[N(N_3)_2]^- + H^+ \rightarrow HN(N_3)_2$	-1425.9
11	$HN(N_3)_2 + H^+ \rightarrow [N(N_3)H_2]^+$	-771.7
12	$2[N(N_3)_2H_2]^+ \rightarrow [NH_4]^+ + [N(N_3)_4]^+$	-60.2
13	$[NH_2]^- + H^+ \rightarrow NH_3$	-1726.5
14	$NH_3 + 2HN_3 \rightarrow [N(N_3)_2]^- + H^+ + 2H_2$	1721.7

Table 12. Experimental and Calculated Heats of Formation (298 K) in kJ/mol

Molecule	ΔH_f			
H_2	0.0 (expt)			
NH_3	-46 (expt)			
$[NH_2]^-$	113 ± 4 (expt)			
$[NH_4]^+$	630 (expt)			
$[H]^+$	1530 (expt)			
HN_3	294 (expt)			
$HN(N_3)_2$	811 (MO/Rxn2)	838 (DFT/Rxn2)		
$N(N_3)_3$	1232 (MO/Rxn3)	1280 (DFT/Rxn3)		
$[N(N_3)_2]^-$	649 (MO/Rxn4)	740 (MO+/Rxn4)	734 (DFT/Rxn10)	697 (DFT/Rxn4)
	780 (MO/Rxn14)	732 (MO+/Rxn14)	734 (DFT/Rxn14)	
$[N(N_3)_4]^+$	2429 (MO/Rxn5)	2552 (DFT/Rxn5)	2503 (DFT/Rxn12)	
H_2NN_3	407 (DFT/Rxn6)			
$[H_2N(N_3)_2]^+$	1597 (DFT/Rxn11)			

Figure Captions

Figure 1.   Geometry of $N(N_3)_2^-$ at the MP2/6-31G* level of theory.

Figure 2.   Total valence electron density plot calculated at the DFT level for the molecular plane of $N(N_3)_2^-$. The calculation was done with effective core potentials so as to eliminate the effects of the 1s orbitals on the density. The plot is for electron densities from 0.0 to 4.4 e/Å^3 in 0.2 e/Å^3 increments.

Figure 3   (a) Geometry of $HN(N_3)_2$ (C_s symmetry) at the MP2/6-31G* level of theory. (b) C_1 symmetry structure for $HN(N_3)_2$.

Figure 4.   Geometry of $N(N_3)_3$ at the MP2/6-31G* level of theory.

Figure 5.   Geometry of $N(N_3)_4^+$ at the MP2/6-31G* level of theory.

Figure 6.   Geometry of $HN(N_3)_2$ transition state at the HF/6-31G* level of theory.

Figure 7.   Geometry of $N(N_3)_3$ transition state at the HF/6-31G* level of theory.
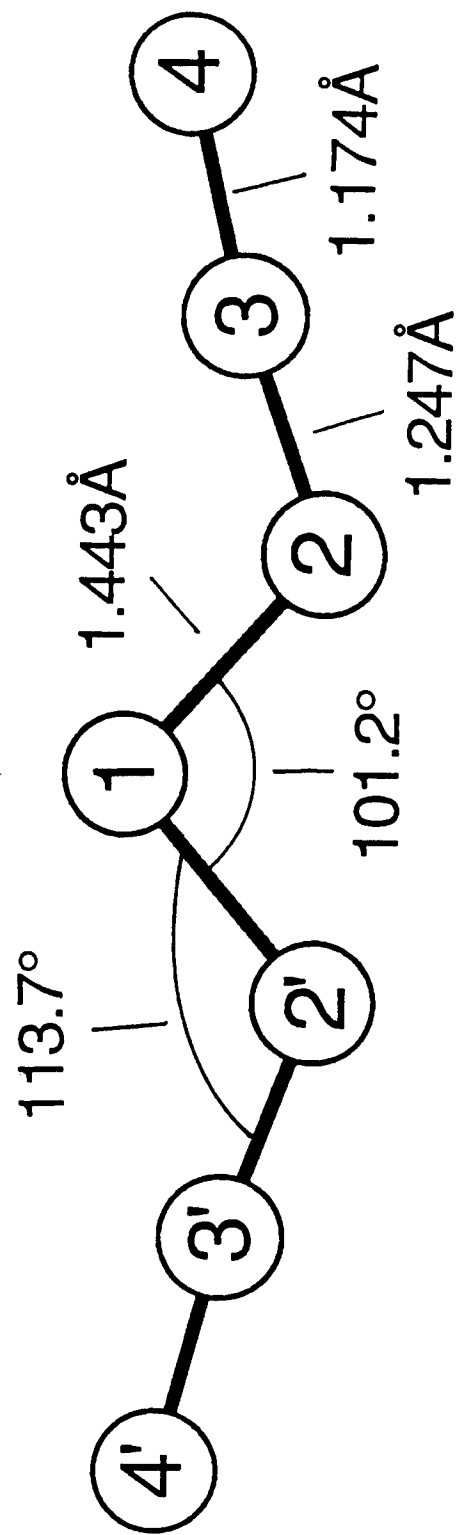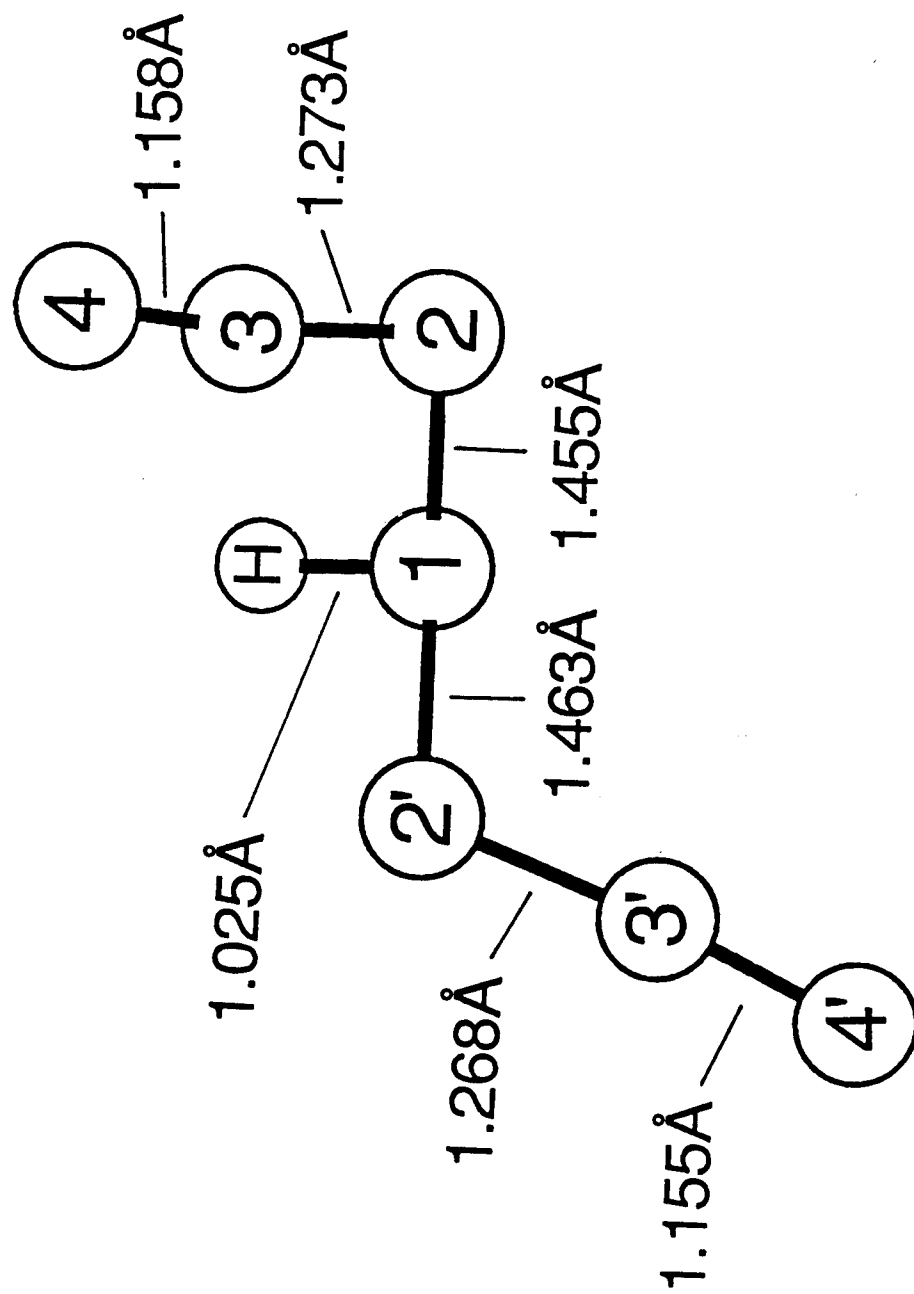
FIGURE 1
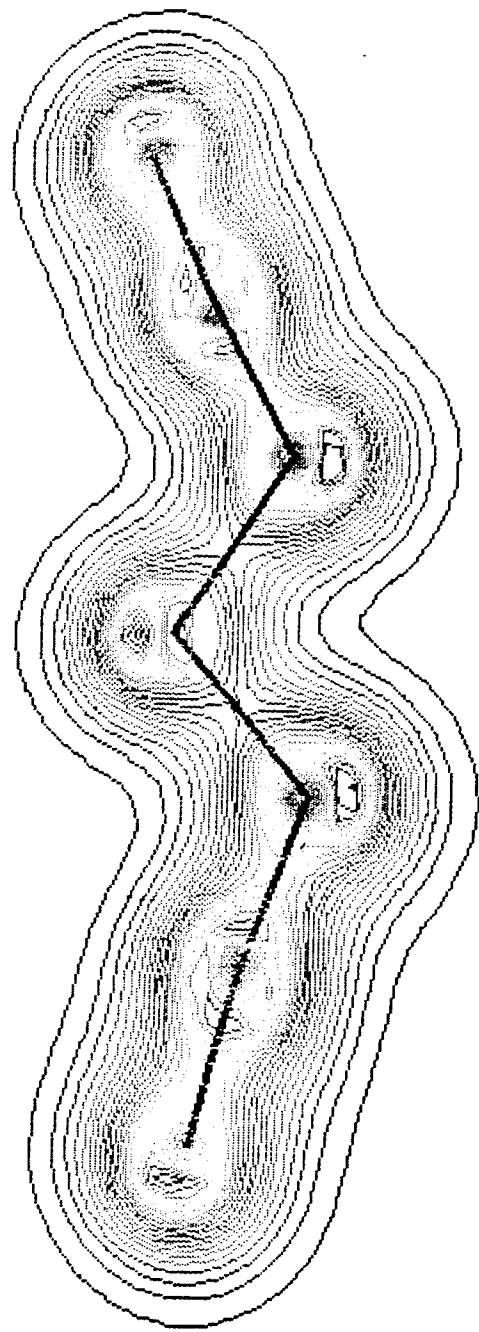
FIGURE 2
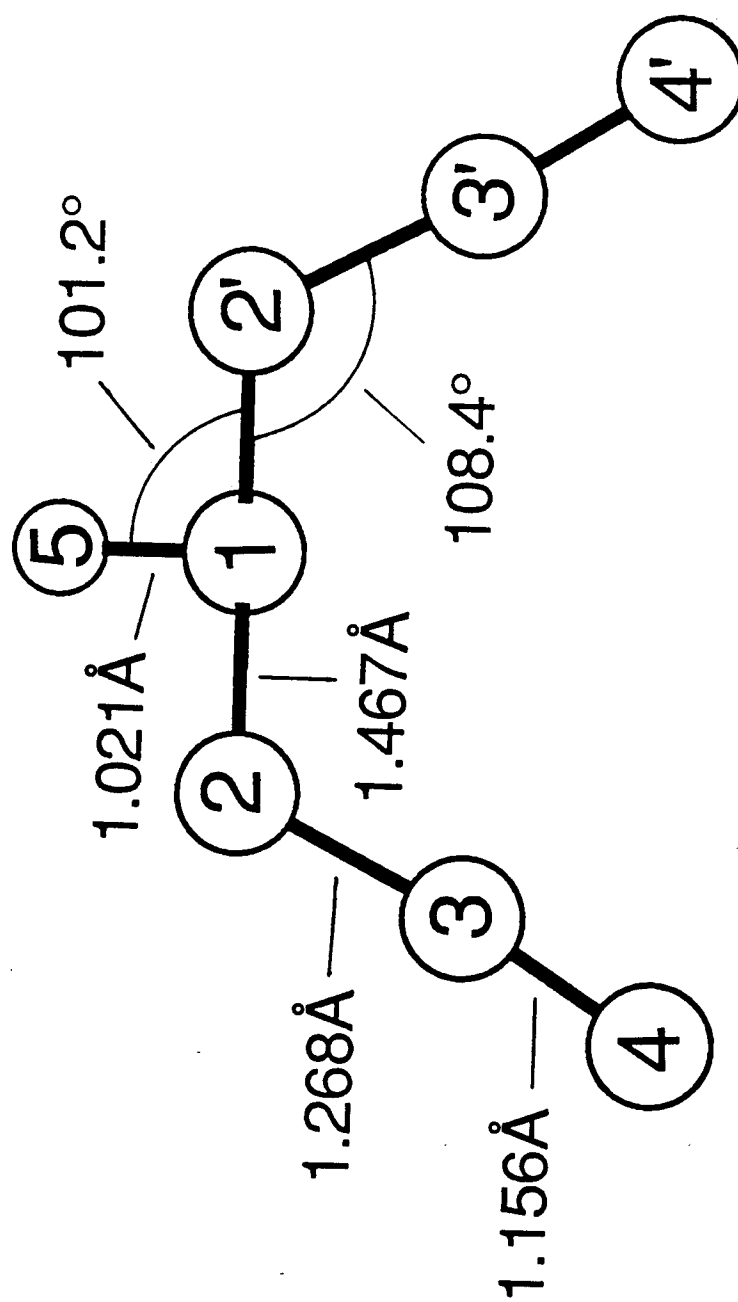
FIGURE 3a

FIGURE 3b

1.271Å

1.155Å

103.9°

1.463Å

FIGURE 4

1.465Å
1.292Å
1.149Å
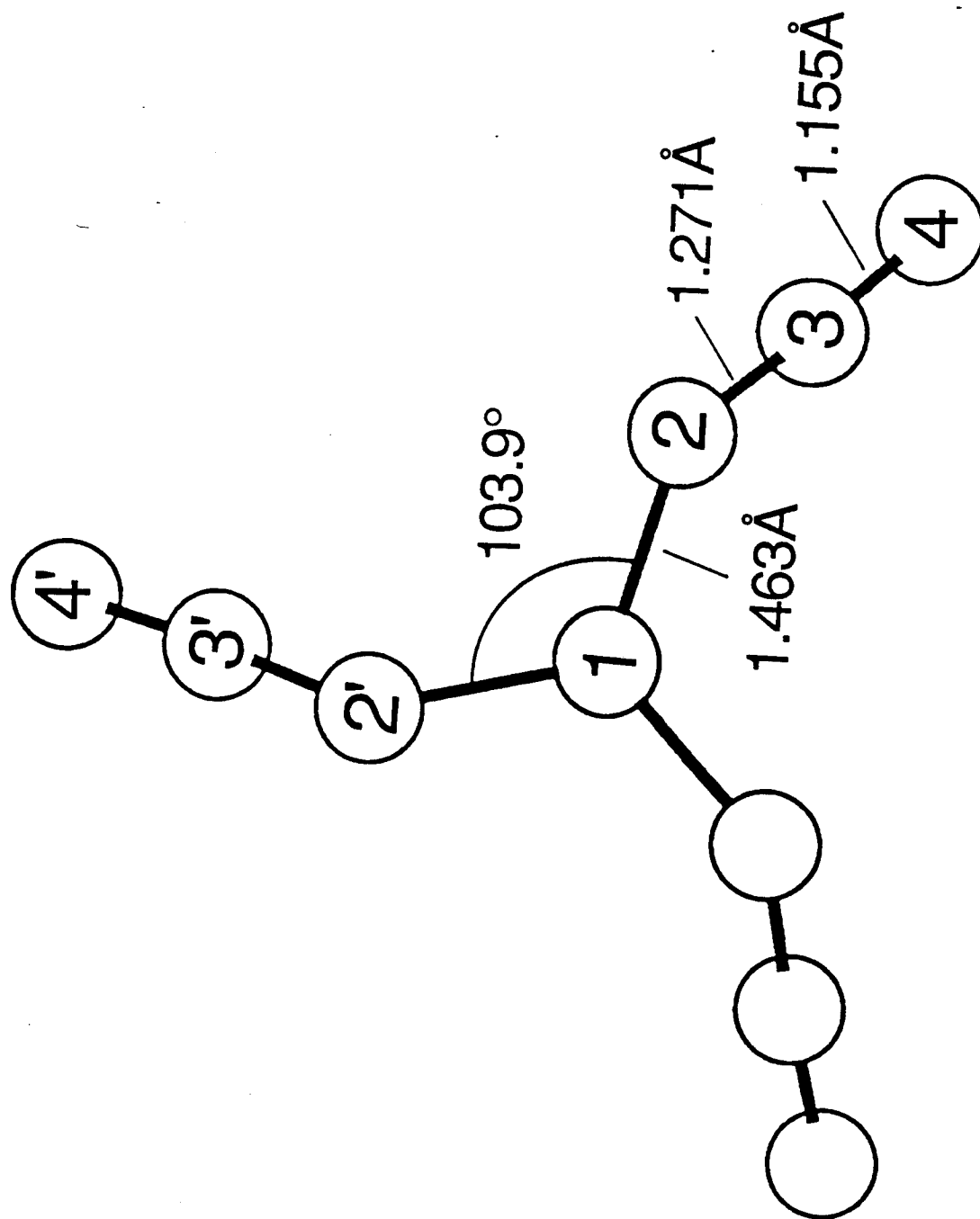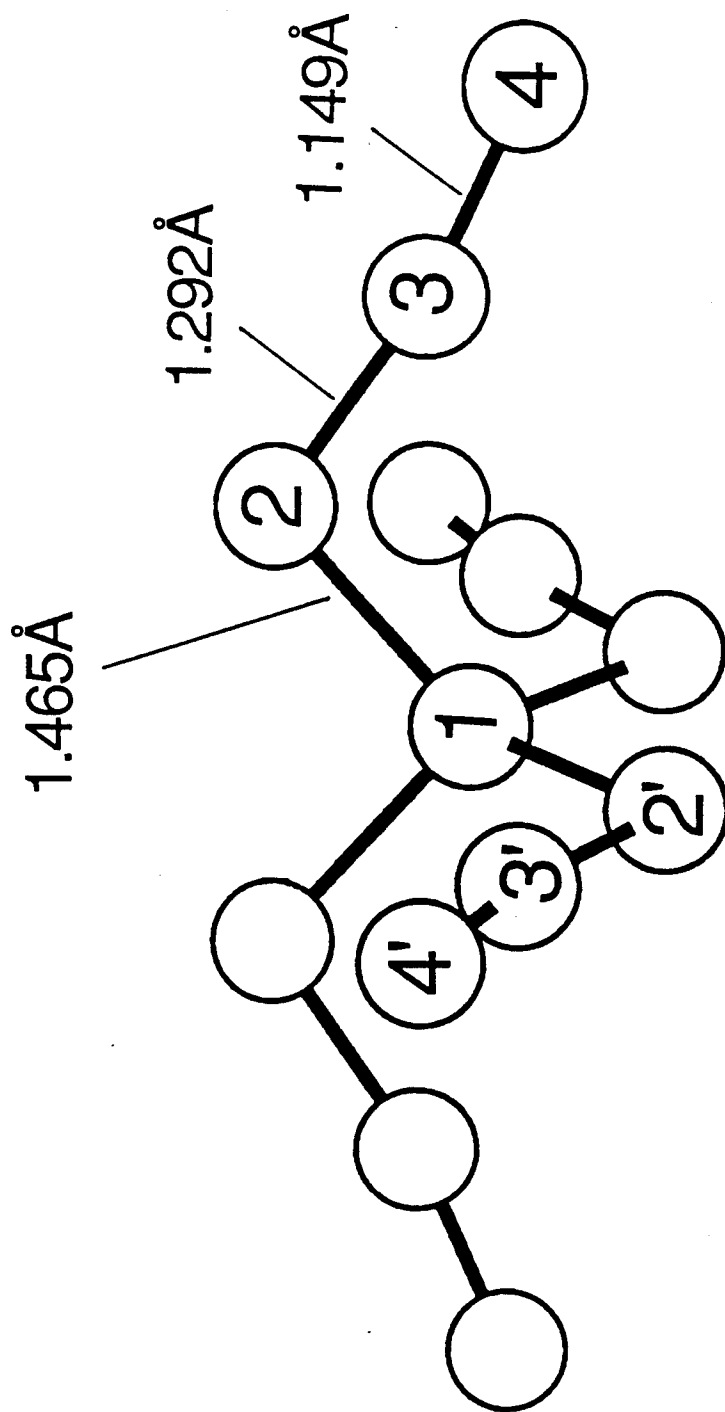
FIGURE 5
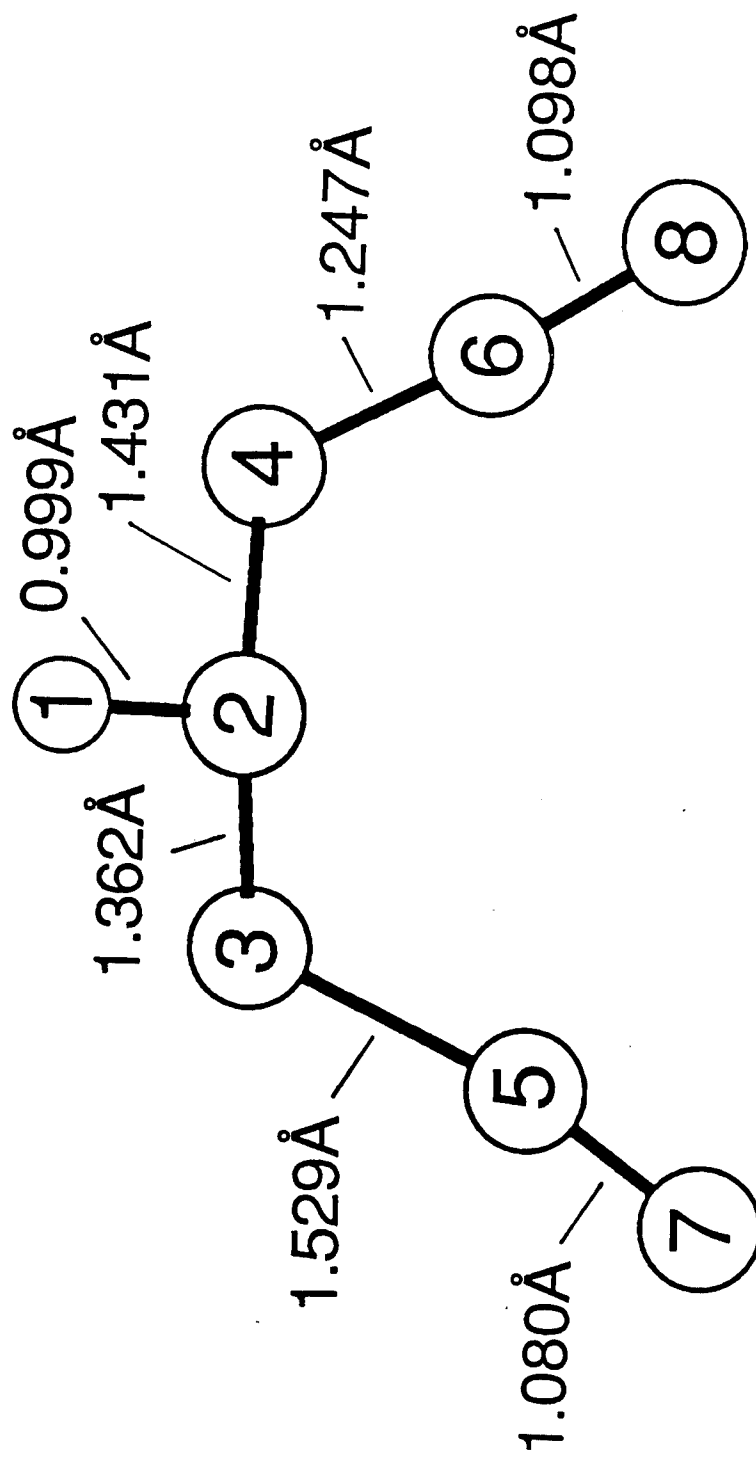
FIGURE 6

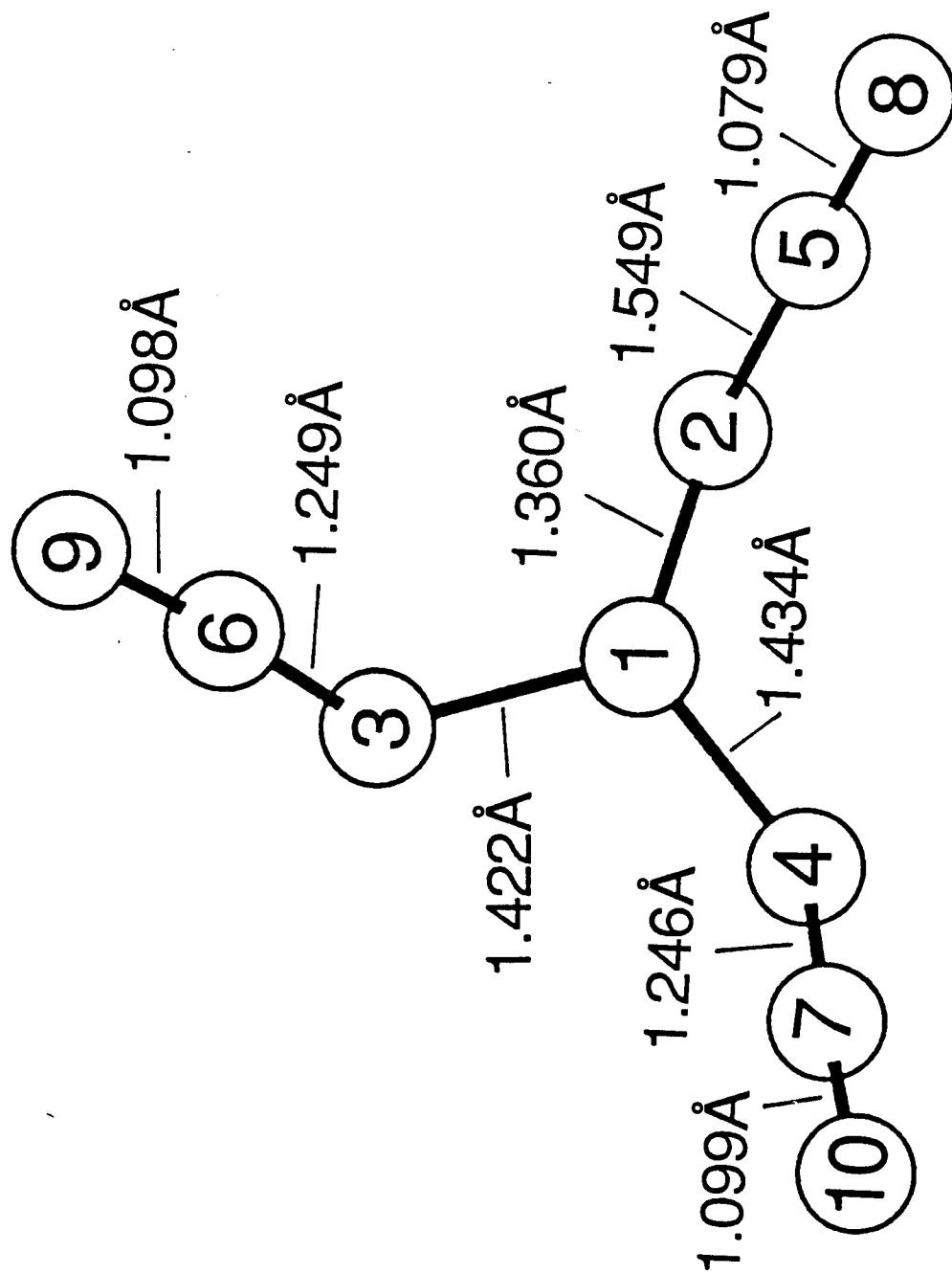**FIGURE 7**

Theoretical Prediction of the Structures and Stabilities of Azidamines

H. Harvey Michels, John A. Montgomery, Jr., Karl O. Christe, and David A. Dixon

Cartesian coordinates, geometry parameters and vibrational frequencies for the transition states for Reaction (16) for $HN(N_2)_3$ and $N(N_3)_3$ at the HF/6-31G* level.

Table S1. Cartesian Coordinates (Å) of transition state for reaction (16) for $HN(N_3)_2$ and $N(N_3)_3$.

$HN(N_3)_2$

8			
1	-0.149231	-1.825059	0.942977
7	-0.066652	-0.958596	0.453121
7	1.056179	-0.993034	-0.316386
7	-1.264849	-0.806294	-0.313698
7	1.804366	0.303467	-0.002720
7	-1.754083	0.313406	-0.062748
7	2.505994	1.123774	0.026426
7	-2.259638	1.278000	0.081294

$N(N_3)_3$

10			
7	0.091467	-0.074976	-0.377425
7	-0.995091	-0.615223	0.991632
7	1.268060	-0.767182	0.774514
7	0.261154	1.296259	0.760747
7	-1.820420	-1.235136	-0.162857
7	2.065440	-0.753238	-0.186313
7	-0.330084	2.001972	-0.078735
7	-2.542397	-1.769580	-0.760428
7	2.841835	-0.785377	-0.961723
7	-0.839961	2.702481	-0.754261

Table 2S. Molecular geometry parameters (Å and degrees) for the transition state for reaction (16) for $HN(N_3)_2$
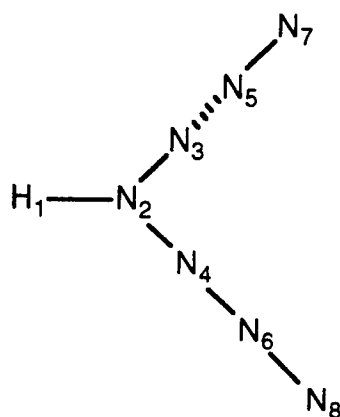
Parameter	Value	Parameter	Value
$r(H_1\text{-}N_2)$	0.999	$\theta(H_1\text{-}N_2\text{-}N_3)$	108.9
$r(N_2\text{-}N_3)$	1.362	$\theta(H_1\text{-}N_2\text{-}N_4)$	106.6
$r(N_2\text{-}N_4)$	1.431	$\theta(N_3\text{-}N_2\text{-}N_4)$	113.0
$r(N_3\bullet\bullet\bullet N_5)$	1.529	$\theta(N_2\text{-}N_3\bullet\bullet\bullet N_5)$	105.4
$r(N_5\text{-}N_7)$	1.080	$\theta(N_3\bullet\bullet\bullet N_5\text{-}N_7)$	165.3
$r(N_4\text{-}N_6)$	1.247	$\theta(N_2\text{-}N_4\text{-}N_6)$	108.4
$r(N_6\text{-}N_8)$	1.099	$\theta(N_4\text{-}N_6\text{-}N_8)$	174.3

Table 3S. Molecular geometry parameters (Å and degrees) for the transition state for reaction (16) for $(N_3)_3$
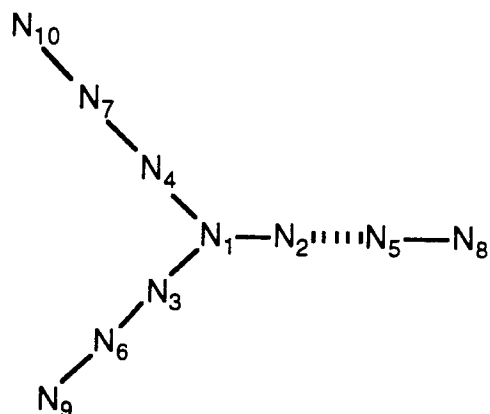
Paramter	Value	Parameter	Value
$r(N_1\text{-}N_2)$	1.360	$\theta(N_2\text{-}N_1\text{-}N_3)$	110.7
$r(N_1\text{-}N_3)$	1.422	$\theta(N_2\text{-}N_1\text{-}N_4)$	110.0
$r(N_1\text{-}N_4)$	1.434	$\theta(N_3\text{-}N_1\text{-}N_4)$	107.0
$r(N_2\bullet\bullet\bullet N_5)$	1.549	$\theta(N_1\text{-}N_2\bullet\bullet\bullet N_5)$	102.4
$r(N_5\text{-}N_8)$	1.079	$\theta(N_2\bullet\bullet\bullet N_5\text{-}N_8)$	165.4
$r(N_3\text{-}N_6)$	1.249	$\theta(N_1\text{-}N_3\text{-}N_6)$	107.9
$r(N_6\text{-}N_9)$	1.098	$\theta(N_3\text{-}N_6\text{-}N_9)$	174.2
$r(N_4\text{-}N_7)$	1.246	$\theta(N_1\text{-}N_4\text{-}N_7)$	107.8
$r(N_7\text{-}N_{10})$	1.099	$\theta(N_4\text{-}N_7\text{-}N_{10})$	174.7

Table S4. Vibrational frequencies (cm^{-1}) for the transition states for reaction (16) for HN(N$_3$)$_2$ and N(N$_3$)$_3$.

HN(N$_3$)$_2$	N(N$_3$)$_3$
3804	2667
2650	2465
2454	2442
1647	1267
1260	1229
1166	1184
1065	1138
974	1022
741	805
668	748
621	652
553	643
417	609
292	505
205	495
91	430
50	376
735i	245
	212
	128
	69
	38
	29
	667i

CHAPTER CONTRIBUTED TO THE NEW EDITION OF HOUBEN-WEYL'S METHODS OF ORGANIC CHEMISTRY
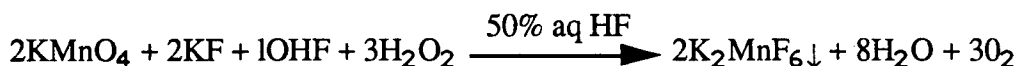
2.2 CHEMICAL METHODS FOR THE GENERATION OF FLUORINE

Generally, the electrochemical production of fluorine which involves only low cost chemicals and electricity in a single step process, is simpler and cheaper than the chemical generation of fluorine and, therefore, is used exclusively when larger amounts of fluorine are needed on a routine basis. However, occasions may arise when commercially sold fluorine gas or electrochemical cells for its production are either not available or not desirable for reasons such as logistics or safety. Under these circumstances, fluorine can be generated by chemical methods.

These methods can be classified into two categories. The first one is a purely chemical synthesis which excludes either techniques such as electrolysis, photolysis, electric discharge, etc. or the use of elemental fluorine for the synthesis of any of the required starting materials. The second category encompasses compounds which have been prepared from fluorine but can be decomposed by either mild heating or displacement reactions to evolve fluorine. Although, from a purist's point of view, this second category is better defined as a chemical storage and regeneration scheme of fluorine, it nevertheless is frequently included in the chemical methods for the generation of fluorine. In the following section, both categories of fluorine generation will be briefly described.
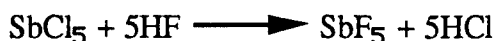
2.2.1. PURELY CHEMICAL SYNTHESIS OF FLUORINE

Attempts to prepare elemental fluorine by chemical methods preceded Moissan's electrochemical synthesis by at least 73 years [1] and did not succeed until 1986, [2] exactly 100 years after Moissan's famous discovery. [3] These failures by many notable chemists had led to the widespread misconception that fluorine, because of its status as the most electronegative element, could not be prepared by chemical means.

The first purely chemical synthesis of fluorine was accomplished in 1986 by Christe[2] and is remarkable for its simplicity and elegance. The two starting materials, K_2MnF_6 and SbF_5, had been known [4,5] for almost a century and can be readily prepared from HF solutions according to:

$$2KMnO_4 + 2KF + 10HF + 3H_2O_2 \xrightarrow{50\% \text{ aq HF}} 2K_2MnF_6\downarrow + 8H_2O + 3O_2$$

and

$$SbCl_5 + 5HF \longrightarrow SbF_5 + 5HCl$$

The original literature yield of 30% reported [4] for the K_2MnF_6 preparation was increased to 73% by using acetone in place of HF for the final washing of the product.[2] A simple Lewis acid displacement reaction was used to liberate MnF_4 which is thermodynamically

$$K_2MnF_6 + 2SbF_5 \xrightarrow{190°C} 2KSbF_6 + MnF_4$$
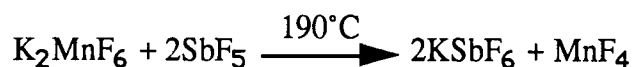
unstable and decomposes to lower manganese fluorides and elemental fluorine with yields in excess of 30%.

$$2MnF_4 \longrightarrow 2MnF_3 + F_2$$

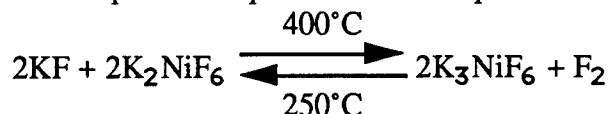The following procedure describes a typical preparation.

Fluorine: A prepassivated (with ClF_3) 0.75 inch o.d. Teflon-FEP U-trap, which was closed by two stainless steel valves, was loaded in the dry N_2 atmosphere of a glove box with 8 mmol of K_2MnF_6. The U-trap was connected to a stainless steel Teflon vacuum manifold,[6] the connections were leak checked and passivated, and about 35 mmol of SbF_5 was transferred in a dynamic vacuum into the U-trap which was cooled to -78°C. The U-tube was wrapped with a wire spiral to protect it against collapse during heating and, then, was heated in an oil bath for one hour at 190°C. The U-tube was cooled to room temperature and contained about 1.3 mmol of essentially pure fluorine gas. The only detectable impurities in the gas were traces of fluorocarbons from attack of the Teflon reactor by fluorine and of SbF_5. These impurities were eliminated by cooling the Teflon tube to -196°C before withdrawing the fluorine. Yield of fluorine: 30-35% based on

$$2K_2MnF_6 + 4SbF_5 \longrightarrow 4KSbF_6 + 2MnF_3 + F_2.$$

2.2.2. CHEMICAL STORAGE AND REGENERATION OF FLUORINE

The problems associated with the storage and handling of larger amounts of fluorine at high pressures can be avoided by the use of fluorine gas generators which are based on stable solids. Two practical approaches have been demonstrated,[7,8] out of which one is commercially available.[9] Both approaches are based on high oxidation state complex fluoro anions of transition metals such as Ni, Cu or Mn.

In the first approach,[7] the temperature dependence of the equilibrium

$$2KF + 2K_2NiF_6 \underset{250°C}{\overset{400°C}{\rightleftharpoons}} 2K_3NiF_6 + F_2$$

is exploited. The K_2NiF_6 is readily formed at 250°C and decomposes above 400°C to regenerate the fluorine at autogenous pressures as high as 25 atm. The following procedure describes the hardware required for the construction and operation of such a fluorine gas regenerator.

Fluorine Gas Regenerator (Asprey Model): A heliarc-welded, all nickel can of 850 mL volume was filled with an intimate mixture of 3 mol of NiF_2 and 9 mol of dry KF. The can was valved to a tank of F_2 gas and a vacuum pump and was heated by an electric resistance furnace. The can was heated slowly to 500°C under 10 atm of F_2 and then cooled to 250°C, while still under several atm of F_2. Several such cycles were carried out before using the device for the regeneration of F_2. For the regeneration of F_2, the salt was fluorinated at 250°C until no more F_2 was taken up. The can was then cooled to 225°C and evacuated to remove the excess fluorine and any volatile impurities. The temperature was then raised until the desired F_2 pressure (at 400°C, 25 atm) was achieved.

In a commercially available modification of this concept, the Kurchatov Institute of Atomic Energy is offering aluminum cylinders filled with $CaNiF_6$ which on heating evolve fluorine.[9] The main characteristics of these cylinders are operating temperatures of 140-260°C, maximum pressure at 260°C=2 atm, and a weight of a 100 L F_2 unit =2.4 kg. Due to the marginal thermal stability of $CaNiF_6$, these cylinders must be kept and transported at temperatures below 60°C.

In the second approach,[8] the high oxidation state transition metal fluoroanion salts are reacted with a solid Lewis acid. The underlying chemical principle is the same as that used for the purely chemical synthesis of fluorine. A stronger Lewis acid displaces the high oxidation state transition metal fluoride from its salt to form the thermodynamically unstable free parent molecule which, then, rapidly decomposes to a lower oxidation state fluoride and elemental fluorine. A typical generator, containing 1 mol of K_2NiF_6 and 3 mol of BiF_5, generates 0.75 mol of F_2 at superatmospheric pressure when heated to temperatures above 70°C. The fluorine evolution rate is temperature dependent and, therefore, can easily be controlled. The stoichiometry for the above reaction is:

$$K_2NiF_6 + 2BiF_5 \longrightarrow 2KBiF_6 + NiF_2 + F_2$$

In place of K_2NiF_6, other salts, such as Cs_2CuF_6, Cs_2MnF_6 or K_2MnF_6, or other Lewis acids, such as TiF_4, can be used. The following procedure describes a typical fluorine generator.

Fluorine Gas Generator (Christe Model): A 100 ml stainless steel cylinder, equipped with a valve and a pressure transducer, was loaded inside a dry box with an intimate mixture of 60 mmol of K_2NiF_6 and 180 mmol of BiF_5. The cylinder was evacuated at room temperature and then heated until F_2 evolution set in at about 60-70°C. The heating rate was followed by observation of the pressure build-up and adjusted to provide the desired amounts and pressures of F_2 (maximum F_2 yield and pressure, about 45 mmol of F_2 and 10 atm).

REFERENCES

(1) H. Davy, *Phil. Trans. R. Soc.* London 103, 263 (1813).

(2) K.O. Christe, *Inorg. Chem.* 25, 3721 (1986).

(3) H. Moissan; *C.R. Hebd. Seances Acad. Sci.* 102, 1543 (1886).

(4) R.F. Weinland, O. Lauenstein, *Z. Anorg. Allg. Chem.* 20, 40 (1899).

(5) O. Ruff, *Ber. Dtsch. Chem. ges.* 39, 4310 (1906).

(6) K.O. Christe, R.D. Wilson, C.J. Schack, *Inorg. Synth.* 24, 3 (1986).

(7) L.B. Asprey, *J. Fluorine Chem.* 7, 359 (1976).

(8) K.O. Christe, R.D. Wilson, *Inorg, Chem.* 26, 2554 (1987).

(9) Available from: I.V. Kurchatov Institute of Atomic Energy, Department of Chemical Physics, 123182 Kurchatov Square, Moscow, Russia.

On the Structure of the [XeOF$_5$]$^-$ Anion and of Heptacoordinated Complex Fluorides Containing One or Two Highly Repulsive Ligands or Sterically Active Free Valence Electron Pairs[‡]

Karl O. Christe,[*1] David A. Dixon,[2] Jeremy C. P. Sanders,[3] Gary J. Schrobilgen,[3] Scott S. Tsai,[3] and William W. Wilson[1]

Contribution from Rocketdyne, A Division of Rockwell International, Canoga Park, California 91309, The DuPont Company, Central Research and Development, Experimental Station, Wilmington, Delaware 19880-0328, and the Department of Chemistry, McMaster University, Hamilton, Ontario L8S 4 MI, Canada

ABSTRACT

The new [XeOF$_5$]$^-$ salt, N(CH$_3$)$_4$XeOF$_5$, was prepared. This highly explosive compound was characterized by infrared, Raman, and multinuclear NMR spectroscopy. The electronic structure, vibrational frequencies, and force field of the free [XeOF$_5$]$^-$ anion in C$_{4v}$ and C$_{5v}$ symmetry were calculated at the LDFT/PP/DZVP, NLDFT/PP/DZVP, HF/ECP/DZP, and MP2/ECP/DZP levels of theory. Except at the Hartree Fock level, all of the calculations predict for free [XeOF$_5$]$^-$ a pseudooctahedral C$_{4v}$ structure with a sterically inactive free valence electron pair on Xe to be lower in energy than a C$_{5v}$ structure in which the oxygen and the sterically active free valence electron pair on Xe occupy the two axial positions of a pseudopentagonal-bipyramid. The vibrational spectra which were experimentally observed for solid [XeOF$_5$]$^-$ salts agree only with the spectra predicted from the C$_{5v}$ model. The C$_{5v}$ structure of [XeOF$_5$]$^-$ is analogous to those found for IF$_7$, [IOF$_6$]$^-$, and [XeF$_5$]$^-$, but differs from the distorted octahedral C$_s$ structures found for XeF$_6$ and [IF$_6$]$^-$ and previously also proposed for [XeOF$_5$]$^-$. The preferences of heptacoordinated molecules for either pentagonal-bipyramidal or distorted octahedral structures and the fluxionality of some of these structures can be rationalized by the presence or absence of unequal ligand repulsion effects.

INTRODUCTION

The $XeOF_4$ molecule can form 1:1 and 3:1 complexes with strong Lewis bases, such as KF, RbF, CsF, and NOF.[4-6] The structure of the 3:1 complexes was established by X-ray crystallography and shown to contain the $[F(XeOF_4)_3]^-$ anion which consists of three $XeOF_4$ molecules bridged to a central $[F]^-$ anion.[7,8] For the $[XeOF_5]^-$ anion which is present in the 1:1 adducts, structure I of C_s symmetry was proposed[7,8] based on the observed Raman spectrum. The free valence electron pair on Xe was assumed to be sterically active and to occupy an XeF_3 face.

I (C_s)
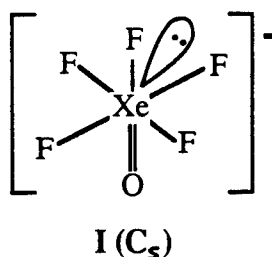
This structural model was based on the structures found for XeF_6[9] and $[IF_6]^-$.[10] However, by analogy with the recently determined structures of $[XeF_5]^-$[11] and $[IOF_6]^-$,[12]
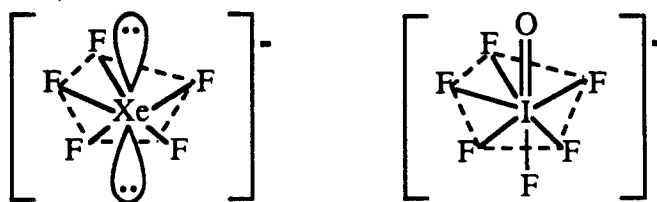

structure II of C_{5v} symmetry also needs to be considered for $[XeOF_5]^-$.

II (C_{5v})
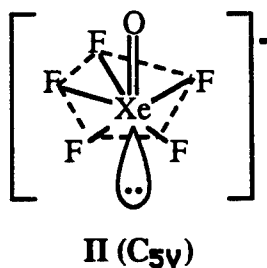
This structure can be derived from that of $[XeF_5]^-$ by replacement of a sterically active free valence electron pair on Xe by a doubly bonded oxygen ligand.

Another structure for $[XeOF_5]^-$ which might also be of low energy is **III** in which the free valence electron pair on Xe is sterically inactive resulting in C_{4v} symmetry.
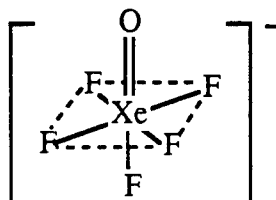
III (C_{4v})

It was, therefore, of interest, to reexamine the structure of the $[XeOF_5]^-$ anion. To minimize anion-anion interactions and to increase the solubility of the $[XeOF_5]^-$ salts for NMR studies and possible growth of single crystals for X-ray diffraction, a larger counter cation was desired. This prompted us to attempt the synthesis of $N(CH_3)_4XeOF_5$ and, if successful, to study its structure.

EXPERIMENTAL SECTION

Caution! The $XeOF_4$ - CH_3CN - $N(CH_3)_4F$ system is hazardous and explosions have occurred several times when either rapidly cooling this system or handling solid $N(CH_3)_4XeOF_5$. Its handling should be limited to small quantities and appropriate safety precautions and shielding should be used at all times.

Materials and Apparatus. Literature methods were used for the syntheses of $XeOF_4$,[12] anhydrous $N(CH_3)_4F$,[13] the $^{17,18}O$-enriched $XeOF_4$ (oxygen isotopic composition: ^{16}O, 36.5%, ^{17}O, 26.5%, and ^{18}O, 37.0%),[14] and the drying of CH_3CN.[15]

Acetonitrile was transferred in a flamed out Pyrex glass vacuum line that was equipped with Kontes glass-Teflon valves and a Heise pressure gauge. The oxidizers were handled in a stainless steel vacuum line equipped

with Teflon-FEP U-traps, 316 stainless steel bellows-seal valves, and a Heise pressure gauge.[16] The metal line and the reactor were passivated before use with ClF_3, BrF_5 and XeF_6. Nonvolatile materials were handled in the dry nitrogen atmosphere of a glove box.

The infrared, Raman, and MNR spectrometers that were used in this study have previously been described.[15] A Perkin-Elmer differential scanning calorimeter, Model DSC-1B, was used to determine the thermal stability of the salt. The samples were crimp-sealed in aluminum pans, and a heating rate of $10°C/min$ in N_2 was used.

**Synthesis of $N(CH_3)_4XeOF_5$.** A 3/4" o.d. Teflon-FEP ampule, that was closed by a stainless valve, was loaded in the dry box with $N(CH_3)_4F$ (1.724 mmol), and CH_3CN (7.35 ml) was added on the glass vacuum line. The ampule was connected to the steel vacuum line and $XeOF_4$ (1.938 mmol) was added at -196°C. The mixture was allowed to warm behind a blast shield to room temperature with occasional gentle agitation. All material volatile at 20°C was pumped off for 4 hours leaving behind a white solid (549 mg, weight calculated for 1.724 mmol of $N(CH_3)_4XeOF_5$ = 545.3 mg), that was identified by vibrational spectroscopy as $N(CH_3)_4XeOF_5$.

Computational Methods. A variety of electronic structure calculations were performed in order to calculate the geometries, relative energies and vibrational frequencies of $[XeOF_5]^-$. The electronic structure calculations were done at four different levels and all calculations were done on a Cray YMP computer. The first set of calculations were done at the Hartree-Fock (HF/ECP/DZP) level with the program GRADSCF.[17] A polarized double zeta valence basis set[18] (DZP) was used for all of the atoms with the inner shell electrons on Xe being treated by an effective core potential (ECP).[19] The geometries and frequencies at this level were calculated by using analytic derivative methods.[20,21] Calculations were then performed at the second order Møller-Plesset (MP2/ECP/DZP) level with only the valence electrons correlated.[22] The same basis set as used for the Hartree-Fock calculations was used for the MP2 calculations. The geometries were optimized and frequencies were calculated by numerical differentiation of the first derivatives at the MP2 level. The MP2 calculations were done with the program Gaussian92.[23]

4

Density functional calculations were done with the program DGauss[24] at the local (LDFT) and nonlocal (NLDFT) (gradient-corrected) levels with two basis sets, one in which all of the electrons are included in a double zeta valence polarized (DZVP)[25] basis set and one in which the Xe core electrons are treated with a pseudopotential[26] (PP) and the remaining electrons are treated with a polarized valence double zeta basis set. The local potential fit of Vosko, Wilk and Nusair[27] was used at the local level (VWN/DZVP and VWN/PP/DZVP). The gradient corrected or non-local density functional calculations were done with the non-local exchange potential of Becke[28] together with the non-local correlation functional of Perdew[29] (BP/DZVP and BP/PP/DZVP). The geometries were optimized by using analytic gradient methods. The second derivatives at the all-electron, LDFT level (VWN/DZVP) were calculated analytically[30] whereas at the NLDFT level or when pseudopotentials were used the second derivatives were calculated by numerical differentiation of the analytic first derivatives. A 2 point method with a finite difference of 0.01 a.u. was used.

RESULTS AND DISCUSSION

Synthesis and Properties of $N(CH_3)_4XeOF_5$. The synthesis of $N(CH_3)_4XeOF_5$ was achieved according to reaction (1).

$$N(CH_3)_4F + XeOF_4 \xrightarrow[20°C]{CH_3CN} N(CH_3)_4XeOF_5 \qquad (1)$$
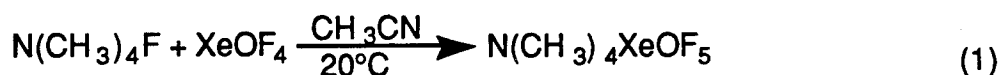
The compound is a white, highly sensitive solid that can explode when touched with a spatula. Rapid freezing of CH_3CN mixtures has also resulted in explosions. Its thermal stability was examined by differential scanning calorimetry. It undergoes a strongly exothermic, violent decomposition at 145°C. The compound's solubility in CH_3CN at 25°C is very low and strongly decreases with decreasing temperature. This poor solubility in CH_3CN has limited the NMR studies to room temperature and has frustrated attempts to grow single crystals for an X-ray diffraction study.

^{129}Xe, ^{17}O, and ^{19}F NMR Study of XeOF$_5^-$. The solubility of N(CH$_3$)$_4$XeOF$_5$ in CH$_3$CN was sufficient to allow the observation of ^{129}Xe, ^{17}O and ^{19}F NMR spectra at room temperature.

The ^{129}Xe NMR spectrum of a saturated solution of N(CH$_3$)$_4$XeOF$_5$ (oxygen isotope composition: ^{16}O, 35.4%; ^{17}O, 21.9%; ^{18}O, 42.7%) in CH$_3$CN at 30°C [Figure (1)] reveals a broad singlet ($\Delta\upsilon_{1/2}$ = 2707 Hz) at δ(^{129}Xe) = 357.9 ppm. The lack of resolved spin-spin coupling to the five ^{19}F ligand nuclei can be attributed to intermolecular fluorine exchange which has also previously been observed, although to a much lesser extent, in the structurally related [XeF$_5$]$^-$ anion.[11] Attempts to reduce the rate of exchange by cooling the sample or by adding excess N(CH$_3$)$_4^+$F$^-$ were unsuccessful owing to the very low solubility of N(CH$_3$)$_4$XeOF$_5$ in CH$_3$CN below room temperature. The ^{129}Xe chemical shift is substantially more shielded (i.e., by -357.9 ppm) than that of neat XeOF$_4$[δ(^{129}Xe) = 0.0 ppm] This follows the expected trend of increased shielding with an increase in negative charge which is also observed for the ^{129}Xe shielding of XeF$_5^-$ with respect to that in XeF$_4$.[11,31]

The ^{17}O NMR spectrum of the same sample [Figure (2)] shows a broad singlet ($\Delta\upsilon_{1/2}$ = 327 Hz) at δ (^{17}O) = 270.8 ppm. In addition, shoulders are observed at the base of the resonance which are attributed to natural abundance (26.44%) ^{129}Xe satellites and demonstrate the nonlability of the Xe=O bond. Gaussian deconvolution of the spectrum allows the extraction of ^{1}J(^{17}O-^{129}Xe) as 566 Hz. This coupling is significantly smaller than the ^{1}J(^{17}O-^{129}Xe) coupling in XeOF$_4$ and [XeOF$_3$]$^+$ (viz., 704 Hz[14] and 619 Hz,[32] respectively) which may be a consequence of the more polar bonds in the anion.

The ^{19}F NMR spectrum of a saturated solution of N(CH$_3$)$_4$XeOF$_5$ in CH$_3$CN at 30°C [Figure (3)] reveals two resonances: an intense broad singlet ($\Delta\upsilon_{1/2}$ = 975 Hz) at δ(^{19}F) = 118.9 ppm and a weak sharp singlet flanked by ^{129}Xe satellites [^{1}J(^{19}F-^{129}Xe) = 1570 Hz] at δ(^{19}F) = 92.5 ppm. The broad resonance is attributed to the [XeOF$_5$]$^-$ anion with the fluoride ligands undergoing intermolecular exchange in agreement with the findings in the ^{129}Xe spectrum; the weak sharp resonance results from a small amount of solvated XeOF$_4$. The high frequency ^{19}F chemical shift of [XeOF$_5$]$^-$ with respect

6

to $XeOF_4$ parallels the similar behavior of the ^{19}F chemical shifts of the pentagonal plane of F ligands in XeF_4 and IOF_5.[11,15] This chemical shift trend appears to be characteristic of a pentagonal planar arrangement of fluorine ligands around a heavy main-group atom[11,15,33] and indicates that the $[XeOF_5]^-$ anion adopts a pentagonal-bipyramidal structure, in agreement with the data from the vibrational spectra of $N(CH_3)_4XeOF_5$ (see below).

Vibrational Spectra and Electronic Structure Calculations. The vibrational spectra of $N(CH_3)_4XeOF_5$ were recorded and are summarized in Table 1. They are in good agreement with the Raman spectra previously reported[6-8] for $CsXeOF_5$ for which a distorted octahedral structure of C_s symmetry had been proposed.[7,8] In the absence of a crystal structure, the vibrational spectra were thoroughly analyzed to distinguish between the different possible structural models. Since the previously reported[6] Raman spectrum of $CsXeOF_5$ at low temperatures exhibited splitting into numerous extra bands,[7,8] the number of observed bands alone does not permit a positive distinction between the different symmetries of the proposed models. To overcome this problem, electronic structure calculations were carried out for $[XeOF_5]^-$ at a number of theoretical levels.

Before we discuss the calculations, we first describe our results on the model compound $XeOF_4$ whose structure and vibrational spectra are well -understood. Calculations were done at the HF/ECP/DZP, MP2/ECP/DZP, VWN/DZVP, VWN/PP/DZVP, BP/DZVP, and BP/PP/DZVP levels. The geometry results[33] are shown in Table 2 and the frequencies[34] are shown in Table 3. The geometry results show some interesting trends. The HF/ECP/DZP and MP2/ECP/DZP calculations predict the Xe=O bond to be too long by less than 0.02 Å. The Xe-F bond length is bracketed by the two methods with the HF results short by 0.02 Å and the MP2 value long by 0.055 Å. At the LDFT and NLDFT levels, neither all-electron calculation can reproduce the experimental geometry. However, the use of a pseudopotential on Xe leads to much better results. At both the LDFT and NLDFT levels, the Xe=O bond length is shorter than the experimental value. The VWN/PP/DZVP value for the Xe-F bond length is short by 0.02 Å whereas the BP/PP/DZVP result is slightly longer. The best prediction of the geometry is at the BP/PP/DZVP level. The vibrational spectra show some interesting trends. Although the Xe=O bond length is

7

predicted reasonably well at the HF level, the Xe=O harmonic stretch is predicted to be too low by almost 150 cm^{-1}. Scaling the stretches (excluding the Xe=O stretch) at the HF level by 0.89 and the bends by 0.84 brings the results into better agreement with the experimental values. The MP2 level predicts the Xe=O stretch to be high by 75 cm^{-1}, consistent with the fact that the theoretical value is harmonic and the experimental value includes anharmonic effects. As would be expected based on the geometries, the DFT calculations with the DZVP basis set do a poor job at predicting the frequencies for XeOF$_4$. Use of the unscaled VWN values seems to give the best agreement with experiment. The only differences between the calculated and experimental values at the VWN level that are greater than 20 cm^{-1} are υ_3, υ_7 and υ_9 with the largest error of 46 cm^{-1} found for υ_7. Based on these results for XeOF$_4$, we only performed calculations on [XeOF$_5$]$^-$ with either pseudopotentials or effective core potentials at the HF, MP2, VWN, and BP levels.

The calculations on [XeOF$_5$]$^-$ were done for the C$_{5v}$ (II) and C$_{4v}$ (III) structures. An attempt to find a vibrationally stable structure of C$_s$ symmetry for Model I was unsuccessful. Both the C$_{5v}$ (II) and C$_{4v}$ (III) structures were found to be stable vibrational minima at all levels of theory except at the HF level where the C$_{4v}$ structure essentially dissociated into XeOF$_4$ and [F]$^-$. In the three cases where correlation energy is included at some level in the calculation, the C$_{4v}$ structure is actually predicted to be more stable than the C$_{5v}$ structure by 15.1, 8.4 and 12.9 kcal/mol at the MP2, VWN and BP levels, respectively. The geometry parameters for [XeOF$_5$]$^-$ in C$_{5v}$ symmetry are given in Table 4. By using appropriately chosen scale factors from XeOF$_4$, we can estimate an "experimental" structure of [XeOF$_5$]$^-$. The Xe=O bond distance is not predicted to change significantly from that in XeOF$_4$. However, there is a significant lengthening of the Xe-F bonds by 0.08 Å on addition of [F]$^-$ to XeOF$_4$. The Xe-F distance is predicted to be slightly shorter than the average value of r(Xe-F) = 2.01 Å found experimentally in the crystal for [XeF$_5$]$^-$.

The vibrational spectra which were experimentally observed for the solid XeOF$_5^-$ salts (see Table 1), are in accord only with the C$_{5v}$ results and not with those[35] predicted for the energetically favored C$_{4v}$ structure. This disagreement is deemed insignificant because (1) the energy differences between the C$_{5v}$ and C$_{4v}$ structures are not large; (2) the energies were

calculated for the free gaseous $XeOF_5^-$ ion and not for solid $XeOF_5^-$ salts; (3) the electronic structure calculations at these levels of theory might not reliably predict effects as subtle as the steric activity of a free valence electron pair, and (4) the steric activity of a free valence electron pair of an ion in a solid salt can be strongly influenced by the nature of the counterion, as has been demonstrated[36] for the structurally closely related SeX_6^{2-} and TeX_6^{2-} salts. Depending on the symmetry of the crystal field, the free valence electron pair on the central atom of these anions can be sterically either active or inactive. As an example of the difficulty in predicting the geometry of these ions, we calculated the electronic structure of the isoelectronic $[IF_6]^-$ ion. At the HF level,[37] it has been shown that the structure with C_{3v} symmetry is lower in energy by 23.5 kcal/mol compared to the O_h structure and the C_{2v} symmetry structure is 21.6 kcal/mol lower in energy than the octahedral structure. This result is consistent with the experimental measurements on this compound.[10,38] At the VWN/PP/DZVP level, $[IF_6]^-$ is predicted to be very close to an octahedron although there may be a slight distortion to C_{3v} symmetry. Beginning from a structure of C_{2v} symmetry, the structure collapsed to a structure of O_h symmetry whereas beginning from C_{3v} symmetry, the structure relaxed to a nearly octahedral structure with C_{3v} symmetry which is only 0.5 kcal/mol more stable than the O_h structure. A structure of C_{5v} symmetry was found to be a minimum for $[IF_6]^-$ but was found to be 16.0 kcal/mol less stable than the structure of near O_h symmetry.

A normal coordinate analysis was also carried out for $[XeOF_5]^-$ in point group C_{5v}. The nine fundamental vibrations can be classified as $\Gamma = 3A_1(IR,Ra) + 3E_1(IR,Ra) + 3E_2(Ra)$. The internal coordinates and symmetry coordinates used for $[XeOF_5]^-$ are analogues to those previously given for the closely related $[XeF_5]^{-11}$ and $[IOF_6]^{-15}$ anions. The symmetry force constants and the potential energy distribution for $XeOF_5^-$ are summarized in Table 5. The listed force field is based on the A_1 and E_2 blocks from the VWM/PP/DZVP calculation and the E_1 block from the HF/ECP/DZP calculation because their scaled frequencies showed the smallest deviations from the experimental values. The use of symmetry blocks from two different sets of calculations is permissible since the symmetry blocks are completely independent of each other. The internal stretching force constants of $[XeOF_5]^-$ are compared in Table 6 to those of

9

closely related molecules[11,34,39] and ions and exhibit the expected trends, i.e., the addition of a negatively charged $[F]^-$ ligand to $XeOF_4$ or XeF_4 causes a weakening of both the Xe=O and the Xe-F bonds due to an increase of the polarities of the Xe-ligand bonds. The addition of an oxygen ligand to $[XeF_5]^-$ or XeF_4 results in a slight strengthening of the Xe-F bonds, but the effect is small and indicates that the electron withdrawing effect of the oxygen ligand is weak i.e., the effective electronegativities of the oxygen ligand and the $[XeF_5]^-$ or XeF_4 groups must be similar.

DISCUSSION

The above results and their analysis strongly support for $[XeOF_5]^-$ a pseudopentagonal-bipyramidal structure of C_{5v} symmetry with a localized free valence electron pair on Xe. This structure is analogous to those known for $[XeF_5]^-$ and $[IOF_6]^-$ but differs from that of free XeF_6 which is a highly fluxional, dynamically distorted octahedron with six fluorine ligands and a delocalized sterically active free valence electron pair on xenon. This raises the question as to what causes this different behavior of the free valence electron pair in these heptacoordinated species. The following rationale provides a ready answer. If in a heptacoordinated species all seven ligands are identical, as for example in IF_7,[40] $[TeF_7]^-$ or $[XeF_7]^+$,[41] the resulting structure is a highly fuxional pentagonal-bipyramid in which axial and equatorial ligands can easily exchange positions. If one of the seven ligands is replaced by a more repulsive or space filling ligand, such as a doubly bonded oxygen atom in $[IOF_6]^-$,[15] this more repulsive ligand will be restricted to one of the less crowded axial positions because a positional exchange with an equatorial ligand is energetically unfavorable. This results in a rigid structure of C_{5v} symmetry. If, however, this more repulsive ligand is a free valence electron pair which can be easily delocalized, the resulting structure can readily undergo dynamic distortion and intramolecular fluorine exchange and one obtains the dynamically distorted octahedral XeF_6 type structures. Another example of this type of structure is $[IF_6]^-$.[10,38] This type of structure, however, is only observed if there is enough room around the central atom for seven ligands. If the maximum coordination number is reduced to six, as in $[ClF_6]^{-42}$ or $[BrF_6]^-$,[38,43,44] the free valence electron pair becomes sterically inactive resulting in a rigid octahedron.

Replacement of two fluorine ligands in XF_7 by more repulsive ligands invariably leads to a rigid pentagonal bipyramid since these two ligands can minimize their mutual repulsion by occupation of the two opposing axial positions. Typical examples for such cases are either $[XeF_5]^{-11}$ which possesses two free valence electron pairs on Xe or $[XeOF_5]^-$ which possesses one free pair and one doubly bonded oxygen ligand. This rationale can account for all the experimentally observed geometries and the presence or absence of fluxionality in these heptacoordinated species and allows the following general predictions where E and R signify free valence electron pairs and more repulsive ligands, respectively:

XF_7:	Fluxional pentagonal-bipyramid
XF_6E:	Fluxional distorted octahedron
XF_5E_2:	Semirigid pentagonal-bipyramid with two axial free electron pairs
XF_6R:	Rigid pentagonal-bipyramid with a more repulsive axial ligand
XF_5R_2:	Rigid pentagonal-bipyramid with two more repulsive axial ligands
XF_5ER:	Rigid pentagonal-bipyramid with a more repulsive axial ligand and axial-free electron pair.

ACKNOWLEDGMENT

REFERENCES

‡ Dedicated to Dr. Roland Bougon on the occasion of his 60th birthday.

1. Rocketdyne; new address Hughes STX-Phillips Laboratory, Building 8451, Edwards Air Force Base, CA 93524, and Loker Hydrocarbon Research Institute, University of Southern California, Los Angeles, CA 90089.

2. DuPont

3. McMaster University

4. Moody, G. J.; Selig, H. *Inorgn. Nucl. Chem. Lett.* **1966**, *2*, 319.

5. Selig, H. *Inorg. Chem.* **1966**, *5*, 183.

6. Waldman, M. C.; Selig, H. *J. Inorg. Nucl. Chem.* **1973**, *35*, 2173.

7. Schrobilgen, G. J.; Martin-Rovet, D.; Charpin, P.; Lance, M. *J. Chem. Soc. Chem. Commun.* **1980**, 894.

8. Holloway, J. H.; Kaucic, V.; Martin-Rovet, D.; Russell, D. R.; Schrobilgen, G. J.; Selig, H. *Inorg. Chem.* **1985**, *24*, 678.

9. Burbank, R. D.; Jones, G. R. *J. Am. Chem. Soc.* **1974**, *96*, 43.

10. Majhoub, A. R.; Seppelt, K. *Angew. Chem. Int. Ed. Engl.* **1991**, *30*, 323.

11. Christe, K. O.; Curtis, E. C.; Dixon, D. A.; Mercier, H. P.; Sanders, J. C. P.; Schrobilgen, G. J. *J. Am. Chem. Soc.* **1991**, *113*, 3351.

12. Christe, K. O.; Wilson, W. W. *Inorg. Chem.* **1988**, *27*, 1296.

13. Christe, K. O.; Wilson, W. W.; Wilson, R. D.; Bau, R.; Feng, J. *J. Am. Chem. Soc.* **1990**, *112*, 7619.

14. Schumacher, G. A.; Schrobilgen, G. J. *Inorg. Chem.* **1984**, *23*, 2923.

15. Christe, K. O.; Dixon, D. A.; Majhoub, A. R.; Mercier, H. P. A.; Sanders, J. C. P.; Seppelt, K.; Schrobilgen, G. J.; Wilson, W. W. *J. Am. Chem. Soc.* **1993**, *115*, 2696.

16. Christe, K. O.; Wilson, R. D.; Schack, C. J. *Inorg. Synth.* **1986**, *24*, 3.

17. GRADSCF is an ab initio program system designed and written by A. Komornicki at Polyatomics Research, Mountain View, CA..

18. Dunning, T. H., Jr.; Hay, P. J. in *Methods of Electronic Structure Theory*, Schaefer, H. F., III, Ed., Plenum Press: New York, 1977, Ch. 1.

19. Wadt, W. R.; Hay, P. J. *J. Chem. Phys.* **1985**, *82*, 284.

20. (a) Komornicki, A.; Ishida, K.; Morokuma, K.; Ditchfield, R.; Conrad, M. *Chem. Phys. Lett.* **1977** *45*, 595. (b) McIver, J. W., Jr.; Komornicki, A. *Chem. Phys. Lett.* **1971**, *10*, 202. (c) Pulay, P. in *Applications of Electronic Structure Theory*, Schaefer, H. F. III, Ed.; Plenum Press: New

York, 1977, p. 153; (d) Breidung, J.; Thiel, W.; Komornicki, A. *Chem. Phys. Lett.* **1988**, *153,* 76.

21.   (a) King, H. F.; Komornicki, A. *J. Chem. Phys.* **1986**,*84*, 5465. (b) King, H. F.; Komornicki, A. in *"Geometrical Derivatives of Energy Surfaces and Molecular Properties'*, Jorgenson, P.; Simons, J. Eds. NATO ASI Series C. Vol. 166, D. Reidel: Dordrecht 1986, p. 207.

22.   *Gaussian 92./DFT, Revision F.3*, Frisch, M. J.; Trucks, G. W.; Schlegel, H. B.; Gill, P. M. W.; Johnson, B. G.; Wong, M. W.; Foresman, J. B.; Robb, M. A.; Head-Gordon, M.; Replogle, E. S.; Gomperts, R.; Andres, J. L.; Raghavachari, K.; Binkley, J. S.; Gonzalez, C.; Martin, R. L.; Fox, D. J.; Defrees, D. J.; Baker, J.; Stewart, J. J. P.; and Pople, J. A., Gaussian, Inc., Pittsburgh PA, 1993.

23.   (a) Møller, C.; Plesset, M. S. *Phys. Rev.* **1934**, *46*, 618; (b) Pople, J. A.; Binkley, J. S.; Seeger, R. *Int. J. Quantum Chem. Symp.* **1976**, *10*, 1; Pople, J. A.; Krishnan, R.; Schlegel, H. B.; Binkley, J. S.; *Int. J. Quantum Chem. Symp.* **1979**, *-13*, 325; Handy, N. C.; Schaeferr, III *J. Chem. Phys.* **1984**, 81, 5031.

24.   (a) Andzelm, J.; Wimmer, E.; Salahub, D. R. In *The Challenge of d and f Electrons: Theory and Computation*; Salahub, D. R.; Zerner, M. C., Eds.; ACS Symposium Series, No. 394, American Chemical Society: Washington D. C., 1989; p228.   (b) Andzelm, J. In *Density Functional Theory in Chemistry*; Labanowski, J.; Andzelm, J., Eds.; Springer-Verlag: New York, 1991, p 155. (c) Andzelm, J. W.; Wimmer, E. *J. Chem. Phys.* **1992**, *96*, 1280.   DGauss is a density functional program available via the Cray Unichem Project.

25.   Godbout, N.; Salahub, D. R.; Andzelm, J.; and Wimmer, E. *Can. J. Chem.* **1992**, *70*, 560.

26.   Chen, H.; Kraskowski, M.; Fitzgerald, G., *J. Chem. Phys.* **1993**, *98*, 8710; (b) Troullier, N.; Martins, J. L. *Phys. Rev. B* **1991**,*43*, 1993.

27.   Vosko, S. J.; Wilk, L.; Nusair, W. *Can. J. Phys.* **1980**, *58*, 1200.

28.   (a) Becke, A. D. *Phys. Rev. A* **1988**, *38*, 3098. (b) Becke, A. D. In *The Challenge of d and f Electrons: Theory and Computation*; Salahub, D. R.; Zerner, M. C., Eds.; ACS Symposium Series, No. 394, American Chemical Society: Washington D. C., 1989; p166. (c) Becke, A. D. *Int. J. Quantum Chem. Symp.* **1989**, *23*, 599.

29.   Perdew, J. P. *Phys. Rev. B* **1986**, *33*, 8822.

30. Komornicki, A.; Fitzgerald, G. *J. Phys. Chem.* **1993**, *98*, 1398 and references therein.

31. Jameson, C. J.; Mason, J. in Multinuclear NMR; Mason, J., Plenum press:New Yrok, **1987**; Chapter 3, pp 66-68.

32. Mercier, H. P. A.; Sanders, J. C. P.; Schrobilgen, G. J.; Tsai, S. S. *Inorg. Chem.* **1993**, *32*, 386.

33. Jacob, E. J.; Bradford Thompson, H.; Bartell, L. S. *J. Mol. Struct.* **1971**, 8, 383, and references cited therein.

34. Begun, G. M.; Fletcher, W. H.; Smith, D. F. *J. Chem. Phys.* **1965**, *42*, 2236; Tsao, P.; Cobb, C. C.; Claassen, H. H. *J. Chem. Phys.* **1971**, *12*, 5247, and references cited therein.

35. For example, the following geometry and unscaled vibrational frequencies were obtained for C_{4v} $XeOF_5^-$ at the LDFT/ECP/DZVP level: r(Xe=O), 1.713 Å; $r(XeF_{eq})$=1.980 Å; $r(XeF_{ax})$=2.038 Å; $\angle OXeF_{eq}$=92.8°; $\angle F_{eq}XeF_{eq}$=89.8; A_1:υ_1=873 (167), υ_2=533 (75), υ_3=417 (88), υ_4=210 (3); B_1:υ_5=406 (O), υ_6=164 (O); B_2:υ_7=156 (O); E:υ_8=525 (640), υ_9=266 (O), υ_{10}=143 (O), υ_{11}=124 (O) cm^{-1} (IR intensity in km/mol).

36. Abriel, W. *Acta Crystallogr.*, Sect. B **1986**, *B42*, 449.

37. Klobukowski, M.; Huzinaga, S.; Seijo, L.; Barandiarán, Z. *Theor. Chim Acta.*, **1987**, *71*, 237.

38. (a) Christe, K. O.; Wilson, W. W. *Inorg. Chem.* **1989**, *28*, 3275. (b) Christe, K. O. *Inorg. Chem.* **1972**, *11*, 1220.

39. Christe, K. O.; Naumann, D. *Inorg. Chem.* **1973**, *12*, 59.

40. Christe, K. O.; Dixon, D. A.; Sanders, J. C. P.; Schrobilgen, G. J.; Wilson, W. W. *J. Am. Chem. Soc.* **1993**, *115*, 9461.

41. Christe, K. O.; Curtis, E. C.; Dixon, D. A. *J. Am. Chem. Soc.*; **1993**, *115*, 1520.

42. Christe, K. O.; Wilson, W. W.; Chirakal, R. V.; Sanders, J. C. P.; Schrobilgen, G. J. *Inorg. Chem.* **1990**, *29*, 3506.

43. Bougon, R.; Charpin, P.; Soriano, M. *C. R. Acad. Sci. Ser. C* **1972**, *272*, 565.

44. Mahjoub, A. R.; Hoser, A.; Fuchs, J.; Seppelt, K. *Angew. Chem. Int. Ed-Engl.* **1989**, *28*, 1526.

DIAGRAM CAPTIONS

Figure 1. ^{129}Xe NMR spectrum (139.051 MHz) of a saturated solution of $N(CH_3)_4^+XeOF_5^-$ in CH_3CN at 30°C.

Figure 2. ^{17}O NMR spectrum (67.801 MHz) of a saturated solution of $N(CH_3)_4^+XeOF_5^-$ (oxygen isotopic composition: ^{16}O, 36.5%, ^{17}O, 26.5% and ^{18}O, 37.0%) in CH_3CN at 30°C.

Figure 3. ^{19}F NMR spectrum (470.599 MHz) of a saturated solution of $N(CH_3)_4^+XeOF_5^-$ in CH_3CN at 30°C: (A) $XeOF_5^-$; (B) $XeOF_4 \cdot CH_3CN$. Asterisks denote ^{129}Xe satellites.
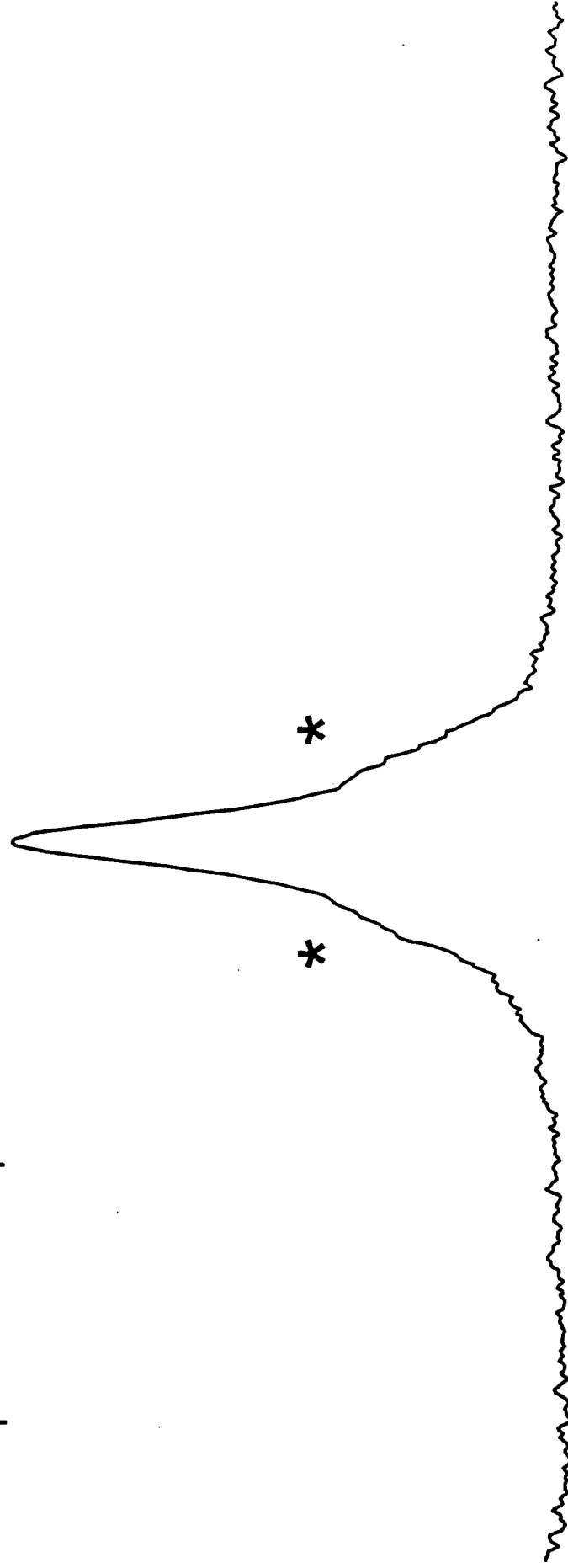
2500 Hz
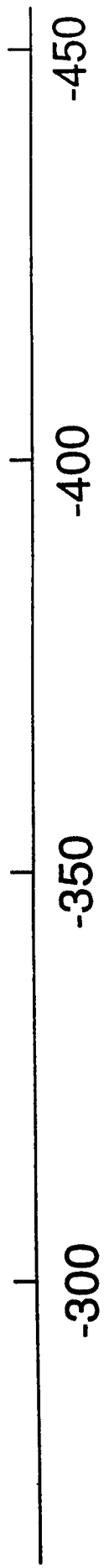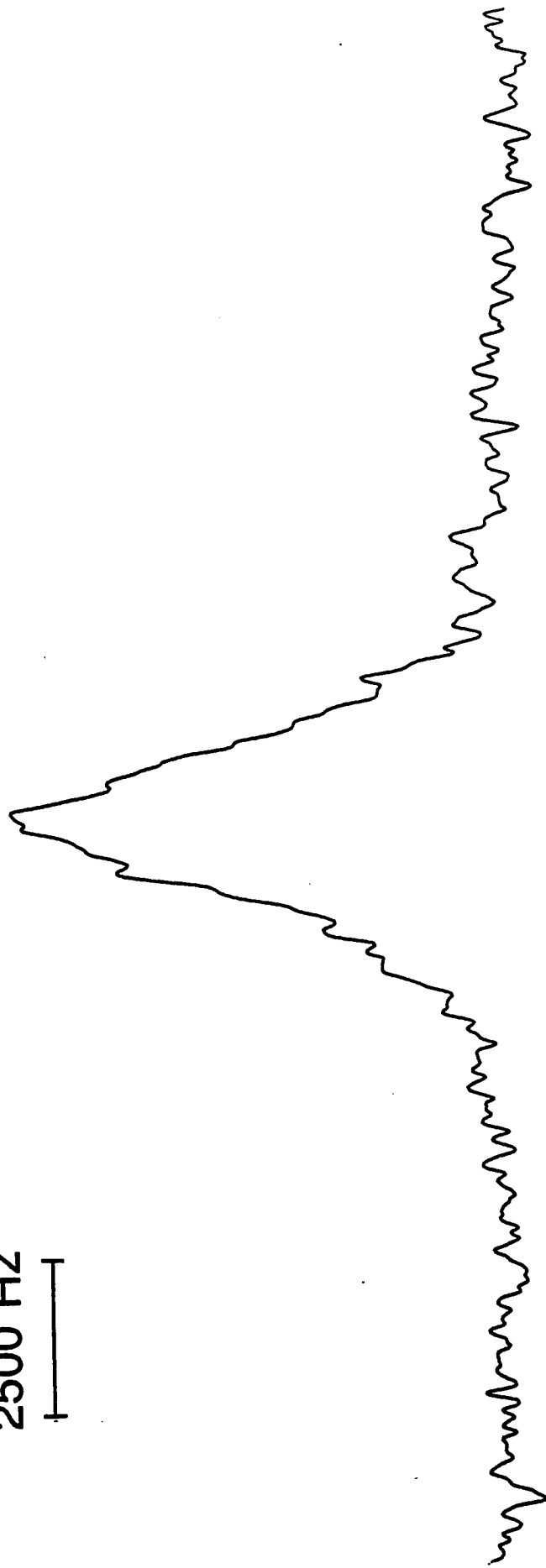
$\delta_{^{129}Xe}$ (ppm from $XeOF_4$)

FIGURE 1

1000 Hz

$\delta_{17}O$ (ppm from H_2O)

FIGURE 2

5000 Hz

A

B

*

*

90

100

110

120

$\delta_{19}F$ (ppm from $CFCl_3$)

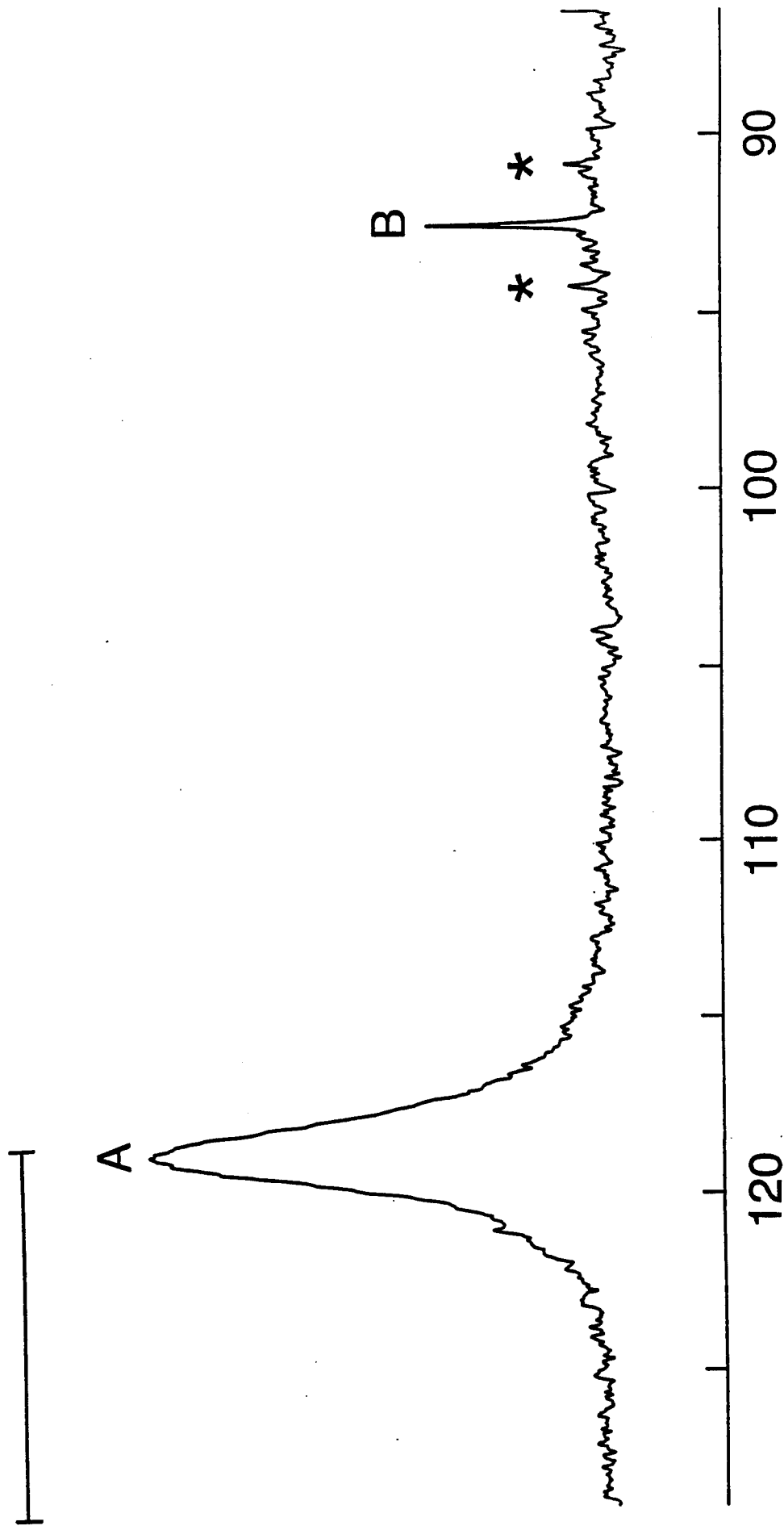FIGURE 3

TABLE 1. Vibrational Spectra of the XeOF₅⁻ Anion in Different Salts and their Assignments in Point Group C₅ᵥ Compared to Those of the Closely Related XeF₅⁻ and IOF₆⁻ Anions and IF₇

Column groups: columns 3–9 are **Calcd freq, cm⁻¹ (IR int)** for XeOF₅⁻ (C₅ᵥ); columns 10–14 are **Observed freq, cm⁻¹**.

Assign (activity)	Approx Mode Description	VWN/PP/DZVP Unscaled	VWN/PP/DZVP Scaled[a]	BP/PP/DZVP Unscaled	BP/PP/DZVP Scaled[b]	MP2/ECP/DZP Unscaled	HF/ECP/DZP Unscaled	HF/ECP/DZP Scaled[c]	N(CH₃)₄XeOF₅[e] IR 30°C	N(CH₃)₄XeOF₅ Ra room temp. and −150°C	CsXeOF₅ Ra[f] room temp.	CsXeOF₅ Ra ^{16}O[g] −196°C	CsXeOF₅ Ra ^{18}O[g] −196°C	XeF₅⁻(D₅ₕ) obsd freq, cm⁻¹ int (IR,Ra)[h]	IOF₆⁻(C₅ᵥ) obsd freq, cm⁻¹ int (IR,Ra)[j]	IF₇(D₅ₕ) obsd freq, cm⁻¹ int (IR,Ra)[k]
A₁(IR,Ra) ν₁	ν Xe=O	904(70)	870	865(66)	904	950(97)	759(16)	759[d]	878ms	880(32)	883(64)	883	839(66)	—	873(vs, 53)	
ν₂	ν sym XeF₅	535(3)	515	478(12)	500	465(2.9)	593(1.0)	516	516m	515(100)	525(100)	524	524(100)	502(-, 100)	584(-, 100)	635(-, 100)
ν₃	δ umbrella XeF₅	309(35)	297	288(36)	301	273(61)	362(84)	315	290ms	296(7)	290(7)	293	290(13)	290(m, -)	359(s, 4)	365(s, -)
E₁(IR,Ra) ν₄	ν as XeF₅	575(671)	553	503(604)	526	506(813)	565(1094)	492	495vs			{410, 396}	{407(7), 390(24)}	450(vs, -)	585(vs,)	670(vs, -)
ν₅	δ wag Xe=O	367(45)	353	342(68)	358	343(23)	407(42)	354	370m	370sh	368(20)	{384, 365}	{378(24), 352(15)}	—		
ν₆	δ as in plane XeF₅	279(8)	269	259(17)	271	259(12)	314(4.3)	273	273vw	270sh	275(5)	274	267(8)	274(s, -)	{407(vs, -); 341(-, 62); 260(s, 2)}	{425(vs, -); 319(-, 6); 257(w, -)}
E₂(−,Ra) ν₇	ν as XeF₅	458(0)	441	430(0)	460	406(0)	511(0)	445	—	{470(18), 450(10)}	{469(35), 439(2)}	{473, 468, 435}	{473(34), 468(29), 435(12)}	423(-, 16)	530(-, 4)	396(-, 2)
ν₈	δ sciss in plane XeF₅	417(0)	401	376(0)	393	376(0)	463(0)	403	—	397(54)	397(47)	{420, 390, 361}	{420(10), 390(40), 361(17)}	377(-, 23)	457(-, 49)	510(-, 17)
ν₉	δ pucker XeF₅	119(0)	115	97(0)	101	87(0)	148(0)	129	—	—	—	—	—	—	—	

(a) Scaled by empirical factor of 0.9653 to maximize the fit with the observed frequencies.
(b) Scaled by empirical factor of 1.0455
(c) Scaled by empirical factor of 0.8704.
(d) Unscaled frequency value.
(e) In addition to the listed bands, the following bands were observed. N(CH₃)₄XeOF₅: XeOF₅⁻, Ra, 840(4) = ν₇ (E₂) + ν₈(E₂) = 847 (A₁+A₂+E₁) being in Fermi resonance with ν₁(A₁); 560(2) = 2 ν₆(E₁) = 546 (A₁+E₂) being in Fermi resonance with ν₂(A₁); Ir, 834mw, (ν₇+ν₈); 655mw, (ν₆+ν₈); N(CH₃)₄⁺, Ra, 3054(4), 3037(2), 2990(2), 2965(3), 2930(1), 1464(12,) 1416(2), 1290(1), 1178(1), 951(14), 759(19), Ir, 3050mw, 2969w, 1486s, 1443w, 1416m, 1290mw, 1178w, 951s, 455sh. For the assignments of the N(CH₃)₄⁺ bands, see references 11,13,15, and 40 and references cited therein.
(f) Data from Reference 6.
(g) Data from Reference 8.
(h) Data from Reference 11.
(i) Data from Reference 15.
(k) Data from Reference 41.

Table 2. Observed and Calculated Geometries for XeOF$_4$

	Experimental[35]	HF/ECP/ DZP	MP2/ECP/ DZVP	VWN/ DZVP	VWN/ PP/DZVP	BP/ DZVP	BP/ PP/DZVP
rXe=O(Å)	1.7053 (0.00089)	1.720	1.722	1.786	1.676	1.814	1.688
rXe-F(Å)	1.9040 (0.00002)	1.879	1.959	2.002	1.883	2.035	1.908
∠O=Xe=F(°)	91.66 (0.072)	90.6	92.7	92.6	92.4	92.7	92.7

Table 3. Observed and Calculated Vibrational Frequencies (cm^{-1}) for XeOF$_4$

		Expt[36] (cm^{-1})	I(IR)	HF/ ECP/DZP Unscaled	HF/ ECP/DZP Scaled[a]	MP2/ ECP/DZP Unscaled	VWN/ DZVP Unscaled	VWN/ PP/DZVP Unscaled	BP/ DZVP Unscaled	BP/ PP/DZVP Unscaled
a$_1$	ν_1	926.3	(s)	778(9.6)	778	1001(62)	828(28)	945(44)	787(26)	904(40)
	ν_2	576.9	(m)	650(1.3)	581	542(3.4)	495(3.2)	595(2.4)	490(3.5)	559(2.4)
	ν_3	285.9	(s)	364(72)	307	276(48)	224(32)	314(30)	233(31)	304(29)
b$_1$	ν_4	543	(-)	614(0)	549	511(0)	467(0)	544(0)	464(0)	501(0)
	ν_5		(-)	239(0)	202	180(0)	141(0)	211(0)	153(0)	203(0)
b$_2$	ν_6	225	(-)	261(0)	220	215(0)	172(0)	231(0)	177(0)	229(0)
e	ν_7	609	(vs)	667(772)	596	614(478)	564(410)	655(481)	567(381)	619(461)
	ν_8	362	(s)	394(27)	333	341(19)	226(13)	351(23)	274(12)	339(10)
	ν_9	161		196(0.5)	165	173(5.6)	133(3.1)	195(0.8)	138(3.7)	195(0.7)

a Empirical scaling factors of 0.8947 and 0.8442 used for stretching and bending frequencies, respectively, ν_1 unscaled.

Table 4. Calculated Geometries of C_{5v} [XeOF$_5$]$^-$

	HF/ ECP/DZP	MP2/ ECP/DZP	VWN/ ECP/DZVP	BP/ ECP/DZVP	Predicted[a]
r Xe = O(Å)	1.733	1.737	1.691	1.703	1.72
r Xe-F(Å)	1.955	2.048	1.969	2.005	1.99
∠O=Xe-F(°)	91.0	92.8	92.2	92.6	92.2
∠F=Xe-F(°)	72.0	71.9	71.8	71.8	71.9

a Predicted values based on scale factors from XeOF$_4$ calculations.

Table 5. Symmetry Force Constants[a] and Potential Energy Distribution[b] of C_{5v} [XeOF$_5$]$^-$ Calculated from the Scaled VWN/PP/DZVP (A$_1$ and E$_2$) and HF/ECP/DZP (E$_1$) Second Derivatives

	freq (cm^{-1})			symmetry force constants			PED
	obsd	calcd					
A$_1$	880	870	F_{11}	F_{11} 6.334	F_{22}	F_{33}	98.2(1) + 1.8(3)
	515	515	F_{22}	0.067	2.953		99.3(2) + 0.3(3)
	296	297	F_{33}	0.065	0.357	2.394	96.8(3) + 2.7(2) + 0.1(1)
E$_1$	495	492	F_{44}	F_{44} 2.030	F_{55}	F_{66}	91.7(4) + 5.3(6) + 2.9(5)
	370	354	F_{55}	-0.358	2.183		85.0(5) + 14.1(6) + 0.9(4)
	273	273	F_{66}	0.083	-0.182	0.906	54.4(5) + 45.4(6) + 0.1(4)
E$_2$	460	441	F_{77}	F_{77} 2.132	F_{88}	F_{99}	90.2(7) + 9.5(8)
	397	401	F_{88}	0.119	1.966		88.9(8) + 10.6(7)
	—	115	F_{99}	0.173	0.050	0.587	99.1(9)

(a) Stretching constants in mdyn/Å, deformation constants in mdyn Å/rad^2, and stretch-bend interaction constants in mdyn/rad.

(b) PED in percent.

Table 6. Comparison of the Stretching Force Constants (mdyn/Å) of $[XeOF_5]^-$ to Those of Similar Molecules and Ions

	$f_{Xe=O}$	$f_{r(XeF)}$	f_{rr}	$f_{rr'}$
$XeOF_5^-$	6.33	2.25	0.15	0.20
XeF_5^{-a}	---	2.10	0.14	0.22
$XeOF_4^b$	7.08	3.26		
XeF_4^c	---	3.06		

(a) Data from ref. 11.
(b) Data from ref. 34.
(c) Data from ref. 39.

Karl O. Christe,* David A. Dixon,
Jeremy C.P. Sanders, Gary J. Schrobilgen,
Scott S. Tsai, and William W. Wilson

On the Structure of the [XeOF₅]⁻ Anion and of
Heptacoordinated Complex Fluorides Containing
One or Two Highly Repulsive Ligands or
Sterically Active Free Valence Electron Pairs

The new, highly explosive [XeOF₅]⁻ salt, N(CH₃)₄XeOF₅, was prepared and characterized by multinuclear NMR and vibrational spectroscopy. Theoretical calculations show that the observed spectra of [XeOF₅]⁻ agree only with a pseudopentagonal-bipyramidal structure of C₅ᵥ symmetry and not with the previously proposed, distorted octahedral structure of Cₛ symmetry. The preferences of heptacoordinated molecules for either pentagonal-bipyramidal or distorted octahedral structures and the fluxionality of some of these structures are rationalized by the presence or absence of unequal ligand repulsion effects.

C₅ᵥ

Cₛ